UNIVERSITÀ DEGLI STUDI DI MILANO

Dottorato di Ricerca in Scienze della Terra
Ciclo XXVI

Paleoceanographic and paleoclimatic reconstructions of the late Albian – early Turonian time interval: from an unstable to a stable ocean

Ph.D. Thesis

Gabriele Gambacorta
Matricola R09005

Tutore	**Anno Accademico**	*Coordinatore*
Prof.ssa Elisabetta Erba	**2012-2013**	**Prof.ssa Elisabetta Erba**

Co-Tutore
Prof. Riccardo Bersezio

“When someone leaves, it's because someone else is about to arrive.”
— Paulo Coelho, The Zahir

This doctoral dissertation is dedicated to Matilde,
The most beautiful of my discoveries

Index

Abstract

Earth during the Cretaceous (145.5-65.5 My) experienced long-lasting periods of warm climate with temperatures much higher than today. The continuous development of Large Igneous Provinces and the global rearrangement of plate boundaries led to an increase in atmospheric levels of greenhouse gasses (CO_2 and possibly CH_4), and times of restricted ocean circulation. Global warming and the abnormal increase in CO_2 changed the equilibria of the carbon cycle thus altering the hydrologic cycle, nutrients distribution, upwelling intensity and deep water formation. The geological record of the late Albian to early Turonian (~104-92 My) time interval represents a particularly intriguing natural laboratory to understand the physical, chemical and biological processes that acted during a period of alternated phases of relative equilibrium and carbon cycle perturbations. The late Albian to early Turonian time interval is characterized by three major geochemical anomalies corresponding to positive excursions of the stable carbon isotope profile: the Oceanic Anoxic Event 1d (OAE1d), the Mid-Cenomanian Event (MCE) and the Oceanic Anoxic Event 2 (OAE2).

This study, combining sedimentological, geochemical (C and O isotopes, inorganic and organic geochemistry) and high-resolution cyclostratigraphic data, provides an integrated investigation of paleoenvironmental and climatic dynamics accompanying these major events. The interplay of surface water changes and sea bottom processes are here discussed with the purpose of better defining how water masses react during highly stressed climatic/environmental conditions.

Five pelagic Tethyan key-sections, four from the Umbria-Marche Basin (Furlo, Contessa, Le Brecce, Monte Petrano – central Italy) and one from the Belluno Basin (Cismon – northern Italy), were chosen as natural archives of the past oceanographic and environmental conditions.

The extremely detailed field- to microscopic-scale sedimentological description of the five sections allowed a better comprehension of the physical processes that acted on the sea-floor during the deposition of the studied sequences. Peculiar sedimentary structures and facies indicate that settling of biogenic particles wasn't the only physical process controlling pelagic sedimentation. Waning and waxing cycles of bottom currents actively redistributed sediments, forming specific facies. In order to account for this process, a new depositional model for calcareous pelagic contourites was established.

New high-resolution oxygen, carbonate- and organic-carbon isotope record were produced for Monte Petrano and Cismon sections. High-resolution $\delta^{13}C$ record exhibits three positive excursions in correspondence of OAE1d, MCE and OAE2. The detailed correlation with published and unpublished isotopic data from the other studied sections better defines the basin-scale stratigraphic framework.

Detailed correlations of the $\delta^{13}C$ profiles through the OAE2 interval revealed the presence of a significant hiatus at the top of the Bonarelli Level in all studied sections. Even if the amount of missing sequence slightly differs from site to site, the hiatus affects both the Umbria-Marche and Belluno basins.

Important lithological changes are associated with the observed carbon isotopic excursions (CIEs). Few centimeter thick black shale layers are associated with the Pialli Event (OAE1d) and the impressive Bonarelli Level is the lithologic expression of the OAE2. The MCE corresponds, instead, to more subtle and intriguing conundrum. Starting from this event up to the Bonarelli Level the studied successions are characterized by the lithologic alternation of organic-rich shales and black chert bands with whitish limestones. A stratigraphic vertical variation of the identified facies was reconstructed and linked to the major geologic events. The interplay of the paleoceanographic processes controlling the sediment composition combined with current-driven sediment distribution resulted in characteristic cyclic patterns. Recurrent stacking patterns, from layer- to lamina-scale, are the result of alternated phases of slackish conditions with times of enhanced circulation. Sedimentological evidence above the Pialli Level (OAE1d) and above the Bonarelli Level (OAE2) indicates that intense bottom-current activity characterized the recovery phases from these major climatic/oceanographic perturbations. In particular, the diffused sedimentary structures indicative of particularly intense bottom-current traction above the Bonarelli Level suggest that the observed hiatus might have been produced by major erosions and reworking of the sediments on the sea-floor during the recovery from anoxic conditions.

Major and trace element geochemical data were produced for Cismon and Monte Petrano sections in order to better understand the paleoenvironmental changes that characterized these two adjacent basins. Element/Al ratios of Ti, Mg, K, Rb, and Zr are fairly constant, indicating a mostly homogeneous source area. Ba and P are present in high concentrations in both sections indicating relatively high-productivity conditions in both areas. The Bonarelli Level is severely depleted in Mn, suggesting oxygen-depleted bottom water conditions in an open marine environment in both the Umbria-Marche and Belluno Basins, while the Cenomanian rhythmic black levels seem to have been deposited in a much more restricted setting. At Cismon, with the exception of the Bonarelli Levels, the depositional environment was dysoxic without ever reaching truly anoxic conditions. However, redox-sensitive elements from both analyzed sections indicate that the MCE marked the onset of more unstable conditions, with alternate times of dysoxic/anoxic and well-oxygenated bottom-waters. Zn and Cu concentrations rise up to high values in the interval between the MCE and the Bonarelli Level, presumably indicating hydrothermal activity.

The application of cyclostratigraphic techniques to all the studied sections from the Umbria-Marche Basin shows that primary productivity variations, represented by the cyclic alternation of carbonate and siliceous lithologies, reflect the climatic, oceanographic and depositional response to orbital cycles. In particular, sediment production and deposition were controlled by short eccentricity (about 100ky) and obliquity (about 40ky) forcing. The applied probabilistic approach allows the determination of a proper sedimentation rate model for the studied sections. The results show a general increase in the sedimentation rate after the MCE and a progressive reduction of sedimentation rates in the OAE2 interval. Spectral analyses of mm-scale sedimentological logs of the Bonarelli Level at Furlo and Contessa indicate very low sedimentation rates for the OAE2, and confirm the presence of hiatuses. According to the sedimentation rate model, and deriving an age of 94My for the beginning of the OAE2, the OAE1d started at about 102.4My and lasted for about 1.2My, while the age of the MCE is about 97My and lasted about 200ky.

Highly detailed sedimentological characterization was central to fully comprehend the pelagic sedimentation in Western Tethys during times of stable and perturbed conditions. Based on bio-chemo- and cyclostratigraphy, facies evolution was precisely dated and event duration was estimated. This multi-proxy approach was proved vital to characterize an apparently homogenous and monotonous sedimentary environment that was indeed extremely dynamic. The vertical repetitive stacking of facies belonging to contrasting depositional suites (settled and tractive) and to opposite oxygenation regimes (oxic vs. anoxic) suggests that the environmental resilience of the pelagic system recovers from perturbations through various instability stages, such as sediment erosion, winnowing and redistribution by bottom currents. This kind of adaptive behavior can be considered an autocyclic process (the recovery), forced by allo-cyclic factors (the perturbations).

This study provides an important step towards a more comprehensive understanding of the mechanisms at the origin of ‘mid-Cretaceous’ paleoceanographic events, including feedbacks to trigger anoxia-dysoxia and re-establish normal conditions at various time scales. The multi-proxy approach used here to decipher the geological record demonstrates that the onset, transition and recovery from anoxia didn’t happen instantaneously but was the result of a continuous subtle variation of processes in an extremely dynamic setting.

Abstract

La Terra durante il Cretaceo (145.5-65.5 Ma) ha sperimentato lunghi periodi di clima caldo con temperature molto più elevate rispetto ad oggi. Il continuo sviluppo di Grandi Province Ignee (LIP) e il riassetto globale dei confini di placca ha portato ad un aumento dei livelli atmosferici di gas serra (CO_2 e in alcuni casi CH_4) e fasi di limitata circolazione oceanica. Il riscaldamento globale e l'aumento abnorme di CO_2 hanno cambiato sensibilmente gli equilibri del ciclo del carbonio, alterando così il ciclo idrologico, la distribuzione dei nutrienti, l'intensità dell'upwelling e la formazione di acque profonde. Il record geologico dell'intervallo di tempo compreso tra il tardo Albiano e il Turoniano basale (~ 104-92 Ma) rappresenta un laboratorio naturale particolarmente intrigante per comprendere i processi fisici, chimici e biologici che hanno agito nel corso di questo periodo, caratterizzato dall'alternarsi di fasi di relativo equilibrio e fasi di alterazione del ciclo del carbonio. L'intervallo tra il tardo Albiano e il Turoniano basale è caratterizzato da tre grandi anomalie geochimiche corrispondenti alle escursioni positive della curva isotopica del carbonio: l'Evento Anossico 1d (OAE1d), l'Evento Cenomaniano Medio (MCE) e l'Evento Anossico 2 (OAE2).

Questo studio, tramite l'integrazione di dati sedimentologici, geochimici (isotopi del carbonio e dell'ossigeno, geochimica inorganica e organica) e ciclostratigrafia ad alta risoluzione, offre un'indagine integrata delle dinamiche paleo-ambientali e climatiche che accompagnarono questi grandi eventi. Particolare enfasi è volta alla comprensione dell'interazione tra i cambiamenti che avvengono nelle acque superficiali e i processi che agiscono sul fondo mare, con lo scopo di meglio definire il comportamento delle masse d'acqua in condizioni ambientali /climatiche estreme.

Come archivi naturali delle passate condizioni oceanografiche e ambientali sono state scelte cinque sezioni pelagiche Tetidee chiave: quattro dal Bacino Umbro-Marchigiano (Furlo, Contessa, Le Brecce, Monte Petrano - Italia centrale) e una dal Bacino di Belluno (Cismon - Italia settentrionale).

La descrizione sedimentologica ad alta risoluzione delle cinque sezioni – dalla scala di terreno fino alla scala microscopica- ha condotto ad una migliore comprensione dei processi fisici che hanno agito sul fondo marino durante la deposizione delle sequenze studiate. La presenza di peculiari strutture e facies sedimentarie indica che la sedimentazione pelagica non è esclusivamente governata dalla decantazione di particelle biogeniche. Correnti di fondo di intensità crescente e calante in modo ciclico ridistribuiscono attivamente i sedimenti presenti, formando facies specifiche e riconoscibili. Al fine di considerare anche questo processo, è stato definito un nuovo modello deposizionale per le contouriti carbonatiche pelagiche.

Nuovi dati isotopici ad alta risoluzione dell'ossigeno e del carbonio sia su carbonato che su materia organica sono stati prodotti per le sezioni del Monte Petrano e del Cismon. Il profilo ad alta risoluzione di $\delta^{13}C$ presenta tre escursioni positive in corrispondenza dell'OAE1d, MCE ed OAE2. Inoltre, la correlazione dettagliata con ulteriori profili isotopici editi ed inediti disponibili per le altre sezioni studiate ha permesso di definire con maggiore accuratezza l'inquadramento stratigrafico a scala di bacino.

Correlazioni dettagliate dei profili di $\delta^{13}C$ attraverso l'intervallo OAE2 rivelano la presenza di uno hiatus significativo nella parte superiore del Livello Bonarelli presente in tutte le sezioni studiate. Anche se la quantità di sequenza mancante differisce leggermente da sito a sito, lo hiatus interessa sia il Bacino Umbro-Marchigiano che il Bacino di Belluno.

Importanti variazioni litologiche sono associate alle escursioni isotopiche del carbonio (CIE). Alcuni strati spessi pochi centimetri di scisto nero sono associati all'Evento Pialli (OAE1d) mentre l'impressionante livello Bonarelli è l'espressione litologica dell'OAE2. L'evento MCE costituisce, invece, un enigma più sottile e intrigante. A partire da questo evento fino al Livello Bonarelli le successioni studiate sono caratterizzate dall'alternanza litologica di scisti ricchi di materiale organico e bande di selce nera intercalate a calcari biancastri. E' stata così ricostruita la variazione verticale stratigrafica delle facies identificate e messa in relazione ai principali eventi geologici. L'interazione dei processi paleoceanografici che controllano la composizione dei sedimenti in combinazione con la distribuzione dei sedimenti da parte delle correnti ha provocato caratteristiche sequenze cicliche. Stacking pattern ricorrenti, da scala di strato a scala di lamina, sono il risultato dell'alternarsi di fasi dominate da condizioni di acque stagnanti con fasi caratterizzate da circolazione intensificata. Evidenze sedimentologiche provenienti dagli strati al di sopra del livello Pialli (OAE1d) e al di sopra del livello Bonarelli (OAE2) testimoniano l'intensa azione di correnti di fondo durante le fasi di recupero da questi grandi perturbazioni climatiche/oceanografiche. In particolare, le diffuse strutture sedimentarie indicative di correnti di trazione al fondo particolarmente intense nella successione sopra al livello Bonarelli suggeriscono che lo hiatus osservato possa essere stato prodotto dalla significativa azione di erosione e ridistribuzione dei sedimenti sul fondo marino durante la fase di recupero dalle condizioni anossiche.

Per le sezioni del Cismon e del Monte Petrano sono stati prodotti anche dati geochimici degli elementi maggiori e in traccia (XRF), al fine di comprendere meglio i cambiamenti paleoambientali che hanno caratterizzato questi due bacini adiacenti tra loro. I valori abbastanza costanti delle concentrazioni di Ti, Mg, K, Rb, e Zr normalilizzate all'alluminio (elemento/Al) indicano una sorgente dei sedimenti prevalentemente omogenea. Le alte concentrazioni di Ba e P in entrambe le sezioni evidenziano

condizioni di produttività primaria relativamente elevata in entrambe le aree. Il Livello Bonarelli è severamente impoverito in Mn, suggerendo che la sua deposizione avvenne sia per il Bacino Umbro-Marchigiano che per il Bacino di Belluno in ambiente marino aperto, caratterizzato da acque profonde impoverite di ossigeno, mentre i livelli neri ritmici del Cenomaniano sembrano essere stati depositati in un ambiente molto più ristretto. I dati relativi alla sezione del Cismon indicano che, ad eccezione del Livello Bonarelli, l'ambiente deposizionale fu generalmente disossico, senza mai raggiungere condizioni veramente anossiche. Tuttavia, gli elementi redox-sensibili di entrambe le sezioni analizzate indicano che l'Evento MCE segnò l'instaurarsi di condizioni più instabili, caratterizzate da fasi alternate di disossia/anossia e fasi con acque profonde ben ossigenate. Concentrazioni di Zn e Cu raggiungono valori elevati nell'intervallo tra l'evento MCE e il livello Bonarelli, indicando presumibilmente l'esistenza di attività idrotermale.

Tutte le sezioni del Bacino Umbro-Marchigiano sono state analizzate con tecniche ciclostratigrafiche, che hanno potuto mettere in luce quanto le variazioni di produttività primaria, rappresentata dalla variazione ciclica di carbonato e litologie silicee, riflettano la risposta climatica, oceanografica e deposizionale ai cicli orbitali. In particolare, la produzione e la deposizione di sedimenti risultano essere controllate dall'eccentricità breve (circa 100ka) e dall'obliquità (circa 40ka). L'approccio ciclostratigrafico di tipo probabilistico qui seguito consente la determinazione di un modello di velocità di sedimentazione adeguato per ciascuna sezione studiata. Tali modelli di sedimentazione sono caratterizzati da un generale aumento del tasso di sedimentazione dopo l'evento MCE e da una successiva progressiva riduzione nell'intervallo OAE2. L'analisi spettrale del log litologico a scala millimetrica del livello Bonarelli al Furlo e alla Contessa indicano infatti tassi di sedimentazione molto bassi per l'OAE2 e confermano la presenza di hiatus. Secondo quanto stimato dal modello di sedimentazione e fissando l'inizio dell'OAE2 a 94Ma, si stima l'OAE1d sia iniziato a circa 102.4Ma e sia durato per circa 1.2Ma, mentre si valuta l'inizio del MCE intorno a 97Ma con una durata di approssimativamente 200ka.

La caratterizzazione sedimentologica altamente dettagliata è stata fondamentale per comprendere appieno la sedimentazione pelagica nella Tetide occidentale, durante le fasi di condizioni sia stabili che perturbate. Sulla base dei dati bio-, chemo- e ciclostratigrafici, l'evoluzione delle facies è stata datata con precisione ed è stata stimata la durata degli eventi.

Questo approccio *multi-proxy* si è dimostrato fondamentale per caratterizzare un ambiente sedimentario apparentemente omogeneo e monotono ma in realtà estremamente dinamico. La sovrapposizione ripetitiva di facies appartenenti a suite deposizionali contrastanti (decantazione e trazione) e di regimi di ossigenazione opposti (ossico vs anossico) suggerisce che la resilienza

ambientale del sistema pelagico si riprende dalle perturbazioni attraverso differenti fasi di instabilità, come ad esempio erosione, *winnowing* e redistribuzione dei sedimenti da parte di correnti di fondo. Questo tipo di comportamento adattattivo può essere considerato un processo auto-ciclico (il recupero), forzato da fattori allociclici (le perturbazioni).

Questo studio fornisce un importante passo verso una più completa comprensione dei meccanismi all'origine degli eventi paleoceanografici del 'Cretaceo medio', tra cui i fattori che innescano i cambiamenti anossia-disossia e ristabiliscono condizioni stabili a varie scale temporali. L'approccio *multi-proxy* utilizzato qui per decifrare il record geologico dimostra che l'insorgenza, la transizione e il recupero da condizioni di anossia non è accaduto istantaneamente, ma è stato il risultato di una continua e sottile variazione di processi in un ambiente estremamente dinamico.

Chapter 1

Introduction

"Time does not efface what noble men leave behind, and their prowess shines forth even when they are dead." (Euripides, Andromache 775). This is what Euripides said about 2500 years ago. The sense of time passing by have fascinated and scared the human mind at the dawn of history.

In the “Allegory of Time governed by Prudence” Tiziano painted the sense of time with three human heads. On the left, slightly in the shade, an old man looks towards the past living of his own memories. An adult man, in the middle, is daring the present, while on the right, well-lighted, a youth looks with hope to the future. An inscription adds: "Ex praeterito praesens prudenter agit, ni futurum actione deturpet", “From the (experience of the) past, the present acts prudently, lest it spoil future action". It doesn’t’ simply represents a hymn to the flow of time but an invitation to the value of the past as an infinite source of inspiration for the present and the future.

The vastness of Earth’s history can lead us immeasurable inspirational secrets.

1.1 The climate system of the Cretaceous

Cretaceous Earth was, by comparison with the present, an alien world (Sellwood and Valdes, 2006).

During this time interval Earth was experiencing a global plate boundary re-arrangement (Blakey, 2012) (Fig. 1.1). The supercontinent Pangaea completed its tectonic breakup into present day continents. Southern continents (Gondwana and the Antarctic) were separated from the northern ones (Laurasia/North America), thus allowing a circumglobal oceanic connection (Hay et al., 1999; Skelton et al., 2003; Sellwood and Valdes, 2007). During the Cretaceous Gondwana broke up as South America, Antarctica and Australia rifted away from Africa, thus forming the South Atlantic and the Indian Oceans. The convergent-margin orogenies continued in the North American Cordillera and Tethys Sea continued to narrow. The concurrence of a greenhouse climate and intense rifting raised eustatic sea levels worldwide (Haq et al., 1987; Takashima et al., 2006; Selwood and Valdes, 2007); wide shallow seas were present in North America (the Western Interior Seaway) and Europe (Mutterlose and Kessels, 2000). At the peak of the Cretaceous transgression, one-third of Earth's present land area was submerged.

Earth during the Cretaceous experienced long-lasting periods of warm climate (Jenkyns, 1999, 2003, 2010; Hu et al., 2012) with temperatures much higher than today (Hay, 2008) (Fig. 1.2). The whole planet was 6°C or more warmer than now, with warm ocean depths and widespread aridity in the equatorial region (Norris et al., 2002; Sellwood and Valdes, 2006) and a consequent reduction of latitudinal thermal gradients (Huber, 1995; Skelton et al., 2003; Donnadieu et al., 2006; Hay, 2008) with ensuing low seasonality.

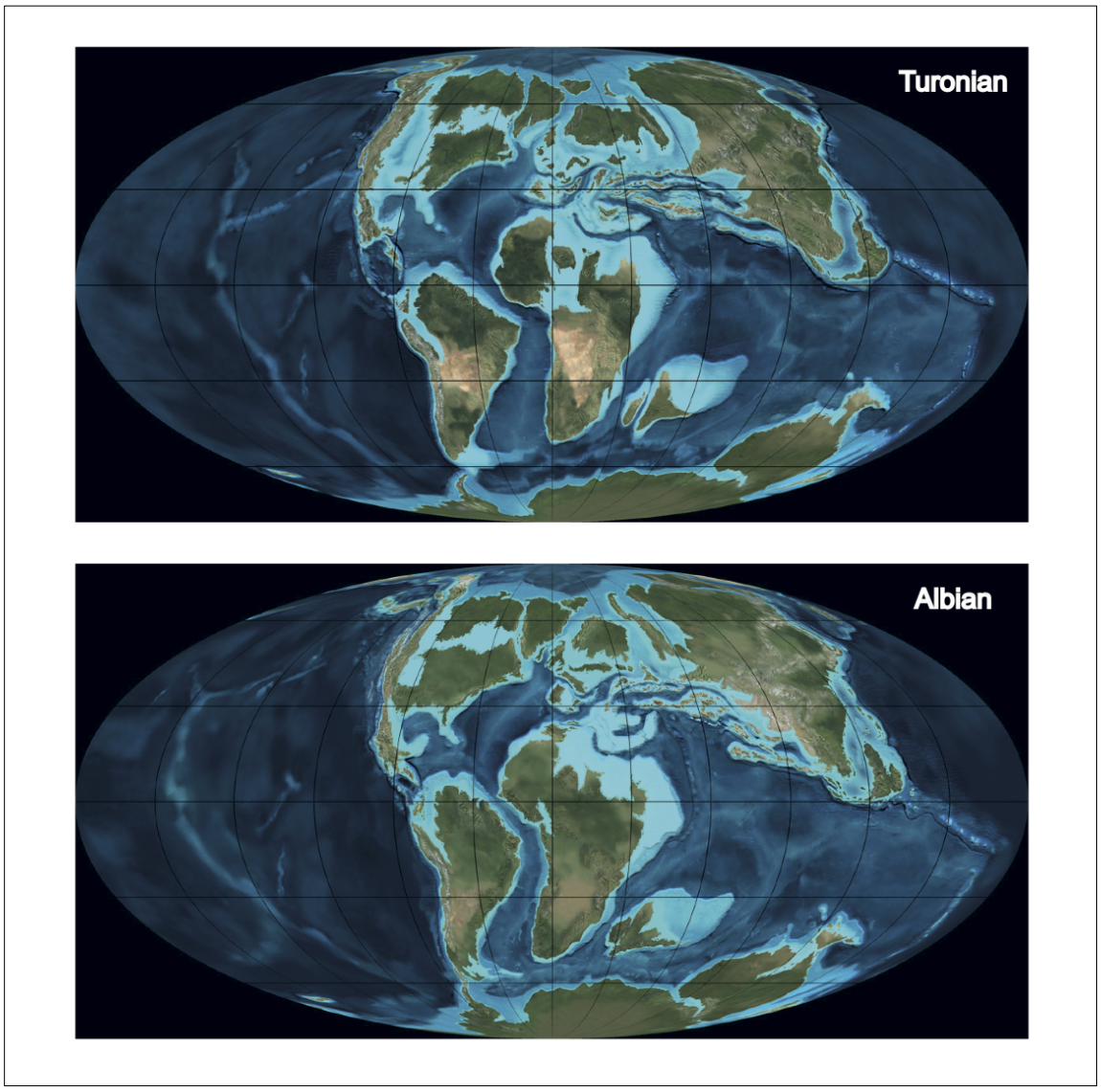

Figure 1.1: *Palaeogeographic reconstructions of the Albian and Turonian time interval (after Blakey, 2012).*

Polar regions were supposed to be ice-free for most of the time (e.g. Hallam, 1985 and Hallam, 1994; Takashima et al., 2006). Price (1999), according to sedimentological data (abraded rock surfaces,

generally unsorted stone-rich beds and the presence of dropstones), faunal and floral evidence and palaeoclimatic modeling, suggested that Mesozoic was surely much warmer than today, but punctuated by a number of episodes of cold or sub-freezing polar climates. According to Price (1999) the extent of polar ice during the Mesozoic is likely to have been approximately one third the size of the present day. The poles weren't thus probably permanently covered by ice caps but received winter snow and probably at least seasonal sea ice was formed (Hay, 2002; Selwood and Valdes, 2007). A weak point to be solved in order to reach a wider acceptance of a common theory on the presence or absence of ice at poles, lies in the inconsistency of the results coming from climate models and what proxy data seem to suggest. Partially, these differences in results are related to the instability of solutions of the models at the poles making them less reliable together with a possible incorrect interpretation of proxy data.

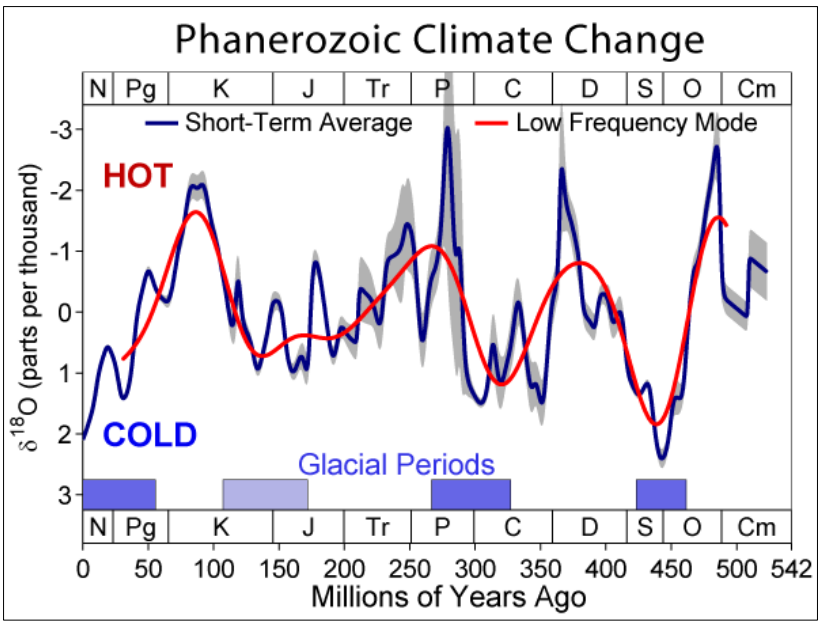

Figure 1.2: *Oxygen isotope ratios over the last 500+ million years used to estimate past climates (after Robert A. Rohde, Global Warming Art).*

On Earth, the distribution of the areas with precipitation exceeding evaporation is controlled by the Inter Tropical Convergence Zone (ITCZ, Selwood and Valdes, 2007) and the associated atmospheric circulation system of the Hadley cells (Wang, 2009; Hay and Floeger, 2012; Wagner et al., 2013). According to Hasegawa et al. (2012), during the Early and Late Cretaceous the reduced latitudinal thermal gradient led to an expansion of the Hadley cells circulation poleward in response to the increase in global temperatures. According to this model, as a consequence a correspondent shifting to higher latitudes of the subtropical high-pressure belt happened. Instead, according to the same authors, during the mid-Cretaceous the global temperatures and/or atmospheric CO2 levels exceeded a certain

threshold that led to a drastically shrinking equatorwards of the Hadley circulation. These major expansion and shrinking of the Hadley convection cells might have had a major impact on the global Cretaceous climatic system, affecting the prevailing surface-wind patterns and thus controlling indirectly the latitudinal distribution of deserts and monsoons.

Many reasons are supposed to be at the origin of the particularly high-temperatures experienced during the Cretaceous. The palaeogeographical distribution of the continental masses must have played an important role in the global temperature flow balance (Donnadieu et al., 2006). The particular disposal of the continents must have affected the thermal heating regime thanks to the thermal conductivity of landmasses and different oceanic circulation.

Incredibly huge submarine and subaerial volcanic episodes were occurring, with emission of extraordinary masses of magma on wide areas and huge volumes of CO_2 as well as other gases and particulates. The most important of these events, called Large Igneous Provinces (LIPs), were: North Atlantic Volcanic Province (NAVP) (Saunders et al., 1997), Deccan event (Eldholm and Coffin, 2000), Maud Rise event (Eldholm and Coffin, 2000), Madagascar event (Storey et al., 1997), Caribbean-Colombian Cretaceous Igneous Province (CCCIP) (Kerr et al., 1997), Alpha Ridge-Queen Elizabeth Islands event (Embry and Osadetz, 1988; Ernst and Buchan, 1997), Kerguelen event (Coffin et al., 2002), Ontong Java event (Neal et al., 1997; Eldholm and Coffin, 2000), Manihiki Plateau event (Eldholm and Coffin, 2000), Paranà-Etendeka event (Peate, 1997).

Moreover, reduced chemical weathering of Ca-silicate rocks, and relative CO_2 drawdown effect (Vaughan, 2007; Skelton et al., 2003), was probably quite reduced during Cretaceous due to the lack of major mountain belts.

Several evidences suggest that the global rearrangement of plate boundaries cannot be considered alone as a sufficient cause, but that other processes must have concurred in the origin of such an anomalous climate. Barron and Washington (1985) run experiments with a general circulation model of the atmosphere coupled to a simple ocean model and estimated that two to tenfold increase in CO_2 with respect to present day values are needed to explain the geologic data (Barron and Washington, 1985) (Fig. 1.3). Haworth et al. (2005) from stomatal characteristics of an extinct Cretaceous conifer (*Pseudofrenelopsis parceramosa*) estimated pCO_2 levels for the Hauterivian-Albian interval ranging from about 560 up to 1200 ppm.

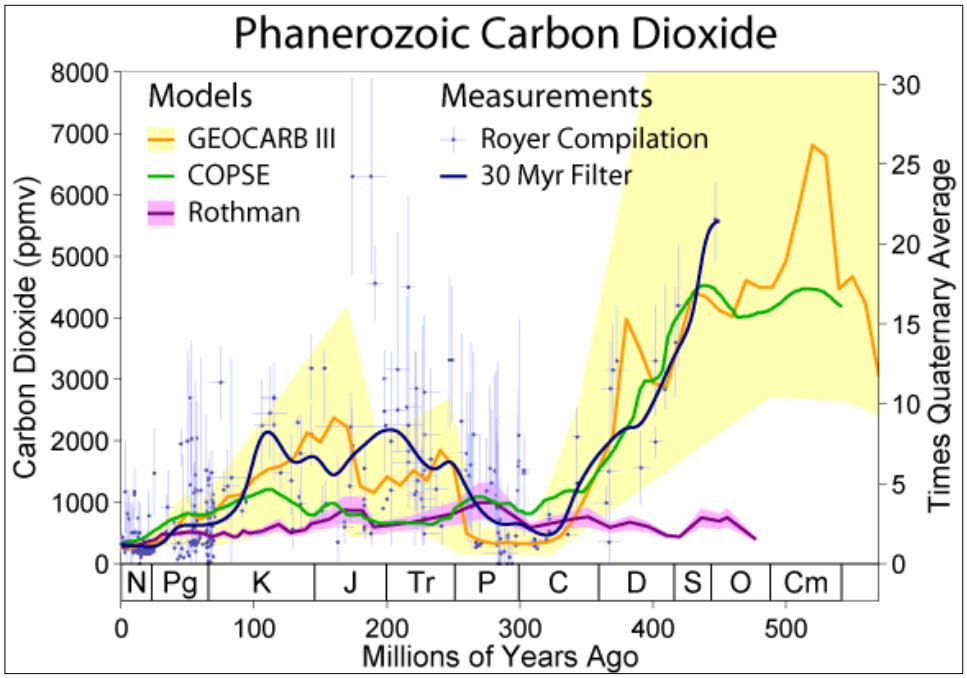

Figure 1.3: *Changes in carbon dioxide concentrations during the Phanerozoic era. Three estimates are based on geochemical modelling: GEOCARB III (Berner and Kothavala 2001), COPSE (Bergmann et al. 2004) and Rothman (2002). These are compared to the carbon dioxide measurement database of Royer et al. (2004) and a 30 Ma filtered average of those data. Error envelopes are shown when they were available. The right hand scale shows the ratio of these measurements to the estimated average for the last several million years (the Quaternary) (after Robert A. Rohde, Global Warming Art)).*

The continuous development of LIPs and the global rearrangement of plate boundaries led to an increase in atmospheric levels of greenhouse gasses, CO_2 and possibly CH_4, and times of restricted ocean circulation (Jenkyns, 2010). Local anoxia occurred during the earlier Cretaceous and became regional to global during the middle Cretaceous (Hay, 2008), with times of widespread production and burial of organic matter. Oceanic currents and climatic conditions might have been very different from that of today considering that in the modern oceans it's impossible for large areas to become anoxic (Hay, 2008).

The Russian research group headed by Nicolai Chumakov of the Geological Institute of the Russian Academy of Sciences produced fantastic maps documenting the climatic patterns throughout the Cretaceous with the support of palaeontological, sedimentological and mineralogical data (Chumakov, 1995, 2004; Chumakov et al., 1995; Hay and Floegel, 2012) (Fig. 1.4).

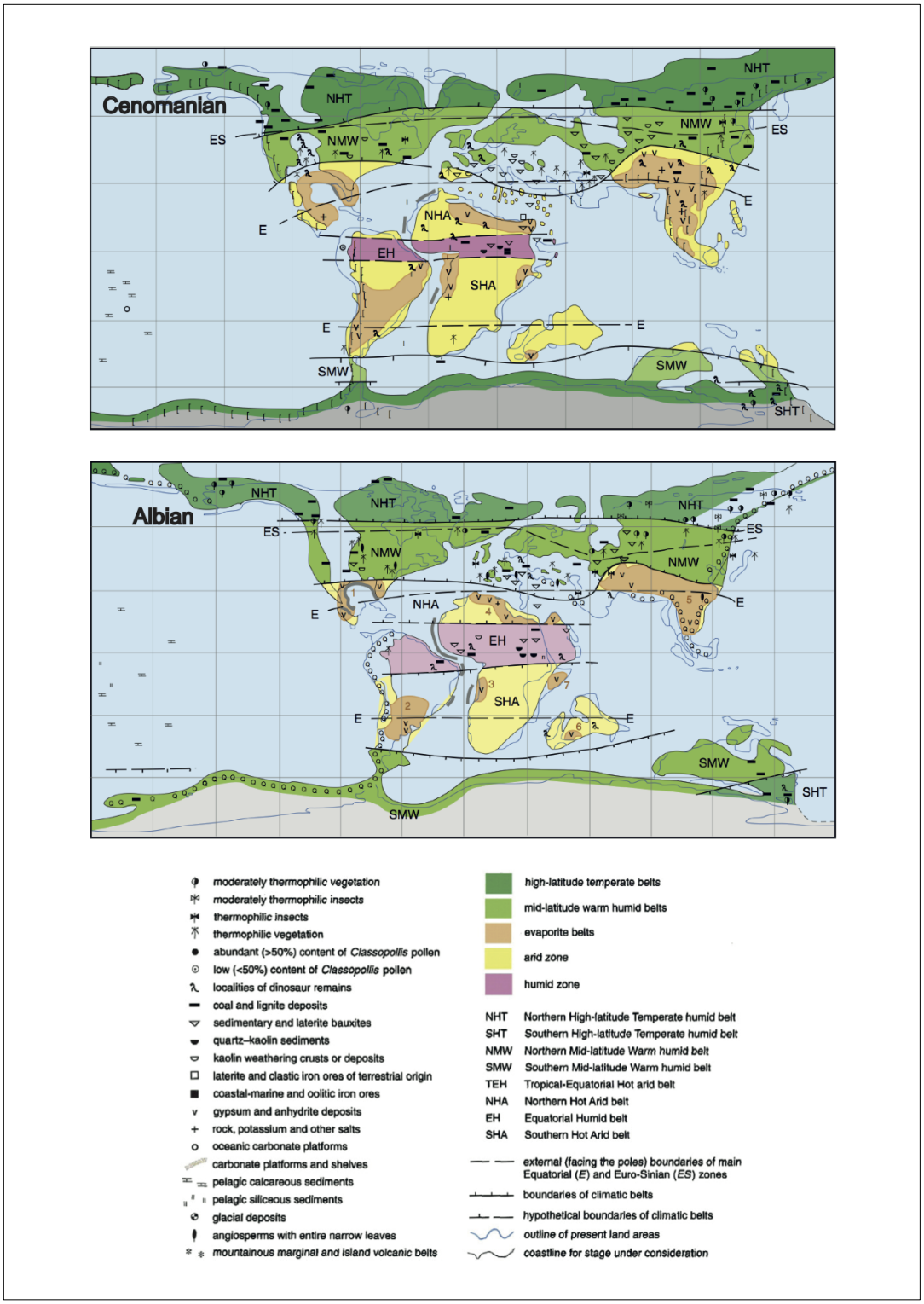

Figure 1.4: *Albian and Cenomanian climatic indicators and zone, after Chumakov et al. (1995) (after Hay and Floegel, 2012).*

1.2 Carbon cycle and the climate system

Carbon, the fourth most abundant chemical element in the universe by mass after hydrogen, helium, and oxygen, plays an important role on the climate system (Vaughan, 2007). In particular, its gaseous form carbon dioxide represents a powerful greenhouse gas.

Huge volumes of carbon dioxide were stored in the mantle when the Earth formed and outgassed from the Earth's interior at mid-ocean ridges and hot-spot volcanoes to form the present day atmosphere (Robock and Oppenheimer, 2003).

Due to a complexity of different biogeochemical processes, carbon passes through time into a series of different geochemical reservoirs. Such kind of cyclic exchange goes under the name of Global Carbon Cycle (Figs. 1.5 and 1.6).

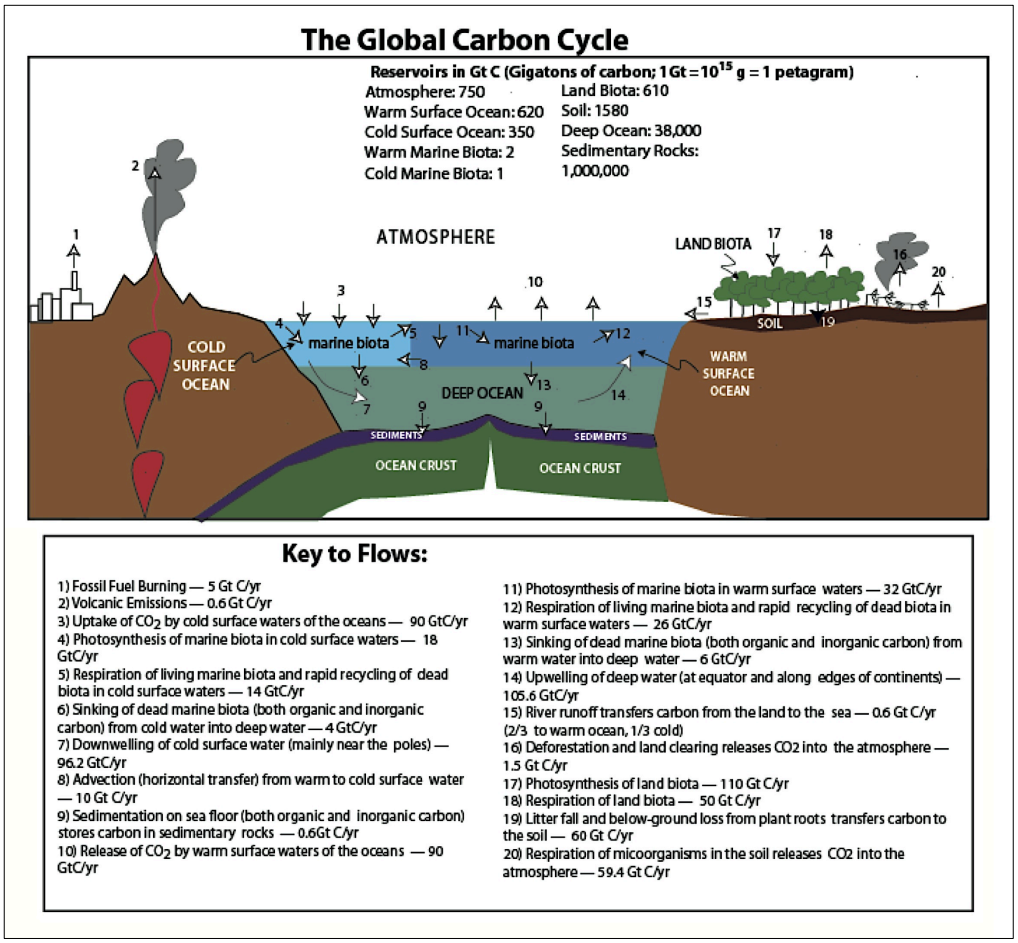

Figure 1.5: The Global Carbon Cycle, as best estimated, in 1994 (after Bice, D. (a)).

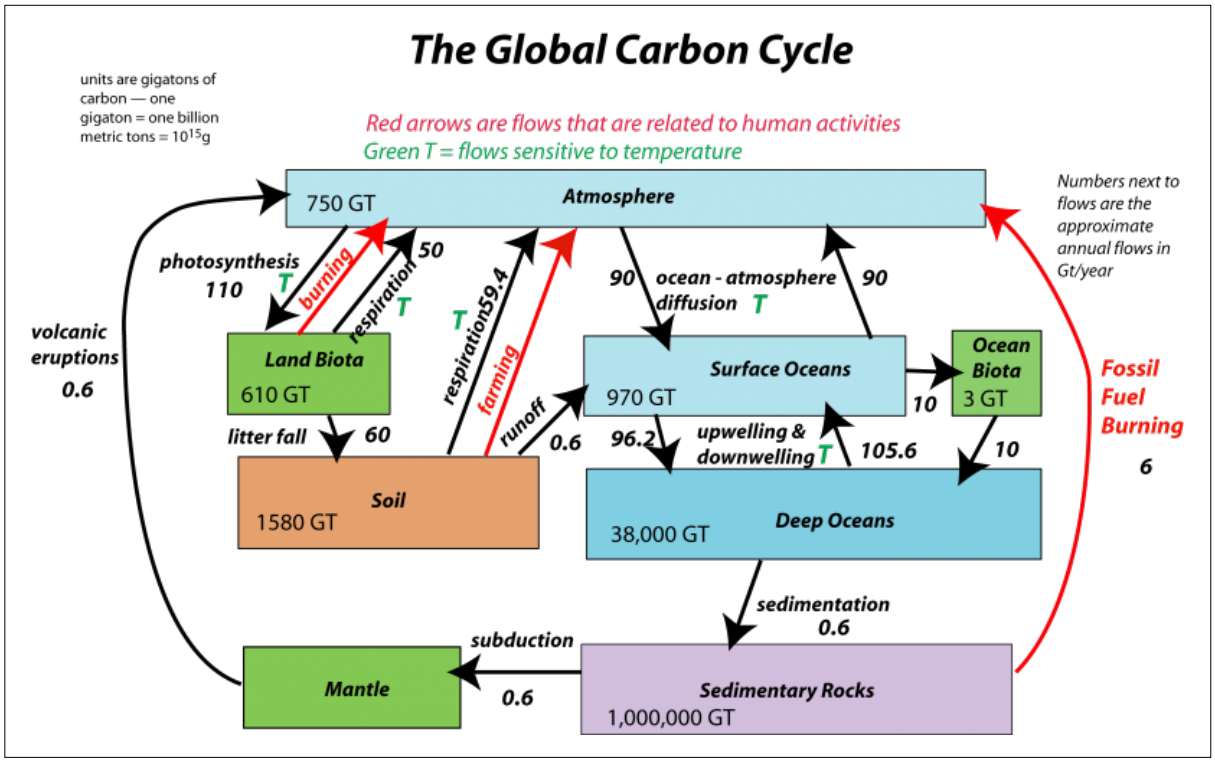

Figure 1.6: *Volumes of carbon for each major reservoir involved in the Global Carbon Cycle (after Bice, D. (b)).*

The carbon cycle takes place at different time scales: a 'Short-term Carbon Cycle' working on day to years scale where carbon is rapidly exchanged only within the superficial system and a 'Long-term Carbon Cycle' that operates from 100ky up to millions of years (Skelton et al., 2003).

The 'Short-term carbon cycle', is the so-called 'breathing of the biosphere'. The reservoirs involved in this cycle are the atmosphere, the biosphere and the oceans, with the last ones containing the largest amount of carbon. Oceanic masses act as the primary regulator of atmospheric carbon dioxide, being the two reservoirs in chemical equilibrium. The atmosphere-biosphere cycle is then mainly controlled by organic carbon via photosynthesis and respiration, and soil formation carbon uptake.

During photosynthesis plants, marine algae and bacteria use sunlight as source of energy forming carbohydrates thanks to the combination of carbon dioxide with water and the release of oxygen as waste:

$$CO_2 + H_2O + \text{sunlight} \rightarrow CH_2O + O_2$$

The sequestration in the ocean of carbon dioxide from the atmosphere acted by marine organisms is called 'biological pump'.

Heterotroph organisms are instead able to extract the energy stored in the carbohydrates by combining them with oxygen and releasing carbon dioxide and oxygen as bio-products:

$CH_2O + O_2 \rightarrow$ energy + $CO_2 + H_2O$

The combination of these processes recycles carbon between the atmosphere, the land and the ocean quite rapidly in terms of years to 100 years. So this cycle does not really sink carbon because carbon is returned to the atmosphere as plants and animal decay and die.

The 'Long-term carbon cycle', or 'geologic carbon cycle' is instead related to longer lasting processes and thus extended residency time in each reservoir (Fig. 1.7).

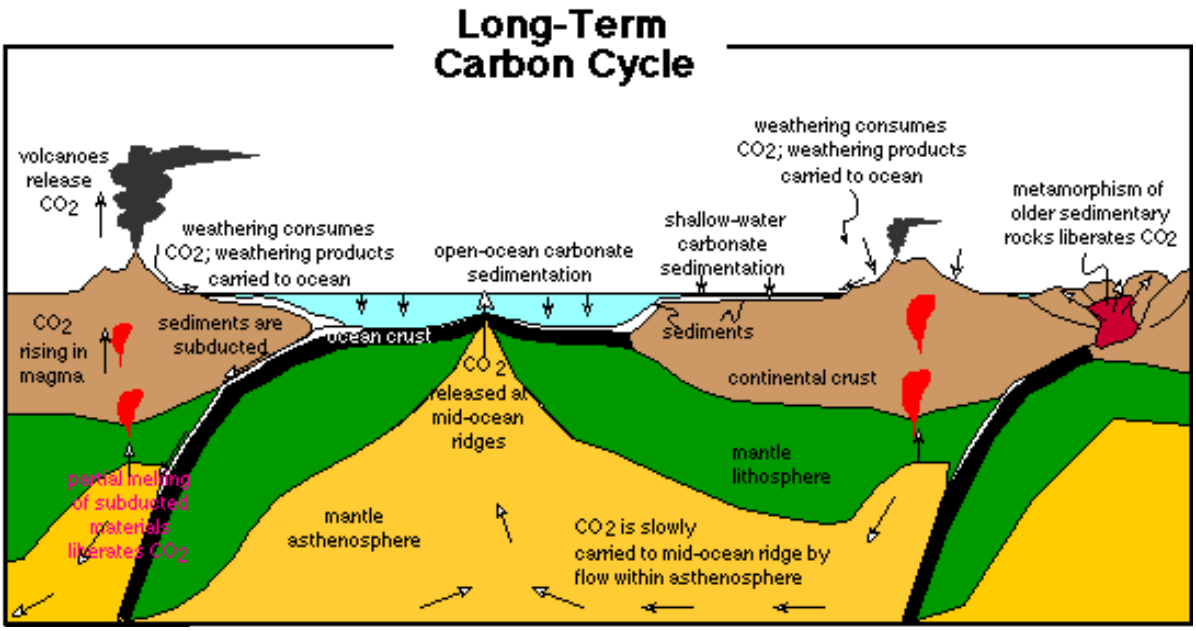

Figure 1.7: *Schematic representation of the long-term carbon cycle showing the flows of carbon that are important on timescales of more than 100kyr (after Bice, D. (a)).*

Both organic and inorganic carbonate carbon are involvolved in this cycle through the sedimentation processes. Generally tiny fractions of the organic carbon escape the decay process, but when it happens the organic carbon enter in the long-term cycle that involves the formation and destruction of fossil fuels and other organic-rich sediments.

The main actor involved by sedimentation in the long-term carbon cycle is instead the inorganic carbonate carbon. Many organisms during their life fix calcium carbonate in their body in the form of shells, plates or more complex biocalcifications both in the continental shelf and in pelagic

depositional settings. Most of the $CaCO_3$ is biologically produced in surface waters and then exported after death of the organism to depth thus removing carbon from the atmosphere-ocean reservoir. This process, called 'carbonate pump', is biologically controlled and for this reason is coupled to the removal of nutrients (e.g., N and P).

Carbonate species (H_2CO_3, HCO_3^- and CO_3^{2-}) reach in water a pH dependent chemical equilibrium with carbon dioxide, with total dissolved carbonate increasing with pH.

First, gaseous CO_2 dissolves in seawater (dissolved free carbon dioxide)

$$CO_2\,(g) \leftrightarrow CO_2\,(aq)$$

forming carbonic acid

$$CO_2\,(aq) + H_2O \leftrightarrow H_2CO_3\,(aq)$$

Then this carbonic acid dissociates in acqueous solutions reaching a pH dependent chemical equilibrium (Fig. 1.8):

$$H_2CO_3\,(aq) \leftrightarrow H^+\,(aq) + HCO_3^-\,(aq)$$
$$HCO_3^-\,(aq) \leftrightarrow H^+\,(aq) + CO_3^{2-}\,(aq)$$

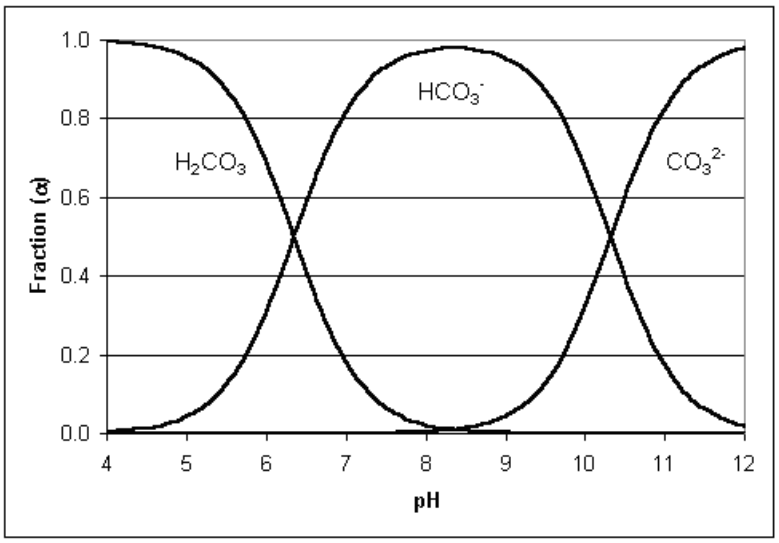

Figure 1.8: *Equilibria of carbonate species fraction in an aqueous media as a function of pH.*

Some of the bicarbonate ions combine with dissolved calcium ions to form calcium carbonate:
$Ca^{2+} + 2HCO_3^- \rightarrow CaCO_3 + H_2CO_3$

This process acts as a fantastic buffering system.

Thus, ocean productivity affects atmospheric CO_2 by both the sequestration of organic carbon and calcium carbonate ($CaCO_3$) from the ocean surface and atmosphere to the deep sea. The two processes act in two different directions: the former lowers atmospheric CO_2, while the latter raises it more modestly (Archer 2003, Sarmiento and Gruber 2006).

The calcium ions needed to form the carbonates reach the oceans thanks to another important process in the long-term carbon cycle: the weathering of rocks. As previously mentioned, carbon dioxide together with other atmospheric gases is able to dissolve in surface waters forming carbon acid, bicarbonate and hydrogen ions. This weakly acid solution is able to react and alter the most common minerals (silicates and carbonates). The products of weathering are predominantly clays and soluble ions such as calcium, iron, sodium, and potassium. Thus, the proportions of silicate and carbonate weathering at the Earth's surface are important in long-term global CO_2 balances (Berner et al., 1983; Liu et al., 2012).

Long-term carbon cycle includes also storage and release of CO_2 by magmatic intrusions, melting and metamorphism. Degassing of magma at mid-ocean ridges and hot-spot volcanoes release massive volumes of carbon dioxide. Melting and metamorphism of carbonates, generally in subduction zones, represent another important contribute to the long-term carbon cycle. Most of the CO_2 from the volcanic arcs come from the recycling of the carbonate subducted.

So, the long-term carbon cycle can be simplified as a cycle in which the atmospheric CO_2 is lowered and used during the weathering of silicate rocks. The ions produced on land during the alteration are carried by rivers to the ocean, where, together with the deposition of organic matter, are fixed to build calcium carbonate shells. The carbonate once subducted and melted release the stored CO_2 back to the atmosphere where the cycle can start again (Fig. 1.9).

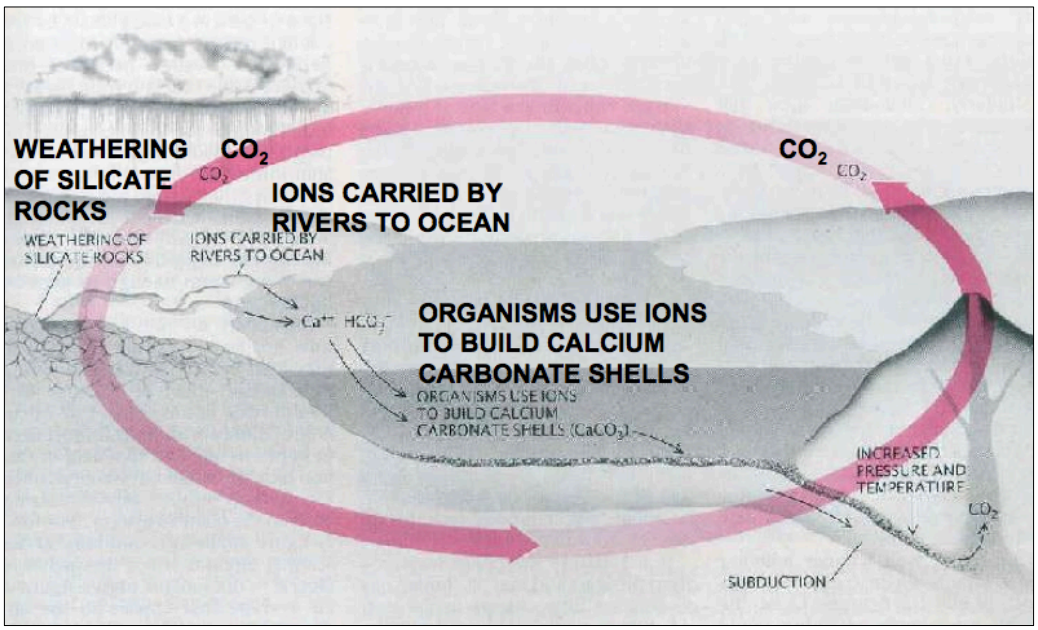

Figure 1.9: *Long-term carbon cycle simplification (after DeConto, 2012; original source unknown).*

1.3 Oceanic Anoxic Events (OAEs)

The modern climate setting represents a rather exceptional condition in the Phanerozoic, with an average global mean temperature of 13.9°C (NOAA, 2012) and about 380 ppm of atmospheric pCO_2 (Foster et al., 2007). As previously described, Mesozoic, and in particular Cretaceous, was a time of extreme greenhouse (Sellwood and Valdes, 2007; Willis and McElwain, 2002). The formation of LIPs (Jenkyns, 2003), submarine volcanism (Larson, 1991a, 1991b; Leckie et al., 2002) or methenogenic sources (Jenkyns, 2010) raised the CO_2 to extremely high levels leading the Earth to experience the most extreme warm episode in the past 150My (Larson, 1991a, 1991b; Erba, 1994, Kerr, 1998; Larson and Erba, 1999; Jenkyns, 1999; Wignall, 2001; Leckie et al., 2002).

Global warming and the abnormal increase in CO_2 changed the equilibria of the carbon cycle thus altering the hydrologic cycle (Weissert et al., 1998; Wortmann, 2004), nutrients distribution, upwelling intensity and deep water formation (Leckie et al., 2002, Takashima et al., 2006; Jenkyns 2010). In such a stressed environment burial of organic carbon represented a significant mechanism of carbon removal and pCO_2 drawdown (Jenkyns 2010).

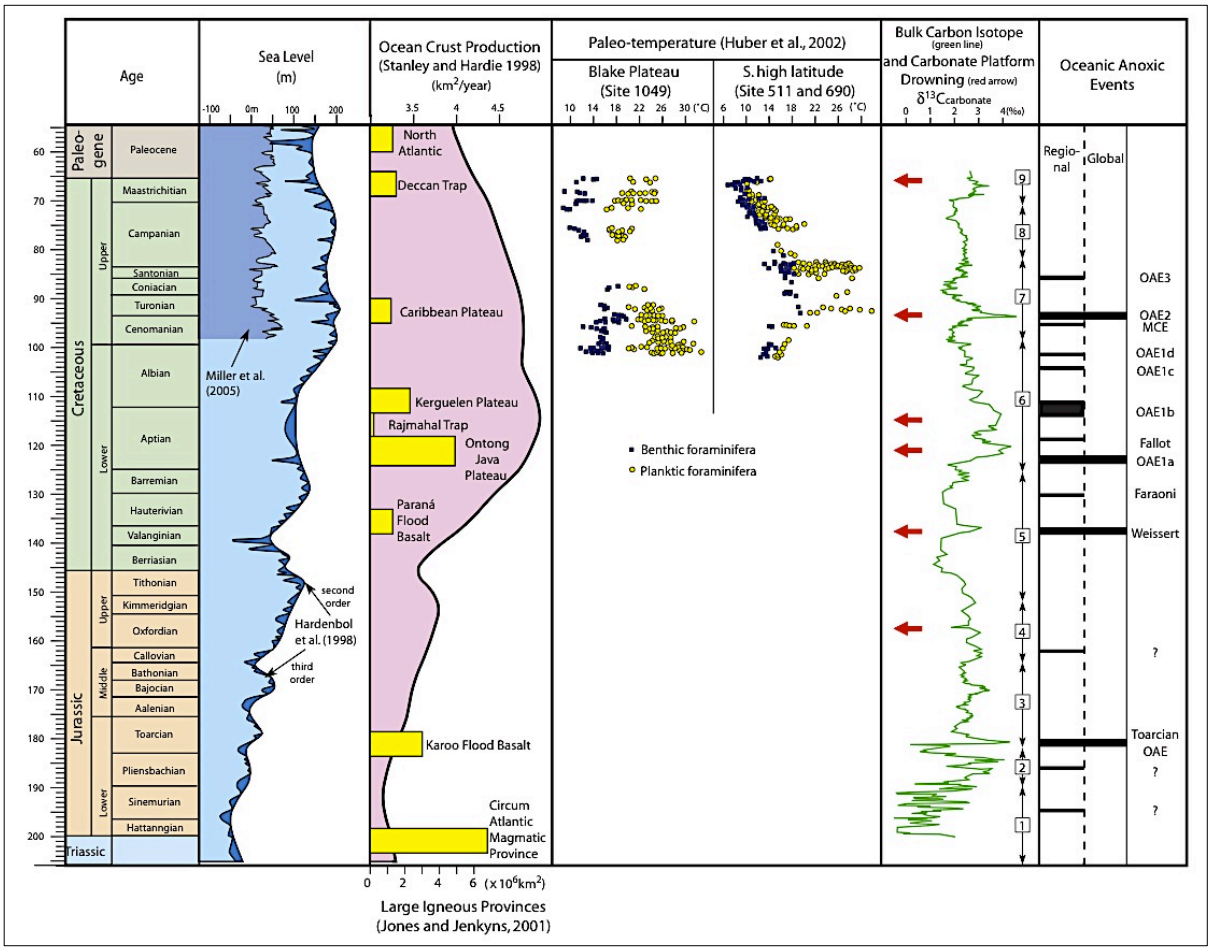

Figure 1.10: C*ompilation showing Jurassic–Cretaceous changes in sea level, oceanic-crust production, paleo-temperature, bulk carbon isotopes, carbonate- platform drowning events and OAEs (after Takashima, 2006). Large Igneous Province data are from Jones and Jenkyns (2001). Bulk carbon isotopes are from (1) van de Schootbrugge et al. (2005); (2) Hesselbo et al. (2000); (3) Morettini et al. (2002); (4) Dromart et al. (2003); (5) Weissert et al. (1998); (6) Erbacher et al. (1996); (7) Jenkyns et al. (1994); (8) Jarvis et al. (2002); and (9) Abramovich et al. (2003). Carbonate-platform drowning data are from Simo et al. (1993) and Weissert and Mohr (1996).*

The evidence of such a kind of process arrived in the early phases of ocean exploration. Many sediments incredibly rich in organic matter were recovered in the Pacific, Atlantic and Indian Oceans from Cretaceous successions coeval with black shales interval previously described in the Thetyan domain. Schlanger and Jenkyns (1976) hypothesized the existence of events characterized by widespread deposition of organic matter: they named them as Oceanic Anoxic Events (OAEs) (Schlanger and Jenkyns, 1976; Scholle and Arthur, 1980). The original definition was applied to two time intervals, namely the Aptian-Albian (OAE1) and Cenomanian-Turonian (OAE2 or Bonarelli Event) (Bonarelli, 1891; Schlanger and Jenkyns, 1976; Arthur et al., 1990; Bralower et al., 1993). Starting from that moment many other events were identified during the years. First, a third event (OAE3) Coniacian-Santonian in age was discovered in the ‘80s (Jenkyns, 1980; Arthur et al., 1990),

followed by the Toarcian OAE (Jenkyns, 1988). Another anoxic event was found in the Valanginian and named Weissert Event (Erba et al., 2004). It represents the first time interval of the Early Cretaceous showing a severe global carbon cycle anomaly (e.g. Lini et al., 1992; Weissert and Erba, 2004; Föllmi et al., 2006). Thanks to improved stratigraphic analyses and research the long OAE1 has been subdivided into four subevents: OAE1a or Selli Event (Arthur et al., 1990, Erba, 1994; Menegatti et al., 1998; Erba et al., 1999; Beerling et al., 2002), OAE1b (Arthur et al., 1990; Leckie et al., 2002; Tiraboschi et al., 2009), OAE1c (Arthur et al., 1990; Leckie et al., 2002; Tiraboschi et al., 2009) and OAE1d also called Pialli or Breistoffer Event (Wilson and Norris, 2001) (Fig. 1.10).

Of all the OAEs, four are certainly global in nature (OAE1a, OAE2, Toarcian OAE and Weissert OAE), whereas other OAEs (OAE1b, OAE1c, OAE1d) have most probably a regional significance. The most spectacular sedimentary expression of the Early Aptian and latest Cenomanian events are respectively the Livello Selli and Livello Bonarelli. The type-area for these two levels is the Umbria-Marche Basin (central Italy), that has been used as main area of study for the present PhD thesis.

Common characteristic of many OAEs is the deposition of C_{org}-rich black shales, with extremely low or absent carbonate and locally abundant radiolarian layers (Bralower, 1988; Bralower et al., 1993; Erbacher et al., 1996; Bucefalo Palliani et al., 1998, 2002; Jenkyns, 1999, 2010; Bellanca et al., 2002; Erba, 2004).

Two main extreme models have been proposed to explain the presence of black shales during OAEs: the ‘stagnant ocean model’ and the ‘expanded oxygen minimum model’ (Sarmiento et al., 1988; Takashima, 2006). According to the ‘stagnant ocean model’ an inefficient mixing of the water column would lead to a stratification of the water masses and the consequent formation of bottom water anoxia. In such kind of environment the enhanced preservation would drive the accumulation of organic matter (Schlanger and Jenkyns, 1976; Rullkötter, 2000; Wakeham and Canuel, 2006). A present day analogue is represented by the Black Sea. The ‘expanded oxygen minimum model’ is instead based on the idea that increased surface ocean primary productivity would produce under particular conditions, such as upwelling, the expansion of the oxygen-minimum zone (OMZ). The increased production of organic matter together with its accumulation in the OMZ would allow the deposition and preservation of organic-rich deposits (Erbacher et al., 2001; Hasegawa, 2003). A present day analogue for this kind of environment can be the Peruvian and Moroccan upwelling margins (Fig. 1.11).

According to Föllmi (2012) one model prevail respect to the other depending on the presence of arid or humid climatic conditions. Föllmi hypothesize that arid conditions were associated with time of intensified evaporation, reduced weathering and consequently lowered nutrient fluxes, and partly

stratified oceans. Humid conditions instead would increase weathering and runoff, intensify oceanic and atmospheric circulation with consequent widespread upwelling with formation of expanded oxygen-minimum zones. “normal” greenhouse, predominantly arid conditions, and intensified greenhouse, predominantly humid conditions.

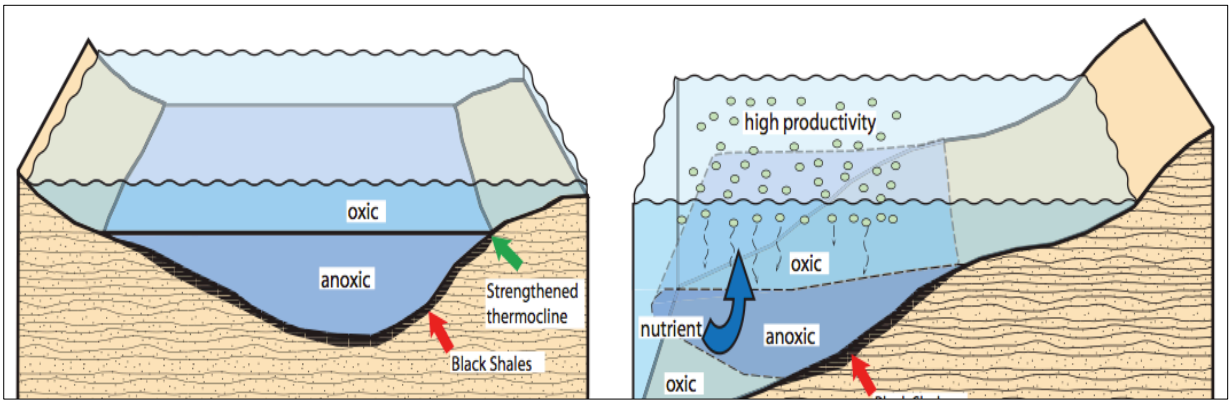

Figure 1.11: *Representative models for black shale deposition: (A) the stagnant ocean model, and (B) the oxygen-minimum-layer model (after Takashima, 2006).*

The major perturbation to the global carbon cycle is recorded by a large carbon isotope excursion in carbonate and organic matter (Jenkyns, 1980; Jenkyns and Clayton, 1986, 1997; Weissert, 1989; Menegatti et al., 1998; Weissert et al., 1998; Erba et al., 1999; Leckie et al., 2002; Erba, 2004; Erba et al., 2004; Jarvis et al., 2006). The connection of these events and major volcanic/tectonic episodes is proven by large, positive and negative excursions in the $^{87}Sr/^{86}Sr$ curve reconstructed for the Cretaceous (Bralower et al., 1997; Jones and Jenkyns, 2001; Leckie et al., 2002).

Three remarks have to be done. First, the term oceanic in Oceanic Anoxic Event can be misleading. OAEs were not episodes of worldwide oceanic anoxia, meaning that not all the oceans were anoxic, but OAEs were global geochemical perturbations of the carbon cycle. Second, as described in Tsikos et al. (2004) for OAE2, the deposition of organic-rich deposit wasn’t coeval in every basin. Then OAEs cannot be defined on a lithological base but should be defined by the geochemical excursions (e.g. Erba et al., 2004; Tsikos et al., 2004; Föllmi, 2012). Third and last remark, even if it can sound obvious, a Carbon Isotope Excursion (CIE) in the geological record do not necessarily relate with an oceanic anoxic events (Föllmi, 2012). An OAE describes a phenomenon characterized by anomalously high burial rates of marine organic carbon with a consequent increase in the $\delta^{13}C$ (Jenkyns, 2010). However, the consequence of many other events that have changed the equilibrium of the one or more of the reservoirs involved in the global carbon cycle can produce a CIE. Moreover, a stratigraphic

interval rich in black shales it's necessarily the result of a perturbation of the global carbon cycle (with the resulting CIE), but simply the result of local to regional factors.

Durinhg OAEs, also the biosphere was affected by such paleoenvironmental perturbations with important biotic variations and evolutionary changes (Bralower, 1988; Jarvis et al., 1988; Coccioni et al., 1992a; Bralower et al., 1993, 1994; Larson et al., 1993; Erba, 1994, 2004; Premoli Silva and Sliter, 1994; Claps et al., 1995; Erbacher et al., 1996, 2001; Bucefalo Palliani et al., 1998, 2002; Salvini and Marcucci Passerini, 1998; Hochuli et al., 1999; Paul et al., 1999; Premoli Silva et al., 1999; Leckie et al., 2002; Monaco et al., 2012). Paleontological evidence suggests that OAE1a and OAE2 where characterized by meso- to eutrophic conditions (Coccioni et al., 1992a; Erba, 1994, 2004; Erbacher et al., 1996; Premoli Silva and Sliter, 1999; Leckie et al., 2002; Kuypers et al., 2002, 2004; Snow et al., 2005; van Breugel et al., 2007). Biostratigraphic studies reveal that during OAEs an important shift of the biogenic components from carbonate-dominated organisms to siliceous- and organic-walled organisms dominated (e.g. Premoli Silva et al., 1999). In particular OAE1a and OAE2 are characterized by huge declines in calcareous nannofossils. These intervals have been termed by Weissert and Erba (2004) 'biocalcification crisis'. Also, many carbonate platforms drowned during the Mesozoic, probably as a result of too rapid eustatic variations and/or as the result of excessive eutrophication and diffused anoxia in the photic zone (Takashima et al., 2006), and possibly ocean acidification (Weissert and Erba, 2004).

Elemental analyses have suggested another possible factor that could have affected the geochemical equilibrium and triggered eutrophism at a global scale. Coastal nutrification due to increased continental weathering and run-off and/or local upwelling cannot explain alone the dimensions of the OAEs. Many authors (Brumsack, 1980; Larson and Erba, 1999; Turgeon et al., 2002; Erba, 2004; Snow et al., 2005; Takashima et al., 2006; Turgeon and Brumsack, 2006) propose that incredibly high volumes of trace-metals produced by submarine volcanic eruptions could be considered a convenient additional factor. For example, during the OAE1a and OAE2 higher trophic levels were probably induced and maintained by hydrothermal inputs of biolimiting metals (Fe and Zn for example) during the construction of the Ontong Java (and Manihiki) and Caribbean Plateaus, respectively.

According to many authors (Weissert and Erba, 2004; McElwain et al., 2005; Takashima et al., 2006; Forster et al., 2007a), the fact that the massive organic matter deposition played a major role in the CO_2 drawdown is proven by the existence of short episodes of climatic cooling after the OAEs.

OAEs represented a real revolution for the Earth System. The global nature of these events and the fact that they are recorded in every geochemical and biological proxy, prove the massive entity of these crises and bear witness of the major impact they had on climate.

1.4 Upper Albian – lower Turonian perturbations to the carbon cycle

During this PhD project the late Albian - Cenomanian interval has been chosen to investigate the depositional processes and environmental dynamics during a time of major carbon cycle perturbations.

In this stratigraphic interval three major geochemical events corresponding to positive excursions in the stable carbon isotope content are recognized at global scale: the Oceanic Anoxic Event 1d, the Middle Cenomanian Event (MCE) and the Oceanic Anoxic Event 2. During this stratigraphic interval together with these three events a series of minor events have been described, such as the Lower Cenomanian Events (LCE I, II and III), the Crippsi Beds Event, and so on (Jarvis et al., 2006) (Fig. 1.12).

A brief description of each one of these events are presented in the following sub-chapters.

1.4.1 Pialli or Breistoffer Event (OAE1d)

The so called Pialli or Breistoffer Event corresponding to the OAE 1d (Wilson and Norris, 2001; Leckie et al., 2002) is characterized by a long positive excursion of the $\delta^{13}C$ records of about 1‰, reaching values of about 2.5‰ in carbonate carbon (C_{carb}) (Wilson and Norris, 2001; Gröcke et al., 2006; Petrizzo et al., 2008; Giorgioni et al., 2012).

As can be seen in Fig. 1.13, in high resolution datasets the isotopic excursion displays three separate peaks (from a to c) (Gale et al., 2006; Jarvis et al., 2006). The carbon anomaly crosses the base of the Cenomanian Stage as defined at the GSSP. The chronostratigraphic limit is defined at 36 meters below the top of the Marnes Bleues Formation on the south side of Mont Risou, east of Rosans (Haute-Alpes, France). This level coincides with the first appearance of the planktonic foraminifer *Rotalipora globotruncanoides* (Kennedy et al., 2004).

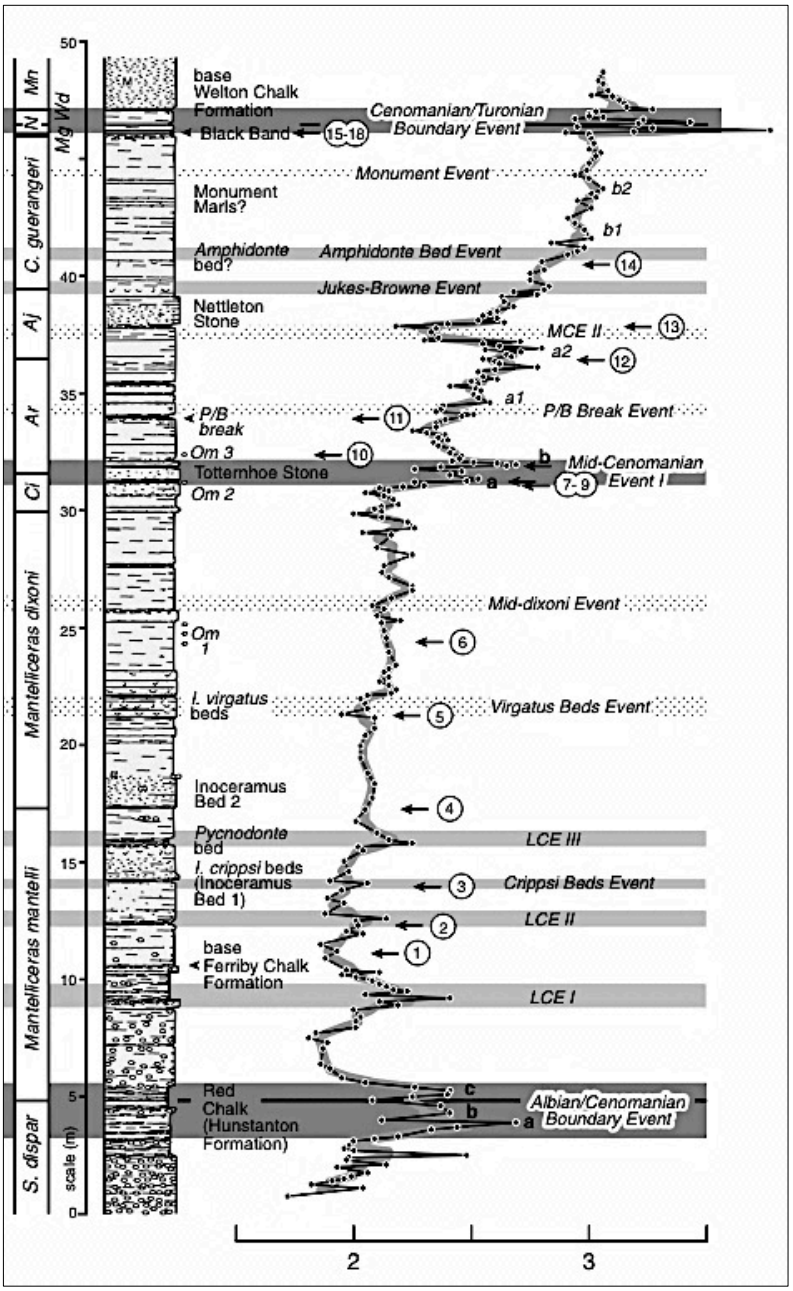

Figure 1.12: $\delta^{13}C$ variation across the Upper Albian – Lower Turonian in the Speeton section (North Yorkshire, UK(North Yorkshire, UK) (after Jarvis et al., 2006, for greater details on the figure see paper).

Many biostratigraphic data have been produced through time (Norris and Wilson, 1998; Bellier et al., 2000; Wilson and Norris; 2001; Leckie et al., 2002; Bornemann et al., 2005; Watkins et al., 2005; Petrizzo et al., 2008). Few authors (Wilson and Norris, 2001, Leckie et al., 2002; Watkins et al., 2005) indicate that the early late Albian well-stratified upper water column collapsed abruptly during OAE1d, with the deposition of black shales and a positive carbon isotope excursion. The intensified winter

mixing and reduced summer stratification was probably the cause of the progressively reduction of the vertical thermal gradient (Wilson and Norris, 2001). According to Bornemann et al. (2005) the black shales deposition occurred instead during times of increased surface-water stratification and decreased deep-water formation due to orbitally induced increase in monsoonal activity.

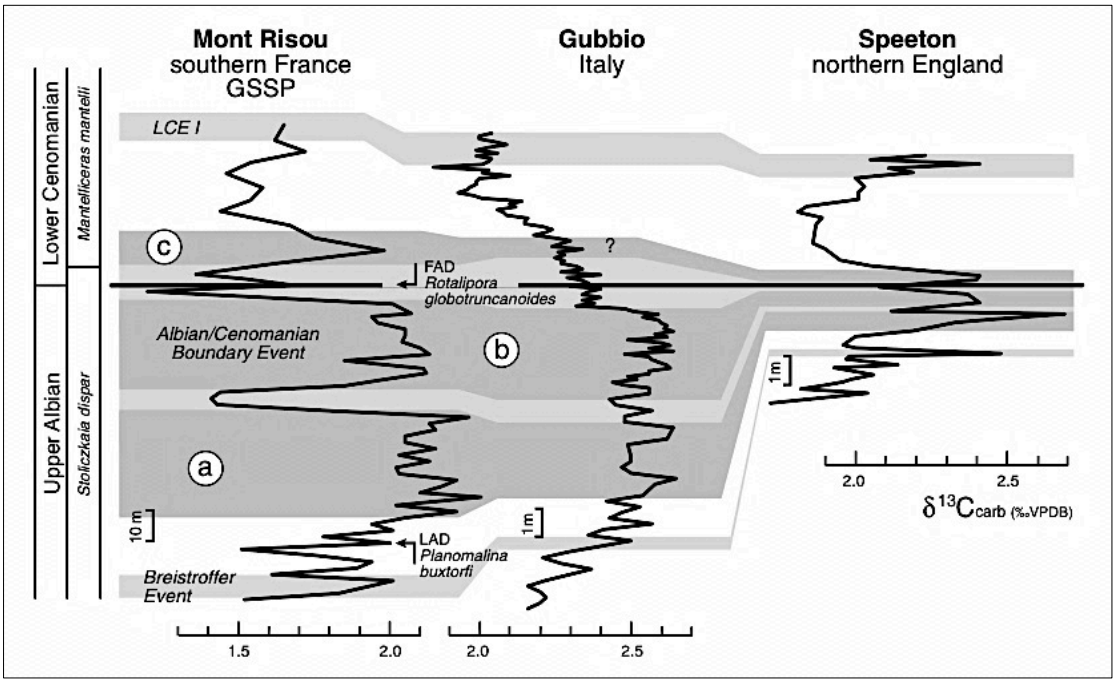

Figure 1.13: Correlation of the Albian/Cenomanian Boundary $\delta^{13}C$ event between the GSSP section of Mont Risou (Gale et al., 1996), Gubbio and Speeton (after Jarvis et al., 2006, for greater details on the figure see paper)

1.4.2 Mid-Cenomanian Event (MCE)

The Mid-Cenomanian Event (MCE) has been interpreted by some authors as the precursor of a global palaeoclimatic and palaeoceanographic change that led to the catastrophic Bonarelli Event (OAE2) (e.g. Coccioni and Galeotti, 2001, 2003).

The term Mid-Cenomanian Event (MCE) was first used by Ernst et al. (1983) and later by Meyer (1990) to describe a nodular limestone layer in the Cenomanian of NW Germany (Friedrich et al., 2009). In 1994 Paul et al. identified a small carbon isotope excursion slightly above the layer described by Ernst et al. (1983) and defined it as MCE.

A pair of two closely spaced $\delta^{13}C_{carb}$ positive excursions in the middle of the *Rotalipora cushmani* Zone characterizes the MCE. The first peak is the MCE Ia that corresponds to a modest increase of

about +0.5‰ in $\delta^{13}C$. After a minor trough, the $\delta^{13}C$ curve rises again to form a second peak called MCE Ib reaching values slightly higher than MCE Ia. The MCE doesn't have to be confused with the stratigraphically higher MCE II marked by a negative excursion of around -0.3‰ (Mitchell et al., 1996). As can be clearly seen in Fig. 1.12, the positive excursion of the MCE I represents a major break on the long-term C isotopic profile separating the very slowly rising $\delta^{13}C$ trend of lower Cenomanian from the evident increasing values of the upper Cenomanian (Jarvis et al., 2006) (Fig. 1.12).

The MCE $\delta^{13}C$ excursion has been widely observed in both the Boreal and Tethyan Realms and within the Atlantic Ocean (Friedrich et al., 2009 and references therein). The MCE has also been described by Gertsch et al. (2010) in shallow and deeper shelf environments of western Morocco. The MCE is not characterized by widespread formation of organic-rich sediments like in the OAE2 (Jenkyns et al., 1994), but is frequently associated with distinctive lithological changes (Jenkyns et al., 1994; Coccioni and Galeotti, 2003).

Related to the MCE changes in the marine biota affected dinoflagellates, radiolarians, benthic and planktic foraminifera, bivalves, ammonites, and belemnites (e.g. Paul et al., 1994; Erbacher et al., 1996; Erbacher and Thurow, 1997; Mitchell and Carr, 1998; Coccioni and Galeotti, 2001, 2003; Wilmsen, 2007; Friedrich et al., 2009; Hardas et al., 2012; Giraud et al., 2013).

The MCE seems to represent a turning point in Cenomanian paleoceanography. There are indications that starting from this event the ecosystem switched towards generally less oxygenated bottom-water conditions (Coccioni et al., 1995; Friedrich et al., 2009). Indications of a change towards more eutrophic surface-water conditions connected with increased water mixing culminating at OAE 2 come from the planktonic foraminiferal record (Premoli Silva and Sliter, 1994, 1999; Leckie et al., 2002), coincident with decreased ventilation of the sea floor (Coccioni and Galeotti, 2003). Hardas et al. (2012), according to calcareous nannofossil and benthic foraminiferal assemblages and supported by TEX86 data produced by Forster et al. (2007b), suggest increased water-column stratification starting with the MCE and lasting to the end of the Cenomanian stage. Giraud et al. (2013), thanks to quantitative analyses of calcareous nannofossil, ammonoid and clay mineral assemblages evidenced important climatic changes within the MCE. According to their data, general humid and mesotrophic conditions were present before the MCE and during the MCE Ib. On the contrary, the authors highlighted strongly oligotrophic levels in sea-surface during the MCE Ia, related both to arid climatic conditions and a major sea-level fall.

It's still not clear whether a cooling event was or not associated with the MCE. Several authors have suggested the existence of a climate cooling on the basis of biostratigraphical and geochemical evidence (Paul et al., 1994; Gale and Christensen, 1996; Stoll and Schrag, 2000; Huber et al., 2002; Miller, 2003, 2005; Wilmsen, 2003; Voigt et al., 2004). Other authors (e.g. Moriya et al., 2007; Ando et al., 2009) question the cooling across the MCE on the basis of biostratigraphic, isotopic and TEX86 data.

According to many authors (Paul et al., 1994; Mitchell, 1996; Mitchell and Carr, 1998; Voigt et al., 2004) the MCE was caused by a general change of the oceanic circulation and sea level that probably led to increased oceanic ventilation and upwelling of nutrient-rich waters.

1.4.3 Oceanic Anoxic Event 2 (OAE2)

The most spectacular sedimentary expression of the OAE2 is the Bonarelli Level in the Italian Central-Appennines (Bonarelli, 1891); it is a bituminous and radiolarian-rich interval that testifies widespread distribution of anoxic conditions in the oceans during the latest Cenomanian (Schlanger and Jenkyns, 1976; Arthur et al., 1990; Bralower et al., 1993; Jenkyns, 2010).

The OAE2 is characterized by a positive excursion of the $\delta^{13}C$ records of about 2-3‰ in carbonates and up to 6‰ in organic carbon (Jenkyns, 1980; Scholle and Arthur, 1980; Schlanger et al., 1987). This event is conventionally interpreted as the consequence of accelerated burial of marine organic matter (Herbin et al. 1986; Arthur et al. 1990; Kuypers et al. 2002, 2004; Jarvis et al., 2006). The OAE2 $\delta^{13}C$ profile has a typical shape characterized by a first rapid rise to a maximum peak 'a' followed by slow decrese to a trough before reaching a second peak called 'b'. After 'b' the $\delta^{13}C$ remains stable at high values for a stable interval informally called 'plateau'. The last point before the decrease to lower values is called peak 'c'. The small spike within the first descending part of the $\delta^{13}C$ curve is called peak 'd' (e. g. Voigt et al., 2007) (Fig. 1.14).

The $\delta^{13}C$ anomaly spans the base of the Turonian Stage according to the definition of the GSSP. The stratigraphic limit is officially defined as the base of Bed 86 of the Bridge Creek Limestone Member at the western end of the Denver and Rio Grande Western Railroad cut near the north boundary of the Pueblo Reservoir State Recreation Area, west of Pueblo, Colorado, USA. The GSSP coincides with the first occurrence of the ammonite *Watinoceras devonense* (Kennedy et al., 2005) and is very close to peak "c" of the C isotopic anomaly (Tsikos et al., 2004).

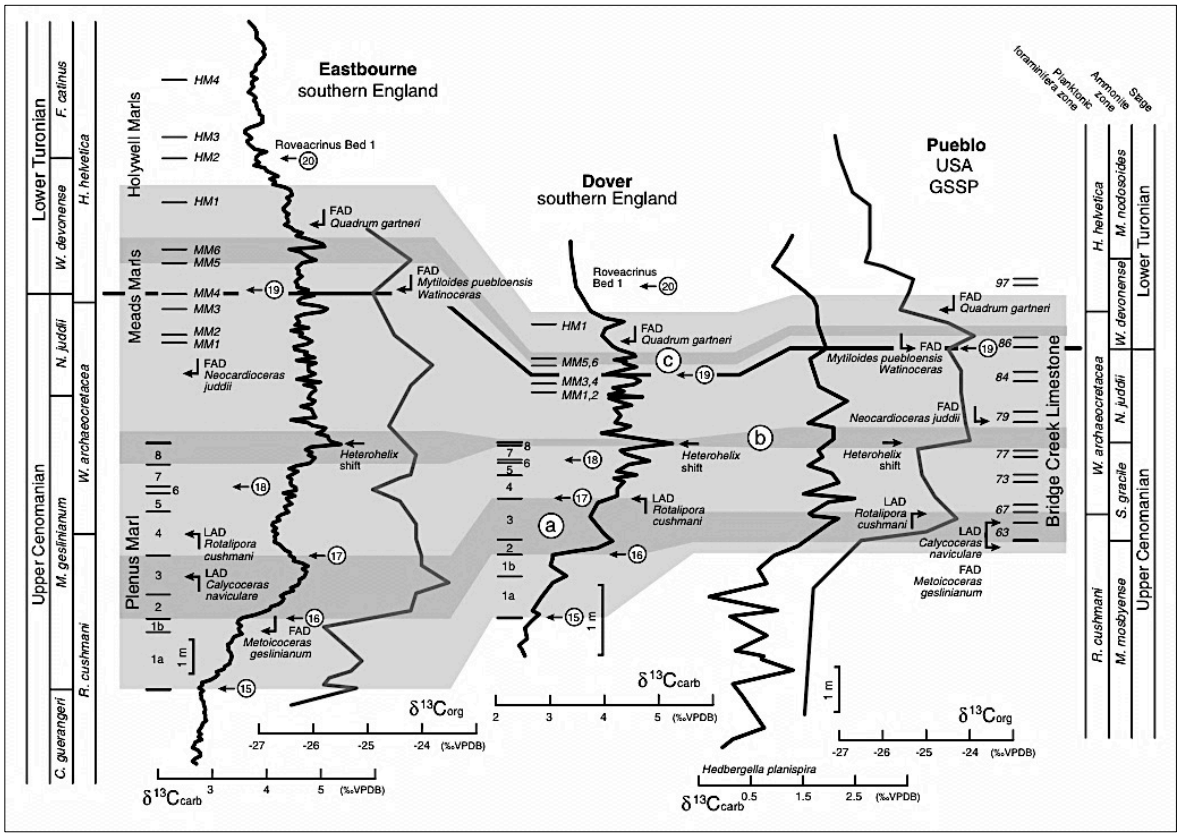

Figure 1.14: Correlation of the Cenomanian/Turonian Boundary δ13C event between England (Eastbourne and Dover) and the GSSP at Pueblo, Colorado, USA (after Jarvis et al., 2006, for greater details on the figure see paper).

The geochemical behavior of OAE2 has been widely studied (e.g. Scholle and Arthur, 1980; Summerhayes, 1981, 1987; Pratt and Threlkeld, 1984; Arthur et al., 1987, 1988, 1990; Schlanger et al., 1987; Jarvis et al., 1988; Hilbrecht et al., 1992; Thurow et al., 1992; Gale et al., 1993; Pratt et al., 1993; Jenkyns et al., 1994; Hasegawa, 1997; Sugarman et al., 1999; Holbourn and Kuhnt, 2002; Kuypers et al., 2004; Tsikos et al., 2004; Scopelliti et al., 2004, 2006, 2008, 2010; Bowman and Bralower, 2005; Erbacher et al., 2005; Jarvis et al., 2006; Yilmaz et al., 2010; Westermann, et al. 2010; Zobaa et al., 2011; Dale et al., 2012; Mitchell et al., 2012; van Bentum et al., 2012). The occurrence of the $\delta^{13}C$ anomaly throughout many different depositional settings, ranging from continental to marine, highlights the global nature of the event and its massive impact on the global carbon cycle.

Many groups were strongly affected by this event (Luciani and Cobianchi, 1999; Leckie et al., 2002; Erba, 2004; Keller et al., 2004, 2008; Coccioni and Luciani, 2005; Caron et al., 2006; Friedrich et al., 2006; Hardas and Mutterlose, 2007; Musavu-Moussavou et al., 2007; Duque-Botero and Maurrasse, 2008; Pearce et al., 2009; Linnert et al., 2010; Sánchez Quiñónez, 2010; El-Sabbagh et al., 2011; Linnert et al., 2011; Prauss, M.L., 2012; Lebedel et al., 2013; Melinte-Dobrinescu et al., 2013).

According to the biodiversity patterns of ammonoids in Europe, Tunisia, and the Western Interior Monnet (2009) question the global scale character of the so-called Cenomanian–Turonian mass extinction. Similarly, calcareous plankton did not suffer a mass-extinction event across OAE2 (Premoli Silva et al., 1999; Erba, 2004).

The OAE2 lasted about 500ka (Sageman et al., 2006) and was charactherized by diffused anoxia with times of free hydrogen sulfide (e.g. Scoppeliti et al., 2006; Hetzel et al., 2009; Owens et al., 2012) and widespread deposition of organic matter (Fig. 1.15) in a time of important rise in sea level (Voigt et al., 2006). According to $\delta^{238}U$ data, used as a paleoredox proxy to quantify the extent of marine anoxia, the global increase of anoxic conditions during OAE2 was at least three times as compared to the present day or to periods before and after OAE2 (Montoya-Pino et al., 2010). However, anoxia wasn't equally distributed: while the Atlantic was heavily subjected to the deposition and preservation of massive volumes of organic matter, on the contrary the continental margins of the Pacific ocean were oxic for most of the OAE2 interval (Takashima et al., 2011). According to Tsandev and Slomp (2009) only the deep-sea became completely anoxic, while the shelves experienced only partial anoxia. Owens et al. (2013) using combined carbon- and sulfur-isotope data showed that merely a small portion of the ocean contained toxic and metal-scavenging hydrogen sulfide, but sufficiently large to deeply change the ocean's chemistry and biology.

Two major group of hypotheses have been made for the huge accumulation of organic matter in sediments representing OAE2: an increase in primary productivity (productivity model) and the presence of a sluggish oceanic circulation with consequent enhanced stratification of the water column and increased preservation of the organic matter (preservation model). Many models produced by computer simulations (e.g. Trabucho Alexandre et al., 2010; Flögel et al., 2011; Monteiro et al., 2012) try to reproduce the data observed on the stratigraphic record in order to better define the mechanism at the origin of the OAE2.

According to some authors the particular paleogeographic and paleoclimatic settings played at least in few areas an important role in generating an inefficient oceanic circulation (Tsandev and Slomp, 2009; Linnert et al., 2011). Other authors identify the increase in primary productivity as the cause of the deposition of organic matter. The mechanisms that triggered this increase in fertility are still debated.

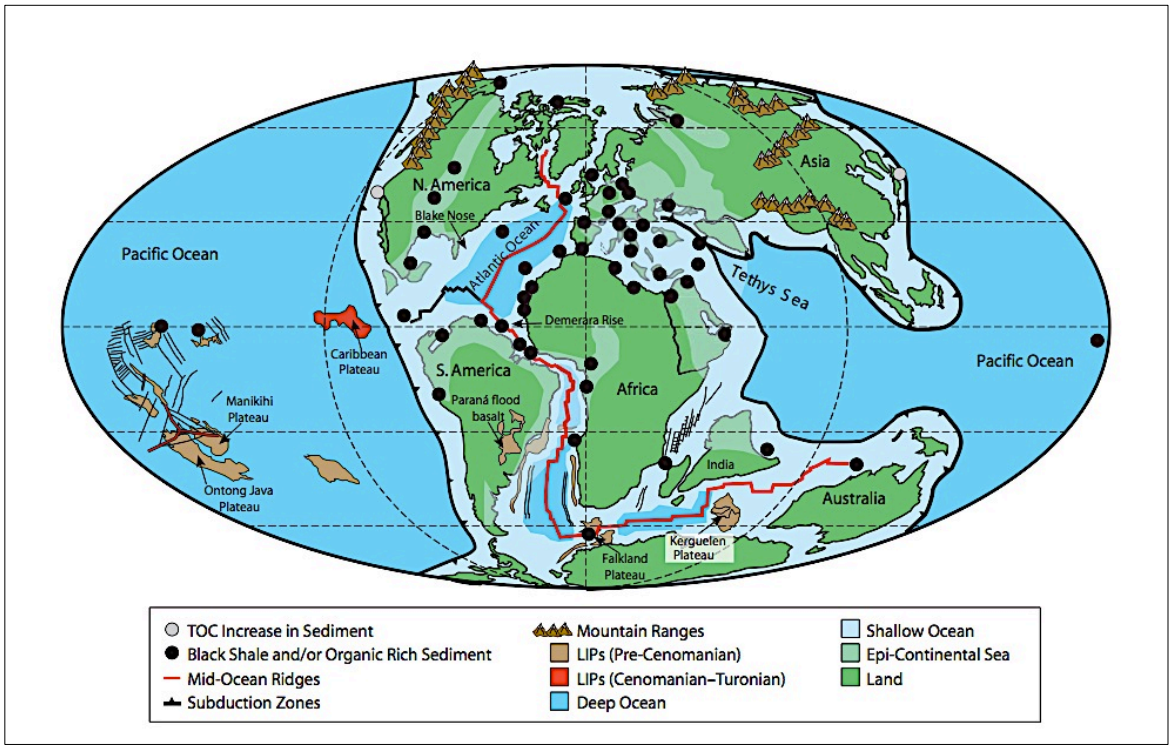

Fig. 1.15 – Distribution of black shales and/or increased organic carbon sediments at OAE 2 (after Takashima et al., 2006). Data are from Schlanger et al. (1987); Arthur et al. (1987, 1988); Jenkyns, (1991); Thurow et al. (1992); Kassab and Obaidalla (2001); Wang et al. (2001); Lebedeva and Zverev (2003); Yurtsever et al. (2003); Coccioni and Luciani (2005); Fisher et al. (2005); and Takashima and Nishi (unpublished data) (after Takashima et al., 2006).

According to Scopelliti et al. (2004) the high-productivity event was driven by increasingly warm and humid climatic conditions that promoted an accelerated hydrological cycle with consequent greater fluvial input of nutrients.

In the stratigraphic record multiple proxies suggest a crucial role of massive volcanism and the related hydrothermal activity as major trigger for the increase in primary productivity. Ashfall deposits (bentonites) throughout the Cenomanian/Turonian boundary are common (e.g. Kauffman, 1984; Kauffman and Caldwell, 1993). It's accepted by many authors (Arthur et al., 1985, 1987; Schlanger et al., 1987; Arthur et al., 1990; Sinton and Duncan, 1997; Kerr, 1998; Jenkyns, 1999; Wignall, 2001; Snow et al., 2005; Turgeon and Creaser, 2008) that major submarine volcanism occurred in the Cenomanian/Turonian boundary interval. An important decrease in the $^{87}Sr/^{86}Sr$ isotopic values has been interpreted as the result of intense submarine volcanism (Ingram et al., 1994; Bralower et al., 1997; Jones and Jenkyns, 2001). Evidence of hydrothermal activity comes from elevated levels of trace metals just below and within sediments representing OAE2 at several localities (Brumsack, 1980; Arthur et al., 1990; Orth et al., 1993; Leckie et al., 1998; Turgeon et al., 2002; Snow et al., 2005; Turgeon and Brumsack, 2006; Elrick et al., 2009). The release by hydrothermal plumes of important

biolimiting metals in the oceans is considered by several authors a possible mechanism for the increase in the primary productivity (e.g. Sinton and Duncan, 1997; Kerr, 1998; Leckie et al., 2002; Erba, 2004; Snow et al., 2005).

As an alternative mechanism, other authors (Arthur et al., 1987; Arthur and Natland, 1979; Tucholke and Vogt, 1979; Summerhayes, 1981, 1987; Cool, 1982; Zimmerman et al., 1987; Leckie et al., 1998; Huber et al., 1999; Poulsen et al., 1999, 2001; Kuypers et al., 2002, 2004) suppose that changes in intermediate and deep water circulation may have led to upwelling of water-masses enriched in nutrients and biolimiting metals with the consequent increase in fertility and expansion of oxygen minima. Neodymium isotopic data suggest that the circulation patterns during the greenhouse interval were different from those of the subsequent relatively temperate interval (MacLeod, K.G. et al., 2008, 2011; Berrocoso et al., 2010).

Few authors (Friedrich et al., 2006; Jarvis et al., 2011; van Bentum et al., 2012; Zheng et al., 2013) have documented a short-lived cooling event during the early stage of OAE2, termed Plenus Cold Event (Gale and Christiansen, 1996; Jarvis et al., 2011). The rates of organic matter burial were probably sufficiently high to lead to major atmospheric CO_2 drawdown resulting in an associated cooling event (Forster et al., 2007a; Sinnighe Damsté et al., 2010), interrupted by renewed volcanogenic CO_2 (Jarvis et al., 2011).

The OAE2 was one of the most extreme events that characterized Cretaceous time. The accumulation of organic carbon played a major role in the CO_2 drawdown and the switch back into 'normal' operational mode (e.g. Brumsack, 2006). Accelerated weathering might also have acted as an important process in the removal of the CO_2 (e.g. Blättler et al., 2011; Pogge von Strandmann et al., 2013). A combination of the two processes is probably at the origin of the mitigation of the mid-Cretaceous greenhouse climatic conditions.

1.5 Aims and objectives of this study

During the present PhD research project the upper Albian – lower Turonian stratigraphic interval (about 104-92 Ma) has been studied. This period of time represents an intriguing phase of Earth history. After the latest Albian OAE 1d, the early Cenomanian oceans reached stage of relative stability. This equilibrium was interrupted by the MCE, an episode that anticipated the impressive OAE 2. The latest Cenomanian OAE2 represented a turning point for the Cretaceous world.

The upper Albian – lower Turonian pelagic successions of the Thethys Ocean represent a perfect laboratory in order to understand the processes that acted during the onset, duration and recovery from local to widespread sea-bottom anoxic conditions. Five key sections from the Umbria-Marche and Belluno basins in Italy have been investigated with a multidisciplinary approach in order to better understand their stratigraphic evolution and characterize the recorded major events. On the basis of sedimentology, paleontology, as well as organic, inorganic and isotopic geochemistry the interplay of surface-water changes (such as rate of nutrients input, salinity, temperature) and sea-bottom processes have been studied, in order to better understand how highly stressed climatic conditions impacted on the entire ocean system.

Key objectives of this study are:

- an extremely detailed characterization of the sedimentary structures and processes that acted on the sea-floor at the time of the deposition of the Scaglia Bianca;
- a better comprehension of the relationships between sedimentary structures (sea bottom processes) and superficial water-masses changes;
- understanding of the processes that acted during the onset, development and recovery from anoxia: how do the sea bottom processes interact with anoxia?
- linking of bottom and surface processes that acted before, during and after the major events : were they in phase, out of phase or decoupled?
- a better understanding of the possible connections between the the Pialli/Breistoffer Event (OAE1d), the MCE and OAE 2.

1.6 Outline of the thesis

Chapter 1 introduces into the Cretaceous greenhouse climate system and illustrates the theory of Cretaceous carbon cycle perturbations.

In Chapter 2 the regional geological setting of the studied areas is presented and the studied sections are briefly illustrated.

Chapter 3 is a synthesis of all the materials and methods applied during this research project.

Chapter 4 deals with the physical processes that acted at the sea-bottom during the deposition of the studied pelagic sequences. All the sedimentary structures identified are here presented and illustrated in

detail. Then the distinguished facies have been organized in an innovative facies framework. A new depositional model for thin-grained carbonate pelagic sediments is developed and presented.

Chapter 5 provides an extremely high-resolution Oxygen, inorganic and organic Carbon stable isotope record for Monte Petrano and Cismon sections. The resulting data represent the first high-resolution geochemical log for these two sections for the late Albian – early Turonian time interval. Moreover, Rock-Eval/TOC Pyrolysis analyses of selected samples are presented. The resulting characterization of organic matter supports the understanding of the origin, depositional environment, and diagenesis of organic matter. The two outcrops are then correlated and the results interpreted in relation to the global carbon cycle perturbations.

In Chapter 6, on the basis of the process described in chapter 4, the stratigraphic vertical variation of the distinguished facies is reconstructed and linked to the major geologic events. Recurrent stacking pattern types or "sequences" have been identified and discussed. Finally, the interplay of superficial water changes and sea bottom processes are here discussed with the purpose of better defining how water masses react during highly stressed climatic conditions.

In Chapter 7 a high-resolution X-Ray Fluorescence (XRF) stratigraphy for the Cismon section is presented. Moreover, additional data produced for the Bonarelli Level at Monte Petrano section are shown. Detrital, biogenic and redox-sensitive elements are used as proxies of palaeoenvironmental processes and their relation with the major palaeoclimatic events.

Chapter 8 deals with the application of cyclostratigraphic techniques to all the studied sections in order to investigate the astronomical signature possibly recorded. The followed approach consists in the probabilistic determination of a proper sedimentation rate model (Malinverno et al., 2010) in order to convert the stratigraphic record from the depth domain to the time domain. Then, whether possible, more insights about duration and timing of the key geological events are obtained.

In Chapter 9 all the data are discussed together with the available literature in order to build an integrated stratigraphic framework and interpret overall trends. Moreover, on the basis of sedimentology, paleontology, as well as organic, inorganic and isotopic geochemistry, all the results coming from the multidisciplinary investigations have been merged to characterize each of the major geochemical events (OAE1d, MCE, OAE2).

In Chapter 10 the final conclusions are drown and an overall discussion of the work is reported.

The project was supervised by Prof. Elisabetta Erba (University of Milan, Italy) and Prof. Riccardo Bersezio (University of Milan, Italy). Collaborational work has been done with Prof. Hugh Jenkyns (University of Oxford, UK), Dr. Alberto Malinverno (Lamont-Doherty Earth Observatory, Columbia University, USA), Prof. Hans Brumsack (Institut für Chemie und Biologie des Meeres (ICBM), University of Oldenburg) and Dr. Bernhard Schnetger (Institut für Chemie und Biologie des Meeres (ICBM), University of Oldenburg).

The individual chapters of this thesis are discrete manuscripts, prepared for submission to international peer- reviewed journals or already in review. Repetitions are therefore unavoidable.

References

Abramovich, S., Keller, G., Stüben, D., Berner. Z. (2003) – Characterization of late Campanian and Maastrichtian planktonic foraminiferal depth habitats and vital activities based on stable isotopes. *Palaeogeography, Palaeoclimatology, Palaeoecology*, 202, 1-29.

Ando, A., Huber, B.T., MacLeod, K.G., Ohta, T., Khim, B. (2009) – Blake Nose stable isotopic evidence against the mid-Cenomanian glaciation hypothesis. *Geology*, 37, 451-454.

Archer, D. (2003) – Biological Fluxes in the Ocean and Atmospheric pCO_2. *In:* Elderfield, H., Holland, H.D., Turekian, K.K. (Eds.), *Treatise on Geochemistry*, Volume 6, 275-291.

Arthur, M.A. and Natland, J.H. (1979) – Carbonaceous sediments in the North and South Atlantic: The role of salinity in stable stratification of Early Cretaceous basins, *In:* Talwani, M., Hay, W., Ryan, W.B.F. (Eds.), Deep Drilling Results in the Atlantic Ocean: Continental Margins and Paleoenvironment. *Geophysical Monograph, Maurice Ewing Series, American Geophysical Union*, 3, 375-401.

Arthur, M.A., Dean, W.E., Schlanger, S.O. (1985) – Variations in the global carbon cycle during the Cretaceous related to climate, volcanism, and changes in atmospheric CO_2. *In:* Sundquist, E.T. and Broecker, W.S. (Eds.), *The Carbon Cycle and Atmospheric CO_2: Natural Variations Archean to Present*, *American Geophysical Union*, *Geophysical Monograph* Series, 32, 504-529.

Arthur, M.A., Schlanger, S.O., Jenkyns, H.C. (1987) – The Cenomanian-Turonian oceanic anoxic event II, paleoceanographic controls on organic matter production and preservation. *In:* Brooks, J. and Fleet, A. (Eds.), *Marine Petroleum Source Rocks*, Geological Society Special Publications, 24, 399-418.

Arthur, M.A., Dean, W.E., Pratt, L.M. (1988) – Geochemical and climatic effects of increased marine organic carbon burial at the Cenomanian/Turonian boundary. *Nature*, 335, 714-717.

Arthur, M.A., Brumsack, H.-J., Jenkyns, H.C., Schlanger, S.O. (1990) – Stratigraphy, geochemistry, and paleoceanography of organic carbon-rich Cretaceous sequences. *In:* Ginsburg, R., Beaudoin, B. (Eds.), *Cretaceous Resources Events, and Rhythms*, 75-119.

Barron, E.J. and Washington, W.M. (1985) – Warm cretaceous climates: High atmospheric CO2 as a plausible mechanism. *In:* Sundquist, E.T. and Broecker, W.S., *The carbon cycle and atmospheric CO2: natural variations archean to present*, Proceedings of the Chapman Conference on Natural Variations in Carbon Dioxide and the Carbon Cycle, 32, 546-553.

Beaudoin, B., M'Ban, E.P., Montanari, A., Pinault, M. (1996) – Lithostratigraphie haute résolution (<20 ka) dans le Cénomanien du bassin d'Ombrie-Marches (Italie). *Comptes Rendus de l'Académie des Sciences Paris*, 323 Series Iia, 689-696.

Beerling, D.J., Lomas, M.R. and Gröcke, D.R. (2002) – On the nature of methane gas-hydrate dissociation during the Toarcian and Aptian oceanic anoxic events. *American Journal of Science*, 302, 28-49.

Bellanca A., Claps, M., Erba, E., Masetti, D., Neri, R., Premoli Silva, I. and Venezia F. (1996) – Orbitally induced limestone/marlstone rhythms in the Albian-Cenomanian Cismon section (Venetian region, northern Italy): sedimentology, calcareous and siliceous plankton distribution, elemental and isotope geochemistry. *Palaeogeography, Palaeoclimatology, Palaeoecology*, 126, 227-260.

Bellanca, A., Erba, E., Neri, R., Premoli Silva, I., Sprovieri, M., Tremolada, F., Verga, D. (2002) – Paleoceanographic significance of the Tethyan "Livello Selli" (Early Aptian) from the Hybla Formation, northwestern Sicily: biostratigraphy and high-resolution chemostratigraphic records. *Palaeogeography, Palaeoclimatology, Palaeoecology*, 185, 175-196.

Bellier, J.-P., Moullade, M., Huber, B.T. (2000) – Mid-Cretaceous planktonic foraminifers from Blake Nose: revised biostratigraphic framework. *In:* Kroon, D., Norris, R.D., Klaus, A. (Eds.), *Proc. ODP, Sci. Results, 171B* [Online]. Available from World Wide Web: http://www-odp.tamu.edu/publications/171B_SR/chap_03/chap_03.htm

Bergman, N.M., Lenton, T.M., Watson, A.J. (2004) – COPSE: A new model of biogeochemical cycling over Phanerozoic time. *American Journal of Science*, 304, 397-437.

Berner, R.A., Lasaga, A.C., Garrels, R.M. (1983) – The carbonate-silicate geochemical cycle and its effect on atmospheric carbon dioxide over the past 100 million years. *American Journal of Science*, 283, 641-683.

Berner, R.A. and Kothavala, Z. (2001) – GEOCARB III: a revised model of atmospheric CO_2 over Phanerozoic time. *American Journal of Science*, 301, 182-204.

Berrocoso, Á.J., MacLeod, K.G., Martin, E.E., Bourbon, E., Londoño, C.I., Basak, C. (2010) – Nutrient trap for Late Cretaceous organic-rich black shales in the tropical North Atlantic. *Geology*, 38, 1111-1114.

Bice, D. (a) Exploring the Dynamics of Earth Systems a guide to constructing and experimenting with computer models of Earth systems using STELLA [Online]. Available from World Wide Web: http://www3.geosc.psu.edu/~dmb53/DaveSTELLA/entrance.htm

Bice, D. (b) Overview of the Carbon Cycle From the Systems Perspective [Online]. Available from World Wide Web: https://www.e-education.psu.edu/earth103/node/692

Blackey, R. (2012) – Web library of palaeogeographic maps: Colorado Plateau Geosystems Inc. [Online]. Available from World Wide Web: http://cpgeosystems.com/paleomaps.html

Blätter, C.L., Jenkyns, H.C., Reynard, L.M., Henderson, G.M. (2011) – Significant increases in global weathering during Oceanic Anoxic Events 1a and 2 indicated by calcium isotopes. *Earth and Planetary Science Letters*, 309, 77-88.

Bonarelli, G. (1891) – Il territorio di Gubbio. *Notizie geologiche*, 1-38.

Bornemann, A., Pross, J., Reichelt, K., Herrle, J.O., Hemleben, C., Mutterlose, J. (2005) – Reconstruction of short-term palaeoceanographic changes during the formation of the Late Albian 'Niveau Breistroffer' black shales (Oceanic Anoxic Event 1d, SE France). *Journal of the Geological Society, London,* 162, 2005, 623-639.

Bowman, A.R. and Bralower, T.J. (2005) – Paleoceanographic significance of high-resolution carbon isotope records across the Cenomanian–Turonian boundary in the Western Interior and New Jersey coastal plain, USA. *Marine Geology*, 217, 305-321.

Bralower, T.J. (1988) – Calcareous nannofossil biostratigraphy and assemblages of the Cenomanian–Turonian boundary interval: implications for the origin and timing of oceanic anoxia. *Paleoceanography*, 3, 275-316.

Bralower, T.J., Sliter, W.V., Arthur, M.A., Leckie, R.M., Allard, D., Schlanger, S.O. (1993). Dysoxic/anoxic episodes in the Aptian-Albian (Early Cretaceous). *In:* Pringle, M., Sager, W.W., Sliter, W.V., Stein, S. (Eds.), *The Mesozoic Pacific: Geology, Tectonics, and Volcanism. American Geophysical Union Monograph*, 77, 5-37.

Bralower, T.J., Arthur, M.A., Leckie, R.M., Sliter, W.V., Allard, D.J., Schlanger, S.O. (1994) – Timing and paleoceanography of dysoxia/anoxia in the Late Barremian to Early Aptian, *Palaios*, 9, 335-369.

Bralower, T.J., Fullagar, P.D., Paull, C.K., Dwyers, G.S., Leckie, R.M. (1997) – Mid-Cretaceous strontium-isotope stratigraphy of deep-sea sections. *Geologica Society of America Bulletin*, 109, 1421-1442.

Bréhéret, J.-G. (1988) - Épisodes de sédimentation riche en matière organique dans les marnes bleues d' âge aptien et albien de la partie pélagique du bassin vocontien. *Bulletin de la Société Géologique de France*, 8, 349-356.

Bréhéret, J.-G. (1994) – The Mid-Cretaceous organic-rich sediments from the Vocontian Zone of the French Southeast Basin. *In:* Mascle, A. (Ed.), *Hydrocarbon and Petroleum Geology of France. Special Publication of the European Association of Petroleum Geoscientists*, 4, 295-320.

Bréhéret, J.-G. (1997) – L'Aptien et l'Albien de la Fosse vocontienne (des bordures aubassin): évolution de la sédimentation et enseignements sur les événements anoxiques. *Société Géologique du Nord*, 25.

Brumsack, H.-J. (1980) – Geochemistry of Cretaceous black shales from the Atlantic Ocean (DSDP Legs 11, 14, 36 and 41). *Chemical Geology*, 31, 1–25.

Brumsack, H.-J. (2006) – The trace metal content of recent organic carbon-rich sediments: Implications for Cretaceous black shale formation. *Palaeogeography, Palaeoclimatology, Palaeoecology*, 232, 344-361.

Bucefalo Palliani, R., Cirilli, S., Mattioli, E. (1998) – Phytoplankton response and geochemical evidence of the lower Toarcian sea level rise in the Umbria-Marche basin (Central Italy). *Palaeogeography, Palaeoclimatology, Palaeoecology*, 142, 33-50.

Bucefalo Palliani, R., Mattioli, E., Riding, J.B. (2002) – The response of marine phytoplankton and sedimentary organic matter to the early Toarcian (Lower Jurassic) oceanic anoxic event in northern England. *Marine Micropaleontology*, 46, 223-245.

Caron, M., Dall'Agnolo, S., Accarie, H., Barrera, E., Kauffman, E.G., Amédro, F., Robaszynski, F., (2006) – High-resolution stratigraphy of the Cenomanian–Turonian boundary interval at Pueblo (USA) and wadi Balhoul (Tunisia): stable isotope and bio-events correlation. *Geobios*, 39, 171-200.

Chumakov, N.M. (1995) – The problem of the warm biosphere. *Stratigraphy and Geological Correlation*, 3, 205-215.

Chumakov, N.M. (2004) – Climatic zones and climate of the Cretaceous period. *In:* Semikhatov, M.A., Chumakov, N.M. (Eds.), Climate in the epochs of major biospheric transformations. *Transactions of the Geological Institute of the Russian Academy of Sciences*, 550, 105-123.

Chumakov, N.M., Zharkov, M.A., Herman, A.B., Doludenko, M.P., Kalandadze, N.N., Lebedev, E.A., Ponomarenko, A.G., Rautian, A.S. (1995) – Climate belts of the Mid- Cretaceous time. *Stratigraphy and Geological Correlation*, 3, 241-260.

Claps, M., Erba, E., Masetti, D., Melchiorri, F. (1995) – Milankovitch-type cycles recorded in Toarcian black shales from the Belluno Trough (Southern Alps Italy). *Memorie di Scienze Geologiche Padova*, 47, 179-188.

Coccioni, R., Erba, E., Premoli Silva, I. (1992) – Barremian-Aptian calcareous plankton biostratigraphy from the Gorgo Cerbara section (Marche, central Italy) and implications for plankton evolution. *Cretaceous Research*, 13, 517-537.

Coccioni, R., Galeotti, S., Gravili, M. (1995) – Latest Albian–early Turonian deep-water agglutinated foraminifera in the Bottaccione section (Gubbio, Italy) — biostratigraphic and palaeoecologic implications. *Revista Espanola de Paleontologia Homenaje al Dr. Guillermo Colom*, 135–152.

Coccioni, R. and Galeotti, S. (2001) – The mid-Cenomanian Event the Prelude to the OAE 2. *EOS Trans. AGU* 82(47), Fall Meet. Suppl.

Coccioni, R. and Galeotti, S. (2003) – The mid-Cenomanian Event: prelude to OAE 2. *Palaeogeography, Palaeoclimatology, Palaeoecology*, 190, 427-440.

Coccioni, R. and Luciani, V. (2005) – Planktonic foraminifers across the Bonarelli Event (OAE2, latest Cenomanian): The Italian record. *Palaeogeography, Palaeoclimatology, Palaeoecology*, 224, 167-185.

Coffin, M.F., Pringle, M.S., Duncan, R.A., Gladczenko, T.P., Storey, M., Müller, R.D., Gahagan, L.A. (2002) – Kerguelen hotspot magma output since 130Ma. *Journal of Petrology*, 43, 1121-1139.

Cool, T.E. (1982) – Sedimentological evidence concerning the paleoceanography of the Cretaceous western North Atlantic Ocean, *Palaeogeography, Palaeoclimatology, Palaeoecology*, 39, 1-35.

Dale, A.W., Meyers, S.R., Aguillera, D.R., Arndt, S., Wallmann, K. (2012) – Controls on organic carbon and molybdenum accumulation in Cretaceous marine sediments from the Cenomanian–Turonian interval including Oceanic Anoxic Event 2. *Chemical Geology*, 324-325, 28-45.

DeConto, R. (2012) – 9th Urbino Summer School of Paleoclimatology 2012, course notes, July, 11-31, Urbino, Italy.

Donnadieu, Y., Pierrehumbert, R., Jacob, R., Fluteau, F. (2006) – Modelling the primary control of paleogeography on Cretaceous climate. *Earth and Planetary Science Letters*, 248, 426-437.

Dromart, G., Garcia, J.-P., Gaumet, F., Picard, S., Rousseau, M., Atrops, F. Lecuyer, C., Sheppard, S.M.F. (2003) – Perturbation of the carbon cycle at the Middle/Late Jurassic transition: Geological and geochemical evidence. *American Journal of Science*, 303, 667-707.

Duque-Botero, F. and Maurrasse, F.J.-M.R. (2008) – Role of cyanobacteria in C_{org}-rich deposits: an example from the Indidura Formation (Cenomanian-Turonian), northeastern Mexico. *Cretaceous Research*, 29, 957–964.

El-Sabbagh, A., Tantawy, A.A., Keller, G., Khozyem, H., Spangenberg, J., Adatte, T., Gertsch, B. (2011) – Stratigraphy of the CenomanianeTuronian Oceanic Anoxic Event OAE2 in shallow shelf sequences of NE Egypt. *Cretaceous Research*, 32, 705-722.

Eldholm, O., and Coffin. M.F. (2000) – Large igneous provinces and plate tectonics. *In:* M.A. Richards, M.A., Gordon, R.G., van der Hilst, R.D. (Eds.), *The history and dynamics of global plate motions*, American Geophysical Union Geophysical Monograph Series, 121, 309–326

Elrick, M., Molina-Garza, R., Duncan, R. and Snow, L. (2009) – C-isotope stratigraphy and paleoenvironmental changes across OAE2 (mid-Cretaceous) from shallow-water platform carbonates of southern Mexico. *Earth and Planetary Science Letters*, 277, 295-306.

Embry, A.F. and Osadetz, K.G. (1988) – Stratigraphy and tectonic significance of Cretaceous volcanism in the Queen Elizabeth Islands, Canadian Arctic Archipelago. *Canadian Journal of Earth Sciences*, 25, 1209-1219.

Ernst, R.E. and Buchan, K.L. (1997) – Giant radiating dyke swarms: their use in identifying pre-Mesozoic large igneous provinces and mantle plumes. *In:* Mahoney, J.J. and Coffin, M.F. (Eds.), *Large igneous provinces: continental, oceanic and planetary flood volcanism*, American Geophysical Union Geophysical Monograph Series, 100, 297-333.

Erba, E. (1994) – Nannofossils and superplumes: the early Aptian 'nannoconid crisis'. *Paleoceanography*, 9, 483-501.

Erba E. (2004) – Calcareous nannofossils and Mesozoic oceanic anoxic events. *Marine Micropaleontology*, 52, 85-106.

Erba, E., Channell, J.E.T., Claps, M., Jones, C., Larson, R., Opdyke, B., Premoli Silva, I., Riva A., Salvini, G., Torricelli, S. (1999) – Integrated stratigraphy of the Cismon APTICORE (Southern Alps, Italy): a 'reference section' for the Barremian – Aptian interval at low latitude s. Journal of Foraminiferal Research, 29, 371-391.

Erba, E., Bartolini, A., Larson, R.L. (2004) – Valanginian Weissert oceanic anoxic event. *Geology*, 32, 149-152.

Erbacher, J., Thurow, J., Littke, R. (1996) – Evolution patterns of radiolaria and organic matter variations: A new approach to identify sea-level changes in Mid-Cretaceous pelagic environments. *Geology*, 24, 499-502.

Erbacher, J. and Thurow, J. (1997) – Influence of oceanic anoxic events on the evolution of mid-Cretaceous radiolaria in the North Atlantic and western Tethys. *Marine Micropaleontology*, 30, 139-158.

Erbacher, J., Huber, B.T., Norris, R.D., Markey, M. (2001) – Increase thermohaline stratification as a possible cause for an oceanic anoxic event in Cretaceous period. *Nature*, 409, 325-327.

Erbacher, J., Friedrich, O., Wilson, P.A., Birch, H., Mutterlose, J. (2005) – Stable organic carbon isotope stratigraphy across Oceanic Anoxic Event 2 of Demerara Rise, western tropical Atlantic. *Geochemistry, Geophysics, Geosystems*, 6, 1-9.

Ernst, G., Schmid, F., Seibertz, E. (1983) – Event-Stratigraphie im Cenoman und Turon von NW-Deutschland. *Zitteliana*, 10, 531-554.

Fisher, J.K., Price, G.D., Hart, M.B., Leng M.J. (2005) – Stable isotope analysis of the Cenomanian–Turonian (Late Cretaceous) oceanic anoxicevent in the Crimea. *Cretaceous Research*, 26, 853-863.

Flögel, S., Wallmann, K., Poulsen, K., Zhou, J., Oschlies, A., Voigt, S., Kuhnt, W. (2011) – Simulating the biogeochemical effects of volcanic CO2 degassing on the oxygen-state of the deep ocean during the Cenomanian/Turonian Anoxic Event (OAE2). *Earth and Planetary Science Letters*, 305 371-384.

Föllmi, K., Godet, A., Bodin, S., Linder, P. (2006) – Interactions between environmental change and shallow water carbonate buildup along the northern Tethyan margin and their impact on the Early Cretaceous carbon isotope record. *Paleoceanography*, 21, 1-6.

Föllmi K.B. (2012) – Early Cretaceous life, climate and anoxia. Cretaceous Research, 35, 230-257.

Forster, A., Schouten, S., Moriya, K., Wilson, P.A., Sinninghe Damsté, J.S. (2007a) – Tropical warming and intermittent cooling during the Cenomanian/Turonian oceanic anoxic event 2: sea surface temperature records from the equatorial Atlantic. *Paleoceanography*, 22, doi:10.1029/2006PA001349.

Forster, A., Schouten, S., Baas, M., Sinninghe Damsté, J.S. (2007b) – A mid-Cretaceous (Albian–Santonian) sea surface temperature record of the tropical Atlantic Ocean. *Geology*, 35, 919-922.

Foster, P., Ramaswamy, V., Artaxo, P., Berntsen, T., Betts, R., Fahey, D.W., Haywood, J., Lean, J., Lowe, D.C., Myhre, G., Nganga, J., Prinn, R., Raga, G., Schulz, M., Van Dorland, R. (2007) – Changes in Atmospheric Constituents and in Radiative Forcing. *In:* Solomon, S., Quin, D., Manning, M., Chen, Z., Marquis, M., Averyt, K.B., Tignor, M., Miller, H.L. (Eds.), *Climate Change 2007: The Physical Science Basis*, Contribution of Working Group I to the Fourth Assessment Report of the Intergovernmental Panel on Climate Change, 129-234.

Friedrich, O., Erbacher, J., Mutterlose, J. (2006) – Paleoenvironmental changes across the Cenomanian/Turonian Boundary Event (Oceanic Anoxic Event 2) as indicated by benthic foraminifera from the Demerara Rise (ODP Leg 207). *Revue de Micropaléontologie*, 49, 121-139.

Friedrich, O., Erbacher, J., Wilson,P.A., Moriya, K., Mutterlose, J. (2009) – Paleoenvironmental changes across the Mid Cenomanian Event in the tropical Atlantic Ocean (Demerara Rise, ODP Leg 207) inferred from benthic foraminiferal assemblages. *Marine Micropaleontology*, 71, 28-40.

Gale, A.S. and Christensen, W.K. – (1996) – Occurrence of the belemnite Actinocamax plenus in the Cenomanian of SE France and its significance. *Bulletin of the Geological Society of Denmark*, 43, 68-77.

Gale, A.S., Jenkyns, H.C., Kennedy, W.J., Corfield, R.M. (1993) – Chemostratigraphy versus biostratigraphy: Data from around the Cenomanian-Turonian boundary, *Journal of the Geological Society of London*, 150, 29-32.

Gale, A.S., Kennedy, W.J., Burnett, J.A., Caron, M., Marshall, J.D. (1996) – The Late Albian to Early Cenomanian succession near Rosans (Drôme, SE France), an integrated study (ammonites,

inoceramids, planktonic Foramini-fera, nannofossils, oxygen and carbon isotopes). *Cretaceous Research*, 17, 515-606.

Gertsch, B., Adatte, T., Keller, G., Tantawy, A.A.M., Berner Z., Mort, H.P., Fleitmann, D. (2010) – Middle and late Cenomanian oceanic anoxic events in shallow and deeper shelf environments of western Morocco. *Sedimentology*, 57, 1430-1462.

Giorgioni, M., Weissert, H., Bernasconi, S.M., Hochuli, P.A., Coccioni, R., Keller, C.E. (2012) – Orbital control on carbon cycle and oceanography in the mid-Cretaceous greenhouse. *Paleoceanography*, 27, PA1204, doi:10.1029/2011PA002163.

Giraud, F., Olivero, D., Baudin, F., Reboulet, S., Pittet, B., Proux, O. (2003) – Minor changes in surface-water fertility across the oceanic anoxic event 1d (latest Albian, SE France) evidenced by calcareous nannofossils. *International Journal of Earth Sciences*, 92, 267-284.

Giraud, F., Reboulet, S., Deconinck, J.F., Martinez, M., Carpentier, A., Bréziat, C. (2013) – The Mid-Cenomanian Event in southeastern France: evidence from palaeontological and clay mineralogical data. *Cretaceous Research*, 46, 43-58.

Gröcke, D.R., Ludvigson, G.A., Witzke, B.L., Robinson, S.A., Joeckel, R.M., Ulnar, D.F., Ravn, R.L. (2006) – Recognizing the Albian-Cenomanian (OAE1d) sequence boundary using plant carbon isotopes: Dakota Formation, Western Interior Basin, USA. *Geology*, 34 193-196.

Hallam, A. (1985) – A review of Mesozoic climates. *Journal of the Geological Society*, 142 433-445.

Hallam, A. (1994) – Jurassic climates as inferred from the sedimentary and fossil record. *In:* Allen, J.R.L., Hoskins, B.J., Sellwood, B.W., Spicer, R.S., Valdes, P.J. (Eds.), *Palaeoclimates and their Modelling: With Special Reference to the Mesozoic Era*, 79-88.

Haq, B.U., Hardenbol, J., Vail, P.R. (1987) – Chronology of fluctuating sea levels since the Triassic. *Science*, 235, 1156-1167.

Hardas, P. and Mutterlose, J. (2007) – Calcareous nannofossil assemblages of Oceanic Anoxic Event 2 in the equatorial Atlantic: Evidence of an eutrophication event. *Marine Micropaleontology*, 66, 52-69.

Hardas, P., Mutterlose, J., Friedrich, O., Erbacher, J. (2012) – The Middle Cenomanian Event in the equatorial Atlantic: The calcareous nannofossil and benthic foraminiferal response. *Marine Micropaleontology*, 96-97, 66-74.

Hasegawa, H., Tada, R., Jiang, X., Suganuma, Y., Imsamut, S., Charusiri, P., Ichinnorov, N., Khand, Y. (2012) - Drastic shrinking of the Hadley circulation during the mid-Cretaceous Supergreenhouse. *Climate of the Past*, 8, 1323-1337.

Hasegawa, T. (1997) – Cenomanian-Turonian carbon isotope events recorded in terrestrial organic matter from northern Japan. *Palaeogeography, Palaeoclimatology, Palaeoecology*, 130, 251-273.

Hasegawa, **T.** (2003) – Cretaceous terrestrial paleoenvironments of northeastern Asia suggested from carbon isotope stratigraphy: Increased atmospheric pCO_2-induced climate. *Journal of Asian Earth Sciences*, 21, 849-859.

Hay, W.W. (2002) – A new view of Cretaceous paleoceanography. *In:* J. Michalik (Ed.), Tethyan/Boreal Cretaceous Correlation, *VEDA Publishing House of the Slovak Academy of Sciences,* 11-37.

Hay, W.W. (2008) – Evolving ideas about the Cretaceous climate and ocean circulation. *Cretaceous Research*, 29, 725-753.

Hay, W.W., DeConto, R.M., Wold, C.N., Wilson, K.M., Voigt, S., Schulz, M., Wold-Rossby, A., Dullo, W.-C., Ronov, A.B., Balukhovsky, A.N., and Söding, E. (1999) – Alternative global Cretaceous paleogeography. *In:* Barrera, E. and Johnson, C.C. (Eds.), *Evolution of the Cretaceous Ocean-Climate System*, Geological Society of America Special Paper 332, 1-47.

Hay, W.W. and Floegel, S. (2012) – New thoughts about the Cretaceous climate and oceans. *Earth-Science Reviews*, 115, 262-272.

Haworth , M., Hesselbo, S.P., McElwain, J.C., Robinson, S.A. and Brunt, J.W. (2005) – Mid Cretaceous pCO_2 based on stomata of the extinct conifer *Pseudofrenelopsis* (Cheirolepidiaceae). *Geology*, 33, 749-752.

Herbin, J.P., Montadert, L., Muller, C., Gomez, R., Thurow, J., Wiedmann, J. (1986) – Organic-Rich Sedimentation at the CenomanianeTuronian Boundary in Oceanic and Coastal Basins in the North Atlantic and Tethys. *Geological Society, London, Special Publications*, 21, 389-422.

Hesselbo, S.P., Gröcke, D., Jenkyns, H.C., Bjerrum, C.J., Farrimond, P., Bell, H.S.M., Green, O.R. (2000) – Massive dissociation of gas hydrate during a Jurassic oceanic anoxic event. *Nature*, 406, 392-395.

Hetzel, A., Böttcher, M.E., Wortmann, U.G., Brumsack, H.-J. (2009) – Paleo-redox conditions during OAE 2 reflected in Demerara Rise sediment geochemistry (ODP Leg 207). *Palaeogeography, Palaeoclimatology, Palaeoecology*, 273, 302-328.

Hilbrecht, H., Hubberten, H.-W., Öberänsli, H. (1992) – Biogeography of planktonic foraminifera and regional carbon isotope variations: Productivity and water masses in Late Cretaceous Europe. *Palaeogeography, Palaeoclimatology, Palaeoecology*, 92, 407-421.

Hochuli, P., Menegatti, A.P., Riva, A., Weissert, H., Erba, E., Premoli Silva, I. (1999) – High-productivity and cooling episodes in the early Aptian Alpine Tethys, *Geology*, 27, 657-660.

Holbourn, A. and Kuhnt, W. (2002) – Cenomanian-Turonian palaeoceanographic change on the Kerguelen Plateau: a comparison with Northern Hemisphere records. *Cretaceous Research*, 23, 333-349.

Hu, X., Wagreich, M., Yilmaz, I.O. (2012) – Marine rapid environmental/climatic change in the Cretaceous greenhouse world. *Cretaceous Research*, 38, 1-6.

Huber, B.T., Hodell, D.A., Hamilton, C.P. (1995) – Middle – Late Cretaceous climate of the southern high latitudes: stable isotopic evidence for minimal equator-to-pole thermal gradients. *Geological Society of America Bulletin*, 107, 1164–1191.

Huber, B.T., Leckie, R.M., Norris, R.D., Bralower, T.J., CoBabe, E. (1999) – Foraminiferal assemblage and stable isotopic change across the Cenomanian– Turonian boundary in the subtropical North Atlantic. *Journal of Foraminiferal Research*, 29, 392-417.

Huber, B.T., Norris, R.D., MacLeod, K.G. (2002) – Deep-sea paleotemperature record of extreme warmth during the Cretaceous. Geology, 30, 123–126.

Ingram, B.L., Coccioni, R., Montanari, A., Richter, F.M. (1994) – Strontium isotopic composition of mid-Cretaceous seawater, Science, 264, 546-550.

Jarvis, I., Carson, G.A., Cooper, M.K.E., Hart, M.B., Leary, P.N., Tocher, B.A., Horne, D., Rosenfeld, A. (1988) – Microfossil Assemblages and the Cenomanian-Turonian (late Cretaceous) Oceanic Anoxic Event. Cretaceous Research, 3, 3-103.

Jarvis, I., Mabrouk, A., Moody, R.T.J., Cabrera, S.D. (2002) – Late Cretaceous (Campanian) carbon isotope events, sea-level change and correlation of the Tethyan and Boreal realms. *Palaeogeography, Palaeoclimatology, Palaeoecology*, 188, 215-248.

Jarvis, I., Gale, A.S., Jenkyns, H.C. and Pearce M.A. (2006) – Secular variation in Late Cretaceous carbon isotopes: a new δ13C carbonate reference curve for the Cenomanian–Campanian (99.6–70.6 Ma). *Geological Magazine*, 143, 561-608.

Jarvis, I., Lignum, J.S., Gröcke, D.R., Jenkyns, H.C., Pearce, M.A. (2011) – Black shale deposition, atmospheric CO2 drawdown, and cooling during the Cenomanian-Turonian Oceanic Anoxic Event. *Paleoceanography*, 26, PA3201, doi:10.1029/2010PA002081.

Jenkyns, H.C. (1980) – Cretaceous anoxic events: From continents to oceans. *Journal of the Geological Society of London*, 137, 171-188.

Jenkyns, H.C. (1988) – The Early Toarcian (Jurassic) anoxic event: stratigraphic, sedimentary and geochemical evidence. *American Journal of Science*, 288, 101-151.

Jenkyns, H.C. (1991) – Impact of Cretaceous sea level rise and anoxic events on the Mesozoic carbonate platform of Yugoslavia. *American Association of Petroleum Geologists Bulletin*, 75, 1007-1017.

Jenkyns, H.C. (1995) – Carbon-isotope stratigraphy and paleoceanographic significance of the lower Cretaceous shallow-water carbonates of Resolution Guyot, Mid-Pacific Mountains, Proc. Ocean Drill. Program Sci. Results, 143, 99-108.

Jenkyns, H.C. (1999) – Mesozoic anoxic events and paleoclimate. *Zentralblatt für Geologie und Paläontologie, Teil.* I, 943-949.

Jenkyns, H.C. (2003) – Evidence for rapid climate change in the Mesozoic–Palaeogene greenhouse world. *Philosophical Transactions of the Royal Society of London A*, 361, 1885-1916.

Jenkyns, H.C. (2010) – Geochemistry of oceanic anoxic events. *Geochemistry Geophysics Geosystems*, 11, Q03004, doi:10.1029/2009GC002788.

Jenkyns, H.C and Clayton, J.C. (1986) – Black shales and carbon isotopes in pelagic sediments from the Tethyan Lower Jurassic. *Sedimentology*, 33, 87-106.

Jenkyns, H.C., Gale, A.S., Corfield, R.M. (1994) – Carbon- and oxygen-isotope stratigraphy of the English Chalk and Italian Scaglia and its palaeoclimatic significance. *Geological Magazine*, 131, 1-34.

Jenkyns, H.C. and Clayton, J.C. (1997) – Lower Jurassic epicontinental carbonates and mudstones from England and Wales: chemostratigraphic signals and the early Toarcian anoxic event. *Sedimentology*, 44, 687-706.

Jones, C.E. and Jenkyns, H.C. (2001) – Seawater strontium isotopes, oceanic anoxic events, and seafloor hydrothermal activity in the Jurassic and Cretaceous. *American Journal of Science,* 301, 112-149.

Kassab, A.S., and Obaidalla, N.A. (2001) – Integrated biostratigraphy and inter-regional correlation of the Cenomanian-Turonian deposits of Wadi Feiran, Sinai, Egypt. *Cretaceous Research*, 22, 105-114.

Kauffman, E.G. (1984) – Paleobiogeography and evolutionary response dynamic in the Cretaceous Western Interior Seaway of North America. *In:* Westermann, G.E.G. (Ed.) Jurassic-*Cretaceous Biochronology and Paleogeography of North America*, Geological Association of Canada, Special Paper, 27, 273-306.

Kaufmann, E.G. and Caldwell, W.G.E. (1993) – The western interior basin in space and time. *In:* Caldwell, W.G.E. and Kauffman, E.G. (Eds.), *Evolution of the Western Interior Basin*, Geological Association of Canada, Special Paper, 39, 1-30.

Keller, G., Berner, Z., Adatte, T., Stueben, D. (2004) – Cenomanian–Turonian and $\delta^{13}C$, and $\delta^{18}O$, sea level and salinity variations at Pueblo, Colorado. *Palaeogeography, Palaeoclimatology, Palaeoecology*, 211, 19-43.

Keller, G., Adatte, T., Berner, Z., Chellai, E.H., Stueben, D. (2008) – Oceanic events and biotic effects of the Cenomanian-Turonian anoxic event, Tarfaya Basin, Morocco. *Cretaceous Research*, 29, 976-994.

Kennedy, W. J., Gale, A. S., Lees, J. A., Caron, M. (2004) – The Global Boundary Stratotype Section and Point (GSSP) for the base of the Cenomanian Stage, Mont Risou, Hautes-Alpes, France. Episodes, 27/1, 21-32.

Kennedy, W. J., Walaszcyk, I., Cobban, W. A. (2005) – The Global Boundary Stratotype Section and Point for the base of the Turonian Stage of the Cretaceous: Pueblo, Colorado, U.S.A. Episodes 28/2, 93-104.

Kerr, A.C. (1998) – Oceanic plateau formation: A cause of mass extinction and black shale deposition around the Cenomanian-Turonian boundary. *Journal of the Geological Society, 155*, 619-626.

Kerr, A.C., Tarney, J., Marriner, G.F., Nivia, A., Saunders, A.D. (1997) – The Caribbean-Colombian Cretaceous Igneous Province: The Internal Anatomy of an Oceanic Plateau. *In:* Mahoney, J.J. and Coffin, M. (Eds.), *Large Igneous Provinces: Continental, Oceanic, and Planetary Flood Volcanism*, American Geophysical Union, Geophysical Monograph Series, 100, 123-144.

Kuhnt, W. (1992) – Abyssal recolonization by benthic Foraminifera after the Cenomanian/Turonian boundary anoxic event in the North Atlantic. *Marine Micropaleontology*, 19, 257-274.

Kuypers, N.M.M, Pancost, R.D., Nijenhuis, I.A., Sinnighe Damsté, J.S. (2002) – Enhanced productivity led to increased organic carbon burial in euxinic North Atlantic basin during the late Cenomanian Oceanic Anoxic Event. Paleoceanography, 17, doi: 10.1029/2000PA000569.

Kuypers, M.M.M., van Bruegel, Y., Shouthen, S., Erba, E., Sinnighe Damsté, J.S. (2004) – N2-fixing cyanobacteria supplied nutrient N for Cretaceous oceanic anoxic events. *Geology*, 32, 853-856.

Larson, R.L. (1991a) – Latest pulse of the Earth: evidence for a mid-Cretaceous superplume. Geology, 19, 547–550.

Larson, R.L. (1991b) – Geological consequences of superplumes. *Geology*, 19, 963–966.

Larson, R.L., Fischer, A.G., Erba, E., Premoli Silva, I. (1993) – APTICORE-ALBICORE: A workshop Report on Global Events and Rhythms of the mid-Cretaceous, 4-9 October, Perugia, Italy, 56.

Larson, R.L. and Erba, E. (1999) – Onset of the mid-Cretaceous greenhouse in the Barremian-Aptian: Igneous events and the biological, sedimentary, and geochemical responses. *Paleoceanography*, 14, 663-678.

Lebedel, V., Lezin, C., Andreu, B., Wallez, M.-J., Ettachfini, E.M., Riquier, L. (2013) – Geochemical and palaeoecological record of the Cenomanian–Turonian Anoxic Event in the carbonate platform of the Preafrican Trough, Morocco. *Palaeogeography, Palaeoclimatology, Palaeoecology*, 369, 79-98.

Lebedeva, N.K. and Zverev, K.V. (2003) – Sedimentological and palynological analysis of Cenomanian-Turonian event in northern Siberia. *Geologiya I Geofizika*, 44, 769-780.

Leckie, R.M., Yuretich, R.F., West, O.L.O., Finkelstein, D., Schmidt, M. (1998) – Paleoceanography of the southwestern Western Interior Sea during the time of the Cenomanian-Turonian boundary (Late Cretaceous). *In:* Dean, W.E. and Arthur, M.A. (Eds.), *Stratigraphy and Paleoenvironments of the Cretaceous Western Interior Seaway, USA*, Concepts in Sedimentology and Paleontology, 6, 101-126.

Leckie, R.M., Bralower, T.J., Cashman, R. (2002) – Oceanic anoxic events and plankton evolution: Biotic response to tectonic forcing during the mid-Cretaceous. *Paleoceanography*, 17, 13-29.

Lini, A., Weissert, H., Erba, E. (1992) – The Valanginian carbon isotopic event: A first episode of greenhouse climate conditions during the Cretaceous. *Terra Nova*, 4, 374-384.

Linnert, C., Mutterlose, J., Erbacher, J. (2010) – Calcareous nannofossils of the Cenomanian/Turonian boundary interval from the Boreal Realm (Wunstorf, northwest Germany). *Marine Micropalaeontology*, 74, 38-58.

Linnert, C., Mutterlose, J, Mortimore, R. (2011) – Calcareous nannofossils from Eastbourne (Southeastern England) and their paleoceanography of the Cenomanian/ Turonian boundary interval. *Palaios*, 26, 298-313.

Liu, Z., Dreybrodt, W., Liuc H. (2011) – Atmospheric CO_2 sink: Silicate weathering or carbonate weathering? *Applied Geochemistry*, 26, S292-S294.

Luciani, V. and Cobianchi, M. (1999) – The Bonarelli Level and other black shales in the Cenomanian-Turonian of the northeastern Dolomites (Italy): calcareous nannofossil and foraminiferal data. *Cretaceous Research*, 20, 135-167.

MacLeod, K.G., Martin, E.E., Blair, S.W. (2008) – Nd isotopic excursion across Cretaceous ocean anoxic event 2 (Cenomanian–Turonian) in the tropical North Atlantic. *Geology*, 36, 811-814.

MacLeod, K.G., Londono, C.I., Martin, E.E., Berrocoso, A.J., Basak, C. (2011) Changes in North Atlantic circulation at the end of the Cretaceous greenhouse interval. *Nature Geoscience*, 4, 779-782.

McElwain, J.C., Wade-Murphy, J., Hesselbo, S.P. (2005) – Changes in carbon dioxide during an oceanic anoxic event linked to intrusion into Gondwana coals. *Nature*, 435, 479-482.

McElwain, J.C. and Punyasena, S.W. (2007) – Mass extinction events and the plant fossil record. *Trends in Ecology and Evolution*, 22, 548-557.

Melinte-Dobrinescu, M.C., Bernárdez, E., Kaiho, K., Lamolda, M.A. (2013) – Cretaceous Oceanic Anoxic Event 2 in the Arobes section, northern Spain: nannofossil fluctuations and isotope events.

In: Bojar, A.-V., Melinte-Dobrinescu, Smit, J. (Eds.), *Isotopic Studies in Cretaceous Research, Geological Society, London*, Special Publications, 382.

Menegatti, A.P., Weissert, H., Brown, R.S., Tyson, R.V., Farrimond, P., Strasser, A., Caron, M. (1998) – High-resolution $\delta^{13}C$ stratigraphy through the early Aptian 'Livello Selli' of the Alpine Tethys. *Paleoceanography*, 13, 530-545.

Meyer, T. (1990) – Biostratigraphische und sedimentologische Untersuchungen in der Plänerfazies des Cenoman von Nordwestdeutschland. *Mitteilungen aus dem Geologischen Institut der Universität Hannover*, 30, 1-114.

Miller, K.G., Sugarman, P.J., Browning, J.V., Kominz, M.A., Hernández, J.C., Olsson, R.K., Wright, J.D., Feigenson, M.D., Van Sickel, W. (2003) – Late Cretaceous chronology of large, rapid sea-level changes: Glacioeustasy during the greenhouse world. *Geology*, 31, 585-588.

Miller, K.G., Wright, J.D., Browning, J.V. (2005) – Visions of ice sheets in a greenhouse world. *Marine Geology*, 217, 215-231.

Mitchell, K., Mason, P.R.D., Van Cappellen, P., Johnson, T.M., Gill, B.C., Owens, J.D., Diaz, J., Ingall, E.D., Reichart, G.-J., Lyons, T.W. (2012) – Selenium as paleo-oceanographic proxy: A first assessment. *Geochimica et Cosmochimica Acta*, 89, 302-317.

Mitchell, S.F. (1996) – Foraminiferal assemblages from the late Lower and Middle Cenomanian of Speeton (North Yorkshire, UK): relationships with sea-level fluctuations and water mass distribution. *Journal of Micropalaeontology*, 15, 37–54.

Mitchell, S.F., Paul, C.R.C., Gale, A.S. (1996) – Carbon isotopes and sequence stratigraphy. *In:* Howell, J.A. and Aitken, J.F. (Eds.), High Resolution Sequence Stratigraphy: Innovations and Applications. *Geological Society of London, Special Publication, 104*, 11-24

Mitchell, S.F. and Carr, I.T. (1998) – Foraminiferal response to mid-Cenomanian (Upper Cretaceous) palaeoceanographic events in the Anglo-Paris Basin (Northwest Europe). *Palaeogeography, Palaeoclimatology, Palaeoecology*, 137, 103-125.

Monaco, P., Rodríguez-Tovar, F.J., Uchman, A. (2012) – Ichnological analysis of lateral environmental heterogeneity within the Bonarelli level (uppermost Cenomanian) in the classical localities near Gubbio, central Appennines, Italy. *Palaios*, 27, 48-54.

Monnet, C. (2009) – The Cenomanian–Turonian boundary mass extinction (Late Cretaceous): New insights from ammonoid biodiversity patterns of Europe, Tunisia and the Western Interior (North America), *Palaeogeography, Palaeoclimatology, Palaeoecology*, 282, 88-104.

Monteiro, F.M., Pancost, R.D., Ridgwell, A., Donnadieu, Y. (2012) – Nutrients as the dominant control on the spread of anoxia and euxinia across the Cenomanian-Turonian oceanic anoxic event (OAE2): Model-data comparison. *Paleoceanography*, 27, doi: 10.1029/2012PA002351.

Montoya-Pino, C., Weyer, S., Anbar, A.D., Pross, J., Oschmann, W., van de Schootbrugge, B., Arz, H.W. (2010) – Global enhancement of ocean anoxia during Oceanic Anoxic Event 2: A quantitative approach using U isotopes. *Geology*, 38, 315-318.

Morettini, E., Santantonio, M., Bartolini, A., Cecca, F., Baumgartner P.O., Hunziker J.C. (2002) – Carbon isotope stratigraphy and carbonate production during the Early–Middle Jurassic: Examples from the Umbria-Marche-Sabina Apennines (central Italy). *Palaeogeography, Palaeoclimatology, Palaeoecology*, 184, 251-273.

Moriya, K., Wilson, P.A., Friedrich, O., Erbacher, J., Kawahata, H. (2007) – Testing for ice sheets during the mid-Cretaceous greenhouse using glassy foraminiferal calcite from the mid-Cenomanian tropics on Demerara Rise. *Geology*, 35, 615–618.

Musavu-Moussavou, B., Danielian, T., Baudin, F., Coccioni, R. (2007) – The Radiolarian biotic response during OAE2. A high-resolution study across the Bonarelli level at Bottaccione (Gubbio, Italy). *Revue de Micropaléontologie*, 50, 253-287.

Mutterlose, J. and Kessels, K. (2000) – Early Cretaceous calcareous nannofossils from high latitudes: Implications for palaeo- biogeography and palaeoclimate. *Palaeogeography, Palaeoclimatology, Palaeoecology*, 160, 347-372.

Neal, C.R., Mahoney, J.J., Kroenke, L.W., Duncan, R.A., Petterson, M.G. (1997) – The Ontong Java Plateau. *In:* Mahoney, J.J. and Coffin, M. (Eds.), *Large Igneous Provinces: Continental, Oceanic, and Planetary Flood Volcanism*, American Geophysical Union, Geophysical Monograph Series, 100, 183-216.

Nederbragt, A.J., Fiorentino, A., Klosowska, B. (2001) – Quantitative analysis of calcareous microfossils across the Albian – Cenomanian boundary oceanic anoxic event at DSDP Site 547 (North Atlantic). *Palaeogeography, Palaeoclimatology, Palaeoecology*, 166, 401-421.

NOAA National Climatic Data Center (2012) – Global surface temperature anomalies [Online]. Available from World Wide Web: http://ncdc.noaa.gov/

Norris, R.D. and Wilson, P.A. (1998) – Low-latitude sea-surface temperatures for the mid-Cretaceous and the evolution of planktic foraminifera, *Geology*, 26, 823-826.

Norris, R.D., Bice, K.L., Magno, E.A., Wilson, P.A. (2002) – Jiggling the tropical thermostat in the Cretaceous hothouse. *Geology*, 30, 299-302.

Orth, C.J., Attrep, M., Quintana, L.R., Elder, W.P., Kauffman, E.G., Diner, R., Villamil, T. (1993) – Elemental abundance anomalies in the late Cenomanian extinction interval – A search for the source(s). *Earth and Planetary Science Letters*, 117, 189-204.

Owens, J.D., Lyons, T.W., Li, X., MacLeod, K., Gordon, G., Kuypers, M.M.M., Anbar, A., Kuhnt, W., Severmann, S. (2012) – Iron isotope and trace metal records of iron cycling in the

proto-North Atlantic during the Cenomanian-Turonian oceanic anoxic event (OAE-2). *Paleoceanography*, doi:10.1029/2012PA002328.

Owens, J.D., Gill, B.C., Jenkyns, H.C., Bates, S.M., Severmann, S., Kuypers, M.M.M., Woodfine, R.G., Lyons, T.W. (2013) – Sulfur isotopes track the global extent and dynamics of euxinia during Cretaceous Oceanic Anoxic Event 2, *Proceedings of the National Academy of Sciences*, published ahead of print.

Paul, C.R.C., Mitchell, S.F., Marshall, J.D., Leary, P.N., Gale, A.S., Duane, A.M. and Ditchfield, P.W. (1994) – Paleoceanographic events in the Middle Cenomanian of Northwest Europe. *Cretaceous Research*, 15, 707-738.

Paul, C.R.C., Lamolda, M.A., Mitchell, S.F., Vaziri, M.R., Gorostidi, A., Marshall, J.D. (1999) – The Cenomanian-Turonian boundary at Eastbourne (Sussex, UK): a proposed European reference section. *Palaeogeography, Palaeoclimatology, Palaeoecology*, 150, 83-121.

Pearce, M.A., Jarvis, I., Tocher, B.A. (2009) – The Cenomanian–Turonian boundary event, OAE2 and palaeoenvironmental change in epicontinental seas: New insights from the dinocyst and geochemical records. *Palaeogeography, Palaeoclimatology, Palaeoecology*, 280, 207-234.

Peate, D.W. (1997) – The Parana-Etendeka Province. *In:* Mahoney, J.J. and Coffin, M. (Eds.), *Large Igneous Provinces: Continental, Oceanic, and Planetary Flood Volcanism*, American Geophysical Union, Geophysical Monograph Series, 100, 217–245.

Petrizzo, M.R., Huber, B.T., Wilson, P.A. MacLeod, K.G. (2008) Late Albian paleoceanography of the western subtropical North Atlantic. *Paleoceanography*, 23, PA1213, doi:10.1029/2007PA001517.

Pogge von Strandmann, P.A.E., Jenkyns, H.C., Woodfine, R.G. (2013) – Lithium isotope evidence for enhanced weathering during Oceanic Anoxic Event 2. *Nature Geoscience*, 6, 668-672.

Poulsen, C.J., Barron, E.J., Johnson, C.C., Fawcett, P. (1999) – Links between major climatic factors and regional oceanic circulation in the mid- Cretaceous. *In:* Barrera, E. and Johnson, C.C. (Eds.) *Evolution of the Cretaceous Ocean-Climate System*, Geological Society of America Special Papers, 332, 73-89.

Poulsen, C.J., Barron, E.J., Arthur, M.A., Peterson, W.H. (2001) – Response of the mid-Cretaceous global ocean circulation to tectonic and CO_2 forcings. *Paleoceanography*, 16, 576-592.

Pratt, L. M., and Threlkeld, C.N. (1984) – Stratigraphic significance of $^{13}C/^{12}C$ ratios in mid-Cretaceous rocks of the Western Interior, U.S.A.. *In:* Stott, D.F. and Glass, D.J. (Eds.), *The Mesozoic of Middle North America*, Canadian Society Petroleum Geologists Memory, 9, 305-312.

Pratt, L.M., Arthur, M.A., Dean, W. E., Scholle, P.A. (1993) – Paleo-oceanographic cycles and events during the Late Cretaceous in the Western Interior Seaway of North America. *In:* Caldwell,

W.G.E. and Kauffman, E.G. (Eds.), Evolution of the Western Interior Basin, *Special Paper of the Geological Association of Canada*, 39, 333-354.

Prauss, M.L. (2012) – Potential freshwater dinocysts from marine upper Cenomanian to upper Coniacian strata of Tarfaya, northwest Africa: Three new species of *Bosedinia*. *Cretaceous Research*, 37, 246-260.

Premoli Silva, I. and Sliter, W.V. (1994) – Cretaceous planktonic foraminiferal biostratigraphy and evolutionary trends from the Bottaccione section, Gubbio, Italy. *Palaeontographica Italica*, 82, 1-89.

Premoli Silva, I. and Sliter, W.V. (1999) – Cretaceous paleoceanography: Evidence from planktonic foraminiferal evolution. In: Barrera, E., and Johnson, C.C. (Eds.), *Evolution of the Cretaceous Ocean-Climate System,* Geological Society of America Special Paper, *332*, 301-328.

Premoli Silva, I., Erba, E., Salvini, G., Verga, D., Locatelli, C. (1999) – Biotic changes in Cretaceous Anoxic Events. *Journal of Foraminiferal Research*, 29, 352-370.

Price, G.D. (1999) – The evidence and implications of polar ice during the Mesozoic. *Earth-Science Reviews*, 48, 183-210.

Robock, A., and Oppenheimer, C. (2003) – Volcanism and the Earth's Atmosphere. Geophysical Monograph Series, 139, 1-360.

Rohde, R.A. – Web resource: Global Worming Art [Online]. Available from World Wide Web: http://www.globalwarmingart.com/

Rothman, D.H. (2002) – Atmospheric carbon dioxide levels for the last 500 million years. *Proceedings of the National Academy of Sciences*, 99, 4167–4171.

Royer, D.L., Berner, R.A., Montañez, I.P., Tabor, N.J., Beerling, D.J. (2004) – CO_2 as a primary driver of Phanerozoic climate. *GSA Today*, 14, 4-10.

Rullkötter, J. (2000) – Organic matter: the driving force of early diagenesis. *In:* Zabel, M. (Ed.), *Marine Geochemistry*, 129-172.

Sageman, B.B., Meyers, S.R., Arthur, M.A. (2006) – Orbital time scale and new C-isotope record for Cenomanian-Turonian boundary stratotype. *Geology*, 34, 125-128.

Salvini, G. and Marcucci Pesserini, M. (1998) – The radiolarian assemblages of the Bonarelli Horizon in the Umbria-Marches Apennines and Southern Alps, Italy. *Cretaceous Research*, 19, 777-804.

Sánchez Quiñónez, C.A., Alegret, L., Aguado, R., Delgado, A., Larrasoaña, J.C., Martín-Algarra, A., O'Dogherty, L., Molina, E. (2010) - Foraminíferos del tránsito Cenomaniense-Turoniense en la sección de El Chorro, Cordillera Bética, sur de España. *Geogaceta*, 49, 23-26.

Sarmiento, J.L., Herbert, T.D., Toggweiler, J.R. (1988) – Causes of anoxia in the world ocean. *Global Biogeochemical Cycles*, 2, 115-128.

Sarmiento, J.L. and Gruber, N. (2006) – *Ocean Biogeochemical Dynamics*, Princeton, Woodstock: Princeton University Press, 1-503.

Saunders, A.D., Fitton, J.G., Kerr, A.C., Norry, M.J., Kent, R.W. (1997) – The North Atlantic Igneous Province. *In:* Mahoney, J.J., and Coffin, M.F. (Eds.), *Large Igneous Provinces: Continental, Oceanic, and Planetary Flood Volcanism*, American Geophysical Union, Geophysical Monograph Series, 100, 45-94.

Schlanger, S.O. and Jenkyns, H.C. (1976) – Cretaceous oceanic anoxic events: causes and consequence. *Geologie en Mijnbouw*, 55, 179-184

Schlanger, S.O., Arthur, M.A., Jenkyns, H.C., Scholle, P.A. (1987) – The Cenomanian-Turonian oceanic anoxic event, I, Stratigraphy and distribution of organic carbon-rich beds and the marine C excursion. *In:* Brooks, J. and Fleet, A.J. (Eds.), Marine Petroleum Source Rocks, *Geological Society Special Publications*, 26, 371-399, 1987.

Scholle, P.A. and Arthur, M.A. (1980) – Carbon isotope fluctuations in Cretaceous pelagic limestones: potential stratigraphic and petroleum exploration tools. *AAPG Bulletin*, 64, 67-87.

Scopelliti, G., Bellanca, A., Coccioni, R., Luciani, V., Neri, R., Baudin, F., Chiari, M., Marcucci, M. (2004) – High-resolution geochemical and biotic records of the Tethyan 'Bonarelli Level' (OAE2, latest Cenomanian) from the Calabianca–Guidaloca composite section, northwestern Sicily, Italy. *Palaeogeography, Palaeoclimatology, Palaeoecology*, 208, 293-317.

Scopelliti, G., Bellanca, A., Neri, R., Baudin, F., Coccioni, R. (2006) – Comparative high-resolution chemostratigraphy of the Bonarelli Level from the reference Bottaccione section (Umbria–Marche Apennines) and from an equivalent section in NW Sicily: Consistent and contrasting responses to the OAE2. *Chemical Geology*, 228, 266-285.

Scopelliti, G., Bellanca, A., Erba, E., Jenkyns, H.C., Neri, R., Tamagnini, P., Luciani, V., Masetti, D. (2008) – Cenomanian–Turonian carbonate and organic-carbon isotope records, biostratigraphy and provenance of a key section in NE Sicily, Italy: Palaeoceanographic and palaeogeographic implications. *Palaeogeography, Palaeoclimatology, Palaeoecology*, 265, 59-77.

Scopelliti, G., Bellanca, A., Neri, R., Sabatino, N. (2010) – Phosphogenesis in the Bonarelli Level from northwestern Sicily, Italy: petrographic evidence of microbial mediation and related REE behavior. *Cretaceous Research*, 31, 237-248.

Sellwood, B.W. and Valdes, P.J. (2006) – Mesozoic climates: General circulation models and rock record. *Sedimentary Geology*, 190, 269-287.

Sellwood, B.W. and Valdes, P.J. (2007) – Mesozoic climates. *In:* Williams, M., Haywood, A.M., Gregory, F.J., Schmidt, D.N. (Eds.), *Deep-Time Perspectives on Climate Change: Marrying the Signal from Computer Models and Biological Proxies*, The Micropalaeontological Society, Special Publications, 201-224.

Simo, J.A., Scott, R.W., Masse, J.-P. (1993) – Cretaceous carbonate platforms: An overview. Pp. 1–14 *In:* Toni Simo, J.A., Scott, R.W., Masse, J.-P. (Eds.), *American Association of Petroleum Geologists, Memoir 56*, 1-14.

Sinnighe-Damsté, J.S., van Bentum, E.C., Reichart, G.-J., Pross, J., Schouten, S. (2010) – A CO_2 decrease-driven cooling and increased latitudinal temperature gradient during the mid-Cretaceous Oceanic Anoxic Event 2. *Earth and Planetary Science Letters*, 293, 97-103.

Sinton, C.W., and Duncan, R.A. (1997) – Potential links between ocean plateau volcanism and global ocean anoxia at the Cenomanian-Turonian boundary, *Economic Geology*, 92, 836-842.

Skelton, P. W., Spicer, R. A., Kelley, S. P., Gilmour, I. (2003) – *The Cretaceous World*. Cambridge University Press, 360 pp.

Snow, L.J., Duncan, R.A., Bralower, T.J. (2005) – Trace element abundances in the Rock Canyon Anticline, Pueblo, Colorado, marine sedimentary section and their relationship to the Caribbean plateau construction and osygen anoxic event 2. *Paleoceanography*, 20, doi:10.1029/2004PA001093.

Stoll, H.M. and Schrag, D.P. (2000) – High-resolution stable isotope records from the Upper Cretaceous rocks of Italy and Spain: glacial episodes in a greenhouse planet? *Bulletin of the Geological Society of America*, 112, 308-319.

Storey, M., Mahoney, J.J., Saunders, A.D. (1997) – Cretaceous basalts in Madagascar and the transition between plume and continental lithosphere mantle sources. *In:* Mahoney, J.J. and Coffin, M. (Eds.), *Large Igneous provinces: Continental, Oceanic, and Planetary Flood Volcanism*, American Geophysical Union, Geophysical Monograph Series, 95–122.

Sugarman, P.J., Miller, K.G., Olsson, R.K., Browning, J.V., Wright, J.D., De Romero, L.M., White, T.S., Muller, F.L., Uptegrove, J. (1999) – The Cenomanian/Turonian carbon burial event, Bass River, NJ, USA: Geochemical, paleoecological, and sea-level changes. *In:* Huber, B.T., Bralower, T.J., Leckie, R.M. (Eds.), *Paleoecological and Geochemical Signatures of Cretaceous Anoxic Events; A Tribute to William Sliter*, Journal of Foraminiferal Research, 29, 438-452.

Summerhayes, C.P. (1981) – Organic facies of middle Cretaceous black shales in the deep North Atlantic, AAPG Bulletin, 65, 2364-2380.

Summerhayes, C.P. (1987) – Organic-rich Cretaceous sediments from the North Atlantic. *In:* Brooks, J. and Fleet, A.J. (Eds.), Marine Petroleum Source Rocks, *Geological Society Special Publications*, 26, 301-316.

Takashima, R., Nishi, H., Huber, B.T., Leckie, R.M. (2006) – Greenhouse world and the Mesozoic ocean. *Oceanography*, 19, 82-92.

Takashima, R., Nishi, H., Yamanaka, T., Tomosugi, T., Fernando, A.G., Tanabe, K., Moriya, K., Kawabe, F., Hayashi, K. (2011) – Prevailing oxic environments in the Pacific ocean during the mid-Cretaceous oceanic Anoxic Event 2. *Nature communications*, 2, article number 234, doi: 10.1038/ncomms1233.

Thurow, J., Brumsack, H.-J., Rullkötter, J., Littke, R., Meyers, P. (1992) – The Cenomanian/Turonian boundary event in the Indian Ocean – A key to understand the global picture, in Synthesis of Results From Scientific Drilling in the Indian Ocean. *American Geophysical Union, Geophysical Monograph Series*, 70, 253-273, AGU, Washington, D.C.

Tiraboschi, D., Erba, E., Jenkyns, H.C. (2009) – Origin of rhythmic Albian black shales (Piobbico core, central Italy): Calcareous nannofossil quantitative ans statistical analyses and paleoceanographic reconstructions. *Paleoceanography*, 19, doi:10.1029/2008PA001670.

Trabucho Alexandre, J., Tuenter, E., Henstra, G.A., Van der Zwan, K.J., Van de Wal R.S.W., Dijkstra, H.A., De Boer, P.L. (2010) – The mid-Cretaceous North Atlantic nutrient trap: Black shales and OAEs. *Paleoceanography*, 25, doi:10.1029/2010PA001925.

Tsandev, I. and Slomp, C.P. (2009) – Modeling phosphorus cycling and carbon burial during Cretaceous Oceanic Anoxic Events, *Earth and Planetary Science Letters*, 286, 71-79.

Tsikos, H., Jenkyns, H.C., Walsworth-Bell, B., Petrizzo, M.R., Forster, A., Kolonic, S., Erba, E., Premoli Silva, I., Baas, M., Wagner, T. and Sinnighe Damsté, J.S. (2004) – Carbon-isotope stratigraphy recorded by the Cenomanian-Turonian Oceanic Anoxic Event: correlation and implications based on three key localities. *Journal of the Geological Society, London,* 161, 711-719.

Tucholke, B.E., and Vogt, P.R. (1979) – Western North Atlantic: Sedimentary evolution and aspects of tectonic history, *Initial Report Deep Sea Drilling Project*, 43, 791-825.

Turgeon, S., Brumsack, H.-J., Kuypers, M., Bottcher, M.E. (2002) – How extreme can you get? A closer look at sediment geochemistry of the Upper Cenomanian and Lower Turonian at Gubbio and Furlo in Italy. *Organic-carbon burial, climate change and ocean chemistry (Mesozoic-Paleogene), Geological Society of London, Dec. 9-11, London, UK,* 19.

Turgeon, S. and Brumsack, H.-J. (2006) – Anoxic vs dysoxic events reflected in sediment geochemistry during the Cenomanian–Turonian Boundary Event (Cretaceous) in the Umbria–Marche Basin of central Italy. *Chemical Geology*, 234, 321-339.

Turgeon, S.C. and Creaser, R.A. (2008) – Cretaceous oceanic anoxic event 2 triggered by a massive magmatic episode. *Nature*, 454, 323-326.

van Bentum, E.C., Reichart, G.-J., Forster, A., Sinnighe Damsté, J.S. (2012) – Latitudinal differences in the amplitude of the OAE-2 carbon isotopic excursion: pCO_2 and paleo productivity. *Biogesciences*, 9, 717-731.

van Breugel, Y., Schouten, S., Tsikos, H., Erba, E., Price, G.D., Sinnighe Damstè, J.S. (2007) – Synchronous negative carbon isotope shifts in marine and terrestrial biomarkers at the onset of the early Aptian oceanic anoxic event 1a: Evidence for the release of 13C-depleted carbon into the atmosphere. *Paleoceanography*, 22, PA1210, doi:10.1029/2006PA001341.

van de Schootbrugge, B., McArthur, J.M., Bailey, T.R., Rosenthal, Y., Wright, J.D. and Miller, K.G. (2005). Toarcian oceanic anoxic event: An assessment of global causes using belemnite C isotope records. *Paleoceanography,* 20, doi: 10.1029/2004PA001102.

Vaughan, A.P.M. (2007) – Climate and geology – a Phanerozoic perspective. *In:* Williams, M., Haywood, A.M., Gregory, F.J., Schmidt, D.N. (Eds.), *Deep-Time Perspectives on Climate Change: Marrying the Signal from Computer Models and Biological Proxies*, The Micropalaeontological Society, Special Publications, 5-59.

Voigt, S., Gale, A.S., Flögel, S. (2004) – Midlatitude shelf seas in the Cenomanian–Turonian greenhouse world: temperature evolution and North Atlantic circulation. *Paleoceanography*, 19, doi:10.1029/2003PA001015.

Voigt, S., Gale, A.S., Voigt, T. (2006) – Sea-level change, carbon cycling and palaeoclimate during the Late Cenomanian of northwest Europe; an integrated palaeoenvironmental analysis. *Cretaceous Research*, 27, 836-858.

Voigt, S., Aurag, A., Leis, F., Kaplan, U. (2007) – Late Cenomanian to Middle Turonian high-resolution carbon isotope stratigraphy: New data from the Münsterland Cretaceous Basin, Germany. *Earth and Planetary Science Letters*, 253, 196-210.

Wagner, T., Hofmann, P., Flögel, S. (2013) – Marine black shale deposition and Hadley Cell dynamics: A conceptual framework for the Cretaceous Atlantic Ocean. *Marine and Petroleum Geology*, 43, 222-238.

Wakeham S. G. and Canuel E. A. (2006) – Degradation and preservation of organic matter in marine sediments. *In:* J. K. Volkman (Ed.), *The Handbook of Environmental Chemistry*, 295-321.

Wang, C.S., Hu, X.M, Jansa, L., Wan, X.Q., Tao, R. (2001) – The Cenomanian–Turonian anoxic event in southern Tibet. *Cretaceous Research*, 22, 481-490.

Wang, P. (2009) – Global monsoon in a geologic perspective. *Chinese Science Bulletin*, 54, 1113-1136.

Watkins, D.K., Cooper, M.J., Wilson, P.A. (2005) – Calcareous nannoplankton response to late Albian oceanic anoxic event 1d in the western North Atlantic. Paleoceanography, 20, doi:10.1029/2004PA001097.

Weissert, H. (1989) – C-isotope stratigraphy, a monitor of paleoenvironmental changes: A case study from the Early Cretaceous. *Survey in Geophysics*, 10, 1-16.

Weissert, H. and Mohr, H. (1996) – Late Jurassic climate and its impact on carbon cycling. *Palaeogeography, Palaeoclimatology, Palaeoecology*, 122, 27-43.

Weissert, H., Lini, A., Föllmi, K.B., Kuhn, O. (1998) – Correlation of Early Cretaceous carbon isotope stratigraphy and platform drowning events: a possible link? *Palaeogeography, Palaeoclimatology, Palaeoecology*, 137, 189–203.

Weissert, H. and Erba E. (2004) – Volcanism, CO2 and palaeoclimate: a Late Jurassic-Early Cretaceous carbon and oxygen isotope record. *Journal of the Geological Society*, 161, 695-702.

Westermann, S., Caron, M., Fiet, N., Fleitmann, D., Matera, V., Adatte, T., Föllmi, K.B. (2010) – Evidence for oxic conditions during oceanic anoxic event 2 in the northern Tethyan pelagic realm. *Cretaceous Research*, 31, 500-514.

Wignall, P.B. (2001) – Large igneous provinces and mass extinctions. *Earth Science Reviews*, 53, 1-33.

Willis, K.J. and McElwain, J.C. (2002) – The Evolution of Plants. *Oxford University Press, Oxford, New York, United States*, 1-378.

Wilmsen, M. (2003) – Sequence stratigraphy and palaeoceanography of the Cenomanian Stage in northern Germany. *Cretaceous Research*, 24, 525-568.

Wilmsen, M. (2007) – Integrated stratigraphy of the upper Lower–lower Middle Cenomanian of northern Germany and southern England. *Acta Geologica Polonica*, 57, 263-279.

Wilson, P.A. and Norris, **R.D.** (2001) – Warm tropical ocean surface and global anoxia during the mid-Cretaceous period, *Nature*, 412, 425-429.

Wortmann, U.G., Herrle, J.O., Weissert, H. (2004) – Altered carbon cycling and coupled changes in Early Cretaceous weathering pattern: evidence from integrated Tethyan isotope and sandstone records. *Earth and Planetary Science Letters*, 220, 69–82.

Yilmaz, I.O., Altiner, D., Tekin, U.K., Tuysuz, O., Ocakoglu, F., Acikalin, S. (2010) – Cenomanian–Turonian Oceanic Anoxic Event (OAE2) in the Sakarya zone, northwestern Turkey: sedimentological, cyclostratigraphic, and geochemical records. *Cretaceous Research*, 31, 207-226.

Yurtsever, T.S., Tekin, U.K., Demirel, Í.H. (2003) – First evidence of the Cenomanian/Turonian boundary event (CTBE) in the Alakirçay Nappe of the Antalya Nappes, southwest Turkey. *Cretaceous Research*, 24, 41-53.

Zheng, X.Y., Jenkyns, H.C., Henderson, G.M., Gale, A.S., Ward, D.J. (2013) – Changing ocean circulation and hydrothermal inputs during Ocean Anoxic Event 2 (Cenomanian–Turonian): Evidence from Nd-isotopes in the European shelf sea. *Earth and Planetary Science Letters*, 375, 338-348.

Zimmerman, H.B., Boersma, A., McCoy F.W. (1987) – Carbonaceous sediments and paleoenvironment of the Cretaceous South Atlantic Ocean. *In:* Brooks, J. and Fleet, A.J. (Eds.), *Marine Petroleum Source Rocks*, Geological Society Special Publications, 24, 271-286.

Zobaa, M.K., Oboh-Ikuenobe, F.E., Ibrahim, M.I. (2011) – The Cenomanian/Turonian oceanic anoxic event in the Razzak Field, north Western Desert, Egypt: Source rock potential and paleoenvironmental association. *Marine and Petroleum Geology*, 28, 1475-1482.

Chapter 2

Studied sections

The pelagic sediments of five key-localities in Italy have been used as study areas: Furlo, Contessa, Monte Petrano and Le Brecce sections in the Umbria-Marche Basin and the Cismon section in the Belluno Basin. As shown in Fig. 2.1 the five measured sections do not homogeneously cover the investigated time interval (about 12 My; 104-92 Ma, after the timescale of Gradstein et al., 2012).

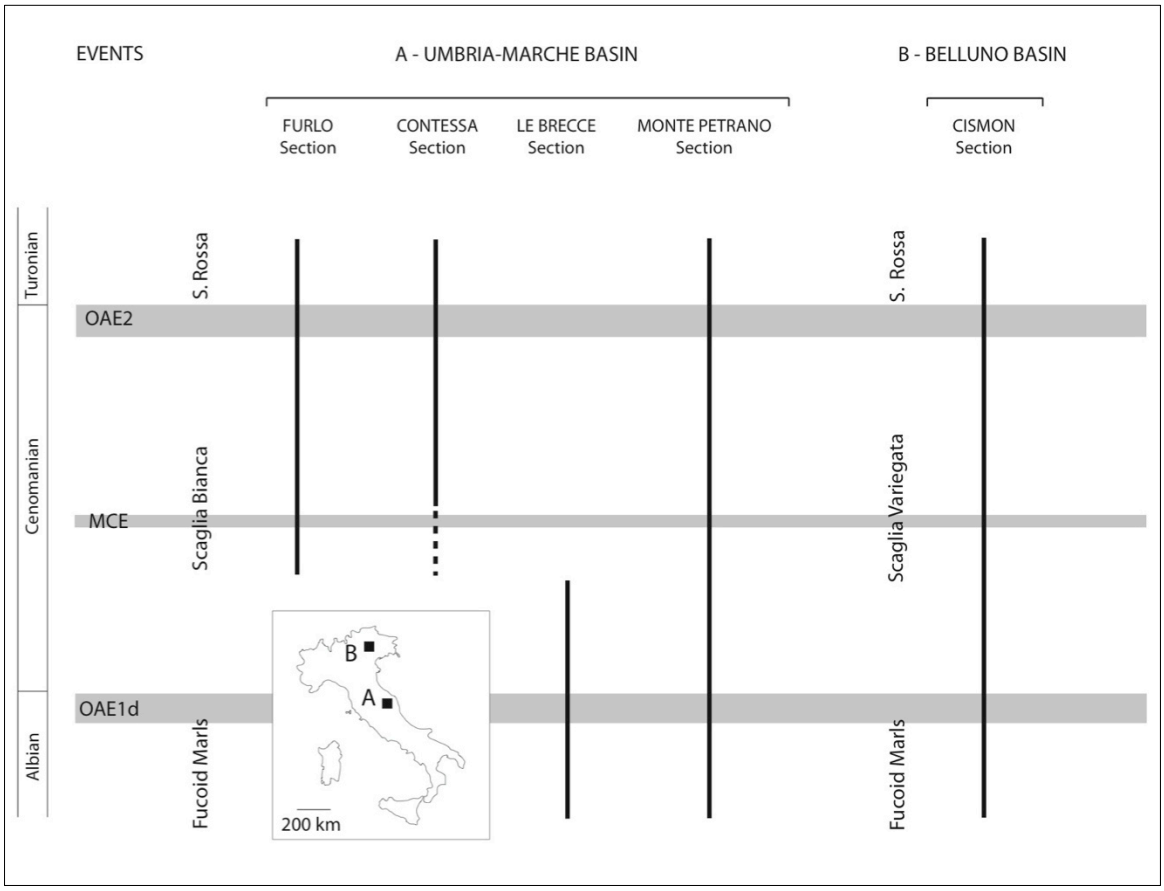

Figure 2.1: *Stratigraphic distribution of the studied sections.*

The selected sections have been dated using calcareous nannofossil and planktonic foraminiferal biostratigraphy (Bellanca et al., 1996; Tamagnini, 2007; Tiraboschi, 2009; Lanci et al., 2010; Erba, unpublished data; Russo, PhD Thesis 2013),

Both basins during the studied time interval were located in the southern part of the Thethys Ocean, in the northern tropical climatic belt (Dercourt et al., 2000; Skelton et al., 2003). These basins were characterized by a strongly irregular bathimetry, owing to their configuration in structural highs and lows inherited from the Jurassic rifting stages. Both the Umbria-Marche and Belluno Basins were relatively close to elevated plateaus and/or to emergent lands. These are relevant features to be accounted for the geological interpretations that will be discussed later on.

2.1 Umbria-Marche Basin

The Umbria-Marche Basin is at present located in the Central Apennines fold and thrust belt, located in the central-eastern part of Italy. This area represents a unique place where an almost continuous Jurassic up to Oligocene pelagic sequence is well preserved and exposed. The Umbria-Marche sequence was entirely deposited on the continental crust of the Adria microplate (Channell et al., 1979a), in a basins and swells setting with a complex palaeobathimetry (Alvarez, 1990). The studied time interval corresponds to the so-called Scaglia Bianca Formation, a mainly calcareous pelagic sequence resulting from lithification of nannofossil-planktonic foraminiferal oozes (Arthur and Premoli Silva, 1982) deposited at a water depth of about 1500-2000m (Arthur and Premoli Silva, 1982; Kuhnt, 1990). The Scaglia Bianca (Late Albian – Early Turonian; in Italian the word Scaglia literally means “scale” or “flake” and refers to the thin, tabular stratification of this formation) lies above the Marne a Fucoidi Formation (Early Aptian – Late Albian) and is overlied by the Scaglia Rossa Formation (Early Turonian – Middle Eocene) (Parisi, 1989; Coccioni and Galeotti, 2003). The Scaglia Bianca lower boundary is conventionally placed at the first chert nodule while the upper limit is conventionally defined by the occurrence of pinkish lithologies (Parisi, 1989).

The Scaglia Bianca Formation can be subdivided, from bottom to top, into four informal members (Coccioni et al., 1992, 2003):

- W1 Lower Yellowish-Grey member: yellowish-grey limestone with nodules and lenses of greenish-grey chert; pink to reddish micritic and marly limestones occur in the lowermost part and greenish-grey to black, marlstone/shale layers are interbedded in the lower portion;
- W2 Reddish member: pink to reddish micritic limestones with subordinate yellowish-grey marlstone layers;

- W3 Upper Yellowish-Grey member: yellowish-grey micritic limestones with nodules and lenses of greenish-grey chert;
- W4 Greyish member: light-grey micritic limestones with nodules and lenses of dark grey to black chert; black marlstone/shale layers are interbedded in the upper part of the member.

About 6-8 meters below the boundary between Scaglia Bianca and Scaglia Rossa formations lies the so called 'Livello Bonarelli', an approximately 1m thick black interval consisting of bituminous argillites and siltstones ('scisti ittiolitici' of Bonarelli, 1891). Slightly below the Livello Bonarelli, there is a first continuus bed of black chert, that can be found throughout the Umbria-Marche area, called "Black Marker" as originally described by Montanari (1985).

2.1.1 Furlo section

The Furlo abandoned quarry (Beaudoin et al 1996; Turgeon and Brumsack, 2006; Mitchell et al, 2008; Turgeon and Craser, 2008; Lanci et al, 2010) is located in the homonymous gorge, 25km south-east of Urbino and is part of a dismissed quarry (43°38'40.82''N, 12°42'40.23''E) (Fig. 2.2a and b). The measured sequence is 30m thick. During the present PhD project the outcrop has been sedimentologically described in great detailed, including the Bonarelli Level logged at a mm-scale. In this outcrop, right above the studied interval, the so called "Bonarelli 2" can be observed. This layer is simply the result of a structural repetition of the Bonarelli due to slumping (Alvarez and Lowrie, 1984 and Alvarez, 2009).

Figure 2.2a: *Furlo section.*

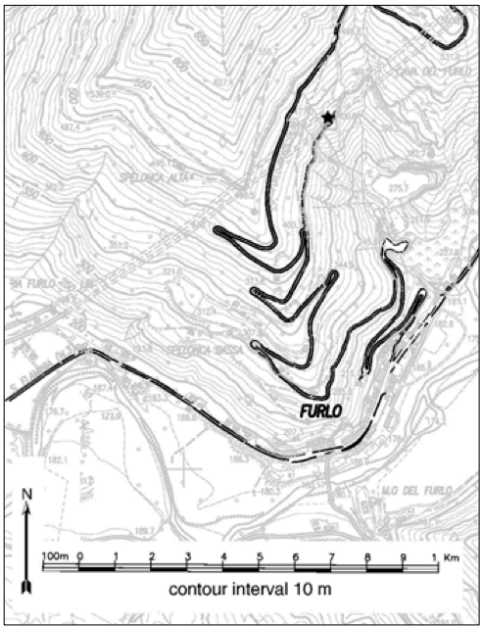

Figure 2.2b: *Furlo section location (after Mitchell et al., 2008).*

2.1.2 Contessa section

The Contessa outcrop (Monechi and Parisi, 1989; Coccioni and Galeotti, 2003; Monaco et al., 2012) is located about 2 km from the town of Gubbio, in the Vispi active quarry, close to the homonymous Highway that gives the informal name to the outcrop (43°22'31.62''N, 12°33'38.54''E). The interval studied is 29m thick. As an additional dataset I analyzed the 40.05m-long Gubbio 2 core (Tsikos et al, 2004) collected from a borehole drilled right in front of the quarry within the framework of the C/T-Net research project by the Milano Research Group. During the present PhD project this core has been described in great detail and correlated to the outcrop data (Fig. 2.3a, b and c). Moreover, as for the Furlo section, the Bonarelli Level has been sedimentologically described at a mm-scale.

Figure 2.3a: *Contessa section. The Gubbio2 core was drilled approximately where the truck on the left is located.*

Figure 2.3b: *Positions of the various drilling-sites at Contessa secion. The Gubbio2 core was drilled in correspondence of Site 2.*

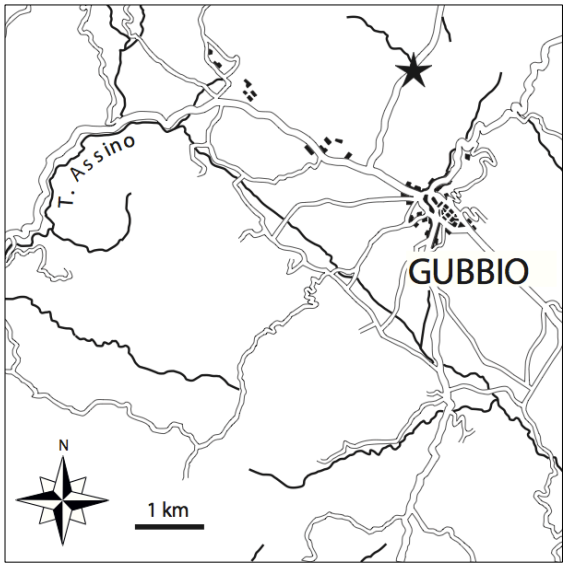

Figure 2.3c: *Contessa section location.*

2.1.3 Le Brecce section

The 20m-thick section at Le Brecce is located inside a gorge, at 3 km from the Piobbico village (43°34'59.93''N, 12°29'04.29''E) (Fig. 2.4 a and b). The studied outcrop is at the km 34 of the state road 257-Apecchiese, close to the Piobbico drillsite (Tiraboschi, 2009). This section was previously studied by Erba and Tiraboschi (unpublished data) and within my PhD project was logged in great detailed.

Figure 2.4a: *Le Brecce section.*

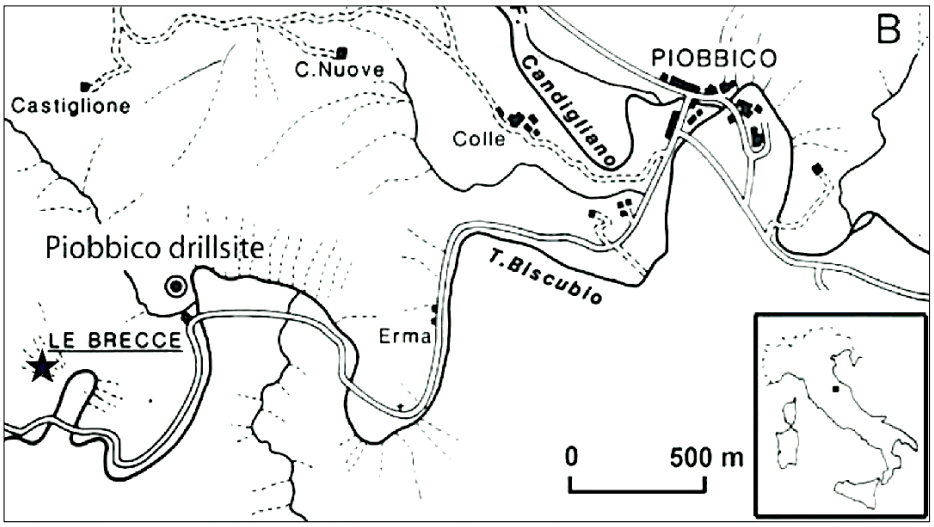

Figure 2.4b: *Le Brecce section location.*

2.1.4 Monte Petrano section

The Monte Petrano measured section, not far from the top of the Petrano Mountain and the Moria village (43°30'24.89''N, 12°36'49.02''E), is 70.5m thick (Fig. 2.5 a and b). This outcrop has never been studied in detail, except for the lowermost part of this section studied by Giorgioni et al. (2012).

Figure 2.5a: *Monte Petrano section.*

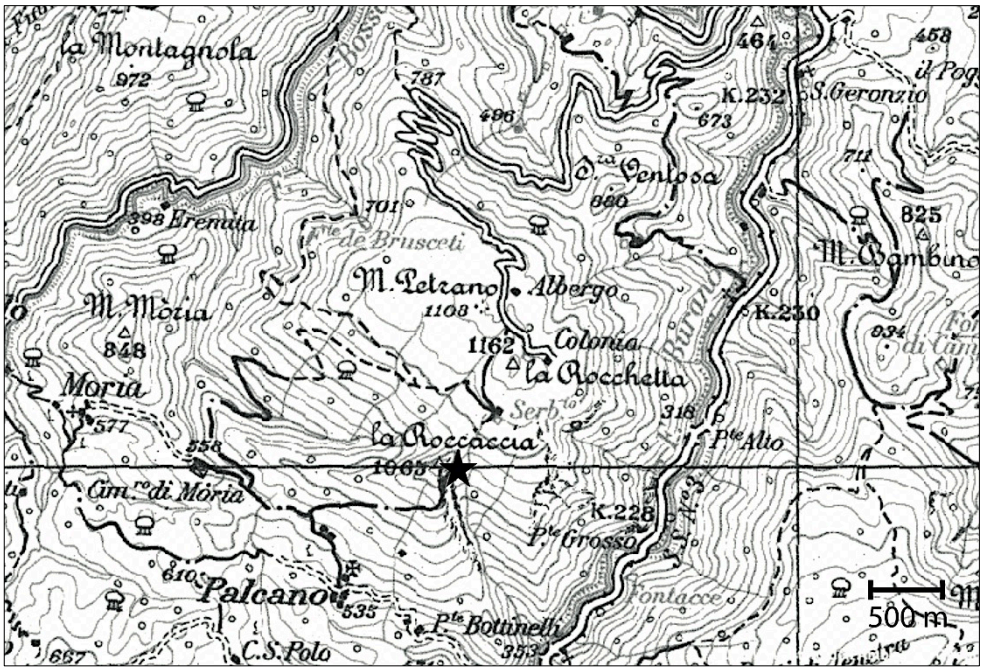

Figure 2.5b: *Monte Petrano section location.*

2.2 Belluno Basin

The Belluno Basin, at present exposed in the Southern Alps fold and thrust belt, was located in the southern margin of the Tethys. During the Cretaceous this passive margin represented a subsiding domain inherited from the Jurassic, at the eastern side of the Trento Plateau (Bernoulli and Jenkyns, 1974; Winterer and Bosellini, 1981; Sarti et al., 1992; Bellanca et al, 1996). The basin was dominated by the deposition of calcareous oozes, starting from the latest Jurassic with the deposition of the Biancone Formation up to the Eocene with the Scaglia Cinerea. The time interval of interest is represented by the upper part of the Scaglia Variegata Formation (Channell et al., 1979a). The succession consists of an alternation of yellowish to grey limestones, chert bands and shales/black shales (Channell et al., 1979b; Claps et al., 1991; Bellanca et al., 1996) that reflects Milankovith cyclicity (Claps et al., 1991; Claps and Masetti, 1994; Bellanca et al, 1996).

2.2.1 Cismon section

The 60m thick Cismon section (Bosellini et al., 1978; Channell et al., 1979a; Bellanca et al., 1996) is located in the Venetian Southern Alps, north-eastern Italy, along the SS50 (State Highway 50) not far from the village of Lamon and along the Cismon stream (46°02’43.00’’, 11°45’40.34’’) (Fig. 2.6 a and b). The base of the analyzed section coincides with the first bed of whitish limestone just above a reddish interval of middle Albian age (Erba et al., 1999).

Figure 2.6a: *Cismon section. The logged interval starts at the first whitish limestone bed above the reddish interval.*

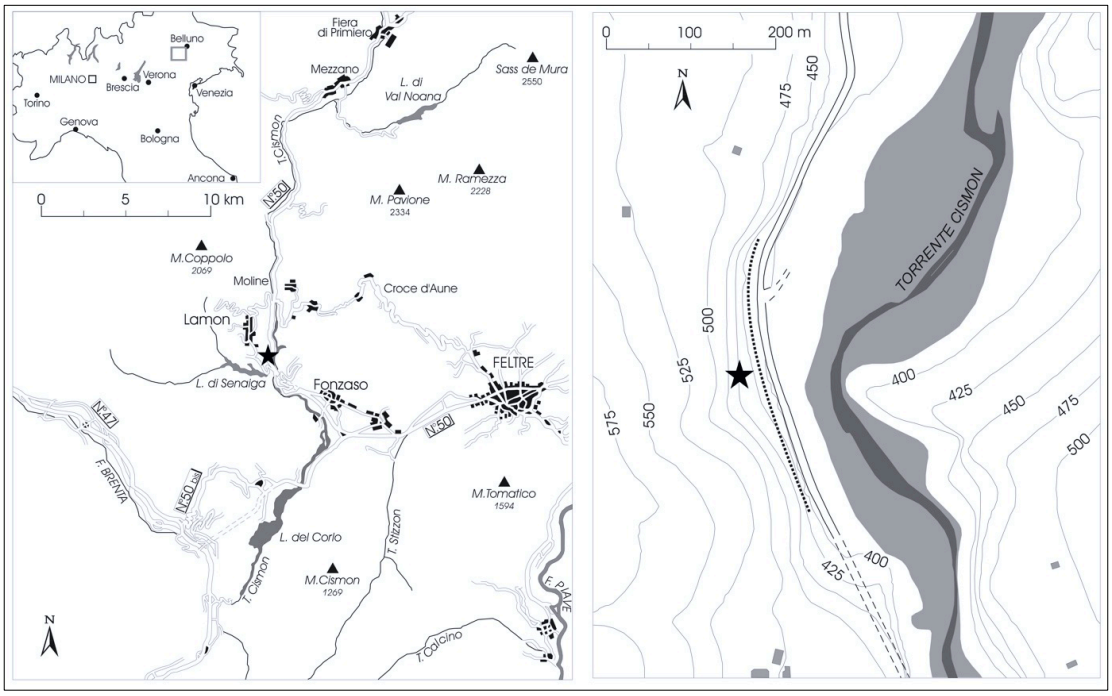

Figure 2.6b: *Cismon section location.*

Table 2.7 reports a complete list of the dataset used for this PhD project. The data directly produced during the present PhD project are flagged with V, while results of previous investigations are marked with X (see individual chapters for references).

	Furlo	Contessa	Le Brecce	Monte Petrano	Cismon
Detailed sedimentological log	V	V	V	V	V
Biostratigraphic data	X	X	X	X	X
Stable oxygen and inorganic carbon isotopes	X	X	X	V	V
Stable organic carbon isotopes	X	X		V	V
Calcimetry	XV			V	V
Rock Eval/TOC Pyrolysis	X			V	V
XRF	X			V	V
Cyclostratigraphy	XV	V	V	V	V

Table 2.7: *Dataset available at the end of the present PhD project.*

References

Alvarez, W. (1990) – Pattern of extensional faulting in pelagic carbonates of the Umbria-Marche Apennines of central Italy. *Geology*, 18, 407-410.

Alvarez, W. (2009) – The historical record in the Scaglia limestone at Gubbio: magnetic reversals and the Cretaceous-Tertiary mass extinction. *Sedimentology*, 56, 137-148.

Alvarez, W. and Lowrie, W. (1984) – Magnetic stratigraphy applied to synsedimentary slumps, turbidites, and basin analysis: The Scaglia limestone at Furlo (Italy). *Geological Society of America Bulletin*, 95, 324–336.

Arthur, M.A. and Premoli Silva, I. (1982) – Development of widespread organic carbon-rich strata in the Mediterranean Tethys. *In:* Schlanger, S.O. and Cita, M.B. (Eds.), *Nature and Origin of Cretaceous Carbon-rich Facies*, 7-54.

Beaudoin, B., M'Ban, E.P., Montanari, A., Pinault, M. (1996) – Lithostratigraphie haute résolution (<20 ka) dans le Cénomanien du bassin d'Ombrie-Marches (Italie). *Comptes Rendus de l'Académie des Sciences Paris*, 323 Series Iia, 689-696.

Bellanca A., Claps, M., Erba, E., Masetti, D., Neri, R., Premoli Silva, I. and Venezia F. (1996) – Orbitally induced limestone/marlstone rhythms in the Albian-Cenomanian Cismon section (Venetian region, northern Italy): sedimentology, calcareous and siliceous plankton distribution, elemental and isotope geochemistry. *Palaeogeography, Palaeoclimatology, Palaeoecology*, 126, 227-260.

Bernoulli, D. and Jenkyns, H.C. (1974) – Alpine, Mediterranean, and Central Atlantic Mesozoic facies in relation to the early evolution of the Tethys. In: Dott, R.H. and Shaver, R.H. (Eds.), Modern and Ancient Geosynclinal Sedimentation. Society of Economic Paleontologists and Mineralogists, Special Publication, 19, 129-160.

Bonarelli, G. (1891) – Il territorio di Gubbio. *Notizie geologiche*, 1-38.

Bosellini, A., Broglio Loriga, C., and Busetto, C. (1978) - I bacini cretacei del Trentino. *Riv. Ital Paleont. Strat*, 84.4, 897-946.

Channell J.E.T., D'Argenio, B., Horvath, F. (1979a) – The African Promontory, in Mesozoic Mediterranean Paleogeography. *Earth Science Review*, 15, 213-272.

Channell, J. E. T., Lowrie, W. and Medizza, F. (1979b) – Middle and Early Cretaceous magnetic stratigraphy from the Cismon section, northern Italy. *Earth and Planetary Science Letters*, 1979, 42.2, 153-166.

Claps, M., Masetti, D., Pedrielli, F., Garavello, A. (1991) – Analisi spettrale e cicli di Milankovitch in successioni cretaciche del Sudalpino orientale. Rivista Italiana di Paleontologia e Stratigrafia, 97, 153-174.

Claps, M. and Masetti, D. (1994) – Milankovitch periodicities recorded in Cretaceous deep-sea sequences from the Southern Alps (Northern Italy). Special Publications International Association of Sedimentologists, 19, 99-107.

Coccioni, R., Galeotti, S., Ragni, D. (1992) – Litho- and biostratigraphy of the Scaglia Bianca Formation (Late Albian-Late Cenomanian) in the Umbria-Marche Apennines (Italy). 6th Annual Meeting of IGCP 262 (Tethyan Cretaceous Correlation) - 'Cretaceous Facies in Orogenic Belts', Athens, 22-26 May, 1992, p. 4.

Coccioni, R., Galeotti, S. (2003) – The mid-Cenomanian Event: prelude to OAE 2. *Palaeogeography, Palaeoclimatology, Palaeoecology*, 190, 427-440.

Coccioni, R., Galeotti, S. (2003) – The mid-Cenomanian Event: prelude to OAE 2. *Palaeogeography, Palaeoclimatology, Palaeoecology*, 190, 427-440.

Dercourt, J., Gaetani, M., Vrielinck, B., Barrier, E., Biju-Duval, B., Brunet, M.F., Cadet, J.P., Crasquin, S., Sandulescu, M. (2000) – *Atlas of Peri-Tethys, Palaeogeographical Maps. Commission de la Carte Geologique du Monde (CCGN/CGMW)*, Paris, pp. 1-269.

Erba, E., Channell, J.E.T., Claps, M., Jones, C., Larson, R., Opdyke, B., Premoli Silva, I., Riva A., Salvini, G., Torricelli, S. (1999) – Integrated stratigraphy of the Cismon APTICORE (Southern Alps, Italy): a 'reference section' for the Barremian – Aptian interval at low latitude s. Journal of Foraminiferal Research, 29, 371-391.

Giorgioni, M., Weissert, H., Bernasconi, S.M., Hochuli, P.A., Coccioni, R., Keller, C.E. (2012) – Orbital control on carbon cycle and oceanography in the mid-Cretaceous greenhouse. *Paleoceanography*, 27, PA1204, doi:10.1029/2011PA002163.

Gradstein, F.M., Ogg, J.G., Schmitz, M.D., Ogg, G.M. (2012) – *The Geologic Time Scale 2012*, vol. 2, Elsevier, 1176pp.

Kuhnt, W., Herbin, J.P., Thurow, J., Wiedmann, J. (1990) – Distribution of Cenomanian-Turonian Organic Facies in the Western Mediterranean and along the Adjacent Atlantic Margin. *In:* Huc, A. Y. (Eds.), *Deposition of Organic Facies*, AAPG Studies in Geology, 30, 133-160.

Lanci L., Muttoni, G., Erba E. (2010) – Astronomical tuning of the Cenomanian Scaglia Bianca Formation at Furlo, Italy. *Earth and Planetary Science Letters*, 292, 231-237.

Mitchell, R.N., Bice, D.M., Montanari, A., Cleaveland, L.C., Christianson, K.T., Coccioni, R., Hinnov, L.A. (2008) – Oceanic anoxic cycles? Orbital prelude to the Bonarelli Level (OAE2). *Earth and Planetary Science Letters*, 267, 1-16.

Monechi, S. and Parisi, G. (1989) – Da Gubbio a Cantiano. *In:* Cresta, S., Monechi, S., Parisi, G. (Eds.), *Stratigrafia del Mesozoico e Cenozoico nell'area umbro-marchigiana*, *Memorie Descrittive della Carta Geologica* d'Italia, 39, 96-102.

Montanari, A. (1985) – Cenomanian anoxic foreslope inferred from turbiditic cherts in the pelagic basin of the Northern Apennines, Italy. *Geological Society of America*, Abstract with programs., 17, 1-667, USA

Parisi, G. (1989) – Stratigrafia del Cretacico-Paleogene. *In:* Cresta, S., Monechi, S., Parisi, G. (Eds.), *Stratigrafia del Mesozoico e Cenozoico nell'area umbro-marchigiana*, *Memorie Descrittive della Carta Geologica* d'Italia, 39, 23-29.

Sarti, M., Bosellini, A. and Winterer, E. L. (1992) - Basin geometry and architecture of a Tethyan passive margin (Southern Alps, Italy): implications for rifting mechanisms. *Geology and geophysics of continental margins*, 53, 241-258.

Skelton, P. W., Spicer, R. A., Kelley, S. P., Gilmour, I. (2003) – *The Cretaceous World*, pp.1-360.

Tamagnini, P. (2007) – Calcareous nannofossils as tracers of paleoceanographic changes associated to Oceanic Anoxic Event 2: records from the Tethys and Atlantic Oceans. *Università degli Studi di Milano, PhD thesis*.

Tiraboschi, D. (2009) – Variazioni quantitative del nannoplancton calcareo durante il Cretacico medio: paleoecologia, paleoceanografia e produzione di carbonato in condizioni di anossia globale ed eccesso di pCO_2. *Università degli Studi di Milano, PhD thesis*.

Tsikos, H., Jenkyns, H.C., Walsworth-Bell, B., Petrizzo, M.R., Forster, A., Kolonic, S., Erba, E., Premoli Silva, I., Baas, M., Wagner, T., Sinnighe Damsté, J.S. (2004) – Carbon-isotope stratigraphy recorded by the Cenomanian–Turonian Oceanic Anoxic Event: correlation and implications based on three key localities. *Journal of the Geological Society, London*, 161, 711-719.

Turgeon, S. and Brumsack, H.-J. (2006) – Anoxic vs dysoxic events reflected in sediment geochemistry during the Cenomanian–Turonian Boundary Event (Cretaceous) in the Umbria–Marche Basin of central Italy. *Chemical Geology*, 234, 321-339.

Turgeon, S.C. and Creaser, R.A. (2008) – Cretaceous oceanic anoxic event 2 triggered by a massive magmatic episode. *Nature*, 454, 323-329.

Winterer, E.L. and Bosellini, A. (1981) – Subsidence and sedimentation on a Jurassic passive continental margin (Southern Alps, Italy). AAPG Bulletin, 65, 394-421.

Chapter 3

Materials and methods

During the PhD research project many analyses have been run. Calcimetry analyses, thin sections and peels were performed at the Earth Science Dept. Labs of the University of Milan. Oxygen and carbon stable isotopes on carbonates and RockEval were measured in the Stable Isotope Laboratory at the Department of Earth Sciences, University of Oxford (UK). Organic carbon stable isotopes were measured at the School of Archeology, University of Oxford (UK). X-ray fluorescence analyses were run at the Institut für Chemie und Biologie des Meeres (ICBM), University of Oldenburg. Ciclostratigraphy has been performed in collaboration with the Earth Science Dept. of the Columbia University.

Comments on the methods are presented in each chapter and are described in detail in Appendix A.

In particular the main methods that have been applied are:

- Field logging and sampling
- Thin sections
- Acetate unstained rock peels
- Calcimetry
- Oxygen and carbon stable isotopes (carbonates)
- Organic carbon stable isotopes
- Rock-Eval/TOC Pyrolysis
- X-ray Fluorescence (XRF)
- Cyclostratigraphy: orbital tuning by means of a probabilistic approach

Chapter 4

Sedimentation in the Thethyan pelagic realm during the Cenomanian: monotonous settling or active redistribution?

Abstract

Sea bottom processes of the pelagic realm are still not completely understood and represent an intriguing subject. This paper focuses on the relationships between "normal" settling processes, redistribution of sediments and oceanographic parameters in a pelagic setting, during the Cenomanian. Five key Thethyian localities in the Cenomanian Umbria-Marche and Belluno Basins have been studied in order to understand the interplay among sea bottom processes that acted on the sea floor. The dataset consists of the mm-scale sedimentological description of the sections complemented by microfacies analysis on selected samples. Different sedimentological indications, such as presence of intraclasts, lined forams, pervasive plane-parallel lamination, suggest a continuos reworking under action of bottom-currents with varying intensity and direction. All the identified facies are here illustrated in detail and organized in a comprehensive schematic facies framework, the "facies matrix", that leads to recognize two depositional facies suites: the "settling dominated" and the "traction current dominated", under different oxygenation conditions. Our results suggest that settling of biogenic and inorganic particles represents the main source of pelagic sediments, but not the unique depositional process: under the action of sea-bottom currents of different intensity, sediments are continuously redistributed on the sea floor. All the collected evidences contribute to the proposal of a comprehensive depositional model for these reworked and redistributed fine-grained sediments, that represent true

This chapter is submitted to *Palaeogeography, Palaeoclimatology, Palaeoecology* as: Gambacorta, G., Bersezio, R., Erba, E., Sedimentation in the Thethyan pelagic realm during the Cenomanian: monotonous settling or active redistribution?, PALAEO 7618.

calcareous pelagic contourites. The model suggests that the identified traction-related facies can be used as a proxy for bottom current intensity and, indirectly, as an indicator of changing ventilation regimes at the sea floor through time.

Key-words: bottom currents, calcareous pelagic contourites, Cenomanian, OAE, pelagic environment, Scaglia

4.1 Introduction

Carbonate pelagic sediments are interpreted as deposited mainly by monotonous and continuous settling of biogenic particles through time. The transfer of these fine-grained biota and minor fine-grained clastics from surface water masses to the seafloor originates the calcareous oozes, that can be eventually replaced by siliceous oozes under specific palaeoceanographic conditions. Likewise, chalk or pelagic limestone sequences are normally regarded as the result of a monotonous homogenized succession of biogenic particles settled throughout the water column and differently lithified during burial diagenesis. The main controls on pelagic sedimentation that are usually taken into account are: 1) production rates and type of biogenic particles (including organic matter) in surface waters; 2) dissolution rates of biogenic particles in the water column, at the sea floor and during burial; 3) rates of dilution by fine grained mineral particles (either of terrigenous or volcanic origin). The resulting lithofacies are differently affected by the diagenetic processes that involve the biogenic component (calcareous and siliceous), the organic matter and the extrabasinal silicatic component; the same processes may introduce newly formed minerals (mostly clay minerals). Hence, in any sedimentological study oriented to unravel the depositional processes of the pelagic realm, the primary and diagenetic features of the rocks must be preliminarily separated.

This paper is focused on the relevance of sea-floor currents redistribution that could be equally important to fully describe the depositional processes of pelagic facies. Specifically, we provide the facies evidence of redistribution of ooze particles and soft mud-chips by sea-bottom currents.

Starting from the pioneering paper of Stow and Lowell (1979), many Authors have studied sea-bottom currents and their effects both in siliciclastic and carbonate environments, ranging from tropical to glacial climatic conditions (e.g. Faugéres et al., 1993, 1999, 2008; Rebesco and Stow, 2001, Stow and Faugéres, 1993; Stow et al., 1998, 2002a; Viana and Rebesco, 2007; Wynn and Stow, 2000; Gao et al., 1998; Mienert, 1998; Stoker et al., 1998; Maldonado and Nelson, 1999; Nowell and Hollister, 1985; McCave et al., 1988; Shanmungam et al., 1993; Shanmungam, 2003, 2006, 2008). Many papers describe calcareous muddy and silty contourites as well as siliceous bioclastic contourites (e.g. Stow et

al., 1998; Stow and Faugéres, 2008, Hüneke and Stow, 2008), but a lot of work has still to be done in order to fully understand the sea-bottom processes that acted on the deep-sea deposition of ancient oozes in "purely pelagic" environments. As defined by Stow et al. (2002b) "contourites are the sediments deposited by or significantly affected by the action of bottom currents". Being this process semi-permanent, it also affects the hemipelagic and pelagic settling (Stow and Faugéres, 2008) and might have a huge impact on the continuous redistribution of pelagic sediments on the sea floor.

Pelagic calcareous and siliceous oozes are mainly formed by biogenic particles with a minor shale input from either volcaniclastic activity (e.g. Klein, 1975), river discharge (e.g. Hemming et al. 1998), eolian dust (e.g. Pratt & King, 1986) or even hydrothermal activity (e.g. Jarvis et al, 2001). The biogenic component is represented by nannofossil-micrite and sand-silt sized planktonic foraminifera with the bigger and more ornamented ones typically linked to less stressed environments (k-selected species) with oligotrophic conditions, normal salinity, warm to mild water temperature and oxygenated conditions (Premoli Silva et al., 1999). Together with planktonic foraminifera, and usually sparse benthic foraminifera, calcareous nannoplankton represent the vast majority of the carbonate fraction providing the clay-size micrite (micarb) of pelagic oozes. The siliceous organisms are mainly represented by radiolaria, diatoms and silicoflagellates. Differently degraded and/or modified organic matter (marine vs. allochtonous continental-derived particles) can also be preserved, both as a particulate minor component of clays, marls and limestone burrows, and as a lithogenetic one (e.g. black shales or black cherts).

The hydrodynamic behavior of most of these components has been tested by a few flume experiments (Southard et al., 1971; Young and Southard, 1978; Black et al., 2003). In any experiment, the boundary conditions and the scale factors play an important role in limiting the possible considerations, even more when the process to be simulated occurs at an oceanic scale. However, Black et al. (2003) have clearly demonstrated that a larger winnow stress is necessary to erode large benthic and planktonic foraminifera tests than to remove fine-grained small foraminifera and coccoliths. Seemingly, it is plausible that also radiolaria, with their vitreous, vacuolar and very light structures, are easily removable and transportable. Cooke et al. (2004), describing current winnowing of early-late Miocene sediments on Challenger Plateau, showed preferential removal of the 3-13µ micrite fraction from the local pelagic succession, concluding that "winnowing of pelagic carbonate ooze is more likely a reflection of the hydrodynamic properties of nannofossil placoliths and the ease with which they are mobilized by fluctuating water velocity" so that "during extreme winnowing events it is the fine silt to very coarse clay material (3-13 µm) that is preferentially removed, suggesting the 10 µm cohesive silt boundary reported for siliciclastic sediments does not apply to calcitic skeletal grains". So, the role of

even delicate bottom currents in reworking the unconsolidated or semi-consolidated pelagic sediments might be reassessed, primarily from the perspective of field observations and facies analysis.

Widespread pelagic sedimentation characterized the southern Tethyan margin during the Cretaceous. Therefore, some well-known Tethyan sections from the Italian basins provide good case-histories to study the deep-sea processes, during time intervals of paleoceanographic stability as well as relative to paleoenvironmental stress. Specifically, the late Albian-Cenomanian interval was a time of intermittent major carbon cycle perturbations. Three positive excursions in the stable carbon isotope content are recognized at global scale: the so called Pialli or Breistoffer Event corresponding to the Oceanic Anoxic Event 1d (Wilson and Norris, 2001; Leckie et al., 2002), the Middle Cenomanian Event (MCE) (Coccioni and Galeotti, 2001, 2003) and the Oceanic Anoxic Event 2 (see Jenkyns 2010 for a synthesis). The most spectacular sedimentary expression of OAE2 is the Bonarelli Level (Bonarelli, 1891), a bituminous radiolaria-rich interval that testifies to widespread anoxic conditions in the oceans during the latest Cenomanian (Schlanger and Jenkyns, 1976; Arthur et al., 1990; Bralower et al., 1993; Jenkyns, 2010).

The goals of this paper are to: 1) describe the fine-grained pelagic facies association of the Cenomanian “Scaglia” of two Tethyan basins, focusing on the evidence of redistribution of sediments; 2) interpret the facies in terms of traction stress intensity; 3) propose a comprehensive facies model for the combination of passive settling and reworking/redistribution processes of oozes by sea-bottom currents, in the peculiar oceanographic setting of these Tethyan basins during the Cenomanian.

4.2 Case histories and methods

Five key-sections from two Tethyan Cretaceous basins in Italy represent the study sites (Fig. 4.1): Furlo (Beaudoin et al 1996; Turgeon & Brumsack, 2006; Mitchell et al, 2008; Turgeon & Craser, 2008; Lanci et al, 2010), Contessa (Monechi & Parisi, 1989; Coccioni & Galeotti, 2003), Monte Petrano (Giorgioni et al., 2012) and Le Brecce (Tiraboschi, 2009) sections in the Umbria-Marche Basin, and the Cismon section in the Belluno Basin (Bosellini et al., 1978; Channell et al., 1979a; Bellanca et al., 1996). The latest Albian to earliest Turonian time interval has been studied at these sites. The schematic stratigraphy of the five studied sections is presented in Fig. 4.1. The partial overlap between the sections permits tight comparisons in the upper part of the Cenomanian succession.

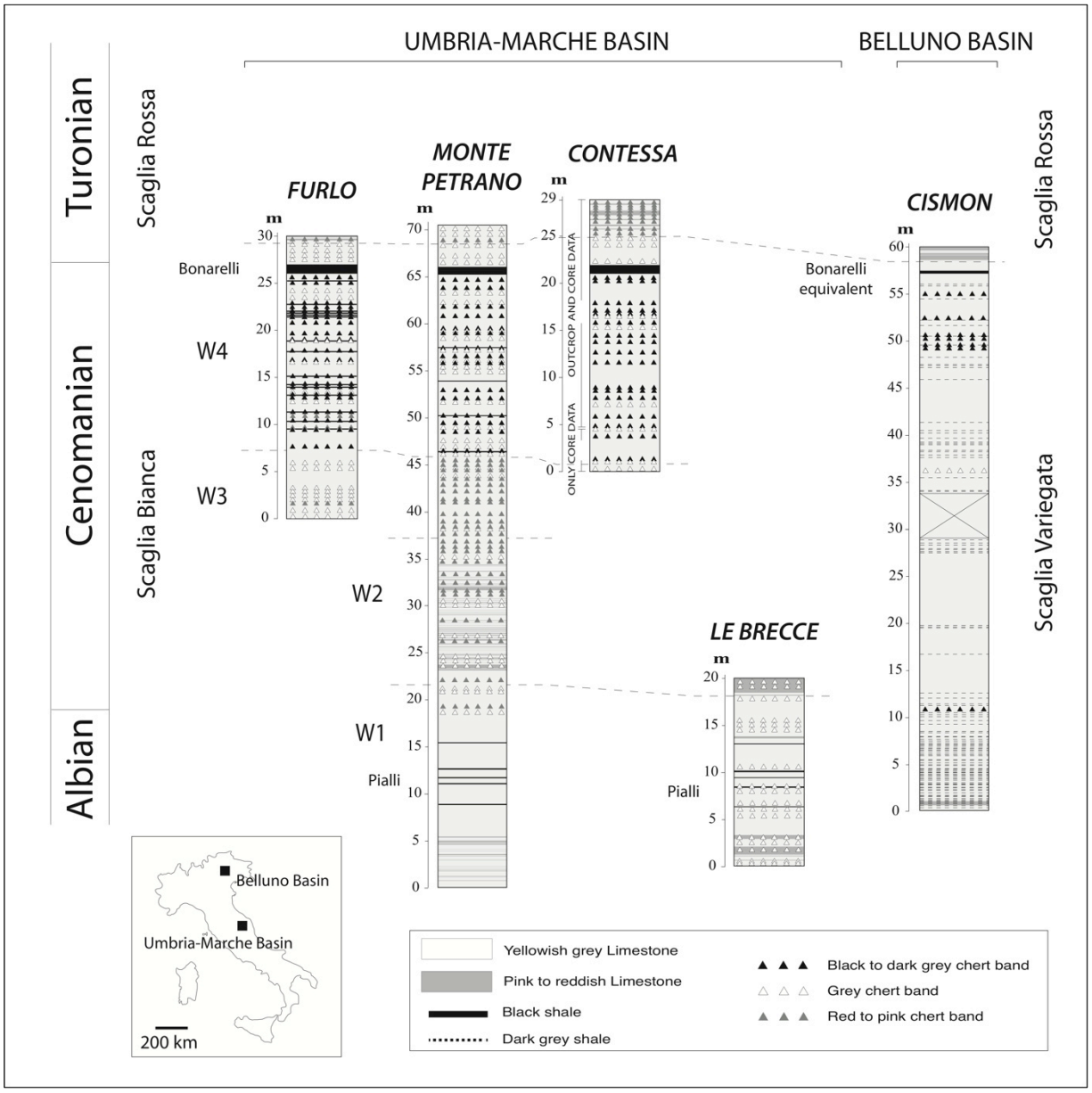

Figure 4.1: Stratigraphy of the studied sections in the framework of the Umbria-Marche and Belluno Basins.

Four sections belong to the Umbria – Marche Basin (Fig. 4.1):

1) The Furlo measured sequence is 30m thick and outcrops in a dismissed quarry located 25km south-east of Urbino. 2) The Contessa section in the Vispi Quarry is about 2 km away from Gubbio (Monechi & Parisi, 1989). The outcrop is close to the coring site of the Gubbio 2 borehole (Tsikos et al, 2004; Turgeon & Brumsack, 2006). The interval of interest is 29m thick. To integrate the field data, we studied the Gubbio 2 core that recovered a 40.05m long section (Fig. 4.1). The Gubbio 2 core was re-described in high resolution and correlated with outcrop data. 3) The Le Brecce section, close to the village of Piobbico is 20m thick and covers only the lower part of the stratigraphic interval of interest.

4) The Monte Petrano section, not far from the top of the Petrano Mountain and the Moria village, is 90m thick. This is a new section in the frame of the Umbria-Marche Basin; previously only the lowermost 20 meters of this section were studied by Giorgioni et al. (2012).

One section was studied in the Belluno Basin (Fig. 4.1): the 60m thick Cismon section is located in the north-eastern part of Italy, not far from the village of Lamon (Channell et al., 1979b; Bellanca et al., 1996).

We decided to focus our attention on the pelagic deposits of the upper Albian-lower Turonian stratigraphic interval, covering a time span of about 12 My (104-92 My).

Both the Tethyan Umbria-Marche and Belluno Basins were located in the northern tropical climatic belt during the studied time interval (Dercourt et al., 2000; Skelton et al., 2003). The Umbria-Marche Basin is at present exposed in the Central Apennines fold and thrust belt. It represents a worldwide known basin for its unique preservation of an almost continuous stratigraphic record starting from the Calcare Massiccio Formation, Hettangian in age, up to the upper Oligocene Scaglia Cinerea Formation. The Umbria-Marche sequence was entirely deposited on the continental crust of the Adria microplate, that probably represented a portion of the major African plate (Channell et al., 1979a). The physiography of the basin is still not fully known, even if, considering the regional structural setting, a complex palaeobathymetry can be assumed (Alvarez, 1990). At the time of deposition of the studied sequence the basin was dominated by pelagic carbonate sedimentation, at a water depth of about 1500-2000m (Arthur and Premoli Silva, 1982; Kuhnt, 1990). In this area we studied the Scaglia Bianca Formation, that consists of an alternation of calcareous beds, marlstones/shales, black shales, and chert beds and nodules ranging from black, grey up to red in color (Parisi, 1989; Coccioni & Galeotti, 2003). The dominant litothype is the fine-grained limestone, resulting from lithification of nannofossil-planktonic foraminiferal oozes (Arthur and Premoli Silva, 1982).

The Belluno Basin, at present exposed into the Southern Alps fold and thrust belt, was located in the southern margin of the Tethys. During the Cretaceous inversion of this passive margin, it represented a subsiding domain inherited from the Jurassic palaeogeography at the eastern side of the Trento plateau (Bernoulli and Jenkyns, 1974; Winterer and Bosellini, 1981; Doglioni & Bosellini, 1987; Sarti et al., 1992; Bellanca et al, 1996). The basin was dominated by the deposition of calcareous oozes, starting from the latest Jurassic (Biancone Formation) up to the Eocene (Scaglia Cinerea). The Cismon section was located close to the hinge between the Trento Plateau and the Belluno Basin (Claps et al, 1991; Claps & Masetti, 1994; Erba and Larson, 1998). The studied time interval is represented by the upper part of the Scaglia Variegata Formation (Channell et al., 1979a). It consists of alternating yellowish to grey limestones, chert bands and shales/black shales (Channell et al., 1979b; Claps et al., 1991;

Bellanca et al., 1996) that are interpreted to reflect Milankovitch cyclicity (Claps et al., 1991; Claps & Masetti, 1994; Bellanca et al, 1996).

It is worth remarking that both the studied basins are plausibly characterized by an irregular morphology of the sea-bottom, owing to their configuration in structural highs and lows inherited from the Jurassic rifting stages. In both cases sharp intrabasinal bathymetric changes occur, as well as both areas were relatively close to elevated plateaus and/or to emergent lands. These are relevant features to be accounted for the sedimentological interpretation of facies that will be discussed later on.

The facies association of the Scaglia Bianca and Scaglia Variegata has been studied bed by bed, based on texture, composition and structures at a mm-scale, thanks to detailed field lithological description, complemented by microfacies analysis.

Field-work has been extremely time consuming. All the outcrops have been preliminarily subdivided into intervals of 1m each. Within them every single layer has been numbered and described by 10-20x hand-lens. Sedimentological logging was oriented to describe every recognizable litho-textural unit, characterized by observable lithological changes (either gradual or abrupt) that we shall define from here and onwards "layer". As a matter of fact, in this kind of successions, "layering" is mostly a diagenetic feature, due to both enhancing of compositional/textural changes, and to segregation of clay, carbonate and silica minerals along newly formed interfaces. However, many of the described sedimentary intervals show an array of macro- and microscopic features that permit to recognize the individual events of deposition (such as erosion contacts, grain sorting, packing and orientation of particles, traction and traction plus fall-out structures and so on). For all of these cases we shall adopt the term of "beds". It is apparent that "layering" is the most easily observed feature during field-work, and that bedding in some cases will be identified only after additional microfacies analysis. Hundreds of oriented samples have been collected for different analyses. Microfacies analysis has been performed in thin section and on acetate unstained rock peels (Wilson and Palmer, 1989). This technique is very fast in providing a large number of thin negatives covering wide surfaces of the samples and worth for expeditious investigation under the microscope.

Considering how difficult it is working with this kind of fine grained sediments and how delicate it is to recognize the eventual occurrence of ancient contourites, we have tried to account for the approach and the criteria recommended by Lovell and Stow (1981) and Stow et al. (1998) in order to properly characterize and interpret the observed structures. This approach required to reconsider several times some ambiguous field observations and/or interpretations on many layer- and bed-types. To do that, the measured sections have been subjected to at least a second run of field investigation after microfacies analysis, to obtain a satisfactory match between the two scales of observations.

Microfacies analyses permitted also to recognize the primary sedimentary structures that were not affected by incipient dissolution or diagenetic effects. A general facies scheme, that is valid for the two basins, could be established. In the next chapter, the facies association will be presented separating the carbonate, siliceous and clayey facies.

4.3 Facies association of the Scaglia Bianca and Scaglia Variegata in the Umbria-Marche and Belluno Basins

The facies association we obtained is presented in Fig. 4.2. In this chapter we describe separately the limestone facies, the shaly facies and the siliceous facies, that form the overall association of the "Scaglia" in the two studied basins. Concerning the siliceous facies, because of the diagenetic overprint, we separated the "depositional facies", whose primary features were only mildly modified during diagenesis and can be recognized both in the field and under the microscope, from the "diagenetic facies". As an exception, we included into the diagenetic facies group some beds (e.g. facies G4a, "Bedded black cherts) that still show some relic primary features under the microscope, so that their depositional significance can be assessed at least by micro-analysis. The scheme proposed in Fig. 4.2 presents also our final interpretation of the facies association, as a function of the interplay between sea-floor traction energy, sea-bottom oxygenation and redeposition processes. This will be the subject of the discussion section 4.4.

4.3.1 Fine-grained limestone-dominated facies

Eight fine-grained limestone-dominated facies have been recognized (Fig. 4.2):

- homogeneous marly limestone (A1)
- homogeneous limestones (A2a and A2b)
- marly-limestone beds (B2)
- limestones with pervasive plane-parallel lamination (C2)
- limestones with oblique and wavy lamination (D2)
- foraminiferal-intraclastic lags (E2)
- alternating micritic and organic-rich laminasets (A4)
- graded-laminated limestones (Ra and Rb).

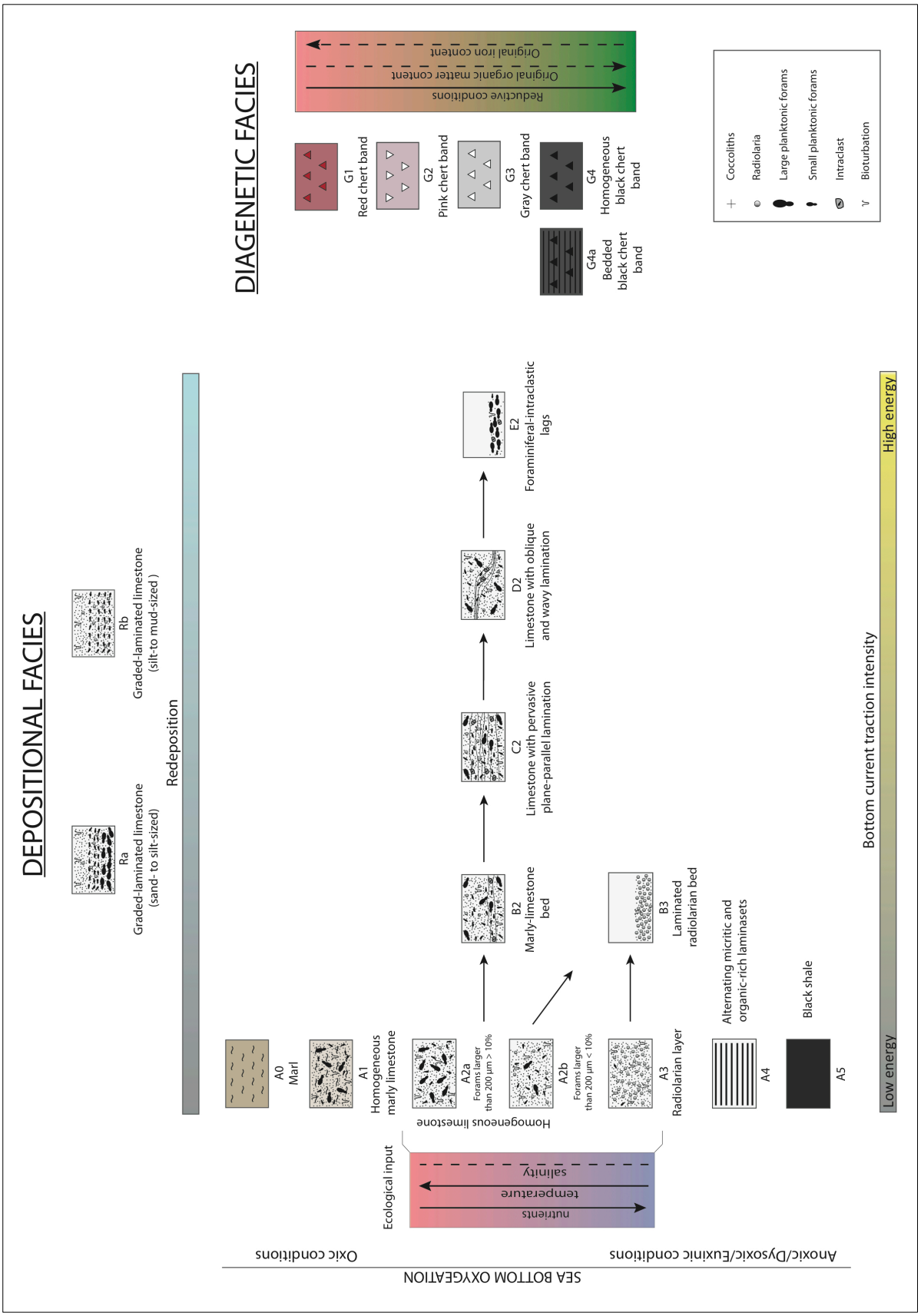

Figure 4.2: Schematic facies framework. See text for explanations.

4.3.1.1 Homogeneous marly limestone layers (A1)

The homogeneous marly limestones are very thin to thin layers, with flat or slightly undulating transitional boundaries. They are composed by at least 40% clay, mixed with micrite and planktonic biota (forams and rare radiolaria). Grey to dark grey mottles are diffuse in these layers, that differ from the homogeneous limestone facies (A2; Fig. 4.2) by their composition, and from the marly limestone beds facies (B2; Fig. 4.2) by the gradual boundaries and the homogeneous structure, that yields no traction evidence. These layers are transitionally associated to the A2 facies layers, in some cases passing to the marlstone layers (facies A0; Fig. 4.2), rarely to the black shale facies (A5; Fig. 4.2). Settling of biogenic calcareous particles (micarb and foraminifera) and rare siliceous organisms (radiolaria) mixed with clay and very fine silty particles is the trivial depositional process. A "hemipelagic" contribution to these layers cannot be excluded, even if the input of very fine-grained clastics was mostly eolian anyway. The A0-A1-A2 transitions that are recurrently observed through all the sections should represent dilution cycles, during which carbonate productivity and extrabasinal input recurrently competed.

4.3.1.2 Homogeneous limestones (A2)

The homogeneous limestones are thin to very thin layers of light coloured (white, grey, pink) calcilutite (Fig. 4.3 a-c). This is the most abundant facies through all the five sections. It represents the "typical" pelagic carbonate facies to which all the others must be compared, in order to appreciate the differences.

These homogeneous limestone layers are mostly composed of micrite and a minor amount of clay, resulting in mudstones/wackestones (Fig. 4.3f). The layers' boundaries are flat to mildly undulating surfaces, either gradual or sharp depending on the overlaying facies type. The color can vary from whitish to reddish, if iron rich (Hu et al., 2009), or grey, in the case of pyrite or diffused organic matter.

In the studied sections the homogeneous limestones are composed by "large" foraminifera (larger than 200μ, e.g. Rotalipora spp., Praeglobotruncana spp., Whiteinella spp., etc.), "small" foraminifera (Heteroelix spp., Guembelitria spp., Muricohedbergella spp., etc.) and a few radiolarian, that are dispersed into a vast majority of micarb with a very subordinate variable amount of clay (the abundance of the biogenic particles is expressed as an area percentage in thin sections and peels). We separated an A2a type, that shows more than 10% of "large" foraminifera from an A2b type, where the latter are less than 10% and generally are as abundant as about 5% of the total area in thin section. Under the microscope no preferential orientation of the largest particles can be observed (Fig. 4.3f). Changes in composition are determined by the variable amount of clays (that determines the transition to the homogeneous marly limestone facies) or silica (homogeneous cherty limestone, Fig. 4.3d).

Pyrite is diffused in those homogeneous limestone layers that are in contact with black shales or black cherts bands or nodules (Fig. 4.3e). Diffuse pervasive mottling and discrete bioturbation is frequent due to the reworking of the sediment by faunal activities (Fig. 4.3c).

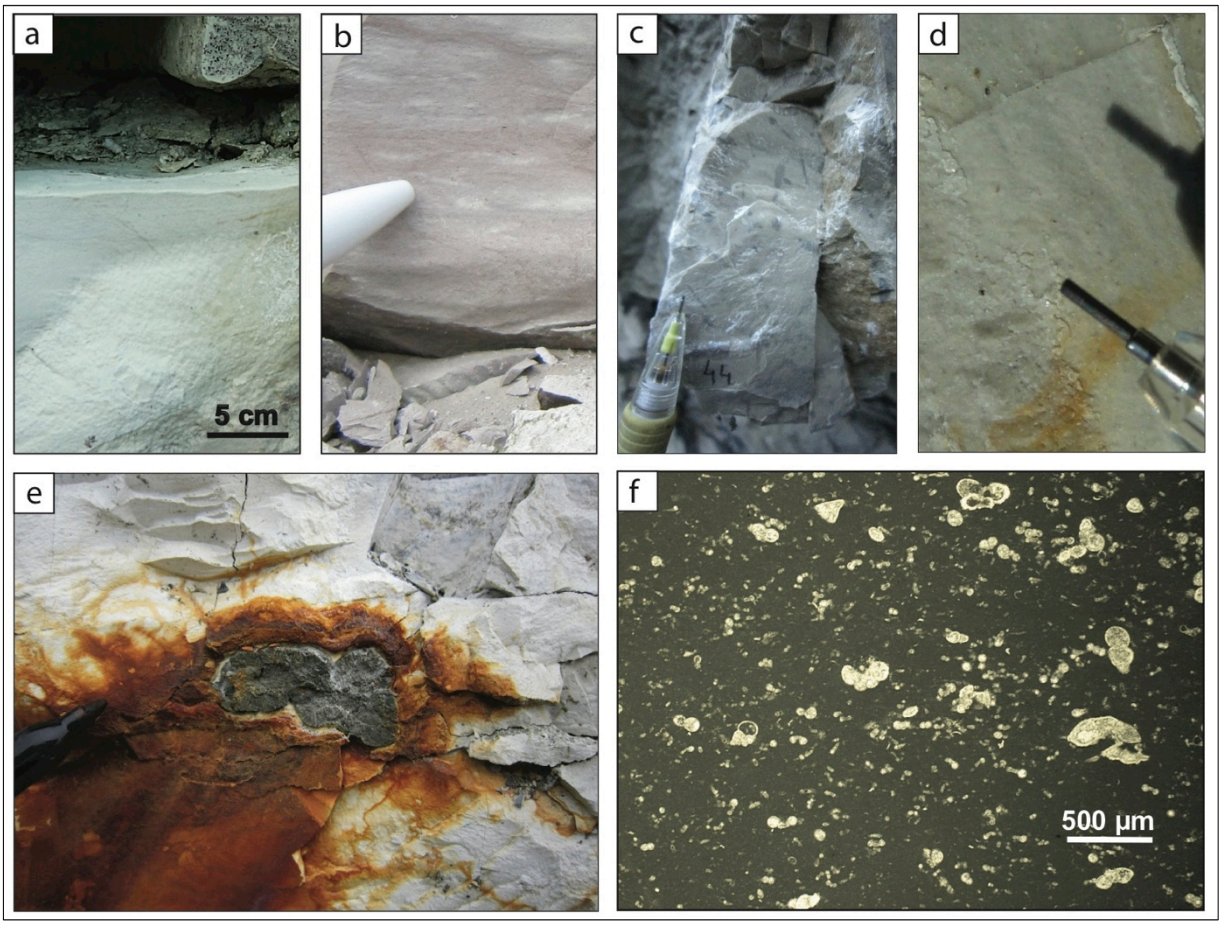

Figure 4.3: Homogeneous limestones facies (A2). a) Yellowish/grey homogeneous limestone (Contessa section). b) Pinkish homogeneous limestone pervasively mottled (Le Brecce section). c) White homogeneous limestone with discrete bioturbation (Cismon section). d) Homogeneous, partly silicified limestonewith 'glassy' brightness (Furlo section). e) Pyrite nodules within a yellowish/grey limestone; marker tip for scale (Contessa section). f) A2b microfacies type in thin section (parallel nicols): rare large foraminifera, common small foraminifera and some radiolarians are sparse within micarb with no preferential orientation (Monte Petrano section).

Trace fossils (Chondrites, Planolites, Thalassinoides and Zoophycos) are most easily observed below the black shale layers thanks to the color contrast generated by darker, probably organic-rich clay introduced into the burrows by dwelling organisms (Fig. 4.3b and Fig. 4.4). Considering the low average sedimentation rate of 0.6-1.4 cm/ka estimated for the Cismon Section (Claps et al., 1991; Claps and Masetti, 1994) and of about 1 cm/ka for the sections in the Umbria-Marche Basin (Lanci et al., 2010) bioturbation should play a major role in the preservation/destruction of structures in pelagic sediments.

The homogeneous limestones facies can be interpreted as the product of planktonic settling throughout the water column. In absence of effective shear stress at the sea-floor, the compositional modulation by productivity cycles, variable input of clay and oxygenation determines the conditions for the origin of the diagenetical (-enhanced) layering. The homogeneous structure is either a syn-genetic feature (where discrete bioturbation traces are observed) or a post-genetic one (where diffuse mottling dominates).

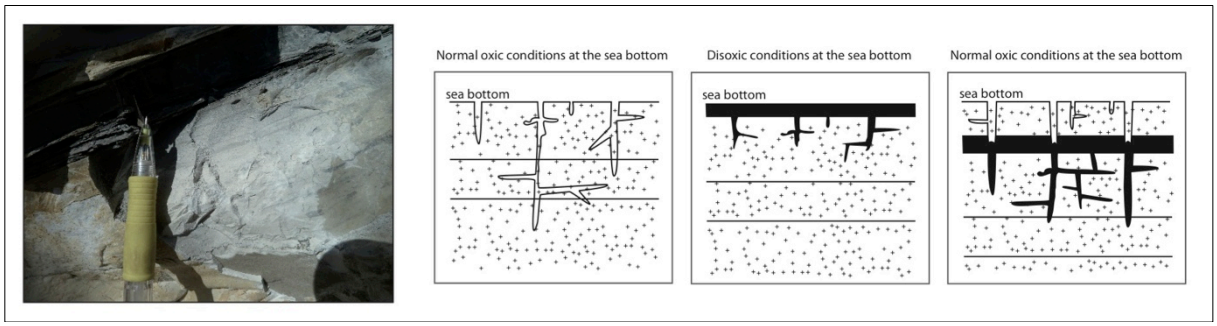

Figure 4.4: Schematic representation of the possible origin of best developed bioturbations. The bioturbation is hardly observable in strata deposited in oxygenated conditions, due to the lack of color contrast; only microfacies analysis will reveal bioturbation. After the deposition of organic-rich shales in at least dysoxic conditions, dwelling organisms will transport the dark sediments in their borrows that will result clearly observable thanks to the color contrast.

4.3.1.3 Marly-limestone beds (B2)

Very thin to thin marly-limestone beds, usually grey and always slightly darker in color than the embedding layers, are recurrently observed. The difference in color pattern is related to a slightly higher concentration of clay within the beds (Fig. 4.5a,b).

Under the microscope an erosive base and a sharp flat to mildly undulating transition at the top are observed. These beds are characterized by homogeneous structure or faint laminae loosely defined by preferential dimensional orientation of foraminifera. These beds share the plankton composition with the bounding calcareous layers, from which they differ by the higher clay component and internal structure (Fig. 4.5c). They are preferentially embedded within layers of the homogeneous limestone facies (A2).

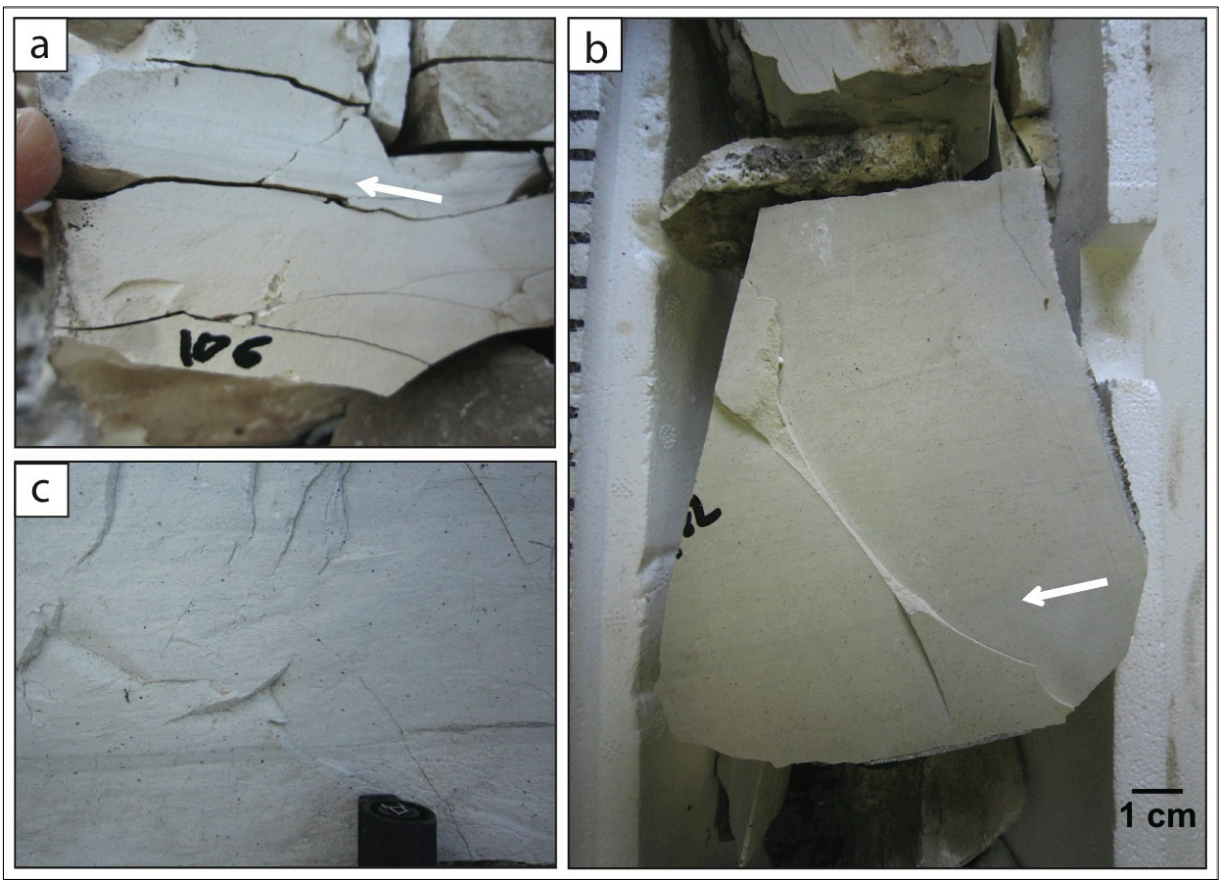

Figure 4.5: a) Single marly-limestone bed (B2) on outcrop, finger for scale (Furlo section). b) A single marly-limestone bed on core (Contessa core section). The bed, at about 4cm from the base of the core, is about 0.5cm thick. Diffused mottling occurs in the upper part of the core. c) Another single-marly limestone bed with a sharp base and top, marker for scale (Monte Petrano section)

The marly-limestone beds can be interpreted as generated by current winnowing and redistribution, close to the critical shear stress threshold (Cooke et al, 2004). The relevant features for this interpretation are the sharp erosive base, the occurrence of laminae and the undulating top. Under increasing shear stress, the most mobile biogenic particles, together with some of the micritic matrix, could be removed (even in the form of soft mud chips), so a basal erosion surface could originate. The clay content within these beds can be considered as a "residue" of the traction process, because of the poor mobility of cohesive clay particles compared to the micarb particles. The current vanishing could also be responsible for the undulating depositional top of the beds themselves. If this interperetation is correct, these beds could reveal episodes of sea-floor traction by slightly intensified bottom currents. Nowadays the intensification of bottom currents has been observed at a seasonal scale (such as deep-water oceanic tides, benthic storms, etc.; Shanmugam, 2006a; 2008; 2013, for a review). The systematic intercalation of these marly-limestone beds within the homogeneous limestone layers is here considered a witness of such a recurrent intensification of bottom currents; their occurrence

should be related to crossing the shear stress selective thresholds of particles' mobility (Cooke et al., 2004).

4.3.1.4 Limestones with pervasive plane-parallel lamination (C2)

In some limestone layers a pervasive plane-parallel lamination has been observed (Fig. 4.6a, b, c). Every lamina has a sharp contact both at the base and at the top. The thickness of the laminae varies between about 1 and 15 mm and their separation varies between about 2 and 10mm. The laminae are internally homogeneous and lack almost completely of large foraminifera, testifying the possible tractive redeposition of the micritic fraction.

Inside the laminae it is common to find whitish intraclasts that share composition and texture with the surrounding sediment (Fig. 4.6d). The presence of intraclasts in pelagic sediments was described in Bersezio (1993), Bersezio et al. (2002), Hüneke and Stow (2008) among many others. Under the microscope, in our case-studies, the intraclasts frequently show sub-angular shape and in some cases they can include broken bioclasts, truncated at the clasts' borders (Fig. 4.6e). In most layers intraclasts tend to concentrate at the top of the lamina, suggesting that they probably floated during the flow.

The presence of intraclasts testifies the presence not only of a loose ooze but also of semi-consolidated sediments close to the interface, so that both could be eroded by the most intense bottom current activity. Fig. 4.6f shows some floating intraclasts within a lamina together with the eroded underlying layer from which some slices are being removed. In summary, the sharp and erosional boundaries, the presence of intraclasts and the winnowing of the most easily floating particles point to erosion, reworking and redistribution by intense bottom currents.

4.3.1.5 Limestones with oblique and wavy lamination (D2)

A few limestone beds with oblique and wavy lamination, ranging from about 2cm up to 20 cm in thickness, occur within the succession (Fig. 4.7a, b). They present a sharp wavy top and/or a sharp wavy bottom. The laminasets are generally curve, sometimes sigmoidal, oblique and/or wavy. They can occur either as isolated, divergent sets (Fig. 4.7b, d), or as superimposed cosets, similar to current ripple laminasets (Fig. 4.7 a, c). Recurrently the sets and cosets of laminae cross-cut to one another and the sigmoidal laminasets are draped by dark-grey, marly lenses, that look very similar to mud offshoots (Shanmugam et al., 1993). (Fig. 4.7c). These features can be observed also under the microscope where their primary origin is clearly documented. Some clay-enriched laminae are formed by silt- to sand-sized intraclasts, foraminifera, radiolaria within a micritic/clayey matrix. The D2 facies beds are almost always associated to the C2 facies beds (limestones with pervasive plane-parallel lamination).

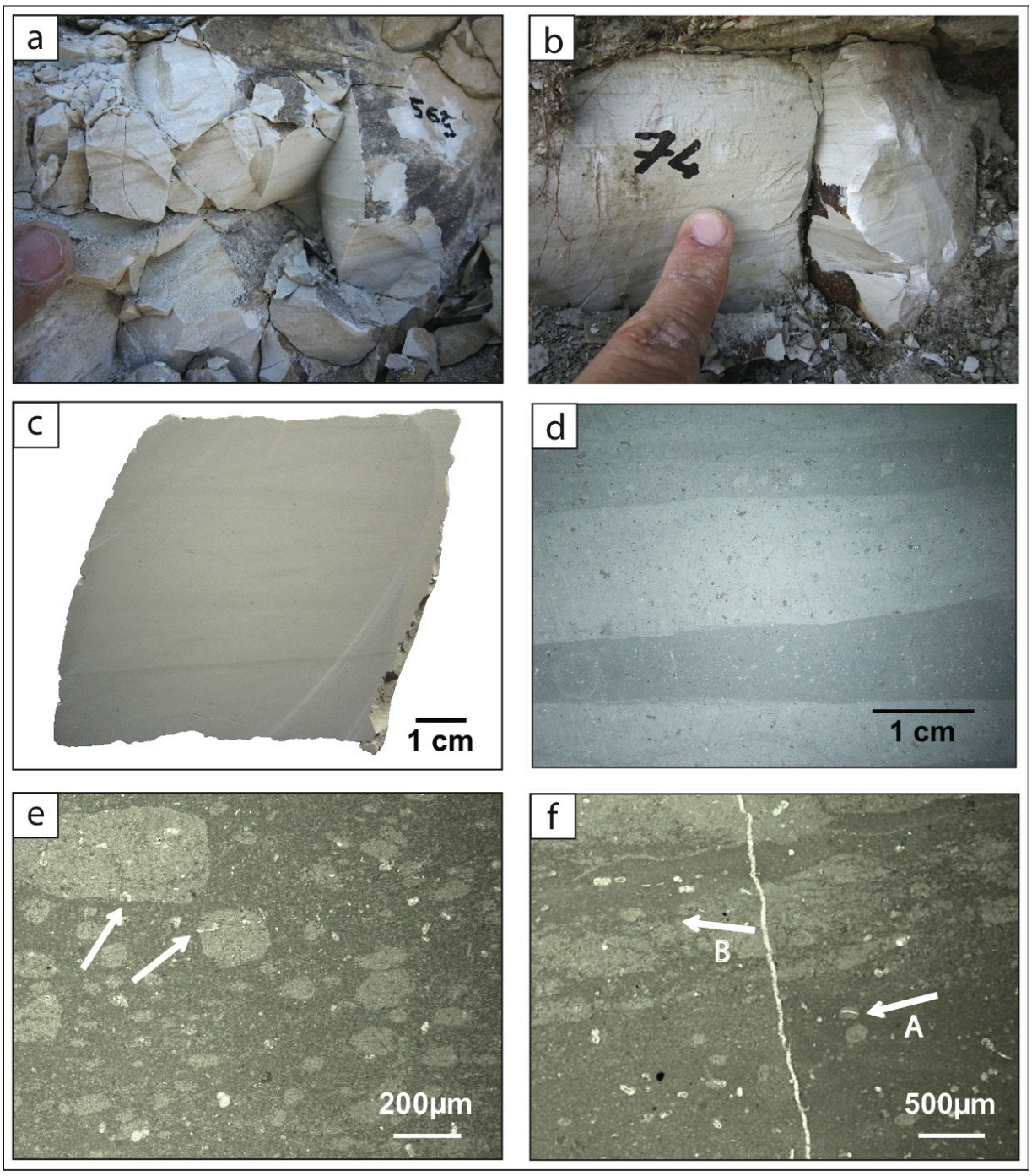

Figure 4.6: Limestone with pervasive plane parallel lamination (C2): a) and b) Monte Petrano section, finger for scale; b) c) polished surface of sample (Furlo section). d) Peel of a pervasive plane parallel laminated sample (Furlo section). Both laminae contain micritic intraclasts. e), f), thin sections, parallel nicols:sub-angular to rounded intraclasts within laminae of pervasive plane-parallel laminated limestone facies. Note the broken bioclasts at the intraclasts' margins (arrows) documenting their erosive origin (Furlo section); In the upper part of sample in f) intraclasts are detached from a lamina (arrow B) that suffered disruption and removal of newly formed intraclasts.

The geometry of beds, the sharp boundaries, the shape and the relationships between the laminasets point to deposition by very low-relief migrating bedforms under sea-floor current traction. The oblique

laminated beds are very similar to migrating current ripples, with mud offshoots documenting fluctuations of current velocity.

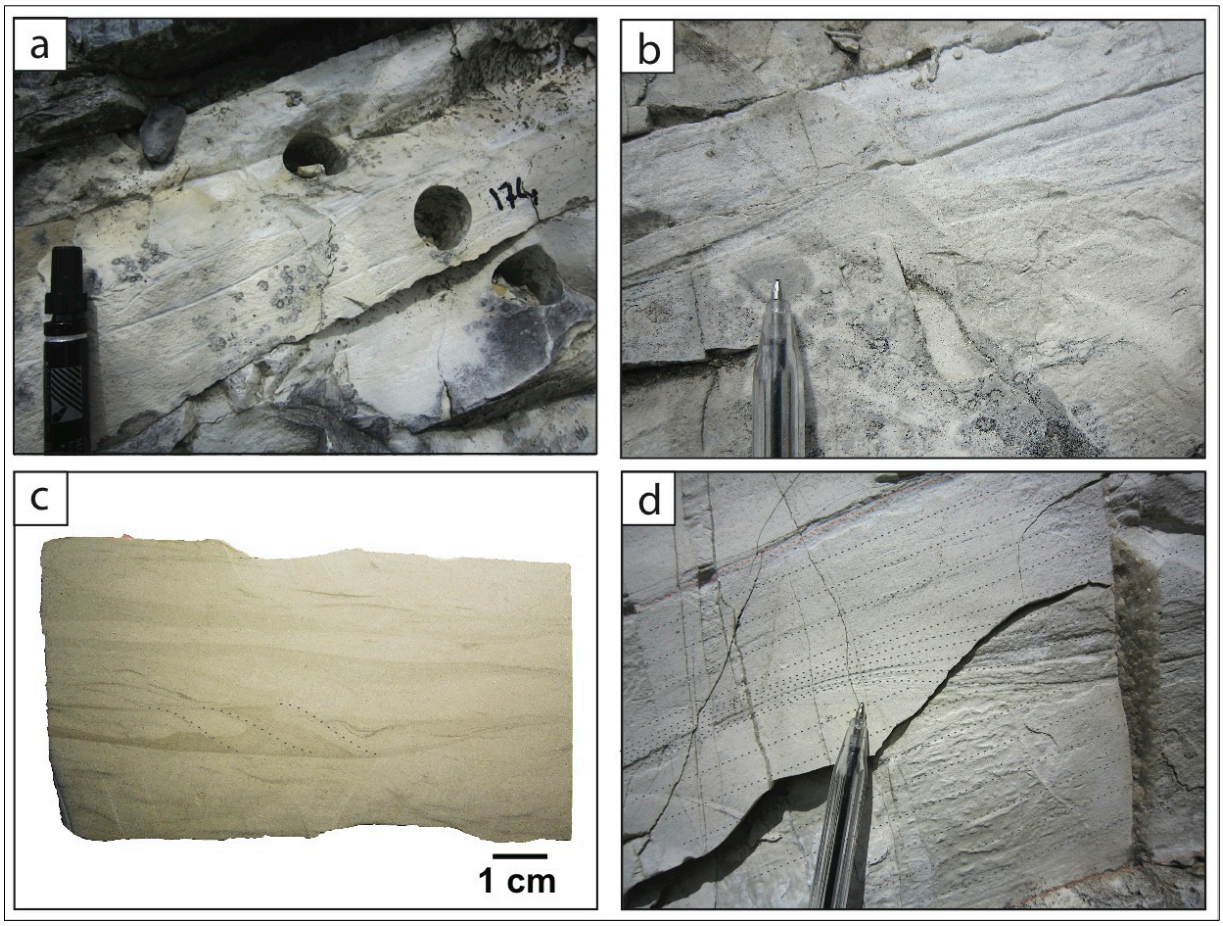

Figure 4.7: Limestones with oblique and wavy lamination (D2), a) Furlo section, marker for scale; b) Furlo section, pen for scale. The wavy and oblique laminasest areclearly visible. c) Oblique and wavy lamination on a polished surface (Le Brecce section). In the lower part, the laminasets are clearly visible (dotted lines to highlight some sets). Just above the dotted lines, dark coloured, clayey, very small lenses look very similar to the suspension mud offshoots within traction sand-sized oblique and sigmoidal laminae (Shanmugam et al., 1993). d) Wavy, divergent lamination (Furlosection). The D2 facies laminaset is pinched in between two C2 beds (limestones with pervasive plane-parallel lamination) that are bounded by erosional surfaces. Some very fine intraclasts occur at the base of the D2 bed.

4.3.1.6 Foraminiferal-intraclastic lags (E2)

In some layers we have observed concentrations and/or alignments of large foraminifera and/or, more rarely, intraclasts (Fig. 4.8 a, b, c, d). They form laminae or flat lenses of packstone/wackestone and/or floatstone with abrupt base, frequently embedded within the layers of the C2 and D2 facies (limestones with pervasive plane-parallel lamination and limestones with oblique and wavy lamination). In thin section a clear preferential orientation and sometimes imbrication of particles is observed (Fig. 4.8e, f). The large foraminifera are always disposed with the major axes parallel to the lamination planes and small particles (silt-sized foraminifera and radiolaria) are rare. These features suggest winnowing of

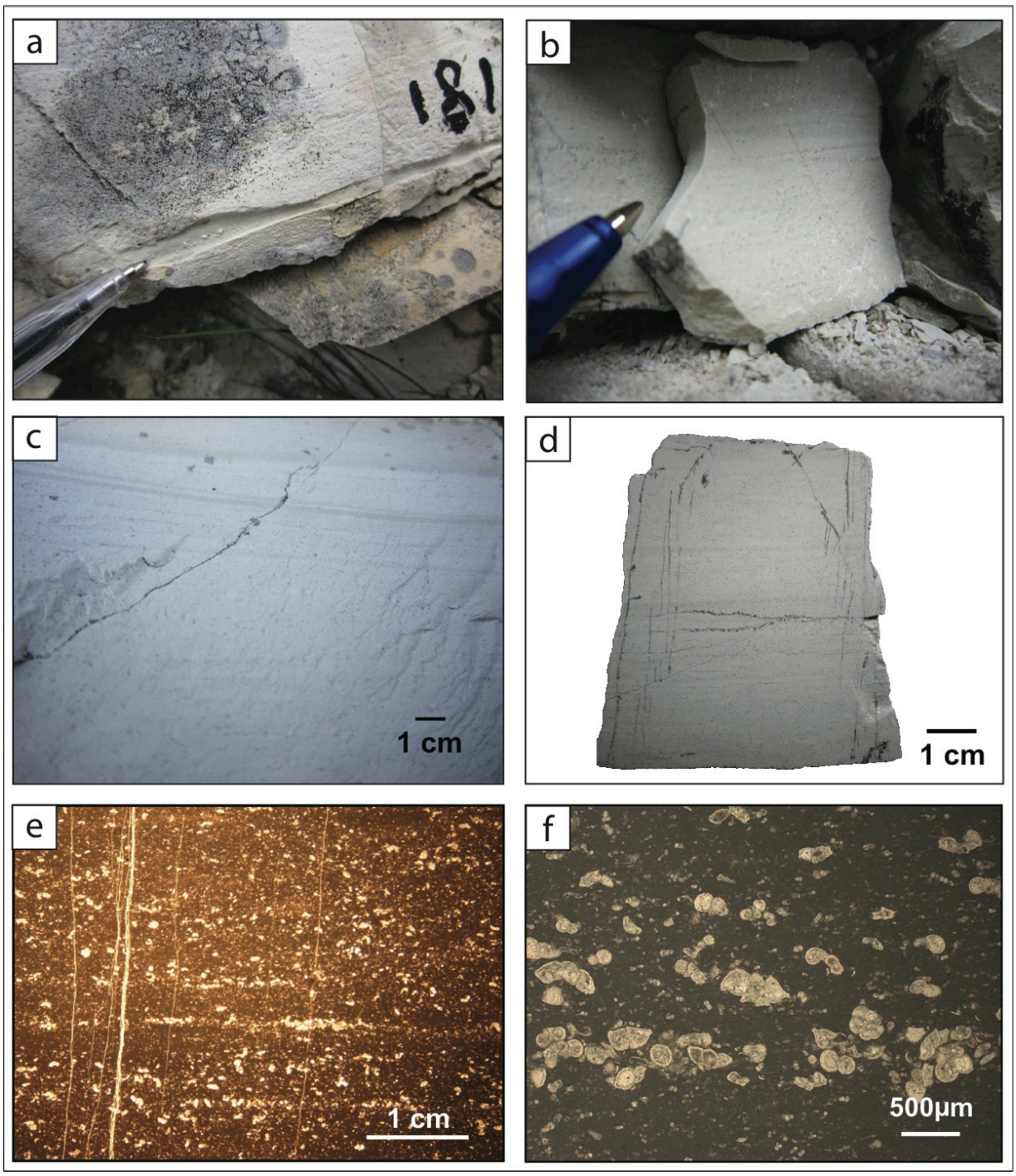

Figure 4.8: Foraminiferal-intraclastic laminated limestones (E2) – a) Intraclastic lag, pointed by the pen for scale (Furlo section). b) Foraminiferal lags; the pen for scale points to these less than 1 mm-thick laminae (Contessa section). c) Foraminiferal lags just below the grey lamina (Monte Petrano section). d) Repetitive foraminiferal lags on a polished surface (Contessa section). The lenticular alignments of forams are observable at a centimeter scale. e) Peel and f) thin section of the same sample of Fig. 7d (parallel nicols). The clustering in lenses and laminae and the preferential orientation of foraminifera are apparent.

the micrite and of the finest particles, together with the most mobile large ones (i.e. empty radiolaria tests). We interpret these packstones and floatstones as tractions lags. Removal of the fine fraction

resulted in the origin of these foraminiferal lags (Cooke et al., 2004) and implies the down-current redistribution of the displaced sediments.

Intervals with a high concentration of bioclasts due to traction effects in pelagic deposits have been already described by Hüneke and Stow (2008).

4.3.1.7 Alternating micritic and organic-rich laminasets (A4)

Plane-parallel laminated, layers characterized by alternating dark grey -yellowish grey laminaae with variable composition are recurrent. Thickness of these plane-parallel and loosely defined laminae ranges from less than 1mm to about 1cm (Fig. 4.9 a, c, e). Under the microscope the compositional lamination is an alternation of wackestones and mudstones with a variable amount of organic matter flakes and some clay, that concentrate to define flat lenses and/or laminae (Fig. 4.9b, d). The A4 facies layers are invariably associated with the black shale (A5) or black chert (G4) facies (Fig. 4.2), to which they grade progressively. Generally the organic-rich laminae get more frequent and thick close to the contact with the overlying black shale or black chert layer. The A4 compositional alternation is here interpreted as due to the onset of dysoxic/anoxic conditions. The general lack of bioturbation throughout the A4 layers, detectable both on hand-sample and at the microscope, supports the interpretation of a progressive shift to poorly oxygenated conditions. In some A4 layers a concentration of partially corroded foraminifera has been observed (Fig. 4.8f). It suggests incipient dissolution by aggressive water at the sediment/water interface, related to the oxydation/decomposition of the organic matter, and a reduction of the sedimentation rate leading to long exposure to aggressive bottom water.

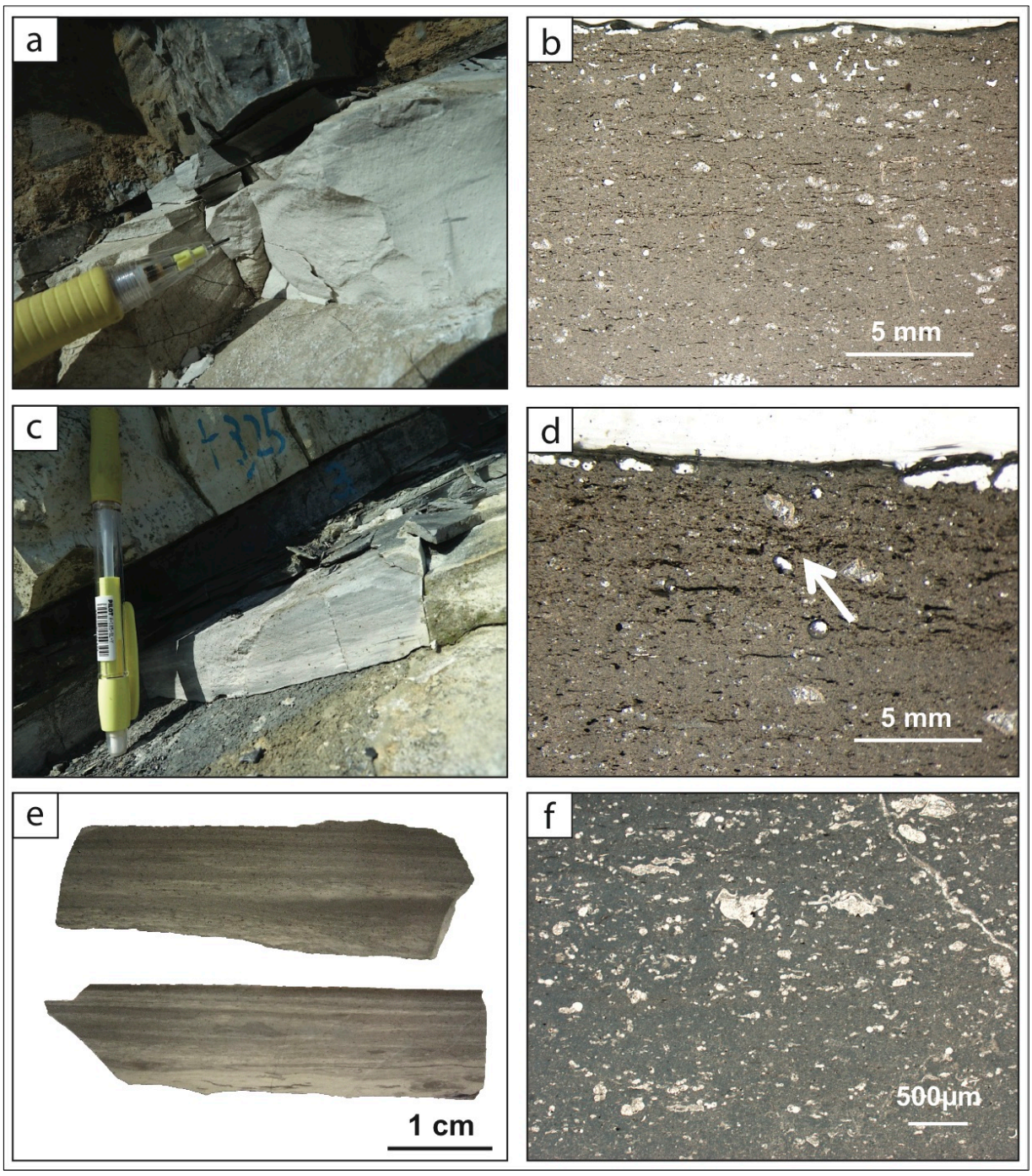

Figure 4.9: Alternating micritic and organic-rich laminasets – a) Compositional lamination (organic rich- and poor laminae) is present in the upper part of the layer, as indicated by the pencil (Furlo section). b) Peel of the layer shown in Fig. 8a. This foraminiferal – radiolarian wackestone lacks of bioturbation and shows concentrations of aligned organic matter flakes forming loosely defined laminae in the upper part of the picture. c) Compositional lamination as in (a) (Furlo, section) defined by changes of organic matter content. d) Peel of the layer shown in Fig.8c. The lack of bioturbation preserves the alignement of the organic flakes along loosely defined laminae. The arrow points to the soft sediment deformation around foraminifera. e) Polished surfaces of the layers in Fig.8a (upper) and 8c (lower). f) Thin section showing fragmentation and erosion of many large foraminifera in a compositionally laminated sample (Furlo section). See text for explanation.

4.3.1.8 Graded-laminated limestones (R)

In the studied sections some thin to very thin, graded and laminated limestone beds occasionally occur (Fig. 4.10), with a flat, sharp base and a transitional top. We separate the Ra type beds (Fig. 4.2; 10a; 10b), graded and laminated fine calcarenites grading to homogeneous or mottled marlstone/calcilutite, from the Rb type beds, that are graded and very faintly plane-parallel laminated calcisiltite-mudstone/marlstone beds (Fig. 4.10c). Both are graded foraminiferal wackestones, with

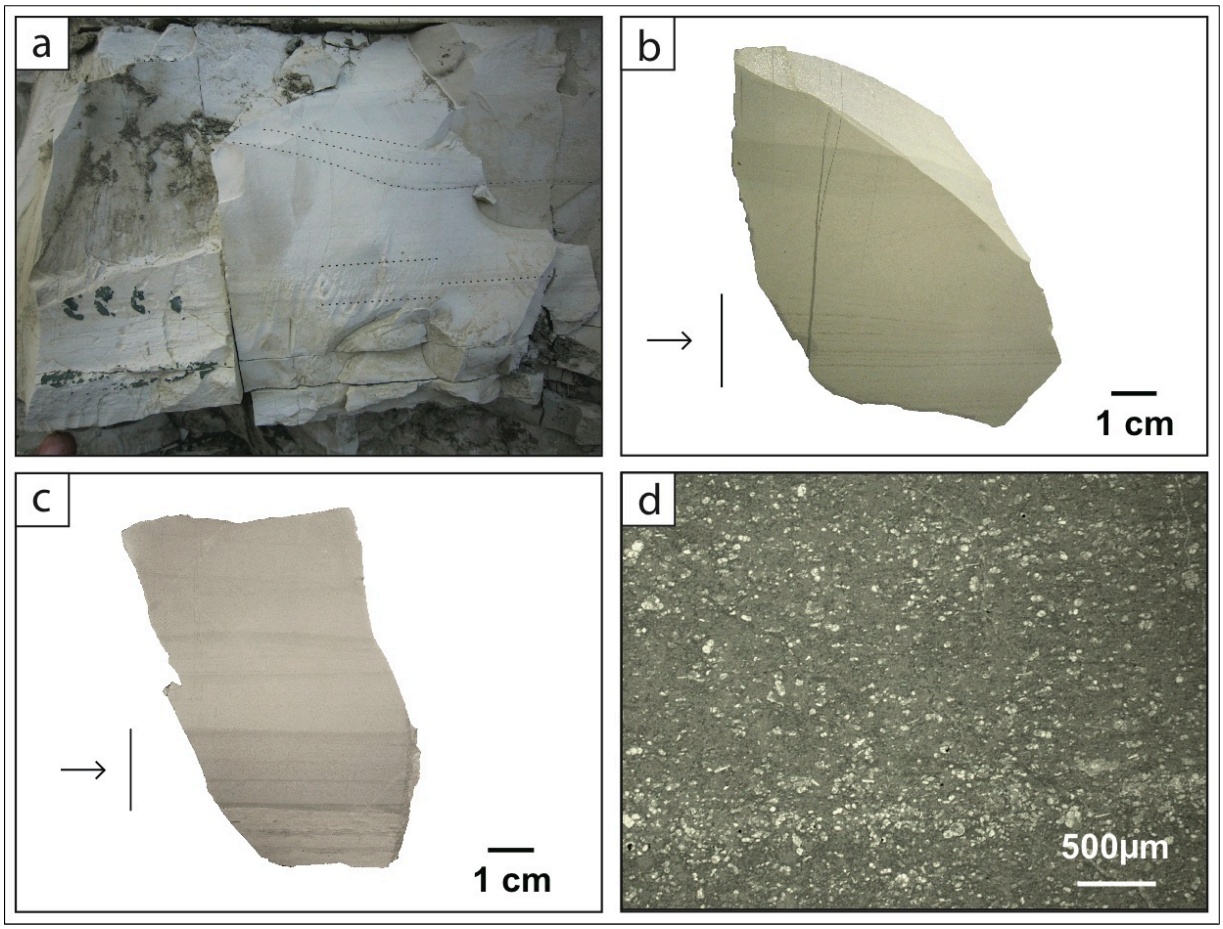

Figure 4.10: a) Example of a resedimented bed (Ra) (Furlo section). The bed shows a graded and plane parallel laminated division (very fine calcarenite to calcisitite) followed by a hardly visible oblique-laminated division (see 10b) and then by a homogeneous division of calcilutite (see drawings on the pictures). On top of the homogeneous division a new oblique laminaset deeply cuts the Ra layer, suggesting reworking of these sediments by sea-floor currents. b) Polished surface of a sample collected from the Ra bed in Fig. 10 a. The arrow points to the laminated divisions, highlighting the oblique laminaset above the plane-parallel laminae. c) Polished surface of a Rb bed (Furlo section). The faintly laminated calcisiltite division is overlain by homogeneous calcilutite and clayey calcilutite (grey). Note the sharp base and the transitional top of the bed; d) Thin section of the graded and faintly laminated division of sample of Fig. 10 a (parallel nicols). Only small foraminifera and small radiolarian represent the coarsest granules of this bed, forming wackestone/packstone laminae grading to mudstone.

plane-parallel lamination that slightly fades towards the top to homogeneous mudstone (Fig. 4.10d). Sometimes, an oblique laminated division can occur in the Ra type, above the plane-paralle laminated division (Fig. 4.10 b). In the four Umbria-Marche sections these beds contain some micaceous

fragments and rare displaced benthic foraminifera, suggesting mixing of some extrabasinal siliciclastic and displaced forams with the autochtonous components. In all the sections, the uppermost mudstone division contains some clay (marly calcilutite). The interpretation of very fine grained graded and laminated limestone beds within a pelagic environment can be considered controversial: they could represent fine grained pelagic turbidites, contourites, internal wave or internal tide deposits linked to a pycnocline, or even tempestites (Shanmungam, 1997, 2002; 2013). We interpret these beds as fine-grained pelagic turbidites on the base of their flat shape, sharp base, transitional top, sequence of depositional intervals and composition (presence of some extrabasinal components). Even if rare, such beds are typical of the Cretaceous pelagic environment of the two studied basins. Their origin is tightly linked to the uneven topography of the sea-floor of these two rift-related basins. They occur in many scattered positions through the Cenomanian succession, generally embedded within the typical pelagic facies A2, sometimes showing top reworking by sea-floor currents (D2 facies).

4.3.2 Siliceous facies

The siliceous facies of the Cenomanian Scaglia have either a direct diagenetic origin or consist of deposits that have been strongly modified by the diagenetic processes. In the latter case it is frequently difficult to recognize the eventual primary transport and deposition processes, both in the field and under the microscope. For this reason we separated the Diagenetic facies (G) from the more or less extensively modified depositional facies (A3, B3; Fig. 4.2), with the exception of facies G4a (a very strongly modified depositional facies, see the following paragraph) that cannot be unambiguously detected during field-work.

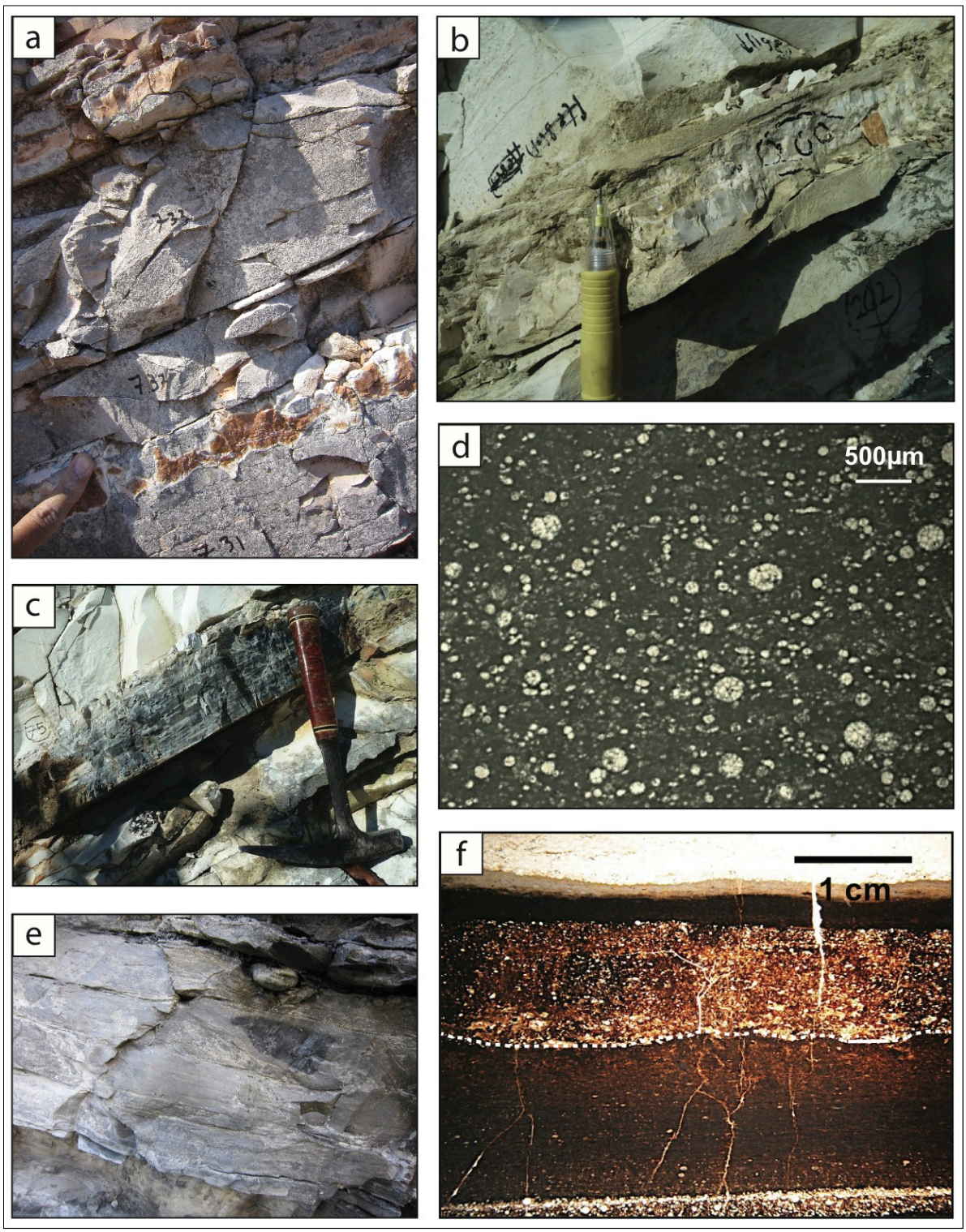

Figure 4.11: Siliceous facies. Chert bands of different colours: a) homogeneous and vitreous red cherts (G1; Monte Petrano section); b) homogeneous and vitreous grey cherts (G3; Furlo section); c) bedded black chert (G4a, Furlo section); d) Thin section of a radiolarian layer (parallel nicols); the biogenic part is composed exclusively by radiolaria within a shale matrix (Contessa section); e) isolated black chert nodule (Cismon section); f) thin section of the bedded black chert of Fig. 11c. Note the alternation of siliceous, radiolarian-rich beds and laminated, organic matter-radiolaria-rich shale interbeds, bounded by an erosivelower surface and by a sharp top.

4.3.2.1 Diagenetic facies (G1, G2, G3, G4)

Diagenetic facies are represented by chert bands, layers and nodules. Chert layer and band thickness ranges between about 0.5cm and about 20cm. They have abrupt, plane-parallel or undulating boundaries. The colour varies from reddish (G1; Fig. 4.11a) to pink (G2), gray (G3; Fig. 4.11b) and black (G4). These cherts are normally vitreous and homogeneous, with no primary structures observable both in the field and under the microscope. Diagenetic chert may form principally where solution and redeposition of silica from biogenic opal (radiolaria) occurs. It may also form during replacement of chalk, alteration of pyroclastic debris and precipitation from hydrothermal sources (Calvert, 1974), the latter two conditions being extremely difficult to ascertain for the depositional setting of the Scaglia in both the studied basins. Isolated chert nodules are diffused within the limestone facies in the studied sections; they are interpreted as the result of a diagenetic concentration of the siliceous components within the carbonate fraction (Fig. 4.11e). Differently, the chert bands and layers are thought to represent the diagenetic transformation of siliceous oozes that correspond to time spans dominated by deposition of siliceous organisms. The differences in colour within the bands are plausibly related mainly to different redox conditions, and to variations of the original content of organic matter, iron and manganese (Jones and Murchey, 1986) (Fig. 4.2). The G4 facies (black chert) is here considered as the "siliceous" equivalent of a black shale. The original sediment was presumably formed by radiolarian tests mixed with a variable amount of clay that could be transformed in a vitreous chert band.

Among the black cherts of the G4 facies, we separated the "Bedded black cherts" (G4a; Fig. 4.11c). In the outcrops this kind of bands shows a very thin bedding (<1 cm), that is highlighted by colour changes (gray vs.black) and differential weathering (Fig. 4.11 c). Under the microscope the bedding is formed by silt- to sand-sized, radiolarian-rich, parallel-laminated beds, with erosional base and sharp top, that alternate with very fine grained, plane-parallel laminated interbeds of clay- and organic matter-rich chert, with radiolarians (Fig. 4.11f). We interpret this G4a facies as the diagenetic modification of a primary interbedding of black shales (A5; Fig. 4.2, see the following chapter) and laminated radiolarian layers (B3; Fig. 4.2, see the following paragraph). This bedding is the result of a compositional alternation between mainly settled organic-rich shales and winnowed/redeposited radiolarian beds. Such alternation suggests the existence of feeble currents even during times of at least dysoxic sea-bottom conditions (black cherts and dark-grey to black radiolarian layers). Generally, we can assume that radiolaria, thanks to their glassy and vacuolar structure are easily transported by bottom currents and accumulated in drifts in areas with lower energy or during times of decreased bottom current activity. They can be redistributed both while produced in the surface water mass or even dispersed from different areas at a later stage.

4.3.2.2 Depositional facies (A3, B3)

Radiolaria-rich layers are frequent in the studied sections (Fig. 4.11d). They are cm-thick layers, mainly formed by Spumellaria specimens. Due to the spherical shape and equigranular size of these microfossils, the radiolarian layers mostly show the compositional alternation of laminae with different clay content (Fig. 4.11d). The A3 radiolarian layers (Fig. 4.2 and 11d) are homogeneous layers, with gradual boundaries, that were deposited under normal settling conditions, during periods of high nutrients input and primary productivity. The B3 laminated radiolarian beds are very thin, partly silicified beds, invariably gray to black coloured, with plane-parallel compositional lamination and sharp base and top. They are formed by radiolaria mixed with variable amounts of clay and minor carbonate. These B3 beds are the less strongly silicified equivalents of the radiolarian beds that alternate with siliceous shale interbeds to form Facies G4a. The only difference is the less extensive diagenetic transformation that makes these beds recognizable in the field as well as under the microscope. They are interpreted as the product of winnowing and/or down-current redeposition of radiolarian tests during times feeble activity of sea-floor currents. Together with the G4a facies they suggest that delicate currents could winnow the radiolarian-rich deposits at the bottom and/or redeposit downcurrent the light spumellaria tests, even during times of sea-bottom dysoxia to anoxia.

4.3.3 Marlstone, claystone and black shale facies

4.3.3.1 Marlstone layers (A0)

Marlstone layers (Facies A0) are common through all the studied sections (Fig. 4.12 a, b, d, e), showing a carbonate content ranging from 30 to 60%. Rare claystones or clayey marlstone layers can also occur; in these cases the clay content is higher than 70-90%. Both seams (less than 1cm thick and sometimes lens-shaped) and layers are present, the latter ranging between 1cm and 30cm in thickness. The lower and upper boundaries are generally flat or undulating and sharp, because of the diagenetic overprint, with few exceptions, such as in the gradual transition to the marly limestone layers (A1). The colour of these marlstones can vary from light brown, light grey to purplish/greenish (as at the transition with the underlaying Marne a Fucoidi Formation in the Umbria-Marche Basin) (Fig. 4.12 c, d). Settling of pelagic particles mixed with clay and some organic matter, in oxic conditions both in the water column and at the bottom, is the typical depositional process of these layers. The origin of clay is plausibly eolian in the Umbria-Marche Basin, while fluvial input cannot be excluded for the Cismon section in the Belluno Basin, that was relatively close to the continental land.

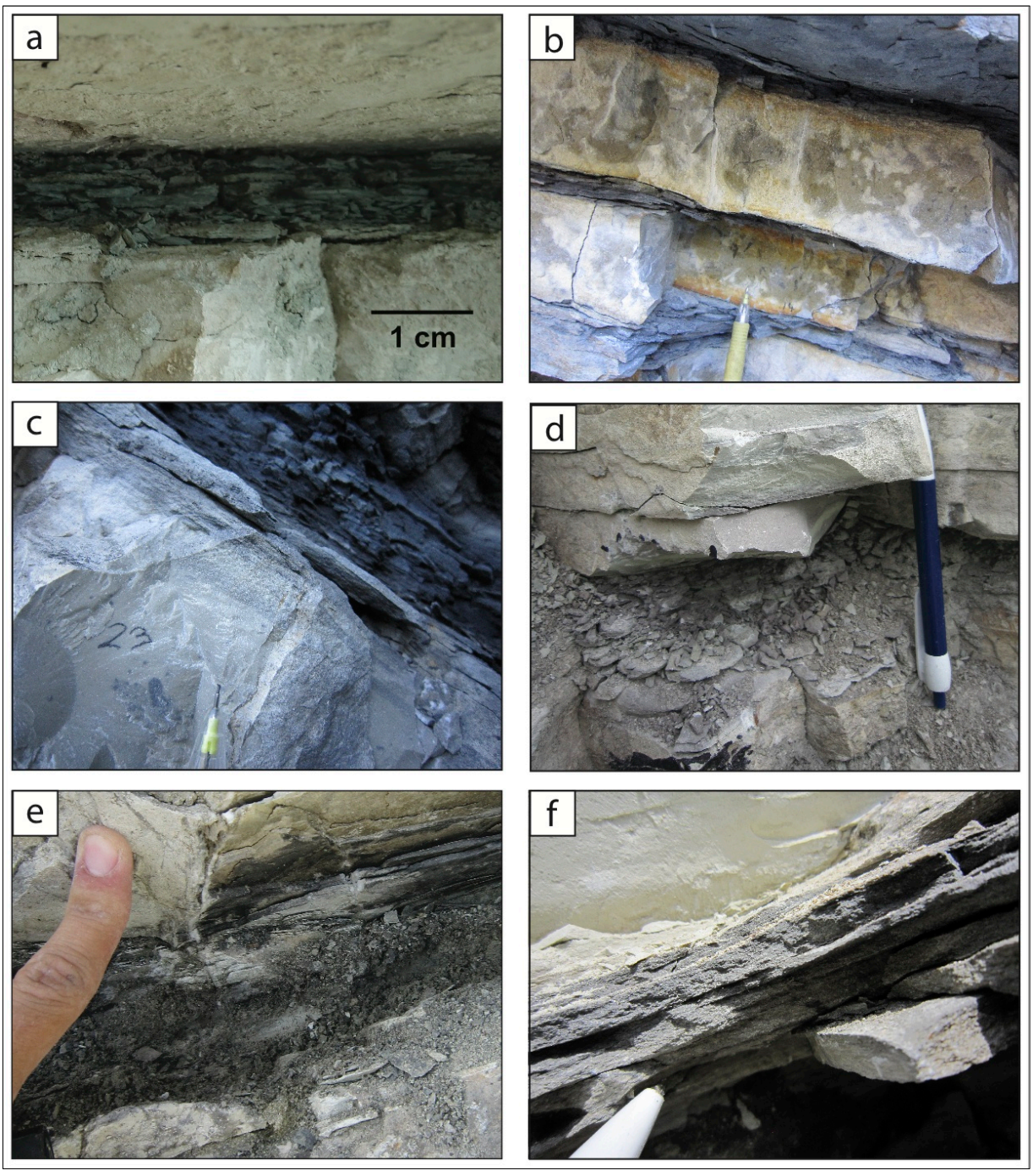

Figure 4.12: Marlstone – shale facies (A0, A5) a) Very thin marlstone layer (A0; Furlosection). b) Marlstone layers (A0) alternating with homogeneous limestone layers (A2), pencil for scale (Cismon section). c) Dark grey shale layer (A5) overlaying a grey homogeneous limestone (A2) with discrete bioturbation in the upper part (Cismon section). d) Purplish/greenish marlstone layer (A0; Le Brecce section). e) Brown marl layer (A0) overlain by a black shale layer (A5) (Monte Petrano section). f) Black shale layer (A5) (Le Brecce section).

4.3.3.2 Black shales (A5)

True black shales (A5) form layers whose thickness ranges from the seam scale (less than 1cm) up to about 5cm (Fig. 4.12c, e, f). They are frequently enriched in redox-sensitive trace metals due to both scavenging and adsorption onto clay particles (Turgeon and Brumsack, 2006). Their carbonate content varies from 20% up to 80% while the total organic carbon content ranges from 1 up to about 20% in the Bonarelli Level (Jenkyns et al., 2007). The black shales are generally thinly laminated with high variable TOC and carbonate content among the laminae. Lamina-scale variations suggest that a single black shale does not represent a single sedimentary episode but the changes through time of many oceanographic controls on deposition, in an anoxic environment. The systematic association of the black shales (or black cherts) with the alternating micritic and organic-rich laminasets (A4) suggests that the latter could represent the transition to deposition in a poorly oxygenated environment. The latest Cenomanian Bonarelli Level (Bonarelli, 1891; Tsikos et al., 2004; Mort et al., 2007; Turgeon and Brumsack, 2008; Monaco et al., 2012), a 35cm up to about 1m thick bituminous radiolarian-rich interval represents the most impressive accumulation of black shales in both basins. In the Umbria-Marche Basin, the lithological expression of the OAE1d, the so-called Pialli Event, is instead represented by 5-6 black shales each on the order of a few centimeters thick (e.g. Giorgioni et al., 2012). Very thin to thin black shale layers also occur below the Bonarelli Level, both at the Monte Petrano section and, as already described in literature, at the Furlo section (e.g. Lanci et al., 2010; Mitchell et al., 2008).

4.4 Schematic facies framework

The results of facies analysis permitted to describe the facies association that characterizes the pelagic depositional setting of the Umbria-Marche and Belluno Basins during the Cenomanian (Fig. 4.2). Because the focus of the paper is on the evidence of sea-floor current activity and redistribution processes in the Cenomanian palaeoceanographic setting of the two selected Tethyan regions, we disregard the siliceous diagenetic facies, and discuss all the other “depositional facies”, that preserve the documentation of the depositional processes.

4.4.1 Controls on sedimentation: the “depositional matrix”

The depositional facies association we described, suggests that among the palaeoceanographic controls on deposition (nurients availability, salinity, oxygenation, current activity, temperature, extrabasinal input), two factors played a major role: oxygenation and sea-floor current intensity. In fact, the limestone, the “shaly” and the non-diagenetic siliceous facies groups can be ordered into two major

"suites": the "pelagic/hemipelagic settling dominated" suite and the "traction current dominated" suite. This concept is represented in Fig. 4.2, where the facies of the Cenomanian Scaglia basins have been ordered into a sort of "depositional matrix". On the horizontal axis all the depositional facies have been ordered in terms of increasing traction intensity, from left to right; on the vertical axis they have been ordered in terms of increasing upwards oxygenation conditions. All the facies deposited by settling, under null or very low traction intensity, have been labeled as A while the facies deposited by progressively increasing current intensity have been labeled B to E, from left to right.

Within the lowest energy suite, that is characterized by no current-related structures (A0 – A5), the A0 – A3 group (claystone/marlstones, A0 – A1; homogeneous limestones, A2; radiolarian layers, A3) are indicative of settling in oxic environment, under the concurrent control of increasing nutrients and decreasing water temperature (Fig. 4.2). The "settling dominated" suite is progressively enriched in TOC, under conditions of progressive oxygen depletion and very low carbonate production, that leads to deposition of interlaminated mudstones and organic-rich shales (A4) and then to black shales (A5) in anoxic conditions.

The "traction current dominated" suite includes the facies types showing evidences of increasing shear stress on the sea-floor sediments, resulting in partly to totally winnowed beds, laminated beds, sometimes with very small current bedforms, and foraminiferal lags (B2 – E2 suite in Fig. 4.2). The parent sediments of these limestone beds are the A2 type pelagic foraminiferal oozes, at normal nutrients conditions, and/or the A1 pelagic/hemipelagic marlstone layers, after productivity/temperature/salinity perturbations with increased eolian/fluvial input. In this latter case, the laminated marly limestone beds (B2) would result from delicate winnowing of the micarb and of the lightest organisms, suggesting a first step in increasing shear stress on the sea-floor by current activity.

Laminated radiolarian beds (B3) have been interpreted as the result of traction acting both on a purely radiolarian layer (A3) or on a radiolaria-rich limestone, thanks to hydrodynamic selection during flow. Considering that the shear stress necessary to remove a radiolarian test compares to that capable to remove micrite we consider these laminated radiolarian beds as deposited under comparable shear stress intensity as the marly-limestone beds (B2).

The G4a "bedded blak chert" facies is the product of the diagenetic transformation of interbedded laminated radiolarian beds and black shales. This coupling indicates recurrent traction and concentration of radiolaria, under anoxic conditions, so revealing a segment of the "traction current dominated" suite also in correspondence of poor oxygenation at the sea-bottom (Fig. 4.2).

Some sporadic redeposited facies (Ra, sand- to silt-sized pelagic turbiditic beds; Rb, silt- to mud-sized highly diluted turbiditic beds) randomly occur, plausibly under the control of instability of intrabasinal and marginal slopes in both the basins (Doglioni & Bosellini, 1987; Alvarez, 1990).

4.4.2 Facies association

In the studied sections the most common facies are the homogeneous limestones (A2), alternated with radiolarian layers (A3; B3), marlstones (A0) and chert bands (G1,G2,G3, G4 and G4a). So, the most repetitive and frequent evidence of sea-floor current activity is represented by marly-limestone beds (B2) and laminated radiolarian beds (B3), that punctuate regularly the stratigraphy, with cm- to dm-vertical spacing. The bedded black chert facies (G4a) is less frequently represented. The siliceous tractive facies represent current activity concomitant with a perturbed state of the water column, either due to high nutrients input or to salinity (Fig. 4.2), the G4a only occurring in at least dysoxic conditions.

In the sections of the Umbria-Marche Basin, the calcareous facies belonging to the "traction current dominated" suite (B2 – E2) are generally more abundant than in the Cismon section of the Belluno Basin. Along the whole stratigraphic interval, from the Albian up to the lower Turonian, the Furlo and Monte Petrano sections are the richest of facies related to bottom current traction (C2, D2 and E2). In the entire Umbria – Marche Basin these facies punctuate the succession with dm-scale vertical separation, generally clustering every 3-6 m. The tractive beds are either isolated among the calcareous facies indicative of normal settling, or vertically associated to one another, with no apparent order, in the major clusters. Frequently the C2 and D2 tractive facies (limestones with pervasive plane-parallel lamination and/or with oblique and wavy lamination) are associated with chert bands (G) and radiolarian layers of the non-tractive type (A3), in oxic conditions, again suggesting that the enhancement of current activity could relate to perturbations of primary productivity, temperature and may be salinity.

In the Cismon section of the Belluno Basin the facies forming the "pelagic/hemipelagic settling dominated" suite are dominant, generally consisting of dark grey limestones, at times mottled or discretely bioturbated (A1-A2), but still the "traction dominated suite facies" occurs, with a larger vertical spacing than in the Umbria – Marche Basin, and without major clustering. These differences are plausibly explained by the palaeogeographic location of this area closer to the growing and initially emerging Eo-alpine chain (Doglioni & Bosellini, 1987).

With the exception of the Bonarelli layer that is not discussed in this paper, black shales are not homogeneously distributed in the analyzed sections. They occur in the upper half of the Furlo section

and, less frequently, at Monte Petrano. Black shales are present also in the Pialli Level (Fig. 4.1) both at Monte Petrano and Le Brecce sections. At the Cismon outcrop no "true" black shales have been observed; in this case, dark grey marlstones and dark marly claystones with higher TOC than the other fine grained marlstone and claystone layers are common.

4.4.3 Depositional model of the "traction current dominated" facies suite: the "calcareous pelagic contourites"

The two facies suites described within the two studied Tethyan settings, derive from competition between settling and bottom current shear stress, in a framework that is modulated primarily by oxygenation and by the other palaeoceanographic controls. The facies matrix (Fig. 4.2) of the Cenomanian "Scaglia l.s." and the vertical distribution of the "traction current dominated" facies, permit to infer a depositional model for the limestone facies of the "traction dominated" suite, that we consider as "calcareous pelagic contourites" (Fig. 4.13), in analogy with the fine-grained contourite depositional models (Stow et al., 1998).

To propose this interpretative model, beside all the data presented in the previous chapters, we also account for these preliminary considerations:

1) bottom currents, like a "wind", rework pelagic deposits with varying intensity and direction. All the calcareous facies we described in the "tractive" suite probably represent the fossil record of extended events that might have lasted for days, months (seasons) and/or years. The preservation of these facies is the result of the interplay among grain-size contrasts, traction intensity, bioturbation, burial and early cementation. The diagenetic overprint makes difficult to recognize the siliceous facies from the diagenetic chert facies, with the field observations yielding uncertain interpretations in a lot of cases. Besides recognizing the tractive structures of the best preserved siliceous layers (laminated radiolarian beds, B3, and bedded black cherts, G4a) we are not yet sufficiently confident to propose a depositional model for this case.

2) There is evidence that a partially cemented bottom of the calcareous layers underlays the uppermost ooze. In fact, in thin section, we found partly cemented aggregates of mudstone and wackestone on the way to be disrupted and eroded from their parent bed (e.g. Fig. 4.6 d, e and f). The transitions from ooze to chalk and than to limestone is gradual (Scholle, 1977) and is related to many factors, including heat flow (Wetzel, 1989), depositional depth, original composition, etc. (Schlanger and Douglas, 1974). Schlanger and Douglas (1974) noticed that soft plastic oozes could occur below stiff but friable chalks due to local reversal in the degree of lithification, but that the general trend is reasonably towards an increasing lithification with length and depth of burial.

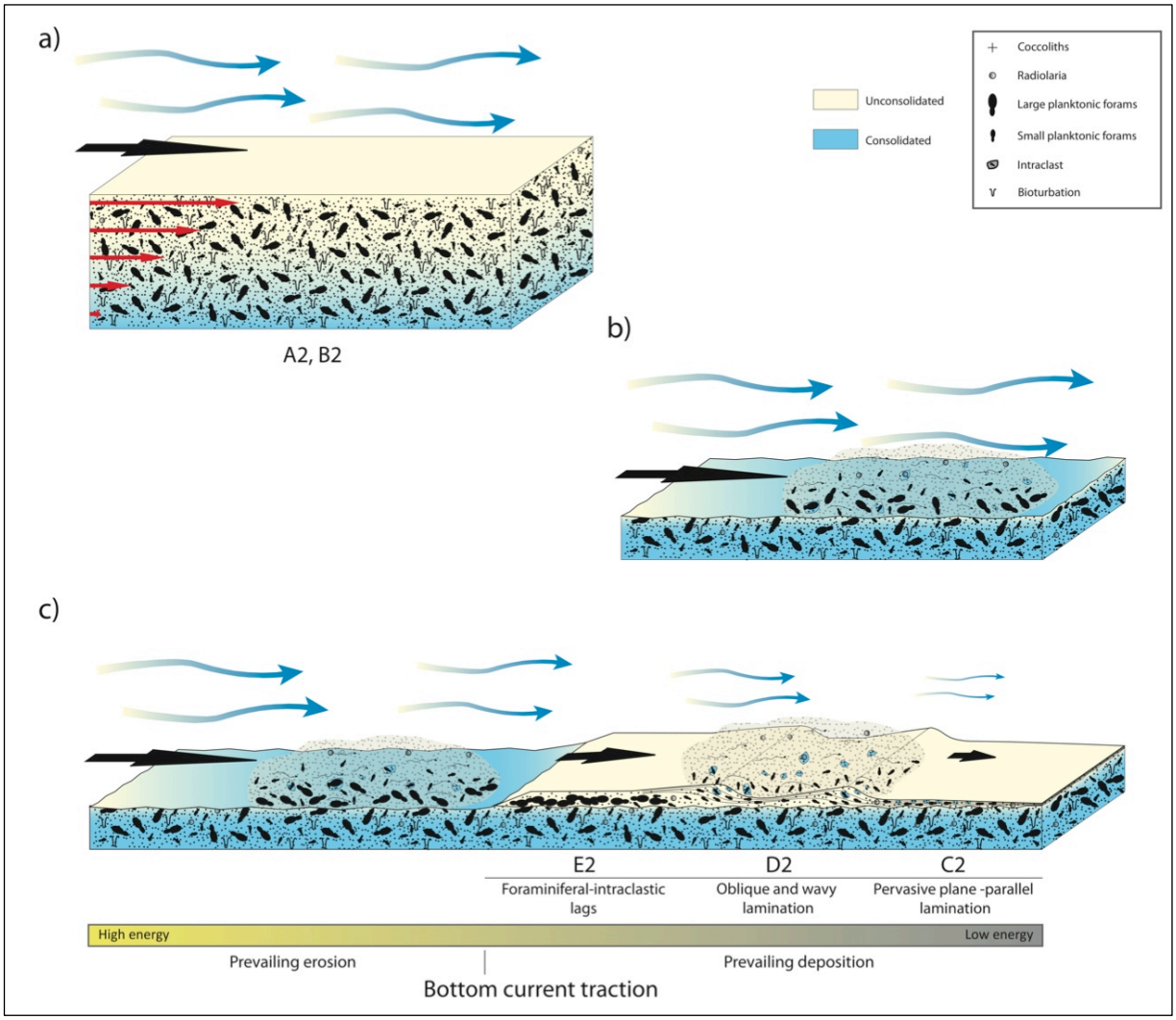

Figure 4.13: Out of scale proposal of a depositional model for the "traction current dominated" calcareous facies suite. a): a carbonatic ooze is subjected to shear stress by sea bottom-current. The ooze has a loose upper part and a partiallly cemented interval below. Shear stress gets progressively less efficient (red arrows) towards the lower part of the ooze layer. b): the unconsolidated sediment together with some intraclasts from the partly cemented lower interval are removed and transported, both at the interface and as a semi-suspended cloud. d): because of shear stress reduction through time and space, after a time span of prevailing erosion at a fixed site, and/or downcurrent of it, the sediment is re-deposited. At the erosion site a winnowed and reworked formainiferal lag (E2) is laid down. The moving sediment cloud is depleted first in the coarser components and deposits oblique to wavy laminated beds, by traction and some traction plus fall-out (D2). The finest and most light suspended sediments of the claud are finally deposited downcurrent under waning current velocity forming the pervasive plane parallel laminated limestones (C2).

Considering all the described features, and accounting for the previous two points, the depositional process we infer for the calcareous "traction dominated" facies suite can be described as an erosion-redeposition process, occurring through time and involving an erosion site that relates down-current to a redistribution site (Fig. 4.13).

In presence of sea-floor current, the shallow ooze is continuously moved and the light particles are uplifted from the bottom and suspended. Winnowing of a homogeneous foraminiferal limestone (facies A2) might progressively lead to the development of a foraminiferal lag, like it is suggested by

experiments and observations (Black et al., 2003; Cooke et al., 2004). The shear stress is also transmitted to the underlaying partly cemented sediment that, at this stage, starts to be deformed (Fig. 4.13a). Under increasing bottom current velocity and shear stress intensity at the interface, even the largest particles and the least mobile ones can be progressively mobilized and transported down-current. At the maximum shear stress stage, even the lag can be removed and consequently the top of the buried partly cemented sediment, may be exposed and disrupted so that erosion can start to deliver limestone intraclasts. Down current of the winnowing/erosion site, the coarsest grains (large foraminifera, intraclasts) probably travel at the base of a "winnowing cloud" and the small and light grains (small foraminifera, radiolaria, coccoliths and micarb) are incorporated into the temporaneously suspended top of the cloud itself. The sediment cloud can deposit different beds down current, according to the different hydrodynamic behavior of the grains and to the waning or waxing stage of the current. In a waning stage scenario (Fig. 4.13b and c) the first particles to be re-deposited are the largest foraminifera and intraclasts, incorporated after erosion of the winnowed foraminiferal lag. Depleted of its coarsest fraction, the cloud of sediment with radiolaria, coccoliths, small foraminifera and the smallest intraclasts, deposits traction plus fall-out beds, with ripple-type and wavy lamination (C2 facies). At last the finest-grained beds with pervasive plane-parallel lamination are deposited (D2 facies; Fig. 4.13c) by the slowed-down current.

Even if we did not directly observe a clear association that could lead to recognize a waxing current scenario, it might be considered that the reverse horizontal facies trend should be theoretically produced moving down current, in that case.

The waning facies trend looks to be typical of the major traction facies clusters that we observed, whose vertical spacing suggests low-frequency recurrency of strong bottom current activity. The most frequent episodes of slight intensification of bottom currents produces the isolated tractive facies, in the form of discrete beds showing winnowing of the mud component and/or laminations. Most of these beds belong to the B2 facies (marly-limestone beds) and some are represented by B3 facies (laminated radiolarian beds).

It is interesting to note that there are evidences of traction current activity also besides this model, that refers to the oxic and calcareous environmental setting, in the anoxic siliceous suite of the "bedded black chert" facies (G4a). A plausibly delicate traction current activity is documented by the alternation of black shale and laminated radiolarian beds even if it is hidden by diagenetic silicization.

4.5 Conclusions

Our results show how settling of biogenic particles, mixed with variable amounts of very fine grained extrabasinal materials, represents the main source of sediments to be delivered to the pelagic realm, but not the unique depositional process within the studied Cenomanian settings of the Tethyan domain. Evidence of bottom currents activity at the sea floor, with varying intensity, has been shown. Currents operate winnowing and redistribute particles with variable frequency of recurrence times. For this reason, pelagic sequences should be interpreted not only in terms of a two-dimensional vertical stacking of palaeoceanographic events but also as the four-dimensional expression of different depositional settings through space and time.

During the latest Albian-Cenomanian, the palaeoceanographic controls on pelagic sedimentation in the Umbria-Marche and Belluno Tethyan Basins, forced deposition to occur primarily along two major suites, the “settling dominated” and the “traction dominated” suite. Oxygenation, primary productivity, nutrients and extrabasinal input modulate the compositional fingerprint of the facies forming the two suites, from purely calcareous to shaly or siliceous and from oxic to anoxic (light limestones, cherts and shales vs. dark marly limestones, black shales and black cherts).

The interplay between the sea-floor current intensity and the grain-size and type of the available sediments at the sea floor modulated the tractive facies types: from the delicately laminated and poorly-sorted marly-limestone beds (B2) and radiolarian beds (B3) to the extremely winnowed foraminiferal lags, via the pervasively laminated well sorted limestones, recurrently with current ripples, as well as from the radiolarian layers and black shales to the tractive “bedded black cherts”. The latter show episodes of sea-floor traction that punctuate black shale deposition. In any case, the type of traction structure can be used as a proxy for bottom current intensity, provided that we can rely on the experimental definition of the hydraulic behavior of the pelagic particles (Southard et al., 1971; Young and Southard, 1978; Black et al., 2003; Cooke et al., 2004).

The vertical repetitive stacking of the facies belonging to the two opposite depositional suites (settled and tractive) and to the two opposite oxygenation regimes (oxic vs. anoxic) suggests that the environmental resilience of the pelagic system can lead to recover perturbations, passing through different instability stages, one of which is represented by sea-floor erosion, winnowing and redistribution of sediments by currents. This kind of adaptative behavior can be considered an autocyclic process (the recovery), forced by allocyclic factors (the perturbations).

As a general conclusive remark, we believe that sedimentation in the pelagic realm is still largely under-known, with complex processes and facies that remain to be properly understood. The deep-sea

deposition is not simply the result of homogeneous and monotonous settling, but the sum of many different processes. The interplay of physiography, bathymetry and paleoceanographic conditions controls bottom currents intensity and direction and then the resulting sediment redistribution. For this reason only a precise characterization of local depositional processes, regional palaeoceanographic settings and global climatic background might allow for a correct interpretation of the stratigraphic record. A better defintition of the interplay between all of these factors is the goal of our ongoing research, aiming to define a comprehensive depositional model of auto- and allocyclical controls on deposition in the pelagic realm in the “Mid-Cretaceous” Tethys.

References

Alvarez, W. (1990) – Pattern of extensional faulting in pelagic carbonates of the Umbria-Marche Apennines of central Italy. *Geology*, 18, 407-410.

Arthur, M.A. and Premoli Silva, I. (1982) – Development of widespread organic carbon-rich strata in the Mediterranean Tethys. *In:* Schlanger, S.O. and Cita, M.B. (Eds.), *Nature and Origin of Cretaceous Carbon-rich Facies*, 7-54.

Arthur, M.A., Brumsack, H.-J., Jenkyns, H.C. and Schlanger, S.O. (1990) – Stratigraphy, geochemistry, and paleoceanography of organic carbon-rich Cretaceous sequences. *In:* Ginsburg, R. and Beaudoin, B. (Eds.), *Cretaceous Resources Events, and Rhythms*, 75-119.

Beaudoin, B., M'Ban, E.P., Montanari, A., Pinault, M. (1996) – Lithostratigraphie haute résolution (<20 ka) dans le Cénomanien du bassin d'Ombrie-Marches (Italie). *Comptes Rendus de l'Académie des Sciences Paris*, 323 Series Iia, 689-696.

Bellanca A., Claps, M., Erba, E., Masetti, D., Neri, R., Premoli Silva, I. and Venezia F. (1996) – Orbitally induced limestone/marlstone rhythms in the Albian-Cenomanian Cismon section (Venetian region, northern Italy): sedimentology, calcareous and siliceous plankton distribution, elemental and isotope geochemistry. *Palaeogeography, Palaeoclimatology, Palaeoecology*, 126, 227-260.

Bernoulli, D. and Jenkyns, H.C. (1974) – Alpine, Mediterranean, and Central Atlantic Mesozoic facies in relation to the early evolution of the Tethys. *In:* Dott, R.H. and Shaver, R.H. (Eds.), *Modern and Ancient Geosynclinal Sedimentation*. Society of Economic Paleontologists and Mineralogists, Special Publication, 19, 129-160.

Bersezio, R. (1993) - Sedimentary events and rhythms in an Early Cretaceous pelagic environment: the Maiolica Fm. of the Lombardy Basin. *Giornale di Geologia*, 55/1, 5-20, Bologna.

Bersezio, R., Erba, E., Gorza, M. and Riva, A. (2002) - Berriasian - Aptian black shales of the Maiolica Fm. (Lombardian Basin, Southern Alps - Northern Italy): a case study of the Early Cretaceous in the Tethys Ocean. *Palaeogeography, Palaeoclimatology, Palaeoecology,* 180, 253-275.

Black, K.S., Peppe, O.C ., Gust, G. (2003) – Erodibility of pelagic carbonate ooze in the northeast Atlantic. Journal of Experimental Marine Biology and Ecology, 285-286, 143-163.

Bonarelli, G. (1891) – Il Territorio di Gubbio. *Notizie Geologiche*, 1-38.

Bosellini, A., Broglio Loriga, C., and Busetto, C. (1978) - I bacini cretacei del Trentino. *Riv. Ital Paleont. Strat*, 84.4, 897-946.

Bralower, T.J., Sliter, W.V., Arthur, M.A., Leckie, R.M., Allard, D., Schlanger, S.O. (1993) – Dysoxic/anoxic episodes in the Aptian-Albian (Early Cretaceous). *In:* Pringle, M., Sager, W.W., Sliter, W.V., Stein, S. (Eds.), *The Mesozoic Pacific: Geology, Tectonics, and Volcanism. American Geophysical Union Monograph*, 77, 5-37.

Calvert, S.E. (1974) – Deposition and Diagenesis of Silica in Marine Sediments. *In:* Hsu, K.J. and Jenkyns, H.C. (Eds.), *Pelagic Sediments: on Land and under the Sea*, 273-299.

Channell J.E.T., D'Argenio, B., Horvath, F. (1979a) – The African Promontory, in Mesozoic Mediterranean Paleogeography. *Earth Science Review*, 15, 213-272.

Channell, J. E. T., Lowrie, W. and Medizza, F. (1979b) – Middle and Early Cretaceous magnetic stratigraphy from the Cismon section, northern Italy. *Earth and Planetary Science Letters*, 1979, 42.2, 153-166.

Claps, M., Masetti, D., Pedrielli, F., Garavello, A. (1991) – Analisi spettrale e cicli di Milankovitch in successioni cretaciche del Sudalpino orientale. Rivista Italiana di Paleontologia e Stratigrafia, 97, 153-174.

Claps, M. and Masetti, D. (1994) – Milankovitch periodicities recorded in Cretaceous deep-sea sequences from the Southern Alps (Northern Italy). Special Publications International Association of Sedimentologists, 19, 99-107.

Coccioni, R., Galeotti, S. (2001) – The mid-Cenomanian Event: the Prelude to the OAE 2. *EOS Trans. AGU* 82(47), Fall Meet. Suppl.

Coccioni R. and Galeotti S. (2003) – The Mid-Cenomanian Event: prelude to OAE 2. *Palaeogeography, Palaeoclimatology, Palaeoecology*, 190, 427-440.

Cooke J.P., Nelson, C.S., Crundwell M.P., Field, B.D., Elkington, S.E. and Stone, H.H. (2004) - Textural variations in Neogene pelagic carbonate ooze at DSDP Site 593, southern Tasman Sea, and their paleoceanographic implications. *New Zealand Journal of Geology and Geophysics*, 47, 787-807.

Dercourt, J., Gaetani, M., Vrielinck, B., Barrier, E., Biju-Duval, B., Brunet, M.F., Cadet, J.P., Crasquin, S., Sandulescu, M. (2000) – *Atlas of Peri-Tethys, Palaeogeographical Maps. Commission de la Carte Geologique du Monde (CCGN/CGMW)*, Paris, pp. 1-269.

Doglioni C. and Bosellini A. (1987) – Eoalpine and Mesoalpine tectonics in the Southern Alps. *Geologische Rundschau*, 76/3, 735-754.

Erba E. and Larson R.L. (1998) – The Cismon APTICORE (Southern Alps, Italy): a reference section for the Lower Cretaceous at low latitudes. *Rivista Italiana di Paleontologia e Stratigrafia*, 104, 181-192.

Faugéres, J.-C and Stow, D.A.V. (1993) – Bottom-current-controlled sedimentation : A synthesis of the contourite problem. *Sedimentary Geology*, 82, 287-297.

Faugéres, J.-C., Stow, D.A.V., Imbert, P., Viana, A.R. (1999) – Seismic features diagnostic of contourite drifts. *Marine Geology*, 162, 1-38.

Faugéres, J.-C. and Stow, D.A.V. (2008) – Contourite drifts: Nature, evolution and controls. In: Rebesco, M., Camerlenghi, A. (Eds.), *Contourites. Developments in Sedimentology*, 60, 257-288.

Gao, Z., Erikkson, K.A., He, Y., Luo, S., Guo, J. (1998) – Deep-Water Tracton Current Deposits - A study of internal tides, internal waves, contour currents and their deposits. Beijing and New York: Science Press, Utrecht, Tokyo, 128pp.

Giorgioni, M., Weissert, H., Bernasconi, S.M., Hochuli, P.A., Coccioni, R., Keller, C.E. (2012) – Orbital control on carbon cycle and oceanography in the mid-Cretaceous greenhouse. *Paleoceanography*, 27, PA1204, doi:10.1029/2011PA002163.

Graham, A.R. (1963) – Routine preparation of polished thin-sections. *The Canadian Mineralogi*st, 7(3), 375-377.

Hemming, S.R., Biscaye, P.E., Broecker, W.S., Hemming, N.G., Klas, M., Hajdas, I. (1998) – Provenance change coupled with increased clay flux during deglacial times in the western equatorial Atlantic. *Palaeogeography, Palaeoclimatology, Palaeoecology*, 142, 217-230.

Hu, X., Cheng, W., Ji, J. (2009) – Origin of Cretaceous Oceanic Red Beds from the Vispi Quarry Section, Central Italy: Visible Reflectance and Inorganic Geochemistry. In: Hu, X., Wang, C., Scott, R.W., Wagreich, M., Jansa, L. (Eds.), *Cretaceous Oceanic Red Beds: Stratigraphy, Composition, Origins, Paleoceanographic, and Paleoclimatic Significance*, SEPM Special Publication, 91, 183-197.

Hüneke, H. and Stow, D.A.V. (2008) – Identification of ancient contourites: Problems and palaeoceanographic significance. *In:* Rebesco, M., Camerlenghi, A. (Eds.), *Contourites. Developments in Sedimentology*, 60, 323-344.

Jarvis, I., Murphy, A.M., Gale, A.S. (2001) - Geochemistry of pelagic and hemipelagic carbonates: criteria for identifying systems tracts and sea-level change. Journal of the Geological Society,158, 685-696.

Jenkyns, H.C. (2007) – Nitrate reduction, sulfate reduction, and sedimentary iron isotope evolution during the Cenomanian-Turonian oceanic anoxic event. *Paleoceanography*, 22, PA3208, doi:10.1029/2006PA001355.

Jenkyns, H.C. (2010) – Geochemistry of oceanic anoxic events. *Geochemistry Geophysics Geosystems*, 11, Q03004, doi:10.1029/2009GC002788.

Jones, D.L. and Murchey, B. (1986) – Geologic significance of Paleozoic and Mesozoic radiolarian chert. *Annual Review of Earth and Planetary Sciences*, 14, 455-492.

Klein, G. D. (1975) – Resedimented pelagic carbonate and volcaniclastic sediments and sedimentary structures in Leg 30 DSDP cores from the western equatorial Pacific. *Geology*, 3, 39–42.

Kuhnt, W., Herbin, J.P., Thurow, J., Wiedmann, J. (1990) – Distribution of Cenomanian-Turonian Organic Facies in the Western Mediterranean and along the Adjacent Atlantic Margin. *In:* Huc, A. Y. (Eds.), *Deposition of Organic Facies*, AAPG Studies in Geology, 30, 133-160.

Lanci L., Muttoni, G., Erba E. (2010) – Astronomical tuning of the Cenomanian Scaglia Bianca Formation at Furlo, Italy. *Earth and Planetary Science Letters*, 292, 231-237.

Leckie, R.M., Bralower, T.J., Cashman, R. (2002) – Oceanic anoxic events and plankton evolution: Biotic response to tectonic forcing during the mid-Cretaceous. *Paleoceanography*, 17, 13-29.

Lovell, J.P.B. and Stow, D.A.V. (1981) – Identification of ancient sandy contourites. *Geology*, 9, 347-349.

Maldonado and Nelson (1999) – Marine geology of the Gulf of Cadiz. Marine Geology, 155, 346pp.

McCave, I.N., Hollister, C.D., Nowell, A.R.M. (1988) – (Eds.) Deep Ocean Sediment Transport: HEBBLE Collected Reprints 1980-1987. Woods Hole Oceanographic Institute, Woods Hole, 737pp.

Mienert, J. (1998) – (Eds.) European North Atlantic Margin (ENAM): Sediment pathways, processes and flux. Marine Geology, 152, 316pp.

Mitchell, R.N., Bice, D.M., Montanari, A., Cleaveland, L.C., Christianson, K.T., Coccioni, R., Hinnov, L.A. (2008) – Oceanic anoxic cycles? Orbital prelude to the Bonarelli Level (OAE2). *Earth and Planetary Science Letters*, 267, 1-16.

Monaco, P., Rodríguez-Tovar, F.J., Uchman, A. (2012) – Ichnological analysis of lateral environmental heterogeneity within the Bonarelli Level (uppermost Cenomanian) in the classical localities near Gubbio, Central Apennines, Italy. *Palaios*, 27, 48-54.

Monechi, S. and Parisi, G. (1989) – Da Gubbio a Cantiano. *Memorie Descrittive della Carta Geologica* d'Italia, 39, 96-102.

Mort, H.P., Adatte, T., Föllmi, K.B., Keller, G., Steinmann, P., Matera, V., Zsolt, B., Stüben, D. (2007) – Phosphorus and the roles of productivity and nutrient recycling during oceanic anoxic event 2. *Geology*, 35, 483-486.

Nowell and Hollister, (1985) – Deep Ocean Sediment Transport - Preliminary Results of High Energy Benthic Boundary Layer Experiment, Marine Geology, 66, 420pp.

Parisi, G. (1989) – Stratigrafia del Cretacico-Paleogene. *In:* Cresta, S., Monechi, S., Parisi, G. (Eds.), *Stratigrafia del Mesozoico e Cenozoico nell'area umbro-marchigiana*, *Memorie Descrittive della Carta Geologica* d'Italia, 39, 23-29.

Pratt L.M. and King D.J. (1986) - Variable marine productivity and high eolian input recorded by rhythmic black shales in Mid-Cretaceous pelagic deposits from central Italy. *Paleoceanography*, 1, 507–522.

Premoli Silva, I., Erba, E., Salvini, G., Locatelli, C., Verga, D. (1999) – Biotic changes in Cretaceous Oceanic Anoxic Events of the Thethys. *Journal of Foraminiferal Research*, 29, 352-370.

Rebesco, M. and Stow, D.A.V. (2001) – Seismic Expression of Contourites and Related Deposits: A Preface. Marine Geophysical Research, 22, 303-308.

Sarti, M., Bosellini, A. and Winterer, E. L. (1992) - Basin geometry and architecture of a Tethyan passive margin (Southern Alps, Italy): implications for rifting mechanisms. *Geology and geophysics of continental margins*, 53, 241-258.

Schlanger, S.O. and Douglas, R.G. (1974) – The pelagic ooze-chalk-limestone transition and its implication for marine stratigraphy. *In:* Hsü, K.J., and Jenkyns, H.C. (Eds.), *Pelagic Sediments: On Land and Under the Sea*, 117-148.

Schlanger, S.O. and Jenkyns, H.C. (1976) – Cretaceous oceanic anoxic events: causes and consequence. *Geologie en Mijnbouw*, 55(3-4), 179-184.

Scholle, P. (1977) – Chalk diagenesis and its relation to petroleum exploration: oil from chalks, a modern miracle?. *American Association of Petroleum Geologists Bulletin*, 61, 982-1009.

Shanmungam, G. (1997) – The Bouma sequence and the turbidite mind set. *Earth Science Review*, 42, 201-229.

Shanmungam, G. (2002) – Ten turbidite myths. *Earth Science Review*, 58, 311-341.

Shanmungam, G. (2003) – Deep-marine tidal bottom currents and their reworked sands in modern and ancient submarine canyons. *Marine Petroleum Geology*, 20, 471-491.

Shanmungam , G. (2006) – Deep-Water Processes and Facies Models: Implications for Sandstone Petroleum Reservoirs. Elsevier, Amsterdam, 476pp.

Shanmungam, G. (2008) – Deep-water bottom currents and their deposits. *In:* Rebesco, M., Camerlenghi, A. (Eds.), *Contourites. Developments in Sedimentology*, 60, 59-81.

Shanmungam, G. (2013) – Modern internal waves and internal tides along oceanic pycnoclines: challenges and implications for ancient deep-marine baroclinic sands. *AAPG Bull.,* 97/5, 799-843.

Shanmungam, G., Spalding, T.D., Rofheart, D.H. (1993) – Traction structures in deep-marine bottom-current reworked sands in the Pliocene and Pleistocene, Gulf of Mexico. *Geology*, 21, 929-932.

Skelton, P. W., Spicer, R. A., Kelley, S. P., Gilmour, I. (2003) – *The Cretaceous World*, pp.1-360.

Southard, J.B., Young, R.A., Hollister, C.D. (1971) – Experimental erosion of calcareous ooze. *Journal of Geophysical Research*, 76, 5903-5909.

Stoker, M.S., Evans, D., Cramp, A. (1998) – Sedimentation, Mass Wasting and Stability. Geological Society of London. Special Publication, 129, 355pp.

Stow, D.A.V. and Lowell, J.P.B. (1979) – Contourites: their recognition in modern and ancient sediments. *Earth Science Review*, 14, 251-291.

Stow, D.A.V. and Faugéres, J.-C. (1993) – Contourites and bottom-currents. Sedimentary Geology, 82, 310pp.

Stow, D.A.V., Faugéres, J.-C., Viana, A.R., Gonthier, E. (1998) – Fossil contourites: A critical review. Sedimentary Geology, 115, 3-31.

Stow, D.A.V., Pudsey, C.J., Howe, J.A., Faugéres, J.-C., Viana, A.R. (Eds.) (2002a) – Deep-water contourite systems: modern drifts and ancient series, seismic and sedimentary characteristics. *Geological Society of London Memoir*, 22, 464pp.

Stow, D.A.V., Faugéres, J.-C., Gonthier, E., Cremer, M., Llave, E., Hernandez-Molina, F.J., Somoza, L., Diaz-Del-Rio, V. (2002b) – Faro-Albufeira drift complex, northern Gulf of Cadiz. *In:* Stow, D.A.V., Pudsey, C.J., Howe, J.A., Faugéres, J.-C., Viana, A.R., *Deep-water contourite systems: modern drifts and ancient series, seismic and sedimentary characteristics*. Geological Society of London Memoir, 22, 137-154.

Stow, D.A.V. and Faugéres, J.-C. (2008) – Contourite facies and the facies model. *In:* Rebesco, M., Camerlenghi, A. (Eds.), *Contourites. Developments in Sedimentology*, 60, 223-256.

Tsikos, H., Jenkyns, H.C., Walsworth-Bell, B., Petrizzo, M.R., Forster, A., Kolonic, S., Erba, E., Premoli Silva, I., Baas, M., Wagner, T., Sinnighe Damsté, J.S. (2004) – Carbon-isotope stratigraphy recorded by the Cenomanian–Turonian Oceanic Anoxic Event: correlation and implications based on three key localities. *Journal of the Geological Society, London*, 161, 711-719.

Turgeon, S. and Brumsack, H.-J. (2006) – Anoxic vs dysoxic events reflected in sediment geochemistry during the Cenomanian–Turonian Boundary Event (Cretaceous) in the Umbria–Marche Basin of central Italy. *Chemical Geology*, 234, 321-339.

Turgeon and Craser (2008) – Cretaceous oceanic anoxic event 2 triggered by a massive magmatic episode. *Nature*, 454, 323-329.

Viana, A.R. and Rebesco, M. (2007) – Economic and palaeoceanographic significance of conturite deposits. Geological Society of London Special Publication, 276, 350pp.

Wetzel, A. (1989) – Influence of heat flow on ooze/chalk cementation: quantification from consolidation parameters in DSDP sites 504 and 505 sediments. *Journal of Sedimentary Petrology*, 59, 539-547.

Wilson, M.A. and Palmer, T.J. (1989) – Preparation of acetate peels. *In:* Schneidermann, N. and Harris, P.M. (Eds.), *Paleotechniques. The Paleontological Society, Special Publication 4*, 142-145.

Wilson, P.A. and Norris, **R.D.** (2001) – Warm tropical ocean surface and global anoxia during the mid-Cretaceous period, *Nature*, 412, 425-429.

Wilson, P.A., Norris, R.D., Cooper, M.J. (2002) – Testing the Cretaceous greenhouse hypo-thesis using glassy foraminiferal calcite from the core of the Turonian tropics on Demerara Rise. *Geology*, 30, 607-610.

Winterer, E.L. and Bosellini, A. (1981) – Subsidence and sedimentation on a Jurassic passive continental margin (Southern Alps, Italy). AAPG Bulletin, 65, 394-421.

Wynn, R.B. and Stow, D.A.V. (2000) – Recognition and interpretation of deep-water sediment waves. *Marine Geology*, 192, 1-321pp.

Young, R.N. and Southard, J.B. (1978) – Erosion of fine-grained marine sediments: Sea-floor and laboratory experiments. *Geological Society of America Bulletin*, 89, 663-672

Chapter 5

High-resolution Carbon and Oxygen stable isotope records from two mid-Cretaceous Thethyan pelagic sequences: Monte Petrano and Cismon sections (Italy)

Abstract

The late Albian-early Turonian time interval was a time of major environmental changes. The Oceanic Anoxic Event (OAE) 1d and OAE2 and a series of other small carbon isotope excursions indicate important perturbations of the global carbon cycle. In this study we present new high-resolution oxygen and carbon isotope records from two Tethyan sections (Cismon and Monte Petrano, Italy). The two studied sequences deposited in carbonate pelagic settings characterized by the alternation of nannofossil-planktonic foraminiferal oozes, radiolarian-rich intervals and shales. High-resolution $\delta^{13}C$ records exhibit a long positive excursion of about 2.5-3‰ in correspondence of what is interpreted as OAE1d together with a large excursion of about 3-3.5‰ in $\delta^{13}C_{carb}$ and -22 to -21.5‰ in $\delta^{13}C_{org}$ in correspondence of OAE2. Between these two events a double-spiked excursion of about 2.5-3‰ in the $\delta^{13}C_{carb}$, represents the Mid-Cenomanian Event (MCE). Starting from this event up to the Bonarelli Level, the sedimentation shifts to alternated dysoxic/anoxic and well-oxygenated conditions as clearly represented by the lithologic rhythms of black shales/black chert bands and whitish limestones. The $\delta^{18}O_{carb}$ data indicate a general warming trend from late Albian up to Bonarelli Level, then followed by a rapid cooling. Oxygen isotopes indicate that OAE 1d was characterized by a relatively warm phase. The high-resolution $\delta^{13}C$ profiles across the OAE2 interval of both the Cismon and Monte Petrano sections highlight the presence of a hiatus eliding the upper part of the isotopic excursion. Such

hiatuses might be the result of physical and/or chemical phenomena that need further investigations to be unambiguously identified.

Key-words: Cenomanian, high-resolution C-isotope record, high-resolution O-isotope record, MCE, OAE1d, OAE2

5.1 Introduction

The mid-Cretaceous was characterized by temperatures much higher than today (Hay, 2008; Jenkyns, 1999, 2003) with ice-free polar regions for most of the time (e.g. Hallam, 1985 and Hallam, 1994; Takashima et al., 2006). A massive increase in CO_2 from two to ten times higher than present day has been inferred to cause greenhouse conditions (Barron and Washington, 1985). Plate boundary re-arrangement accompanied by massive submarine and subaerial volcanic episodes seems to be at the origin of the excess atmospheric CO_2 (Neal et al., 2008; Jenkyns, 2010).

The Late Albian to Early Turonian represents a peculiar time in Earth history: transient to prolonged perturbations of the global carbon cycle alternated with phases of stable conditions (Jarvis et al., 2006). During the latest Albian the oceans became progressively reduced, favoring the deposition of organic-rich shales. The Pialli Level and the Breistoffer Event are the sedimentary expression of the latest Albian Oceanic Anoxic Event (OAE) 1d (Arthur et al, 1990) characterized by a $\delta^{13}C$ positive excursion of ~1‰ reaching values of about 2.5‰ in carbonate carbon (Ccarb) (Wilson and Norris, 2001; Gröcke et al., 2006; Petrizzo et al., 2008; Giorgioni et al., 2012). Wilson and Norris (2001) suggest that during OAE 1d the well-stratified water column collapsed abruptly due to intensified winter mixing and reduced summer stratification. According to Bornemann et al. (2005) instead, the black shales deposition occurred at times of increased surface-water stratification and decreased deep-water formation due to orbitally induced increase in monsoonal activity.

The Mid-Cenomanian Event (MCE) has been interpreted as the precursor of a global palaeoclimatic and palaeoceanographic change that led to the catastrophic Bonarelli Event (OAE 2) (e.g. Coccioni and Galeotti, 2003). The MCE carbon isotopic excursion has been widely observed in both the Boreal and Tethyan Realms and in the Atlantic Ocean (Friedrich et al., 2009 and references therein). The MCE is not characterized by widespread formation of organic-rich sediments, but is frequently associated with distinctive lithological changes (Coccioni and Galeotti, 2003). Related to this event changes in the marine biota affected dinoflagellates, radiolarians, nannofossils, benthic and planktic foraminifera,

bivalves, ammonites, and belemnites (e.g. Paul et al., 1994; Erbacher et al., 1996; Erbacher and Thurow, 1997; Mitchell and Carr, 1998; Coccioni and Galeotti, 2001; Wilmsen, 2007; Friedrich et al., 2009; Giraud et al., 2013)

The OAE2 is characterized by a positive excursion of the $\delta^{13}C$ record of about 2-3‰ in carbonate carbon (C_{carb}) and up to 6‰ in organic carbon (Jenkyns, 1980, 1985, 2010; Scholle and Arthur, 1980; Schlanger et al. 1987; Elrick et al., 2009). The most spectacular sedimentary expression of the OAE2 is the Bonarelli Level in the Italian Umbria-Marche Basin (Bonarelli, 1891), a bituminous radiolarian-rich interval that testifies widespread distribution of anoxic conditions in the oceans during the latest Cenomanian (Schlanger and Jenkyns, 1976; Arthur et al., 1990; Jenkyns, 2010). This event is conventionally interpreted as the consequence of accelerated burial of marine organic matter (e.g. Herbin et al. 1986; Arthur et al. 1990; Kuypers et al. 2002, 2004; Jarvis et al., 2006). The OAE2 lasted about 500ka with the extintion of approximately 27% of marine invertebrates (Hay, 2008). Many biota were strongly affected by this event (Bralower, 1988; Premoli Silva and Sliter, 1994; Luciani and Cobianchi, 1999; Premoli Silva et al., 1999; Leckie et al., 2002; Erba, 2004; Friedrich et al., 2006; Hardas and Mutterlose, 2007; Monnet, 2009; Lebedel et al., 2013). The OAE2 was charactherized by diffused anoxia with times of free hydrogen sulfide (e.g. Scoppeliti et al., 2006; Hetzel et al., 2009; Owens et al., 2012) and widespread deposition of organic matter.

In this study we present new oxygen and carbon isotopic data from two Italian pelagic sequences deposited during the late Albian-early Turonian time interval, namely the Monte Petrano and Cismon sections from the Umbria-Marche and Belluno Basins, respectively. The high-resolution records, are used to correlate sections at regional to global scale in order to identify and quantify paleoenvironmental perturbations and possible hiatuses

5.2 Geological setting and studied sections

The 70.5m-thick studied interval of the Monte Petrano section is located in the Umbria-Marche Basin not far from the Moria village (Schwarzacher, 1994; Giorgioni et al., 2012) (Fig. 5.1). This basin is characterized by a continuous pelagic sedimentation of Jurassic to Oligocene age. The sedimentary sequence deposited on the continental crust of the Adria microplate (Channell et al., 1979a) in a complex basins and swells setting (Alvarez, 1990).

The studied interval corresponds to the Scaglia Bianca Formation consisting of whitish pelagic limestones resulting from lithification of nannofossil-planktonic foraminiferal oozes (Arthur and

Premoli Silva, 1982) with chert bands, radiolarian layers and shales as minor lithologies (Parisi, 1989). A 80cm thick black shale radiolarian-rich level in the upper part of the section corresponds to the Bonarelli Level.

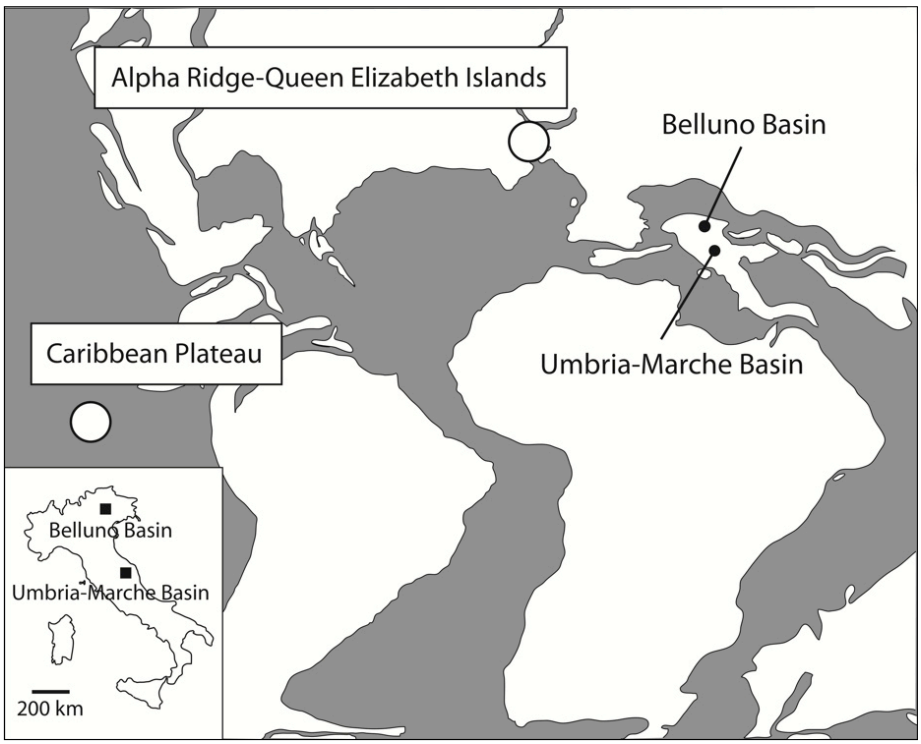

Figure 5.1: Present-day and paleogeographic position of the studied sections.

The Cismon section is located in Southern Alps not far from the Lamon village in north-east Italy (Channell et al., 1979b; Bellanca et al., 1996) (Fig. 5.1). The analyzed sequence consists of a 60m thick interval of the Scaglia Variegata Formation (Channell et al., 1979a), deposited on the southern margin of the Tethys, and is represented by the alternation of yellowish to grayish micritic limestone, radiolarian layers, chert bands and shales (Channell et al., 1979b; Claps et al., 1991, 1994; Bellanca et al., 1996). Few meters before the lithostratigraphic boundary to the overlying Scaglia Rossa, a 35cm thick Bonarelli Level is the lithological expression of the OAE2 in this basin. The sequence is disturbed by frequent faults and ductile structural deformation. In particular, we have identified a major fault at about 45m. At about meter 11 a slump with a clear base surface deforms the sequence.

5.3 Methods

At Monte Petrano section a total of 300 samples were collected for stable oxygen and carbonate carbon isotope. In particular in the lower 50 meters of the section, samples were taken with a sampling step of 25cm, while from 10 meters below to 10 meters above the Bonarelli Level, samples were collected every 10cm. Additionally, 9 regularly-spaced samples from the Bonarelli layer together with 9 black shales from the interval below the Bonarelli were collected for organic carbon stable isotopes.

At Cismon section a total of 209 samples were collected, in particular: from the base of the section to 29m with a sampling rate of 25cm; from about 29m to 34m no samples were recovered due to the presence of coverage; from 34m to 49.75m with a sampling rate of 50cm; from 50.1 to 57.9 every 20cm and finally every 10cm from 58m up to 59.9m. For organic carbon stable isotopes 5 dark grey shales were ollected together with 5 regularly-spaced samples from within the Bonarelli Level.

For both sections sampling was accurately done on fresh surfaces in order to minimise weathering effects. Efforts were made to avoid veins and fractures.

Samples of fine-grained limestones were analysed isotopically for $\delta^{13}C$ and $\delta^{18}O$ using a VG Isogas Prism II mass spectrometer with an on-line VG Isocarb common acid bath preparation system. Samples were dosed with acetone ($(CH_3)_2CO$) and dried at 60°C for at least 30 minutes. In the instrument they were reacted with purified phosphoric acid (H_3PO_4) at 90°C. Calibration to PDB standard via NBS-19 was made daily using the Oxford in-house (NOCZ) Carrara marble standard. Reproducibility of replicated standards is usually better than 0.1‰ for $\delta^{13}C$ and $\delta^{18}O$. Potential memory effects using the VG Isocarb common acid-bath system can be of the order of 1‰. Adjacent samples of widely dissimilar isotopic composition were reanalysed, or run with blanks between. Stable isotope ratios are reported using the conventional δ notation to indicate deviation from the arbitrary PDB standard.

For organic carbon stable isotopes, samples were crushed with an agate mortar and pestle to <125 μm. Carbonate was removed by treating 1-2g of sample with 30ml 1% HCl, and heating on a hot plate for about 2h. This phase was repeated many times replacing the exhausted acid with new one until the colour of the reacted solution became pale yellow. The acid-treated samples were then transferred to a centrifuge tube, and washed with Milli-Q water and centrifuged. Every sample was further washed in order to reach a neutral pH, then dried in an oven at about 60°C for minimum 24h. Few grams of treated sample (from about 5 up to 10mg according to the amount of organic carbon content) were then put into a tin capsule. Stable carbon-isotope composition and C/N ratio were measured on a CF-IRMS

system, which is composed by a combustion elemental analyzer (a Carlo-Erba NA 2000) coupled to a gas source isotope ratio mass spectrometer (Sercon GSL). Samples were combusted and converted to N_2 and CO_2, which are separated in a GC column packed with CarbosieveTM (Supelco G60/80 mesh; Bellefonte, Pennsylvania, USA) packing medium, while water was removed thanks to a chemical trap. Helium was used as carrier gas with a stream of 100 mL/min. Together with the set of samples Alanine was used as internal standard. Sample isotopic ratios are reported as delta per mil relative to the VPDB international standards for carbon (Coplen 1994).

Selected black shale and dark grey shale samples from both sections were measured for carbonate content using the Dietrich-Frühling gas volumetric method by measuring evolved CO_2 after acidification of the bulk sample with HCl. In particular 86 samples from Cismon section and 17 samples from Monte Petrano section were collected.

Rock Eval Pyrolysis was performed on 19 black shales samples from the Monte Petrano section and 23 dark grey shales and black shales from the Cismon section. Additional 7 samples were simply analysed for Total Organic Carbon (TOC) on a Coulomat 702.

5.4 Results

5.4.1 Oxygen- and carbonate carbon-isotope data

For the Monte Petrano section the measured bulk $\delta^{13}C_{carb}$ values vary between 1.7‰ and 3.5‰ (Fig. 5.2). Unpublished nannofossil biostratigraphic data produced by Fabio Russo during his PhD thesis (Russo, 2013) are here used to date the latest Albian to early Turonian time interval.. The lower part of the section, after a slight decrease in $\delta^{13}C$ values from 2.3‰ to 2‰, is characterized by a $\delta^{13}C$ excursion (carbon isotope excursion, CIE) up to values of about 3‰ corresponding to the OAE1d. In this interval four different peaks are ascribable to the four peaks (named ‘a’ to ‘d’) as defined by Kennedy et al. (2004).

The $\delta^{13}C$ background values of about 2‰ reached after the OAE1d are interrupted in the NC11* nannofossil biozone by a brief excursion up to 2.9‰ corresponding to the MCE with two individual peaks ‘a’ and ‘b’ as described by Jarvis et al. (2006). After this event the $\delta^{13}C$ progressively climb up to values of about 2.7‰ before reaching the base of the Bonarelli Level. The lowermost limestones above the Bonarelli, in the NC13** nannofossil biozone, show values of about 3.5‰ and the curve progressively decreases to values of about 2.7 ‰.

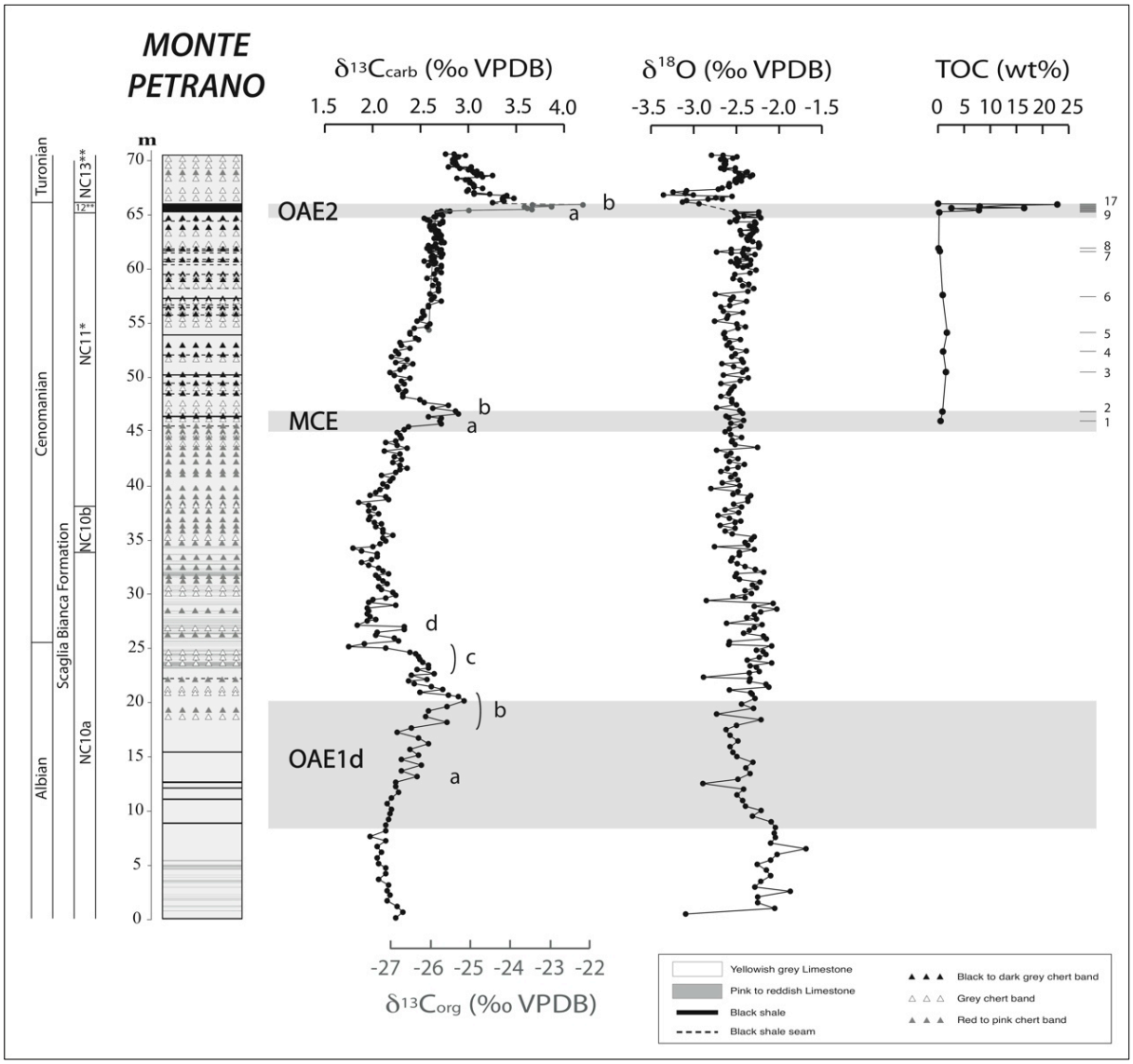

Figure 5.2: Monte Petrano schematic section. Nannofossil biostratigraphy, isotopic composition ($\delta^{13}O_{carb}$, $\delta^{13}O_{org}$ and $\delta^{18}O_{carb}$) and Total Organic Carbon (TOC) are illustrated from left to right. The samples collected for RockEval are numbered from 1 to 17.

Along the section $\delta^{18}O_{carb}$ values range between -1.7‰ and -3.3‰. A minor decrease is observed across the OAE1d and then the profile remains rather stable around 2.5‰. The interval immediately preceding the Bonarelli Level shows an overall shift from lower to slightly higher values. The highest values are reached right after the Bonarelli Level and then rapidly increase back to -2.5‰ about 2 meters above the top of the Bonarelli.

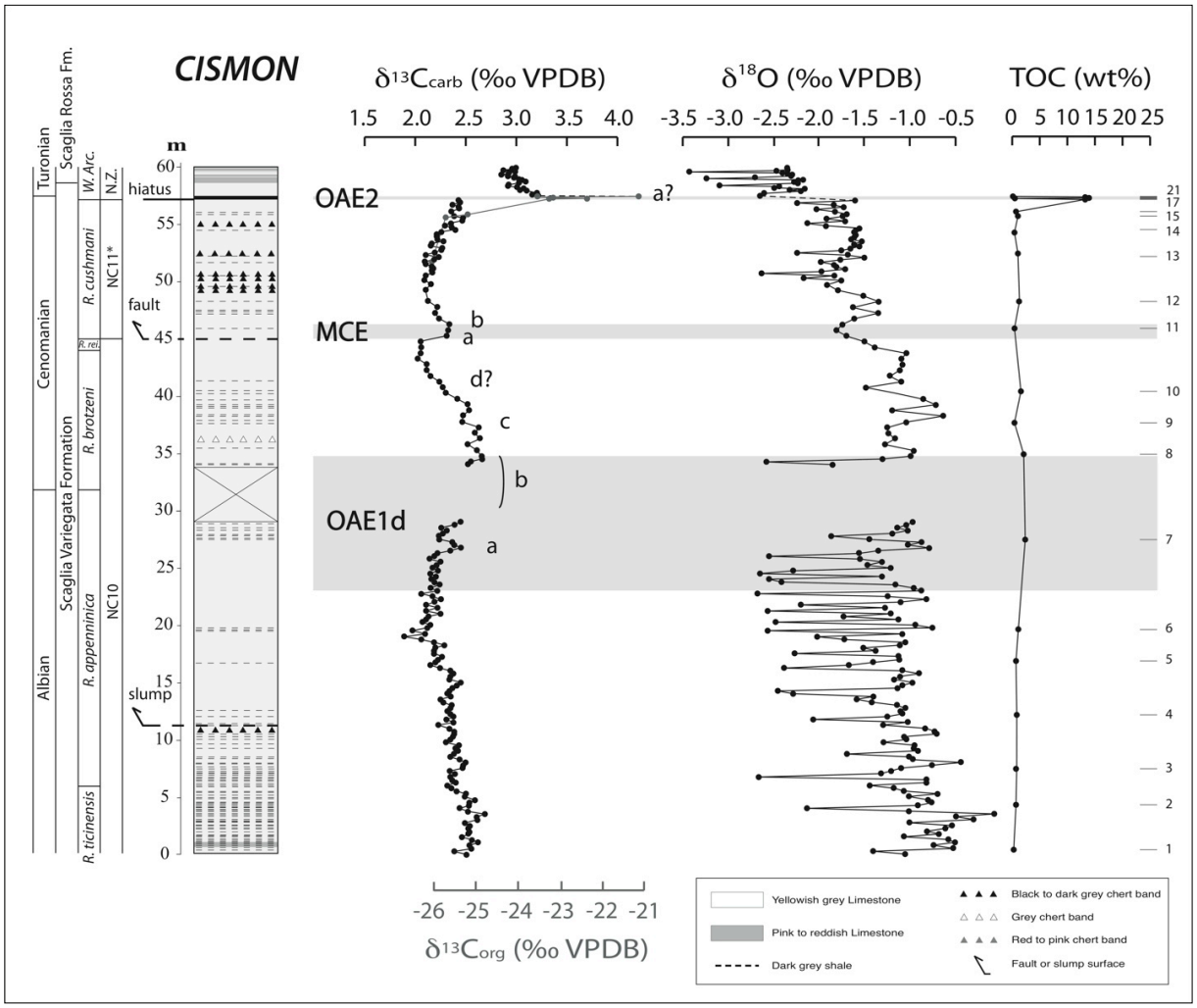

Figure 5.3: Cismon schematic section. Foraminifera and nannofossil biostratigraphy, isotopic composition ($\delta^{13}O_{carb}$, $\delta^{13}O_{org}$ and $\delta^{18}O_{carb}$) and Total Organic Carbon (TOC) are illustrated from left to right. The samples collected for RockEval are numbered from 1 to 21.

In the Cismon section $\delta^{13}C_{carb}$ values range from 1.9‰ up to about 3.2‰ (Fig. 5.3). Both planktonic foraminiferal and nannofossil biozones are partially modified after Bellanca et al. (1996) (Premoli Silva and Erba, unpublished data). The lower part is characterized by a general decrease of the values from about 2.5‰ to about 2‰. The typical shape of the OAE1d long-lasting CIE presents $\delta^{13}C_{carb}$ values of about 2.6‰. Due to the coverage seems that only three of the four peaks described by Kennedy et al. (2004) are recognized. The 'a' peak is not identified and should fall in the part where no samples were collected. The rapid decrease of the values after the OAE1d in the *R. brotzeni* biozone is sharply interrupted by the fault at about 45 m of the sequence. Right after the fault, in the *R.cushmani* foraminiferal biozone, the values jump to about 2.3‰ as a result of what we interpret as the MCE. In the interval preceding the Bonarelli Level, values progressively rise from about 2‰ to about 2.5‰.

After the Bonarelli Level limestones record values from 3.1‰ down to 2.9‰. $\delta^{18}O_{carb}$ values range between -0.5‰ and 3.5‰. The lowermost part is characterized by a progressive decrese towards lower values with an interesting cyclic pattern. Unfortunately not much can be said on the OAE1d due to the presence of the coverage. From this event up to the fault at 45m the trend is almost constant around -1.3‰. Around the MCE the $\delta^{18}O_{carb}$ shows a short negative excursion to about -2‰ followed by values oscillating from -2.5‰ up to -1.5‰. The interval above the Bonarelli Level, apparently still cyclic, is characterized by an overall increasing trend.

5.4.2 Organic carbon-isotope data

In the Monte Petrano section, the bulk $\delta^{13}C_{org}$ values vary between −22.2‰ and −25.9‰ (Fig. 5.2). The lower part of the curve rapidly rise from -25.9‰ up to about -23.4‰ and then gently rise up to -22.2‰ to reach what can be possibly interpreted as the 'a' peak as described in e.g. Jarvis et al. (2006).

In the Cismon section the bulk $\delta^{13}C_{org}$ values range between -21.1‰ and -23.6‰ (Fig. 5.3). Despite the limited number of samples, the curve shows a short increase of the values from about -23.3‰ to about -22.4‰. The middle part exhibits a decrease to values of about -23.6‰ rapidly followed in the upper part by a quick increase to about -21.1‰.

Although the absolute values are slightly different in the two sections, the two curves can be correlated.

5.4.3 Calcimetry and Rock-Eval data

The carbonate content of the collected samples from the Monte Petrano and Cismon sections are schematically presented in Fig. 5.4. Together with these results additional unpublished data relative to the Furlo section (CT-Net, Bombardiere unpublished data) are illustrated. All the samples collected from the different Bonarelli Levels are characterized by extremely low carbonate content. Instead, both at Monte Petrano and at Furlo, the black shale layers below the Bonarelli Level show a quite large range of values, spanning from 10 to 90%. The carbonate content of the dark grey layers at Cismon on the other hand is characterized by a more limited range of values from 30 to 80% with generally more homogeneous values around 50%.

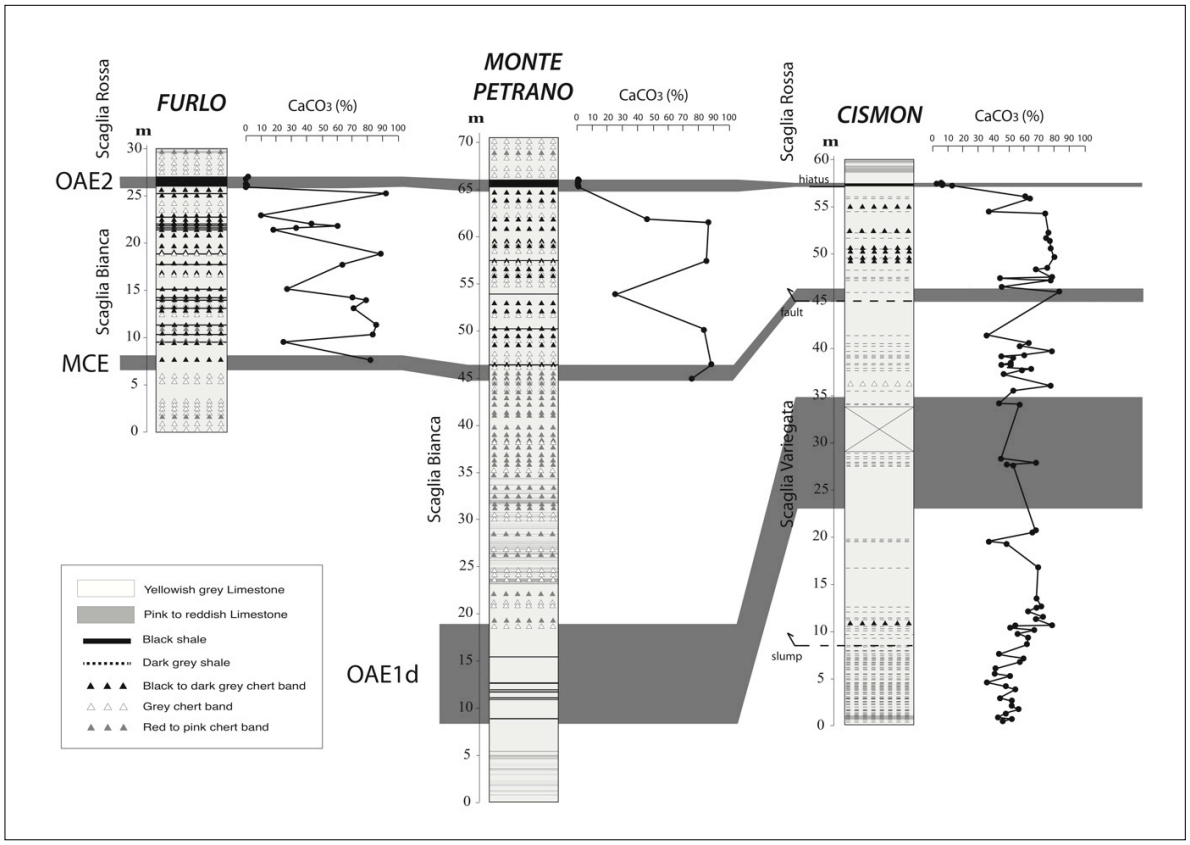

Figure 5.4: Carbonate content variation of the studied black shale and dark grey shales for the Monte Petrano and Cismon sections (present thesis) and by comparison with the Furlo section (Luca Bombardiere post-doc unpublished data).

The measured TOC content is reported in Figs. 5.2 and 5.3. In the Monte Petrano section, the highest TOC values are recorded in the Bonarelli Level ranging between 0.5% and ~23%, with a general increase in organic-carbon content in the upper part of the interval. As regards the black shales from the interval below the Bonarelli Level, TOC distributes between lower than 1% up to 2%. In the Cismon section TOC content of the dark grey shales is quite variable. In the lower part of the section, the highest values are in correspondence of the OAE1d with an average TOC of 2%. Above the MCE the few dark grey shales show a slightly higher organic-carbon content up to about 1.5%. Also in this section the Bonarelli Level is the interval characterized by the highest values ranging from lower than 1% up to about 14%.

In Figs. 5.5a and 5.5b, the van Krevelen diagrams (van Krevelen, 1950) relative to the measured samples from the studied sections are presented. Both black shales and dark grey shales below the Bonarelli Level from both the sections present values lower than 300 mg HC/g C-org. The cross-plot with Oxygen Index (OI) data indicate a type II organic matter for these levels. Samples from the Bonarelli Level at Monte Petrano show quite a large range of Hydrogen Index (HI) values ranging

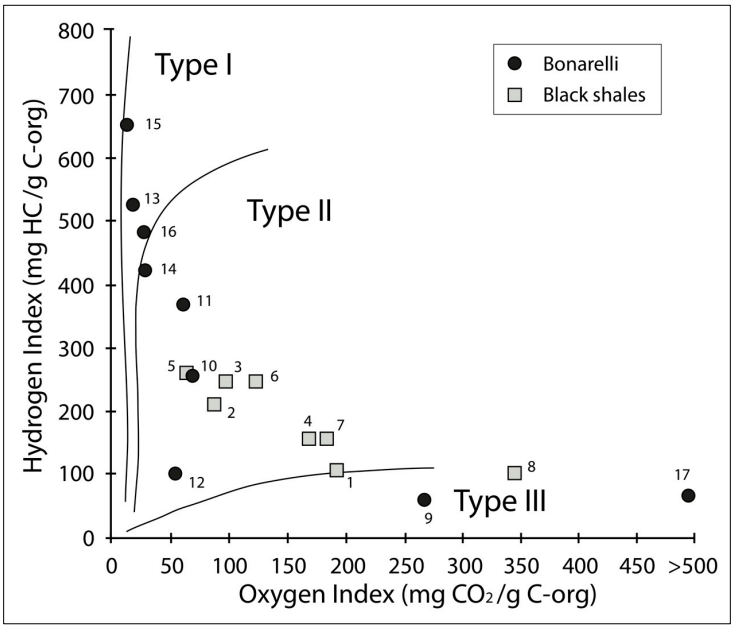

Figure 5.5a: Van Krevelen diagram for the Bonarelli and black shale samples from the Monte Petrano section. The numbers are referred to the collected samples for RockEval as reported in Fig. 5.2.

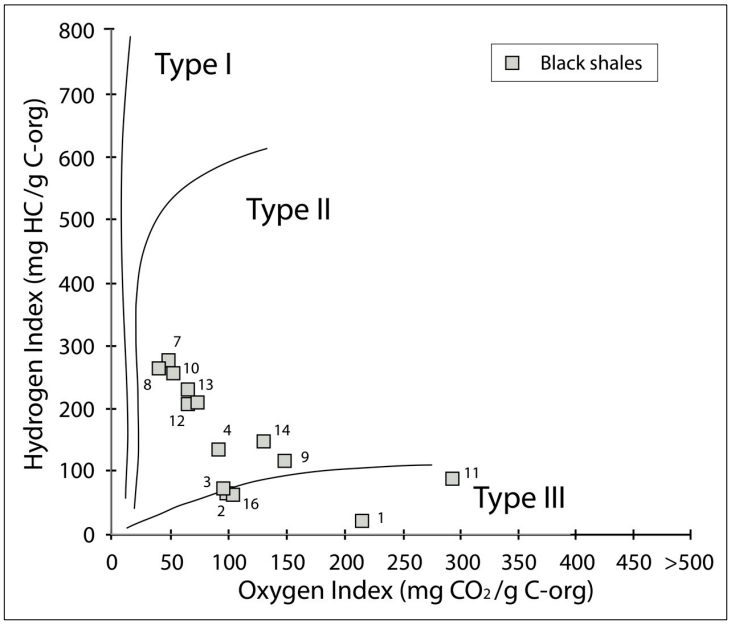

Figure 5.5b: Van Krevelen diagram for the Bonarelli and dark grey shale samples from the Cismon section. The numbers are referred to collected samples for RockEval as reported in Fig. 5.3.

from 100 up to 700 mg HC/g C-org indicative of primary algal and/or bacterial productivity with a type I to type II organic matter. Observed samples lying in the Type III area could represent very oxidised planktonic organic matter (Tissot and Welte, 1978). Measured Tmax in both the sections is about 435°C.

5.5 Discussion

5.5.1 Other sections from the Umbria-Marche Basin

The two studied sections are correlated with other sections in the Umbria-Marche Basin, that were revisited in detail for sedimentology and lithostratigraphy. Additional unpublished and published isotopic data from Furlo, Contessa and Le Brecce sections are here presented.

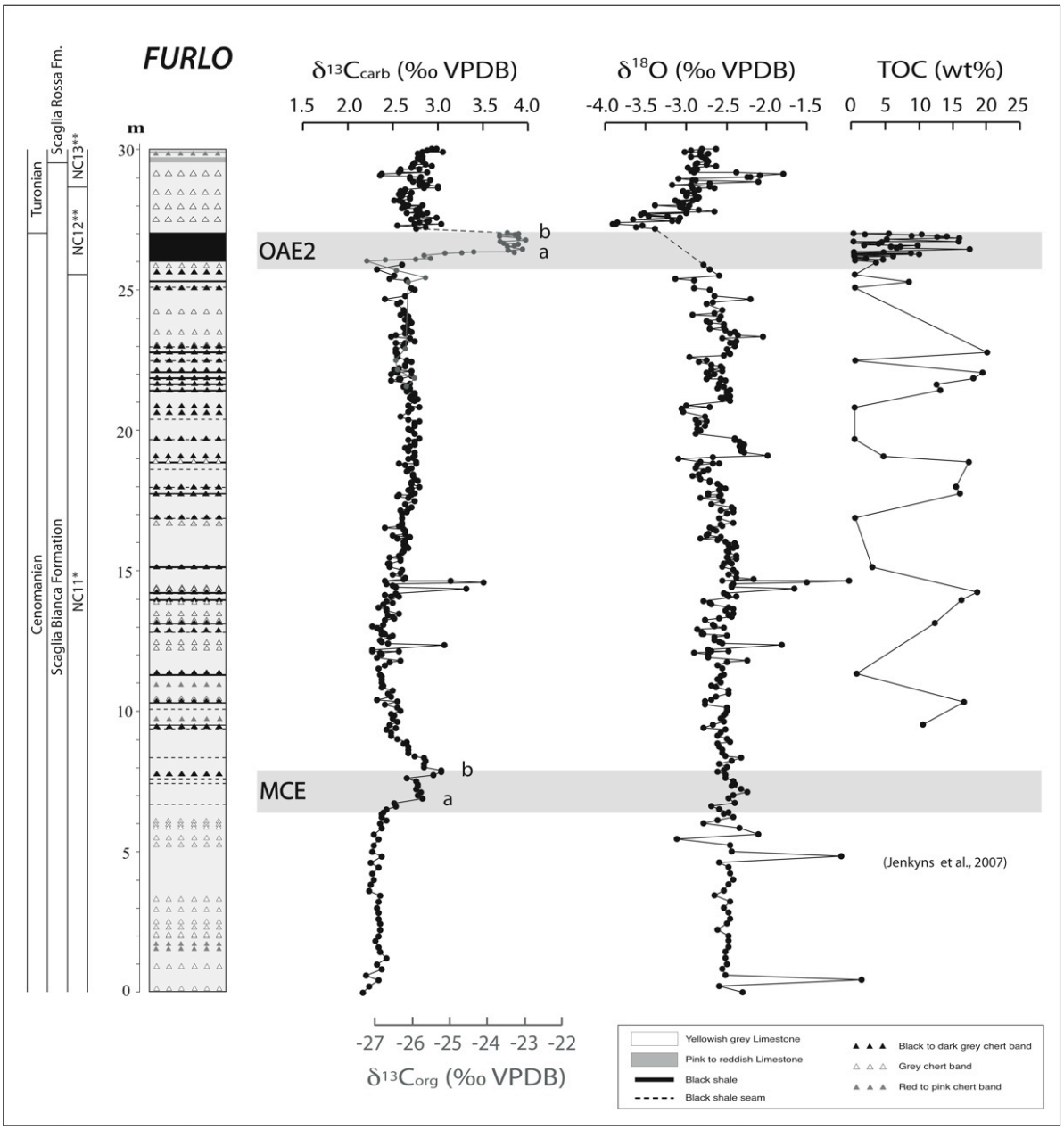

Figure 5.6: Nannofossil biostratigraphy, lithostratigraphy, and isotopic composition ($\delta^{13}O_{carb}$, $\delta^{13}O_{org}$ and $\delta^{18}O_{carb}$) of the Furlo sections. Total Organic Carbon (TOC) from Jenkyns et al. 2007

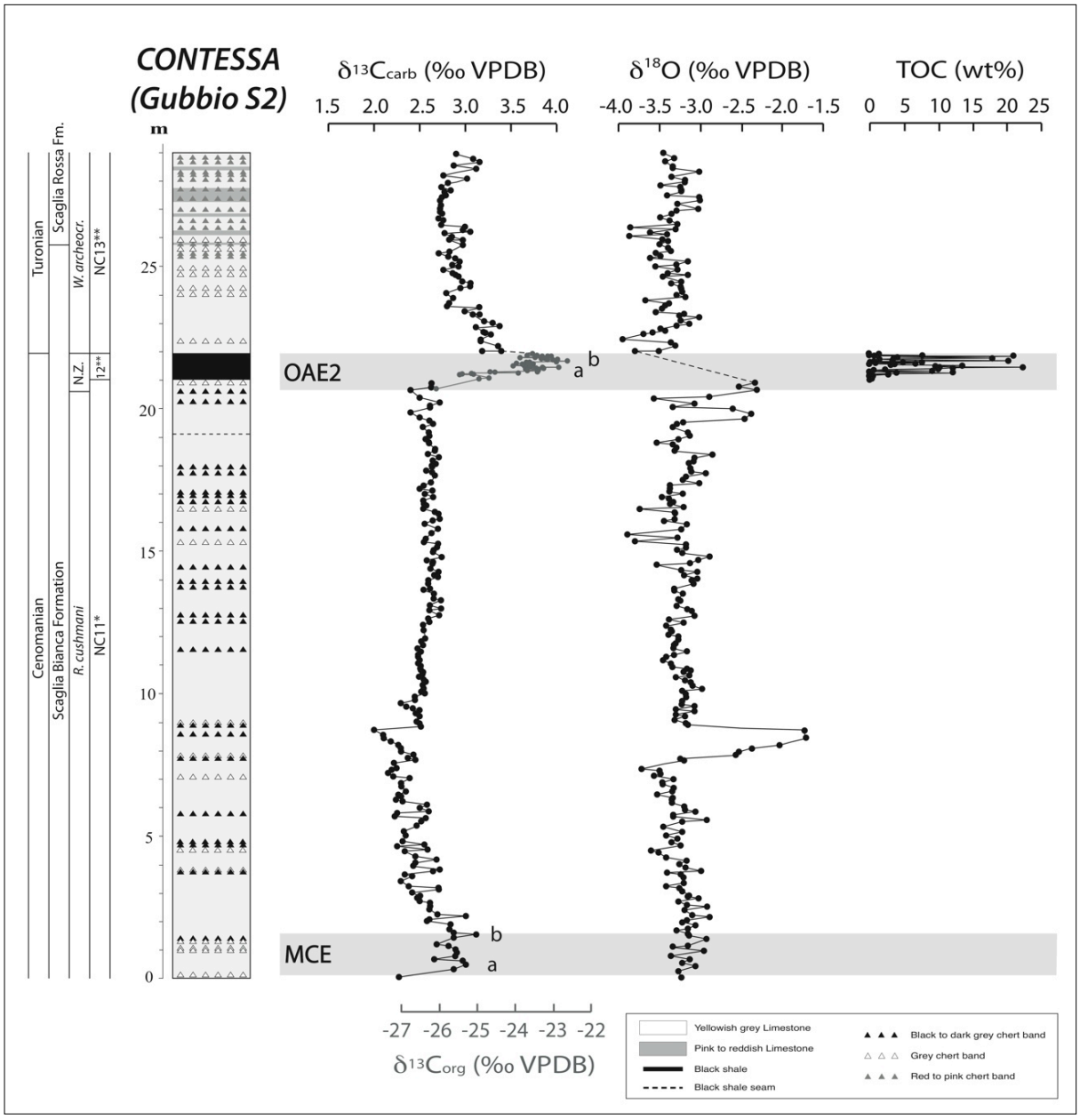

Figure 5.7: Planktonic foramineral and nannofossil biostratigraphy, lithostratigraphy, isotopic composition ($\delta^{13}O_{carb}$, $\delta^{13}O_{org}$ and $\delta^{18}O_{carb}$) and Total Organic Carbon (TOC) of the Contessa section

The Furlo section was studied during the EU CT-Net research program (Turgeon & Brumsack, 2006; Tamagnini, 2007; Lanci et al., 2010). The unpublished isotopic curve is here presented in Fig. 5.6. The biostratigraphic data is slightly modified after Lanci et al. (2010) (Erba, unpublished data). TOC data are from Jenkyns et al. (2007).

Carbon and oxygen isotopic curves for the Contessa section were firstly published by Stoll and Schrag (2000). Additional high-resolution isotopic data focused on the Scaglia Bianca cored at Gubbio site 2

were published by Tsikos et al. (2004) and here illustrated in Fig. 5.7. The planktonic foraminiferal biostratigraphy is extrapolated from Premoli Silva and Sliter (1994). Nannofossil biozonation was described in Tsikos et al. (2004) and partially changed using the revision of Fabio Russo (Russo, PhD thesis 2013). TOC data are from Luca Bombardiere's unpublished data archived within the CT-Net database.

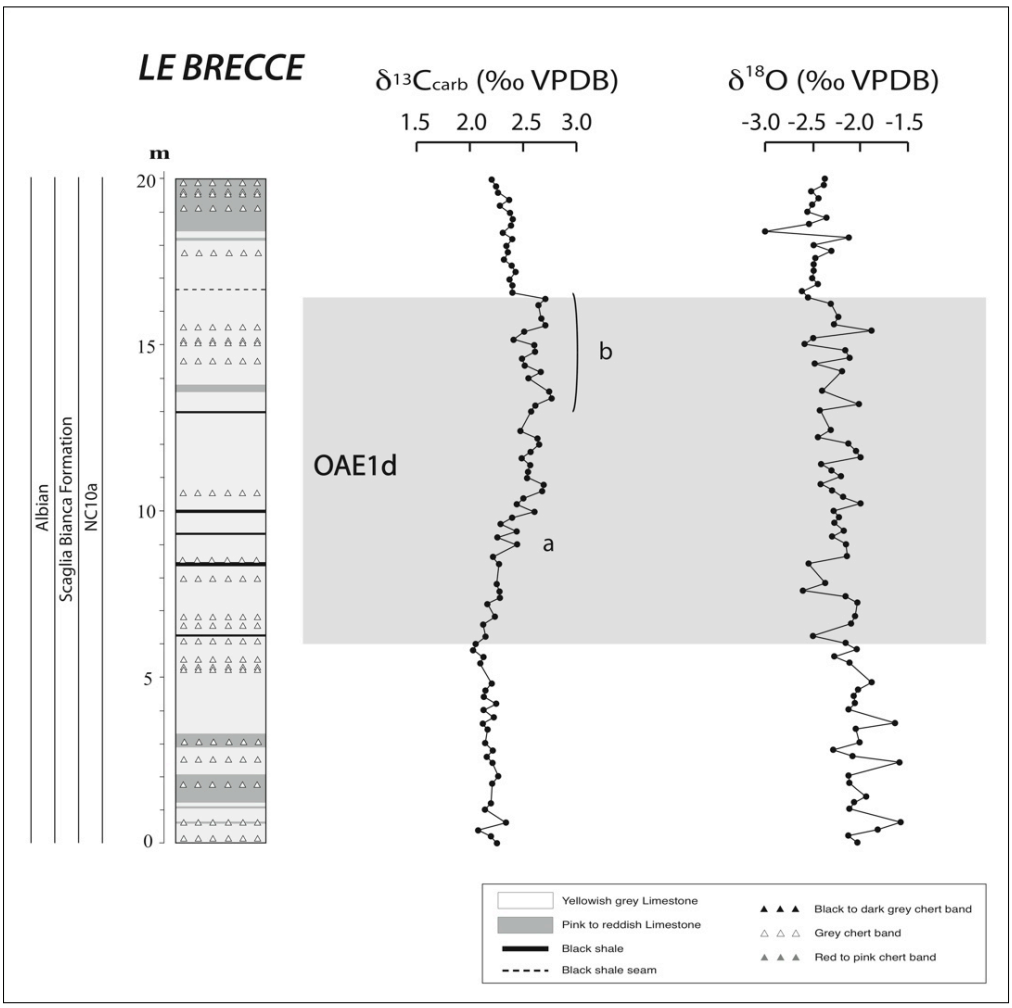

Figure 5.8: Nannofossil biostratigraphy, lithostratigraphy and isotopic composition ($\delta^{13}O_{carb}$, $\delta^{13}O_{org}$ and $\delta^{18}O_{carb}$) of Le Brecce section.

Le Brecce section was studied for biostratigraphy by Daniele Tiraboschi (Tiraboschi, PhD thesis 2009) while isotopes were measured by Paul A.Wilson and reported in Tiraboschi's PhD thesis (Fig. 5.8).

Following Erba et al. (2004) and Tsikos et al. (2004) in all the presented sections we have decided to define OAE1d, MCE and OAE2 on the basis of carbon isotopic stratigraphy. We have identified the

base of the event at the beginning of the $\delta^{13}C$ excursion and its top at the highest value before the decrease to lower values.

Fig. 5.9 illustrates the correlation of all the studied sections. The shape of the $\delta^{13}C$ curve in the latest Albian-earliest Turonian is characterized by reproducible trends that are used for high-resolution dating and correlations. Among the five studied sequences the Cismon section is the only one that is characterized by major discontinuities: a fault removes part of the MCE and the interval preceding it, another hiatus elides the base of the Bonarelli Level and the underlying interval.

The OAE1d carbon isotopic excursion can be well correlated in all the three sections that cover this stratigraphic interval. The MCE with its two peaks, even if with slightly lower absolute values at Cismon, is clearly traceable throughout the various sequences. The high $\delta^{13}C$ values reached during the OAE2 excursion are evident in all the sections both on carbonate- and organic-carbon isotopes.

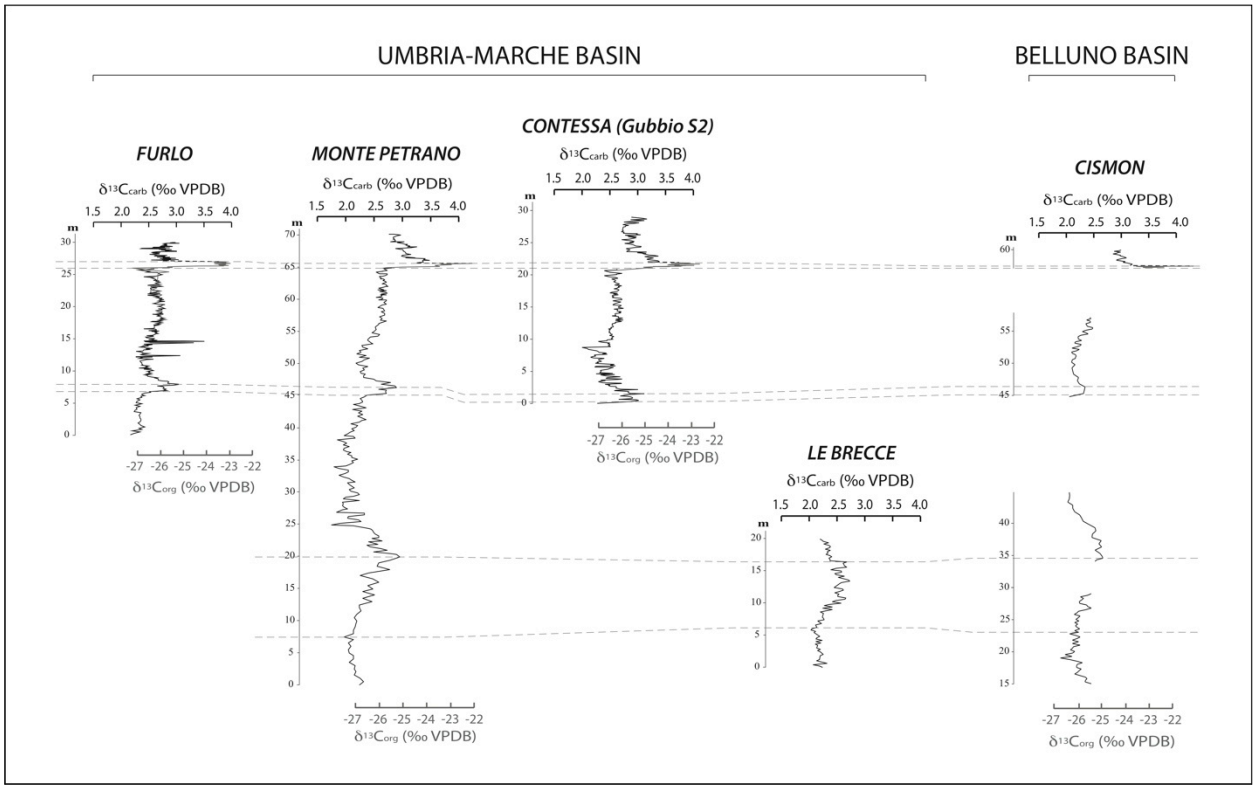

Figure 5.9: Chemostratigraphic correlation of the Monte Petrano and Cismon sections with Furlo, Contessa and Le Brecce sections. The base and the top of the carbon isotopic excursions corresponding to the OAE1d, MCE and OAE2 are correlated in all five sections.

5.5.2 Major perturbations to the global carbon cycle and their relation with lithology and sedimentology

The lithologic expression of the so-called Pialli Level (Coccioni and Galeotti, 2003) is represented by an interval with six and five black shales at Monte Petrano and Le Brecce, respectively. This lithostratigraphic interval doesn't correspond to the whole carbon isotopic excursion, since it is limited to its lowermost ascending part. At Cismon, the same stratigraphic interval does not contain black shales, but few dark grey shales with relatively higher values of TOC (around 2%) have been observed.

The MCE, as already documented (e.g. Jenkyns et al., 1994; Coccioni and Galeotti, 2003), is associated to distinctive lithological changes. Sedimentation shifts to alternate dysoxic/anoxic and well-oxygenated conditions starting from the MCE as clearly represented in the Umbria-Marche Basin at Furlo by the presence of frequent black shales and black chert bands alternated with whitish limestones, corresponding to member W4 sensu Coccioni and Galeotti, 2003. In particular black chert bands start to appear exactly within the MCE and continue to occur up to the Bonarelli Level.

In all the presented sections, after the positive excursion of the MCE the carbon-isotope profile shows a through with lower $\delta^{13}C$ values followed by a progressive increase up to OAE2.

In the Cismon section black chert bands and dark grey shales with slightly higher TOC content up to 1.5% begin from the MCE event. Both at Furlo and Monte Petrano the lowermost part of the MCE excursion is characterized by a thin black shale seam, while in correspondence of the highest $\delta^{13}C_{carb}$ values a black chert band is observed.

A possible correlation of the MCE isotopic excursion with a massive volcanic event is here hypothesized. A precursor activity of the massive Caribbean Large Igneous Province (LIP) or the emplacement of any other major volcanic province, could have been at the origin of the perturbation of the global carbon cycle. The initial development of the Alpha Ridge-Queen Elizabeth Islands LIP (Embry and Osadetz, 1988) could be one of the possible triggers. Tarduno et al. (1998) have supposed an approximate age of about 95My, while Verzhbitsky et al. (2012), on the basis of thermal flow data, have estimated an age of about 97-79 My for the formation of this large structural element of the Amerasian Basin.

Whether or not the MCE was triggered by a major volcanic episode, as already suggested by other authors (Coccioni et al., 1995; Friedrich et al., 2009) it seems to represent a turning point in mid-Cretaceous paleoceanography. Considering the difference of magnitude of this event in comparison to the OAE2, the MCE was probably an independent event not necessarily connected to the OAE2. However, all data indicate that starting from the MCE there was a general switch to more unstable

conditions and rhythmically oxygen-depleted bottom-waters. The $\delta^{13}C$ positive excursions of OAE1d, MCE and OAE2 can be attributable to removal of light organic carbon due to widespread deposition and burial of organic matter although massive Corg-rich black shales are known only for OAE2 (Bonarelli Level and its equivalents). In all the studied sequences the OAE2 isotopic excursion corresponds to black shales with high TOC concentrations (up to more than 20%) and $CaCO_3$ close to zero. As described by Tsikos et al. (2004) the black shales are diachronous with respect to the OAE2 isotopic excursion.

As already stated by Stoll and Schrag (2000) for the Contessa section, we exclude that the general shift of the $\delta^{18}O_{carb}$ from heavier to lighter oxygen-isotopes observed in all the studied sections is the result of diagenesis. It's quite unlikely that diagenetic overprint produces similar artifacts at different sites. We interpret these data as the result of a general shift to warmer conditions from the latest Albian up to the OAE2. The lowest values in $\delta^{18}O_{carb}$ in the limestones right above the Bonarelli Level suggests warm conditions in correspondence of this analysed interval, followed by a general cooling trend towards the uppermost part.

Intervals with higher $\delta^{18}O_{carb}$ well correspond to reddish limestones and red chert bands, thus suggesting that their deposition happened during generally cooler temperatures. The OAE1d is characterized by generally low $\delta^{18}O$ values, indicating warmer conditions associated with this event. Instead no clear $\delta^{18}O_{carb}$ signals seem to be associated with the MCE.

5.5.3 Stratigraphic hiatuses associated with the OAE2

Voigt et al. (2007) noticed that the values reached by the $\delta^{13}C_{carb}$ curve in the interval above the Bonarelli Level at the Contessa site (Core Gubbio 2 in Tsikos et al., 2004) are clearly too low to be considered as the 'c' peak as described in complete Cenomanian/Turonian boundary interval successions (e.g. Sageman et al., 2006). Therefore, they supposed that the upper part of the $\delta^{13}C$ anomaly is elided and that the record immediately above the Bonarelli Level represents the 'd' peak.

Moreover, the organic-carbon curve compared to the GSSP reference section at Pueblo (Colorado) (Sageman et al., 2006) adds further interesting insights. While the 'a' and 'b' peaks and part of the 'plateau' are apparently recorded, the end of the plateau with the 'c' peak and the first part of the decrease seem to be missing. We interpret these results as a clear evidence of an important hiatus in correspondence of the upper part of the OAE2 excursion and the immediately following interval (Fig. 5.10).

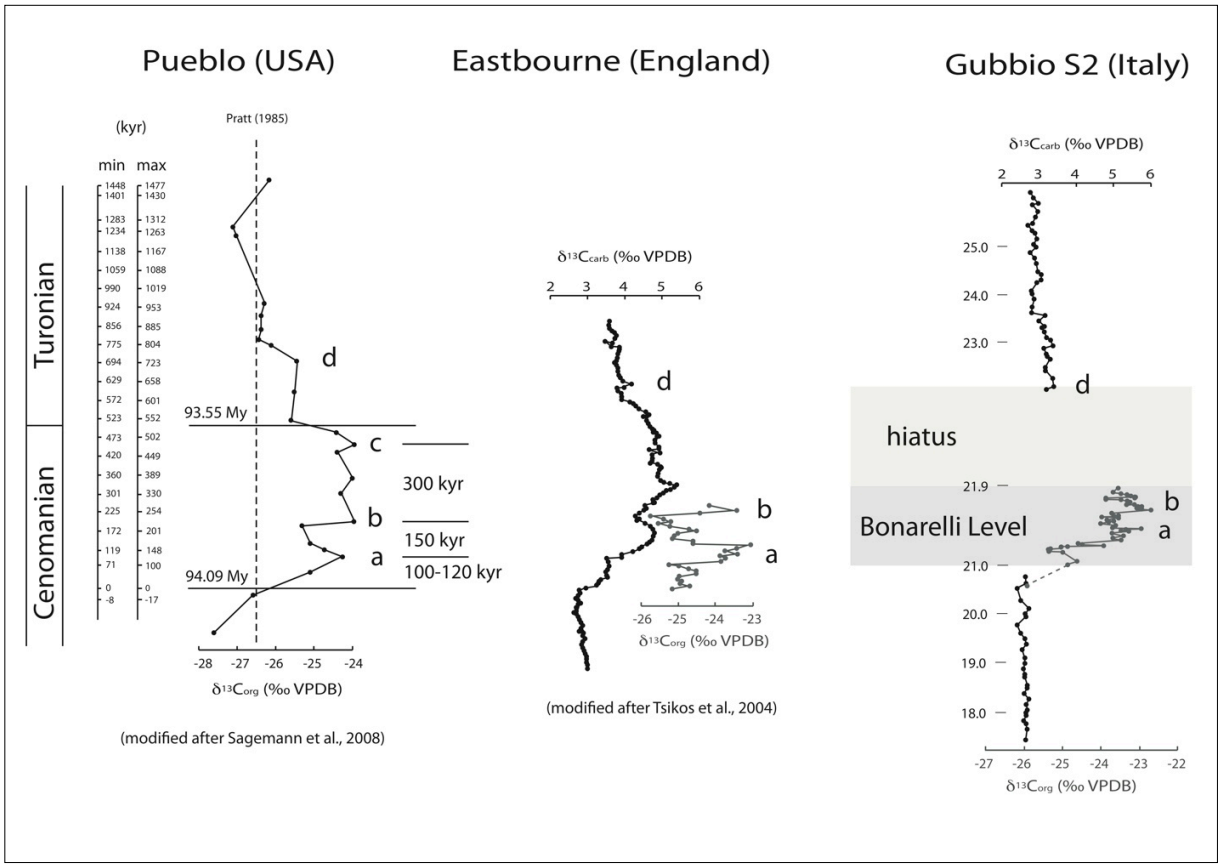

Figure 5.10: Comparison of the carbon isotopic profiles for the OAE2 interval at the GSSP key-locality of Pueblo (Colorado) and the English section of Eastbourne with the Contessa section in Italy (Gubbio S2, Tsikos et al., 2004). Chemostratigraphic correlation suggests the presence of a hiatus at the top of the isotopic excursion. See text for explanation.

The measured carbonate- and organic-carbon isotopic values in correspondence of the OAE2 for the studied sections are illustrated in detail in Fig. 5.11. The $\delta^{13}C_{carb}$ and $\delta^{13}C_{org}$ data show similar patterns and values in all the studied sequences, thus suggesting a widespread hiatus in the upper part of the isotopic excursion, with variable amount of missing sequence from section to section. It is worth mentioning that, in all the studied sections from the Umbria-Marche Basin, the beginning of the isotopic excursion coincides with the so-called 'black marker' as defined by Montanari (1985).

In Fig. 5.12 is shown the comparison between the oxygen isotopic record at Eastbourne (England) (Tsikos et al., 2004) and the already presented record at Gubbio S2 (Tsikos et al., 2004). The alternation between warm and cool phases is highlighted, such as the Plenus cold Event (Jarvis et al., 2011). As a consequence of the hiatus identified thanks to $\delta^{13}C_{carb}$ correlation, an important part of the $\delta^{18}O$ record is missing. The lowermost part of the preserved interval above the Bonarelli Level can be correlated to the early Turonian thermal maximum (Jarvis et al., 2011), and in particular at Contessa it corresponds to the short cooling phase within this thermal event.

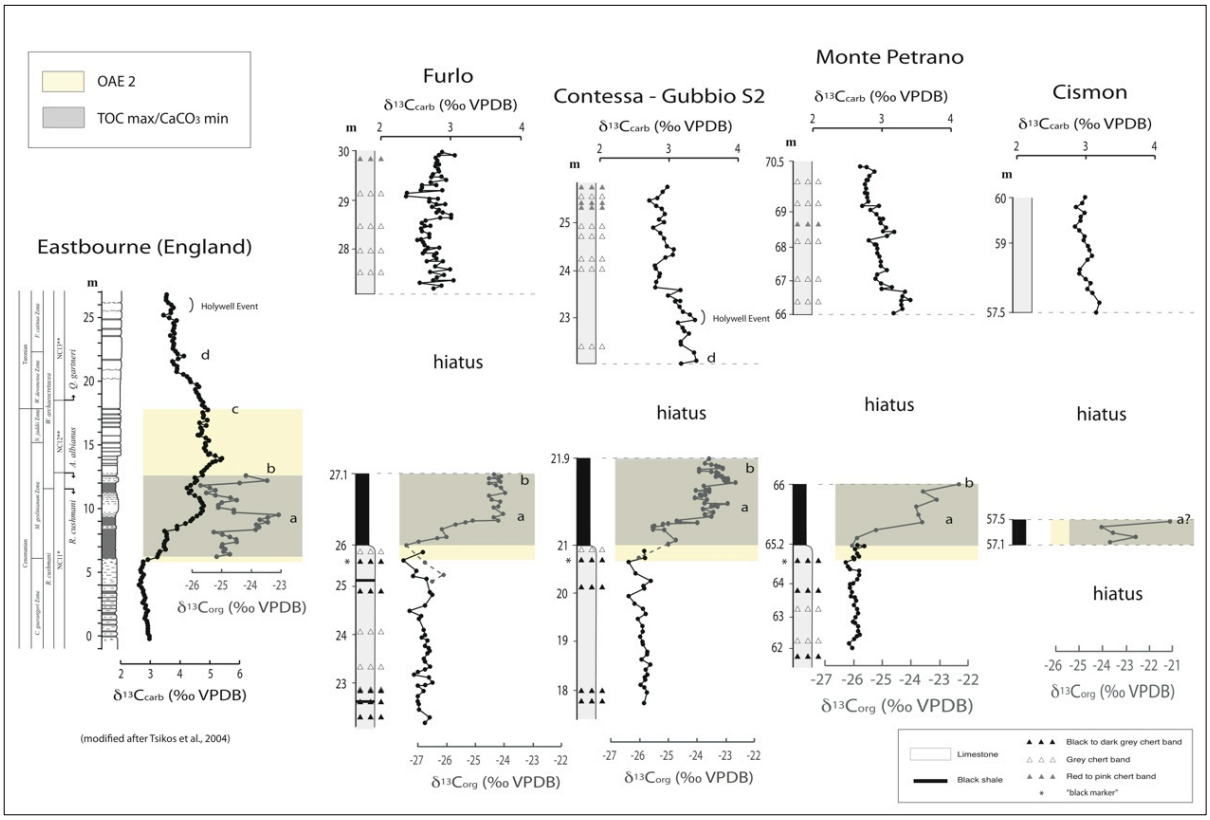

Figure 5.11: Detailed carbonate- and organic-carbon isotopic profiles for the OAE2 at Furlo, Monte Petrano, Contessa-Gubbio2 and Cismon sections. The position of the Bonarelli Level is indicated by a grey band, while the OAE2 interval by a yellow band. The position of the Holywell Event (Voigt et al., 2007; Jarvis et al., 2011) is indicated.

Many processes can be at the origin of the observed OAE2 isotopic records. Hiatuses in correspondence of the OAE2 are frequently described in different depositional settings (e.g. Erbacher et al., 2005; El-Sabbagh et al., 2011). Such discontinuities have been interpreted as the result of frequent erosions or condensations connected with a general regressive trend (e.g. Jaillard and Arnaud-Vanneau, 1993; Gale et al., 2008). Indeed, it's quite difficult to justify an erosion or condensation in a pelagic depositional environment as a consequence of a regressive trend. Such hiatuses imply the occurrence of other physical processes, which could produce intense erosion or not deposition of part of the sequence. The shutdown of the carbonate productivity in favor of dominant siliceous and bacterial organisms during highly eutrophic conditions, as described by van Os et al. (1994) for Mediterranean sapropels, might have led to suppressed sedimentation rates with consequent condensed surfaces. However, an almost complete shutdown or extreme reduction in sedimentation rates seems quite unlikely. Chemical processes may represent another crucial mechanism that simultaneously or alone could be at the origin of the observed results. For example carbonates have a low preservation

potential in high-alkalinity anoxic waters, and in upwelling sediments they are possibly subjected to corrosion effects (Turgeon and Brumsack, 2006).

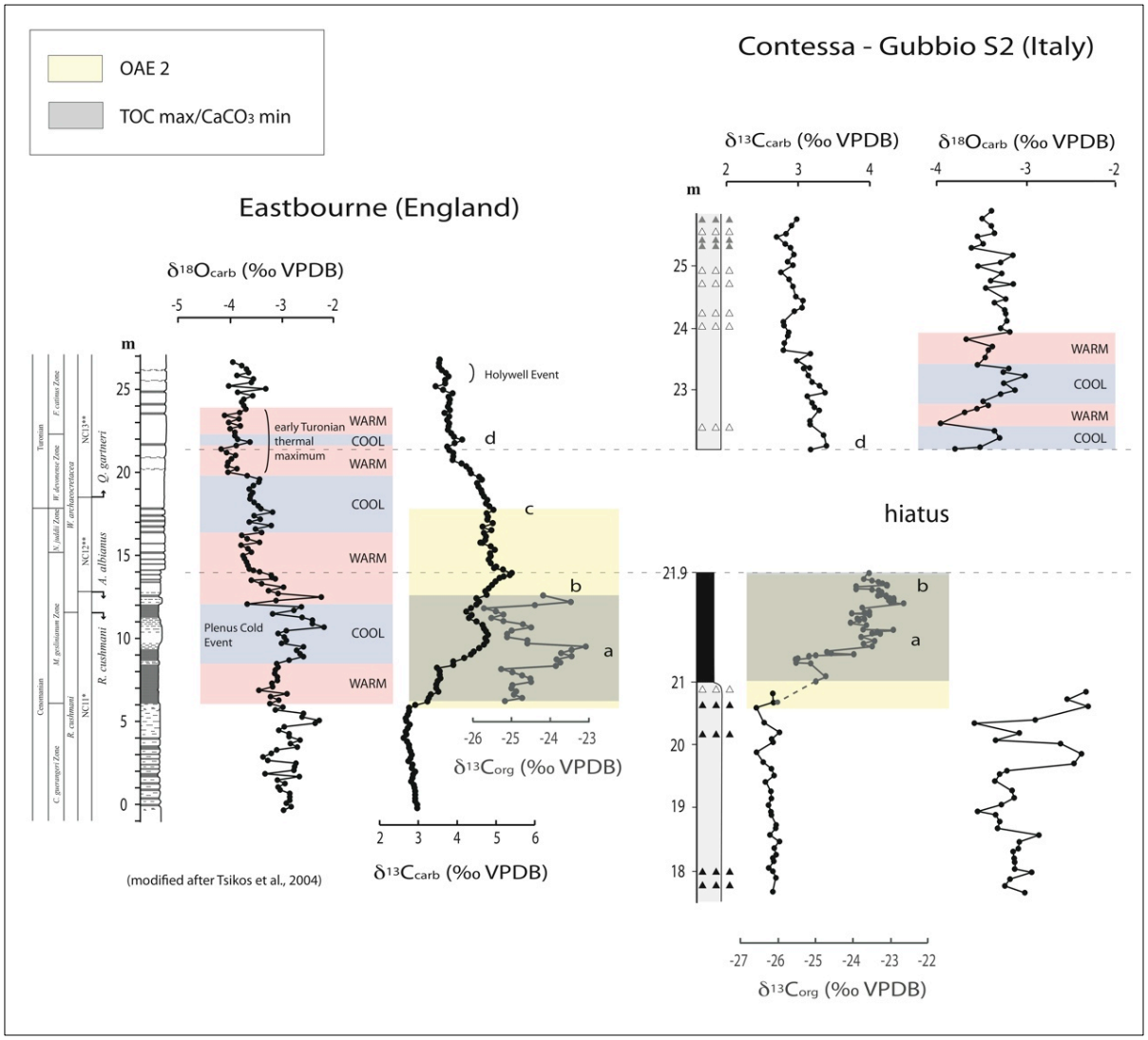

Figure 5.12: Comparison of the carbon and oxygen isotopic profile for the OAE2 interval at Eastbourne (England) on the left (Tsikos et al., 2004) and at Gubbio S2 on the right (Tsikos et al., 2004). The position of the Bonarelli Level is indicated by a grey band, while the OAE2 interval by a yellow band. On the oxygen isotopic curves the warm and cool phases are highlighted with a pink and light blue band respectively. The stratigraphic position of the hiatus is indicated.

Alternatively, widespread dissolution due to a rise of the Carbonate Compensation Depth (CCD) during the OAE2 can be at the origin of a pervasive corrosion. However, even if a rise of the CCD is reasonable, the carbonates are homogeneously low throughout the whole Bonarelli Level, thus indicating that this cannot be at the origin of a non-deposition exclusively in the late part of OAE2 . For these reasons, the observed results need further investigations to be explained. The integration of

additional sedimentological, micropaleontological and geochemical data will possibly give deeper information on the phenomena at the origin of the pervasive latest Cenomanian-early Turonian hiatuses recorded in two adjacent Tethyan basins.

5.6 Conclusions

In this paper high-resolution oxygen, carbonate- and organic-carbon isotopic data for the latest Albian–earliest Turonian time interval from the Monte Petrano and Cismon sections in Italy are presented. The two studied sequences deposited in carbonate pelagic setting in the Tethyan Umbria-Marche and Belluno Basins, respectively. Data have been correlated with other sections from the Umbria-Marche Basin.

Major excursions in the $\delta^{13}C$ profiles correspond to OAE1d and OAE2. The long OAE1d is accompanied by the deposition of 5-6 centimetric black shale layers, corresponding to the so-called Pialli Level, restricted to the lower part of the C isotopic anomaly. The OAE2 instead is associated with organic-rich (TOC more than 20%) and carbonate-lean Bonarelli Level.

Between these two excursions a double-spiked excursion in the $\delta^{13}C_{carb}$ (up to 2.5-3‰) corresponds to the MCE. The lithological alternation of organic-rich shales/black chert bands with whitish limestone layers correlates with the beginning of this event and terminates with the Bonarelli Level, thus confirming that the MCE is associated to significant paleoceanographic (and lithological) changes. This event, even if probably not directly connected to OAE2, in the two studied basins have undoubtedly represented a switch to more unstable conditions much easily subjected to oxygen-depleted bottom-waters.

Measured oxygen isotopic data indicate a general warming trend starting from the latest Albian up to the Bonarelli Level thus followed after the OAE2 by a relatively rapid cooling. Additionally, $\delta^{18}O_{carb}$ indicate that the OAE1d was characterized by generally warm conditions. No clear $\delta^{18}O_{carb}$ signal seems to be associated with the MCEas far as paleotemperature conditions are concerned.

On the basis of both the general trend and the absolute values, the detailed correlation of both $\delta^{13}C_{carb}$ and $\delta^{13}C_{org}$ in the OAE2 interval of the studied section with profiles available in the literature indicate the presence of a hiatus in the upper part of the excursion at the top of the Bonarelli Level. Even if the amount of missing sequence slightly differs from section to section, the hiatus is common in two adjacent Tethyan basins and approximately affects the same stratigraphic interval. The origin of this latest Cenomanian–earliest Turonian discontinuities can be related to a physical and/or a chemical

process. A rise of CCD or reduced sedimentation rates do not justify the observed hiatuses. Further investigations are needed in order to unravel the phenomena connected with the observed geological record.

References

Alvarez, W. (1990) – Pattern of extensional faulting in pelagic carbonates of the Umbria-Marche Apennines of central Italy. *Geology*, 18, 407-410.

Arthur, M.A. and Premoli Silva, I. (1982) – Development of widespread organic carbon-rich strata in the Mediterranean Tethys. *In:* Schlanger, S.O. and Cita, M.B. (Eds.), *Nature and Origin of Cretaceous Carbon-rich Facies*, 7-54.

Arthur, M.A., Brumsack, H.-J., Jenkyns, H.C., Schlanger, S.O. (1990) – Stratigraphy, geochemistry, and paleoceanography of organic carbon-rich Cretaceous sequences. *In:* Ginsburg, R., Beaudoin, B. (Eds.), *Cretaceous Resources Events, and Rhythms*, 75-119.

Barron, E.J. and Washington, W.M. (1985) – Warm cretaceous climates: High atmospheric CO2 as a plausible mechanism. *In:* Sundquist, E.T. and Broecker, W.S., *The carbon cycle and atmospheric CO2: natural variations archean to present*, Proceedings of the Chapman Conference on Natural Variations in Carbon Dioxide and the Carbon Cycle, 32, 546-553.

Bellanca A., Claps, M., Erba, E., Masetti, D., Neri, R., Premoli Silva, I. and Venezia F. (1996) – Orbitally induced limestone/marlstone rhythms in the Albian-Cenomanian Cismon section (Venetian region, northern Italy): sedimentology, calcareous and siliceous plankton distribution, elemental and isotope geochemistry. *Palaeogeography, Palaeoclimatology, Palaeoecology*, 126, 227-260.

Blackman, R.B. and Tukey, J.,W. (1958) – The measurement of power spectra from the point of view of communication engineering. *Dover Publications*, 190 pp.

Bonarelli, G. (1891) – Il territorio di Gubbio. *Notizie geologiche*, 1-38.

Bornemann, A., Pross, J., Reichelt, K., Herrle, J.O., Hemleben, C., Mutterlose, J. (2005) – Reconstruction of short-term palaeoceanographic changes during the formation of the Late Albian 'Niveau Breistroffer' black shales (Oceanic Anoxic Event 1d, SE France). *Journal of the Geological Society, London,* 162, 2005, 623-639.

Channel J.E.T., D'Argenio, B., Horvath, F. (1979a) – The African Promontory, in Mesozoic Mediterranean Paleogeography. *Earth Science Review*, 15, 213-272.

Channel, J. E. T., Lowrie, W. and Medizza, F. (1979b) – Middle and Early Cretaceous magnetic stratigraphy from the Cismon section, northern Italy. *Earth and Planetary Science Letters*, 1979, 42.2, 153-166.

Claps, M., Masetti, D., Pedrielli, F., Garavello, A. (1991) – Analisi spettrale e cicli di Milankovitch in successioni cretaciche del Sudalpino orientale. Rivista Italiana di Paleontologia e Stratigrafia, 97, 153-174.

Claps, M. and Masetti, D. (1994) – Milankovitch periodicities recorded in Cretaceous deep-sea sequences from the Southern Alps (Northern Italy). Special Publications International Association of Sedimentologists, 19, 99-107.

Coccioni, R., Galeotti, S., Gravili, M. (1995) – Latest Albian–early Turonian deep-water agglutinated foraminifera in the Bottaccione section (Gubbio, Italy) — biostratigraphic and palaeoecologic implications. *Revista Espanola de Paleontologia Homenaje al Dr. Guillermo Colom*, 135–152.

Coccioni, R. and Galeotti, S. (2001) – The mid-Cenomanian Event the Prelude to the OAE 2. *EOS Trans. AGU* 82(47), Fall Meet. Suppl.

Coccioni, R. and Galeotti, S. (2003) – The mid-Cenomanian Event: prelude to OAE 2. *Palaeogeography, Palaeoclimatology, Palaeoecology*, 190, 427-440.

Coplen T.B. (1994) – Reporting of stable hydrogen, carbon, and oxygen isotopic abundances. *Pure and Applied Chemistry* 66, 273-6.

El-Sabbagh, A., Tantawy, A.A., Keller, G., Khozyem, H., Spangenberg, J., Adatte, T., Gertsch, B. (2011) – Stratigraphy of the CenomanianeTuronian Oceanic Anoxic Event OAE2 in shallow shelf sequences of NE Egypt. *Cretaceous Research*, 32, 705-722.

Elrick, M., Molina-Garza, R., Duncan, R. & Snow, L. (2009) – C-isotope stratigraphy and paleoenvironmental changes across OAE2 (mid-Cretaceous) from shallow-water platform carbonates of southern Mexico. *Earth and Planetary Science Letters*, 277, 295-306.

Embry, A. and Osadetz, K. (1988) – Stratigraphy and tectonic significance of Cretaceous volcanism. Queen Elizabeth Islands, Arctic Archipelago. *Canadian Journal of Earth Sciences*, 25, 1209-1219.

Erba E. (2004) – Calcareous nannofossils and Mesozoic oceanic anoxic events. *Marine Micropaleontology*, 52, 85-106.

Erbacher, J., Thurow, J., Littke, R. (1996) – Evolution patterns of radiolaria and organic matter variations: A new approach to identify sea-level changes in Mid-Cretaceous pelagic environments. *Geology*, 24, 499-502.

Erbacher, J. and Thurow, J. (1997) – Influence of oceanic anoxic events on the evolution of mid-Cretaceous radiolaria in the North Atlantic and western Tethys. *Marine Micropaleontology*, 30, 139-158.

Erbacher, J., Friedrich, O., Wilson, P.A., Birch, H., Mutterlose, J. (2005) – Stable organic carbon isotope stratigraphy across Oceanic Anoxic Event 2 of Demerara Rise, western tropical Atlantic. *Geochemistry, Geophysics, Geosystems*, 6, 1-9.

Friedrich, O., Erbacher, J., Mutterlose, J. (2006) – Paleoenvironmental changes across the Cenomanian/Turonian Boundary Event (Oceanic Anoxic Event 2) as indicated by benthic foraminifera from the Demerara Rise (ODP Leg 207). *Revue de Micropaléontologie*, 49, 121-139.

Friedrich, O., Erbacher, J., Wilson,P.A., Moriya, K., Mutterlose, J. (2009) – Paleoenvironmental changes across the Mid Cenomanian Event in the tropical Atlantic Ocean (Demerara Rise, ODP Leg 207) inferred from benthic foraminiferal assemblages. *Marine Micropaleontology*, 71, 28-40.

Gale, A.S., Voigt, S., Sageman, B.B., Kennedy, W.J. (2008) – Eustatic sea-level for the Cenomanian (Late Cretaceous) – Extension to the Western Interior Basin, USA. *Geology*, 36, 859-862.

Giorgioni, M., Weissert, H., Bernasconi, S.M., Hochuli, P.A., Coccioni, R., Keller, C.E. (2012) – Orbital control on carbon cycle and oceanography in the mid-Cretaceous greenhouse. *Paleoceanography*, 27, PA1204, doi:10.1029/2011PA002163.

Giraud, F., Reboulet, S., Deconinck, J.F., Martinez, M., Carpentier, A., Bréziat, C. (2013) – The Mid-Cenomanian Event in southeastern France: evidence from palaeontological and clay mineralogical data. *Cretaceous Research*, 46, 43-58.

Gröcke, D.R., Ludvigson, G.A., Witzke, B.L., Robinson, S.A., Joeckel, R.M., Ulnar, D.F., Ravn, R.L. (2006) – Recognizing the Albian-Cenomanian (OAE1d) sequence boundary using plant carbon isotopes: Dakota Formation, Western Interior Basin, USA. *Geology*, 34 193-196.

Hallam, A. (1985) – A review of Mesozoic climates. *Journal of the Geological Society*, 142 433-445.

Hallam, A. (1994) – Jurassic climates as inferred from the sedimentary and fossil record. *In:* Allen, J.R.L., Hoskins, B.J., Sellwood, B.W., Spicer, R.S., Valdes, P.J. (Eds.), *Palaeoclimates and their Modelling: With Special Reference to the Mesozoic Era*, 79-88.

Hardas, P. and Mutterlose, J. (2007) – Calcareous nannofossil assemblages of Oceanic Anoxic Event 2 in the equatorial Atlantic: Evidence of an eutrophication event. *Marine Micropaleontology*, 66, 52-69.

Hay, W.W. (2008) – Evolving ideas about the Cretaceous climate and ocean circulation. *Cretaceous Research*, 29, 725-753.

Herbin, J.P., Montadert, L., Muller, C., Gomez, R., Thurow, J., Wiedmann, J. (1986) – Organic-Rich Sedimentation at the CenomanianeTuronian Boundary in Oceanic and Coastal Basins in the North Atlantic and Tethys. *Geological Society, London, Special Publications*, 21, 389-422.

Hetzel, A., Böttcher, M.E., Wortmann, U.G., Brumsack, H.-J. (2009) – Paleo-redox conditions during OAE 2 reflected in Demerara Rise sediment geochemistry (ODP Leg 207). *Palaeogeography, Palaeoclimatology, Palaeoecology*, 273, 302-328.

Jaillard, E. and Arnaud-Vanneau, A. (1993) The Cenomanian – Turonian transition on the Peruvian margin. *Cretaceous Research*, 14, 585-605.

Jarvis, I., Gale, A.S., Jenkyns, H.C. and Pearce M.A. (2006) – Secular variation in Late Cretaceous carbon isotopes: a new δ13C carbonate reference curve for the Cenomanian–Campanian (99.6–70.6 Ma). *Geological Magazine*, 143, 561-608.

Jarvis, I., Lignum, J.S., Gröcke, D.R., Jenkyns, H.C., Pearce, M.A. (2011) – Black shale deposition, atmospheric CO2 drawdown, and cooling during the Cenomanian-Turonian Oceanic Anoxic Event. *Paleoceanography*, 26, PA3201, doi:10.1029/2010PA002081.

Jenkyns, H.C. (1980) – Cretaceous anoxic events: From continents to oceans. *Journal of the Geological Society of London*, 137, 171-188.

Jenkyns, H.C. (1985) – The early Toarcian and Cenomanian–Turonian anoxic events in Europe – comparisons and contrasts. *Geologische Rundschau* 74, 505-518.

Jenkyns, H.C. (1999) – Mesozoic anoxic events and paleoclimate. *Zentralblatt für Geologie und Paläontologie, Teil.* I, 943-949.

Jenkyns, H.C. (2003) – Evidence for rapid climate change in the Mesozoic–Palaeogene greenhouse world. *Philosophical Transactions of the Royal Society of London A*, 361, 1885-1916.

Jenkyns, H.C. (2010) – Geochemistry of oceanic anoxic events. *Geochemistry Geophysics Geosystems*, 11, Q03004, doi:10.1029/2009GC002788.

Jenkyns, H.C., Gale, A.S., Corfield, R.M. (1994) – Carbon- and oxygen-isotope stratigraphy of the English Chalk and Italian Scaglia and its palaeoclimatic significance. *Geological Magazine*, 131, 1-34.

Jenkyns, H.C., Matthews, A., Tsikos, H., Erel, Y. (2007) – Nitrate reduction, sulfate reduction, and sedimentary iron isotope evolution during the Cenomanian-Turonian oceanic anoxic event. *Paleoceanography*, 22, PA3208, doi:10.1029/2006PA001355

Kennedy, W. J., Gale, A. S., Lees, J. A., Caron, M. (2004) – The Global Boundary Stratotype Section and Point (GSSP) for the base of the Cenomanian Stage, Mont Risou, Hautes-Alpes, France. Episodes, 27/1, 21-32.

Kuypers, N.M.M, Pancost, R.D., Nijenhuis, I.A., Sinnighe Damsté, J.S. (2002) – Enhanced productivity led to increased organic carbon burial in euxinic North Atlantic basin during the late Cenomanian Oceanic Anoxic Event. Paleoceanography, 17, doi: 10.1029/2000PA000569.

Kuypers, M.M.M., van Bruegel, Y., Shouthen, S., Erba, E., Sinnighe Damsté, J.S. (2004) – N2-fixing cyanobacteria supplied nutrient N for Cretaceous oceanic anoxic events. *Geology*, 32, 853-856.

Lanci L., Muttoni, G., Erba E. (2010) – Astronomical tuning of the Cenomanian Scaglia Bianca Formation at Furlo, Italy. *Earth and Planetary Science Letters*, 292, 231-237.

Lebedel, V., Lezin, C., Andreu, B., Wallez, M.-J., Ettachfini, E.M., Riquier, L. (2013) – Geochemical and palaeoecological record of the Cenomanian–Turonian Anoxic Event in the carbonate platform of the Preafrican Trough, Morocco. *Palaeogeography, Palaeoclimatology, Palaeoecology*, 369, 79-98.

Leckie, R.M., Bralower, T.J., Cashman, R. (2002) – Oceanic anoxic events and plankton evolution: Biotic response to tectonic forcing during the mid-Cretaceous. *Paleoceanography*, 17, 13-29.

Luciani, V. and Cobianchi, M. (1999) – The Bonarelli Level and other black shales in the Cenomanian-Turonian of the northeastern Dolomites (Italy): calcareous nannofossil and foraminiferal data. *Cretaceous Research*, 20, 135-167.

Mitchell, S.F. and Carr, I.T. (1998) – Foraminiferal response to mid-Cenomanian (Upper Cretaceous) palaeoceanographic events in the Anglo-Paris Basin (Northwest Europe). *Palaeogeography, Palaeoclimatology, Palaeoecology*, 137, 103-125.

Monnet, C. (2009) – The Cenomanian–Turonian boundary mass extinction (Late Cretaceous): New insights from ammonoid biodiversity patterns of Europe, Tunisia and the Western Interior (North America), *Palaeogeography, Palaeoclimatology, Palaeoecology*, 282, 88-104.

Montanari, A. (1985) – Cenomanian anoxic foreslope inferred from turbiditic cherts in the pelagic basin of the Northern Apennines, Italy. *Geological Society of America*, Abstract with programs., 17, 1-667, USA

Neal C.R ., Coffin M.F., Arndt N.T., Ducan R.A., Eldholm O., Erba E., Farnetani C., Fitton J.G., Ingle S.P., Ohkouchi N., Rampino M.R., Reichow M.K., Self S., Tatsumi Y. (2008) – Investigating large igneous province formation and associated plaeoenvironmental events: A White Paper for scientific drilling. *Scientific Drilling*, 6, 4-18.

Owens, J.D., Lyons, T.W., Li, X., MacLeod, K., Gordon, G., Kuypers, M.M.M., Anbar, A., Kuhnt, W., Severmann, S. (2012) – Iron isotope and trace metal records of iron cycling in the proto-North Atlantic during the Cenomanian-Turonian oceanic anoxic event (OAE-2). *Paleoceanography*, doi:10.1029/2012PA002328.

Paillard, D., Labeyrie, L., Yiou, P. (1996) – Macintosh program performs time-series analysis. *EOS Trans. AGU*, 77, 379.

Parisi, G. (1989) – Stratigrafia del Cretacico-Paleogene. *In:* Cresta, S., Monechi, S., Parisi, G. (Eds.), *Stratigrafia del Mesozoico e Cenozoico nell'area umbro-marchigiana*, *Memorie Descrittive della Carta Geologica* d'Italia, 39, 23-29.

Paul, C.R.C., Mitchell, S.F., Marshall, J.D., Leary, P.N., Gale, A.S., Duane, A.M. and Ditchfield, P.W. (1994) – Paleoceanographic events in the Middle Cenomanian of Northwest Europe. *Cretaceous Research*, 15, 707-738.

Petrizzo, M.R., Huber, B.T., Wilson, P.A. MacLeod, K.G. (2008) Late Albian paleoceanography of the western subtropical North Atlantic. *Paleoceanography*, 23, PA1213, doi:10.1029/2007PA001517.

Premoli Silva, I. and Sliter, W.V. (1994) – Cretaceous planktonic foraminiferal biostratigraphy and evolutionary trends from the Bottaccione section, Gubbio, Italy. *Palaeontographica Italica*, 82, 1-89.

Premoli Silva, I., Erba, E., Salvini, G., Verga, D., Locatelli, C. (1999) – Biotic changes in Cretaceous Anoxic Events. *Journal of Foraminiferal Research*, 29, 352-370.

Russo, F. (2013) – Calcareous nannofossils revised biostratigraphy of the latest Albian-earliest Campanian time interval (Late Cretaceous). *Università degli Studi di Milano, PhD thesis*.

Sageman, B.B., Meyers, S.R., Arthur, M.A. (2006) – Orbital time scale and new C-isotope record for Cenomanian-Turonian boundary stratotype. *Geology*, 34, 125-128.

Schlanger, S.O. and Jenkyns, H.C. (1976) – Cretaceous oceanic anoxic events: causes and consequence. *Geologie en Mijnbouw*, 55, 179-184

Schlanger, S.O., Arthur, M.A., Jenkyns, H.C., Scholle, P.A. (1987) – The Cenomanian-Turonian oceanic anoxic event, I, Stratigraphy and distribution of organic carbon-rich beds and the marine C excursion. *In:* Brooks, J. and Fleet, A.J. (Eds.), Marine Petroleum Source Rocks, *Geological Society Special Publications*, 26, 371-399, 1987.

Scholle, P.A. and Arthur, M.A. (1980) – Carbon isotope fluctuations in Cretaceous pelagic limestones: potential stratigraphic and petroleum exploration tools. *AAPG Bulletin*, 64, 67-87.

Schwarzacher, W. (1994) – Cyclostratigraphy of the Cenomanian in the Gubbio district, Italy: a field study. *In:* de Boer, P.L. and Smith, D.G. (Eds.), *Orbital Forcing and Cyclic Sequences*, Special Publications International Association of Sedimentologists, 19, 99-107.

Scopelliti, G., Bellanca, A., Neri, R., Baudin, F., Coccioni, R. (2006) – Comparative high-resolution chemostratigraphy of the Bonarelli Level from the reference Bottaccione section (Umbria–Marche Apennines) and from an equivalent section in NW Sicily: Consistent and contrasting responses to the OAE2. *Chemical Geology*, 228, 266-285.

Stoll, H.M. and Schrag, D.P. (2000) – High-resolution stable isotope records from the Upper Cretaceous rocks of Italy and Spain: glacial episodes in a greenhouse planet? *Bulletin of the Geological Society of America*, 112, 308-319.

Tamagnini, P. (2007) – Calcareous nannofossils as tracers of paleoceanographic changes associated to Oceanic Anoxic Event 2: records from the Tethys and Atlantic Oceans. *Università degli Studi di Milano, PhD thesis*.

Tarduno J.A., Brinkman D., Renne P., Cottrell R., Scher H., Castillo P. (1998) – Evidence for extreme climatic warmth from Late Cretaceous Arctic vertebrates. *Science*, 282, 2241-2244.

Takashima, R., Nishi, H., Huber, B.T., Leckie, R.M. (2006) – Greenhouse world and the Mesozoic ocean. *Oceanography*, 19, 82-92.

Tiraboschi, D. (2009) – Variazioni quantitative del nannoplancton calcareo durante il Cretacico medio: paleoecologia, paleoceanografia e produzione di carbonato in condizioni di anossia globale ed eccesso di pCO_2. *Università degli Studi di Milano, PhD thesis*.

Tissot, B.P. and Welte, D. H. (1978) – Petroleum formation and occurrence. *Springer-Verlag,* Berlin, 538 pp.

Tsikos, H., Jenkyns, H.C., Walsworth-Bell, B., Petrizzo, M.R., Forster, A., Kolonic, S., Erba, E., Premoli Silva, I., Baas, M., Wagner, T. and Sinnighe Damsté, J.S. (2004) – Carbon-isotope stratigraphy recorded by the Cenomanian-Turonian Oceanic Anoxic Event: correlation and implications based on three key localities. *Journal of the Geological Society, London,* 161, 711-719.

Turgeon, S. and Brumsack, H.-J. (2006) – Anoxic vs dysoxic events reflected in sediment geochemistry during the Cenomanian–Turonian Boundary Event (Cretaceous) in the Umbria–Marche Basin of central Italy. *Chemical Geology*, 234, 321-339.

van Krevelen, D.W. (1950) – Graphical-statistical method for the study of structure and reaction processes of coal. *Fuel*, 29, 269-284.

van Os, B.J.H., Middelburg, J.J., De Lange, G.J. (1991) – Possible diagenetic mobilisation of barium in sapropelic sediment from the Eastern Mediterranean. *Marine Geology*, 100, 125-136.

Verzhbistsky, E.V., Lobkovsky, L.I., Kononov, M.V., Byakov, A.F. (2012) – The age and genesis of the structures in the Amerasian basin. *Izvestiya, Physics of the Solid Earth*, 48, 785-797.

Voigt, S., Aurag, A., Leis, F., Kaplan, U. (2007) – Late Cenomanian to Middle Turonian high-resolution carbon isotope stratigraphy: New data from the Münsterland Cretaceous Basin, Germany. *Earth and Planetary Science Letters*, 253, 196-210.

Wilmsen, M. (2007) – Integrated stratigraphy of the upper Lower–lower Middle Cenomanian of northern Germany and southern England. *Acta Geologica Polonica*, 57, 263-279.

Wilson, P.A. and Norris, **R.D.** (2001) – Warm tropical ocean surface and global anoxia during the mid-Cretaceous period, *Nature*, 412, 425-429.

Chapter 6

Cyclic bottom-currents and extraordinary events in a greenhouse world

Abstract

The Albian-Cenomanian pelagic succession of the Thethyan basins represents a good laboratory to understand the processes that acted during the onset, transition and recovery from local to widespread sea-bottom anoxic conditions in the Cretaceous oceans, between the OAE1d and OAE2 events. Five key sections from the Belluno and Umbria-Marche Basins in Italy have been analyzed at a centimeter-scale resolution in order to recognize the interplay between superficial water changes (such as rate of nutrients input, salinity and so on) and sea-bottom processes. The goal is to understand how the oceanic water masses reacted during highly stressed climatic conditions. The detailed sedimentological description of the five sections is here presented and the role of sea-bottom currents is highlighted. Facies stacking patterns show that sedimentation was controlled by the alternation of periods characterized by slackish water and/or a stratified water column, with periods of enhanced circulation. The basic cyclic sequences deriving from this dynamics have been identified and described. Intriguing mm-scale variability within these sequences suggest that the transitions from and to anoxia did not occur at once but were the result of a series of subtle and continuous variations of depositional processes. Sedimentary facies associated to bottom current activity are present within the OAE1d sedimentary record and in particular above the OAE2 deposits, thus proving that the major anoxia that characterized these two events was followed by a time of enhanced circulation. This intense phase of ventilation was accompanied by intense bottom currents that produced the widespread erosional gap at the upper part of the OAE2.

Key-words: Bonarelli Level, bottom currents, Cretaceous Tethys, OAE, pelagic environment, Scaglia

6.1 Introduction

The Cretaceous Earth was, by comparison with the present, an alien world (Sellwood and Valdes, 2006), experiencing a global plate boundary re-arrangement. The supercontinent Pangaea completed its tectonic breakup into the precursors of the present day continents. Southern continents (Gondwana and the Antarctic) were separated from the northern ones (Laurasia/North America), thus allowing a circumglobal oceanic connection (Hay et al., 1999; Skelton et al., 2003; Sellwood and Valdes, 2007). During Cretaceous Gondwana broke up as South America, Antarctica and Australia rifted away from Africa, thus forming the South Atlantic and the Indian Oceans. The convergent-margin orogenies continued in the North American Cordillera, while the Tethys Ocean continued to narrow.

The concurrence of a greenhouse climate and intense rifting raised eustatic sea levels worldwide (Haq et al., 1987; Takashima et al., 2006; Selwood and Valdes, 2007); wide shallow seas were present in North America (the Western Interior Seaway) and Europe (Mutterlose and Kessels, 2000). At the peak of the Cretaceous transgression, one-third of Earth's present land area was submerged.

Earth during the Cretaceous experienced also long-lasting periods of warm climate (Jenkyns, 1999, 2003, 2010; Hu et al., 2012) with temperatures much higher than today (Hay, 2008). The whole planet was ~6°C warmer than now, with warm ocean depths, widespread aridity in the equatorial region (Norris et al., 2002; Sellwood and Valdes, 2006) and a consequent reduction of latitudinal thermal gradients (Huber, 1995; Skelton et al., 2003; Donnadieu et al., 2006; Hay, 2008) and low seasonality. Polar regions were supposed to be ice-free for most of the time (e.g. Hallam, 1985 and Hallam, 1994; Takashima et al., 2006).

Many reasons are supposed to be at the origin of the particularly high-temperatures experienced during Cretaceous, the most extreme warm episode in the past 150My (Larson, 1991a, 1991b; Erba, 1994, Kerr, 1998; Larson and Erba, 1999; Jenkyns, 1999, 2003; Wignall, 2001; Leckie et al., 2002).

The palaeogeographical distribution of the continental masses must have played an important role in the global temperature balance (Donnadieu et al., 2006). However, geological evidence suggest that the global rearrangement of plate boundaries cannot be alone a sufficient cause. Other processes must have concurred in the origin of such an anomalous climate. Barron and Washington (1985) ran experiments with a general circulation model of the atmosphere coupled to a simple ocean model and estimated that two to tenfold increase in CO_2 with respect to present day values are needed to explain the geologic data (Barron and Washington, 1985). Haworth et al. (2005) from stomatal characteristics of an extinct Cretaceous conifer (Pseudofrenelopsis parceramosa) estimated pCO_2 levels for the Hauterivian-Albian

interval ranging from about 560 up to 1200 ppm. Incredibly huge submarine and subaerial volcanic episodes called Large Igneous Provinces (LIPs) were occurring, with emission of extraordinary masses of magma and volatiles. The frequent development of LIPs (Larson, 1991a,1991b; Leckie et al., 2002) or methanogenic sources (e.g. Jenkyns, 2010) and the global rearrangement of plate boundaries led to an increase in atmospheric levels of greenhouse gasses, CO_2 and possibly CH_4, leading to times of restricted ocean circulation (Jenkyns, 2010). Local anoxia occurred during earlier Cretaceous times and became regional to global during the middle Cretaceous with episodes of widespread production and burial of organic matter (Schlanger and Jenkyns, 1976; Arthur et al., 1990). Oceanic currents and climatic conditions might have been very different from those of today, considering that in the modern oceans it is impossible for large areas to become anoxic (Hay, 2008).

Global warming and the abnormal increase in CO_2 changed the equilibria of the carbon cycle thus altering the hydrologic cycle (Weissert et al., 1998; Wortmann, 2004), nutrients distribution, upwelling intensity and deep water formation (Leckie et al., 2002, Takashima et al., 2006; Jenkyns 2010). In such a stressed environment burial of organic carbon represented a significant mechanism of carbon removal and CO_2 drawdown (Jenkyns 2010).

There is an enormous amount of literature ranging from sedimentology, inorganic/organic and isotopic geochemistry (micropaleontology and biostratigraphy of Cretaceous pelagic successions and anoxic events. Thanks to calcareous plankton biostratigraphy there are huge datasets on primary productivity variations, nutrients availability, surface water temperature and oxygenation (e.g. Premoli Silva et al., 1999; Erba, 2004). The study of benthic organisms has unraveled in many areas the delicate role played by the rate of nutrients reaching the sea-floor, temperature and oxygenation conditions (e.g. Friedrich et al., 2009). Other tiny and precious fragments of information on processes and events that happened millions of years ago are reconstructed by means of detailed geochemical proxies, ranging from organic biomarkers (e.g. Sinnighe Damsté et al., 2010), major and trace elements (e.g. Brumsack, 2006) up to stable isotopes (see Jenkyns, 2010 for a synthesis).

However, very little is still known about sea-bottom physical processes and their links with superficial water masses changes during times of widespread anoxia and in particular during times of major palaeoclimatic perturbations. Hence, the purpose of this work is to combine stratigraphic and sedimentological data to propose an evolutionary model worth to justify the environmental changes and the depositional conditions in the pelagic environment during the onset and vanishing stages of anoxic conditions, under the control of stagnation - ventilation cycles. Two upper Albian – lower-Turonian Tethyan settings have been selected for this study, in the well-known Belluno and Umbria-Marche Basins of Italy.

6.2 Case history

The late Albian – lower Turonian time interval has been selected to investigate the depositional processes and environmental dynamics during a period punctuated by major carbon cycle perturbations, as testified by three positive excursions in the stable carbon isotope record (Jarvis et al., 2006): the upper Albian Pialli Level - or Breistoffer Event - corresponding to the Oceanic Anoxic Event (OAE) 1d (Wilson and Norris, 2001), the Middle Cenomanian Event (MCE) (Coccioni and Galeotti, 2001, 2003) and the OAE 2 (Schlanger and Jenkyns, 1976; Arthur et al., 1990).

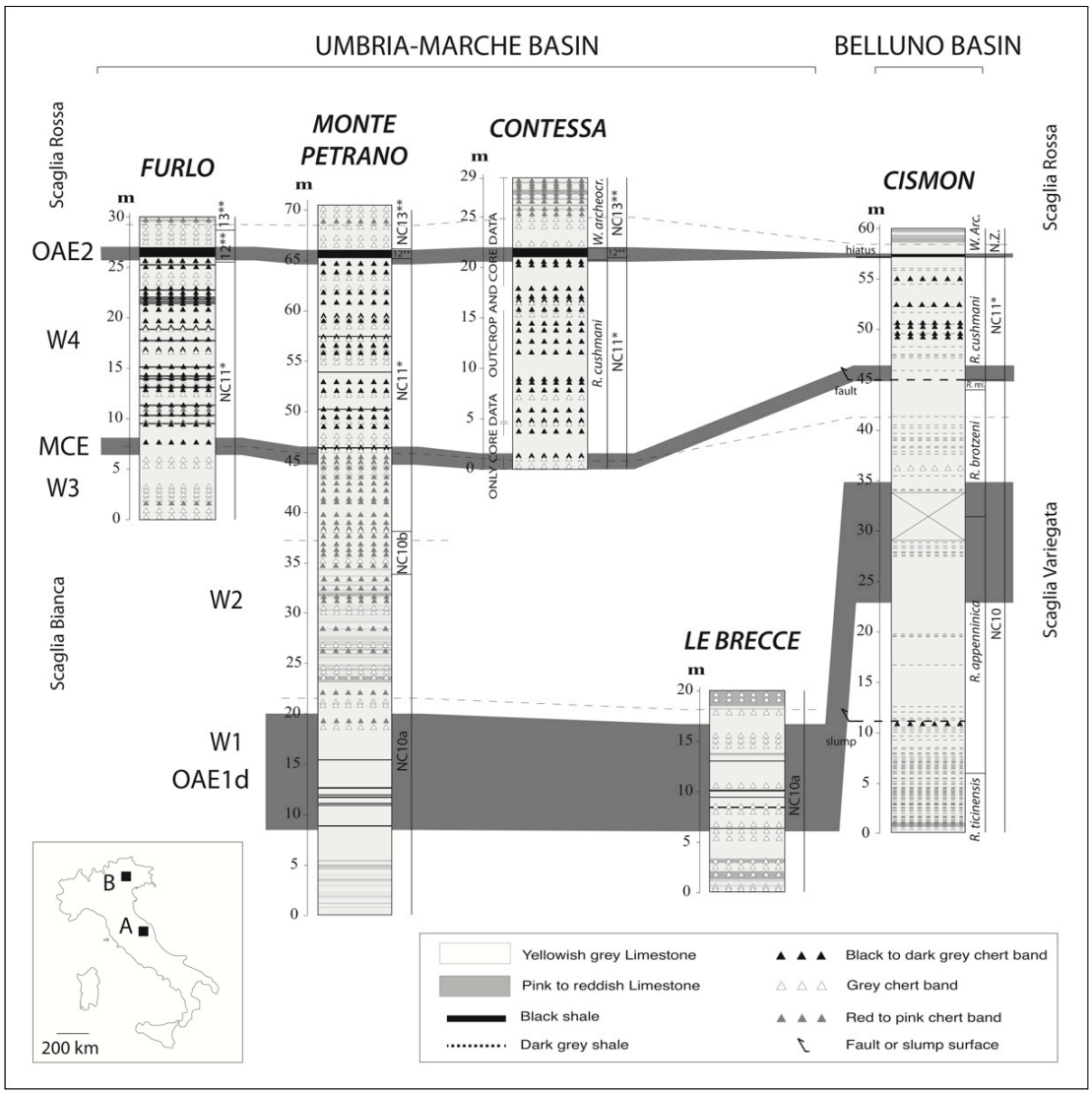

Figure 6.1: Schematic lithostratigraphy and stratigraphic position of the studied sections. Grey bands correspond to carbon isotopic anomalies. Nannofossil and planktonic foraminiferal biostratigraphy (as available) is indicated next to each section. A= Umbria-Marche Basin; B= Belluno Basin.

The pelagic sediments of five localities (Fig. 6.1) in Italy have been used for high-resolution characterization: Furlo, Contessa, Monte Petrano and Le Brecce sections in the Umbria-Marche Basin and the Cismon section in the Belluno Basin. During the studied time interval, both basins were located in the southern part of the Thethys Ocean, in the northern tropical climatic belt (Dercourt et al., 2000; Skelton et al., 2003) (Fig. 6.2).

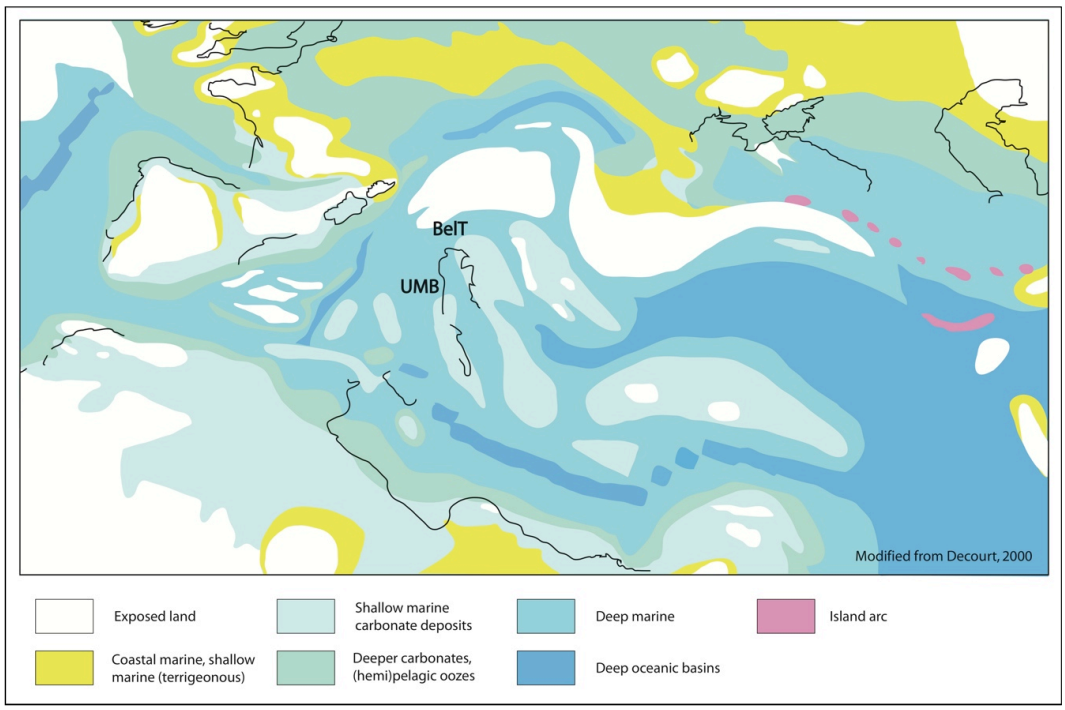

Figure 6.2: *Palaeogeographic reconstruction of studied area during the Cenomanian; UMB=Umbria-Marche Basin, BelT=Belluno Trough (modified after Dercourt, 2000).*

The Umbria-Marche Basin, located today in the central-eastern part of Italy, represents a unique place where an almost continuous Jurassic to Oligocene pelagic sequence is well preserved. The Umbria-Marche sequence was entirely deposited on the continental crust of the Adria microplate, in a basins and swells setting with a complex palaeobathimetry (Alvarez, 1990). The late Albian – early Turonian time interval is represented by the Scaglia Bianca Formation, a mainly calcareous pelagic sequence resulting from lithification of nannofossil-planktonic foraminiferal oozes (Arthur and Premoli Silva, 1982) deposited at bathyal depth. The Scaglia Bianca (in Italian the word “scaglia” literally means “scale” or “flake” and it refers to the thin, tabular stratification of this formation) lies above the Marne a Fucoidi Formation (early Aptian – late Albian) and is followed by the Scaglia Rossa Formation (early Turonian – middle Eocene). The Scaglia Bianca has been informally subdivided into four members (Coccioni et al., 1992, 2003) (Fig. 6.3).

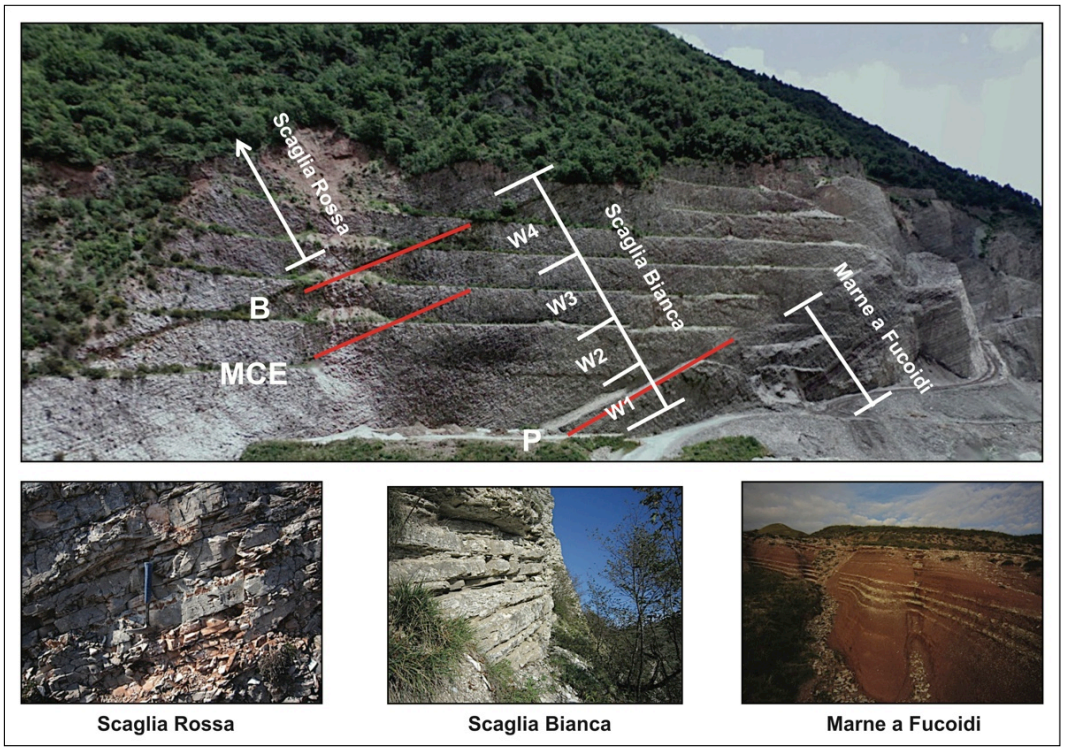

Figure 6.3: *Scaglia Bianca subdivision in members as described by Coccioni et al. (1992, 2003). On the upper picture, taken from the Contessa Highway right in front of the Contessa outcrop (Vispi quarry) it is clearly visible the transition to the Marne a Fucoidi Formation (below) and the Scaglia Rossa Formation (above). The three major events described in this paper are highlighted in red: P, Pialli or Breistoffer Event (OAE1d); MCE, Mid Cenomanian Event; B, Bonarelli (OAE2).*

The Furlo section is located in the homonymous gorge 25km south-east of Urbino and is part of a dismissed quarry (Beaudoin et al 1996; Turgeon and Brumsack, 2006; Mitchell et al, 2008; Turgeon and Craser, 2008; Lanci et al, 2010). The measured sequence is 30m thick.

The Contessa outcrop is located about 2 km from Gubbio in the Vispi active quarry, close to the homonymous Highway that gives the informal name to the outcrop (Monechi and Parisi, 1989; Coccioni and Galeotti, 2003). The interval of interest is 29m thick. As an additional dataset the Gubbio 2 Core collected from a borehole drilled right in front of the quarry during the C/T-Net research project, has been described, correlated to and integrated with the outcrop data.

The 20m-thick section at Le Brecce is located inside a gorge, at 3 km from the Piobbico village. The studied outcrop is at the km 34 of the state road 257-Apecchiese, close to the Piobbico drillsite (Tiraboschi, 2009).

The 90m thick section at Monte Petrano is about 2 km east of the Moria village (Giorgioni et al., 2012).

The 60m thick Cismon section is located in the Venetian Southern Alps, north-eastern Italy, along the SS50 (State Highway 50) not far from the village of Lamon and along the Cismon stream (46°02'43.00'', 11°45'40.34'') (Channell et al., 1979b; Bellanca et al., 1996).

During the Cenomanian the Cismon area was located close to the hinge between the Trento Plateau and the Belluno Basin (Erba and Larson, 1998). The Cenomanian Scaglia Variegata Formation (Channell et al., 1979a) was deposited in a horst and graben extensional setting (Bernoulli and Jenkyns, 1974; Bosellini et al., 1978; Winterer and Bosellini, 1981) with the alternation of yellowish to grey limestones, chert bands and shales/black shales (Channell et al., 1979b; Claps et al., 1991, 1994; Bellanca et al., 1996).

6.3 Methods

The five selected sections have been detailed studied and logged at mm-scale, with the exception of the Bonarelli layer, to which this analysis has not been applied, facies analysis has been based on the objective description of texture, composition, sedimentary structure, shape and features of the bounding surfaces of layers and beds (either depositionl/erosional or diagenetic), complemented by microfacies analysis on samples from selected facies. Field and laboratory facies description led to the identification of a number of facies types (see Chapter 4) interpreted in terms of depositional and lithogenetic processes. The facies stacking patterns have been firstly recognized during field logging, then checked and refined after graphic restitution of the measured lithologic logs. The repetition of some basic types of facies stacking patterns permitted to derive the combination of genetic processes, in the frame of the multiple controls on the dynamics of the pelagic environment. Specific care has been devoted to unravel the "normal and unperturbed" settling processes from any "perturbation", either due to redistribution of sediments by traction or to changes imputable to the basic controlling factors, such as primary productivity, oxygen deficiency linked with bottom water ventilation, non autochtonous inputs, like eolian or volcaniclastic dust or pelagic turbidites.

6.4 Results

For every studied section a schematic panel has been realized. The resulting five composite sections are presented in Fig. 6.5a-e.

For each section the composite log contains three panels: lithology, sedimentary/diagenetic structures and additional features.

The left panel is the comprehensive schematic log with the vertical lithologic variations, distinguishing whitish or reddish limestones from black shales and reporting the differently coloured continuous chert bands.

The right panel instead reports all the additional features in the form of a range chart, where the presence and persistence of a certain feature is indicated by a black bar. The following features are reported, from left to right: position of resedimented layers (facies R as defined in Chapter 4), hardground, chert nodules, cherty intervals, radiolarian layers, marl beds thicker than 0.5cm, intervals with discrete bioturbation, pyrite nodules, sparse lined forams. Concerning discrete bioturbation, we have chosen to split it in two qualitative different classes: a moderate discrete bioturbation class, for the cases where the traces are rare to common within the described interval, and an intense discrete bioturbation class, when the abundant traces dominate a vast area of the investigated interval. The latter is represented in the panel with a black bar larger than the one used for the less intensely bioturbated intervals. Pervasive mottling, i.e. the result of pervasive sediment reworking without any visible discrete biogenic trace, is not included in the graph.

The central panel presents the facies identified by their dominant structures. The panel consists of a vertical facies log following the concept reported in the scheme of Fig. 6.4, where all the facies are plotted as a function of bottom current activity/intensity and oxygenation (x-axis) and nutrients (y-axis). The main aim of the central panel log in Figs. 6.5a-e is to show synthetically the variation of the observed facies and sedimentary structures through time, as a function of the increasing shear stress exerted by sea-bottom currents (as described in Chapter 4). This curve can be used as an indirect indicator of varying regimes of sea-bottom current intensity/persistency. In this qualitative and interpretative log, the traction intensity estimated from the different sedimentary structures is plotted on the vertical axis in the corresponding stratigraphic position. First all the facies are ideally separated according to the sea-bottom oxygenation conditions, following the scheme of Fig. 6.4: the facies related to oxygen depletion, i.e. black shale and black chert layers, are plotted to the left of the central bar, while on the right side all the facies related to conditions of “normal” oxygenation are plotted. Within these two end members two transitional facies of alternating micritic and organic-rich laminasets and bedded black chert bands (Fig. 6.4, Facies A4 and G4a respectively; details in Chapter 4), are reported. The diagram reads in this way: on increasing traction intensity and “normal” oxygenation, the facies bars shift from homogeneous limestone to single marly-limestone beds, limestones with pervasive plane-parallel lamination, limestones with wavy lamination and

foraminiferal-intraclastic lags (as defined in Chapter 4). Within the array of the tractive facies, the micrites with few sparse forams lined by feeble bottom-currents, the laminated radiolarian layers and the laminated chert bands have been merged in the same class of weak traction intensity.

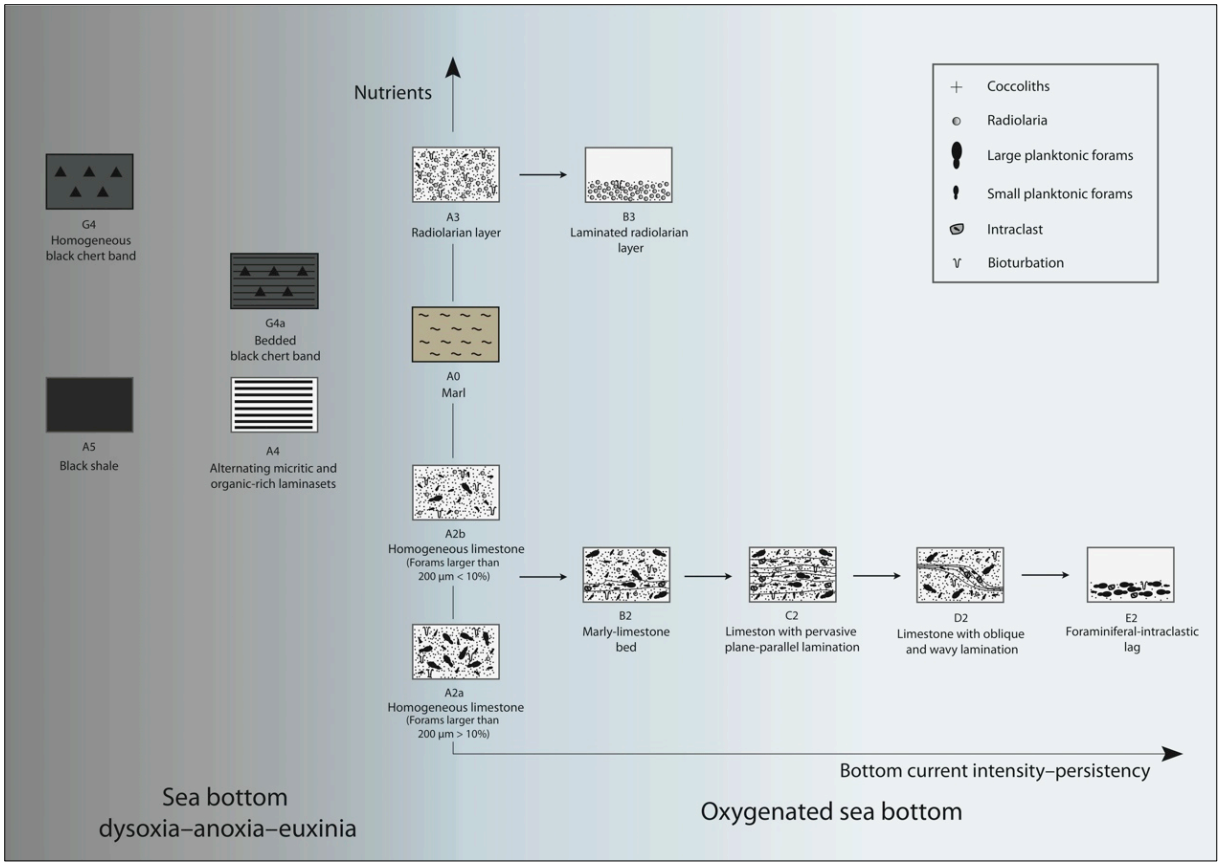

Figure 6.4: Facies scheme representing the ideal transition from anoxic (on the left) to oxygenated facies (on the right). Two transitional facies alternating micritic and organic-rich laminasets and bedded black chert bands, as described in Chapter 4 are distinguished. From left to right all the facies are organized with increasing intensity of the sea-bottom currents shear stress. See legend for symbols explanation.

The first half a meter above the Bonarelli level has been particularly difficult to describe due to the high silica content. Thin sections and peels in that interval where particularly opaque, making microfacies observation particularly difficult and in some cases impossible. Pervasive parallel laminations have been observed in this interval at the field scale, but, due to the above-mentioned technical limits, poor microfacies observation has been done in order to safely exclude a mere compositional origin of the laminae. In Figs. 6.5a-e this half a meter has been interpreted as a tractive, pervasive parallel laminated interval (facies C2 as defined in Chapter 4).

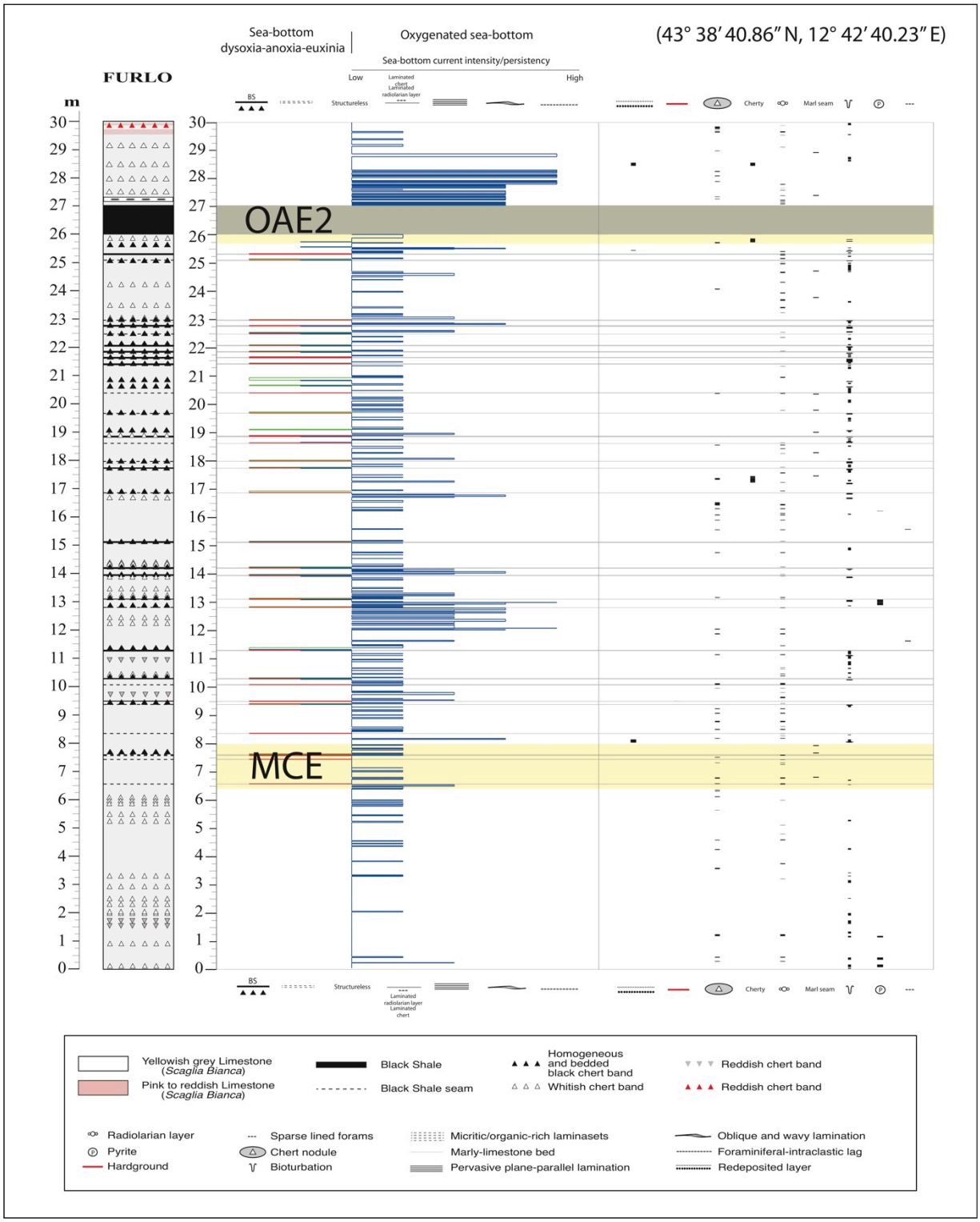

Figure 6.5a: Furlo composite section, see text for explanation. The position of the Bonarelli Level is indicated by a grey band, while the OAE2 and MCE interval by a yellow band.

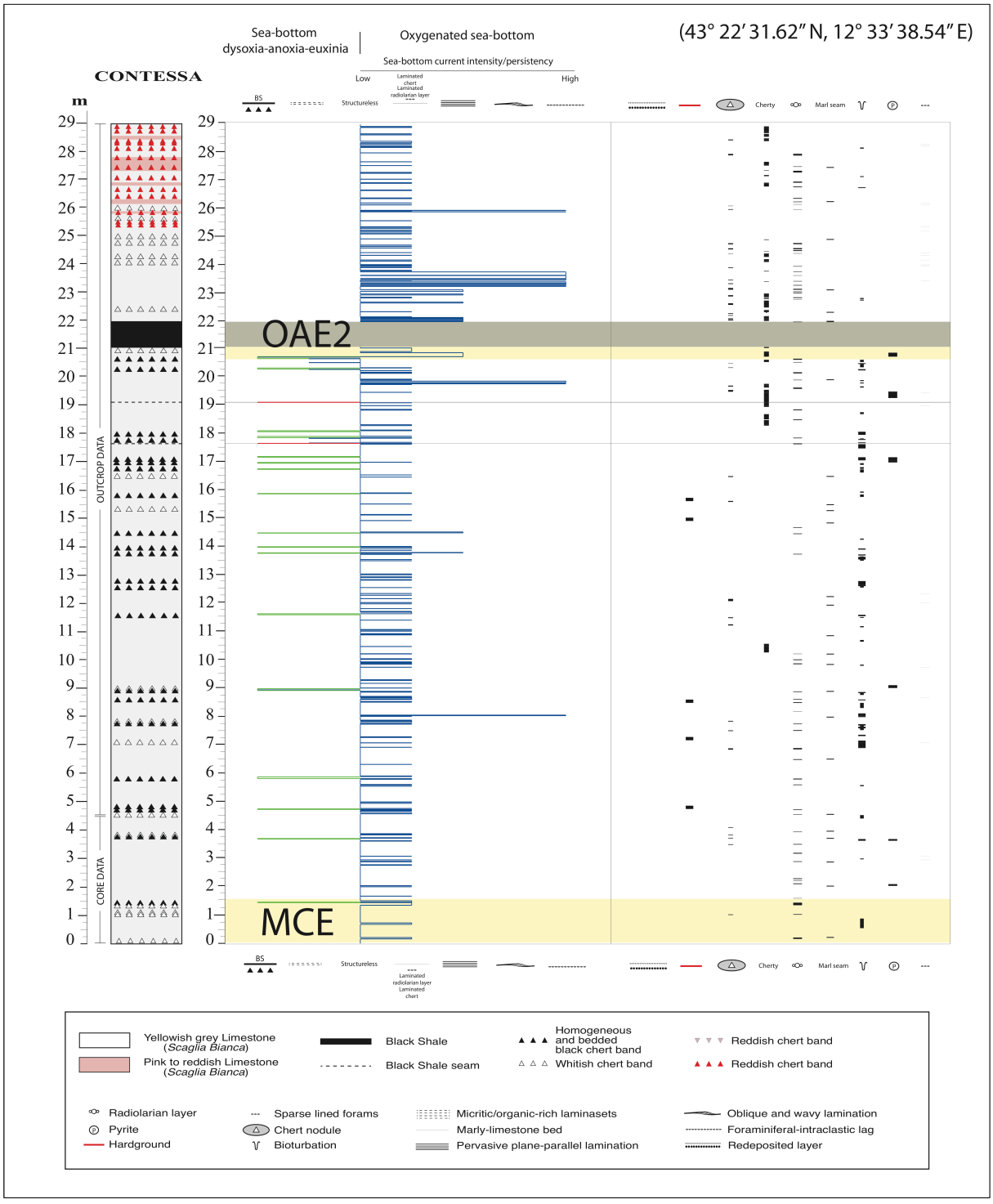

Figure 6.5b: Contessa composite section, see text for explanation. The position of the Bonarelli Level is indicated by a grey band, while the OAE2 and MCE interval by a yellow band.

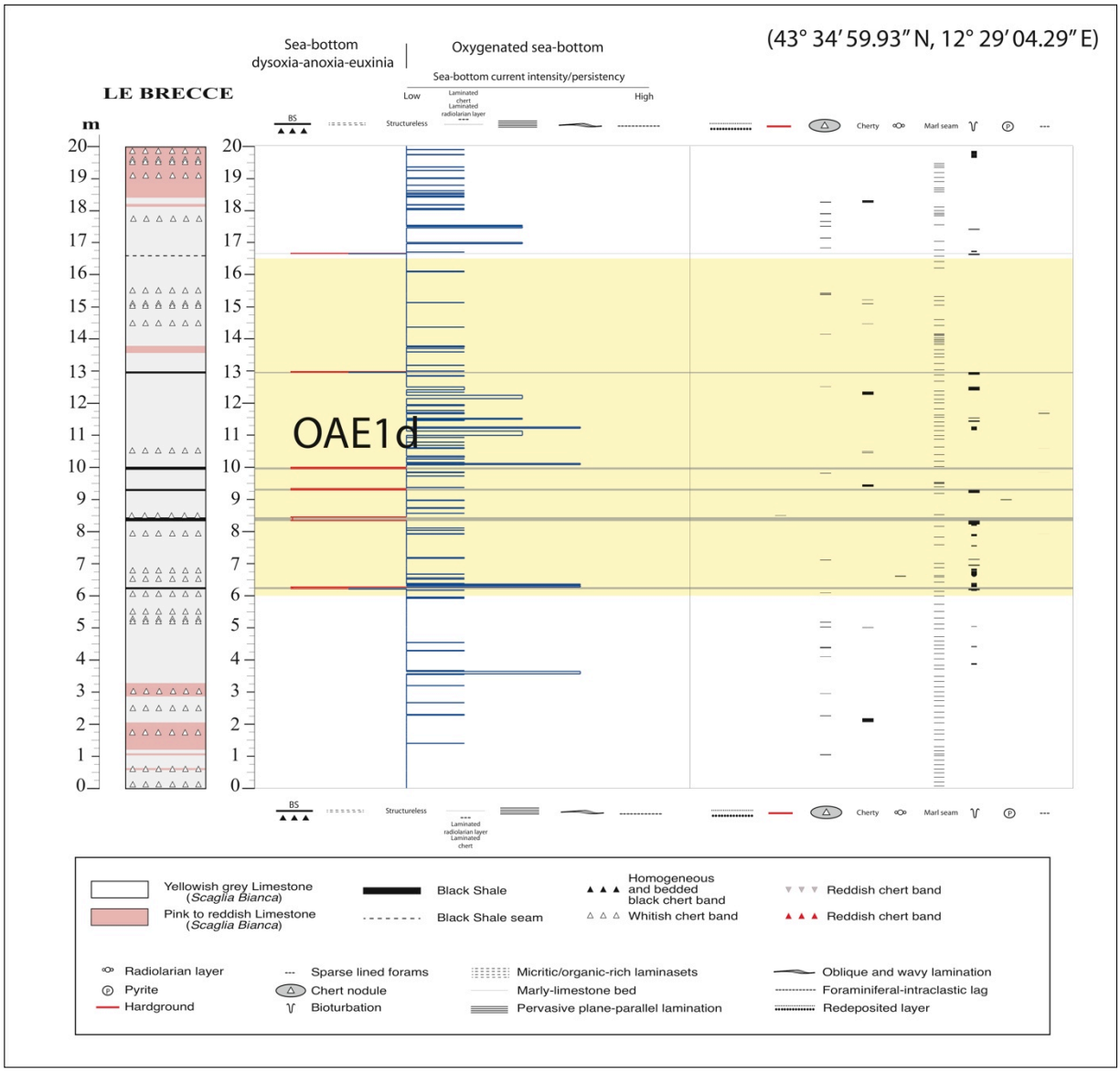

Figure 6.5c: Le Brecce composite section, see text for explanation. The position of the OAE1d is indicated by yellow band.

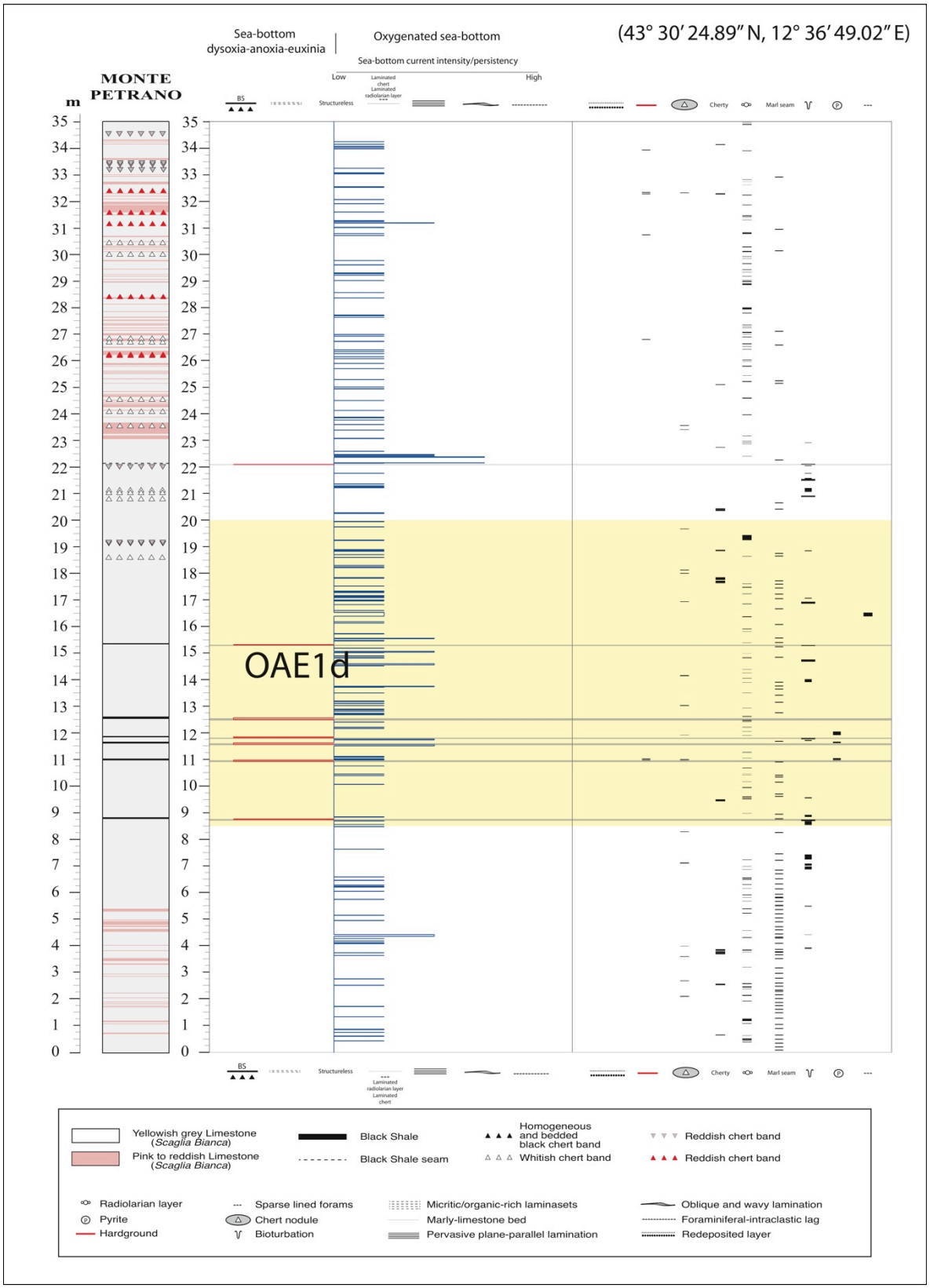

Figure 6.5d: Monte Petrano composite section (lower part), see text for explanation. The position of the OAE1d is indicated by a yellow band.

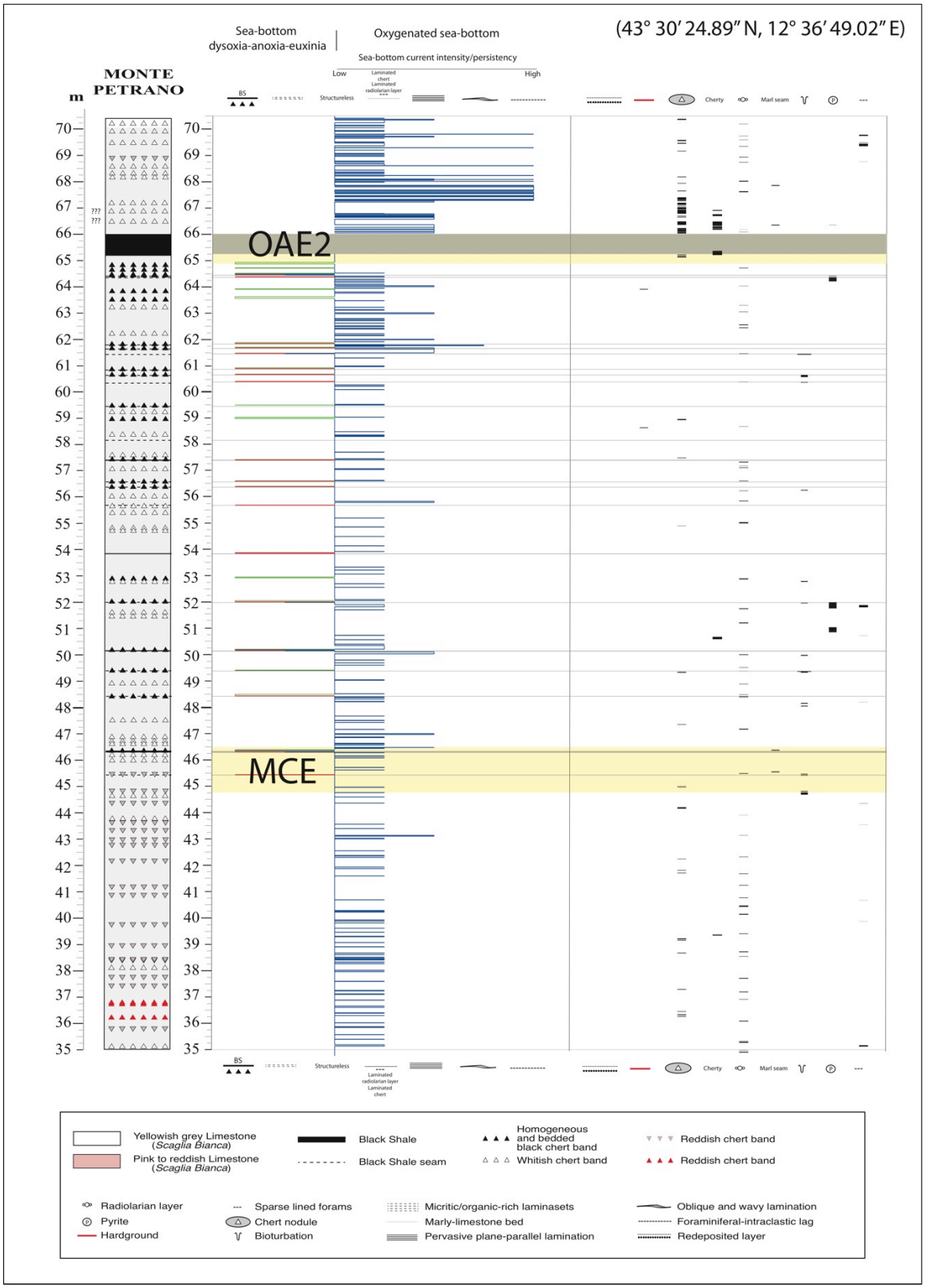

Figure 6.5d bis: Monte Petrano composite section (upper part), see text for explanation. The position of the Bonarelli Level is indicated by a grey band, while the OAE2 and MCE interval by a yellow band.

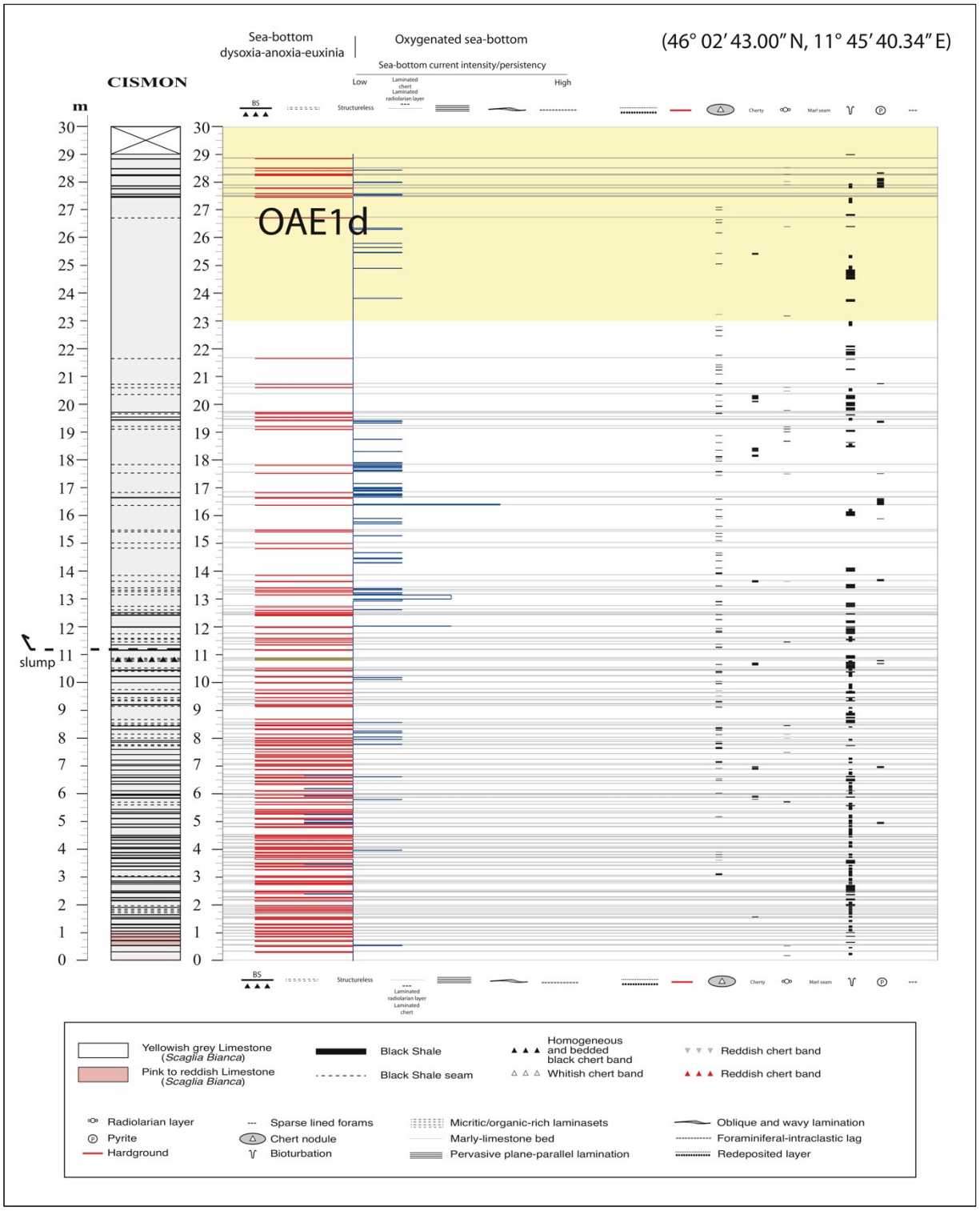

Figure 6.5e: Cismon composite section (lower part), see text for explanation. The position of the OAE1d is indicated by a yellow band.

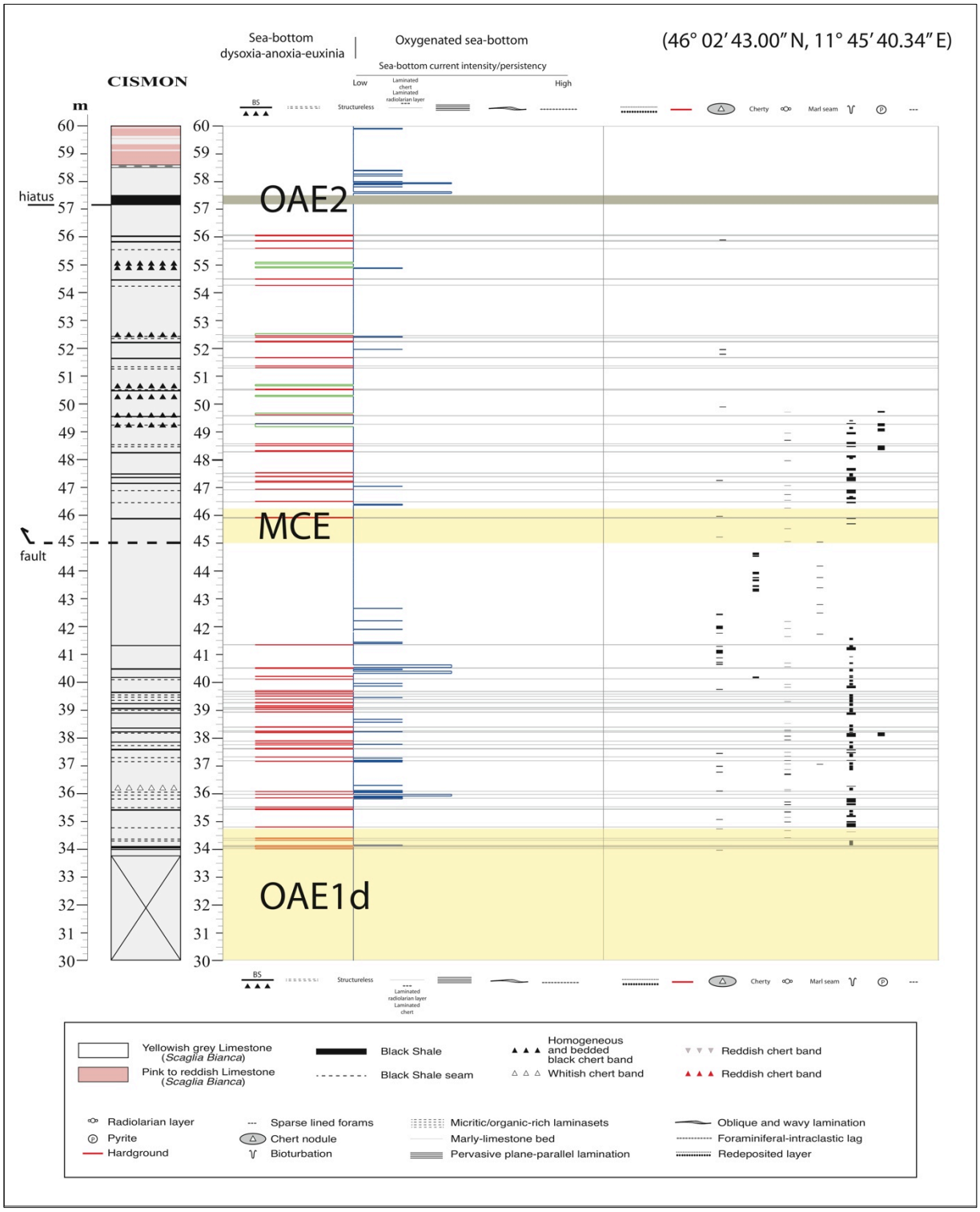

Figure 6.5e bis: Cismon composite section (upper part), see text for explanation. The position of the Bonarelli Level is indicated by a grey band, while the OAE2 and MCE interval by a yellow band.

6.4.1 Stacking patterns

Three repetitive stacking pattern types or "sequences" have been identified in the studied successions thus suggesting the presence of cyclic processes at their origin. These are graphically presented in Figs. 6.6-6.8.

Sequence 1: in the studied sections the most common stacking pattern consists of repetitive cycles of homogeneous calcilutite layers (facies A2), followed by radiolarian layers (facies A3/B3), limestone beds with traction structures (facies B2-E2) and a new homogeneous calcilutite layer. This stacking pattern is represented in Fig. 6.6.

We interpret this pattern as due to cycles of eutrophication in oxic conditions. During times of normal oligotrophic conditions the main producers are foraminifera and coccoliths whose deposition forms a carbonate ooze (A in Fig. 6.6). During time of the increased nutrient availability, for example due to enhanced riverine input, the productivity is dominated by siliceous organisms with the deposition of the radiolarian layer (B in Fig. 6.6), in an environment reasonably characterized by water stratification. Once back to normal oligotrophic conditions an efficient circulation is re-established as highlighted by the tractions structures in the limestone above the radiolarian layer (C in Fig 6.6) that predates deposition of the "normal" calcareous ooze related to oligotrophic conditions.

This kind of stacking pattern is typical of both the Umbria-Marche Basin and the Belluno Basin throughout the whole stratigraphic sequence. This indicates that this pattern represents the so-called "background sedimentation".

Sequence 2: this stacking pattern is recurrent in the intervals characterized by the presence of a black shale and barren of black cherts. The sequence 2 is characterized by a homogeneous calcilutite at the base (facies A2), a transition to anoxic conditions represented by micritic intervals alternatively rich and poor of organic matter (facies A4) followed by a black shale (facies A5). The sequence terminates with a whitish limestone with evidences of traction followed by a shift back to a homogeneous calcilutite (respectively facies B2-E2 and A2). The stacking pattern is represented in Fig. 6.7). Starting from oxic conditions (A in Fig. 6.7) the onset of anoxic conditions (C in Fig. 6.7) occurs gradually with the resulting deposition of alternated micritic and organic-rich laminasets (B in Fig. 6.7). The re-establishment of oxic conditions is accompanied by a phase of enhanced bottom-circulation (D in Fig. 6.7) as testified by the tractive structures. This sequence is characteristic of the studied Pialli layers of the Umbria-Marche Basin (Le Brecce and Monte Petrano sections).

Sequence 3: this stacking pattern forms in two slightly different sequences, sequence 3a and 3b (Fig. 6.8), that share the presence of a black chert band in their core. From bottom to top Sequence 3a is characterized by (Fig. 6.8): homogeneous calcilutite (facies A2), black chert band (facies G4 or G4a), a laminated limestone then back again to a homogeneous calcilutite (respectively B2-E2 and A2). Sequence 3b, quite similar, is characterized from bottom to top by (Fig. 6.8): homogeneous calcilutite (A2), alternated micritic and organic-rich laminasets (A4), a black shale (A5), a frequently bedded black chert band (G4 and/or G4a), a laminated limestone (B2-E2) before getting back again to a homogeneous limestone (A2). The black shale can be represented either by a cm-thick layer or just by a black shale seam only few mm-thick.

Sequence 3 is present in the upper part of the studied successions above the Mid-Cenomanian Event up to the Bonarelli Level. In particular this stratigraphic time interval at Furlo and Monte Petrano is almost completely characterized by type 3b sequences while Contessa and Cismon by exclusively type 3a sequences.

The superposition of black shales and black chert bands was already described by Beaudoin et al. (1996) and Salmon et al. (1998). In the studied outcrops, black chert bands have been distinguished in two main facies: when vitreous with no evident structures they have been defined as “homogeneous” (facies G4), while when characterized by a thin mm-scale alternation of silicified shaly organic-rich beds and radiolarian-rich horizons they have been described as “bedded” (facies G4a). Bedded black chert bands are common in Umbria-Marche Basin while they are absent at Cismon.

We interpret the 3a and 3b patterns as the sedimentary expression of the same depositional process at different basin locations during a time of shift from oligotrophic to eutrophic anoxic conditions.

The deposition in normal oxic conditions (A in Fig. 6.8) is followed by the gradual onset of prevailing anoxic conditions (B in Fig. 6.8) due to enhanced stratification connected after increase of fresh water supply. The deposition of a black chert or a black shale in this conditions depends on the availability of silica related to nutrients and/or clay particles. The distribution of nutrients and clay particles depends on the shape of the fresh water plume that segregates the clay, with the detrital to nutrients ratio decreasing from the proximal to the distal areas (Lalli and Parsons, 1997). The r-opportunist organisms (such as radiolaria) are able to use the incresead available nutrients only at a certain distance from the sediment plume with limited water turbidity. For this reason black shale layers are expected to deposit in the proximal (and eventually confined) settings, while black cherts would be their lateral correspective in the distal locations (B in Fig. 6.8). The progressive reduction of fresh water, nutrients and mud inputs will shrink the fresh water plume and the water column stratification. As a

consequence, the depositional settings will shift landwards leading to the deposition of black cherts in areas previously characterized by the deposition of black shales (C in Fig. 6.8). The subsequent re-establishment of a normal riverine input and the associated normal oxic and oligotrophic conditions is accompanied by a phase of enhanced bottom-circulation (D in Fig. 6.8), as proven by the facies with tractive structures. In this perspective, the depositional meaning of homogeneous black chert bands and bedded black chert bands is different.

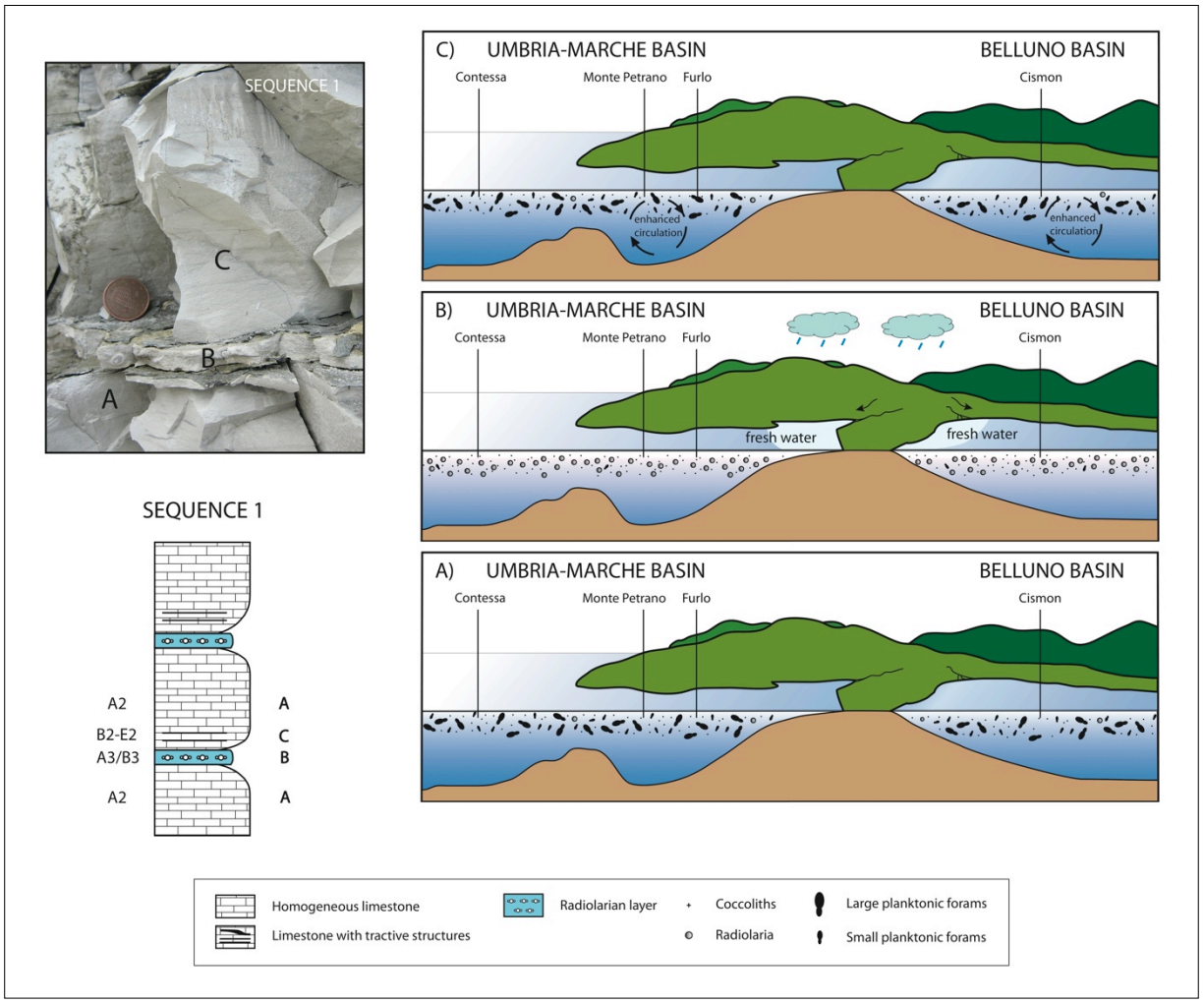

Figure 6.6: Left: Limestone-radiolaria-limestone sequence (Sequence 1). Right: depositional model for Sequence 1. Facies labels as described in Chapter 4. See text for a detailed explanation.

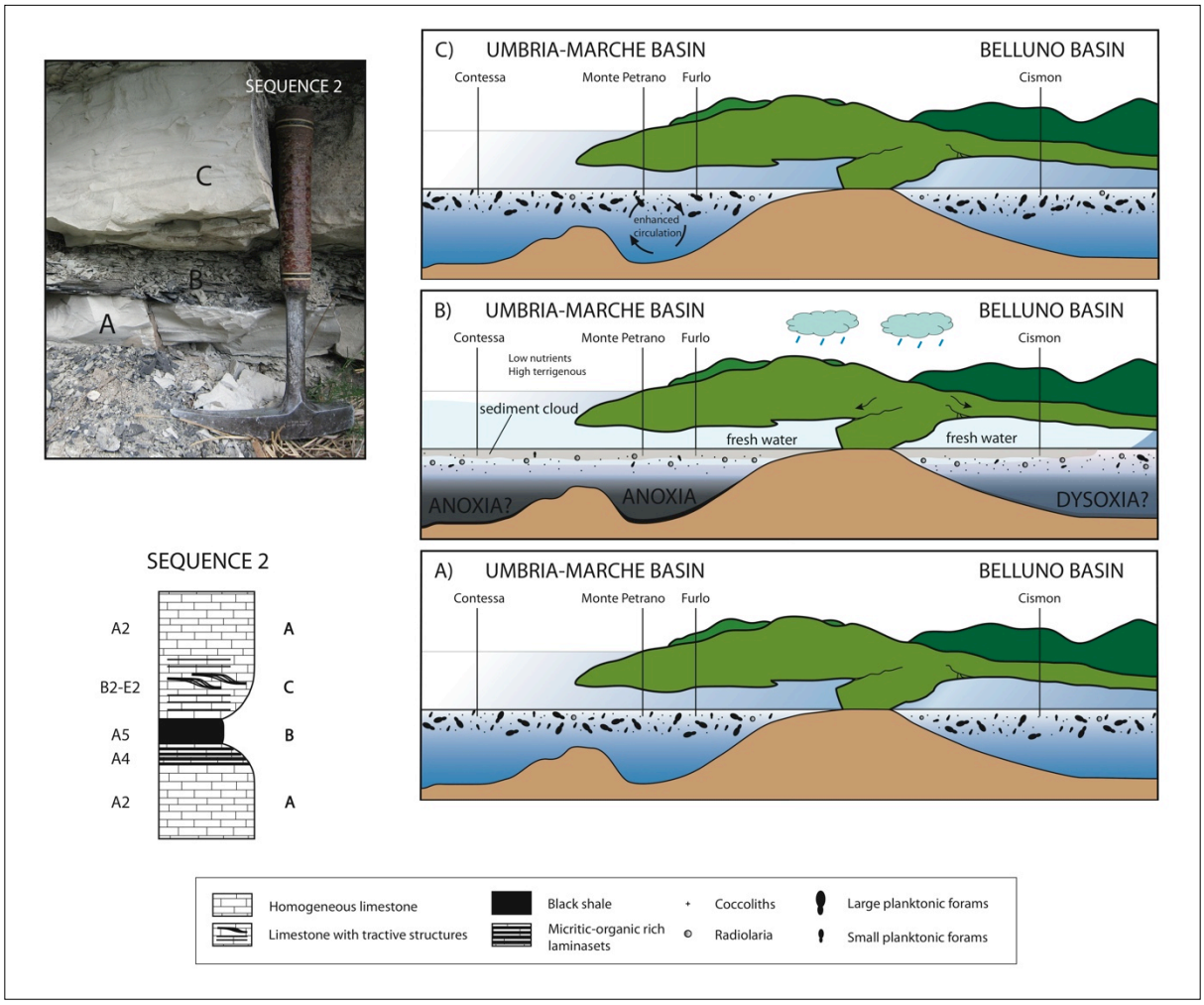

Figure 6.7: Left: Limestone-radiolaria-limestone sequence (Sequence 1). Right: depositional model for Sequence 1. Facies labels as described in Chapter 4. See text for a detailed explanation.

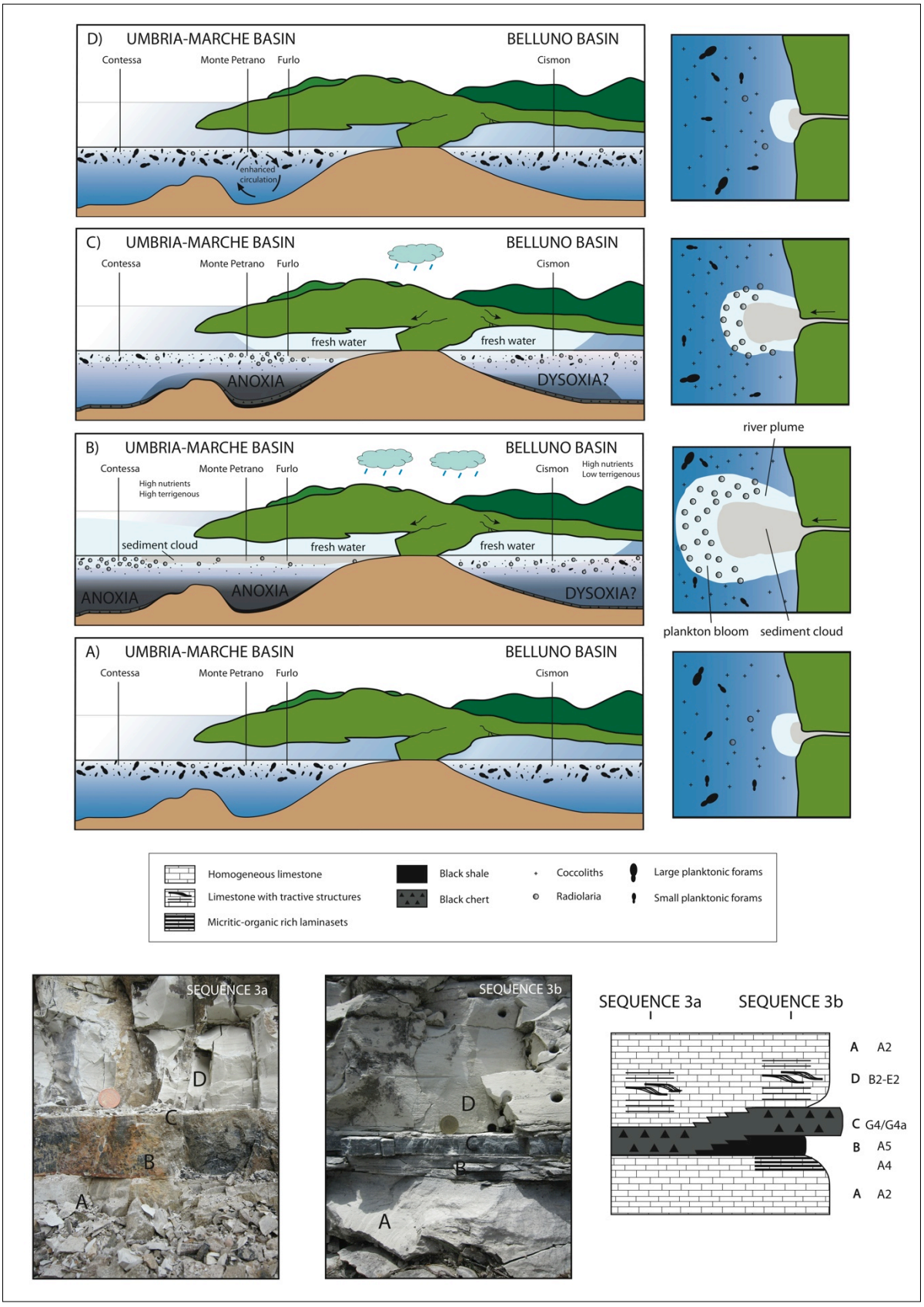

Figure 6.8: Left: Limestone-black shale-black chert-limestone sequence (Sequence 3a and 3b). Right: depositional model for Sequence 3a and 3b. Facies labels as described in Chapter 4. See text for a detailed explanation.

Homogeneous black chert (facies G4, see Chapter 4) is the result of the deposition and preservation of organic matter during a time dominated by biogenic silica and minor terrigenous input. The resulting lithology is thus the siliceous analogue of a black shale. Bedded black chert bands (facies G4a, see Chapter 4) are instead compositional alternations of mainly winnowed radiolarian horizons under the action of sea-bottom currents with settled organic-rich shales. This facies G4a is at the end the silicified alternation of black shale and radiolarian layers (facies A5 and B3 as defined in Chapter 4) produced by prevailing anoxic sea-bottom conditions punctuated by traction events, with a progressive shift from anoxic to dysoxic and finally oxic conditions. Probably this facies is the small-scale expression of the big scale alternation of chert beds and shale intervals described by Hori et al. (1993) as the result of cyclic-rapid accumulation of biogenic SiO_2 under extremely slow accumulative environments of shale. The intriguing mm-scale variability within the sequence suggest that the onset, transition and recovery from anoxia does not occur at once but is a continuous subtle variation of mutually linked processes (Fig. 6.9).

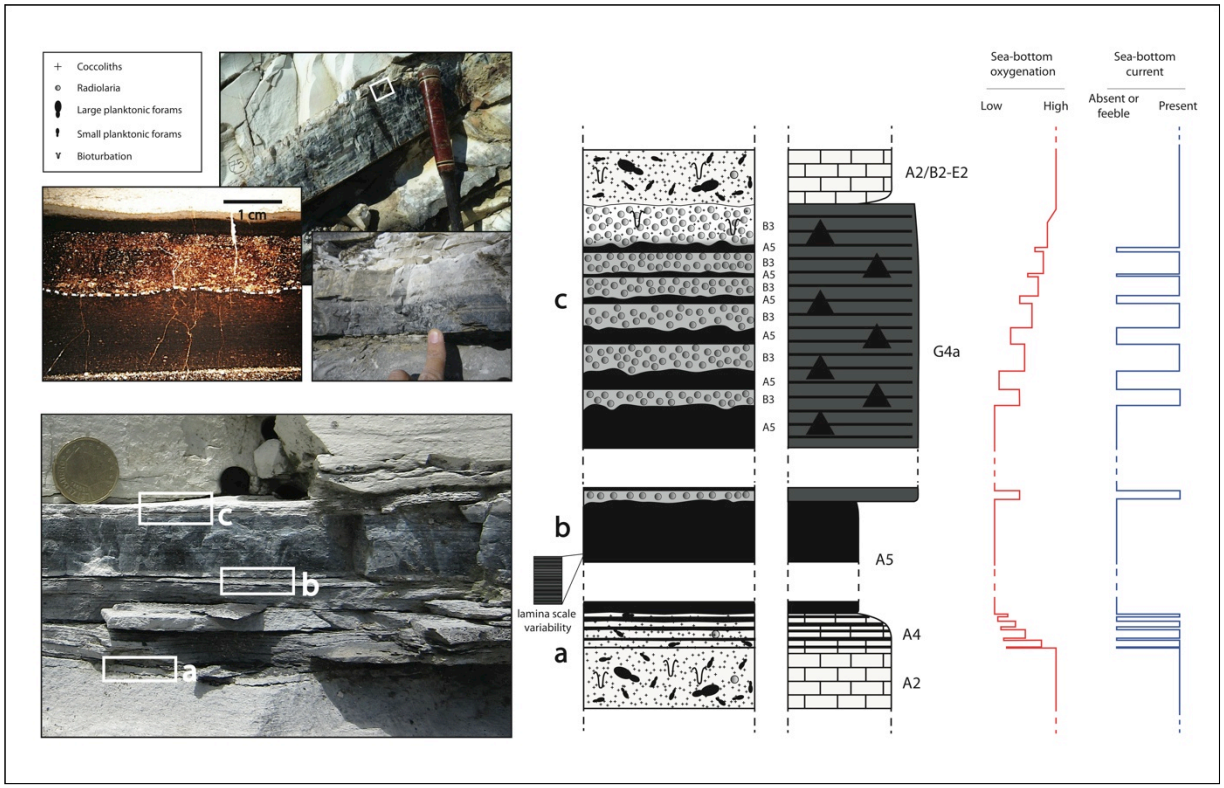

Figure 6.9: Lamina- thin bed scale variation within Sequence 3b. Sea-bottom oxygenation conditions and presence of bottom-currents are ideally sketched on the right. Upper left: picture of a bedded black chert band and thin section of the interval surrounded by the white frame.

6.5 Discussion

6.5.1 Interplay of superficial water masses and sea-bottom conditions

The main components of the studied lithified oozes, forming any kind of stacking pattern are nannofossils, planktonic forams, rare benthic foraminifera and radiolaria (Arthur and Premoli Silva, 1982). Among all the surface water mass parameters, nutrients play the major role in determining the observed biogenic association if compared with temperature and salinity. Planktonic forams have different ornamentation and sizes according to the different trophic level, with the larger and more ornamented ones, implying stratified stable conditions (Premoli Silva et al., 1999). Under mesotrophic conditions the biogenic association is depleted in large planktonic foraminifera (Premoli Silva et al., 1999). Under eutrophic conditions K-strategist calcareous plankton are overwhelmed by r-opportunist diatoms and radiolarians and locally dynoflagellates (Premoli Silva et al., 1999). Under extreme conditions bacterial phytoplankton becomes dominant (Kuypers et al., 2004). Thus we can identify two antagonist worlds: a “carbonate realm” and a “siliceous realm”, as schematically represented in the “lithogenetic” scheme of Fig. 6.10.

How does the transition from one realm to another occur? As a matter of fact, in this kind of successions, "layering" is mostly a diagenetic feature, due to both enhancing of compositional/textural changes, and to segregation of clay, carbonate and silica minerals along newly formed interfaces (see Chapter 4). On the contrary it cannot be denied that, even considering a diagenetic overprint, the sharp boundaries have to be related to primary depositional factors. The sharp changes from carbonate to siliceous sediments observable at a field scale cannot be related to continuous shifts in the carbonate compensation depth (CCD). Changes in the biogenic facies association are most reliably related to changes in the trophic level in the superficial water masses with consequent changes in the association of living organisms.

In the described sections (Figs. 6.5a-e) the transition from a calcareous layer to a radiolarian layer is very frequent, as it is highlighted by the stacking pattern of sequences 1 and 3a. In many cases we have observed a marl/clay interval in between, sometimes thicker than 1cm, that is a thickness sufficient to exclude a diagenetic segregation origin. We speculate whether in a pelagic environment part of these shale layers are explainable as the result of different saturation behavior of calcite and silica along the water column. Sea-water is saturated in calcite above the so-called carbonate compensation depth, while it is generally under-saturated in silica along the whole water column. A high level of siliceous productivity is needed in order to allow the preservation of the siliceous organisms during their settling along the water column preserving them from dissolution once they reach the sea-floor.

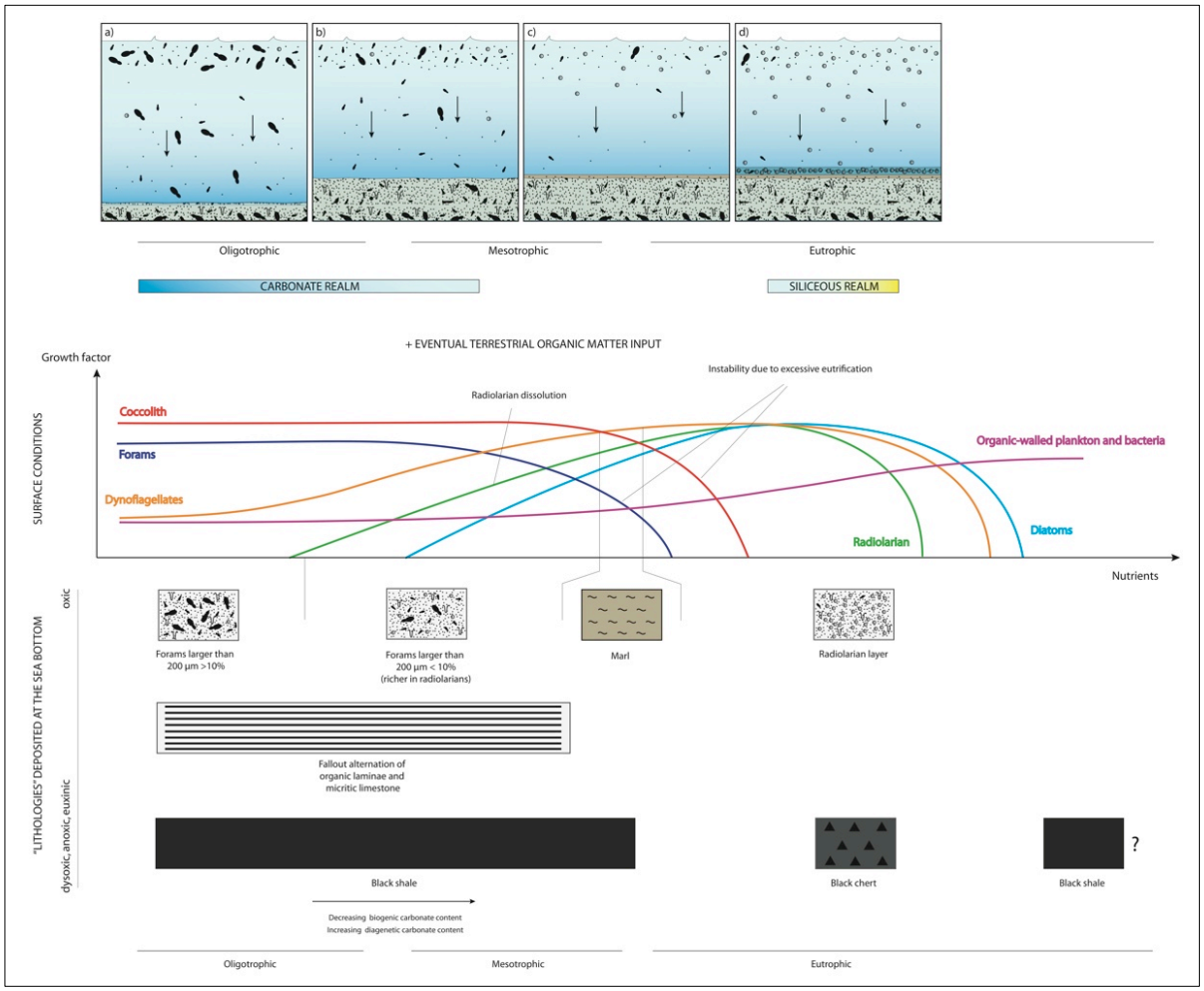

Figure 6.10: Lithogenetic scheme illustrating the shift from a carbonate- to a siliceous-dominated deposition, see text for a detailed explanation.

With the exclusion of exceptional times of higher clay input due to increased riverine supply, large amounts of aeolian dust or volcanic ashes, we can generally assume a continuous input of shale in the basin, diluted within the huge amount of carbonate fraction. During times of gradual shift to mesotrophic/eutrophic conditions the carbonate producers decrease while the increase of the silica producers is still not sufficient to warrant their preservation and their lithogenetic role. The resulting lithology would be a shale/marl facies, poor in radiolaria that is the expression of a low sedimentation rate coupled with silica dissolution, thus mimicking condensation. Only when the increase in silica organisms is sufficient to prevail on silica dissolution the transition to the siliceous realm will be efficient to generate a siliceous-rich layer.

The above described process is connected with oxic bottom-water conditions (stacking pattern 1). A similar sequence of lithologies can be observed under anoxic conditions with the addition of preserved

organic matter diluted within the hosting sediments (stacking patterns 2 and 3b). We can suppose a change from black shale (organic matter diluted by mud/marl) in oligotrophic-mesotrophic and/or eutrophic conditions to a black chert (organic matter diluted by biogenic silica) in eutrophic conditions. Following this idea a black shale deposited during mesotrophic conditions can be considered as the equivalent of a condensed interval (during low mud riverine input), due to both still silica under-saturated waters and to reduced carbonatic productivity and dissolution of the carbonate fraction because of carbon-rich aggressive bottom waters. Under extreme conditions productivity is maintained by bacterial phytoplankton with subsequent very low sedimentation rates, as described for the Bonarelli Level and its equivalents.

Thus, according to the above-described process, continuous variation in surface-water conditions would result in sharp primary lithologic contrasts at the sea-floor. This contrast is then enhanced by the subsequent diagenetic segregation.

6.5.2 Cyclic ventilation events

The three observed stacking pattern types (Figs. 6.6-6.8) result from palaoceanographic changes, as it has been previously described in terms of cyclical and repetitive shifts from oligotrophic to eutrophic conditions and vice-versa of the shallow waters. These changes controlled the repetitive shifts from calcareous to siliceous-dominated deposition and from oxic to anoxic conditions. The observed stacking pattern types show that in any case the recovery towards “normal” oligotrophic and oxic conditions, leading to deposition of a calcareous ooze, are predated by sea-bottom current activity, resulting in the deposition of the current laminated and/or winnowed facies. The current patterns could derive from either regional or local (basin-related) processes or could also be driven by the local to regional palaeoceanographic context, but in any case the link between current activity and repetitive/cyclical reventilation at the sea-floor seems to be ascertained. A wide scale significance cannot be excluded.

Turgeon and Brumsack (2006) proposed a partially silled physiography for the site of the Furlo section. The presence of a sill can be at the origin, or could have enhanced the effect of cycles of vertical water stratification. If we accept the hypothesis of at least partial confinement of the Furlo sequence we might assume that palaeobathymetry and/or distance from the shore might have played a role in the distribution of the sediments corresponding to the stacking patterns type of Sequence 3. Considering the shape of the riverine plume entering the basin the Furlo section could be interpreted as located in a proximal position (see paragraph 6.4.1). Also Monte Petrano, being similar to Furlo but with the deposition of thinner black shales, was reasonably located in a proximal and/or restricted part of the

basin. Contessa on the contrary with its type 3b sequences was probably in a less confined or shallower position.

6.5.3 Extraordinary ventilation events?

Strong sea-bottom storms and strong turnovers have been directly observed and described in the literature. Benthic storms are periodic intensification of normal bottom currents flow and play an important role in the winnowing, transport and redistribution of bottom sediments (Hollister et al., 1980; Nowell and Hollister, 1985; Hollister, 1993; Hernández-Molina et al., 2008). They occur for example in areas subjected to strong climatic contrast between high and low latitude (Hernández-Molina et al., 2008). Generally the mean flow is from two to five times faster than normal current velocities, and in some cases it can reach flow velocities of over 20cm s^{-1} with a very high concentration of suspended matter (up to 5g L^{-1}) and a large erosional capability (Hernández-Molina et al., 2008). Benthic storms have enough velocity to resuspend sediments, produce sedimentary structures at the sea floor, and rework sediments down to a depth of around 0.5m (Kennet, 1982; Bearmon, 1989; Hernández-Molina et al., 2008).

Internal waves, first reported by Ekman (1904), called also baroclinic currents, are another process able to develop high horizontal current velocities up to $2m^{-1}$ and vertical velocities of 20cm s^{-1} (Brandt et al., 2002). These gravity waves result from the oscillation along the interface between two water layers of different densities (Shanmugam, 2008) due to either differences in temperature or salinity.

Evidences of particularly enhanced circulation have been described also in the geological record. In order to explain the frequent erosions observed at the base of the Paleozoic black shale, Baird et al. (1986, 1988, 1991) suggested the existence of deep-storm-waves, density currents and internal waves connected to the existence of a vertical chemical stratification. One of the most known example of exceptional mixing of the water masses is the Permo-Triassic boundary, a time of widespread "superanoxia" as firstly introduced by Isozaki, Y. (1994) and successively described by other authors (Wignall et al., 1992; Brennecka et al., 2011; Payne et al., 2012; Dustira et al., 2013) with a total stratification of the superocean Panthalassa for nearly 20 million years (Isozaki, Y., 1997). According to few authors (Kajiwara et al., 1994; Knoll et al., 1996) the catastrophic overturn of the ocean masses supersaturated in carbon dioxide was at the origin of the impressive Permo-Triassic extinction.

The facies association of the Scaglia and the stacking pattern types document the activity of currents at the sea-bottom. The stratigraphic distribution of the most striking tractive facies shows that there is a

relationship between high traction intensity at the sea-floor and the major perturbations to the global carbon cycle (Fig. 6.11).

In particular we have observed limestones with wavy and pervasive plane-parallel laminations (C2 and D2 facies) within the OAE1d (Fig. 6.11) at Le Brecce, Monte Petrano and Cismon sections (Figs. 6.5c, d and e), thus suggesting strong bottom-current reworking of these beds.

In all the studied sections of the Umbria-Marche Basin, in the stratigraphic interval within the MCE and the OAE2, two main phases of enhanced circulation are evident (Facies C2 and D2). The first is at about one third and the second at about two thirds of the sequence comprised between these two events. For example in the Furlo section the first phase is at about 12m up to 14m and the second from about 22.5m up to 23.5m (Fig. 6.5a).

Particularly intriguing are the structures observed in the interval above the Bonarelli layer. Even if it is less clear in the Cismon section of the Belluno Basin, it is particularly evident in the Umbria-Marche Basin, where about one meter above the Bonarelli in all the sections there are many beds composed mainly of foraminiferal-intraclastic laminated limestones produced by the concentration and alignment of large foraminifera and, more rarely, intraclasts to form flat lenses or laminae of packstone/wackestone and floatstones (Facies E2; Figs. 6.5 and 6.11). These layers, frequently embedded with abrupt base within the pervasive laminated facies are residual lags produced by winnowing of the fine fraction under oxygenated conditions. Moreover, curious slightly deformative structures are common at the top of the Bonarelli layer of all of the studied sections. This is particularly evident in the first 15 cm at the top of the Bonarelli at Furlo Quarry, where the first few limestone layers are widely ondulated, deformed and with multiple hummocks-like geometries. Even if these "calcareous muddy hummocks" are difficult to interpret, because a diagenetic overprint to enhance the curvature of the bed boundaries cannot be excluded, their relation with soft sediment deformation under strong shear stress cannot be neglected. So we consider the systematic presence of this peculiar facies at the top of the Bonarelli as another indication of the activity of the strongest sea-bottom currents.

We then speculate whether in the two basins a time of extraordinary ventilation might have postdated the OAE2. At present we would not state if it's just a local/regional phenomenon or if it occurred at a wider scale. In the literature is frequently described the presence of hiatuses associated with the main OAEs, both in pelagic settings as in coastal environments (e.g. Jones et al., 1994; Drzewiecki and Simo, 1997; McArthur et al., 2000; Jones et al., 2001; Meyers and Sageman, 2004; Erbacher et al., 2005; Robinson et al., 2008; El-Sabbagh et al., 2011; Caswell et al., 2012. Few authors have explained

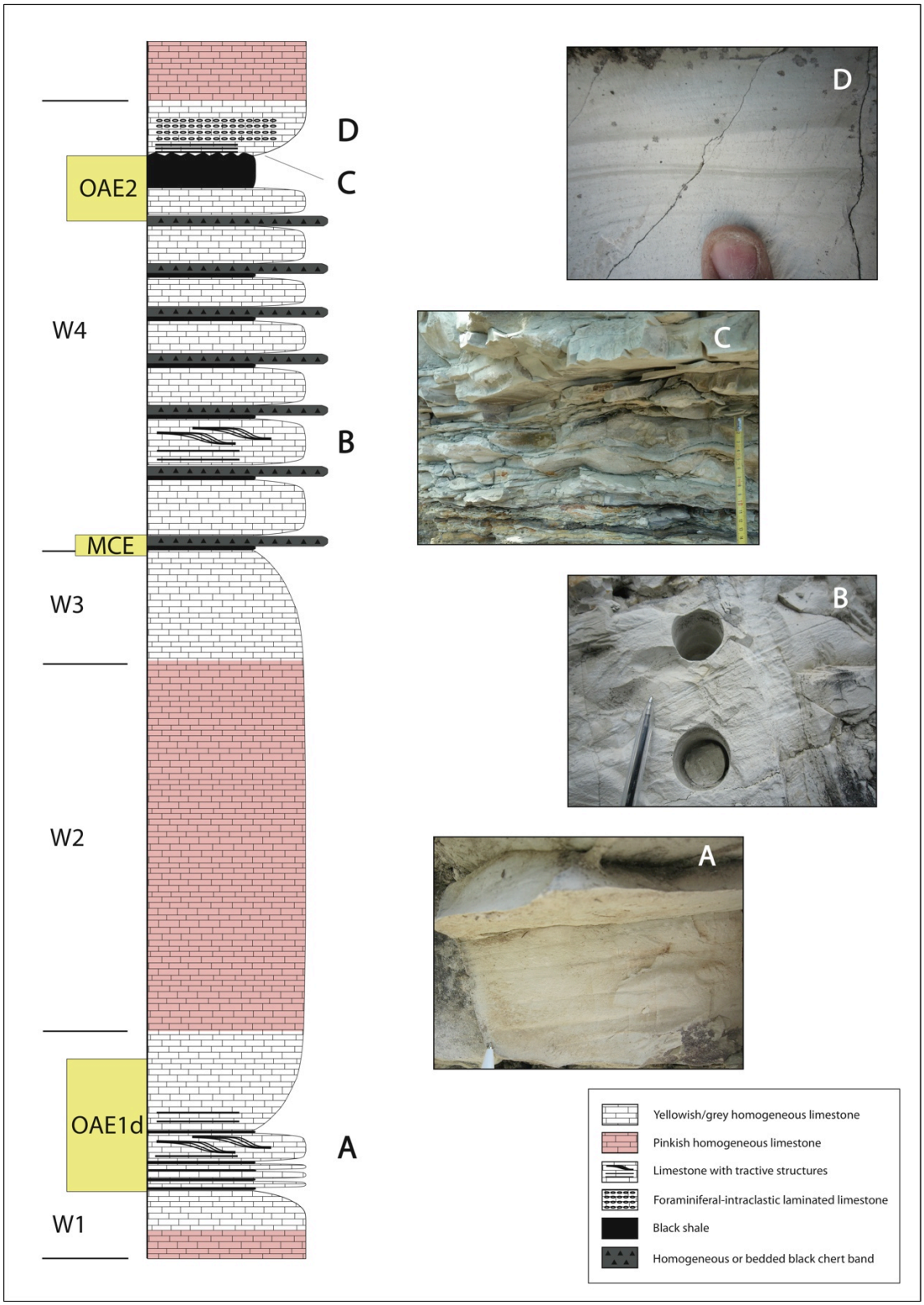

Figure 6.11: Vertical profile illustrating the main lithological variations in the Umbria-Marche Basin across the Scaglia Bianca Formation. The main geochemical events are indicated. In the pictures: A) wavy structures above/within the OAE1d (C2 and D2 facies); B) wavy laminated limestones a few meters above the MCE (C2 and D2 facies); C) wavy structures right at the top of the Bonarelli layer (E2 facies); D) foraminiferal-intraclastic lamination in the limestone about 1 meter above the Bonarelli layer (D2 and E2 facies).

these hiatuses as linked to a general regressive trend (e.g. Jaillard and Arnaud-Vanneau, 1993; Gröcke et al., 2006). We hypothesize that the recurrent gap above the OAE2 and maybe other OAEs could be the result of a geochemical process coupled with complementary physical processes, e.g. activity of bottom currents.

When comparing the $\delta^{18}O$ record (as previously presented in Chapter 5) with the vertical facies log, there is a clear relation between the occurrence of the sedimentary structures connected with the highest sea-bottom current intensity and the $\delta^{18}O$ positive excursions associated with cooling phases. In particular, an important part of the missing portion of the record (see Fig. 5.12 in Chapter 5), when compared with the Eastbourne section isotopic profile (Tsikos et al., 2004), lies within a cooling phase (Fig. 6.12).

As supposed for the Permo-Trias boundary by Knoll et al. (1996), the decrease in atmospheric greenhouse capacity would re-establish a latitudinal thermal gradient thus facilitating the growth of continental glaciers, but after high-latitude cooling reached a critical threshold, vigorous, thermo-haline bottom current circulation would be induced, causing oceanic overturn and the rapid return to normal conditions.

Times characterized by enhanced circulation might have resulted in major erosion and reworking of the sediments on the sea-bottom during the recovery from the anoxic conditions. Moreover an increase in ventilation would produce a great amount of sediment drifts that are frequently subjected to slump and instability (Laberg and Camerlenghi, 2008). In particular when the sediments are rich in siliceous organisms, as in the studied interval above the Bonarelli layer, the intergranular contacts among whole or broken siliceous microfossils prevent normal sediment consolidation, favouring sediment instability and erosion (Volpi et al., 2003; Laberg and Camerlenghi, 2008). The lithologic contrast at the top of the Bonarelli between the black shales-radiolarian layer rich interval and the above limestone facies could act *di per se* both as a preferential boundary for erosion of unconsolidated sediments and as the basal surface for slumping and sediment instability. At the same time an increase in bottom current reworking after the Bonarelli would have accumulated vast drifted deposits easily subjected to slump and resedimentation in the deepest part of the basin.

This process could be at the origin of strong ventilation events during the recovery from the OAE2. The shift of the color from whitish limestones to reddish hematite rich limestones a few meters above the Bonarelli and above the OAE 1d confirms both a change in shale availability and a general shift to an increase of dissolved oxygen in bottom waters due to an intensification of bottom circulation (Hu et al., 2009; Wang et al., 2011; Neuhuber and Wagreich, 2011; Xi et al., 2007).

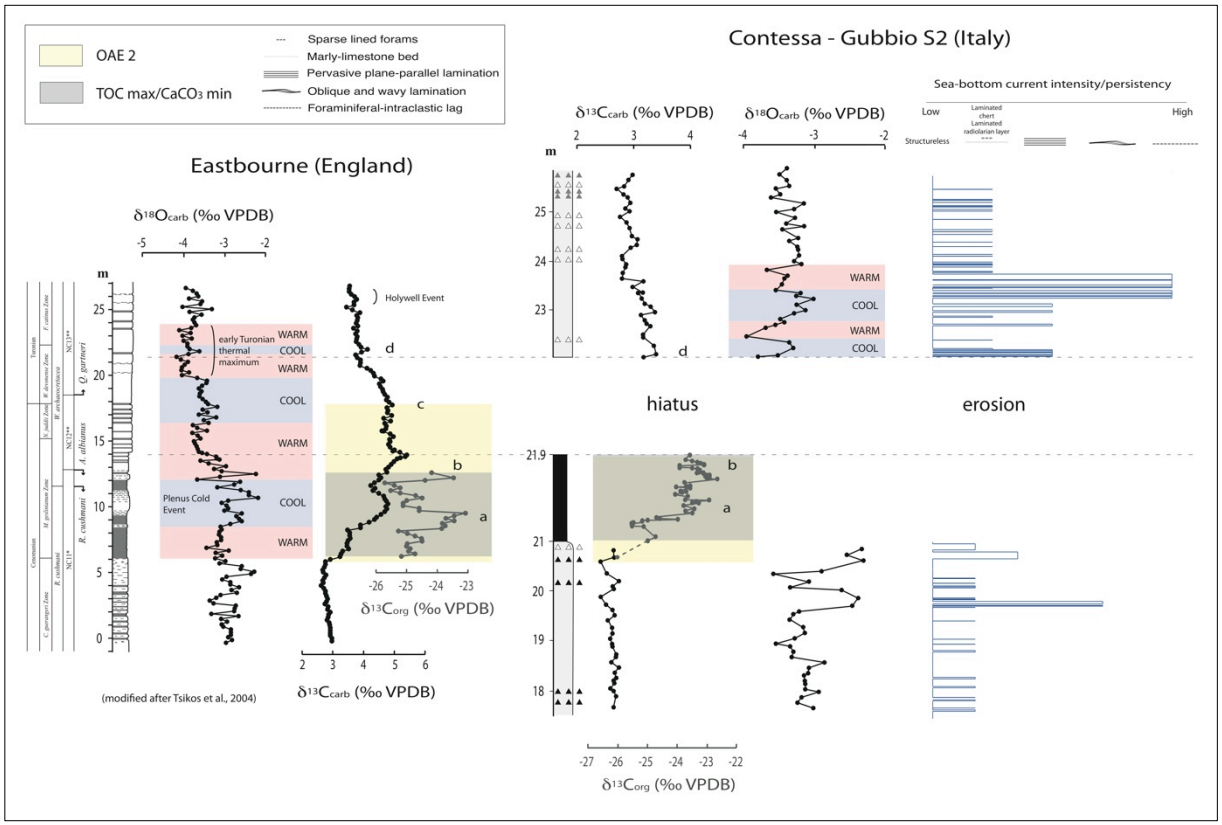

Figure 6.12: Comparison of the carbon and oxygen isotopic profile for the OAE2 interval at Eastbourne (England) on the left (Tsikos et al., 2004) and at Gubbio S2 on the right (Tsikos et al., 2004), together with the vertical facies log. Bottom currents intensity that increases from left to right, is here correlated to cooling phases. The position of the Bonarelli Level is indicated by a grey band, while the OAE2 interval by a yellow band. On the oxygen isotopic curves the warm and cool phases are highlighted with a pink and light blue band respectively. The stratigraphic position of the possibly eroded portion is indicated.

6.6 Conclusions

The data-set from the Cretaceous pelagic successions of the Umbria-Marche and Belluno Tethyan basins permits to draw the imagine of a dynamic sea-bottom, linking the depositional patterns with the oceanographic changes occurring at the surface waters and with the intensity of sea-bottom currents, both during the OAEs 1d, MCE and OAE2 and during the interludes among them.

The switch from oligotrophic to eutrophic conditions of the surface waters controls the shift from calcareous to siliceous deposition, in oxic conditions. At the sites and times of anoxia, siliceous and organic-rich shales (black shales) replace to one another as a function of trophism, black shales corresponding to oligotrophic–mesotrophic/eutrophic and black cherts exclusively to eutrophic conditions.

The stacking patterns of the observed facies show the repetition of three major types, all of them including indications of bottom current activity. Invariably the position of tractive facies within the stacking patterns indicates that they postdate the deposition of the sediments related to the peak perturbation of trophism and/or oxygenation. This systematic association documents the role of bottom currents in the recovery of the "normal" environmental conditions.

According to my data sea-bottom ventilation is a common process, fundamental in order to re-establish the "normal" oceanic conditions after any perturbation. Phases of enhanced circulation seem to represent repetitive events in the normal cycles of stratification and de-stratification of water masses and re-establishment of normal oxyenation conditions. Different depositional patterns within the sedimentary sequence reflect repetitive environmental variations mainly controlled by trophic conditions and oxygenation rate. The identified cyclicity has various orders of magnitude, ranging from the meter scale, as expressed by the described stacking pattern types represented by sequences 1 - 3, down to the mm-scale as expressed by the internal variations observed in the black shale and bedded black chert facies (G4a).

Evidences of traction-related facies after the OAE1d and in particular above the OAE2 suggest that the times of most intense circulation ("extraordinary reventilation events") postdated the major perturbations of the global carbon cycle. These phases of intensified ventilation must have played an important role in re-establishing normal water masses trophism, oxygenation and stratification. Intense sea-bottom currents might have had important effects on the dynamics of sediment redistribution causing the widely observed erosional gap at the top of OAE2, in particular associated with cooling phases that might have enhanced bottom current ventilation.

Oceanic Anoxic Events represent incredible opportunities in order to observe how do Earth system reacts to extreme greenhouse conditions. These events have represented both a physical and a chemical major perturbation and thus only an integrated study of both the physical and chemical process can lead to a better comprehension of the mechanisms at the origin and resolution of these events. The dramatic environmental conditions connected to these global events might have required impressive feedback processes in order to shift back the system to normal climatic conditions.

References

Alvarez, W. (1990) – Pattern of extensional faulting in pelagic carbonates of the Umbria-Marche Apennines of central Italy. *Geology*, 18, 407-410.

Alvarez, W. (2009) – The historical record in the Scaglia limestone at Gubbio: magnetic reversals and the Cretaceous-Tertiary mass extinction. *Sedimentology*, 56, 137-148.

Alvarez, W. and Lowrie, W. (1984) – Magnetic stratigraphy applied to synsedimentary slumps, turbidites, and basin analysis: The Scaglia limestone at Furlo (Italy). *Geological Society of America Bulletin*, 95, 324–336.

Arthur, M.A. and Premoli Silva, I. (1982) – Development of widespread organic carbon-rich strata in the Mediterranean Tethys. *In:* Schlanger, S.O. and Cita, M.B. (Eds.), *Nature and Origin of Cretaceous Carbon-rich Facies*, 7-54.

Arthur, M.A., Brumsack, H.-J., Jenkyns, H.C. and Schlanger, S.O. (1990) – Stratigraphy, geochemistry, and paleoceanography of organic carbon-rich Cretaceous sequences. *In:* Ginsburg, R. and Beaudoin, B. (Eds.), *Cretaceous Resources Events, and Rhythms*, 75-119.

Baird, G.C. and Brett C.E. (1986) – Erosion on an anaerobic seafloor: significance of reworked pyrite deposits from the Devonian of New York State. *Palaeogeography, Palaeoclimatology, Palaeoecology*, 57, 157-193.

Baird, G.C., Brety, C. E., Kirchgasser, W. T. (1988) – Genesis of black shale-roofed discontinuities in the Genesee Formation, western New York State. *In:* McMillan, N.J., Embry, A.F., Glass, D.J. (Eds.), *Devonian of the World*, Canadian Society of Petroleum Geologists Memoir, 14, 357-375.

Baird, G.C. and Brett, C.E. (1991) – Submarine erosion on the anoxic seafloor: stratinomic paleoenvironmental, and temporal significance of reworked pyrite-bone beds. *In:* Tyson, R.V. and Pearson, T.H. (Eds.), Modern and Ancient Shelf Anoxia: Geological Society of London, Special Publication, 58, 233-257.

Barron, E.J. and Washington, W.M. (1985) – Warm cretaceous climates: High atmospheric CO2 as a plausible mechanism. *In:* Sundquist, E.T. and Broecker, W.S., *The carbon cycle and atmospheric CO2: natural variations archean to present*, Proceedings of the Chapman Conference on Natural Variations in Carbon Dioxide and the Carbon Cycle, 32, 546-553.

Bearmon, G. (1989) – Ocean chemistry and deep-sea sediments, 134pp

Beaudoin, B., M'Ban, E.P., Montanari, A., Pinault, M. (1996) – Lithostratigraphie haute résolution (<20 ka) dans le Cénomanien du bassin d'Ombrie-Marches (Italie). *Comptes Rendus de l'Académie des Sciences Paris*, 323 Series Iia, 689-696.

Bellanca A., Claps, M., Erba, E., Masetti, D., Neri, R., Premoli Silva, I. and Venezia F. (1996) – Orbitally induced limestone/marlstone rhythms in the Albian-Cenomanian Cismon section (Venetian region, northern Italy): sedimentology, calcareous and siliceous plankton distribution, elemental and isotope geochemistry. *Palaeogeography, Palaeoclimatology, Palaeoecology*, 126, 227-260.

Bernoulli, D. and Jenkyns, H.C. (1974) – Alpine, Mediterranean, and Central Atlantic Mesozoic facies in relation to the early evolution of the Tethys. In: Dott, R.H. and Shaver, R.H. (Eds.), Modern and Ancient Geosynclinal Sedimentation. Society of Economic Paleontologists and Mineralogists, Special Publication, 19, 129-160.

Bosellini, A., Broglio Loriga, C., and Busetto, C. (1978) - I bacini cretacei del Trentino. *Riv. Ital Paleont. Strat*, 84.4, 897-946.

Brandt, P., Rubino, A., Fischer, J. (2002) – Large-amplitude internal solitary waves in the North Equatorial Countercurrent. Journal of Physical Oceanography, 32, 1567-1573.

Brennecka, G.A., Herrmann, A.D., Algeo, T.J., Anbar, A.D. (2011) – Rapid expansion of oceanic anoxia immediately before the end-Permian mass extinction. *Proc. Natl. Acad. Sci.* USA, 108, 17631–34.

Brumsack, H.-J. (2006) – The trace metal content of recent organic carbon-rich sediments: Implications for Cretaceous black shale formation. *Palaeogeography, Palaeoclimatology, Palaeoecology*, 232, 344-361.

Caswell, B.A. and Coe, A.L. (2012) – A high-resolution shallow marine record of the Toarcian (Early Jurassic) Oceanic Anoxic Event from the East Midlands Shelf, UK. *Palaeogeography, Palaeoclimatology, Palaeoecology*, 365-6, 124-135.

Channel J.E.T., D'Argenio, B., Horvath, F. (1979a) – The African Promontory, in Mesozoic Mediterranean Paleogeography. *Earth Science Review*, 15, 213-272.

Channel, J. E. T., Lowrie, W. and Medizza, F. (1979b) – Middle and Early Cretaceous magnetic stratigraphy from the Cismon section, northern Italy. *Earth and Planetary Science Letters*, 1979, 42.2, 153-166.

Claps, M., Masetti, D., Pedrielli, F., Garavello, A. (1991) – Analisi spettrale e cicli di Milankovitch in successioni cretaciche del Sudalpino orientale. Rivista Italiana di Paleontologia e Stratigrafia, 97, 153-174.

Claps, M. and Masetti, D. (1994) – Milankovitch periodicities recorded in Cretaceous deep-sea sequences from the Southern Alps (Northern Italy). Special Publications International Association of Sedimentologists, 19, 99-107.

Coccioni, R., Galeotti, S., Ragni, D. (1992) – Litho- and biostratigraphy of the Scaglia Bianca Formation (Late Albian-Late Cenomanian) in the Umbria-Marche Apennines (Italy). 6th Annual Meeting of IGCP 262 (Tethyan Cretaceous Correlation) - 'Cretaceous Facies in Orogenic Belts', Athens, 22-26 May, 1992, p. 4.

Coccioni, R., Galeotti, S. (2001) – The mid-Cenomanian Event the Prelude to the OAE 2. EOS Trans. AGU 82(47), Fall Meet. Suppl.

Coccioni, R., Galeotti, S. (2003) – The mid-Cenomanian Event: prelude to OAE 2. *Palaeogeography, Palaeoclimatology, Palaeoecology*, 190, 427-440.

Dercourt, J., Gaetani, M., Vrielinck, B., Barrier, E., Biju-Duval, B., Brunet, M.F., Cadet, J.P., Crasquin, S., Sandulescu, M. (2000) – *Atlas of Peri-Tethys, Palaeogeographical Maps. Commission de la Carte Geologique du Monde (CCGN/CGMW)*, Paris, pp. 1-269.

Donnadieu, Y., Pierrehumbert, R., Jacob, R., Fluteau, F. (2006) – Modelling the primary control of paleogeography on Cretaceous climate. *Earth and Planetary Science Letters*, 248, 426-437.

Drzewiecki, P.A. and Simo, J.A. (1997) – Carbonate platform drowning and oceanic anoxic events on a Mid-Cretaceous carbonate platform, south-central Pyrenees, Spain. *Journal of Sedimentary Research*, 67, 698-714.

Dustira, A.M., Wignall, P.B., Joachimski, M., Blomeier, D., Hartkopf-Fröder, Bond, D.P.G. (2013) – Gradual onset of anoxia across the Permian–Triassic Boundary in Svalbard, Norway. *Palaeogeography, Palaeoclimatology, Palaeoecology*, 374, 303-313.

Ekman, V.W. (1904) – On dead water. Norwegian North Polar Expedition 1893-1896. Sci. Res., 5, 152pp.

El-Sabbagh, A., Tantawy, A.A., Keller, G., Khozyem, H., Spangenberg, J., Adatte, T., Gertsch, B. (2011) – Stratigraphy of the Cenomanian-Turonian Oceanic Anoxic vent OAE2 in shallow shelf sequences of NE Egypt. *Cretaceous Research*, 32, 705-722.

Erba, E. (1994) – Nannofossils and superplumes: the early Aptian 'nannoconid crisis'. *Paleoceanography*, 9, 483-501.

Erba E. (2004) – Calcareous nannofossils and Mesozoic oceanic anoxic events. *Marine Micropaleontology*, 52, 85-106.

Erba, E., Bartolini, A., Larson, R.L. (2004) – Valanginian Weissert oceanic anoxic event. *Geology*, 32, 149-152.

Erba E. and Larson R.L. (1998) – The Cismon APTICORE (Southern Alps, Italy): a reference section for the Lower Cretaceous at low latitudes. *Rivista Italiana di Paleontologia e Stratigrafia*, 104, 181-192.

Erbacher, J., Friedrich, O., Wilson, P.A., Birch, H., Mutterlose, J. (2005) – Stable organic carbon isotope stratigraphy across Oceanic Anoxic Event 2 of Demerara Rise, western tropical Atlantic. *Geochemistry, Geophysics, Geosystems*, 6, Q06010, doi:10.1029/2004GC000850.

Friedrich, O., Erbacher, J., Wilson, P.A., Moriya, K. and Mutterlose, J. (2009) – Paleoenvironmental changes across the Mid Cenomanian Event in the tropical Atlantic Ocean (Demerara Rise, ODP Leg 207) inferred from benthic foraminiferal assemblages. *Marine Micropaleontology*, 71, 28-40.

Gambacorta, G., Bersezio, R., Erba, E. (submitted) – Sedimentation in the Tethyan pelagic realm during the Cenomanian: monotonous settling or active redistribution?

Giorgioni, M., Weissert, H., Bernasconi, S.M., Hochuli, P.A., Coccioni, R., Keller, C.E. (2012) – Orbital control on carbon cycle and oceanography in the mid-Cretaceous greenhouse. *Paleoceanography*, 27, PA1204, doi:10.1029/2011PA002163.

Graham, A.R. (1963) – Routine preparation of polished thin-sections. *The Canadian Mineralogi*st, 7(3), 375-377.

Gröcke, D.R., Ludvigson, G.A., Witzke, B.L., Robinson, S.L., Joeckel, R.M., Ufnar, D.F., Ravn, R.L. (2006) – Recognizing the Albian-Cenomanian (OAE1d) sequence boundary using plant carbon isotopes: Dakota Formation, Western Interior Basin, USA. *Geology*, 34,193-196.

Hallam, A. (1985) – A review of Mesozoic climates. *Journal of the Geological Society*, 142 433-445.

Hallam, A. (1994) – Jurassic climates as inferred from the sedimentary and fossil record. *In:* Allen, J.R.L., Hoskins, B.J., Sellwood, B.W., Spicer, R.S., Valdes, P.J. (Eds.), *Palaeoclimates and their Modelling: With Special Reference to the Mesozoic Era*, 79-88.

Haq, B.U., Hardenbol, J., Vail, P.R. (1987) – Chronology of fluctuating sea levels since the Triassic. *Science*, 235, 1156-1167.

Hay, W.W. (2008) – Evolving ideas about the Cretaceous climate and ocean circulation. *Cretaceous Research*, 29, 725-753.

Hay, W.W., DeConto, R.M., Wold, C.N., Wilson, K.M., Voigt, S., Schulz, M., Wold-Rossby, A., Dullo, W.-C., Ronov, A.B., Balukhovsky, A.N., and Söding, E. (1999) – Alternative global Cretaceous paleogeography. *In:* Barrera, E. and Johnson, C.C. (Eds.), *Evolution of the Cretaceous Ocean-Climate System*, Geological Society of America Special Paper 332, 1-47.

Haworth , M., Hesselbo, S.P., McElwain, J.C., Robinson, S.A. and Brunt, J.W. (2005) – Mid Cretaceous pCO_2 based on stomata of the extinct conifer *Pseudofrenelopsis* (Cheirolepidiaceae). *Geology*, 33, 749-752.

Hernández-Molina, F.J., Maldonado, A., Stow, D.A.V. (2008) – Abyssal plain controurites. *In:* Rebesco, M., Camerlenghi, A. (Eds.), *Contourites. Developments in Sedimentology*, 60, 345-378.

Hollister, C.D. (1993) – The concept of deep-sea contourites. *Sedimentary Geology*, 82, 5-11.

Hollister, C.D., Nowell, A.R.M., Smith, J.D. (1980) – The Third Annual Report of the High Energy Boundary Layer Experiment. WHOI. Tech. Rep., 80, 32-48.

Hori, R.S., Cho, C., Umeda, H. (1993) – Origin of cyclicity in Triassic-Jurassic radiolarian bedded cherts of the Mino accretionary complex from Japan. *The Island Arc*, 3, 170-180.

Hu, X., Cheng, W., Ji, J. (2009) – Origin of Cretaceous Oceanic Red Beds from the Vispi Quarry Section, Central Italy: Visible Reflectance and Inorganic Geochemistry. In: Hu, X., Wang, C., Scott, R.W., Wagreich, M., Jansa, L. (Eds.), *Cretaceous Oceanic Red Beds: Stratigraphy, Composition, Origins, Paleoceanographic, and Paleoclimatic Significance*, SEPM Special Publication, 91, 183-197.

Hu, X., Wagreich, M., Yilmaz, I.O. (2012) – Marine rapid environmental/climatic change in the Cretaceous greenhouse world. *Cretaceous Research*, 38, 1-6.

Huber, B.T., Hodell, D.A., Hamilton, C.P. (1995) – Middle – Late Cretaceous climate of the southern high latitudes: stable isotopic evidence for minimal equator-to-pole thermal gradients. *Geological Society of America Bulletin*, 107, 1164–1191.

Isozaki, Y. (1994) – Superanoxia across the Permo-Triassic boundary: Recorded in accreted deep-sea pelagic chert in Japan. Canadian Society of Petroleum Geologists Memoir, 17, 805-812.

Isozaki, Y. (1997) – Permo-Triassic Boundary Superanoxia and Stratified Superocean: Records from Lost Deep Sea. *Science*, 276, 235-238.

Jacquin, T., Magniez-Jannin, F., Ponsot, C., De Graciansky, P., Vail, P.R. (1991) – The Cretaceous oceanic events (anoxia and hiatus) within a sequence stratigraphic framework. American Association of Petroleum Geologists, Tulsa, OK, United States, *In:* Anonymous, *AAPG 1991 annual convention with DPA/EMD divisions and SEPM, an associated society*, 75 (3), 601, georefid:1991-059486.

Jaillard, E. and Arnaud-Vanneau, A. (1993) – The Cenomanian-Turonian transition on the Peruvian margin. *Cretaceous Research*, 14, 585-605.

Jarvis, I., Gale, A.S., Jenkyns, H.C., Pearce, M.A. (2006) – Secular variation in Late Cretaceous carbon isotopes: a new $\delta^{13}C$ carbonate reference curve for the Cenomanian–Campanian (99.6–70.6 Ma). *Geological Magazine*, 143, 561-608.

Jenkyns, H.C. (1999) – Mesozoic anoxic events and paleoclimate. *Zentralblatt für Geologie und Paläontologie, Teil.* I, 943-949.

Jenkyns, H.C. (2003) – Evidence for rapid climate change in the Mesozoic–Palaeogene greenhouse world. *Philosophical Transactions of the Royal Society of London A*, 361, 1885-1916.

Jenkyns, H.C. (2010) – Geochemistry of oceanic anoxic events, Geochemistry Geophysics Geosystems, pp. doi: 10.1029/2009GC002788

Jones, C.E., Jenkyns, H. C., Coe, A. L., Hesselbo, S. P. (1994) – Strontium isotopic variations in Jurassic and Cretaceous seawater. *Geochimica et Cosmochimica Acta*, 58, 3061–3074.

Jones, C.E. and Jenkyns, H.C. (2001) – Seawater strontium isotopes, oceanic anoxic events, and seafloor hydrothermal activity in the Jurassic and Cretaceous, *American Journal of Science*, 301, 112-149.

Kajiwara, Y., Yamakita, S., Ishida, K., Ishiga, H., Imai, A. (1994) – Development of a largely anoxic stratified ocean and its temporary massive mixing at the Permian-Triassic boundary supported by the sulfur isotopic record. *Palaeogeography, Palaeoclimatology, Palaeoecology*, 111, 367-379.

Kennet, J.P. (1982) – The geologic record of bottom currents. *In:* Kennet, J.P. (Eds.), *Marine Geology*, 505-534.

Kerr, A.C. (1998) – Oceanic plateau formation: A cause of mass extinction and black shale deposition around the Cenomanian-Turonian boundary. *Journal of the Geological Society, 155*, 619-626.

Knoll, A.H., Bambach, R.K., Canfield, D.E., Grotzinger, J.P. (1996) – Comparative Earth history and Late Permian mass extinction. *Science*, 273, 452-57.

Kuypers, M.M.M., van Bruegel, Y., Shouthen, S., Erba, E., Sinnighe Damsté, J.S. (2004) – N2-fixing cyanobacteria supplied nutrient N for Cretaceous oceanic anoxic events. *Geology*, 32, 853-856.

Laberg, J.S. and Camerlenghi, A. (2008) – The significance of contourites for submarine slope stability. *In:* Rebesco, M., Camerlenghi, A. (Eds), *Contourites. Developments in Sedimentology*, 60, 537-556.

Lalli, C.M. and Parsons, T. (1997) – Biological oceanography: an introduction. *Pergamon Press*, 382pp.

Lanci L., Muttoni, G., Erba E. (2010) – Astronomical tuning of the Cenomanian Scaglia Bianca Formation at Furlo, Italy. *Earth and Planetary Science Letters*, 292, 231-237.

Larson, R.L. (1991a) – Latest pulse of the Earth: evidence for a mid-Cretaceous superplume. Geology, 19, 547–550.

Larson, R.L. (1991b) – Geological consequences of superplumes. *Geology*, 19, 963–966.

Larson, R.L. and Erba, E. (1999) – Onset of the mid-Cretaceous greenhouse in the Barremian-Aptian: Igneous events and the biological, sedimentary, and geochemical responses. *Paleoceanography*, 14, 663-678.

Leckie, R.M., Bralower, T.J., Cashman, R. (2002) – Oceanic anoxic events and plankton evolution: Biotic response to tectonic forcing during the mid-Cretaceous. *Paleoceanography*, 17, 13-29.

McArthur, J. M., Donovan, D. T., Thirlwall, M. F., Fouke, B. W., Mattey, D. (2000) – Strontium isotope profile of the Early Toarcian (Jurassic) Oceanic Anoxic Event, the duration of ammonite biozones, and belemnite palaeotemperatures. *Earth and Planetary Science Letters*, 179, 269-285.

Meyers, S.R. and Sageman, B.B. (2004) – Detection, quantification, and significance of hiatuses in pelagic and hemipelagic strata. Earth and Planetary Science Letters, 224, 55-72.

Mitchell, R.N., Bice, D.M., Montanari, A., Cleaveland, L.C., Christianson, K.T., Coccioni, R., Hinnov, L.A. (2008) – Oceanic anoxic cycles? Orbital prelude to the Bonarelli Level (OAE2). *Earth and Planetary Science Letters*, 267, 1-16.

Monechi, S. and Parisi, G. (1989) – Da Gubbio a Cantiano. *In:* Cresta, S., Monechi, S., Parisi, G. (Eds.), *Stratigrafia del Mesozoico e Cenozoico nell'area umbro-marchigiana*, *Memorie Descrittive della Carta Geologica* d'Italia, 39, 96-102.

Mort, H.P., Adatte, T., Keller, G., Bartels, D., Föllmi, K.B., Steinmann, P., Berner, Z., Chellai, E.H. (2008) – Organic carbon deposition and phosphorus accumulation during Oceanic Anoxic Event 2 in Tarfaya, Morocco. *Cretaceous Research*, 29(5-6), 1008-1023.

Mutterlose, J. and Kessels, K. (2000) – Early Cretaceous calcareous nannofossils from high latitudes: Implications for palaeo- biogeography and palaeoclimate. *Palaeogeography, Palaeoclimatology, Palaeoecology*, 160, 347-372.

Neuhuber, S. and Wagreich, M. (2011) – Geochemistry of Cretaceous Oceanic Red Beds – A synthesis. *Sedimentary Geology*, 235, 72-78.

Norris, R.D., Bice, K.L., Magno, E.A., Wilson, P.A. (2002) – Jiggling the tropical thermostat in the Cretaceous hothouse. *Geology*, 30, 299-302.

Nowell, A.R.M. and Hollister, C.D. (1985) – Deep ocean sediment transport – Preliminary results of the high energy benthic boundary layer experiment. *Marine Geology*, 66, 420pp.

Payne, J.L. and Clapham, M.E. (2012) – End-Permian mass extinction in the oceans: an ancient analog for the twenty-first century?. *Annual Review of Earth and Planetary Sciences*, 40, 89-111.

Premoli Silva, I., Erba, E., Salvini, G., Verga, D., Locatelli, C. (1999) – Biotic changes in Cretaceous Anoxic Events. *Journal of Foraminiferal Research*, 29, 352-370.

Robinson, S.R., Clarke, L.J., Nederbragt, A., Wood, I.G. (2008) – Mid-Cretaceous oceanic anoxic events in the Pacific Ocean revealed by carbon-isotope stratigraphy of the Calera Limestone, California, *GSA Bulletin*, 120(11/12), 1416-1427.

Salmon, V., Derenne, S., Lallier-Vergés, E., Largeau, C., Beaudoin, B. (1998) – Alteration of Organic Matter During Chertification of a Cenomanian Black Shale (Umbria-Marche Basin, Central Italy). *Mineralogical Magazine*, 62A(3), 1314-1315.

Schlanger, S.O. and Jenkyns, H.C. (1976) – Cretaceous oceanic anoxic events: causes and consequence. *Geologie en Mijnbouw*, 55(3-4), 179-184.

Sellwood, B.W. and Valdes, P.J. (2006) – Mesozoic climates: General circulation models and rock record. *Sedimentary Geology*, 190, 269-287.

Sellwood, B.W., Valdes, P.J. (2007) – Mesozoic climates. *In:* Williams, M., Haywood, A.M., Gregory, F.J., Schmidt, D.N. (Eds.), *Deep-Time Perspectives on Climate Change: Marrying the Signal from Computer Models and Biological Proxies*, The Micropalaeontological Society, Special Publications, 201-224.

Shanmugam, G. (2008) – Deep water bottom currents and their deposits. *In:* Rebesco, M., Camerlenghi, A. (Eds.), *Contourites. Developments in Sedimentology*, 60, 59-81.

Sinnighe-Damsté, J.S., van Bentum, E.C., Reichart, G.-J., Pross, J., Schouten, S. (2010) – A CO_2 decrease-driven cooling and increased latitudinal temperature gradient during the mid-Cretaceous Oceanic Anoxic Event 2. *Earth and Planetary Science Letters*, 293, 97-103.

Skelton, P. W., Spicer, R. A., Kelley, S. P., Gilmour, I. (2003) – *The Cretaceous World*. Cambridge University Press, 360 pp.

Takashima, R., Nishi, H., Huber, B.T., Leckie, R.M. (2006) – Greenhouse world and the Mesozoic ocean. *Oceanography*, 19, 82-92.

Tiraboschi, D. (2009) – Variazioni quantitative del nannoplancton calcareo durante il Cretacico medio: paleoecologia, paleoceanografia e produzione di carbonato in condizioni di anossia globale ed eccesso di pCO_2. *Università degli Studi di Milano, PhD thesis*.

Tsikos, H., Jenkyns, H.C., Walsworth-Bell, B., Petrizzo, M.R., Forster, A., Kolonic, S., Erba, E., Premoli Silva, I., Baas, M., Wagner, T. and Sinnighe Damsté, J.S. (2004) – Carbon-isotope stratigraphy recorded by the Cenomanian-Turonian Oceanic Anoxic Event: correlation and implications based on three key localities. *Journal of the Geological Society, London,* 161, 711-719.

Turgeon, S. and Brumsack, H.-J. (2006) – Anoxic vs dysoxic events reflected in sediment geochemistry during the Cenomanian–Turonian Boundary Event (Cretaceous) in the Umbria–Marche Basin of central Italy. *Chemical Geology*, 234, 321-339.

Turgeon, S.C. and Creaser, R.A. (2008) – Cretaceous oceanic anoxic event 2 triggered by a massive magmatic episode. *Nature*, 454, 323-326.

Volpi, V., Camerlenghi, A., Hillebrand, C.-D., Rebesco, M., Ivaldi, R. (2003) – The effect of biogenic silica on sediment consolidation and slope instability, Pacific margin of the Antarctic Peninsula. *Basin Res.*, 15, 339-354.

Wang, C., Hu, X., Huang, Y., Wagreich, M., Scott, R., Hay, W. (2011) – Cretaceous oceanic red beds as possible consequence of oceanic anoxic events. *Sedimentary Geology*, 235, 27-37.

Weissert, H., Lini, A., Föllmi, K.B., Kuhn, O. (1998) – Correlation of Early Cretaceous carbon isotope stratigraphy and platform drowning events: a possible link? *Palaeogeography, Palaeoclimatology, Palaeoecology*, 137, 189–203.

Wignall, P.B. (2001) – Large igneous provinces and mass extinctions. *Earth Science Reviews*, 53, 1-33.

Wignall, P.B. and Hallam A. (1992) – Anoxia as a cause of the Permian/Triassic mass extinction: facies evidence from northern Italy and the western United States. *Palaeogeography, Palaeoclimatology, Palaeoecology* , 93, 21-46.

Wilson, M.A. and Palmer, T.J. (1989) – Preparation of acetate peels. *In:* Schneidermann, N. and Harris, P.M. (Eds.), *Paleotechniques. The Paleontological Society, Special Publication 4*, 142-145.

Wilson, P. A., and Norris, R.D. (2001) – Warm tropical ocean surface and global anoxia during the mid-Cretaceous period. *Nature*, 412, 425-429.

Winterer, E.L. and Bosellini, A. (1981) – Subsidence and sedimentation on a Jurassic passive continental margin (Southern Alps, Italy). AAPG Bulletin, 65, 394-421.

Wortmann, U.G., Herrle, J.O., Weissert, H. (2004) – Altered carbon cycling and coupled changes in Early Cretaceous weathering pattern: evidence from integrated Tethyan isotope and sandstone records. *Earth and Planetary Science Letters*, 220, 69–82.

Xi, C., Wang, C., Hu, X., Huang, Y., Wang, P., Jansa, L., Zeng, X. (2007) – Cretaceous Oceanic Red Beds: Distribution, Lithostratigraphy and Paleoenvironments. *Acta Geologica Sinica*, 81, 1070-1086.

Chapter 7

Paleoenvironmental changes across the early Albian–late Turonian time interval inferred from major and trace element geochemistry of sediments from Cismon and Monte Petrano sections (Italy)

Abstract

During the mid-Cretaceous, the Earth was experiencing one of the most extreme climate of the last 150 My. This time interval was characterized by episodes of widespread anoxia, so called Oceanic Anoxic Events (OAEs), with massive organic carbon deposition on vast areas of the oceans. In particular, the late Albian-early Turonian was a time of important changes starting with the latest Albian Oceanic Anoxic Event (OAE) 1d up to the OAE 2 of latest Cenomanian age. Major and minor elements were analyzed by X-ray fluorescence on selected samples from two Italian sections, namely at Cismon in the Belluno Basin (northern Italy) and at Monte Petrano in the Umbria-Marche Basin (central Italy). Major elements show that the sediments consist of various mixtures of clay minerals (Al), quartz, chert (Si), feldspar (Al, Na, K) and carbonates (Ca) mainly from coccoliths and foraminifers. Element/Al ratios of Ti, Mg, K, Rb and Zr are fairly constant, indicating a mostly homogeneous source area of the terrigenous material. After the Mid Cenomanian Event (MCE), a slight rise of the Zr concentrations hints at a gentle increase of coarser sediments, probably related to increased riverine input.

Ba is present in very high concentrations in both sections, as well as P although in smaller proportion. Such elements are indicative of high-productivity conditions in both areas with paleo-water depth deeper than 1000m.

At both the sections, the Bonarelli Level is severely depleted in Mn, indicating dysoxic-anoxic conditions through the water column. Black shales are restricted to specific locations characterized by anoxic waters leading to Mn-enrichments in the sediments. Several minor elements, mostly redox-sensitive or sulphide-forming, are generally enriched in the C_{org}-rich sediments, indicating temporary dysoxic to euxinic conditions in the water column.
At Cismon, with the exception of the Bonarelli Level, the depositional environment was characterized by dysoxic conditions, based on redox-sensitive elements. However, redox-sensitive elements, even with a different extent in the two basins, indicate that starting from the MCE the environment shifted to more unstable conditions with alternate times of dysoxic/anoxic and well-oxygenated bottom-waters. Also, from the MCE high concentrations of Cu and at a minor extent As, associated with diffused Zn and Y, point to the influence of an active submarine hydrothermal activity.

Key-words: anoxia, black shales, MCE, OAEs, trace metal enrichments

7.1 Introduction

The 'mid-Cretaceous' was a time of extreme greenhouse (Sellwood and Valdes, 2007; Willis and McElwain, 2002; Jenkyns 2003). The formation of Large Igneous Provinces (LIP) (Coffin and Eldholm, 1994; Neal et al., 2008) was associated to excess CO_2 leading the Earth to experience the most extreme warm episode in the past 150My (Larson, 1991a, 1991b; Erba, 1994; Kerr, 1998; Larson and Erba, 1999; Wignall, 2001; Leckie et al., 2002; Jenkyns, 2003).

The abnormal rise in CO_2 and the intense warming altered the global carbon cycle equilibria, affecting the hydrologic cycle (Weissert et al., 1998; Weissert, 2000; Wortmann, 2004), nutrients distribution, upwelling intensity and deep water formation (e.g. Takashima et al., 2006; Jenkyns 2010). A series of feedbacks must have happened in order to re-establish the normal climatic conditions. Together with weathering, burial of organic carbon might have represented an important mechanism in driving carbon removal and pCO_2 drawdown (see Jenkyns 2010 for a synthesis). The geological evidence of mid Cretaceous extreme climate and environments arrived in the early phases of ocean exploration. Sediments incredibly rich in organic matter were recovered in the Pacific, Atlantic and Indian Oceans from Cretaceous successions, coeval with black shale intervals previously described in the Thetyan domain. Based on such recoveries, Schlanger and Jenkyns (1976) defined intervals characterized by widespread deposition of organic matter Oceanic Anoxic Events (OAEs).

Across the late Albian-Cenomanian time interval, before the onset of the OAE2, for a few million years, small to medium scale perturbations to the global carbon cycles alternated with times of stable conditions (e.g. Jarvis et al., 2006). In late Albian times, well-stratified oceans collapsed abruptly with widespread deposition of organic matter during OAE 1d (Arthur et al., 1990), characterized by a long positive excursion of the $\delta^{13}C$ records of about 1‰ reaching values of about 2.5‰ in carbonate carbon (C_{carb}) (Wilson and Norris, 2001; Gröcke et al., 2006; Petrizzo et al., 2008; Giorgioni et al., 2012). Intensified winter mixing and reduced summer stratification were probably the main causes that produced the progressive reduction of the vertical thermal gradient (Wilson and Norris, 2001; Leckie et al., 2002; Watkins et al., 2005).

After OAE1d, the Cenomanian oceans reached a phase of relative stability, interrupted by the Mid-Cenomanian Event (MCE), and later on by OAE 2. Geological evidence suggests that MCE correlates with inception of generally relatively decreased ventilation at the sea floor (Coccioni and Galeotti, 2003; Coccioni et al., 1995; Friedrich et al., 2009). The MCE carbon excursion (Jarvis et al., 2006; Friedrich et al., 2009 and references therein) is not associated to general deposition of organic-rich sediments, but correlates with lithological changes (Jenkyns et al., 1994; Coccioni and Galeotti, 2003). Some authors (e.g. Coccioni et al., 2001, 2003; Hardas et al., 2012) consider the MCE as the precursor of a global palaeoclimatic and palaeoceanographic perturbation, culminating with the Bonarelli Level (OAE2). Among the Jurassic-Cretaceous OAEs the latest Cenomanian event (Bonarelli, 1891; Schlanger and Jenkyns, 1976; Arthur et al., 1990) is most impressive being charactherized by widespread to global anoxia (e.g. Jenkyns 2010) and enhanced burial of organic matter (Herbin et al. 1986; Arthur et al. 1990; Kuypers et al. 2002, 2004; Jarvis et al., 2006) The equilibria of many biota were altered (e.g. Leckie et al., 2002; Erba, 2004; Friedrich et al., 2006; Hardas and Mutterlose, 2007; Pearce et al., 2009; Linnert et al., 2011; Prauss, M.L., 2012; Lebedel et al., 2013). OAE2 is further marked by a positive excursion of the $\delta^{13}C$ records of about 2-3‰ in carbonate carbon (C_{carb}) and up to 6‰ in organic carbon (Jenkyns, 1980; Scholle and Arthur, 1980; Schlanger et al. 1987; Arthur et al., 1990; Jenkyns, 2010).

In this paper we present inorganic geochemical data for the late Albian-early Turonian time interval from two different key-localities: the Cismon section and the Monte Petrano section in the Belluno Basin and Umbria-Marche Basin, respectively. Both basins were located in the south-western part of the Thethys Ocean, in the northern tropical climatic belt (Dercourt et al., 2000; Skelton et al., 2003). During the Cenomanian the Cismon area was located in a horst and graben extensional setting (Bernoulli and Jenkyns, 1974; Bosellini et al., 1978; Winterer and Bosellini, 1981) close to the hinge between the Trento Plateau and the Belluno Basin (Erba and Larson, 1998). The Umbria-Marche Basin

was located slightly more to the south in a basins and swells setting (Alvarez, 1990) with a pelagic sedimentation entirely deposited on the continental crust of the Adria microplate.

Major and trace element investigations in these two pelagic sequences are aimed at the reconstruction of paleoenvironmental conditions to better understand the processes that acted in the water column. In particular, elemental enrichments in the Cenomanian interval will provide intriguing insights on the paleoceanographic conditions acting after OAE1d and before OAE2.

Calcareous nannofossil data (Tamagnini, 2009; Erba unpiublished data) will be integrated to discuss bottom-water and surface-water changes and processing prior, during and after OAEs in the late Albian-early Turonian time interval.

7.2 Materials and methods

The 60m thick Cismon section is located in the Venetian Southern Alps, north-eastern Italy, along the SS50 (State Highway 50) facing the Cismon stream (Bosellini et al., 1978; Channell et al., 1979a; Bellanca et al., 1996) (Fig. 7.1). The studied sequence, part of the Scaglia Variegata Formation (Channel et al., 1979a), is characterized by the alternation of yellowish to greyish micritic limestone, radiolarian layers, chert bands and shales (Channel et al., 1979b; Claps et al., 1991; Bellanca et al., 1996). In the upper part of the sequence a thin level of about 35cm of organic-rich shales, radiolarian layers and black cherts represents the Bonarelli Level equivalent. No real black shales have been observed but frequent dark grey shales are interlayered within the sequence. Few isolated black chert bands are present in the interval above the MCE excursion as indicated by carbon isotope stratigraphy (see Chapter 5). The outcrop is characterized by a slump at the meter 11 and by a major fault at meter 45. The fault displaces part of the sequence removing part of the lowermost Cenomanian interval. As highlighted also by carbon-isotopic stratigraphy a hiatus immediately above and below the Bonarelli Level is present (see Chapter 5).

A total of 5 equally-spaced samples from the Bonarelli Level and 81 dark grey shales were collected throughout the sequence. Moreover, 2 additional brown shales above the Bonarelli layer have been collected. According to carbon-isotope stratigraphy and biostratigraphic data, as discussed in Chapter 5, the sequence spans a time interval from late Albian to early Turonian.

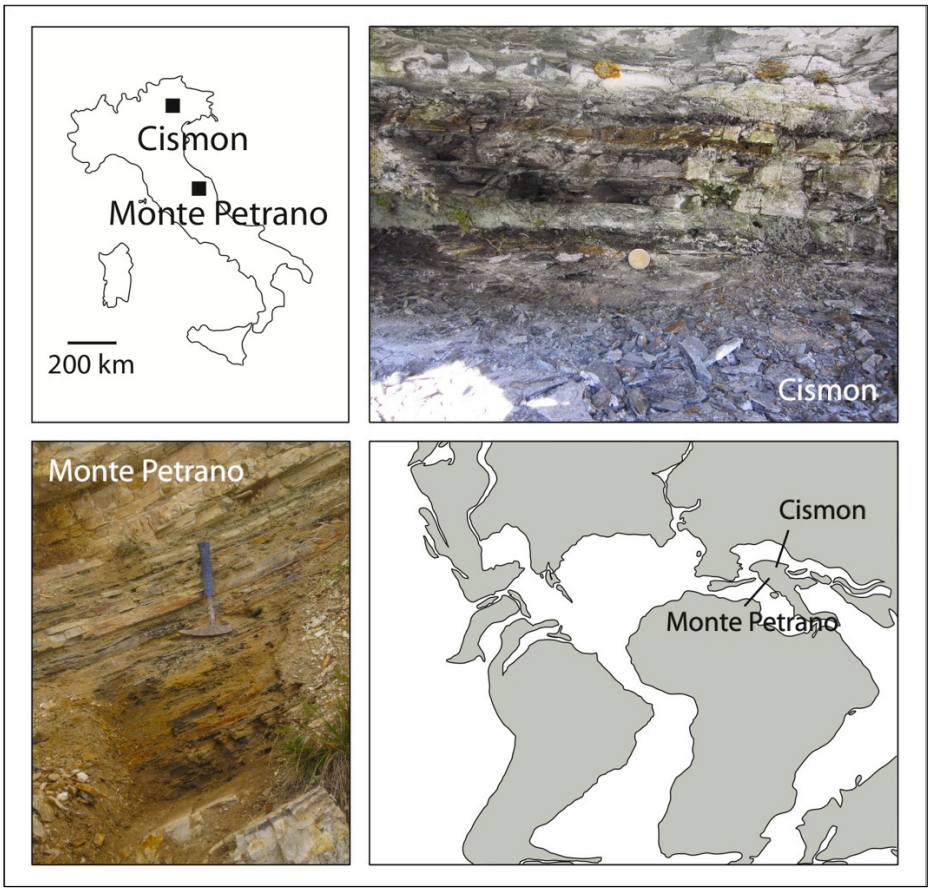

Figure 7.1: Present day (up left) and paleogeographic (down right) position of the studied sections. Up right and down left: Bonarelli Level at Monte Petrano and at Cismon respectively.

The 30m thick studied interval of the Monte Petrano section is located about 2 km east of the Moria village in the Umbria-Marche Basin (Fig. 7.1). The studied Scaglia Bianca Formation is mainly a calcareous pelagic sequence resulting from lithification of nannofossil-planktonic foraminiferal oozes (Arthur and Premoli Silva, 1982) deposited at bathyal depth. From this section 9 equally-spaced samples have been collected from the 80cm thick Bonarelli Level. Moreover, 8 black shale layers and seams have been sampled in the stratigraphic interval below the Bonarelli Level. Sampling was done on fresh surfaces in order to minimise present-day weathering effects. According to chemo- and biostratigraphy (see Chapter 5) the sequence covers a time interval from before the MCE to the early Turonian.

Collected samples have been analyzed by X-ray fluorescence analysis (XRF). About 700 mg of sample powder were mixed with 4200 mg lithium tetraborate, pre-oxidized in oven at 500°C overnight with NH_4NO_3 and then fused to glass beads. The beads were analysed by a spectrometer (Philips PW 2400),

calibrated with selected in-house geostandards. Analytical precision, as checked by parallel analysis of international reference material and in-house standards, is better than 1% for Si, Ti, Al, Fe, Mn, Ca, K, 2% for Na, Mg, and better than 5% for the following minor and trace elements Ba, Cr, Ni, Rb, Sr, V, Y, Zn, Zr, except P, Co, Cu, As, Pb (5-10%) (Schnetger et al., 2000).

Elemental values were normalised to Al in order to account for dilution effects by potential biogenic components such as carbonates, silica, and phosphorites (Brumsack, 2006; Turgeon and Brumsack, 2006). Concentrations are compared to the average shale values (AS) of Wedepohl (1971, 1991) and expressed as enrichments factors ($EF_{element}$) relative to AS. Enrichment factors were calculated as follows:

$$EF_{element} = (element/Al)_{sample} / (element/Al)_{AS}$$

An element with the same Al-normalised ratio as AS would have an EF of 1. On the basis of the different elemental concentrations, we describe a sample as "enriched" when $EF_{element} \geq 5$, while we consider the sample "depleted" when $EF_{element} \leq 0.5$ (Brumsack, 2006).

The non-detrital or 'excess' content of a particular element ($element_{xs}$) (Brumsack, 2006) is calculated using:

$$element_{xs} = element_{sample} - (Al_{sample} * (element/Al)_{AS})$$

7.3 Results

A summary of the results for the Cismon section is reported in Table 7.1a to f, while measured values are plotted in Figs. 7.2a to 7.2c. Detailed results obtained for the Bonarelli Level are reported in Figs. 7.2d. Results for the Monte Petrano section are reported in Table 7.2a and 7.2b. Depth profiles of the various elements are illustrated in Fig. 7.3a and b. Results for the Bonarelli Level are reported in greater detail in Fig. 7.3c and d.

The studied sequences have been divided according to carbon isotopic stratigraphy (as discussed in Chapter 5), in six main intervals: the interval before the OAE1d, the OAE1d, the sequence between the OAE1d and the MCE, the interval from the base of the MCE and the base of the OAE2, the OAE2 and finally the part of the succession above the OAE2. Samples from the lower three intervals and the uppermost interval come exclusively from the Cismon section, while the sequence from the base of the MCE and the top of the OAE2 was investigated in both sections. The results for each interval are

presented in detail in the following paragraphs. Enrichment Factors (EFs) for every element in the various interval are synthetized in Fig. 7.4a and b for Cismon and Monte Petrano, respectively.

7.3.1 Interval below OAE1d

Samples below the OAE1d are generally characterized by concentrations of major elements, such as Ti, Al, Fe, Mg, K and Mn quite similar to AS values, while Mn is slightly lower than AS. Na is well below AS values throughout all the six intervals (Table 7.1a).

Minor elements present values comparable to AS with the exception of Ba that is higher than AS. Cu and Zn in particular show concentrations slightly higher than AS. Particularly high Ca and Sr contents suggest a high dilution effect by carbonate.

7.3.2 OAE1d

Results indicate again an enrichment of Ca and Sr owing to dilution by carbonate. Ba concentration with respect to AS is higher than AS for a factor of 9 (Table 7.1b). The average Mn content of analyzed samples indicates a slight depletion. As for the interval below the OAE1d, we observe Cu and Zn concentrations slightly higher than AS.

7.3.3 Between OAE1d and MCE

Major elements are generally characterized by concentrations comparable to AS with the exception of Ca, Na and Ni (Table 7.1c). As regards minor elements, analyzed samples are enriched in Ba and Sr and depleted in Mo and slightly in Mn. Slightly higher concentrations, but still within the limits, of P and Cu are detected.

7.3.4 Interval between MCE and the Bonarelli Level

At Cismon, sediments from this interval are enriched in Ca, Ba, Cu and Sr. Within the MCE in particular, Zr and Ba are present in very high concentrations (Table 7.1d). Even if at a lower extent than the already mentioned element, Co and Zn and occasionally As show values higher than AS (average EF around 3.3 for Co and Zn and average EF around 2.2 for As).

At Monte Petrano the analyses revealed more extreme characteristics, with several redox-sensitive or sulphide-residing elements present in high concentrations (Table 7.2a). Among major elements Si, Ca, P and Mn are enriched if compared to AS, while Na is depleted. Among minor elements Ba, Co, Cu Sr, V and Zn are the ones with the highest concentrations. As, Cr, Mo, Ni, Pb and U, even if less

extremely concentrated, show values much higher than AS. Y, at the end, has a concentration about 4 times higher than AS.

7.3.5 Bonarelli Level

Samples from the Bonarelli Level at Cismon, are characterized by very high concentrations in As, Ba, Cu, Mo, Ni, V and Zn (Table 7.1e). Both Ba and Mo in particular are extremely high. Mn is instead significantly lower than AS. Calcium values are the lowest, but still with a value of EF equal to 4.33. Slight enrichments in P and Sr are also detected.

At Monte Petrano the Bonarelli Level presents quite similar characteristics to what has been observed for Cismon. Also here Mn is in extremely low concentrations, while Ba and Mo are incredibly high. As, Cu, Ni, Si and Zn are enriched in comparison to AS. Si, Co, Cr and U abundances are higher than AS (Table 7.2b).

7.3.6 Interval above the Bonarelli Level

The two analysed samples from the Cismon section present concentrations similar to AS, apart from Ca that is still quite high. Ba and Cu exceed the AS expected values (Table 7.1f).

	Below OAE1d n=40							**Average shale**	
Elem/Oxide	conc	sigma	min	max	/Al	sigma	EF	conc	/Al
SiO_2	26.60	6.34	14.69	40.68	4.35	0.72	1.40	58.90	3.11
TiO_2	0.24	0.08	0.10	0.39	0.05	0.00	0.93	0.78	0.053
Al_2O_3	5.61	1.75	2.35	8.58	-	-	-	16.70	[1.00]
Fe_2O_3	2.22	0.62	0.89	3.23	0.53	0.07	0.97	6.90	0.55
MgO	1.70	0.44	0.91	2.72	0.35	0.04	1.97	2.60	0.18
CaO	31.68	6.02	21.04	43.23	9.15	5.15	50.82	2.20	0.18
Na_2O	0.17	0.08	0.02	0.32	0.04	0.01	0.31	1.60	0.13
K_2O	1.38	0.47	0.52	2.21	0.38	0.02	1.12	3.60	0.34
P_2O_5	0.155	0.049	0.080	0.280	0.023	0.004	2.89	0.160	0.008
As	2	2	0	7	0.77	0.84	0.70	10	1.10
Ba	1593	470	817	3196	567.20	159.04	8.59	580	66.00
Co	8	3	2	16	2.95	1.47	1.40	19	2.10
Cr	60	26	17	117	19.64	3.40	1.93	90	10.00
Cu	56	34	17	168	18.55	7.94	3.64	45	5.10
MnO	0.019	0.007	0.011	0.035	64	47	0.66	0.008	96.000
Mo	0	1	0	3	0.14	0.26	0.93	1	0.15
Ni	30	11	11	58	10.45	2.61	1.36	68	7.70
Pb	17	6	6	37	5.60	0.94	2.24	22	2.50
Rb	57	20	21	90	19.00	0.98	1.19	140	16.00
Sr	588	140	462	1294	216.53	73.89	6.37	300	34.00
U	2	1	0	4	0.64	0.42	1.52	4	0.42
V	80	26	37	154	28.04	6.88	1.87	130	15.00
Y	34	8	22	54	12.10	2.19	2.63	41	4.60
Zn	82	27	32	155	30.25	12.69	2.75	95	11.00
Zr	54	16	25	82	18.50	1.40	1.03	160	18.00

Table 7.1a: XRF measured values for the interval below OAE1d at Cismon. All oxides and bulk parameters are reported as %, minor elements in µg/g. Standard deviation (σ), minimum and maximum values are shown. All trace element/Al and Mn/Al ratios are expressed as $\times 10^{-4}$. Average shale values from Wedepohl (1971, 1991) are reported in the two rightmost columns.

	OAE1d n=6						
Elem/Oxide	conc	sigma	min	max	/Al	sigma	EF
SiO_2	26.59	3.59	20.33	31.68	3.73	0.28	1.20
TiO_2	0.28	0.05	0.18	0.33	0.05	0.00	0.94
Al_2O_3	6.37	1.15	4.15	7.88	-	-	-
Fe_2O_3	2.59	0.48	1.62	3.08	0.54	0.03	0.98
MgO	1.95	0.26	1.50	2.25	0.35	0.03	1.96
CaO	29.13	4.28	24.49	37.13	6.64	2.61	36.88
Na_2O	0.14	0.04	0.07	0.20	0.03	0.00	0.24
K_2O	1.60	0.31	1.01	1.95	0.39	0.01	1.15
P_2O_5	0.145	0.031	0.104	0.192	0.019	0.004	2.39
As	4	1	2	6	1.19	0.37	1.09
Ba	1918	539	1328	2712	608.28	290.55	9.22
Co	12	4	4	16	3.47	0.96	1.65
Cr	59	12	38	77	17.54	1.47	1.72
Cu	56	15	29	79	16.41	2.48	3.22
MnO	0.018	0.003	0.015	0.023	44	14	0.46
Mo	1	1	0	2	0.14	0.21	0.92
Ni	46	21	19	88	13.31	4.87	1.73
Pb	20	4	13	27	6.02	0.52	2.41
Rb	63	12	40	79	18.55	0.34	1.16
Sr	522	35	450	562	161.65	40.10	4.75
U	3	2	0	5	0.74	0.45	1.77
V	100	31	67	165	29.65	7.07	1.98
Y	30	3	27	37	9.29	1.88	2.02
Zn	117	42	48	189	34.25	10.15	3.11
Zr	59	10	41	68	17.64	0.85	0.98

Table 7.1b: XRF values for the interval within OAE1d at Cismon. All oxides and bulk parameters are reported as %, minor elements in µg/g. Standard deviation (σ), minimum and maximum values are shown. All trace element/Al and Mn/Al ratios are expressed as $\times 10^{-4}$. Average shale values from Wedepohl (1971, 1991).

	Between OAE1d and MCE n=18						
Elem/Oxide	conc	sigma	min	max	/Al	sigma	EF
SiO_2	25.22	5.79	13.66	36.46	4.13	0.40	1.33
TiO_2	0.24	0.07	0.10	0.40	0.05	0.00	0.95
Al_2O_3	5.52	1.63	2.37	9.14	-	-	-
Fe_2O_3	2.14	0.51	1.25	2.94	0.53	0.08	0.96
MgO	1.88	0.42	1.12	2.81	0.40	0.06	2.23
CaO	32.08	5.81	20.45	43.53	9.29	5.38	51.62
Na_2O	0.15	0.06	0.03	0.24	0.04	0.01	0.29
K_2O	1.36	0.41	0.56	2.32	0.38	0.01	1.13
P_2O_5	0.187	0.047	0.089	0.280	0.029	0.004	3.57
As	3	3	0	11	1.34	1.26	1.22
Ba	1069	275	462	1423	377.48	77.94	5.72
Co	10	4	4	17	3.62	1.48	1.72
Cr	55	17	21	92	18.72	1.52	1.84
Cu	56	33	22	176	18.49	5.65	3.63
MnO	0.015	0.003	0.011	0.024	47	26	0.49
Mo	0	0	0	1	0.04	0.11	0.27
Ni	32	12	14	61	11.21	3.24	1.46
Pb	21	9	7	44	7.02	1.45	2.81
Rb	56	18	22	98	18.89	0.67	1.18
Sr	634	78	482	755	244.06	103.25	7.18
U	2	1	0	4	0.66	0.51	1.56
V	93	54	35	275	30.65	9.49	2.04
Y	30	5	19	38	10.85	1.93	2.36
Zn	95	45	42	242	32.21	7.59	2.93
Zr	53	12	28	74	18.43	1.62	1.02

Table 7.1c: XRF values for the interval from the interval between OAE1d and MCE at Cismon. All oxides and bulk parameters are reported as %, minor elements in µg/g. Standard deviation (σ), minimum and maximum values are shown. All trace element/Al and Mn/Al ratios are expressed as $\times 10^{-4}$. Average shale values from Wedepohl (1971, 1991).

	Above MCE n=17						
Elem/Oxide	conc	sigma	min	max	/Al	sigma	EF
SiO_2	21.16	13.27	9.73	64.44	5.01	3.29	1.61
TiO_2	0.17	0.07	0.11	0.43	0.05	0.00	0.91
Al_2O_3	3.92	1.55	2.58	9.34	-	-	-
Fe_2O_3	1.66	0.59	1.12	3.37	0.57	0.10	1.04
MgO	1.22	0.34	0.91	2.43	0.37	0.04	2.03
CaO	38.03	6.53	25.30	45.33	14.78	5.16	82.09
Na_2O	0.09	0.05	0.03	0.19	0.03	0.01	0.23
K_2O	0.97	0.42	0.63	2.42	0.39	0.02	1.14
P_2O_5	0.109	0.035	0.072	0.223	0.023	0.004	2.93
As	5	4	0	16	2.48	1.99	2.25
Ba	1003	968	271	4439	527.44	597.29	7.99
Co	14	8	4	31	6.89	3.53	3.28
Cr	45	20	29	104	21.24	2.62	2.08
Cu	54	37	13	168	25.86	14.77	5.07
MnO	0.029	0.007	0.013	0.042	121	42	1.26
Mo	0	1	0	2	0.12	0.23	0.80
Ni	37	19	10	87	17.93	7.82	2.33
Pb	13	5	5	25	6.23	1.58	2.49
Rb	39	18	24	101	18.58	1.18	1.16
Sr	738	112	517	916	397.10	131.03	11.68
U	1	1	0	2	0.48	0.35	1.14
V	60	26	32	118	28.77	6.01	1.92
Y	20	4	15	36	10.41	2.08	2.26
Zn	74	28	37	131	36.70	11.18	3.34
Zr	42	12	29	83	20.68	2.72	1.15

Table 7.1d: XRF values for the interval from the base of the MCE up to the base of the Bonarelli at Cismon. All oxides and bulk parameters are reported as %, minor elements in µg/g. Standard deviation (σ), minimum and maximum values are shown. All trace element/Al and Mn/Al ratios are expressed as $\times 10^{-4}$. Average shale values from Wedepohl (1971, 1991).

	Bonarelli n=5						
Elem/Oxide	conc	sigma	min	max	/Al	sigma	EF
SiO_2	47.58	7.67	38.95	59.22	4.21	0.45	1.35
TiO_2	0.41	0.09	0.32	0.54	0.05	0.00	0.87
Al_2O_3	10.11	2.07	7.87	12.94	-	-	-
Fe_2O_3	5.65	0.59	4.82	6.60	0.78	0.21	1.42
MgO	2.54	0.56	1.87	3.39	0.29	0.01	1.59
CaO	5.57	1.69	3.40	8.28	0.78	0.30	4.33
Na_2O	0.42	0.06	0.35	0.52	0.06	0.01	0.45
K_2O	2.40	0.51	1.88	3.08	0.37	0.00	1.09
P_2O_5	0.310	0.136	0.185	0.556	0.025	0.008	3.14
As	37	10	19	45	7.45	3.01	6.77
Ba	7714	1484	5791	9875	1506.91	443.65	22.83
Co	30	7	18	40	5.90	1.86	2.81
Cr	153	37	110	198	29.76	8.95	2.92
Cu	129	42	88	205	25.88	11.77	5.07
MnO	0.019	0.004	0.014	0.026	27	3	0.28
Mo	15	12	0	36	3.35	3.02	22.37
Ni	192	83	86	288	40.50	22.43	5.26
Pb	26	3	21	30	5.09	0.96	2.03
Rb	95	22	73	125	17.67	0.48	1.10
Sr	595	108	469	770	114.61	25.41	3.37
U	6	3	2	9	1.09	0.51	2.60
V	504	286	116	908	105.51	72.80	7.03
Y	58	19	41	93	10.86	2.74	2.36
Zn	428	268	79	765	88.38	63.30	8.03
Zr	87	18	72	119	16.25	1.18	0.90

Table 7.1e: XRF values for the Bonarelli Level at Cismon. All oxides and bulk parameters are reported as %, minor elements in µg/g. Standard deviation (σ), minimum and maximum values are shown. All trace element/Al and Mn/Al ratios are expressed as $\times 10^{-4}$. Average shale values from Wedepohl (1971, 1991).

	Above Bonarelli depth = 59.7			depth = 58.5		
Elem/Oxide	conc	/Al	EF	conc	/Al	EF
SiO_2	38.94	3.63	1.17	66.44	5.00	1.61
TiO_2	0.41	0.05	0.92	0.49	0.05	0.89
Al_2O_3	9.47	-	0.57	11.74	-	0.70
Fe_2O_3	4.87	0.68	1.24	4.78	0.54	0.98
MgO	2.34	0.28	1.56	2.92	0.28	1.57
CaO	19.65	2.80	15.57	13.06	1.50	8.34
Na_2O	0.33	0.05	0.38	0.47	0.06	0.43
K_2O	2.61	0.43	1.27	3.06	0.41	1.20
P_2O_5	0.125	0.011	1.36	0.151	0.011	1.33
As	0	0.00	0.00	0	0.00	0.00
Ba	3629	723.99	10.97	6671	1073.55	16.27
Co	10	2.00	0.95	12	1.93	0.92
Cr	99	19.75	1.94	122	19.63	1.92
Cu	54	10.77	2.11	337	54.23	10.63
MnO	0.071	110	1.14	0.044	55	0.57
Mo	1	0.20	1.33	1	0.16	1.07
Ni	55	10.97	1.43	72	11.59	1.50
Pb	12	2.39	0.96	27	4.35	1.74
Rb	103	20.55	1.28	118	18.99	1.19
Sr	563	112.32	3.30	590	94.95	2.79
U	3	0.60	1.43	2	0.32	0.77
V	87	17.36	1.16	111	17.86	1.19
Y	31	6.18	1.34	36	5.79	1.26
Zn	56	11.17	1.02	85	13.68	1.24
Zr	74	14.76	0.82	91	14.64	0.81

Table 7.1f: XRF values for the interval above the Bonarelli Level at Cismon. All oxides and bulk parameters are reported as %, minor elements in µg/g. All trace element/Al and Mn/Al ratios are expressed as $\times 10^{-4}$. Average shale values from Wedepohl (1971, 1991).

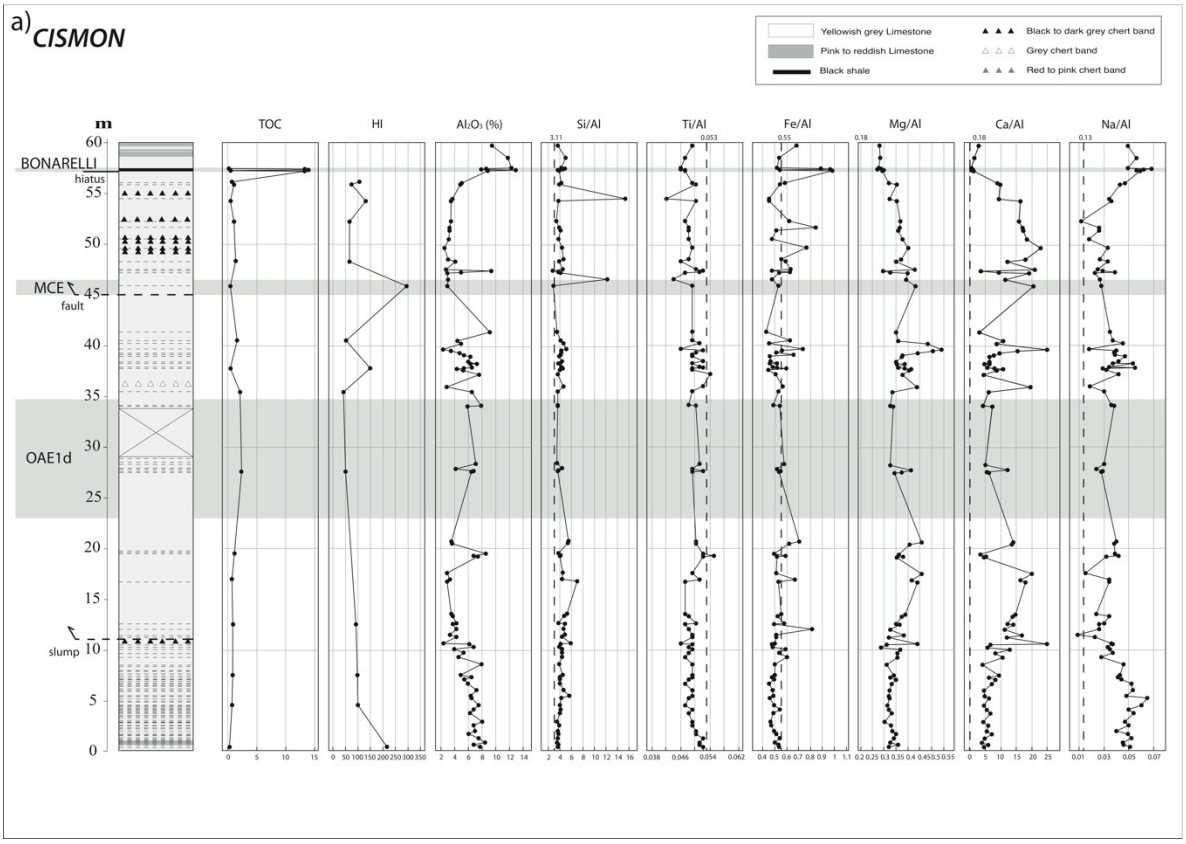

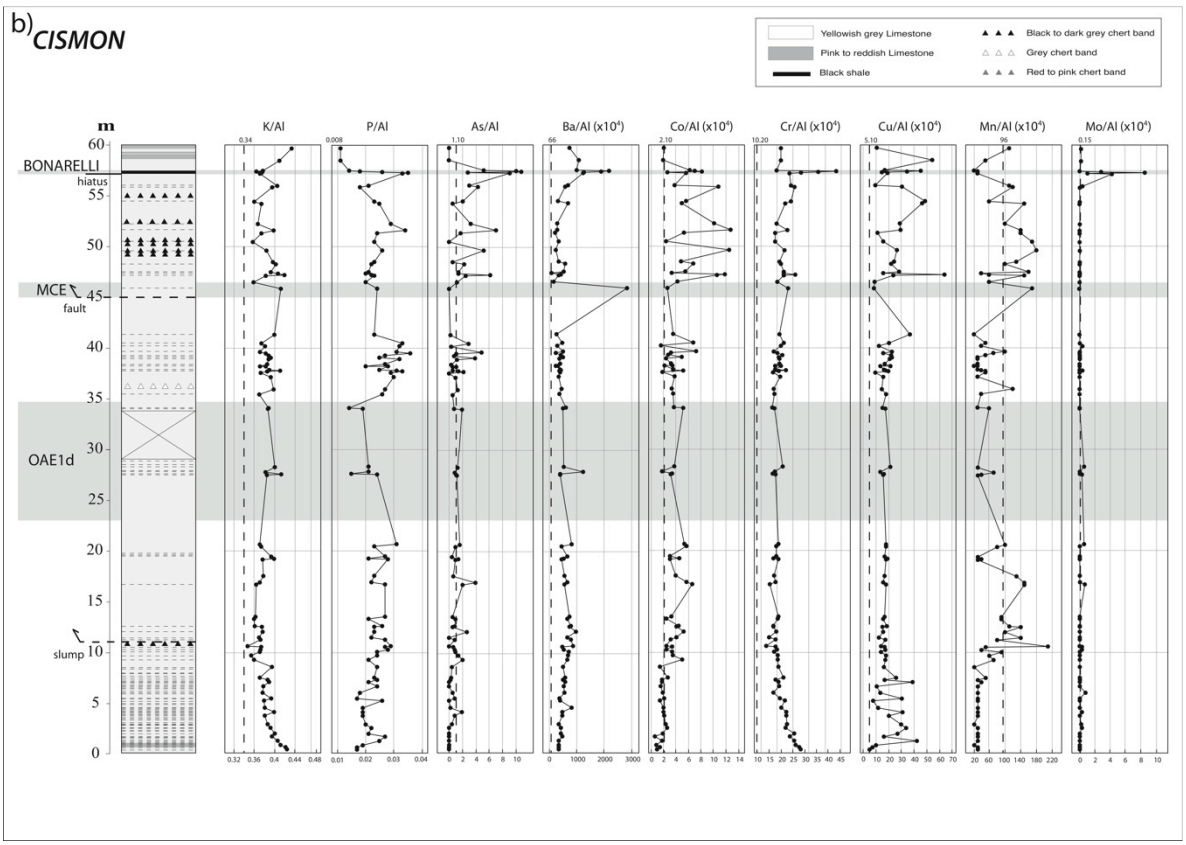

Figs. 7.2a and b: Major and trace element profiles for the Cismon section. Dotted lines refer to average shale values for each element (Wedepohl, 1971). Additionally, TOC and HI measurements are reported.

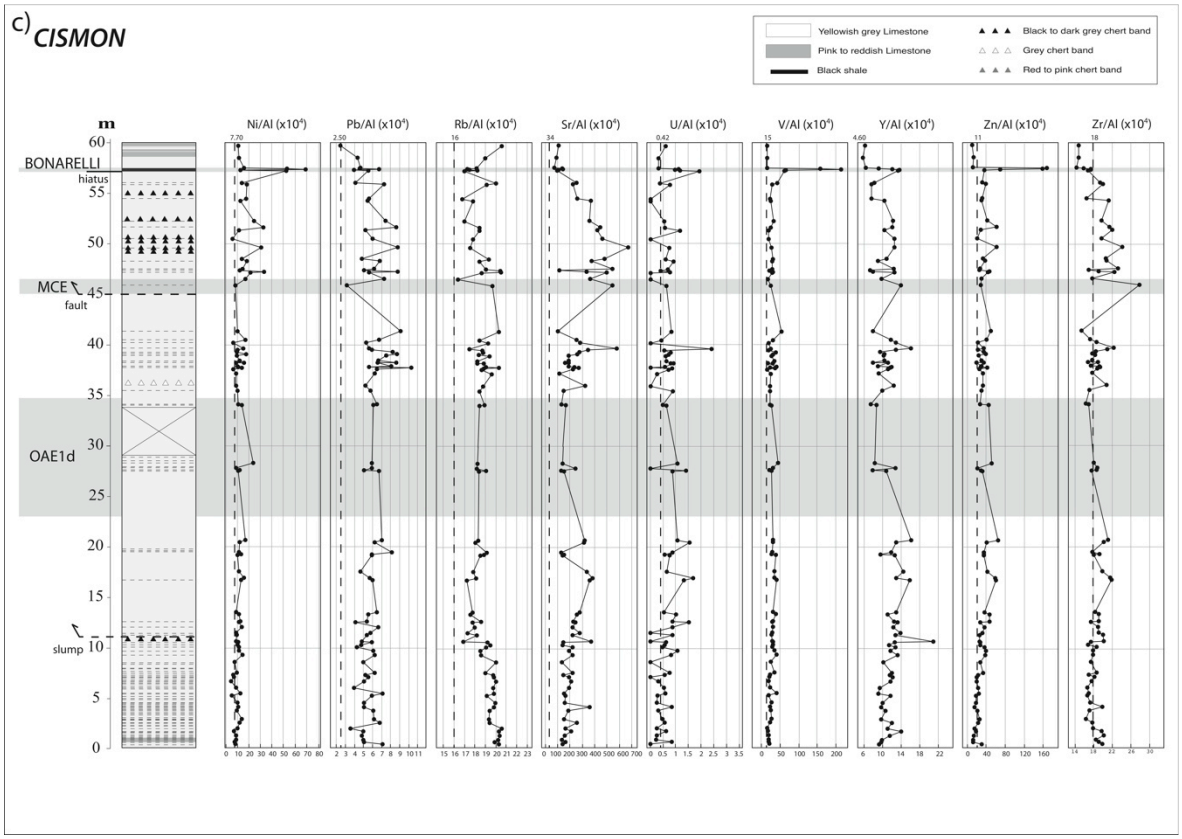

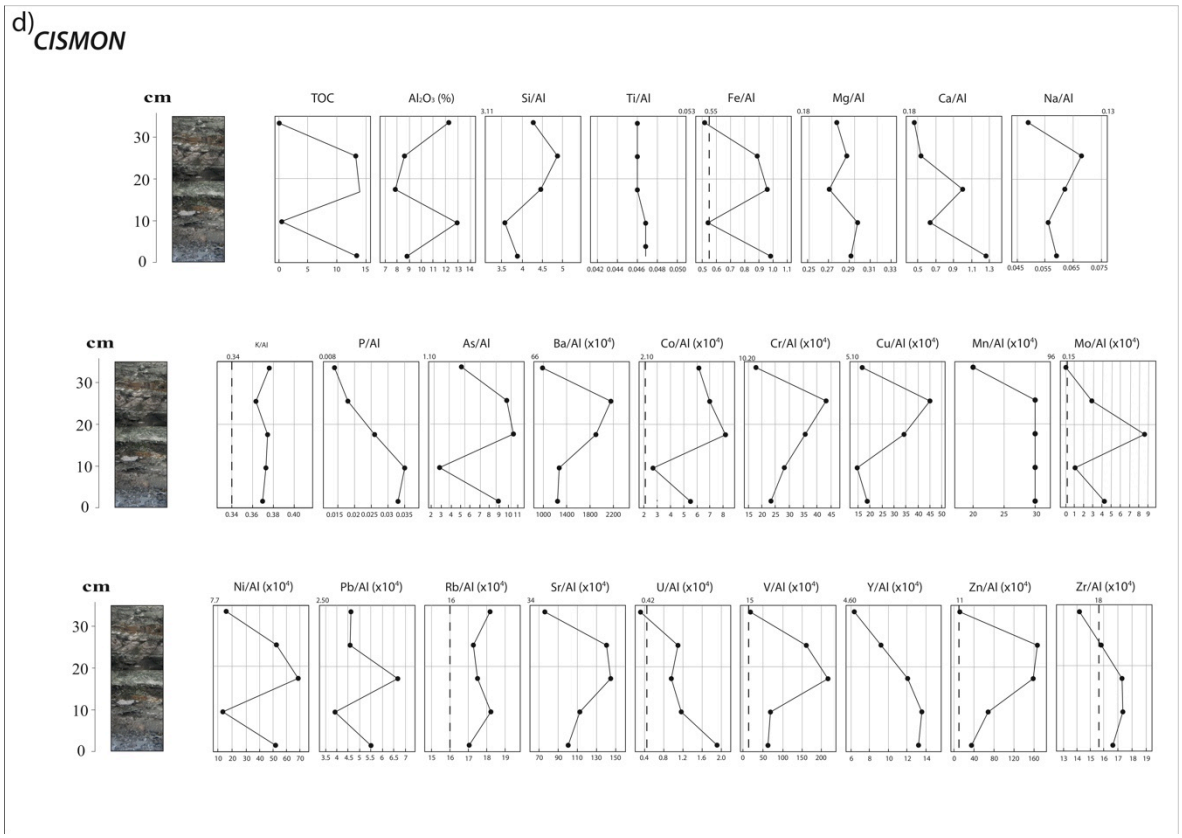

Figs. 7.2c: Trace element profiles for the Cismon section. Dotted lines refer to average shale values for each element (Wedepohl, 1971).
Fig. 7.2d: Detail of the major and trace element profiles in the Bonarelli Level at Cismon. Dotted lines refer to average shale values for each element (Wedepohl, 1971). Additionally, TOC and HI measurements are reported.

	Above MCE n=8							**Average shale**	
Elem/Oxide	conc	sigma	min	max	/Al	sigma	EF	conc	/Al
SiO_2	18.80	19.01	6.62	59.30	8.00	8.01	9.50	58.90	3.11
TiO_2	0.09	0.05	0.05	0.19	0.05	0.01	0.98	0.78	0.053
Al_2O_3	2.04	1.01	1.28	4.15	-	-	-	16.70	[1.00]
Fe_2O_3	1.03	0.50	0.52	1.81	0.71	0.35	2.23	6.90	0.55
MgO	0.55	0.22	0.37	0.90	0.32	0.10	2.18	2.60	0.18
CaO	41.11	16.43	15.00	48.84	31.76	15.37	286.23	2.20	0.18
Na_2O	0.01	0.02	0.00	0.06	0.01	0.01	0.18	1.60	0.13
K_2O	0.52	0.24	0.35	0.99	0.40	0.12	1.26	3.60	0.34
P_2O_5	0.095	0.047	0.047	0.154	0.039	0.015	6.98	0.160	0.008
As	3	3	0	10	3.32	3.88	8.81	10	1.10
Ba	774	296	499	1130	799.86	369.03	19.49	580	66.00
Co	20	11	4	32	20.07	12.73	18.27	19	2.10
Cr	67	42	17	137	60.17	33.20	10.96	90	10.00
Cu	94	66	16.000	230	83.65	47.88	30.43	45	5.10
MnO	0.030	0.010	0	0.048	265	141	5.12	0.008	96.000
Mo	0	0	0	1	0.16	0.44	9.84	1	0.15
Ni	46	26	8	78	44.18	26.33	9.81	68	7.70
Pb	11	7	3	25	9.72	4.77	6.75	22	2.50
Rb	18	10	10	38	16.29	5.03	1.12	140	16.00
Sr	695	277	268	874	749.48	363.20	36.03	300	34.00
U	1	1	0	2	0.58	0.76	5.42	4	0.42
V	168	135	45	459	158.74	120.71	29.65	130	15.00
Y	17	7	12	27	16.71	5.91	4.49	41	4.60
Zn	92	54	34	186	91.00	55.07	16.38	95	11.00
Zr	26	10	15	37	25.88	9.04	1.80	160	18.00

Table 7.2a: XRF values for the interval from the base of the MCE up to the base of the Bonarelli at Monte Petrano. All oxides and bulk parameters are reported as %, minor elements in µg/g. Standard deviation (σ), minimum and maximum values are shown. All trace element/Al and Mn/Al ratios are expressed as $\times 10^{-4}$. Average shale values from Wedepohl (1971, 1991) are reported in the two rightmost columns.

	Bonarelli n=9						
Elem/Oxide	conc	sigma	min	max	/Al	sigma	EF
SiO_2	67.36	8.64	48.93	80.30	13.13	6.39	4.22
TiO_2	0.22	0.12	0.09	0.49	0.04	0.00	0.83
Al_2O_3	5.57	2.45	2.63	10.04	-	-	-
Fe_2O_3	2.96	1.16	1.58	5.58	0.81	0.43	1.48
MgO	0.94	0.51	0.38	1.89	0.18	0.02	1.03
CaO	0.44	0.32	0.11	0.97	0.12	0.10	0.67
Na_2O	0.18	0.07	0.04	0.29	0.05	0.03	0.39
K_2O	1.28	0.56	0.60	2.34	0.36	0.02	1.07
P_2O_5	0.250	0.186	0.041	0.661	0.046	0.036	5.75
As	23	22	4	72	9.02	7.28	8.20
Ba	10070	4196	3857	19268	4293.49	2391.23	65.05
Co	17	16	2	58	6.37	5.42	3.03
Cr	94	39	38	156	37.70	21.21	3.70
Cu	167	111	82.000	460	68.82	42.06	13.49
MnO	0.010	0.010	0	0.024	15	19	0.19
Mo	19	24	0	82	8.99	12.37	59.96
Ni	87	54	32	214	39.19	32.34	5.09
Pb	18	5	9	29	7.24	2.74	2.90
Rb	47	20	21	82	15.82	1.05	0.99
Sr	478	96	291	590	201.76	106.10	5.93
U	4	4	0	14	1.84	1.46	4.38
V	528	265	82	862	228.71	157.55	15.25
Y	23	15	7	51	9.27	5.87	2.02
Zn	413	336	65	1188	192.14	190.86	17.47
Zr	42	14	25	66	14.91	2.09	0.83

Table 7.2b: XRF values for the Bonarelli Level at Monte Petrano. All oxides and bulk parameters are reported as %, minor elements in µg/g. Standard deviation (σ), minimum and maximum values are shown. All trace element/Al and Mn/Al ratios are expressed as $\times 10^{-4}$. Average shale values from Wedepohl (1971, 1991).

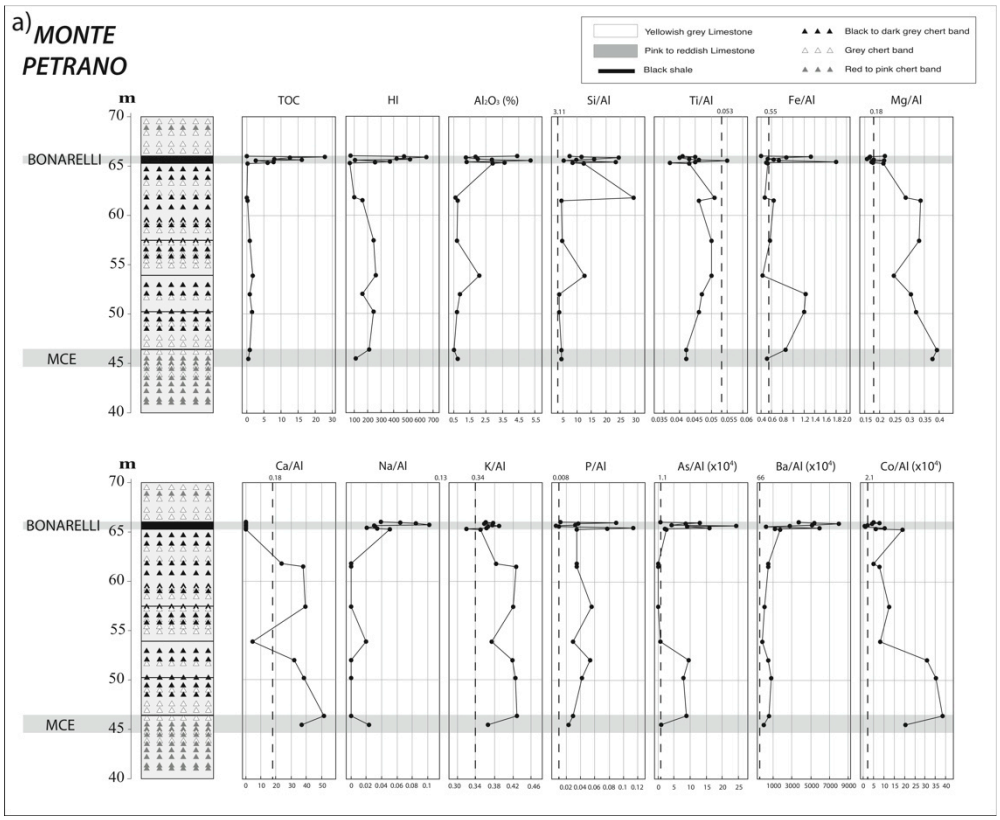

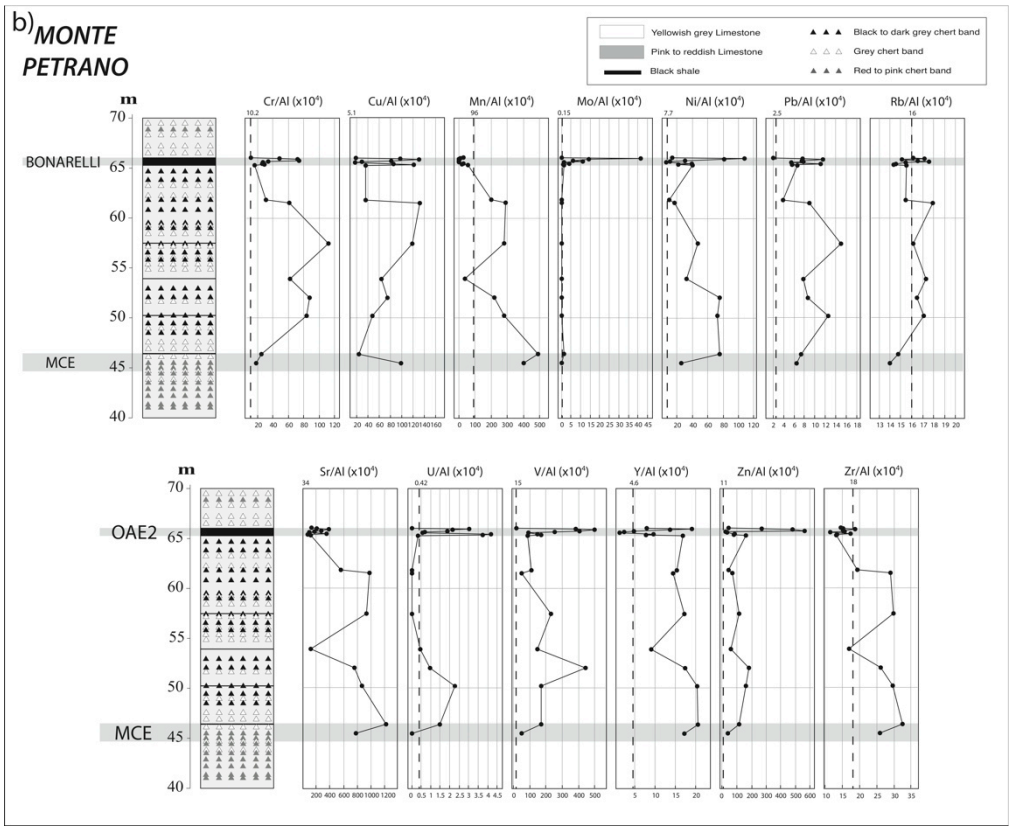

Figs. 7.3a and b: Major and trace element profiles for the Monte Petrano section. Dotted lines refer to average shale values for each element (Wedepohl, 1971). Additionally, TOC and HI measurements are reported.

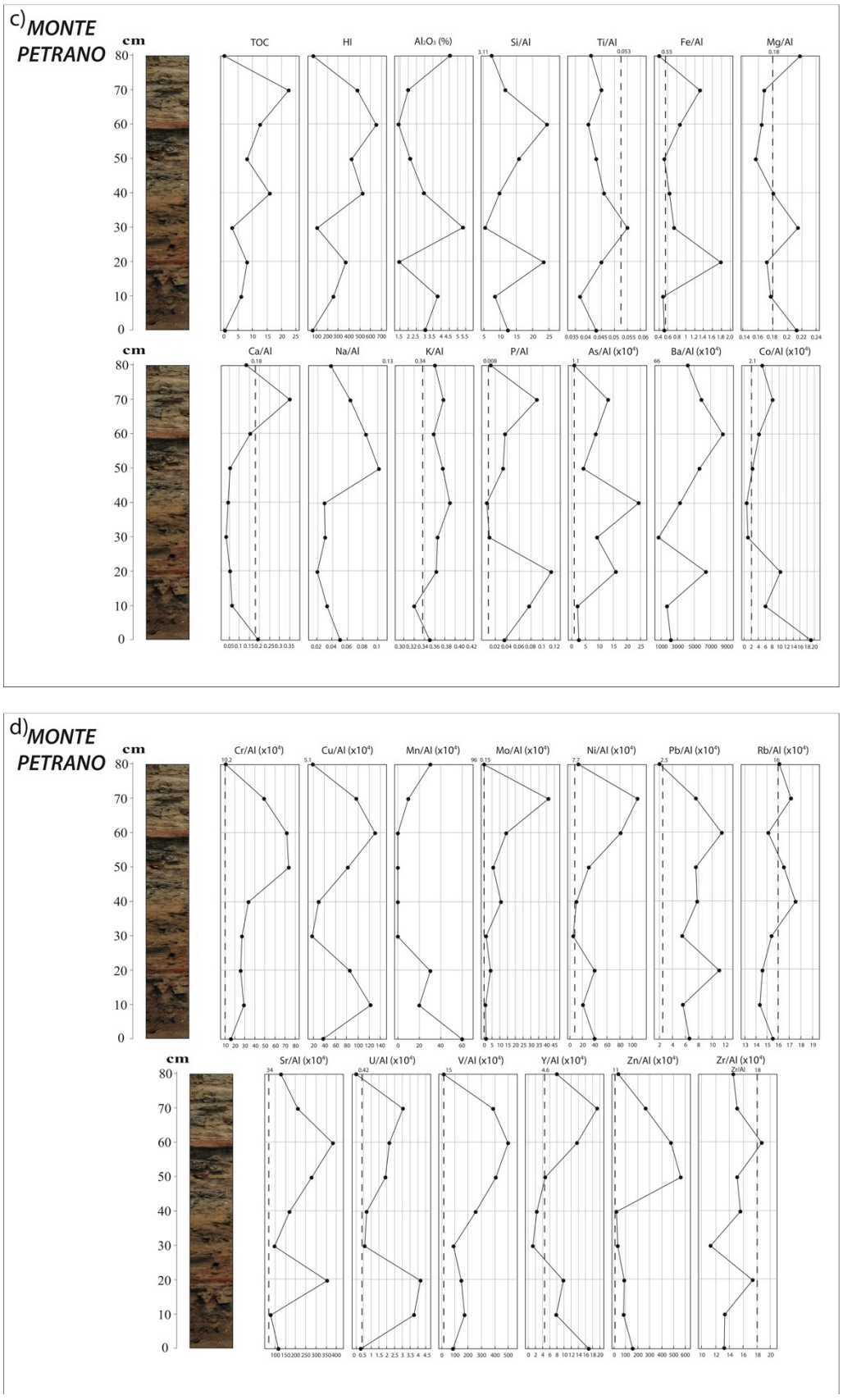

Fig. 7.3c and d: Details of the major and trace element profiles in the Bonarelli Level at Monte Petrano. Dotted lines refer to average shale values for each element (Wedepohl, 1971). Additionally, TOC and HI measurements are reported.

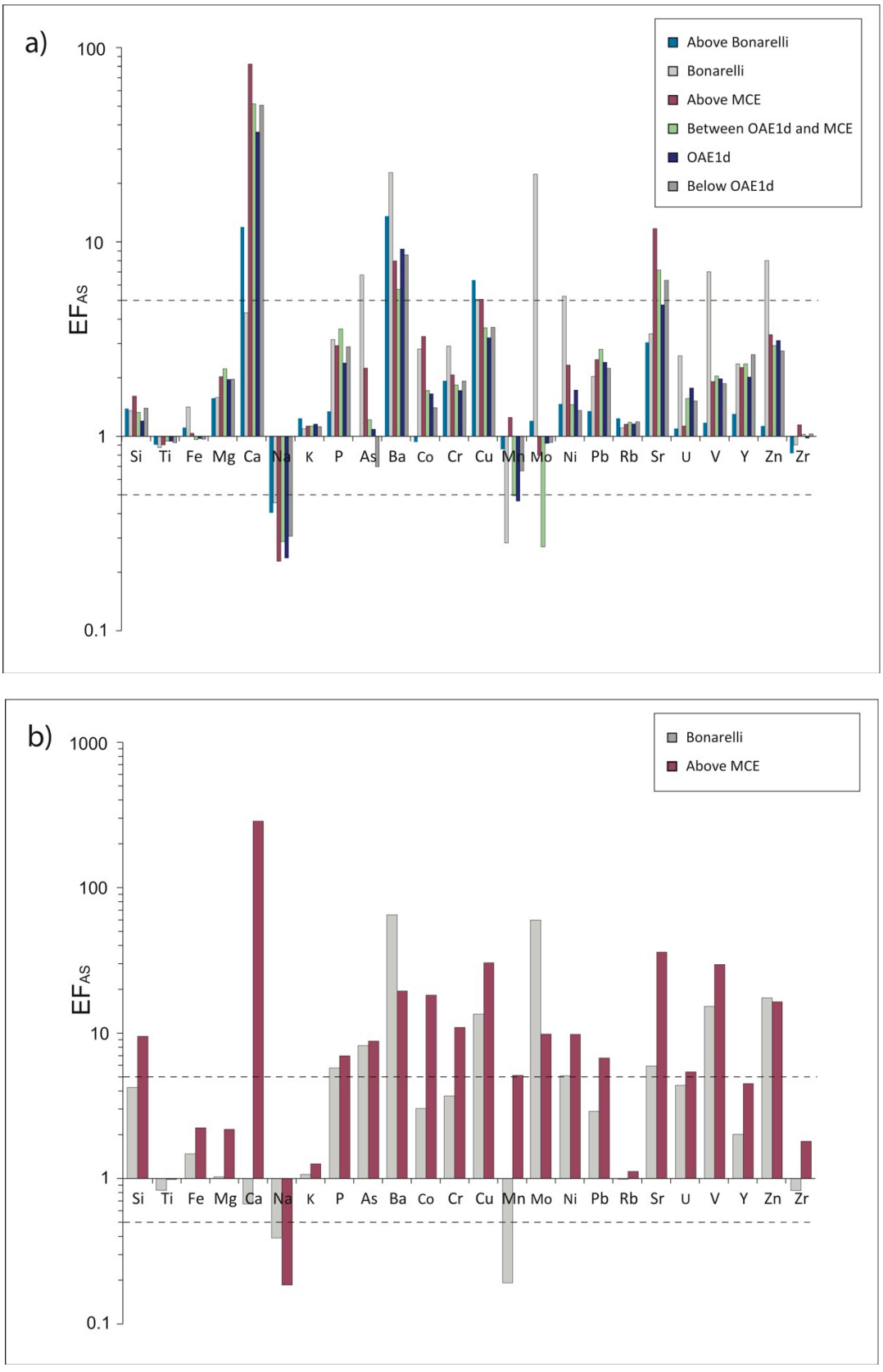

Figs. 7.4a and b: Enrichment factors of analyzed elements at Cismon and Monte Petrano respectively. Upper dashed line represents $EF_{element} \geq 5$ enrichment cut-off, while the lower one represents $EF_{element} \leq 0.5$ cut-off.

7.4 Discussion

7.4.1 Nature of sediments

In both sections, Ti and Zr concentrations, interpreted as proxies for higher energy environments (e.g. Schmitz, 1987; Schneider et al., 1997), are quite similar to AS values, thus indicating that deposition occurred in a pelagic setting distant from the coast and with a low terrigenous detrital input. This observation is in strict accordance with the supposed pelagic depositional environment. Even if the Belluno Basin is supposed to be more proximal to the mainland in comparison to the Umbria-Marche Basin, no evidence of higher proximity is detected. Lithogenetic-conservative elements such as Ti, K, Mg and Rb remain quite constant throughout the studied sections, indicating a mostly homogeneous source area through time. Zr, generally considered an immobile element, shows a sublte increase after the MCE, that can be indicative of coarser sediments (e.g. Pedersen et al., 1992; Ganeshram et al., 1999) transported by more intense riverine input in the basin.

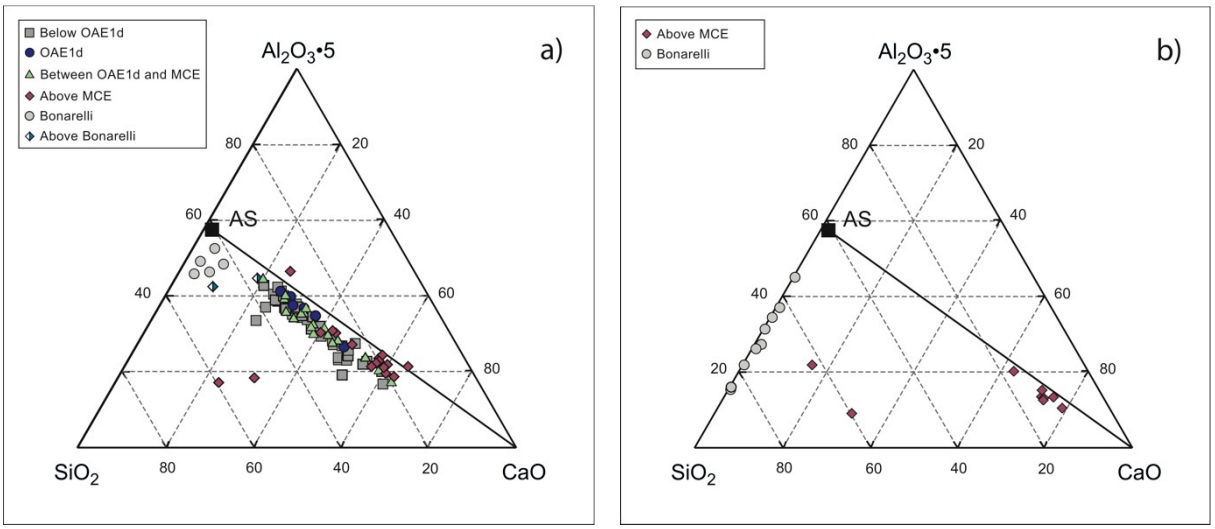

Fig. 7.5a and b: Ternary diagram of relative proportions of Al_2O_3×5, SiO_2, and CaO for Cismon (left) and Monte Petrano (right). An arbitrary multiplier of 5 is used for Al_2O_3 in order to better distribute the data points within the graph. Average shale (AS) composition is also shown (Wedepohl, 1971).

All the data from individual intervals have been plotted on a triangular diagram with axes Al_2O_3, SiO_2, and CaO, as represented in Fig. 7.5a and 7.5b for Cismon and Monte Petrano, respectively. The three oxides used at the different origins represent three of the major chemical components in sedimentary rocks: clays, quartz and/or biogenic silica, and calcium carbonate respectively. All samples from both sections, with the exception of the Bonarelli Level, fall on the so-called 'carbonate dilution line'

connecting the AS point to the CaO pole. This indicates that most samples are the result of a background sedimentation with different dilution by carbonates. The samples from the interval within the MCE and the OAE2 are similar in both sections, with values more shifted towards the CaO pole along the carbonate dilution line. Bonarelli samples, even if slightly more carbonatic at Cismon, are quite similar in both sections and are essentially the result of a bi-component mixing of AS and SiO_2.

7.4.2 Variations in clay mineralogy

High K contents are mainly related to illites/K-feldspars, high Mg values can be considered as representative of chlorite and low K/Al and Mg/Al ratios as indicative of K and Mg poor clay minerals such as kaolinite. Following this approach, clay mineralogy has been investigated plotting the normalized to Al data for K and Mg. The results for Cismon and Monte Petrano are reported in Fig. 7.6a and b, respectively. In general samples cluster around values of K/Al of ~3.8 and Mg/Al values aound ~3.3. Samples from within the OAE1d and the MCE at Cismon are slightly more chloritic, while samples from the Bonarelli in both sections are slightly more kaolinitic with lower K/Al and Mg/Al values at Monte Petrano. Illite is most abundant in the oceans, while chlorite is generally exclusively preserved in cold climates/cold waters or extremely dry climates due to its tendency to be easily weathered when exposed to humid and even temperate conditions (Weaver, 1990). Kaolinite, instead, is generally formed by intense chemical weathering in warm, humid climates where silica is leached out, leaving soils enriched in alumina (Weaver, 1990). According to this general rule, our data suggest cooler conditions before and after the OAE1d. The clay mineralogy of the Bonarelli Level, instead, seems to indicate warmer depositional conditions.

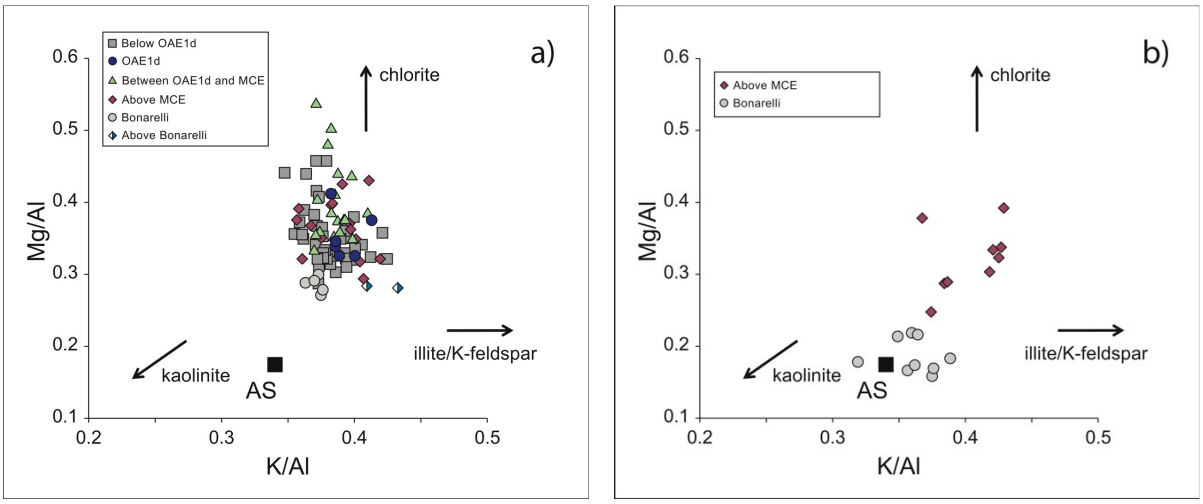

Fig. 7.6a and b: Plot of Mg/Al vs. K/Al for Cismon (left) and Monte Petrano (right).

7.4.3 Redox-sensitive elements as bottom-water oxygenation indicators

Many trace elements accumulate as a result of combined authigenic processes and post-depositional precipitation or adsorption from the bottom waters or from pore waters, mainly under the control of different redox conditions (Algeo and Maynard, 2004; Calvert and Pedersen, 2007).

C_{org}-rich sediments are frequently associated with major and trace metal enrichments (e.g. Brumsack, 1980; Calvert, 1983; Arthur et al., 1990; Warning and Brumsack, 2000; Scopelliti et al., 2004). The generally high concentration in trace metals is interpreted in many cases as a consequence of the oxygen-depleted bottom waters conditions (e.g. Brumsack 1980; Piper, 1994; Tribovillard et al., 2004; Brumsack, 2006; Tribovillard et al., 2006).

Mn represents a useful proxy for bottom-water oxygenation regimes (Landing and Bruland, 1980, 1987). This element is generally depleted in oxygen-poor bottom waters as a consequence of its removal from sediments under reducing conditions at the sediment/water interface. According to Thurow et al. (1992) soluble Mn^{2+} is efficiently removed from sediments under anoxic conditions (Oxygen Minimum Zone) and redeposited as Mn^{4+} in oxygenated waters. Such a process suggests that in open marine settings anoxic conditions, such as in an upwelling area with an expanded oxygen minimum zone (OMZ), C_{org}-rich sediments are depleted in Mn. On the contrary, in areas with scarce circulation, due for example to the presence of a sill, Mn tends to remain trapped within the basin resulting in higher Mn/Al values.

Due to scavenging, under anoxic conditions Mo is accumulated in concentrations higher than AS both in sulphides (Koide et al., 1986; Colodner et al., 1993) and in sulphur-rich organic matter (Tribovillard et al., 2004).

Cr, V and U, generally conservative in oxic waters (Ku et al., 1977; Colodner et al., 1993), are proxies for suboxic conditions due to their tendency to accumulate in conditions of poor-oxygen conditions (e.g. Brumsack and Gieskes, 1983; Emerson and Huested, 1991; Sarkar et al., 1993; Piper and Isaacs, 1995; Rue et al., 1997; Brumsack, 2006). The sedimentary U sink in particular, is strongly controlled by the settling flux of metabolizable organic matter to the sea floor (Calvert and Pedersen, 2007).

Cu, Ni, Zn are all chalcophile elements that are commonly enriched in black shales mainly in the form of sulphides (Calvert and Pedersen, 2007). Ni and Zn in the water column behave as micronutrients, while Cu, even if partially behaves as micronutrient, is also scavenged from solution onto particle surfaces in deep water (Calvert and Pedersen, 2007). These three elements are enriched in modern organic-rich sediments (Jacobs et al., 1987) as well as in black shales (Hulbert et al., 1992; Brumsack, 2006; Piper and Calvert, 2009). However, Ni in oxic environment, like Co, is intensively scavenged in the water column by Mn oxides and released during dissolution of this carrier phase under suboxic conditions (Rachold and Brumsack, 2001).

While Pb can be fixed under reducing conditions in sediments (e.g. Brumsack, 2006), Co diffuse out of sediments under reducing conditions (e.g. Luther, 1991; Huerta-Diaz and Morse, 1992), although it can be fixed as a stable sulphide under sulfidic conditions (Luther, 1991; Huerta-Diaz and Morse, 1992; Turgeon and Brumsack, 2006).

7.4.3.1 Bonarelli Level

The Bonarelli Level at Monte Petrano is highly enriched in As, Cu, Mo, Ni, U, V and Zn and at a lesser in Co and Cr (EF about 3). The Bonarelli at Cismon is characterized by high values of As, Cu, Mo, Ni, V and Zn. The very low concentrations of Mn and Co and the peculiar enrichment in redox-sensitive elements are indicative of severe anoxic conditions in open-marine settings. Additionallys in both studied sections, even if with different extent, Ca concentration reaches minimum values, as previously documented for many localities (e.g. Hilbrecht et al., 1996; Voigt, 2000; Turgeon and Brumsack, 2006; Wagreich et al., 2008).

7.4.3.2 Interval below the Bonarelli Level

At Cismon samples from the intervals below the OAE1d and above the OAE2 are not characterized by enrichment in redox-sensitive elements. Data from the OAE1d and the interval between the OAE1d and the base of the MCE show values in redox-sensitive elements similar to AS.

The interval comprised between the base of the MCE and the base of the OAE2, characterized by frequent organic-rich shales, shows interesting results. Darker and relatively Corg-rich layers are characterized by high concentrations of As, Co, Cu, Cr, Mn, Mo, Ni, Pb, U, V, Y and Zn. The presence of these elements together suggests that these levels deposited under dysoxic to euxinic conditions. The high concentration in Mn indicates that probably their deposition happened in a partially isolated area of the basin where Mn remained trapped. At Cismon no real black shales are present in this interval. The extremely thin dark grey shales collected from this interval show high values of Cu, moderate concentration of Co (EF=3.3) and slightly higher concentrations of As, Mn and Ni (EF about 2). The generally low values of redox-sensitive elements indicate that the sediments never experienced anoxia, but only times of dysoxic conditions. However, it's important to notice that all the mentioned elements start to have higher concentrations exactly at the onset of the MCE and then oscillate from lower to higher values through the interval up to the OAE2. This evidence suggests that, even if at Cismon anoxic conditions were never reached during this time interval, from the onset of the MCE the deposition was subjected to more unstable conditions, with times of alternating dysoxia and well-oxygenated bottom waters.

7.4.4 Excess silica

Silica content is different in the two sections, with the Monte Petrano generally characterized by higher Si concentrations. Excess silica was calculated using 3.11 as average shale Si/Al value as indicated by Wedephol, 1971). Both the dark grey shales and the Bonarelli Level at Cismon indicate that the average concentration of about 25% of the silica hasn't a detrital source. At Monte Petrano excess silica measured in black shales below the Bonarelli Level indicates that about 39% is biogenic silica. Black shales within the Bonarelli Level, instead, contain about 70% of biogenic silica. We interpret this excess values as the result of biosiliceous accumulations of radiolaria, very common throughout the sections and in particular in the Bonarelli Level (Salvini and Passerini, 1998).

7.4.5 Barium and phosphorous as palaeoproductivity proxies

Settling of Ba through the water column is strongly correlated with organic carbon flux out of surface waters under the control of (seasonal) fluctuations in primary productivity (e.g. Jeandel et al., 2000; Balakrishnan Nair et al., 2005; Brumsack, 2006). Ba excess content is considered a proxy for bio-productivity (e.g. Dymond et al., 1992; Fagel et al., 2004). The processes by which barium is transported to the sediments, although not completely clear, seem to be connected with a syngenetic mechanism during decay, aggregation and settling of organic-rich detritus (Bishop, 1988). Analyzing sediments collected from the Peruvian upwelling margin, Von Breymann et al. (1992) have clearly shown that in areas with high primary productivity enhanced barium accumulation can concentrate only in deep-water environments and cannot be extended to shallow-water settings. The Ba enrichments at times can be also the result of great paleo-water depth, scarce dilution as a consequence of the low terrigenous-detrital input and diagenetic mobility (Brumsack, 2006)

In order to compute the barium excess content, as detrital Ba/Al background ratio has been used the value of $27x10^{-4}$ as applied to the Umbria-Marche Furlo section by Turgeon and Brumsack (2006). Barium data indicate that about 89% of the barium is in excess in the dark grey shales of the Cismon section, and about 96% in the black shales at Monte Petrano. The barium non-detrital fraction in the Bonarelli Level is almost equal in the two sections with values of 97% and 99% at Cismon and Monte Petrano, respectively. Our data indicate that the studied sediments deposited at water-depth deeper than 1000m in an environment characterized by mostly continuous high-productivity.

Phosphorous represents an important limiting macro-nutrient for algal growth and its accumulation is considered a proxy for paleoproductuivity (e.g. Ganeshram et al., 2002). It is generally present in deep-sea sediments as francolite (or carbonate fluor-apatite) (Ruttenberg and Berner, 1992). Then concentration of P is generally high in the black shale layers at Monte Petrano, with an average EF of about 7 and about 6 in the Bonarelli Level. At Cismon, instead, both the dark grey shales and the Bonarelli sediments are not particularly enriched in P, with an EF from about 2 to 3.

7.4.6 Comparison with Furlo sediment geochemistry

Extended geochemistry characterization of Cenomanian pelagic sediments were carried out by Turgeon and Brumsack (2006) at the Furlo section, located in the Umbria-Marche Basin. The comparison of the Monte Petrano and Cismon sequences with the Furlo section allows a much better comprehension of our results in the interval comprised from the base of the MCE and the OAE2. Major and trace element measurements obtained for the Furlo section (Turgeon and Brumsack, 2006; original

data kindly provided by Hans Brumsack) are illustrated in Figs. 7.7a to 7.7c, and with a particular focus on the Bonarelli Level in Figs 7.7d and 7.7e.

Data from the Monte Petrano and Furlo sections, being in the same basin, are very similar, while Cismon results are quite different. The nature of sediments and clay mineralogy above the MCE is almost the same in all three sections. Silica excess is in similar concentrations both at Furlo and at Monte Petrano, indicating that biosiliceous accumulation (opal) was relatively homogeneous in the Umbria-Marche Basin. Barium and phosphorous at a lesser extent are very abundant in the three section, suggesting widespread high-productivity conditions in both the Umbria-Marche and Belluno Basins. Zn concentrations in the black shales at Monte Petrano are very similar to the values measured in the black shales at Furlo.

The comparison of the two studied sections with the Furlo sequence indicates generally homogeneous characteristics within the Umbria-Marche Basin. While after the MCE this basin was experiencing locally anoxic conditions, the Cismon area in the Belluno Basin was characterized by generally well oxygenated bottom-water conditions with only temporary dysoxia, with peaks likely in correspondence of the black chert bands. This indication suggests that the deposition of black shales after the MCE represents a lithologic expression of local conditions. During the sedimentation of the Bonarelli Level, instead, the two basins were subjected to very similar environmental conditions with widespread deposition of organic-rich sediments in severely oxygen-depleted conditions.

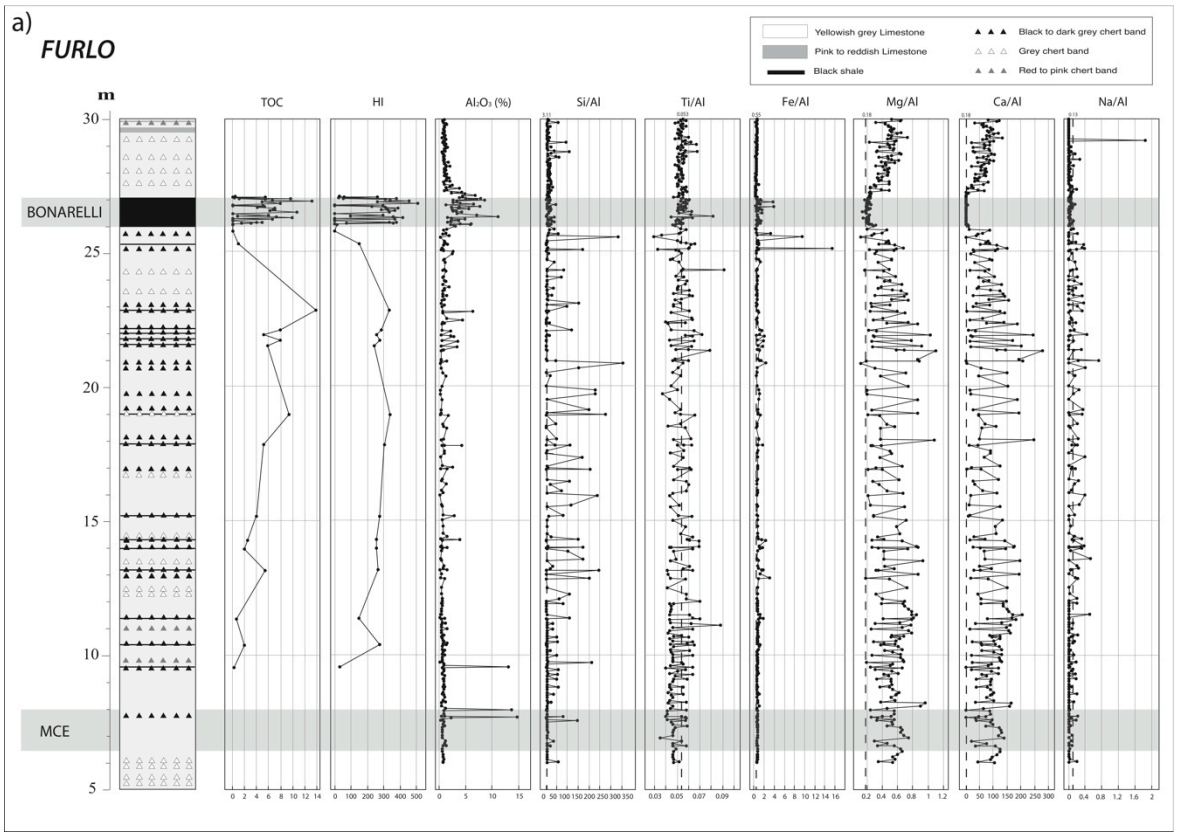

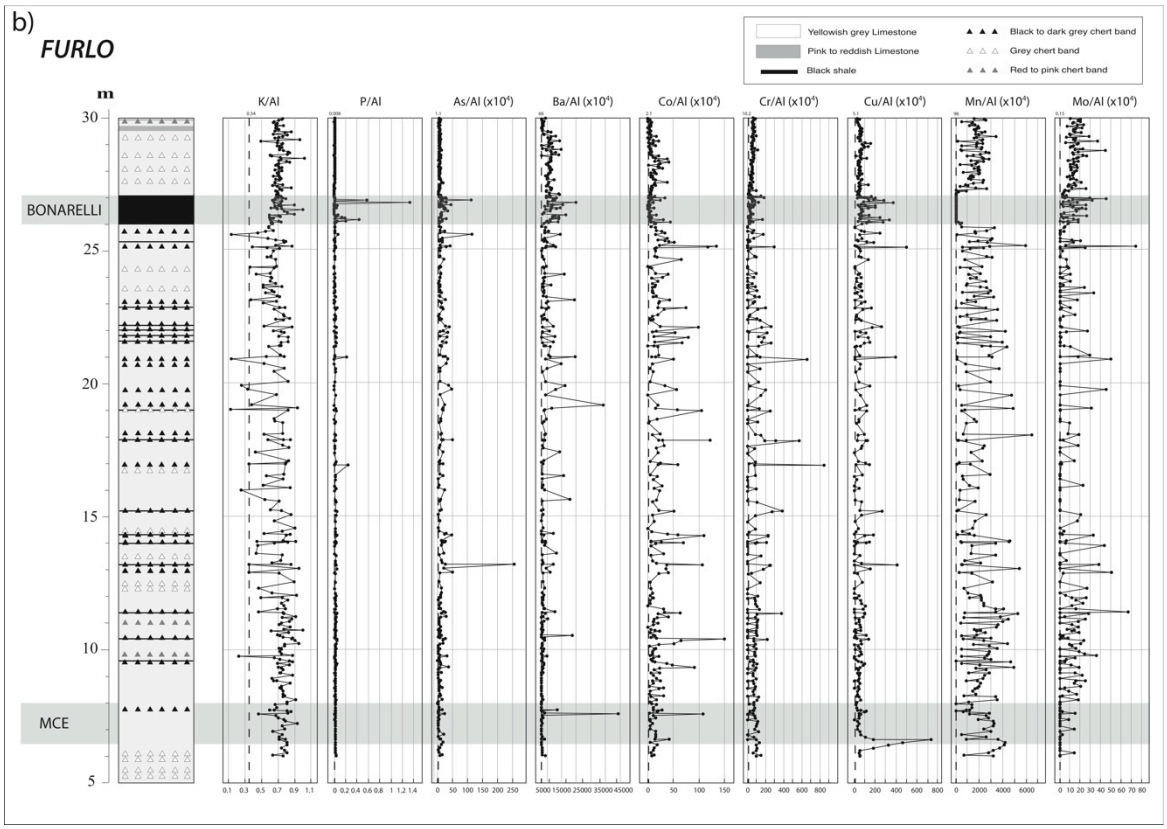

Figs. 7.7a and b: Major and trace element profiles for the Furlo section. Dotted lines refer to average shale values for each element (Wedepohl, 1971). Additionally, TOC and HI measurements are reported.

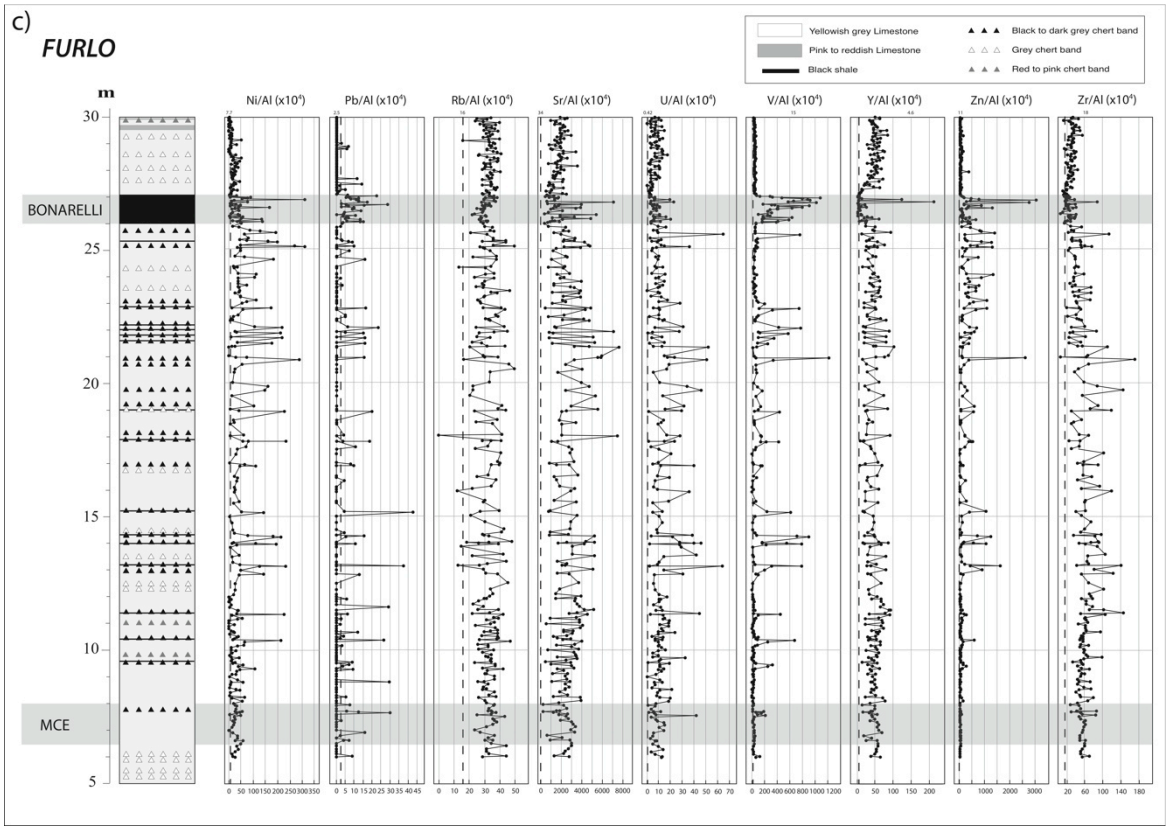

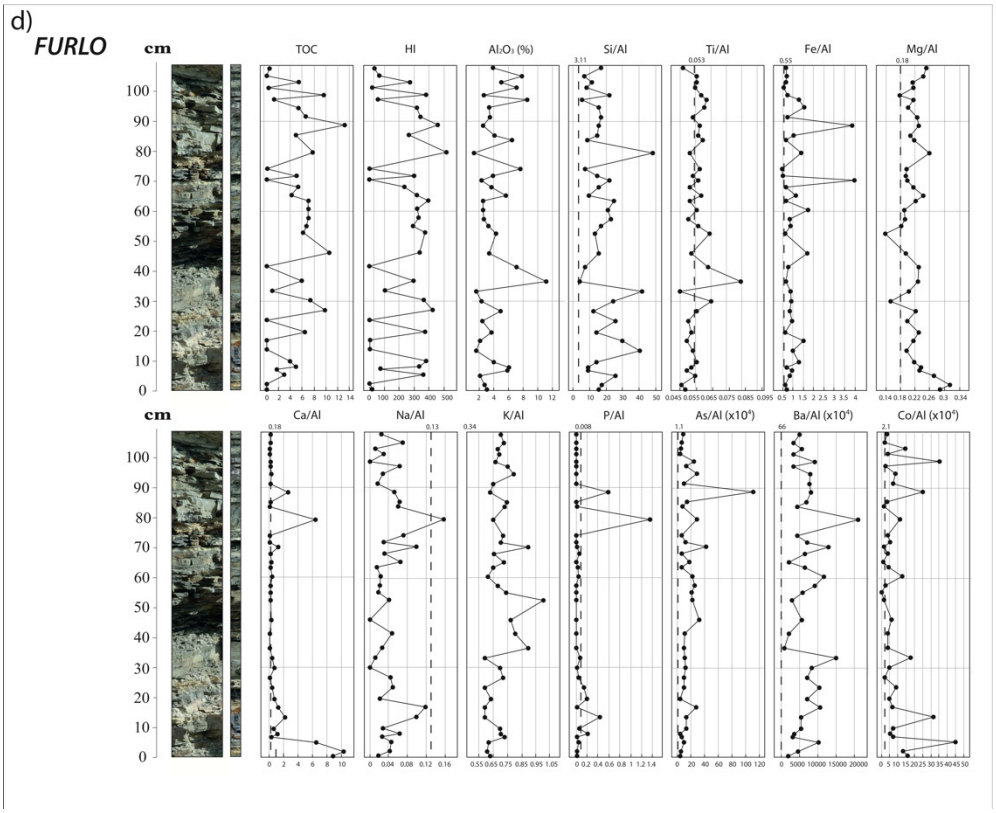

Figs. 7.7c: Trace element profiles for the Furlo section. Dotted lines refer to average shale values for each element (Wedepohl, 1971).
Fig. 7.7d: Detail of the major and trace element profiles in the Bonarelli Level at Furlo. Dotted lines refer to average shale values for each element (Wedepohl, 1971). Additionally, TOC and HI measurements are reported.

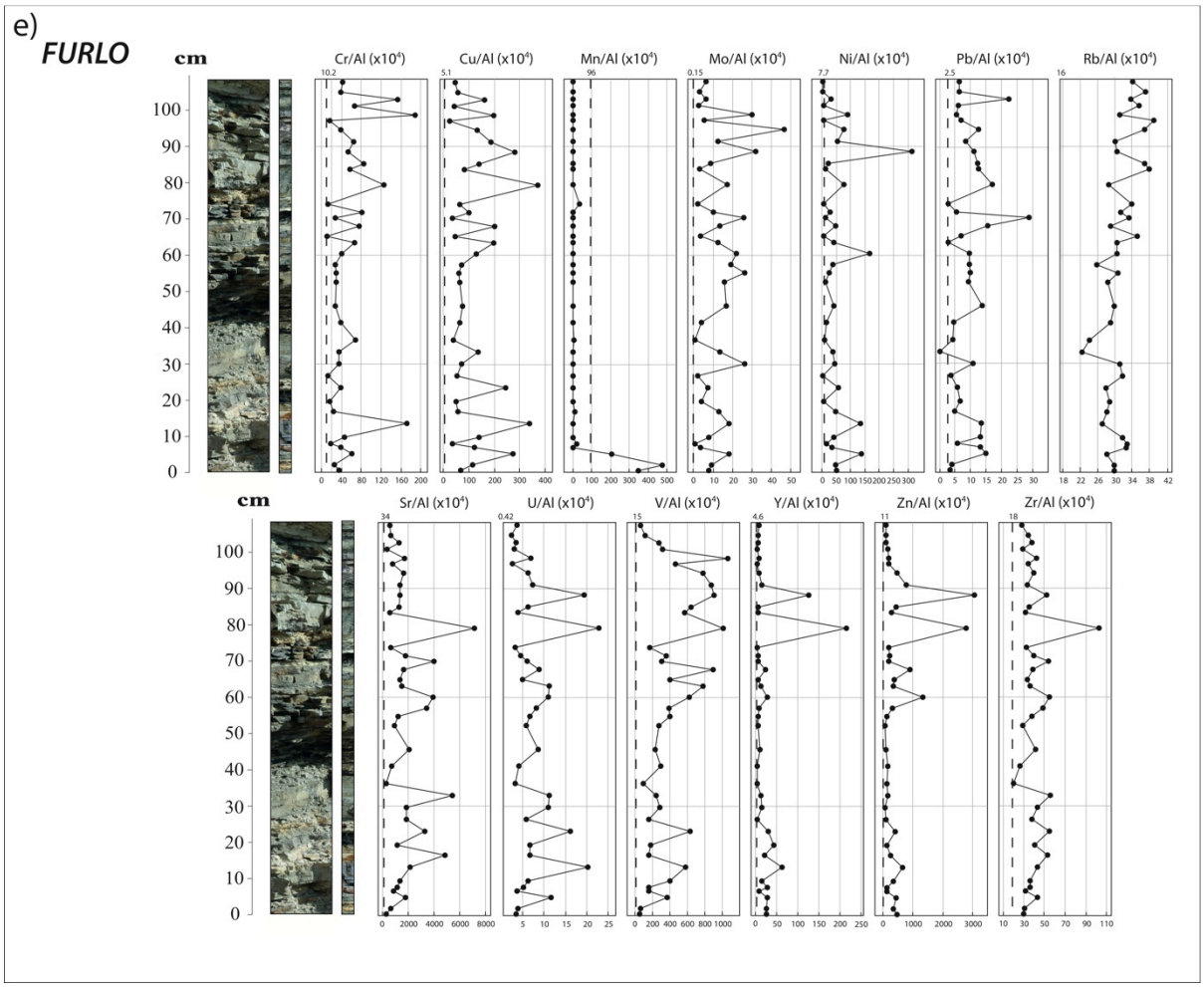

Fig.7.7e: Detail of the trace element profiles in the Bonarelli Level at Furlo. Dotted lines refer to average shale values for each element (Wedepohl, 1971).

Additionally, data on biogenic barite concentrations in the Furlo section (Erba unpublished data) are presented in Fig. 7.8. They were obtained through image analysis of thin sections, counting all single barite crystal with a dimension lower than 8μm. According to Paythan et al. (2002) only the barite with this particular dimensions represents the biogenic fraction connected with the primary productivity.

Also, nannofossil total abundance and temperature- and fertility-related nannofossil indices (Tamagnini, 2009; Erba, unpublished data) are reported. The nannofossil Temperature Index (TI) and the nannofossil Fertility Index (FI) were calculated as follows:

$$TI = \frac{(Z.erectus + B.constans)}{W.barnesiae + (Z.erectus + B.constans)} * 100$$

$$FI = \frac{(E.floralis + R.parvidentatum)}{(Z.diplogrammus + R.asper) + (E.floralis + R.parvidentatum)} * 100$$

More details and discussion is provided by Tamagnini (2009) and Tiraboschi et al. (2009).

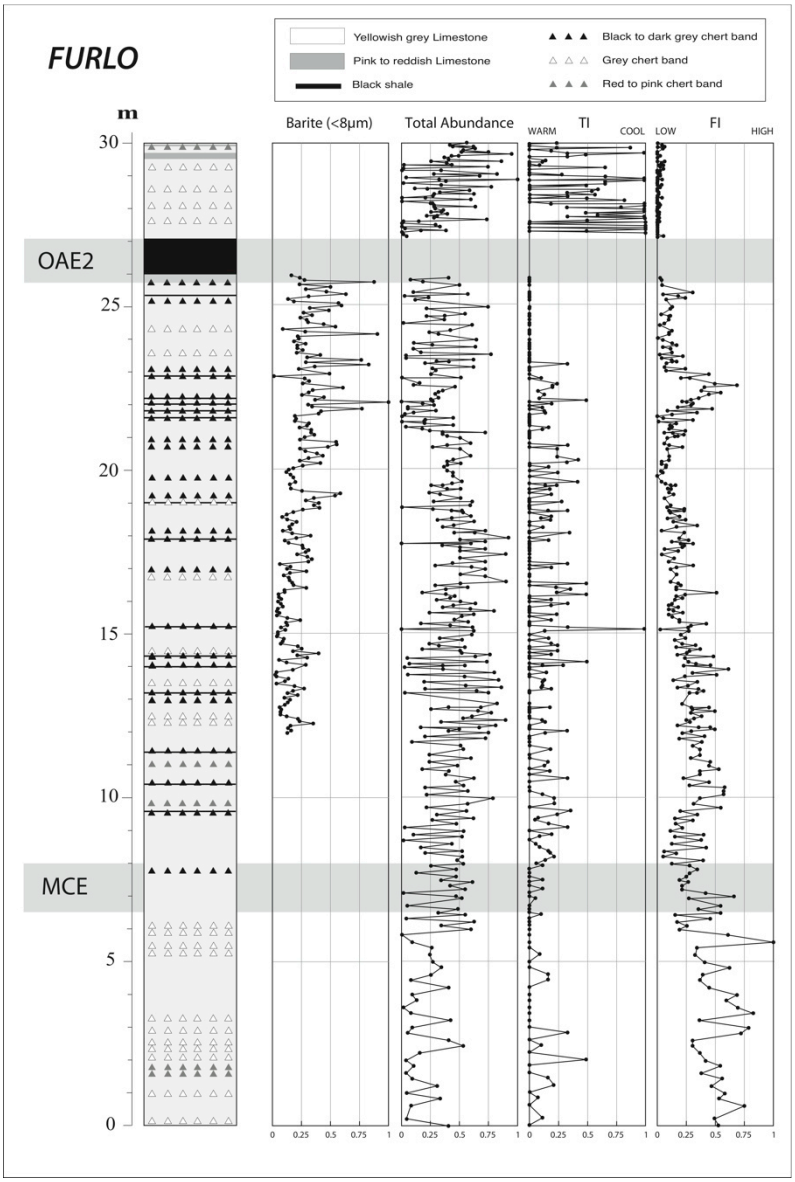

Fig. 7.8: Biogenic barite variations at Furlo based on thin sections image analyses. Data are normalized relative to the maximum value. Nannofossil total abundance, temperature (TI) and fertility (FI) indices are also shown.

In Fig. 7.9 average element enrichments (EF) of selected major and trace elements in black shales at Furlo and Monte Petrano and in dark grey shales at Cismon above the MCE are compared with the EF

values of Pliocene and Pleistocene obtained for Eastern Mediterranean sapropels and Holocene Black Sea sapropels and with the EF values of coastal upwelling C_{org}-rich sediments (Brumsack, 2006). Even if the depletion in P and enrichment in Co resemble the geochemical characteristics of sapropels, all the analyzed Cenomanian sediments show characteristics that are intermediate relative to the composition of organic-rich sediments from coastal upwelling areas and sapropels.

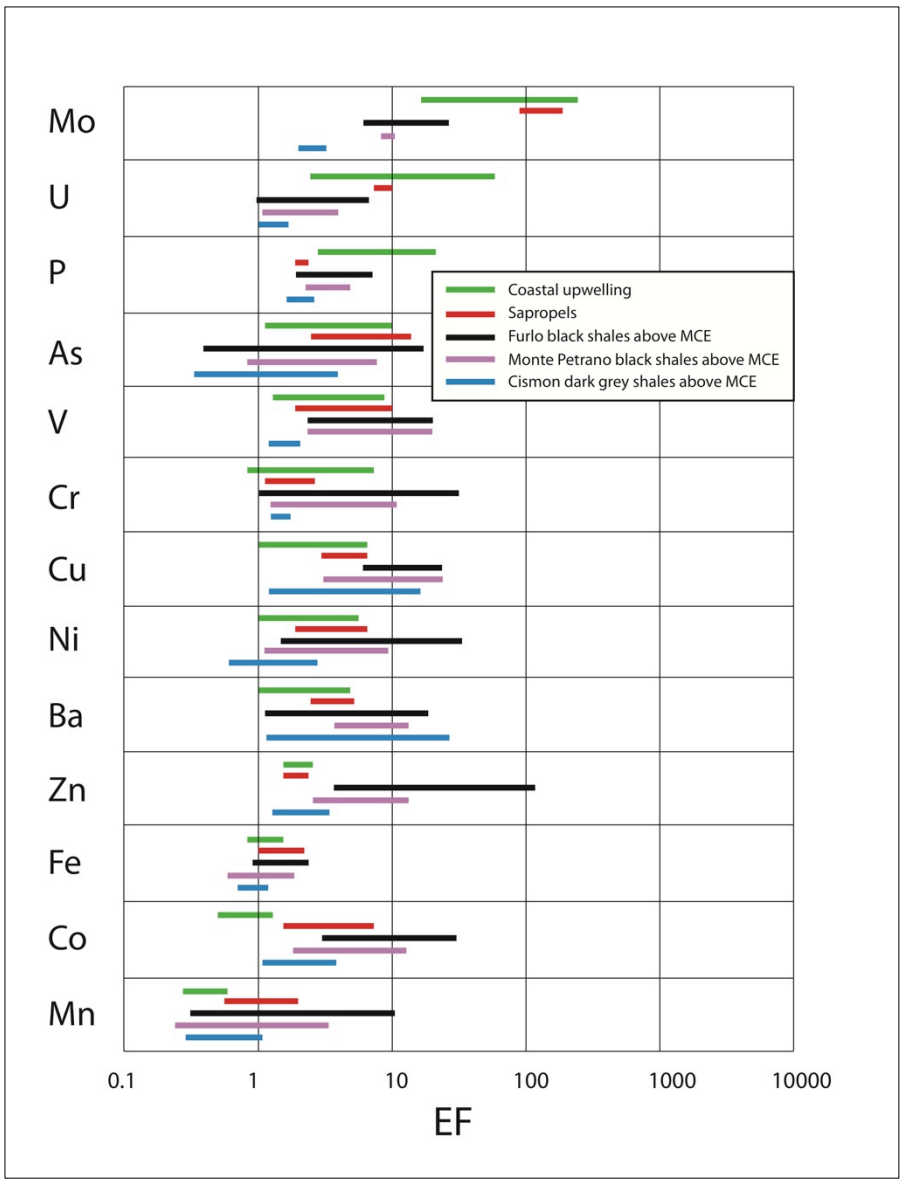

Fig. 7.9: Enrichment of selected major and trace elements in black shales from Furlo and Monte Petrano and in dark grey shales from Cismon compared with the average values for coastal upwelling sediments and sapropels. The length of the bar for each element is extended from the EF minimum to the EF maximum value recorded in the data (modified after Brumsack, 2006).

Zn concentrations are slightly high at Cismon (EF=3) and very high at Monte Petrano (EF=16) below the OAE2, while it becomes highly enriched - with amounts similar in both the sections - in the Bonarelli Level (average EF about 16). Geochemical data present spikes of Ba, Zr and Cu within the MCE, and at Furlo a Cu spike correlates with the onset of the MCE. Generally Cu concentrations, and at a lesser extent As, increase from the MCE up to the OAE2. The presence of Cu, Zn, As and Y points to a possible circulation of metal-rich hydrothermal fluids (e.g. Normark et al., 1983; Arthur et al., 1990; Bao et al., 2008; Sarradin et al., 2009; Breuer and Pichler, 2013).

Even if the MCE is not associated to deposition of C_{org}-rich sediments at Cismon, it's evident that starting from this event more unstable redox conditions developed in both basins, with frequent episodes of anoxia at Furlo and Monte Petrano and dysoxia at Cismon.

The nannofossil temperature index of the Furlo section (Fig. 7.8) documents a shift to more unstable climatic conditions starting from the MCE and persisting up to the OAE2. The nannofossil fertility index suggests decreasing trophic conditions up to some about 400 ky before OAE2. No evidence of high productivity is associated with the MCE.

The onset of submarine volcanism or enhanced spreading rates was probably at the origin of increased hydrothermal activity. On the other hand, submarine volcanism related to LIPs was inducing climate change altering the hydrological cycle equilibrium leading to icreased runoff and consequent enhanced water stratification and stimulation of higher productivity by the introduction of nutrients in surface waters, in particular in those areas physically bounded by sills, or partially isolated. In correspondence of the interval between MCE and OAE2 in many sections from the Umbria-Marche Basin as well as at Cismon in the Belluno Basin, organic-rich sediments are exclusively represented by black chert bands, indicating that black shales represent specific local conditions (Fig. 7.10). A possible explanation of the lack of black shales at Cismon could be related to its possible paleogeographic position in a more open marine setting and/or to a reduced/different terrigenous detrital input.

7.5 Conclusions

Major and trace element geochemistry of the Monte Petrano and Cismon sections gives important information on the processes that acted in two adjacent Tethyan basins during a time of important paleoceanographic changes. The sudied pelagic sections consist of alternate pelagic limestones with radiolarian-rich intervals, dark grey to black shales, and reddish to black chert. Element content

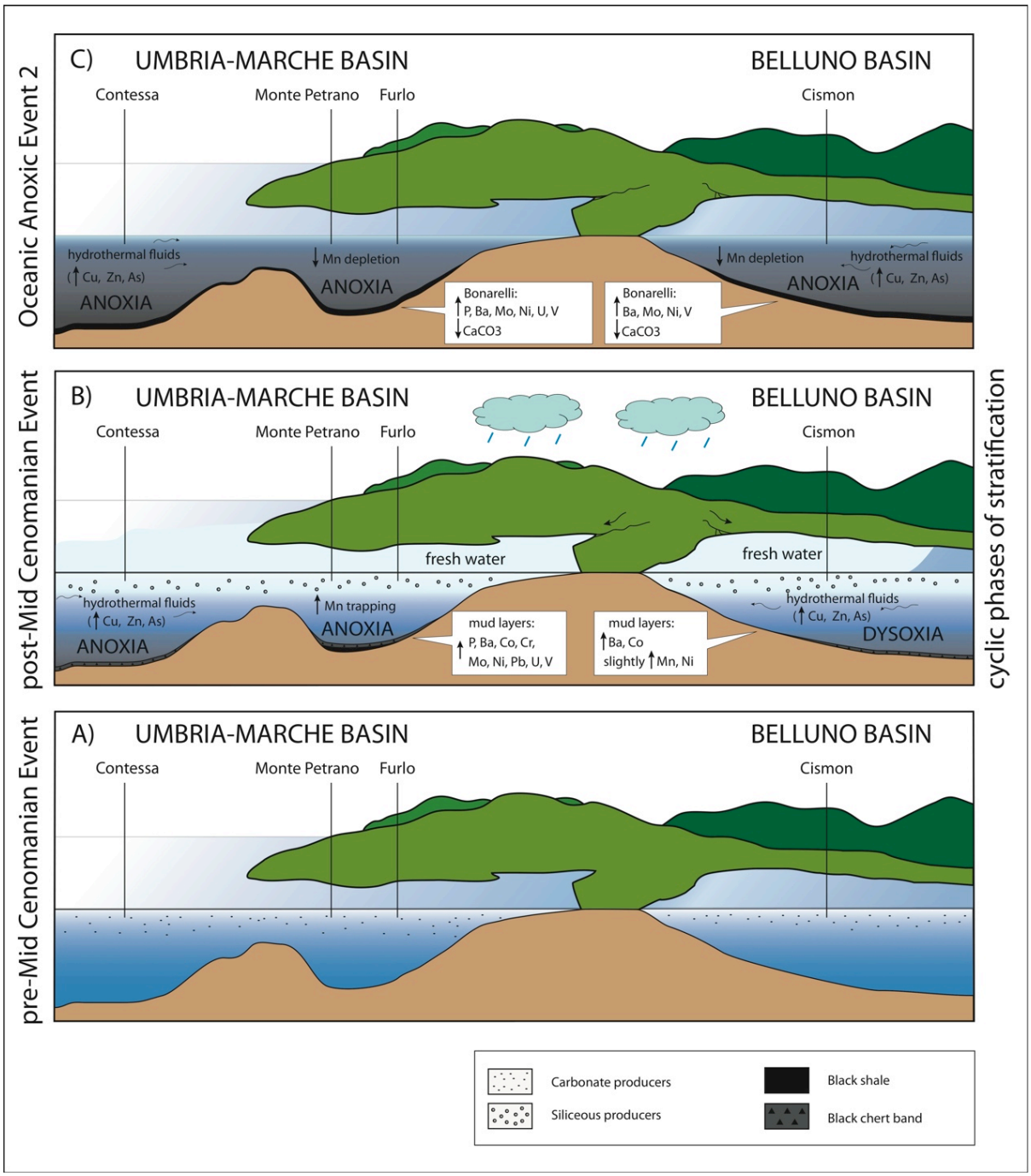

Fig. 7.10: Schematic cartoon illustrating the main geochemical characteristics of the studied sediments throughut the sturied time interval. In particular three different time steps are sketched: A) time interval before the mid-Cenomanian Event characterized by stable conditions; B) time interval between the Mid-Cenomanian Event and the Oceanic Anoxic Event 2; C) Oceanic Anoxic Event 2.

indicates that shales are mainly a mixture of a detrital clay minerals, quartz and feldspar originated from an almost homogeneous source area and various amount of biogenic components such as silica from radiolarian and carbonate from nannofossils and foraminifers.

High Ba and P concentrations indicate that both basins were characterized by bathial depths with enduring high-productivity conditions.

Cu is present in high concentrations starting from the MCE up to the OAE2 indicating, together with a generally high Zn content. The presence of Cu, Zn with slight increase in As and at times Y suggests effective submarine hydrothermal activity.

Starting from late Albian through the time interval preceeding the onset of the OAE2, the Umbria-Marche Basin experienced temporary episodes of anoxia with the deposition of black shale layers and black chert bands alternated to whitish limestones as a result of possible water stratification. During the same time interval at Cismon in the Belluno Basin no deposition of black shales occurred and the only times of organic-matter preservation were exclusively associated to the deposition of few black chert bands. This suggests that the deposition of black shales during and after the MCE was controlled by specific local anoxic conditions. However, even if with different extent, redox-sensitive elements indicate that starting from the MCE paleoenvironmental conditions became generally unstable in both the Umbria-Marche and Belluno Basin.

The Bonarelli Level, strongly Mn-depleted and enriched in many redox-sensitive elements, deposited during pervasive anoxic conditions in open marine settings. The similar geochemical characteristics in both basins are a further evidence that anoxia was widely distributed through south-western Thetys during OAE 2.

Further geochemical investigations focused exclusively on the Mid-Cenomanian Event may reveal important additional information on the origin, extent and paleoclimatic effect of this event and its possible relation with the Oceanic Anoxic Event 2.

References

Algeo, T. and Maynard, J.B. (2004) – Trace-element behavior and redox facies in core shales of Upper Pennsylvanian Kansas-type cyclothems. *Chemical Geology*, 206, 289-318.

Alvarez, W. (1990) – Pattern of extensional faulting in pelagic carbonates of the Umbria-Marche Apennines of central Italy. *Geology*, 18, 407-410.

Alvarez, W. (1990) – Pattern of extensional faulting in pelagic carbonates of the Umbria-Marche Apennines of central Italy. *Geology*, 18, 407-410.

Arthur, M.A. and Premoli Silva, I. (1982) – Development of widespread organic carbon-rich strata in the Mediterranean Tethys. *In:* Schlanger, S.O. and Cita, M.B. (Eds.), *Nature and Origin of Cretaceous Carbon-rich Facies*, 7-54.

Arthur, M.A., Brumsack, H.-J., Jenkyns, H.C., Schlanger, S.O. (1990) – Stratigraphy, geochemistry, and paleoceanography of organic carbon-rich Cretaceous sequences. *In:* Ginsburg, R., Beaudoin, B. (Eds.), *Cretaceous Resources Events, and Rhythms*, 75-119.

Balakrishnan Nair, T.M., Ittekkot, V., Shankar, R., Guptha, M.V. (2005) – Settling barium fluxes in the Arabian Sea: Critical evaluation of relationship with export production. *Deep Sea Research*, 52, 1930-1946.

Bao, S.-X., Zhou, H.-Y., Peng, X.-T., Ji, F.-W., Yao, H.-Q. (2008) – Geochemistry of REE and yttrium in hydrothermal fluids from the Endeavour segment, Juan de Fuca Ridge. *Geochemical Journal*, 42, 359-370.

Bellanca A., Claps, M., Erba, E., Masetti, D., Neri, R., Premoli Silva, I. and Venezia F. (1996) – Orbitally induced limestone/marlstone rhythms in the Albian-Cenomanian Cismon section (Venetian region, northern Italy): sedimentology, calcareous and siliceous plankton distribution, elemental and isotope geochemistry. *Palaeogeography, Palaeoclimatology, Palaeoecology*, 126, 227-260.

Bernoulli, D. and Jenkyns, H.C. (1974) – Alpine, Mediterranean, and Central Atlantic Mesozoic facies in relation to the early evolution of the Tethys. In: Dott, R.H. and Shaver, R.H. (Eds.), Modern and Ancient Geosynclinal Sedimentation. Society of Economic Paleontologists and Mineralogists, Special Publication, 19, 129-160.

Bishop, J.K.B. (1988) – The barite-opal-organic carbon association in oceanic particulate matter. *Nature*, 332, 341-343.

Bonarelli, G. (1891) – Il territorio di Gubbio. *Notizie geologiche*, 1-38.

Bosellini, A., Broglio Loriga, C., and Busetto, C. (1978) - I bacini cretacei del Trentino. *Riv. Ital Paleont. Strat*, 84.4, 897-946.

Breuer, C. and Pichler, T. (2013) – Arsenic in marine hydrothermal fluids. *Chemical Geology*, 348, 2-14.

Brumsack, H.-J. (1980) – Geochemistry of Cretaceous black shales from the Atlantic Ocean (DSDP Legs 11, 14, 36 and 41). *Chemical Geology*, 31, 1-25.

Brumsack, H.-J. (2006) – The trace metal content of recent organic carbon-rich sediments: Implications for Cretaceous black shale formation. *Palaeogeography, Palaeoclimatology, Palaeoecology*, 232, 344-361.

Brumsack, H.-J. and Gieskes, J.M. (1983) – Intertitial water trace-element chemistry of laminated sediments from the Gulf of California, Mexico. *Marine Chemistry*, 14, 89-106.

Calvert, S.E. (1983) – Geochemistry of Pleistocene sapropels and associated sediments from the eastern Mediterranean. *Oceanologica Acta*, 6, 255-267.

Calvert, S.E. and Pedersen, T.F. (2007) – Elemental proxies for palaeoclimatic and paleaeoceanographic variability in marine sediments: interpretation and application. *In:* Hillaire-Marcel, C. and De Vernal, A., *Proxies in Late Cenozoic Paleoceanography*, Developments in Marine Geology, 1, 567-644.

Channell J.E.T., D'Argenio, B., Horvath, F. (1979a) – The African Promontory, in Mesozoic Mediterranean Paleogeography. *Earth Science Review*, 15, 213-272.

Channell, J.E.T., Lowrie, W. and Medizza, F. (1979b) – Middle and Early Cretaceous magnetic stratigraphy from the Cismon section, northern Italy. *Earth and Planetary Science Letters*, 1979, 42.2, 153-166.

Claps, M., Masetti, D., Pedrielli, F., Garavello, A. (1991) – Analisi spettrale e cicli di Milankovitch in successioni cretaciche del Sudalpino orientale. Rivista Italiana di Paleontologia e Stratigrafia, 97, 153-174.

Coccioni, R., Galeotti, S., Gravili, M. (1995) – Latest Albian–early Turonian deep-water agglutinated foraminifera in the Bottaccione section (Gubbio, Italy) — biostratigraphic and palaeoecologic implications. *Revista Espanola de Paleontologia Homenaje al Dr. Guillermo Colom*, 135–152.

Coccioni, R. and Galeotti, S. (2001) – The mid-Cenomanian Event the Prelude to the OAE 2. *EOS Trans. AGU* 82(47), Fall Meet. Suppl.

Coccioni, R. and Galeotti, S. (2003) – The mid-Cenomanian Event: prelude to OAE 2. *Palaeogeography, Palaeoclimatology, Palaeoecology*, 190, 427-440.

Coffin, M.F. and Eldholm, O. (1994) – Large igneous provinces: crustal structure, dimensions, and external consequences. *Reviews of Geophysics*, 32, 1-36.

Colodner, D., Sachs, J., Ravizza, G., Turekian, K., Edmont, J., Boyle, E. (1993) – The geochemical cycle of rhenium: a reconnaissance. *Earth and Planetary Science Letters*, 117, 205-221.

Dercourt, J., Gaetani, M., Vrielinck, B., Barrier, E., Biju-Duval, B., Brunet, M.F., Cadet, J.P., Crasquin, S., Sandulescu, M. (2000) – *Atlas of Peri-Tethys, Palaeogeographical Maps. Commission de la Carte Geologique du Monde (CCGN/CGMW)*, Paris, pp. 1-269.

Dymond, J., Suess, E., Lyle, M. (1992) – Barium in deep-sea sediment: a proxy for paleoproductivity. *Paleoceanography*, 7, 163–181.

Emerson, S.R. and Huested, S.S. (1991) – Ocean anoxia and the concentrations of molybdenum and vanadium in seawater. *Marine Chemistry*, 34, 177-196.

Erba, E. (1994) – Nannofossils and superplumes: the early Aptian 'nannoconid crisis'. *Paleoceanography*, 9, 483-501.

Erba E. (2004) – Calcareous nannofossils and Mesozoic oceanic anoxic events. *Marine Micropaleontology*, 52, 85-106.

Erba E. and Larson R.L. (1998) – The Cismon APTICORE (Southern Alps, Italy): a reference section for the Lower Cretaceous at low latitudes. *Rivista Italiana di Paleontologia e Stratigrafia*, 104, 181-192.

Fagel, N., Dehairs, F., Peinert, R., Andre, L., Antia, A.N. (2004) – Reconstructing export production at the NE Atlantic margin: Potential and limits of the Ba proxy. *Marine Geology*, 204, 11-25.

Friedrich, O., Erbacher, J., Mutterlose, J. (2006) – Paleoenvironmental changes across the Cenomanian/Turonian Boundary Event (Oceanic Anoxic Event 2) as indicated by benthic foraminifera from the Demerara Rise (ODP Leg 207). *Revue de Micropaléontologie*, 49, 121-139.

Friedrich, O., Erbacher, J., Wilson,P.A., Moriya, K., Mutterlose, J. (2009) – Paleoenvironmental changes across the Mid Cenomanian Event in the tropical Atlantic Ocean (Demerara Rise, ODP Leg 207) inferred from benthic foraminiferal assemblages. *Marine Micropaleontology*, 71, 28-40.

Ganeshram, R.S., Calvert, S.E., Pedersen, T.F. and Cowie, G.L. (1999) – Factors controlling the burial of organic carbon in laminated and bioturbated sediments off NW Mexico: Implications for hydrocarbon preservation. *Geochmica et Cosmochimica Acta*, 63, 1723-1734.

Ganeshram, R.S., Pedersen, T.F., Calvert, S.E., François, R. (2002) – Reduced nitrogen fixationin the glacial ocean inferred from changes in marine nitrogen and phosphorus inventories. *Nature*, 415, 156-159.

Giorgioni, M., Weissert, H., Bernasconi, S.M., Hochuli, P.A., Coccioni, R., Keller, C.E. (2012) – Orbital control on carbon cycle and oceanography in the mid-Cretaceous greenhouse. *Paleoceanography*, 27, PA1204, doi:10.1029/2011PA002163.

Gröcke, D.R., Ludvigson, G.A., Witzke, B.L., Robinson, S.A., Joeckel, R.M., Ulnar, D.F., Ravn, R.L. (2006) – Recognizing the Albian-Cenomanian (OAE1d) sequence boundary using plant carbon isotopes: Dakota Formation, Western Interior Basin, USA. *Geology*, 34 193-196.

Hardas, P. and Mutterlose, J. (2007) – Calcareous nannofossil assemblages of Oceanic Anoxic Event 2 in the equatorial Atlantic: Evidence of an eutrophication event. *Marine Micropaleontology*, 66, 52-69.

Hardas, P., Mutterlose, J., Friedrich, O., Erbacher, J. (2012) – The Middle Cenomanian Event in the equatorial Atlantic: The calcareous nannofossil and benthic foraminiferal response. *Marine Micropaleontology*, 96-97, 66-74.

Herbin, J.P., Montadert, L., Muller, C., Gomez, R., Thurow, J., Wiedmann, J. (1986) – Organic-Rich Sedimentation at the CenomanianeTuronian Boundary in Oceanic and Coastal Basins in the North Atlantic and Tethys. *Geological Society, London, Special Publications*, 21, 389-422.

Hetzel, A., Böttcher, M.E., Wortmann, U.G., Brumsack, H.-J. (2009) – Paleo-redox conditions during OAE 2 reflected in Demerara Rise sediment geochemistry (ODP Leg 207). *Palaeogeography, Palaeoclimatology, Palaeoecology*, 273, 302-328.

Hilbrecht, H., Frieg, C., Tröger, K.-A., Voigt, S., Voigt, T. (1996) – Shallow water facies during the Cenomanian-Turonian anoxic event: Bio-Events, isotopes and sea level in southern Germany. *Cretaceous Research*, 17, 229-253.

Huerta-Diaz, M, A. and Morse, J.W. (1992) – Pyritization of trace metals in anoxic marine sediments. *Geochmica et Cosmochimica Acta*, 56, 2681-2702.

Hulbert, L.J., Carne, R.C., Gregoire, D.C., Paktunc, D. (1992) – Sedimentary nickel, zinc, and platinum-group-element mineralization in Devonian black shales at the Nick Property, Yukon, Canada; a new deposit type. *Exploration and Mining Geology*, 1, 39-62.

Jacobs, L., Emerson, S, Huested, S.S. (1987) – Trace metal geochemistry in the Cariaco Trench. *Deep Sea Research*, 34, 965-981.

Jarvis, I., Gale, A.S., Jenkyns, H.C. and Pearce M.A. (2006) – Secular variation in Late Cretaceous carbon isotopes: a new δ13C carbonate reference curve for the Cenomanian–Campanian (99.6–70.6 Ma). *Geological Magazine*, 143, 561-608.

Jeandel, C., Tachikawa, K., Dehairs, F. (2000) – Biogenic barium in suspended and trapped material as a tracer of export production in the tropical NE Atlantic (EUMELI sites). *Marine Chemistry*, 71, 125.

Jenkyns, H.C. (1980) – Cretaceous anoxic events: From continents to oceans. *Journal of the Geological Society of London*, 137, 171-188.

Jenkyns, H.C. (2003) – Evidence for rapid climate change in the Mesozoic–Palaeogene greenhouse world. *Philosophical Transactions of the Royal Society of London A*, 361, 1885-1916.

Jenkyns, H.C. (2010) – Geochemistry of oceanic anoxic events. *Geochemistry Geophysics Geosystems*, 11, Q03004, doi:10.1029/2009GC002788.

Jenkyns, H.C., Gale, A.S., Corfield, R.M. (1994) – Carbon- and oxygen-isotope stratigraphy of the English Chalk and Italian Scaglia and its palaeoclimatic significance. *Geological Magazine*, 131, 1-34.

Kerr, A.C. (1998) – Oceanic plateau formation: A cause of mass extinction and black shale deposition around the Cenomanian-Turonian boundary. *Journal of the Geological Society, 155*, 619-626.

Koide, M., Hodge, V.F., Tang, J.S., Stallard, M., Goldberg, E.G., Calhoun, J., Bertine, K.K. (1986) – Some comparative marine chemistries of rhenium, gold, silver and molybdenum. *Applied Geochemistry*, 13, 705-714.

Ku, T.-L., Knauss, K.G., Mathieu, G.G. (1977) – Uranium in the open ocean: Concentration and isotopic composition. *Deep Sea Research*, 24, 1005-1017.

Kuypers, N.M.M, Pancost, R.D., Nijenhuis, I.A., Sinnighe Damsté, J.S. (2002) – Enhanced productivity led to increased organic carbon burial in euxinic North Atlantic basin during the late Cenomanian Oceanic Anoxic Event. Paleoceanography, 17, doi: 10.1029/2000PA000569.

Kuypers, M.M.M., van Bruegel, Y., Shouthen, S., Erba, E., Sinnighe Damsté, J.S. (2004) – N2-fixing cyanobacteria supplied nutrient N for Cretaceous oceanic anoxic events. *Geology*, 32, 853-856.

Landing, W.M. and Bruland, K.W. (1980) – Manganese in the North Pacific. *Earth and Planetary Science Letters*, 49, 45-56.

Landing, W.M. and Bruland, K.W. (1987) – The contrasting biogeochem- istry of iron and manganese in the Pacific Ocean. *Geochimica et Cosmochimica Acta*, 51, 29-43.

Larson, R.L. (1991a) – Latest pulse of the Earth: evidence for a mid-Cretaceous superplume. Geology, 19, 547–550.

Larson, R.L. (1991b) – Geological consequences of superplumes. *Geology*, 19, 963–966.

Larson, R.L. and Erba, E. (1999) – Onset of the mid-Cretaceous greenhouse in the Barremian-Aptian: Igneous events and the biological, sedimentary, and geochemical responses. *Paleoceanography*, 14, 663-678.

Lebedel, V., Lezin, C., Andreu, B., Wallez, M.-J., Ettachfini, E.M., Riquier, L. (2013) – Geochemical and palaeoecological record of the Cenomanian–Turonian Anoxic Event in the carbonate platform of the Preafrican Trough, Morocco. *Palaeogeography, Palaeoclimatology, Palaeoecology*, 369, 79-98.

Leckie, R.M., Bralower, T.J., Cashman, R. (2002) – Oceanic anoxic events and plankton evolution: Biotic response to tectonic forcing during the mid-Cretaceous. *Paleoceanography*, 17, 13-29.

Linnert, C., Mutterlose, J, Mortimore, R. (2011) – Calcareous nannofossils from Eastbourne (Southeastern England) and their paleoceanography of the Cenomanian/ Turonian boundary interval. *Palaios*, 26, 298-313.

Luther III, G.W. (1991) – Pyrite synthesis via polysulfide compounds. *Geochimica et Cosmochimica Acta*, 55, 2839-2849.

Neal C.R ., Coffin M.F., Arndt N.T., Ducan R.A., Eldholm O., Erba E., Farnetani C., Fitton J.G., Ingle S.P., Ohkouchi N., Rampino M.R., Reichow M.K., Self S., Tatsumi Y. (2008) – Investigating large igneous province formation and associated plaeoenvironmental events: A White Paper for scientific drilling. *Scientific Drilling*, 6, 4-18.

Normark, W.R., Morton, J.L., Koski, R.A., Clague, D.A., Delaney, J.R. (1987) – Active hydrothermal vents and sulfide deposits on the southern Juan de Fuca Ridge. *Geology*, 11, 158-163.

Owens, J.D., Lyons, T.W., Li, X., MacLeod, K., Gordon, G., Kuypers, M.M.M., Anbar, A., Kuhnt, W., Severmann, S. (2012) – Iron isotope and trace metal records of iron cycling in the proto-North Atlantic during the Cenomanian-Turonian oceanic anoxic event (OAE-2). *Paleoceanography*, doi:10.1029/2012PA002328.

Pedersen, T.F., Shimmield, G.B., Price, N.B. (1992) – Lack of enhanced preservation of organic matter in sediments under the intense oxygen minimum on the Oman Margin. *Geochimica et Cosmochimica Acta*, 56, 545-551.

Pearce, M.A., Jarvis, I., Tocher, B.A. (2009) – The Cenomanian–Turonian boundary event, OAE2 and palaeoenvironmental change in epicontinental seas: New insights from the dinocyst and geochemical records. *Palaeogeography, Palaeoclimatology, Palaeoecology*, 280, 207-234.

Petrizzo, M.R., Huber, B.T., Wilson, P.A. MacLeod, K.G. (2008) Late Albian paleoceanography of the western subtropical North Atlantic. *Paleoceanography*, 23, PA1213, doi:10.1029/2007PA001517.

Piper, D.Z. (1994) – Seawater as the source of minor elements in black shales, phosphorites and other sedimentary rocks. *Chemical Geology*, 114, 95-114.

Piper, D.Z. and Isaacs, C.M. (1995) – Geochemistry of minor elements in the Monterey Formation, CA: Seawater chemistry of deposition. *US Geological Survey Professional Paper* No. 1566, Reston, VA, 41pp.

Piper, D.Z. and Calvert, S.E. (2009) – A marine biogeochemical perspective on black shale deposition. *Earth-Science Reviews*, 95, 63-96.

Prauss, M.L. (2012) – Potential freshwater dinocysts from marine upper Cenomanian to upper Coniacian strata of Tarfaya, northwest Africa: Three new species of *Bosedinia*. *Cretaceous Research*, 37, 246-260.

Rachold, V. and Brumsack, H.-J. (2001) – Inorganic geochemistry of Albian sediments from the Lower Saxony Basin NW Germany: palaeoenvironmental constraints and orbital cycles. *Palaeogeography Palaeoclimatology Palaeoecology*, 174, 121-143.

Rue, E., Smith, G., Cutter, G., Bruland, K. (1997) – The response of trace element redox couples to suboxic conditions in the water column. *Deep Sea Research I*, 44, 113-134.

Ruttenberg, K.C., and Berner, R.A. (1992) – Development of a sequential extraction method for different forms of phosphorous in marine sediments. *Limnology and Oceanography*, 37, 991-1007.

Salvini, G. and Passerini, M.M. (1998) – The radiolarian assemblages of the Bonarelli Horizon in the Umbria-Marche Apennines and Southern Alps, Italy. *Cretaceous Research*, 777-804.

Sarkar, A., Bhattacharya, S.K., Sarin, M.M. (1993) – Geochemical evidence for anoxic deep water in the Arabian Sea during the last glaciation. *Geochmica et Cosmochimica Acta*, 57, 1009-1016.

Sarradin, P.-M., Waeles, M., Bernagout, S., Le Gall, C., Sarrazin, J., Riso, R. (2009) – Speciation of dissolved copper within an active hydrothermal edifice on the Lucky Strike vent field (MAR, 37°N). *Science of the Total Environment*, 407, 869-878.

Schlanger, S.O. and Jenkyns, H.C. (1976) – Cretaceous oceanic anoxic events: causes and consequence. *Geologie en Mijnbouw*, 55, 179-184.

Schlanger, S.O., Arthur, M.A., Jenkyns, H.C., Scholle, P.A. (1987) – The Cenomanian-Turonian oceanic anoxic event, I, Stratigraphy and distribution of organic carbon-rich beds and the marine C excursion. *In:* Brooks, J. and Fleet, A.J. (Eds.), Marine Petroleum Source Rocks, *Geological Society Special Publications*, 26, 371-399, 1987.

Schmitz, B. (1987) – Barium, equatorial high productivity, and the northward wandering of the Indian continent. *Paleoceanography*, 2, 63–78.

Schnetger, B., Brumsack, H.-J., Schale, H., Hinrichs, J., Dittert, L. (2000) – Geochemical characteristics of deep-sea sediments from the Arabian Sea: a high-resolution study. *Deep-Sea Research II*, 47, 2735-2768.

Scholle, P.A. and Arthur, M.A. (1980) – Carbon isotope fluctuations in Cretaceous pelagic limestones: potential stratigraphic and petroleum exploration tools. *AAPG Bulletin*, 64, 67-87.

Schmitz, B. (1978) – The TiO_2/Al_2O_3 ratio in the Cenozoic Bengal Abyssal Fan sediments and its use as a paleostream energy indicator. *Marine Geology*, 76, 195-206.

Schneider, R.R., Price, B., Müller, P.J., Kroon, D. Alexander, I. (1997) – Monsoon related variations in Zaire (Congo) sediment load and influence of fluvial silicate supply to marine

productivity in the east equatorial Atlantic during the last 200,000 years. *Paleoceanography*, 12, 463-481.

Scopelliti, G., Bellanca, A., Coccioni, R., Luciani, V., Neri, R., Baudin, F., Chiari, M., Marcucci, M. (2004) – High-resolution geochemical and biotic records of the Tethyan 'Bonarelli Level' (OAE2, Latest Cenomanian) from the Calabianca–Guidaloca composite section, northwestern Sicily, Italy. *Palaeogeography Palaeoclimatology Palaeoecology*, 208, 293-317.

Scopelliti, G., Bellanca, A., Neri, R., Baudin, F., Coccioni, R. (2006) – Comparative high-resolution chemostratigraphy of the Bonarelli Level from the reference Bottaccione section (Umbria–Marche Apennines) and from an equivalent section in NW Sicily: Consistent and contrasting responses to the OAE2. *Chemical Geology*, 228, 266-285.

Sellwood, B.W. and Valdes, P.J. (2007) – Mesozoic climates. *In:* Williams, M., Haywood, A.M., Gregory, F.J., Schmidt, D.N. (Eds.), *Deep-Time Perspectives on Climate Change: Marrying the Signal from Computer Models and Biological Proxies*, The Micropalaeontological Society, Special Publications, 201-224.

Skelton, P. W., Spicer, R. A., Kelley, S. P., Gilmour, I. (2003) – *The Cretaceous World*, pp.1-360.

Takashima, R., Nishi, H., Huber, B.T., Leckie, R.M. (2006) – Greenhouse world and the Mesozoic ocean. *Oceanography*, 19, 82-92.

Tamagnini, P. (2007) – Calcareous nannofossils as tracers of paleoceanographic changes associated to Oceanic Anoxic Event 2: records from the Tethys and Atlantic Oceans. *Università degli Studi di Milano, PhD thesis*.

Thurow, J., Brumsack, H.-J., Rullkötter, J., Littke, R., Meyers, P. (1992) – The Cenomanian/Turonian Boundary Event in the Indian Ocean – a key to understand the global picture. Synthesis of results from scientific drilling in the Indian Ocean. *American Geophysical Union Geophysical Monograph*, 70, 253-273.

Tiraboschi, D. (2009) – Variazioni quantitative del nannoplancton calcareo durante il Cretacico medio: paleoecologia, paleoceanografia e produzione di carbonato in condizioni di anossia globale ed eccesso di pCO_2. *Università degli Studi di Milano, PhD thesis*.

Tiraboschi, D., Erba, E., Jenkyns, H.C. (2009) – Origin of rhythmic Albian black shales (Piobbico core, central Italy): Calcareous nannofossil quantitative ans statistical analyses and paleoceanographic reconstructions. *Paleoceanography*, 19, doi:10.1029/2008PA001670.

Tribovillard, N., Riboulleau, A., Lyons, T., Baudin, F. (2004) – Enhanced trapping of molybdenum by sulfurized marine organic matter of marine origin in Mesozoic limestones and shales. *Chemical Geology*, 213, 385-401.

Tribovillard, N., Algeo, T.J., Lyons, T., Riboulleau, A. (2006) – Trace metals as paleoredox and paleoproductivity proxies: An update. Chemical Geology, 232, 12-32.

Turgeon, S. and Brumsack, H.-J. (2006) – Anoxic vs dysoxic events reflected in sediment geochemistry during the Cenomanian–Turonian Boundary Event (Cretaceous) in the Umbria–Marche Basin of central Italy. *Chemical Geology*, 234, 321-339.

Voigt, S. (2000) – Cenomanian-Turonian composite d13C curve for Western and Cen- tral Europe: the role of organic and inorganic carbon fluxes. *Palaeogeography Palaeoclimatology Palaeoecology*, 160, 91-104.

von Breymann, M.T., Emeis, K.-C., Suess, E. (1992) – Water depth and diagenetic constraints on the use of barium as a palaeoproductivity indicator. *In:* Summerhayes, C.P., Prell, W.L., Emeis, K.-C. (Eds.), *Upwelling Systems: Evolution Since the Early Miocene*, Geological Society Special Publications, 64, 273-284.

Wagreich, M., Bojar, A.-V., Sachsenhofer, R.F., Neuhuber, S., Egger, H. (2008) – Calcareous nannoplankton, planktonic foraminiferal, and carbonate carbon isotope stratigraphy of the Cenomanian–Turonian boundary section in the Ultrahelvetic Zone (Eastern Alps, Upper Austria). *Cretaceous Research*, 29, 965-975.

Warning, B. and Brumsack, H.-J. (2000) – Trace metal signatures of eastern Mediterranean sapropels. *Palaeogeography Palaeoclimatology Palaeoecology*, 158, 293-309.

Watkins, D.K., Cooper, M.J., Wilson, P.A. (2005) – Calcareous nannoplankton response to late Albian oceanic anoxic event 1d in the western North Atlantic. Paleoceanography, 20, doi:10.1029/2004PA001097.

Weaver, C.E. (1990) – Clays, muds and shales. *Developments in sedimentology*, 44, 819pp.

Wedepohl, K.H. (1971) – Environmental influences on the chemical composition of shales and clays. *In:* Ahrens, L.H., Press, F., Runcorn, S.K., Urey, H.C. (Eds.), *Physics and Chemistry of the Earth*, Pergamon, Oxford, UK, 307-331.

Wedepohl, K.H. (1991) – The composition of the upper Earth's crust and the natural cycles of selected elements. Metals in natural raw materials. Natural resources. *In:* Merian, E. (Ed.), *Metals and their compounds in the natural wnvironment*, VCH, Weinheim, Germany, 3-17.

Weissert, H., Lini, A., Föllmi, K.B., Kuhn, O. (1998) – Correlation of Early Cretaceous carbon isotope stratigraphy and platform drowning events: a possible link? *Palaeogeography, Palaeoclimatology, Palaeoecology*, 137, 189–203.

Weissert, H. (2000) – Global change: Deciphering methane's fingerprint. *Nature*, 406, 356-357.

Wignall, P.B. (2001) – Large igneous provinces and mass extinctions. *Earth Science Reviews*, 53, 1-33.

Willis, K.J. and McElwain, J.C. (2002) – The Evolution of Plants. *Oxford University Press, Oxford, New York, United States*, 1-378.

Wilson, P.A. and Norris, **R.D.** (2001) – Warm tropical ocean surface and global anoxia during the mid-Cretaceous period, *Nature*, 412, 425-429.

Winterer, E.L. and Bosellini, A. (1981) – Subsidence and sedimentation on a Jurassic passive continental margin (Southern Alps, Italy). AAPG Bulletin, 65, 394-421.

Wortmann, U.G., Herrle, J.O., Weissert, H. (2004) – Altered carbon cycling and coupled changes in Early Cretaceous weathering pattern: evidence from integrated Tethyan isotope and sandstone records. *Earth and Planetary Science Letters*, 220, 69–82.

Chapter 8

Astronomical forcing on 'mid-Cretaceous' productivity in the Western Tethys

Abstract

Cyclostratigraphic analysis has been applied to the late Albian – early Turonian time interval investigated in four Tethyan sections from the Umbria-Marche Basin (Furlo, Contessa, Le Brecce and Monte Petrano). The Bonarelli Level at Furlo and Contessa has been analyzed in detail. A probabilistic approach, slightly modified from the method of Malinverno et al. (2010), has been used to estimate the optimal distribution of sedimentation rates throughout the various sections. Calcium carbonate contents are the input data for the cyclostratigraphic analysis. The results, obtained by orbital tuning according to short eccentricity and obliquity components, show that there is an influence of astronomical cyclicities on the considered geological record and consistent sedimentation rate trends. An increase in the average sedimentation rates right after the Mid-Cenomanian Event (MCE) is interpreted as the result of an increase in weathering and/or increased carbonate productivity paralleled by decreased primary productivity. The OAE2 is anticipated by an overall decrease in sedimentation rates culminating in minimum rates in the Bonrelli Level. Cyclostratigraphy of the Bonarelli Level at Furlo and Contessa highlights a duration lower than the supposed 500ky thus suggesting the presence of a hiatus in the Bonarelli Level in both the sections. The influence of eccentricity and obliquity might have played an important role in controlling the latitudinal thermal gradients and indirectly the hydrological cycle. Cyclic variations in precipitation rates and runoff coupled with possible variations in the circulation patterns might have led to alternate fluctuations in nutrients availability, thus determining the cyclic deposition of siliceous-dominated and carbonate-dominated sediments.

Key-words: Bonarelli, Cenomanian, cyclostratigraphy, orbital time scale, Scaglia Bianca, spectral analysis

8.1 Introduction

During the Mesozoic greenhouse world the Earth experienced the warmest conditions of the last 150My (Larson and Erba, 1999; Wignall, 2001). Oceans experienced widespread deposition of organic-rich black shales during oceanic anoxic events (OAEs) (Schlanger and Jenkyns, 1976; Arthur et al., 1990). During late Albian–early Turonian time interval the ocean/atmosphere system was characterized by profound perturbations of the global carbon cycle as evidenced by anomalies in the carbon isotope chemostratigrahy: the OAE1d of latest Albian age (Arthur et al., 1990; Wilson and Norris, 2001), the Mid-Cenomanian Event (Paul et al., 1994) and OAE2 at the Cenomanian–Turonian boundary (Jenkyns, 1980; Arthur et al., 1990). The most spectacular sedimentary expression of the OAE2 is the Bonarelli Level, a bituminous radiolarian-rich interval in the Italian Central-Appennines (Bonarelli, 1891). Geological evidence suggests that starting from the MCE less oxygenated bottom-water conditions protracted until the OAE2 (Coccioni et al., 1995; Friedrich et al., 2009). The sedimentary expression of OAE1d are the Pialli Level (Coccioni and Galeotti, 2003) and the Breistroffer Level (Wilson and Norris, 2001).

It is widely accepted that mid Cretaceous lithologic variations and in particular anoxic and oxic rithmic alternations are controlled by orbital cycles (Herbert and Fischer, 1986; Herbert et al., 1986; Claps and Masetti, 1994; Bellanca et al., 1996; Sageman et al., 1997; Grippo et al., 2004; Mitchell et al., 2008; Lanci et al., 2010; Giorgioni et al., 2012). In this study we present the results of a cyclostratigraphic analysis performed on four sections from the Umbria-Marche Basin in Italy, covering a time period from late Albian to early Turonian. A proxy for the carbonate content variations troughout the sedimentary record, were investigated in order to understand the influence of astronomical forcing on the deposition of the studied sequences.

Several previous cyclostratigraphic studies have been performed on sections belonging to the Umbria-Marche Basin (e.g. Furlo, Contessa and Monte Petrano).

Just focusing on the late Albian to lower Turonian time interval, it must be noticed that there is a general agreement about the existence of an interrelationship between orbital forcing and oceanographic conditions and their influence on the occurrence of the main organic-rich sediments depositional events. Unfortunately, the real influence of astronomic periodicities and processes that determine oceanic anoxia are still so poorly understood, that still theories on this subject are often controversial.

Some authors (Mitchell et al. 2008; Batenburg et al., 2012) proposed maxima in eccentricity as controlling factor for the deposition of the Cenomanian organic-rich sediments at Furlo section. According to this paradigm, eccentricity maxima enhance the seasonal contrast, thus causing both an intensification of the monsoons and a consequent increase in estuarine circulation in the Cretaceous North Atlantic. In particular, Mitchell et al. (2008) hypothesized that a time of low variability caused the ocean system to remain stuck in an anoxic state until the variability increased again, thus bringing to upwelling and exceptional productivity possibly enhanced by additional nutrients supply from volcanic activity (Trabucho Alexandre et al., 2010). According to this view, an event like OAE 2 is an extreme protracted version of the briefer orbitally controlled anoxic episodes. For the studied section they obtained a constant sedimentation rate of about 9.6m/My. Analysing lithological, geophysical and stable isotope data from Furlo section, Bateburg et al. (2012) identified a total of five and a half 405-kyr cycles below the Bonarelli Level, stressing that the timing of black chert deposition, as well as the onset of the oceanic anoxic event itself, is related to eccentricity maxima.

On the contrary, Lanci et al. (2010), studying the rock-magnetic properties at Furlo section, suggested minima in eccentricity as governing the black shales deposition and the onset of the Bonarelli Level as predicted by the anti-monsoonal model of Herbert and Fischer (1986). Their tuning of their data with the 405kyr long cycles suggests for the Scaglia Bianca at Furlo a sedimentation rate of about 9.9m/My.

De Vleeschouwer et al. (2012) performed the spectral analyses of the SiO_2 and Al_2O_3 concentrations through the Bonarelli Level in the Bottaccione section at Gubbio, an outcrop next to the here presented Contessa section, revealing four strong ~21 cm thick cycles. The authors indicated a duration of approximately 410kyr for the Bonarelli Level assuming a sedimentation rate of 2.0m/Myr.

Schwarzacher (1994), studying layer thickness variations at Monte Petrano section and at both Contessa and Bottacione sections, obtained a lenght of 6.6My for the whole Cenomanian thanks to the detection of 100ky short eccentricity cyles and assuming a constant velocity of sedimentation of 10m/My. Schwarzacher pointed out that power spectral analysis is of little use while examining long sequences because the recognition of cycles is difficult because of sedimentation rate changes. Moreover he suggested that a better comprehension of the real orbital influence on sedimentation excluding can be obtained by correlating several distant sections thus better filtering the local factors. These indications are at the base of the approach used in the present study.

8.2 Materials

The Umbria-Marche Basin is at present located in the Central Apennines fold and thrust belt in central-eastern Italy. The pelagic studied sequences deposited in the Western Tethys on the continental crust of the Adria microplate (Channell et al., 1979) (Fig. 8.1).

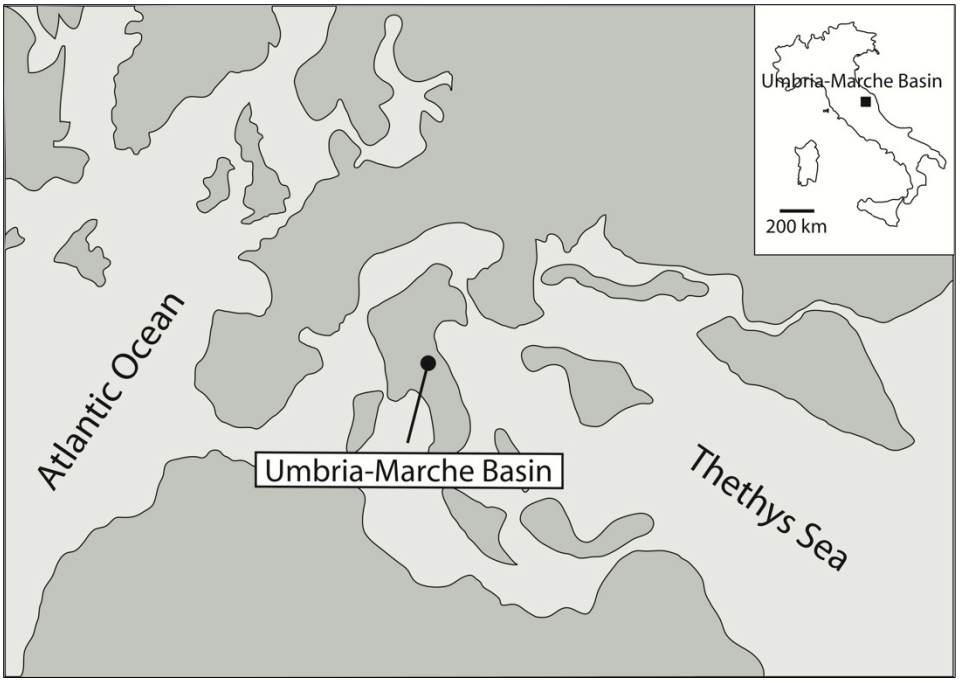

Figure 8.1: *Paleogeographic and present day location of the studied area.*

The so-called Scaglia Bianca Formation, corresponding to the the studied time interval, consists prevalently of alternation of calcareous pelagic sediments resulting from lithification of nannofossil-planktonic foraminiferal oozes (Arthur and Premoli Silva, 1982) and layers rich in siliceous radiolarian tests deposited at water depth of about 1500-2000m (Arthur and Premoli Silva, 1982; Kuhnt, 1990). Below this interval lies the so-called Marne a Fucoidi Formation (Early Aptian – Late Albian) while above there is the Scaglia Rossa Formation (Early Turonian – Middle Eocene) (Parisi, 1989; Coccioni and Galeotti, 2003). Scaglia Bianca has been subdivided by Coccioni et al. (1992, 2003) in four informal members. From base to top has been distinguished: a 'Lower Yellowish-Grey member' (W1) mainly characterized by yellowish-grey limestone with nodules and lenses of greenish-grey chert; a 'Reddish member' (W2) formed by pink to reddish micritic limestones; an 'Upper Yellowish-Grey member' (W3) with yellowish-grey micritic limestones with nodules of greenish-grey chert and a

'Greyish member' (W4) made of light-grey micritic limestones with dark grey to black chert bands and black marlstone/shale layers. About 6-8 meters below the boundary between Scaglia Bianca and Scaglia Rossa Formations the 'Livello Bonarelli' is present. Throughout the basin Beaudoin et al. (1996) identified and correlated the black chert bands within the Scaglia Bianca Formation and in particular he named as 'black marker' the first black chert band slightly below the Livello Bonarelli Montanari (1985).

Four sections have been analyzed:

- the 30m thick Furlo section, (Beaudoin et al 1996; Turgeon and Brumsack, 2006; Mitchell et al, 2008; Turgeon and Craser, 2008; Lanci et al, 2010) is located 25km south-east of Urbino;
- the 29m thick Contessa outcrop (Monechi and Parisi, 1989; Coccioni and Galeotti, 2003; Monaco et al., 2012), located about 2 km from Gubbio in the Vispi active quarry
- the 20m thick section of Le Brecce, close to the Piobbico village;
- the 70.5m thick Monte Petrano section, not far from the Moria village (Schwarzacher, 1994; Giorgioni et al., 2012).

8.3 Methods

Detailed sedimentological logging was oriented to describe every recognizable lithotextural unit, characterized by observable lithological changes. For each section has been produced a cm-scale resolution sedimentological log. Additionally, for the Furlo and Contessa section the Bonarelli Level has been described at mm-scale distinguishing the lithological alternation of bituminous argillites, radiolarian siltstones and black chert layers ('scisti ittiolitici' of Bonarelli, 1891).

Cyclostratigraphic analysis devoted to orbital tuning is commonly applied to continuous profiles of data, e.g. petrophysical logs (Locklair and Sageman, 2008), geochemical logs (Westerhold and Röhl, 2009), layer thickness (Claps and Masetti, 1994), bioturbation density (Erba and Premoli Silva, 1994), etc. Many authors have considered the direct or indirect measurement of carbonate content as relevant and convenient for the identification of astronomical forcing on geologic record (e.g. Weedon et al., 1997; Cleaveland et al., 2002; Locklair and Sageman, 2008).

In this work, the detailed sedimentological logs were used as input dataset for the cyclostratigraphic analysis: with the exception of the Bonarelli Level at Furlo and Contessa, where the log was directly analyzed, they were transformed into profiles of carbonate content that can be considered an indirect

proxy of carbonate primary productivity variation (e.g. Rühlemann et al., 1999; Pattan et al., 2003; Barron et al., 2004).

So, for each section, in order to convert the available high-resolution sedimentological description into carbonate profile, seven macro-classes of lithology were identified and characterized by a range of possible carbonate content. In particular, for limestone the carbon content was assumed to be distributed uniformely between 90% and 97%, for cherty limestone the uniform distribution from 60% to 70%, for marly limestone with a uniform distribution from 60% to 80%. Marl carbonate content was assigned the range 40–60%, while for radiolarian layer and chert bands a uniform distribution between 0% and 2% was chosen. As regards black shales, their carbonate content is quite variable and then it is difficult to identify an adequate range of values for their simulation. For this reason direct measurements of carbonate content of the identified black shales for the Furlo and Monte Petrano sections (Fig. 8.2) were used. Only for the few black shales without direct calcimetry data, values randomly distributed within the range of the measured ones were simulated. Calcimetries were measured using a Dietrich-Frühling gas volumetric method by measuring evolved CO_2 after acidification of the bulk sample with HCl.

An example of a portion of a simulated carbonate content profile is shown in Figure 8.3a.

The cyclostratigraphic analysis here applied is divided into two main steps. The first phase consists in the determination of a proper stepwise constant sedimentation rate model that matches cycles in the sedimentary records with characteristic orbital periodicities. The second step concerns the conversion of the stratigraphic record from the depth domain to the time domain, by means of the estimated sedimentation rate model. This exercise is applied independently to the five available sections, which are then correlated in order to get more insights about the timing and duration of the key geological events under study. In this work the approach to orbital tuning suggested in Malinverno et al., 2010 was adopted: it consists in the application of a semi-automatic probabilistic algorithm for the determination of the optimal distribution of the most likely sedimentation rates, based on a ‘likelihood’ function estimation.

The ingredients to evaluate the likelihood are basically: a set of possible tuning frequencies with their uncertainty; the periodogram of the data, relative to a stratigraphic interval that can be assumed homogeneous from the sedimentation rate point of view (such intervals will be called herein after as blocks); and the estimation of the periodogram of the red noise background associated to the data. For more details, refer to Appendix A.

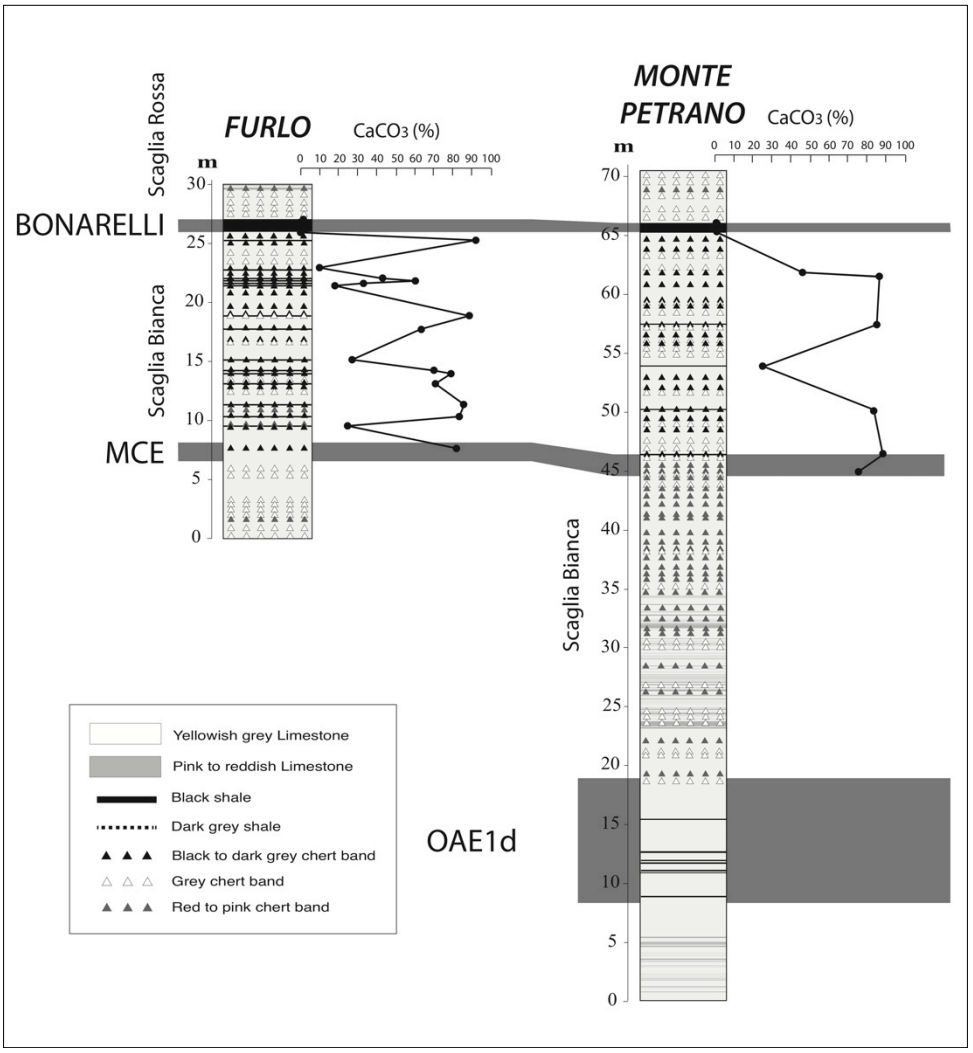

Figure 8.2: *Carbonate content of black shales at Furlo and Monte Petrano.*

The set of possible tuning frequencies with their uncertainty here considered, were evaluated from the orbital solutions of Laskar et al. (2004) in a 10My interval from 100My to 90My. Periodograms of the orbital solutions in 2My windows were used for picking the frequencies of periodogram peaks corresponding to the orbital periods. Then both average peak frequencies and associated standard deviations were computed in the full 10My interval. In Table 8.1 is reported the resulting frequencies and their standard deviations used for tuning.

Orbital cycle	Mean Period (ky)	Mean Frequency (cycles/My)	Standard Deviation (cycles/My)
Long Eccentricity	403.9	2.476	0.050
Short Eccentricity	126.26	7.739	0.047
Short Eccentricity	97.81	10.223	0.075
Obliquity	37.58	26.608	0.082
Precession	22.57	44.305	0.049
Precession	21.39	46.762	0.121
Precession	18.33	54.545	0.094

Table 8.1: Used *tuning frequencies*.

Due to the fact that the carbon content was simulated and not directly measured, in order to refine the periodogram estimation a Montecarlo approach was used. For each section 30 different realizations of the 'calcimetry profile' were generated and the estimation of the "true" periodogram by averaging all the individual realization periodograms was obtained.

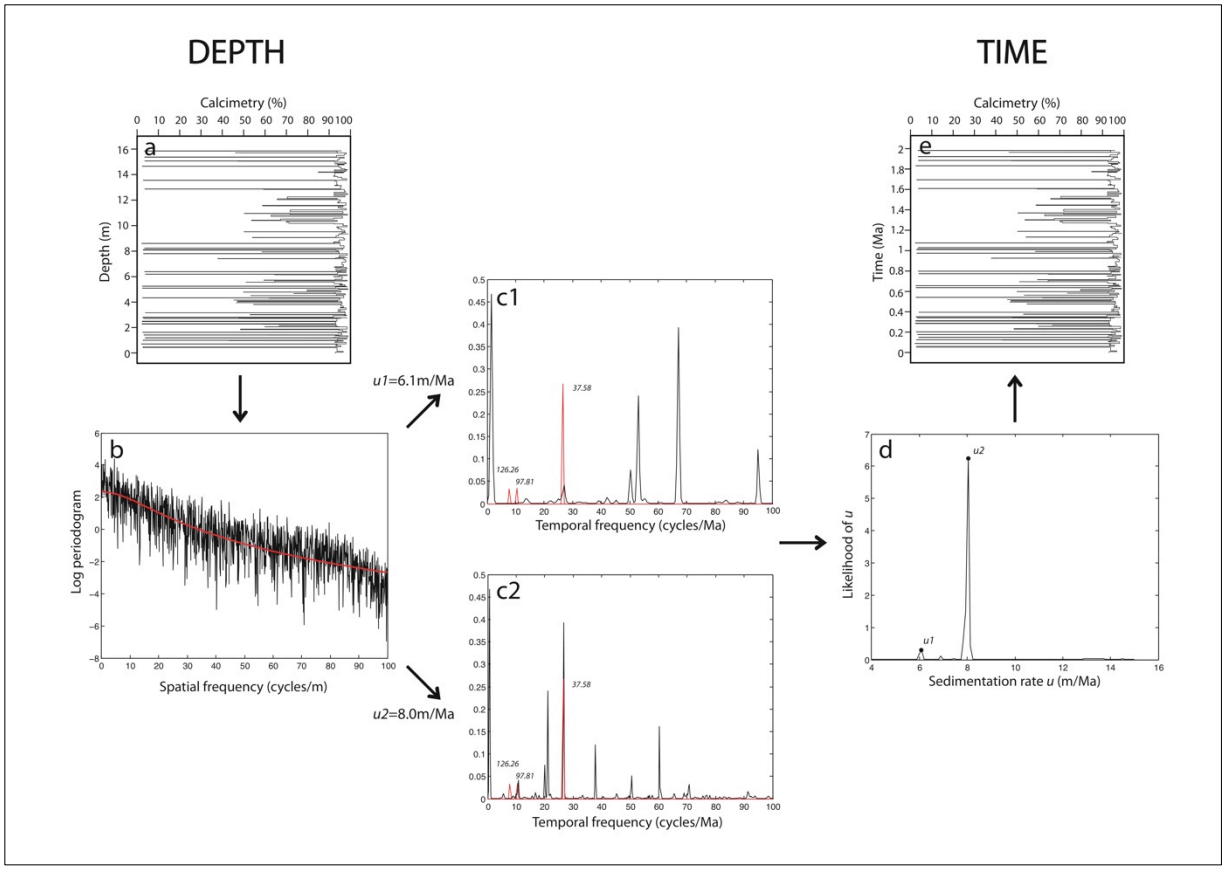

Figure 8.3: *Schematic drawing illustrating the workflow applied for the cyclostratigraphic analyses. In detail: a) input $CaCO_3$ profile; b) log average periodogram of the input data (red line is the fitted red-noise background); c1) and c2) intermediate computation for two different tested sedimentation rate: the more the theoretical orbital frequencies (in red) match the correspondent spectrum (in black) the higher is the likelihood;*

In Fig. 8.3 the used workflow is schematically schetched. For further details about the method, refer to Appendix A.

Regarding the applied methodology, under the hyphotesis that the sedimentation has been continuous (no erosion and no hiatus) (Weedon, 2003), the initial choice of number of blocks and locations of block interfaces has been set according to geological criteria. In particular, the block interfaces have been initially associated to the main lithological changes along the sequence and during the trial and error test phase they have been adjusted in order to optimize the results, as extensively explained in Appendix B.

The common constraints that have been applied to all the sections concerns the set of orbital frequencies for the tuning. Considering the general thickness of the various intervals in the studied sections and according to the average values generally associated to the already studied pelagic sequences in the same basin, the chance of detecting precession periodicities has been considered practically inconsistent. For this reason the two components of short eccentricity and obliquity have been used as tuning frequencies. According to average sedimentation rate described for the same time interval in the Basin, as previously described, it has been chosen to estimate possible sedimentation rates within the range of 4 to 15m/My.

As anticipated before, the Bonarelli Level at Furlo and Contessa was treated according to a different method. In Fig. 8.9, the schematic lithological description of the layer for the two sections is reported. As it can be clearly observed, the Bonarelli level is made of lithological alternations of black chert layers, black shale and radiolarian layers, and is characterized by an average carbonate content almost homogeneous and extremely low. Such poor pattern of variation does not help in highlight the differences among the internal layers. For this reason, in order to stress the distinction between siliceous and poorly siliceous layers, a lithological index was used as input data for the spectral analysis. In particular, such index was defined assigning a value of 0 to both black chert and radiolarian layers, and a value of l to the black shale intervals.

8.4 Results

The results of cyclostratigraphic analysis represent the best solutions after several trial and error runs of the methodology.

The obtained results for each section are summarized in a graphical representation, where plots are organized as follows:

- schematic lithological profile;
- one of the thirty “realizations” of calcimetry;
- spacial frequency;
- obtained sedimentation rates.

The calcimetry profiles have been simulated in order to accurately estimate the power spectrum density of the geological record under study. carbonate content is highly correlated with the lithological description, with high $CaCO_3$ for limestones and very low $CaCO_3$ in cherty intervals. Although calcimetry has been simulated according to uniform distributions, the overall profile still remains “discrete” in character, meaning that it is much more stepwise – like the original lithological description- than continuous and smoothed.

The graphical representation of special frequency is the average periodogram computed on each optimal block expressed in cycles/m. The superimposed red dashed lines are the seven astronomic components of eccentricity, obliquity and precession. They have been rescaled in cycles/m, by considering the optimal sedimentation rate computed for each block, in order to compare them with the proper periodogram. This is the reason why they are lying at different locations for different blocks, although are representing the same astronomical periodicity.

The optimal sedimentation rate for each block (red dashed line) is superimposed to the image of the likelihood. The highest likelihood values correspond to the darkest bars in the image.

In the case of Furlo section (Fig. 8.4) the optimal solution is composed by five blocks without accounting for the Bonarelli Level that has been treated seperately and will be presented later on. The first interface lies at 6.5 m from the base and marks the transition between members W3 and W4 of the Scaglia Bianca. The optimal sedimentation rate is 5.3 m/My. The second block covers an interval from 6.5m and 16.5m and is characterized by an increase of sedimentation rate up to 9.1m/My. The third block ranges from 16.5m and 21.5m with an average sedimentation rate of 6.0m/My. The fourth block starts at 21.5m and terminates at the base of the Bonarelli Level. The estimated sedimentation rate is 4.1m/My. The fifth block corresponds to the portion above the Bonarelli Lavel; the sedimentation rate optimizing the likelihood is 5.3m/My.

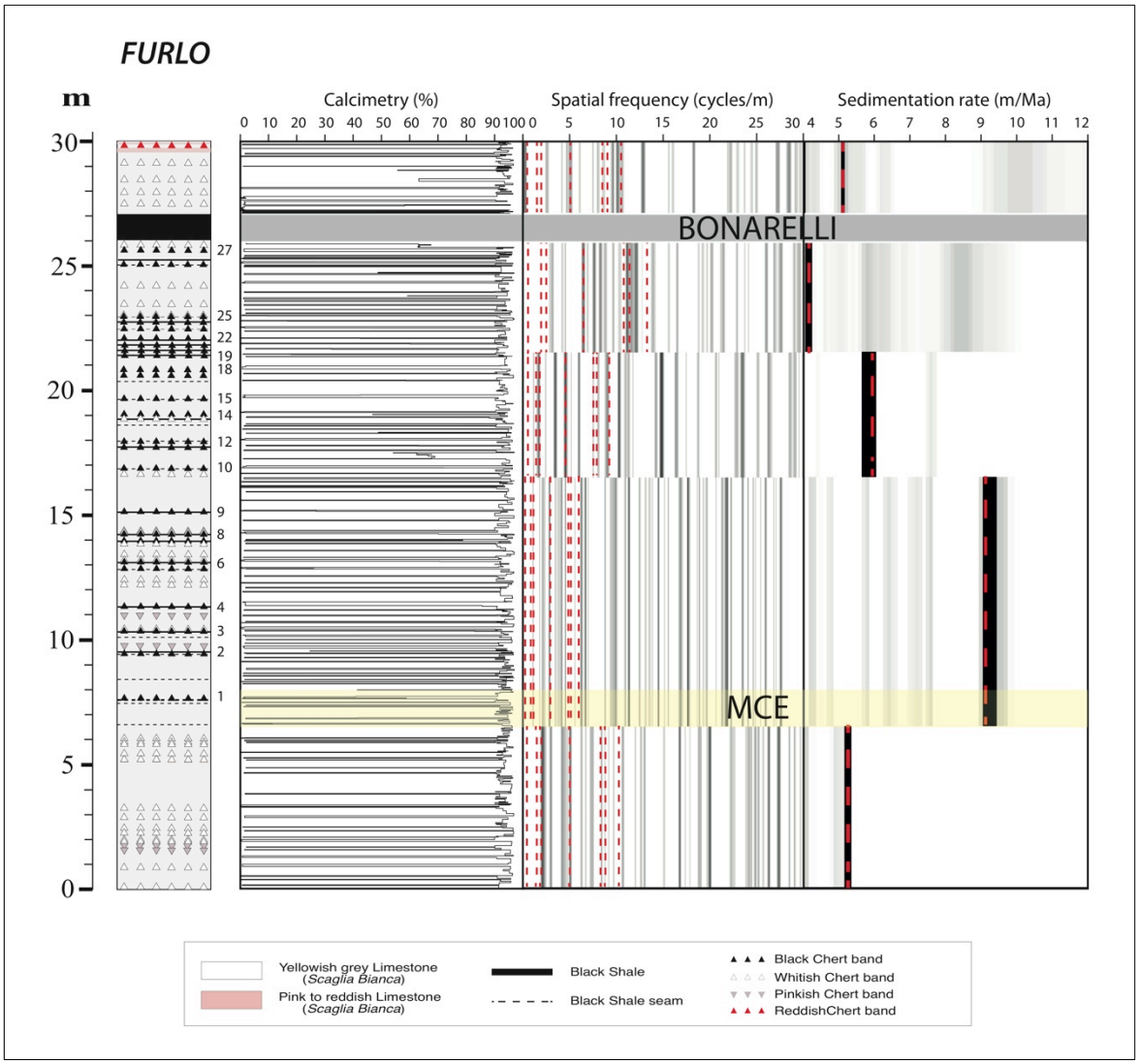

Figure 8.4: *Summary of cyclostratigraphy results on Furlo section. Numbers next to the lithological profile refer to the numeration used by Beaudoin et al. (1996). The Bonarelli Level is highlighted by a gray band, while the MCE position is indicated by a yellow band.*

Lanci et al (2010) used IRM data from the Furlo for cyclostratigraphy, pointing out the occurrence of long eccentricity, about 405ky, among their major peaks of their power spectrum density estimation. They estimated an average value of sedimentation rate for the whole sequence equal to about 9.9m/My. In Fig. 8.5 the power spectrum density of the entire section computed on IRM data of Lanci et al. (2010) (Fig. 8.5a) is compared with power spectrum of the calcimetry profile of the same interval (this study, Fig. 8.5b). The number and the relative intensity of the two power spectra are comparable although they are computed on different datasets. In particular in Lanci et al.'s power spectrum is possible to identify not only the triplette (405ky, 125ky and 98ky) of peaks associated to the 9.9m/My described in their study (and correspondent to the 9.1m/My here estimated), but two additional

triplettes correspondent to two intervals with different sedimentation rates: 6.0m/My and 4.1m/My. These values are in agreement with what was estimated in this study by distinguishing three main blocks. We can conclude that both spectra can be interpreted as the sum of three main spectra associated to three different sedimentation rates.

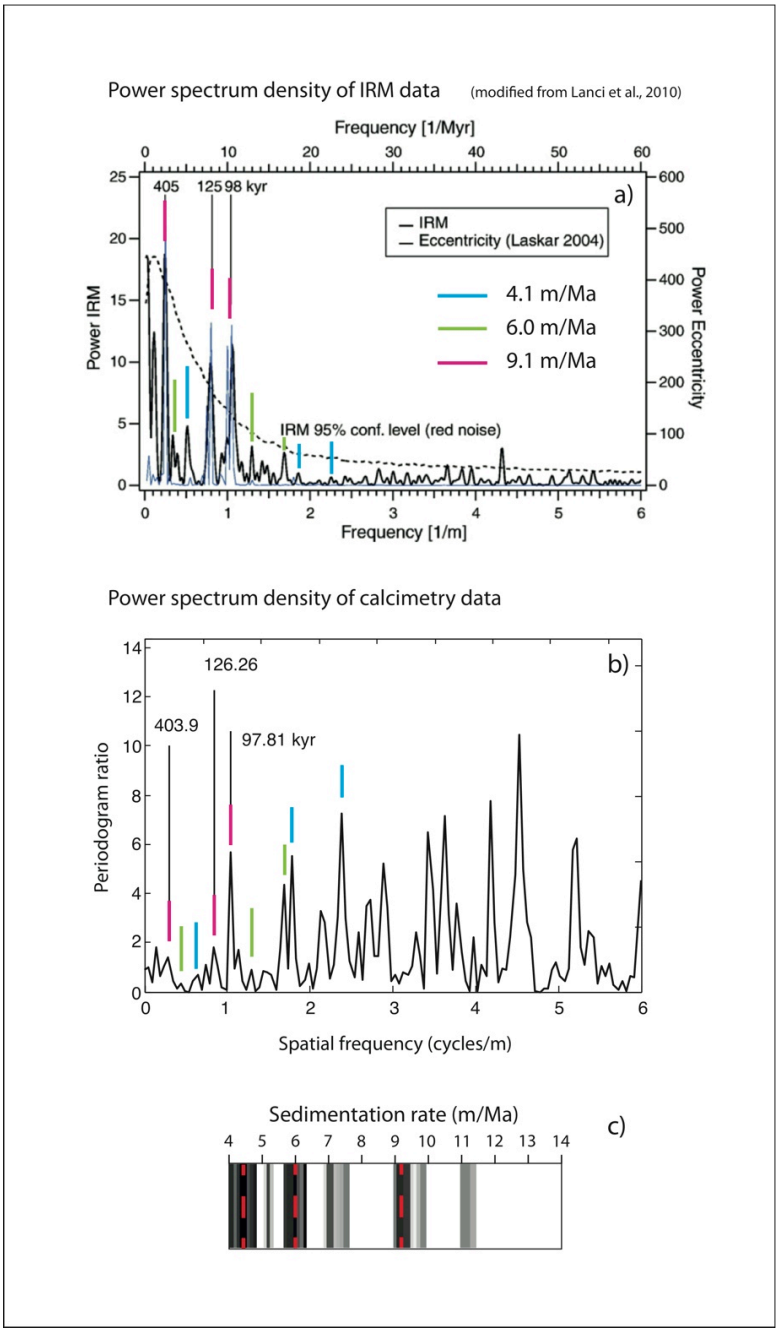

Figure 8.5: *Comparison of Lanci et al. RMI spectrum with $CaCO_3$ spectrum both computed on the entire Furlo sequence. a) IRM spectrum modified after Lanci et al., 2010; b) calcimetry spectrum (this study); c) likelihood of the sedimentation rate distribution obtained from calcimetry data of the entire section.*

The results of cyclostratigraphic analysis of the Contessa section are reported in Fig. 8.6. The geological record has been divided into 3 blocks, excluding the Bonarelli Level. The first block lies from the base of the sequence up to 9.64m with an estimated sedimentation rate of 6.1m/My. The second block, with a very well-defined likelihood peak at 8.7m/My, ranges from 9.64m up to the base of the Bonarelli Level. The third block comprises the portion avove the top of the Bonarelli level. The sedimentation rate is 4.2m/My.

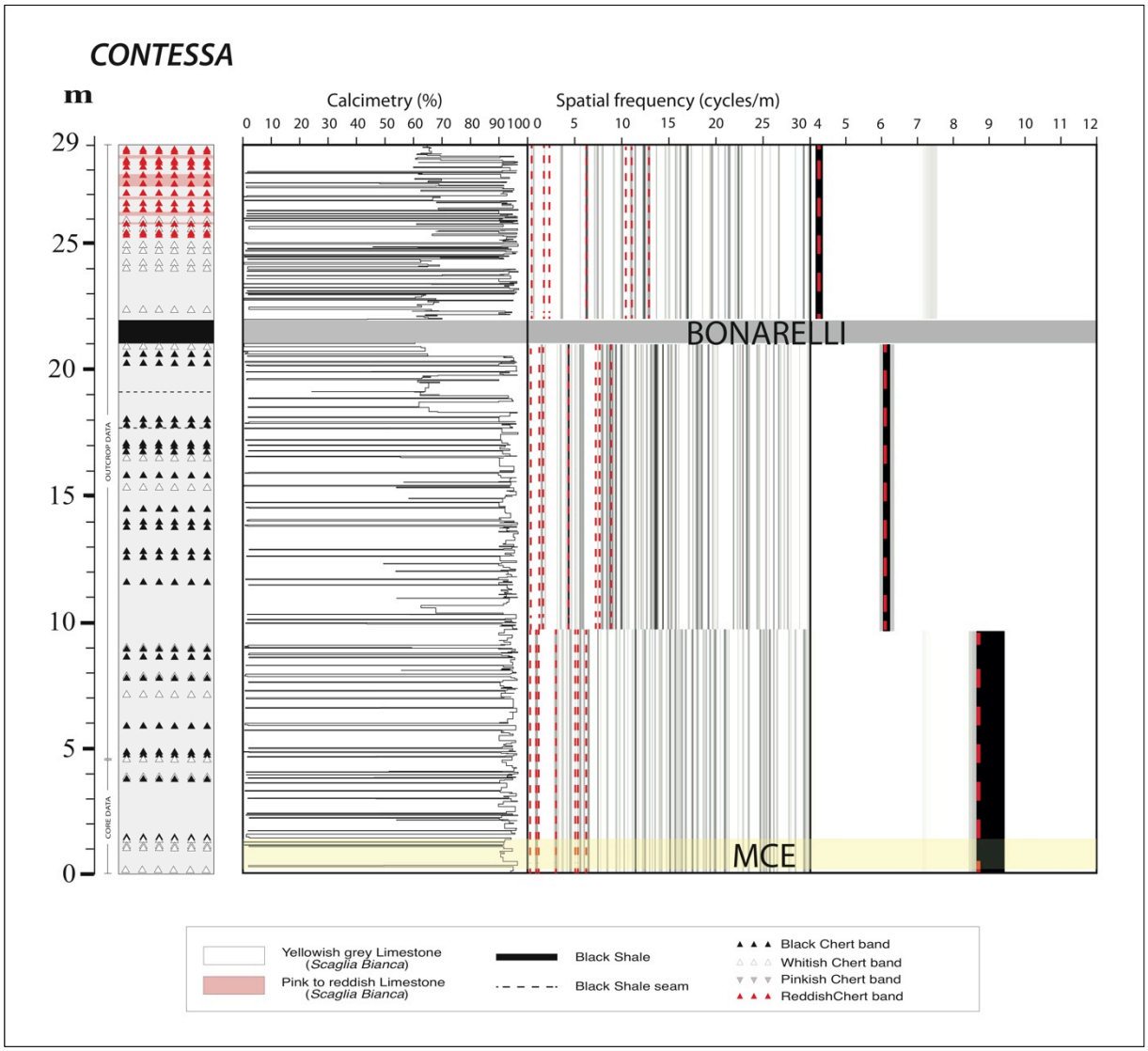

Figure 8.6: *Summary of cyclostratigraphy results for the Contessa section. The Bonarelli Level is highlighted by a gray band, while the MCE position is indicated by a yellow band.*

The interval studied at Monte Petrano is much thicker-longer than at Furlo and Contessa. It starts below the Pialli Level (OAE1d) and extends to the base of the Scaglia Rossa. The section has been divided into 6 blocks, as reported in Figs. 8.7a and b.

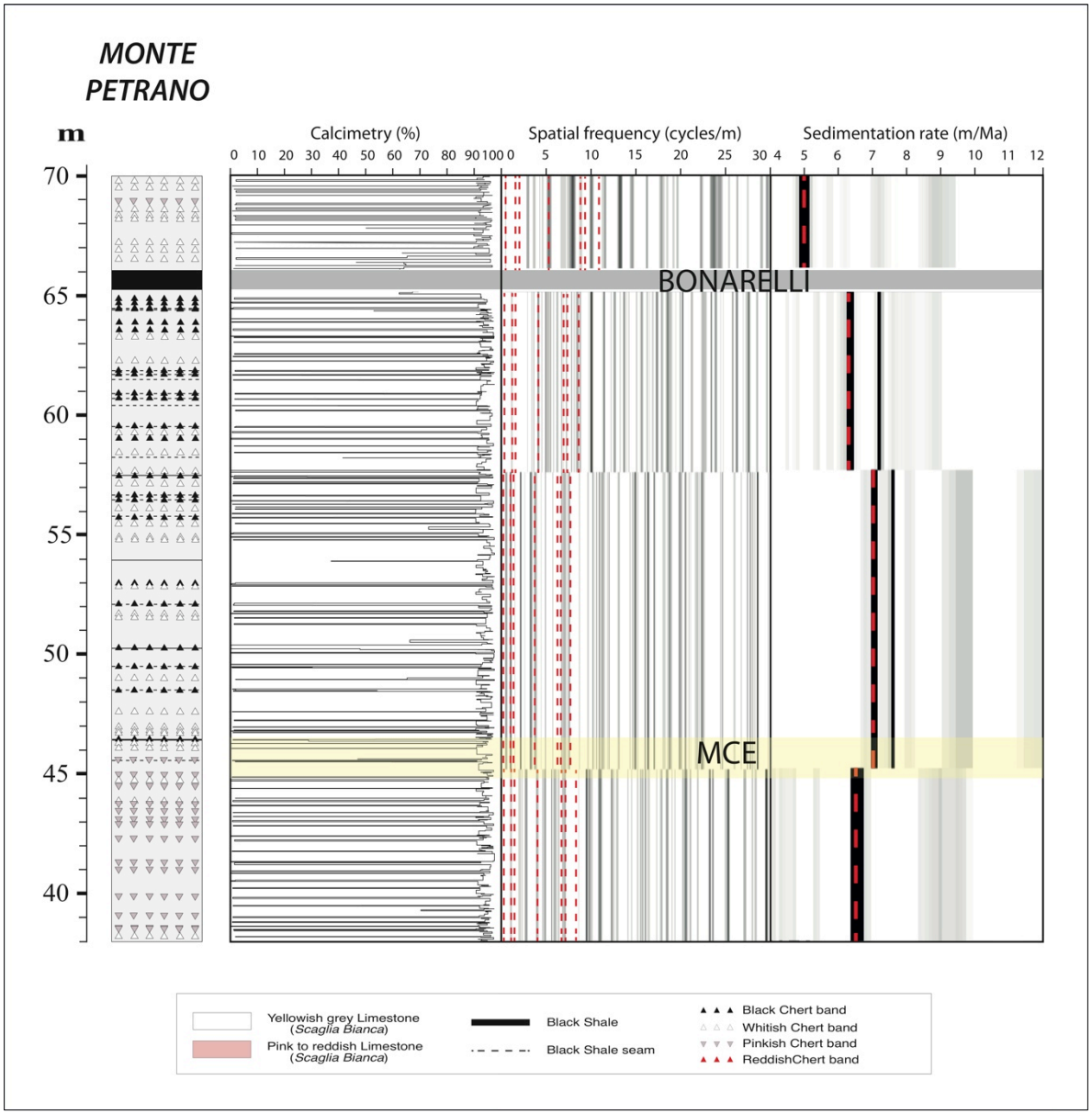

Figure 8.7a: *Summary of cyclostratigraphy results on the upper portion of the Monte Petrano section. The Bonarelli Level is highlighted by a gray band, while the MCE position is indicated by a yellow band.*

The first block includes the first 28m from the base of the section. It shows a well-defined likelihood peak in correspondance of a sedimentation rate of 8.4m/My. An abrupt decrease in sedimentation rate

has been estimated in the following block, which ranges from 28m to 38m. The passage to this block shortly postdates the appearance of red chert bands. The optimal sedimentation rate is 4.8m/My.

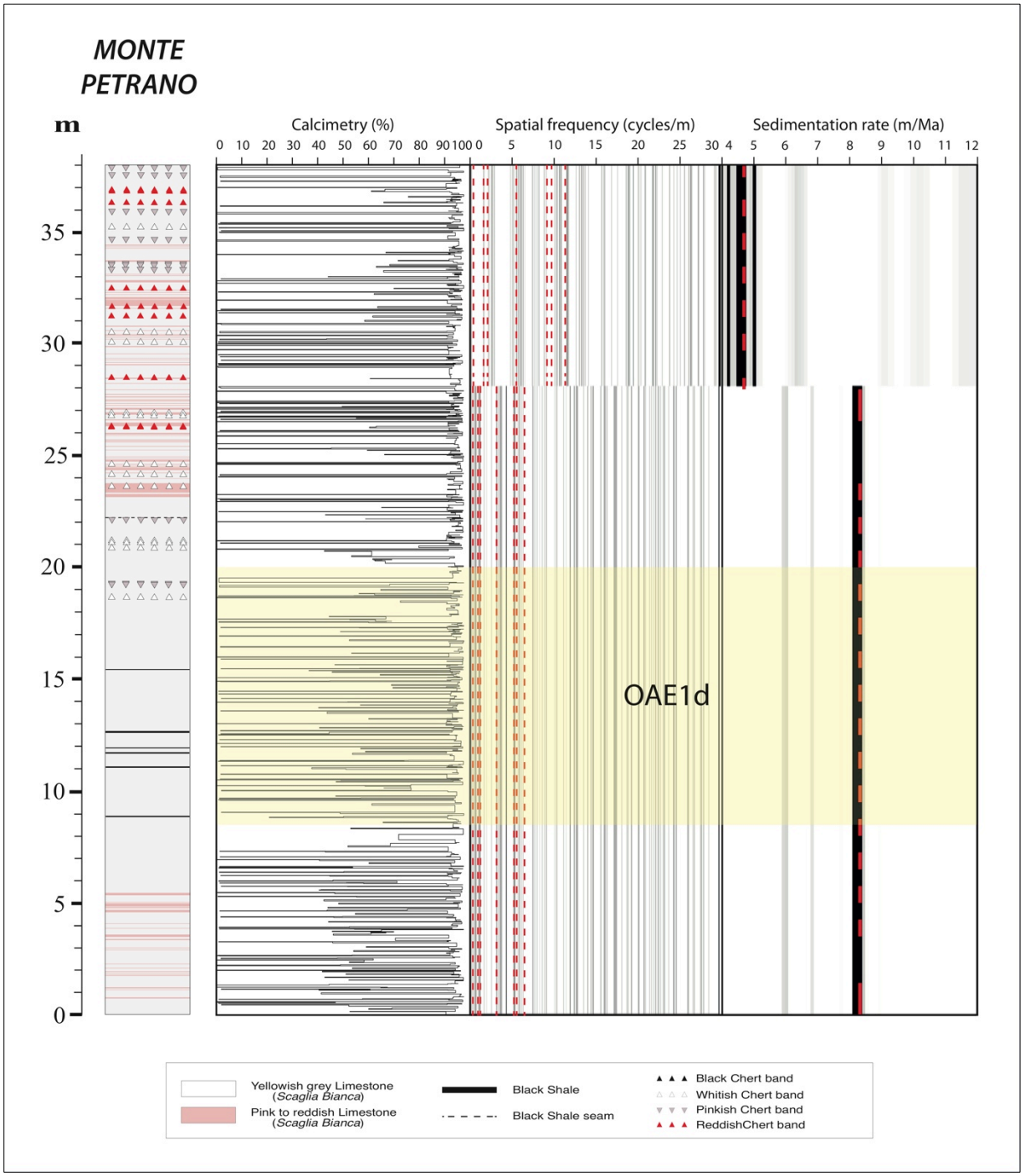

Figure 8.7b: *Summary of cyclostratigraphy results on the lower portion of Monte Petrano section. The OAE1d position is indicated by a yellow band.*

The next two blocks are characterized by an increase of sedimentation velocity, equal respectively to 6.5m/My and 7m/My. The interval from 57.7m up to the base of the Bonarelli Level presents an estimated value of 6.3m/My. The uppermost portion above the Bonarelli Level is chacterized by an estimated sedimentation rate of 5m/My.

Le Brecce section has been analysed for cyclostratigraphic characterization of the OAE1d interval to be compared to the lower part of the Monte Petrano section. The results for Le Brecce section are reported in Fig. 8.8. In this case, the optimal result is obtained by taking into account one single block, with sedimentation rate of 8.3m/My.

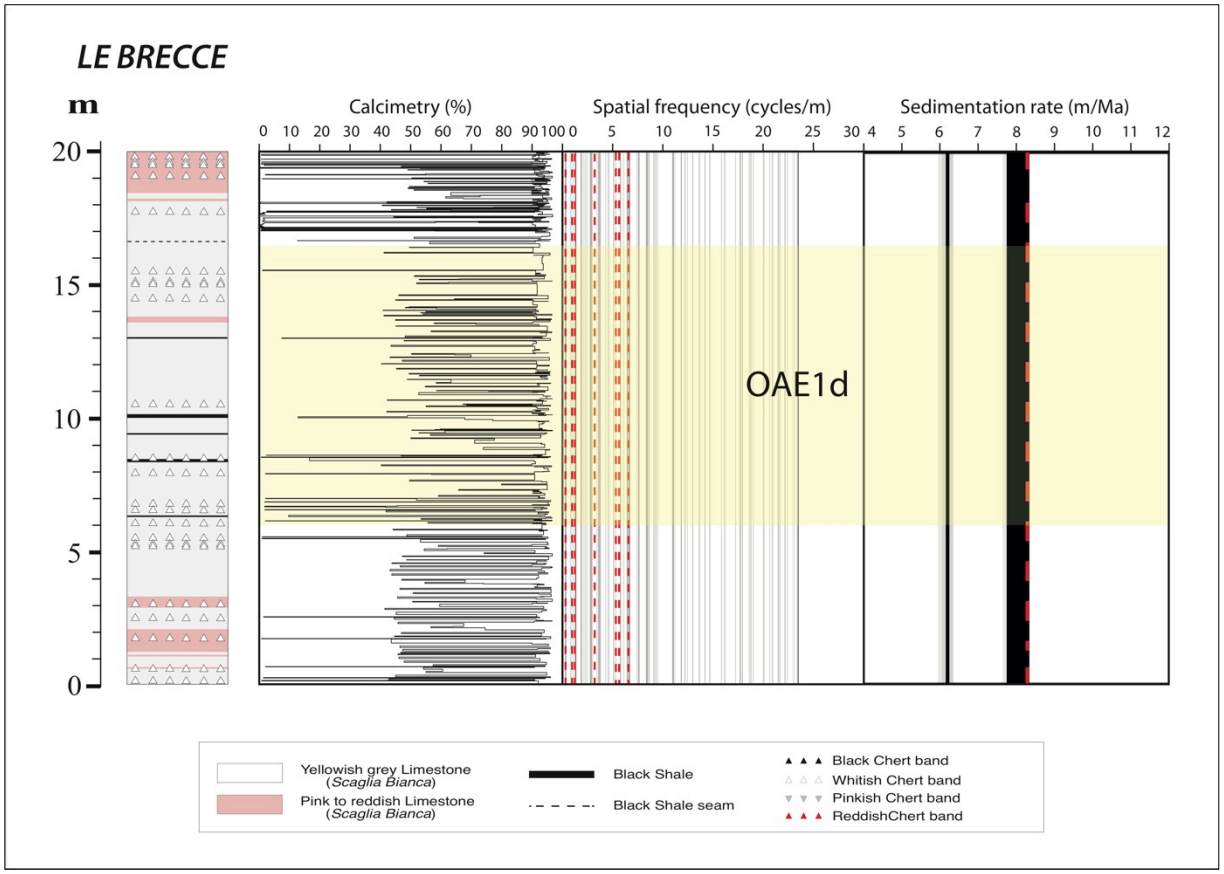

Figure 8.8: *Summary of cyclostratigraphy results on Le Brecce section. The OAE1d position is indicated by a yellow band.*

For the Bonarelli Level at Furlo and Contessa, due to the short record and the limited resolution of the data, it has been chosen to run a different methodology in order to avoid the forcing of the solution. Instead of computing the likelihood for estimating a possible sedimentation rate, the power spectrum density of their lithological index has been directly analysed. The spectra obtained for the two logs are

reported in Fig. 8.9. For the Bonarelli at Furlo the spectrum shows a major peak at 14.62 cycles/m, while at Contessa it is characterized by two peaks of comparable heights, respectively at 15.60 cycles/m and 19.43cycles/m.

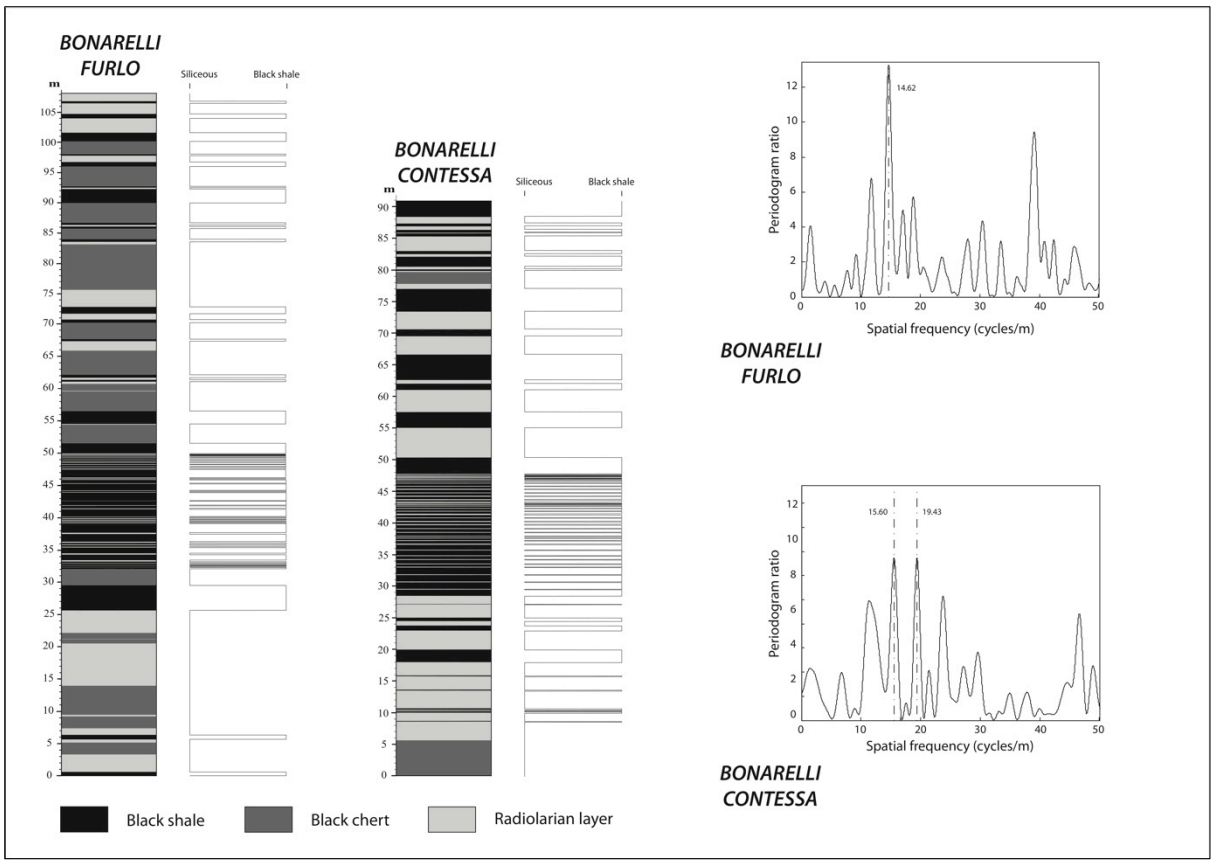

Figure 8.9: *On the left: schematic lithological logs of the Bonarelli Level at Furlo and Contessa each with the correspondent curve used for spectrum estimation. On the right: associated periodograms (dotted lines refer to major peaks).*

8.5 Discussion

The optimal sedimentation rates obtained through cyclostratigraphy are here used to convert depth domain to time domain (Figs. 8.9 and 8.10). It should be stressed that the time conversion has been performed assuming an age of 94My for the base of the Bonarelli Level, based on the age of the Cenomanian/Turonian boundary (93.5 My after Gradstein et al., 2012) and the cyclostratigraphically constrained duration of OAE in the GSSP Pueblo section (~500ky after Sageman et al., 2006).

In Fig. 8.10 a representative calcimetry profile for each studied section is represented in time domain, together with the correspondent ETP profile. The Le Brecce section has been correlated with the Monte Petrano section fixing the position of the former record according to the maximum carbon isotopic excursion of the OAE1d (peak 'b' according to the definition of Kennedy et al., 2004).

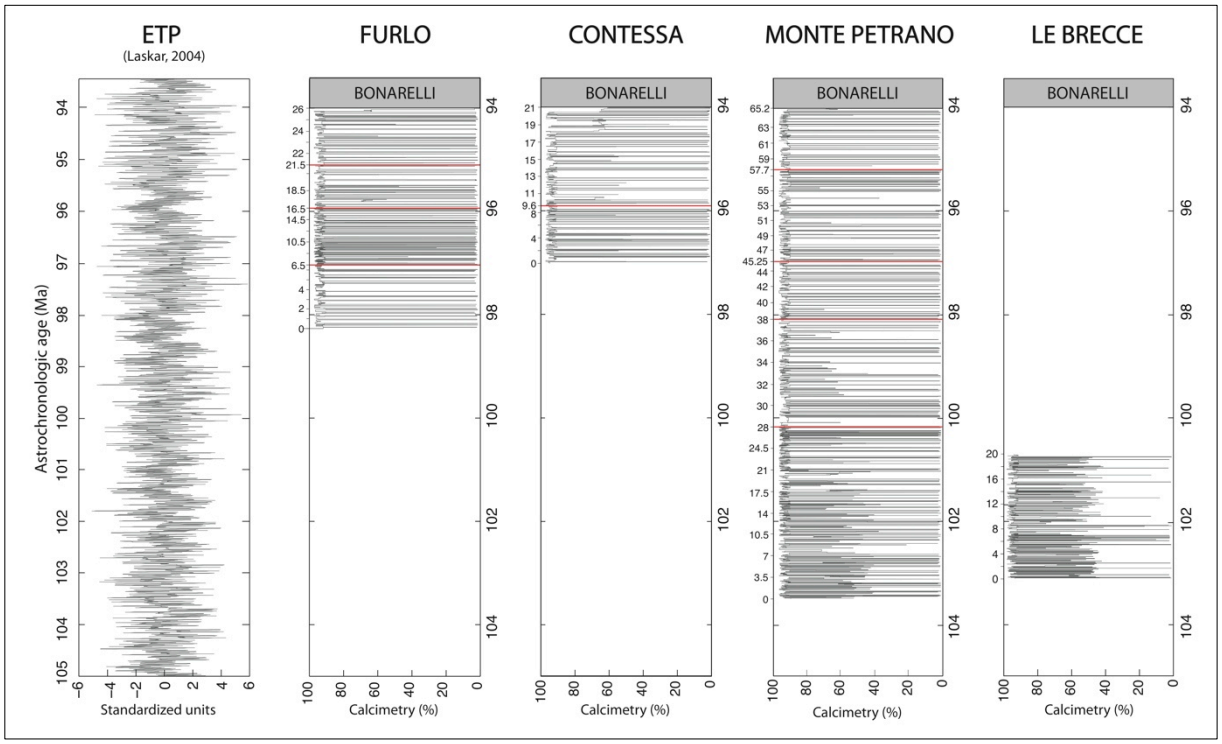

Figure 8.10: *Simulated calcimetry profiles converted in time domain. On the left the ETP curve obtained from Laskar's 2004 solution is reported. For each section, block boundaries in time domain are represented in red.*

In Fig. 8.11 the various sedimentation rates for each section are plotted in time domain: a high consistency is evident In fact the timing of the MCE is consistent in the analysed sectiond, reinforcing the goodness of the obtained results. Moreover, the increasing-decreasing trends of sedimentation rates are reproducible in all studied section. In particular, the sedimentation rates estimated for the OAE1d interval are similar at Monte Petrano and Le Brecce (~8m/My). For the interval between OAE1d and the MCE two blocks were distinguished, with sedimentation rates of ~4.5m/My in the lower reddish portion (Monte Petrano), and values of ~6m/My in the overlying portion (Furlo and Monte Petrano). Above the MCE sedimentation rates show a significant increase, reaching values of ~9m/My at Furlo and Contessa and ~7m/My at Monte Petrano. In all sections, the Bonarelli Level is characterized by suppressed sedimentation rates (about 3m/My). In all sections, sedimenation rates of 5m/My have been estimated for the interval above the Bonarelli Level. (not shown in Fig. 8.11) .

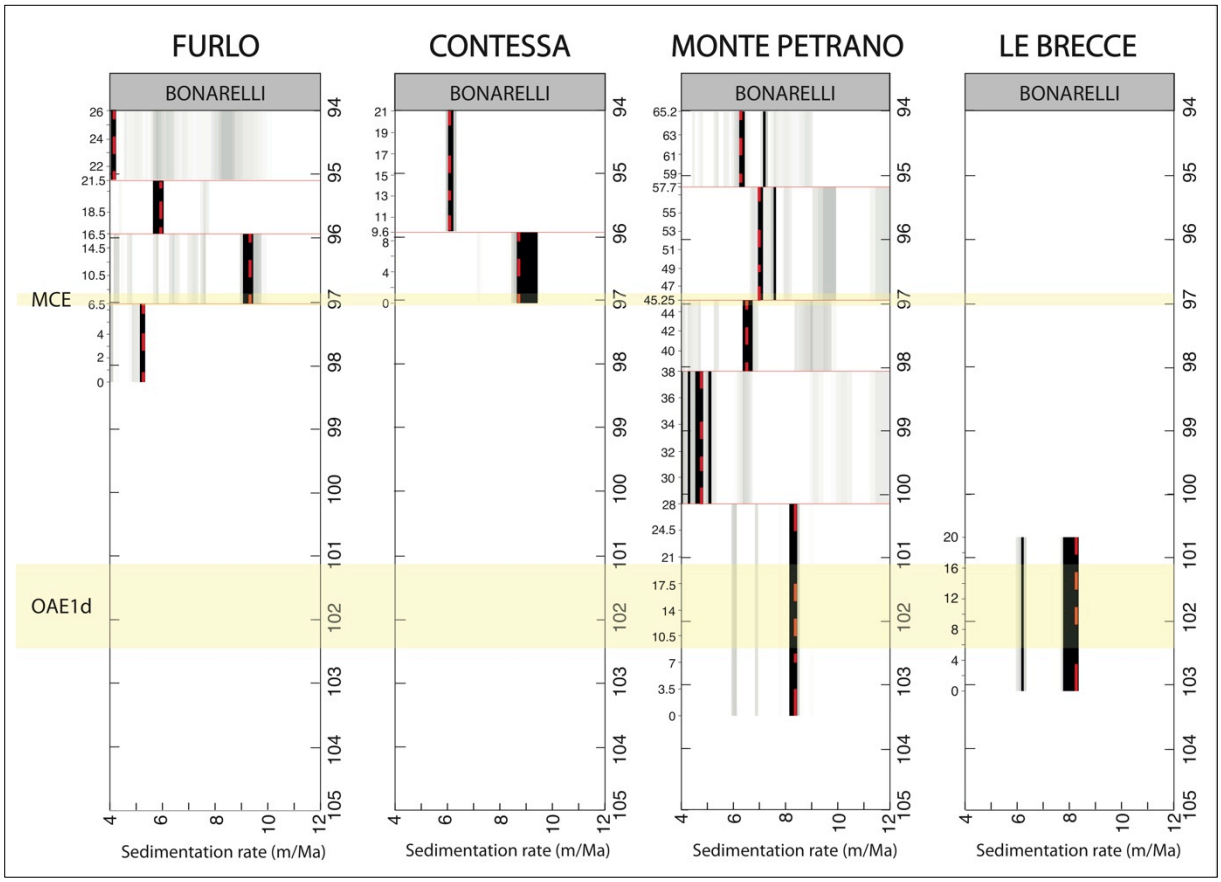

Figure 8.11: *Sedimentation rate best estimates in time domain. The Bonarelli Level is marked by a gray band, while the MCE and the OAE1d positions are indicated by yellow bands.*

In order to explain the common increment in sedimentation rate after the MCE, we can speculate that an increase in weathering or in productivity may have followed this event thus enhancing the average velocity of sedimentation.

According to the sedimentation rate model and supposing an age of 94My for the base of the OAE2, the OAE1d started at about 102.4Ma and lasted for about 1.2My. This result is quite different if compared to the 200-300ky duration obtained by Wilson and Norris (2001). Part of the reason of this difference can be attributed to a different definition of OAE1d and/or the application of a different cyclostratigraphic method.

The estimated age for the MCE is about 97My and its astronomically calibrated duration is of about 200ky.

For the Bonarelli Level, given the high uncertainty of the orbital periodicities to be used, three different scenarios have been tested. Assuming a reasonable duration of OAE2 of about 500ky (Sageman et al., 2006), the long eccentricity component cannot be represented in the Bonarelli Level. Three main

periodicities were tested as representing the various peaks: obliquity (37.58ky), long (22.57ky) and short precession component (18.33ky) (Tab. 8.2). The short eccentricity components were excluded as a possible solution because on one hand the estimated duration would have been extremely too high if compared with the supposed duration of about 500ky described in Sageman et al. (2006) and on the other hand such a frequence would be under-sampled.

For the Bonarelli at Contessa, due to the observed double spikes, both the peaks have been tested separately. Obliquity can be reasonably discarded considering that the duration of the Bonarelli Level in the studied section has to be quite lower than the estimated value supposed by Sageman et al. (2006) as a consequence of the diffused erosion that affects this interval, as described in Chapter 5. Precession seems the only component ascribable to the observed peaks thus indicating a window of values comprised within the long and short precession solution. In particular for the Bonarelli at Furlo a duration of from about 290 to 357ky has been obtained. For the Bonarelli at Contessa a length ranging from 352ky to 434ky for the 19.43 peak and from 283ky to 348ky for the 15.60 peak. Assuming that the Bonarelli Level deposited with similar sedimentation velocities, the solution which guarantees the reciprocal consistency for both the Furlo and Contessa sections, consists in a sedimentation rate of about 3m/My which implies a duration of about 350ky. Such a value is consistent with what has been estimated on the basis of the isotopic record (see Chapter 5). The low velocity of sedimentation can be the result of reduced carbonate deposition during the OAE2.

The common trend in sedimentation rates through the analyzed stratigraphic interval indicates that the general variation cannot be ascribed to local factors but on the contrary to climatically driven processes. The results here presented demonstrate that sedimentation was influenced by astronomical periodicities. In particular carbonate productivity was guided by short eccentricity and obliquity components. Both variations in orbital eccentricity, modulating the amplitude of the precession cycles, and changes in axial tilt influence the relative strength of the seasonal climatic variability. The resulting cyclic variations in precipitation rates and runoff coupled with possible variations in the circulation patterns might have led to alternate variations in nutrients availability, thus determining the cyclic deposition of carbonate-rich sediments and carbonate-poor (black shales, radiolarian layer/chert) sediments.

BONARELLI FURLO				
Thickness	1.082	m	Total cycles on 1,082m	15.81884
Periodogram peak	14.62	cycles/m	Duration	Sedimentation rate
Obliquity	37.58	ky	594.47	1.82
Long precession	22.57	ky	357.03	3.03
Short precession	18.33	ky	289.96	3.73
			Solution	290-357ky

BONARELLI CONTESSA	Peak at 19,43			
Thickness	0.991	m	Total cycles on 0,991m	19.2551
Periodogram peak	19.43	cycles/m	Duration	Sedimentation rate
Obliquity	37.58	ky	723.61	1.37
Long precession	22.57	ky	434.59	2.28
Short precession	18.33	ky	352.95	2.81
			Solution	352-434ky

BONARELLI CONTESSA	Peak at 15,60			
Thickness	0.991	m	Total cycles on 0,991m	15.4596
Periodogram peak	15.60	cycles/m	Duration	Sedimentation rate
Obliquity	37.58	ky	580.97	1.71
Long precession	22.57	ky	348.92	2.84
Short precession	18.33	ky	283.37	3.50
			Solution	283-348ky

Table 8.2: *Estimates of the possible duration of the Bonarelli Level at Furlo and Contessa.*

8.6 Conclusions

The probabilistic approach here applied to cyclostratigraphic characterization provided a very good agreement in the estimated sedimentation rates of the four studied sections. This result demonstrates that the general observed sedimentation patterns are strongly influenced by astronomical cyclicities. Important variations in carbonate primary productivity and/or weathering might have determined an increase in the velocity of sedimentation after the Mid-Cenomanian Event. Moreover, data indicate that the sedimentary conditions before the onset of the OAE2 turned unstable resulting in a progressive decrease of the sedimentation rate. The orbital forcing probably acted on the hydrologic cycle, influencing the latitudinal thermal gradients and the rate of nutrients availability as recorded in the cyclic predominance of carbonate versus siliceous productivity. The estimated average velocity of sedimentation of about 3m/My of the Bonarelli Level at Furlo and Contessa, further document the existence of a hiatus in correspondence of this event.

References

Arthur, M.A., Brumsack, H.-J., Jenkyns, H.C., Schlanger, S.O. (1990) – Stratigraphy, geochemistry, and paleoceanography of organic carbon-rich Cretaceous sequences. *In:* Ginsburg, R., Beaudoin, B. (Eds.), *Cretaceous Resources Events, and Rhythms*, 75-119.

Arthur, M.A. and Premoli Silva, I. (1982) – Development of widespread organic carbon-rich strata in the Mediterranean Tethys. *In:* Schlanger, S.O. and Cita, M.B. (Eds.), *Nature and Origin of Cretaceous Carbon-rich Facies*, 7-54.

Barron, J.A., Bukry, D., Bischoff, J.L. (2004) – High resolution paleoceanography of the Guaymas Basin, Gulf of California, during the past 15 000 years. *Marine Micropaleontology*, 50, 185-207.

Batenburg, S.J., Montanari, A., Sproveri, M., Hilgen, F.J., Coccioni, R., Gale, A.S. (2012) – Astronomical tuning of black cherts in the Cenomanian Scaglia Bianca as precursors of the Bonarelli level (OAE2) at Furlo, Italy. *EGU General Assembly*, Wien, 2691.

Beaudoin, B., M'Ban, E.P., Montanari, A., Pinault, M. (1996) – Lithostratigraphie haute résolution (<20 ka) dans le Cénomanien du bassin d'Ombrie-Marches (Italie). *Comptes Rendus de l'Académie des Sciences Paris*, 323 Series Iia, 689-696.

Bellanca A., Claps, M., Erba, E., Masetti, D., Neri, R., Premoli Silva, I. and Venezia F. (1996) – Orbitally induced limestone/marlstone rhythms in the Albian-Cenomanian Cismon section (Venetian region, northern Italy): sedimentology, calcareous and siliceous plankton distribution, elemental and isotope geochemistry. *Palaeogeography, Palaeoclimatology, Palaeoecology*, 126, 227-260.

Bonarelli, G. (1891) – Il territorio di Gubbio. *Notizie geologiche*, 1-38.

Channell J.E.T., D'Argenio, B., Horvath, F. (1979) – The African Promontory, in Mesozoic Mediterranean Paleogeography. *Earth Science Review*, 15, 213-272.

Claps, M. and Masetti, D. (1994) – Milankovitch periodicities recorded in Cretaceous deep-sea sequences from the Southern Alps (Northern Italy). *In:* de Boer, P.L. and Smith, D.G. (Eds.), *Orbital Forcing and Cyclic Sequences*, Special Publications International Association of Sedimentologists, 19, 99-107.

Cleaveland, L.C., Jensen, J., Goese, S., Bice, D.M., Montanari, A. (2002) – Cyclostratigraphic analysis of pelagic carbonates at Monte dei Corvi (Ancona, Italy) and astronomical correlation of the Serravallian–Tortonian boundary. *Geology*, 30, 931-934.

Coccioni, R., Galeotti, S., Ragni, D. (1992) – Litho- and biostratigraphy of the Scaglia Bianca Formation (Late Albian-Late Cenomanian) in the Umbria-Marche Apennines (Italy). 6th Annual

Meeting of IGCP 262 (Tethyan Cretaceous Correlation) - 'Cretaceous Facies in Orogenic Belts', Athens, 22-26 May, 1992, p. 4.

Coccioni, R., Galeotti, S., Gravili, M. (1995) – Latest Albian–early Turonian deep-water agglutinated foraminifera in the Bottaccione section (Gubbio, Italy) — biostratigraphic and palaeoecologic implications. *Revista Espanola de Paleontologia Homenaje al Dr. Guillermo Colom*, 135–152.

Coccioni, R. and Galeotti, S. (2003) – The mid-Cenomanian Event: prelude to OAE 2. *Palaeogeography, Palaeoclimatology, Palaeoecology*, 190, 427-440.

De Vleeschouwer, D., Montanari, A., Coccioni, R. (2012) – An anchored astronomical time-scale for the Turonian reference sections in the Umbria-Marche Basin, Italy. *EGU General Assembly*, Wien, 6185.

Erba, E. and Premoli Silva, I. (1994) – Orbitally driven cycles in trace-fossil distribution from the Piobbico core (late Albian, central Italy). *In:* de Boer, P.L. and Smith, D.G. (Eds.), *Orbital Forcing and Cyclic Sequences*, Special Publications International Association of Sedimentologists, 19, 211-225.

Friedrich, O., Erbacher, J., Wilson,P.A., Moriya, K., Mutterlose, J. (2009) – Paleoenvironmental changes across the Mid Cenomanian Event in the tropical Atlantic Ocean (Demerara Rise, ODP Leg 207) inferred from benthic foraminiferal assemblages. *Marine Micropaleontology*, 71, 28-40.

Giorgioni, M., Weissert, H., Bernasconi, S.M., Hochuli, P.A., Coccioni, R., Keller, C.E. (2012) – Orbital control on carbon cycle and oceanography in the mid-Cretaceous greenhouse. *Paleoceanography*, 27, PA1204, doi:10.1029/2011PA002163.

Gradstein, F.M., Ogg, J.G., Schmitz, M.D., Ogg, G.M. (2012) – *The Geologic Time Scale 2012*, vol. 2, Elsevier, 1176pp.

Grippo, A., Fischer, A.G., Hinnov, L.A., Herbert, T.D., Premoli Silva, I. (2004) – Cyclostratigraphy and chronology of the Albian stage (Piobbico core, Italy). *In:* D'Argenio, B., Fischer, A.G., Premoli Silva, I., Weissert, H., Ferreri, V. (Eds.), *Cyclostratigraphy: Approaches and Case Histories*, Society for Sedimentary Geology, Special Publication, 81, 57-81.

Herbert, T.D. and Fischer, A.G., (1986) – Milankovitch climatic origin of Mid- Cretaceous black shale rhythms in central Italy. *Nature*, 321, 739-743.

Herbert, T.D., Stallard, R.F., Fischer, A.G. (1986) – Anoxic events, productivity rhythms, and the orbital signature in a Mid-Cretaceous deep-sea sequence from central Italy. *Paleoceanography*, 1, 495-506.

Jenkyns, H.C. (1980) – Cretaceous anoxic events: From continents to oceans. *Journal of the Geological Society of London*, 137, 171-188.

Kennedy, W. J., Gale, A. S., Lees, J. A., Caron, M. (2004) – The Global Boundary Stratotype Section and Point (GSSP) for the base of the Cenomanian Stage, Mont Risou, Hautes-Alpes, France. Episodes, 27/1, 21-32.

Kuhnt, W. (1990) – Agglutinated foraminifera of western Mediterranean Upper Cretaceous pelagic limestones (Umbrian Apennines, Italy, and Betic Cordillera, southern Spain). *Micropaleontology*, 36, 297-330.

Lanci L., Muttoni, G., Erba E. (2010) – Astronomical tuning of the Cenomanian Scaglia Bianca Formation at Furlo, Italy. *Earth and Planetary Science Letters*, 292, 231-237.

Larson, R.L. and Erba, E. (1999) – Onset of the mid-Cretaceous greenhouse in the Barremian-Aptian: Igneous events and the biological, sedimentary, and geochemical responses. *Paleoceanography*, 14, 663-678.

Laskar, J., Robutel, P., Joutel, F., Gastineau, M., Correia, A.C.M., Levrard, B. (2004) – A long-term numerical solution for the insolation quantities of the Earth. *Astronomy and Astrophysics*, 428, 261-285.

Locklair, R.E. and Sageman, B.B. (2008) – Cyclostratigraphy of the Upper Cretaceous Niobrara Formation, Western Interior, U.S.A.: A Coniacian–Santonian orbital timescale. *Earth and Planetary Science Letters*, 269, 540-553.

Malinverno, A., Erba, E., Herbert, T.D. (2010) - Orbital tuning as an inverse problem: Chronology of the early Aptian oceanic anoxic event 1a (Selli Level) in the Cismon APTICORE. *Paleoceanography*, 25, PA2203, doi:10.1029/2009PA001769.

Mitchell, R.N., Bice, D.M., Montanari, A., Cleaveland, L.C., Christianson, K.T., Coccioni, R., Hinnov, L.A. (2008) – Oceanic anoxic cycles? Orbital prelude to the Bonarelli Level (OAE2). *Earth and Planetary Science Letters*, 267, 1-16.

Monaco, P., Rodríguez-Tovar, F.J., Uchman, A. (2012) – Ichnological analysis of lateral environmental heterogeneity within the Bonarelli level (uppermost Cenomanian) in the classical localities near Gubbio, central Appennines, Italy. *Palaios*, 27, 48-54.

Monechi, S. and Parisi, G. (1989) – Da Gubbio a Cantiano. *In:* Cresta, S., Monechi, S., Parisi, G. (Eds.), *Stratigrafia del Mesozoico e Cenozoico nell'area umbro-marchigiana*, *Memorie Descrittive della Carta Geologica* d'Italia, 39, 96-102.

Montanari, A. (1985) – Cenomanian anoxic foreslope inferred from turbiditic cherts in the pelagic basin of the Northern Apennines, Italy. *Geological Society of America*, Abstract with programs., 17, 1-667, USA

Parisi, G. (1989) – Stratigrafia del Cretacico-Paleogene. *In:* Cresta, S., Monechi, S., Parisi, G. (Eds.), *Stratigrafia del Mesozoico e Cenozoico nell'area umbro-marchigiana*, *Memorie Descrittive della Carta Geologica* d'Italia, 39, 23-29.

Pattan, J.N., Masuzawa, T., Naidu, P.D., Parthiban, G., Yamamoto, M. (2003) – Productivity fluctuations in the southeastern Arabian Sea during the last 140 ka. *Palaeogeography, Palaeoclimatology, Palaeoecology*, 193, 575-590.

Paul, C.R.C., Mitchell, S.F., Marshall, J.D., Leary, P.N., Gale, A.S., Duane, A.M. and Ditchfield, P.W. (1994) – Paleoceanographic events in the Middle Cenomanian of Northwest Europe. *Cretaceous Research*, 15, 707-738.

Rühlemann, C., Müller, P.J., Schneider, R.R. (1999) – Organic Carbon and Carbonate as Paleoproductivity Proxies: Examples from High and Low Productivity Areas. *In:* Fisher, G. and Wefer, G. (Eds.), *Use of Proxies in Paleoceanography*, 315-344.

Sageman, B.B., Rich, J., Arthur, M.A., Birchfield, G.E., Dean, W.E. (1997) – Evidence for Milankovitch periodicities in Cenomanian–Turonian lithologic and geochemical cycles, Western Interior U.S.A.. *Journal of Sedimentary Research*, 67, 286-302.

Sageman, B.B., Meyers, S.R., Arthur, M.A. (2006) – Orbital time scale and new C-isotope record for Cenomanian-Turonian boundary stratotype. *Geology*, 34, 125-128.

Schlanger, S.O. and Jenkyns, H.C. (1976) – Cretaceous oceanic anoxic events: causes and consequence. *Geologie en Mijnbouw*, 55, 179-184.

Schwarzacher, W. (1994) – Cyclostratigraphy of the Cenomanian in the Gubbio district, Italy: a field study. *In:* de Boer, P.L. and Smith, D.G. (Eds.), *Orbital Forcing and Cyclic Sequences*, Special Publications International Association of Sedimentologists, 19, 99-107.

Trabucho Alexandre, J., Tuenter, E., Henstra, G.A., Van der Zwan, K.J., Van de Wal R.S.W., Dijkstra, H.A., De Boer, P.L. (2010) – The mid-Cretaceous North Atlantic nutrient trap: Black shales and OAEs. *Paleoceanography*, 25, doi:10.1029/2010PA001925.

Turgeon, S. and Brumsack, H.-J. (2006) – Anoxic vs dysoxic events reflected in sediment geochemistry during the Cenomanian–Turonian Boundary Event (Cretaceous) in the Umbria–Marche Basin of central Italy. *Chemical Geology*, 234, 321-339.

Turgeon, S.C. and Creaser, R.A. (2008) – Cretaceous oceanic anoxic event 2 triggered by a massive magmatic episode. *Nature*, 454, 323-326.

Weedon, G.P. (2003) - *Time-Series Analysis and Cyclostratigraphy: Examining Stratigraphic records of Environmental Cycles*, Cambridge University Press, pp. 1-259.

Weedon, G.P., Shackleton, N.J., Pearson, P.N. (1997) – The Oligocene time scale and cyclostratigraphy f the Ceara Rise, western equatorial Atlantic. *In:* Schackleton, N.J., Curry, W.B.,

Richter, C., Bralower, T.J. (Eds.), *Proceedings of the Ocean Drilling Program, Scientific Results*, 154, 101-114.

Westerhold, T. and Röhl, U. (2009) – High resolution cyclostratigraphy of the early Eocene - new insights into the origin of the Cenozoic cooling trend. *Climate of the Past*, 5, 309-327.

Wignall, P.B. (2001) – Large igneous provinces and mass extinctions. *Earth Science Reviews*, 53, 1-33.

Wilson, P.A. and Norris, **R.D.** (2001) – Warm tropical ocean surface and global anoxia during the mid-Cretaceous period, *Nature*, 412, 425-429.

Chapter 9
Discussion and Conclusions

The alternate phases of paleoceanographic stability and instability that characterized the late Albian–early Turonian time interval in the south-western Tethys represent an incredible laboratory for understanding the Earth System and its delicate equilibria. In particular, the study of the physico-chemical processes that acted on surface waters with those that acted at sea-bottom represents an important step towards a wider comprehension of the different mechanisms of feedbacks that our Planet develops during times of stressed oceanographic regimes.

Pelagic successions of the Umbria-Marche Basin and Belluno Basin were selected to characterize lithology, changes in biogenic and terrigenous components, and sedimentary structures to reconstruct surface conditions and bottom processes and diagenetic modifications. High-resolution chemostratigraphy (C stable isotopes) was calibrated with calcareous plankton biostratigraphy for precise dating and correlations. Anomalies in the $\delta^{13}C$ profiles correspond to OAE1d, MCE and OAE2. The long OAE1d is accompanied by the deposition of 5-6 centimetric black shale layers, corresponding to the so-called Pialli Level, restricted to the lower part of the C isotopic anomaly. The OAE2 instead is associated with organic-rich (TOC more than 20%) and carbonate-lean Bonarelli Level. A double-spiked excursion in the $\delta^{13}C$ corresponds to the MCE that marks the beginning of the W4 member within the Scaglia Bianca formation. Detailed correlations of the $\delta^{13}C$ profiles through the OAE2 interval revealed indicate the presence of a significant hiatus at the top of the Bonarelli Level in all studied sections. Even if the amount of missing sequence slightly differs from site to site, the hiatus affects both the Umbria-Marche and Belluno Basins.

Cyclostratigraphy was used to derive Milankovitch cycles and sedimentation rates. General patterns (increases and decreases) in sedimentation rates were verified in the studied sections, suggesting a common regional control on sediment production during the latest Albian-early Turonian time interval. Specifically type (calcareous versus siliceous) and abundance of biogenic particles and amount of silicoclastic input were affected by bottom current activity and intensity. Orbitally forced climatic fluctuations seem to have determined hydrologic cycles, influencing rates of run-off and nutrients availability. Cyclic increased precipitation and freshwater runoff was effective in producing density stratification of water masses that led to the development of a pycnocline, preventing vertical mixing

and slower rates of deep-water renewal leading to dysaerobic-anaerobic bottom-waters. Proximity of sites to coastlines appears to have determined the abundance of fine-grained terrigenous components and subsequent deposition of black shales. At more distal locations, terrigenous input was less and less abundant and nutrient availability stimulated high productivity of r-opportunist siliceous plankton with sedimentation of radiolarian oozes becoming radiolarian-rich dark grey to black cherts.

For all the studied pelagic sections, sedimentological data have revealed a very dynamic depositional regime with effective bottom currents interacting with settling of mostly biogenic particles (nannofossils and planktonic foraminifers) mixed with variable amounts of very fine grained extrabasinal materials as minor component. While variations in surface-water nutrients availability, salinity, temperature controlled the type and abundance of primary producers and of planktonic communities in general, bottom currents, like a 'wind', reworked pelagic deposits with varying intensity and direction. Extremely high-resolution sedimentological analyses (in the filed and with investigation of thin sections and peels) were central to identify even subtle sedimentary structures resulting from processes at the sea-floor. During the latest Albian-Cenomanian, the pelagic sedimentation in the Umbria-Marche and Belluno Tethyan Basins, occurred primarily along two major suites: the "settling dominated" and the "traction dominated" suite. The interplay between the sea-floor current intensity and the grain-size and type of particles reaching the sea-floor modulated the tractive facies types: from the delicately laminated and poorly-sorted marly-limestone and radiolarian beds, to the extremely winnowed foraminiferal lags, via the pervasively laminated well-sorted limestones, recurrently with current ripples, as well as from the radiolarian layers and black shales to the tractive "bedded black cherts".

Geochemical data indicate that the studied sections deposited at bathial depth in a pelagic setting distant from coast with low terrigenous detrital input and a mostly homogeneous source area through time. The analyzed sediments consist of various mixtures of clay minerals (Al), quartz and biogenic silica (Si) mainly from radiolarian tests, feldspar (Al, Na, K) and carbonates (Ca) mainly from coccoliths and foraminifers. The observed alternation of silica- and calcareous-rich sediments is the result of the competition between two "antagonist" communities primarily controlled by trophic levels: a 'calcareous realm', dominated mainly by coccolithophorids and planktonic foraminifers under oligotrophic to mesotrophic conditions, and by a 'siliceous realm', determined by dominance of r-opportunists such as radiolarians and diatoms under eutrophic. Cyclostratigraphic analysis demonstrated that the continuous switch between these two conditions was influenced by astronomical periodicities, which could have resulted in cyclic changes in climate (temperature and precipitations) and oceanic circulation patterns (stratified of unstable water column).

The well-oxygenated and stable oceanic conditions that characterized the late Albian were interrupted by the Oceanic Anoxic Event 1d (OAE1d), a warm interval with pulses of anoxia-dysoxia and associated deposition of black shale layers. In the Umbria-Marche Basin the lithologic expression of this event, the so-called Pialli Level, doesn't correspond to the whole $\delta^{13}C_{carb}$ excursion, but is limited to its lowermost part. At Cismon, in the same stratigraphic interval, in place of real black shales few dark grey shale layers with relatively higher values of TOC around 2% have been observed. According to the sedimentation rate model defined with the cyclostratigraphic analysis OAE1d started at about 102.4My and lasted for about 1.2My.

During the recovery from this event, climate shifted back to cooler conditions as indicated by $\delta^{18}O_{carb}$ data with the deposition in the Umbria-Marche Basin of reddish limestones and red chart bands with reduced sedimentation rates. Sedimentological evidence of wavy and pervasive plane parallel laminations near the top and above the Pialli Level suggests that a phase of enhanced circulation was associated with the beginning of a relative cooling and the re-establishment of normal oceanographic conditions.

The stable early Cenomanian Tethys Ocean turned unstable during the mid-Cenomanian, at an estimated age of about 97My. Distinctive lithological changes are associated with the double-spiked $\delta^{13}C_{carb}$ positive excursion of about 3‰ of the MCE, with an astronomically calibrated duration of about 200ky. Sedimentation shifted to alternate dysoxic/anoxic and well-oxygenated conditions as represented by the lithologic alternation of black shales and black chert bands with whitish limestones. Geochemical data indicate that the MCE correlates with the onset of metal-rich hydrothermal fluids, thus suggesting that this event probably marked the beginning of increased spreading rate velocities or the emplacement of important volumes of volcanics. It's curious that the $\delta^{13}C_{carb}$ values are characterized by a progressive increase starting from the MCE up to the base of the Oceanic Anoxic Event 2. The release of bio-limiting metals in the oceans and the perturbation of the global carbon cycle changed the system to more unstable conditions, possibly affecting the global hydrologic cycle. Sedimentological and geochemical data suggest that increased rates of precipitation and run-off might have resulted in alternated phases of enhanced stratification of the water column with times of deposition and preservation of organic-rich sediments. The deposition of a black chert or a black shale in this conditions depends on the availability of silica related to nutrients and/or clay particles. The distribution of nutrients and clay particles depends on the shape of the fresh water plume that segregates the clay, with the detrital to nutrients ratio decreasing from the proximal to the distal areas. The r-opportunist organisms (such as radiolaria) are able to use the incresead available nutrients only at a certain distance from the sediment plume with limited water turbidity. For this reason black shale

layers are expected to deposit in the proximal (and eventually confined) settings, while black cherts would be their lateral correspective in the distal locations. The progressive variation in fresh water, nutrients and mud inputs will shift the depositional settings basinwards or landwards. The onset of the anoxic conditions occurred progressively, as testified for example by the alternation of micrite and organic rich laminasets. Also, the recovery from anoxia and the re-establishment of the normal-stratification and/or oxic conditions didn't happen abruptly but, as documented by sediment winnowing, was characterized by intermittent phases of enhanced circulation. Cyclostratigraphic analyses indicate that above the MCE the velocity of sedimentation in the Umbria-Marche Basin significantly increased in all studied sections, probably as the result of enhanced weathering and/or in primary productivity.

In both studied basins the OAE2 was associated to widespread burial of organic matter with the removal of light organic-carbon and the consequent carbon isotope excursion observable both on carbonate- and organic-carbon isotopes. This massive perturbation of the global carbon cycle in all the studied sequences is associated with the presence of black shales, black chert bands and radiolarian layer of the Bonarelli Level, with extremely high TOC concentrations (up to more than 20%). As indicated by the overall decrease of the $\delta^{18}O$ values from the upper Albian to the uppermost Cenomanian, climate progressively shifted towards warmer conditions, with its acme in correspondence of the OAE2 interval. The very low concentration of Mn and Co and the peculiar enrichment in redox-sensitive elements indicate that the deposition of these organic-rich sediments occurred under severe anoxic conditions. The very low carbonate content of the Bonarelli Level tells us that its deposition was probably accompanied by minimum carbonate productivity in favor of dominant siliceous and bacterial organisms during highly eutrophic conditions and a rise of the carbonate compensation depth (CCD). The sedimentation rate drastically reduced to ~3m/My, as suggested by detailed cyclostratigraphic analyses of the Bonarelli Level.

Isotopic $\delta^{18}O$ data indicate that the time interval after the OAE2, represented by the transition from the Bonarelli Level to the reddish limestones and red chert bands of the Scaglia Rossa Formation, was characterized by a maximum warming followed by cooling. Immediately above the Bonarelli Level, beds composed mainly of foraminiferal-intraclastic laminated limestones suggest winnowing of carbonate oozes under the action of intense bottom water currents. A single phase or various different phases of intensified ventilation likely associated with cool thermal conditions must have played an important role in re-establishing normal water masses trophism, oxygenation and stratification. Both $\delta^{13}C_{carb}$ and $\delta^{13}C_{org}$ data and cyclostratigraphic estimate of the duration of the Bonarelli Level indicate that in all the studied sections the topmost part of the OAE2 is affected by a hiatus. Intense sea-bottom

currents might have had important effects on the dynamics of sediment erosion and redistribution resulting in (prolonged) hiatus detected in the Cenomanian/Turonian boundary interval.

The vertical repetitive stacking of the facies belonging to the two opposite depositional suites (settled and tractive) and to the two opposite oxygenation regimes (oxic vs. anoxic) suggests that the environmental resilience of the pelagic system can lead to perturbation recovery, passing through different instability stages, one of which is represented by sea-floor erosion, winnowing and redistribution of sediments by currents. This kind of adaptive behavior can be considered an autocyclic process (the recovery), forced by allocyclic factors (the perturbations).

OAEs provide the opportunity to understand how the Earth System reacts to extreme greenhouse conditions. These events have represented both a physical and a chemical major perturbation and thus only an integrated study of physical, chemical and biological processes can lead to a better comprehension of the mechanisms at the origin of these events. The dramatic environmental conditions connected to these global events might have required impressive feedback processes to re-establish the normal climatic status. The multi-proxy approach used here to decipher the geological record demonstrates that the onset, transition and recovery from anoxia didn't happen instantaneously but was the result of a continuous subtle variation of processes in an extremely dynamic setting. This research opens many intriguing hypotheses that need further investigations.

Appendix A
Materials and methods

All the materials and methods used during the PhD project are here described in detail.

A.1 Field logging and sampling

The sedimentological description of the studied sections has been determined based on texture, composition and structures at a mm-scale thanks to detailed field lithological description, complemented by microfacies analysis on thin sections and peels.

Field work has been extremely time consuming. All the outcrops, avoiding any structural repetition, were first divided in intervals of 1m each. Every single layer has been numbered and described using a lens (10X and 20X magnification), distinguishing any - even subtle - sedimentological variation.

Sedimentological logging was oriented to describe every recognizable litho-textural unit, characterized by observable lithological changes (either gradual or abrupt) that I shall define from here and onwards "layers". As a matter of fact, in this kind of successions, "layering" is mostly a diagenetic feature, due to both enhancing of compositional/textural changes, and to segregation of clay, carbonate and silica minerals along newly formed interfaces. However, many of the described sedimentary intervals show an array of macro- and microscopic features that permit to recognize the individual events of deposition (such as erosion contacts, grain sorting, packing and orientation of particles, traction and traction plus fall-out structures and so on). For all of these cases I shall adopt the term of "beds". It is apparent that "layering" is the most easily observed feature during field-work, and that bedding in some cases can be identified only after additional microfacies analysis.

Due to subtle sedimentary structures in pelagic sediments, the investigated sections have been subjected to many runs of field analyses intergrated by microfacies studies, to obtain a comprehensive characterization at the two scales of observations.

All the studied outcrops have been intensively sampled. Many thousands of oriented samples have been collected for microfacies analyses on thin section and acetate unstained rock peels. Many

hundreds of oriented samples have been also collected for biostratigraphic analyses (e.g. Russo PhD thesis 2013) with a regular spaced sampling rate of 0.5m. The Monte Petrano and Cismon outcrops have been densely sampled for the geochemical analyses with a regular spaced sampling rate of 25cm and of 10cm in the intervals of particular interest.

A.2 Thin sections

Rock chips of the selected samples were cut in a cube shape of 1-2cm in length using a steel saw blade with diamonds fixed on its edge. When the studied material was too fragile, the sample was permeated at about 70-80°C with a bi-component epoxy resin made of Araldite D and catalyzer HY951 in a ratio of 10:2. The obtained rock chip was then preliminary polished using a lapidary mill with water and 400-grit silicon carbide (SiC) as abrasive and then with a 1000-grit silicon carbide. Thin sections (Graham, 1963) were prepared mounting the polished surface of the rock chip on a previously cleaned petrographic slide 28 x 47 mm wide and 1-1.2 mm thick. The used glue consists of Araldite and HV953U catalyzer in a ratio of 1:1. After cementing, the samples were ground to desired thickness (generally 30µm for components, up to about 10µm in case of very fine grain material or matrix) using a Logitech LP 30 polisher (Fig. A.1) for a time ranging from 15 up to 30 minutes. The resulting rock surface was finally polished with a 1000-grit silicon carbide.

A.3 Acetate unstained rock peels

Rock peeling (McCrone, 1963; Germann, 1965; Davies and Till, 1968; Gutteridge, 1985; Abineri, 1986a,b, 1989; Wilson and Palmer, 1989) consists in the removal of a thin layer of rock material. A polished rock surface was obtained from a slabbed rock sample using a lapidary mill with water and 400-grit silicon carbide (SiC) as abrasive. Rock surface was acidified using a 15% hydrochloric acid solution for a period of about 10-15 seconds and then rinsed with distilled water. After few hours acetone was applied on the etched surface immediately followed by the application of a cellulose acetate sheet over the etched surface. After few hours the acetate was gently removed obtaining a negative of the studied surface. The bigger advantages of this technique compared to thin-sectioning is the easily and rapidly production of big amounts of thin negatives observable at the microscope. Moreover, the size of the investigated surface can be much greater than any conventional thin section, covering a wide surface of the sample (Fig. A.2).

Figure A.1: Logitech LP 30 polisher.

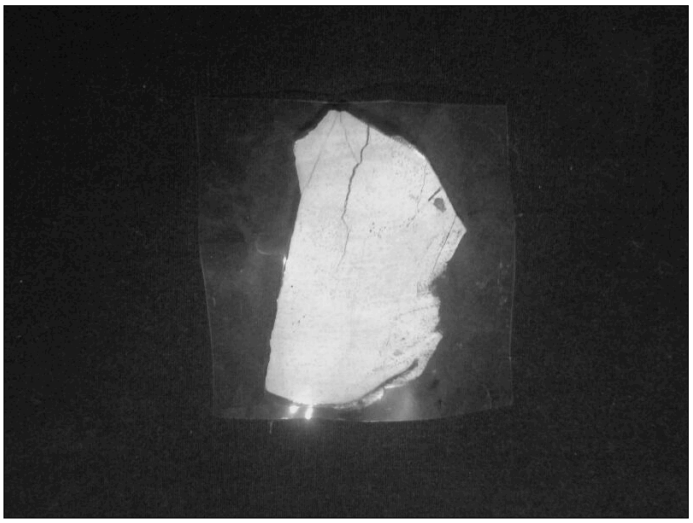

Figure A.2: Example of an acetate unstained rock peel.

A.4 Calcimetry

Many samples have been analyzed for the determination of their carbonate content. In particular 17 samples from the Furlo section, 19 from the Monte Petrano section and 88 from the Cismon section

have been measured. The indirect measure of the carbonate content of a sample was made using the Dietrich-Frühling gas volumetric method by measuring evolved CO_2 after acidification of the bulk sample with HCl. The calcimeter is made of the following parts: a sample container A, a graded glass column B with a valve C on top filled with ethanol or stained distilled water and a connected smaller container D (Fig. A.3).

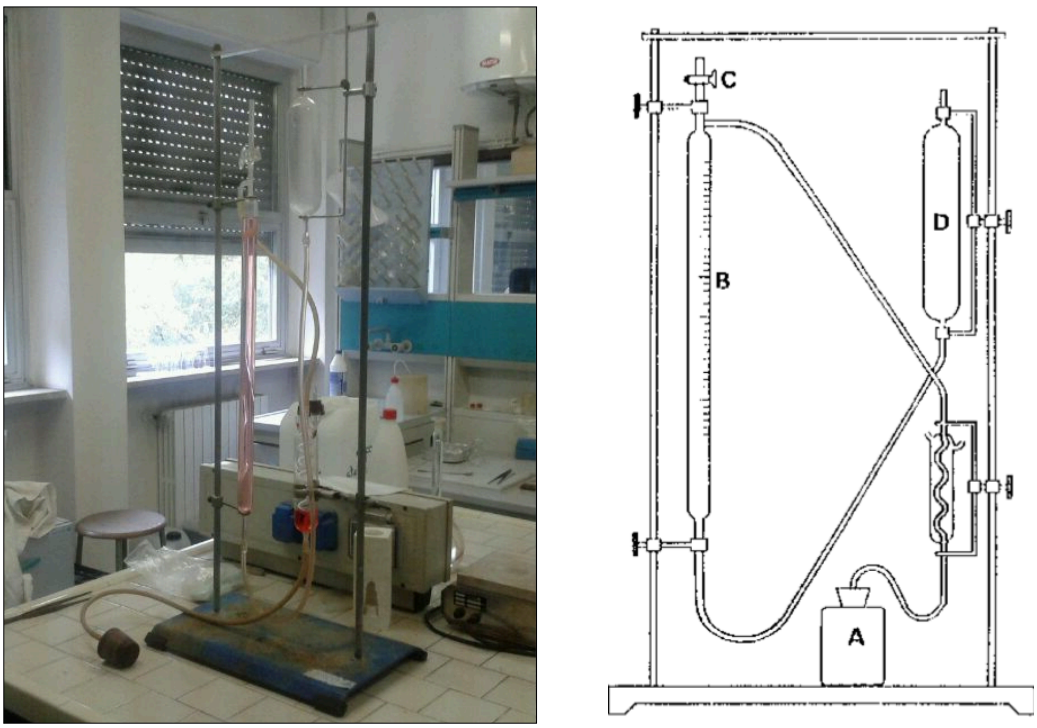

Figure A.3: Dietrich-Frühling calcimeter.

Few grams of sample powder (from 0.5 up to 3 grams in case of a carbonate rock) are inserted in the container A together with a separate vial with 10ml of 50% chloridric acid. The container A is then closed and connected with the calcimeter. The inside pressure of the calcimeter column is equalized to the outside pressure opening the C valve. When the C valve is closed the experiment starts simply flipping the container A thus putting in contact the sample powder with the acid. The resulting CO_2 developed in the reaction acts a pressure on top of the column B lowering its fluid level. Once the reaction is completed the internal pressure is re-equilibrated with the external one, moving the height of the column D until the fluid contained in the B and D columns reach the same level. Once reached the equilibrium the gas-volumetric value can be read on the B column scale.

The analysis is run on a blank sample of both known weight and carbonate content and on the sample to be measured. The carbonate content of the sample is calculated with the following formula:

sample carbonate content (%) = (weight $_{blank}$ x $CO_{2\ sample}$)/(weight $_{sample}$ x $CO_{2\ blank}$) x 100

A.5 Oxygen and carbon stable isotopes (carbonates)

Samples of fine-grained carbonates were analysed isotopically for $\delta^{13}C$ and $\delta^{18}O$ using a VG Isogas Prism II mass spectrometer with an on-line VG Isocarb common acid bath preparation system (Fig. A.4). Samples were dosed with acetone ($(CH_3)_2CO$) and dried at 60°C for at least 30 minutes. In the instrument they are reacted with purified phosphoric acid (H_3PO_4) at 90°C.

Calibration to PDB standard via NBS-19 was made daily using the Oxford in-house (NOCZ) Carrara marble standard. Reproducibility of replicated standards is usually better than 0.1‰ for $\delta^{13}C$ and $\delta^{18}O$. Potential memory effects using the VG Isocarb common acid-bath system can be of the order of 1‰. Adjacent samples of widely dissimilar isotopic composition were reanalysed, or run with blanks between.

A total of 679 samples have been measured, and specifically 380 samples and 299 samples for the Monte Petrano and Cismon section, respectively.

Stable isotope ratios

These are reported using the conventional δ notation to indicate deviation (in parts per thousand, usually known as per mill, with symbol ‰) from the arbitrary PDB (Pee Dee Formation, Belemnite) standard.

$$\delta X = \left[\frac{Rx_{(sample)} - Rx_{(standard)}}{Rx_{(standard)}} \right] \times 1000 \quad = \quad \left[\frac{Rx_{(sample)}}{Rx_{(standard)}} - 1 \right] \times 1000 \quad (‰)$$

where Rx = ($^{13}C/^{12}C$), ($^{18}O/^{16}O$), etc.
So:

$$\delta^{18}O = \left[\frac{^{18}O/^{16}O_{(sample)}}{^{18}O/^{16}O_{(standard)}} - 1 \right] \times 1000 \quad (‰)$$

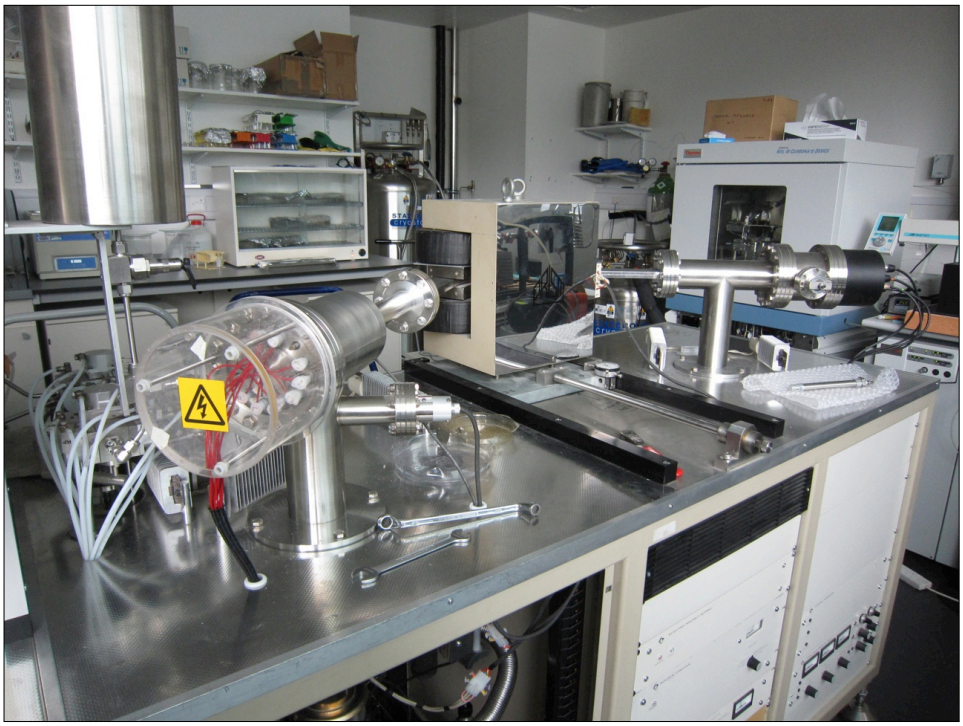

Figure A.4: VG Isogas Prism II mass spectrometer.

A.6 Organic carbon stable isotopes

Organic carbon stable isotopes have been measured on a total of 42 samples, 19 of which coming from the Monte Petrano section and the remaining ones from the Cismon section. Samples were crushed with an agate mortar and pestle to <125 μm. Carbonate was removed by treating 1-2g of sample with 30ml 1% HCl, and heating on a hot plate for about 2h. This phase was repeated many times, replacing the exhausted acid with new one until the colour of the reacted solution was pale yellow (Fig. A.5). The acid-treated sample was then transferred to a centrifuge tube, and washed with Milli-Q water and centrifuged. The sample was further washed in order to reach a neutral pH, then dried in an oven at about 60°C for minimum 24h. Few grams of treated sample (from about 5 up to 10mg according to the amount of organic carbon content) were put into a tin capsule. Stable carbon-isotope composition and C/N ratio were measured with a CF-IRMS system (Fig. A.6), which is composed by a combustion elemental analyzer (e.g. a Carlo-Erba NA 2000) coupled to a gas source isotope ratio mass spectrometer (Sercon GSL). Samples were combusted and converted to N_2 and CO_2 which are separated in a GC column packed with CarbosieveTM (Supelco G60/80 mesh; Bellefonte, Pennsylvania, USA) packing medium, while water was removed thanks to a chemical trap. Helium is used as carrier gas with a stream of 100 mL/min. Together with the set of samples Alanine was used as

internal standard. Sample isotopic ratios are reported as delta per mil relative to the VPDB and AIR international standards for carbon and nitrogen respectively (Coplen 1994).

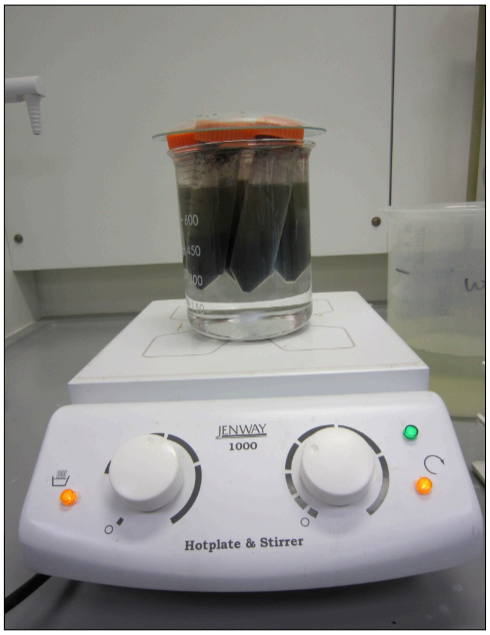

Figure A.5: HCl treated samples on a hot plate.

Figure A.6: CF-IRMS.

A.7 Rock-Eval/TOC Pyrolysis

Rock-Eval pyrolysis is used to identify the type and maturity of organic matter and to detect petroleum potential in sediments (Espitalie et al, 1985; Peters, 1986). Rock Eval pyrolysis was performed using Rock-Eval 6 analyzer (Behar et al., 2001) (Fig. A.7).

The Rock-Eval pyrolysis method consists of a completely automated program temperature heating (in a pyrolysis oven) in an inert atmosphere (helium) of a small sample to quantitatively and selectively determine (1) the free hydrocarbons contained in the sample and (2) the hydrocarbon- and oxygen-containing compounds (CO_2) that are volatilized during the cracking of the unextractable organic matter in the sample (kerogen) (Pimmel and Claypool, 2001).

Figure A.7: Rock-Eval 6 analyser.

19 samples from the Monte Petrano section and 23 samples from the Cismon section have been analyzed. About 60mg of previously milled sample were put in a crucible and measured using a RockEval6 analyzer. Blue Lias Formation (SAB 134) have been run every ten samples as internal standard (between 1 and 2mg). The amount of sample to be used is related to its TOC concentration, so

that the sample and the standard have a similar organic carbon content. The crucible containing the sample passes through the following pyrolysis oven temperature program: in the first phase the oven reaches a temperature of about 300°C thus allowing the volatilizing of the free hydrocarbons, determining the S1 peak detected by the Flame Ionization Detector (FID). In the second phase the temperature is increased from 300° to 550°C. This is the phase of volatilization of the very heavy hydrocarbons compounds (>C40) as well as the cracking of nonvolatile organic matter. The SID detects the hydrocarbons released from this thermal cracking giving rise to the S2 peak (by FID). The temperature at which S2 reaches its maximum is the so-called Tmax, a value that can be correlated with the nature and maturity of the kerogen. The CO_2 issued from kerogen cracking is trapped in the 300°-390°C range and then released and detected on a Thermal Conductivity Detector (TCD) during the cooling of the pyrolysis oven (S3 peak) (Fig. A.8).

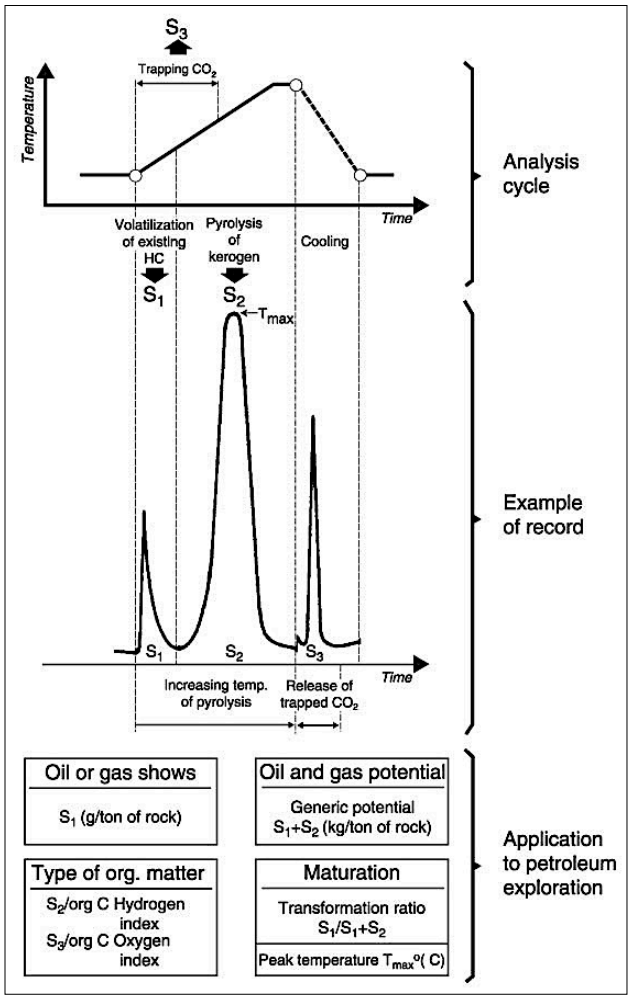

Figure A.8: Rock Eval trace (Pimmel and Claypool, 2001).

From the above-mentioned direct measurements other indirect measurements can be derived (Pimmel and Claypool, 2001):

- HI: Hydrogen Index [HI = (S2/TOC) x 100]. The Hi is a measure of the hydrogen richness of the source rock, and when the kerogen type is known it can be used to estimate the thermal maturity of the rock.
- OI: Oygen Index [OI = (S3/TOC) x 100]. The OI is a measure of the oxygen richness of a source rock. This index is unreliable in rocks with high carbonate content. High OI values (>50 mg/g) are characteristic of immature hydrocarbons.
- PI: Production Index [PI = S 1 /(S 1 + S 2)]. The PI is the ratio of already generated hydrocarbon to potential hydrocarbons. Low ratios indicate either immaturity or extreme postmature organic matter. High PI ratios indicate the mature stage or contamination by migrated hydrocarbons or drilling additives. The PI increases steadily with depth and associated hydrocarbon generation.
- PC: Pyrolyzable Carbon [PC = 0.083 × (S1 + S2)]. The PC corresponds to carbon content of hydrocarbons volatilized and pyrolyzed during the analysis.

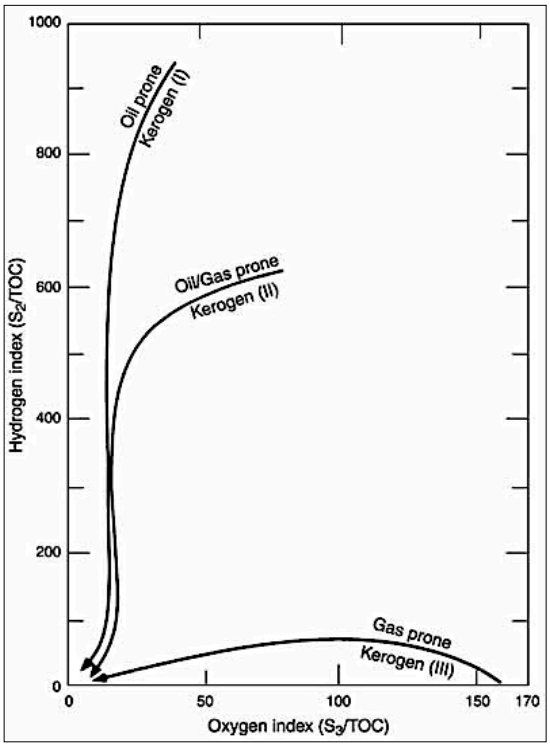

Figure A.9: Van Krevelen diagram (Pimmel and Claypool, 2001).

An important graphical plot is the van Krevelen diagram (van Krevelen, 1950), originally introduced for coals, in which the OI is plotted against the HI. This graph is widely used in order to differentiate the various types of kerogen (Fig. A.9).

A.8 X-ray Fluorescence (XRF)

A total of 23 samples collected from the Monte Petrano section and 96 samples coming from the Cismon section were analyzed by X-ray fluorescence analysis (XRF). For XRF, 700 mg of the sample powder are mixed with 4200 mg lithium tetraborate, pre-oxidized in oven at 500°C overnight with NH4NO3 and then fused to glass beads (Fig. A.10). The beads were analysed by a spectrometer (Philips PW 2400), calibrated with two carefully selected in-house geostandards: Perù-1A and Posidonia Shale-3.1 (Fig. A.11). Perù-1A is a fine-grained sediment taken from the upwelling area dominated by diatoms of the Peruvian margin, while Posidonia Shale is a black shale taken from the Lower Jurassic homonym formation that comprises finely laminated layers of organic-rich shales formed of fine-grained sediments intercalated with bituminous limestones.

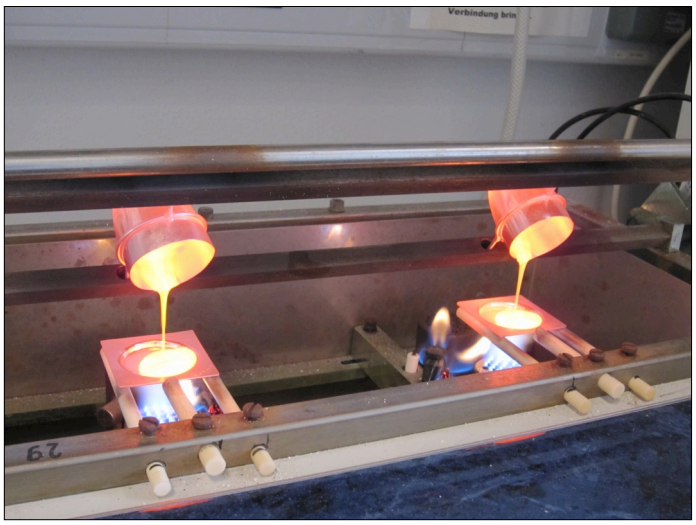

Figure A.10: Melted samples poured to form glass beads.

Analytical precision, as checked by parallel analysis of international reference material and in-house standards, is better than 1% for Si, Ti, Al, Fe, Mn, Ca, K, 2% for Na, Mg, and better than 5% for the following minor and trace elements Ba, Cr, Ni, Rb, Sr, V, Y, Zn, Zr, except P, Co, Cu, As, Pb (5-10%) (Schnetger et al., 2000).

Figure A.11: Philips PW 2400 spectrometer.

A.9 Cyclostratigraphy: orbital tuning by means of a probabilistic approach

In this work, a huge amount of quantitative analyses have been collected. Assuming that these data record astronomic cycles (de Boer and Smith, 1994; Berger and Loutre, 1994), for each studied section a cyclostratigraphic analysis has been performed.

First of all, the analysis consists in the determination of a proper sedimentation rate model by matching cycles in the sedimentary records with characteristic orbital periodicities. Secondly, the estimated sedimentation rate model is used to convert the stratigraphic record from the depth domain (where it was sampled) to the time domain. Whether possible, I tred to get more insights about duration and timing of key geological events recorded in individual sections. The cyclostratigraphic analysis is usually performed on the basis of a spectral analysis of the sedimentary sequence (Weedon, 2003).

In this work I adopted the approach to orbital tuning suggested by Malinverno et al. (2010). This method consists in the application of a semi-automatic probabilistic algorithm for the determination of the optimal distribution of the most likely sedimentation rates. The main actor of the method is the so-called ‘likelihood’, that is a measure of how much the sedimentation rate is likely, assuming an a priori

set of probable orbital frequencies. For every sedimentation rate, the magnitude of the likelihood measures the match between the frequency peaks brought by the data and the known tuning frequencies. The higher is the likelihood, the more likely is the sedimentation rate.

More formally, the likelihood p of a sedimentation rate u is the combination of the probability distribution describing the uncertainty of the *j-th* tuning frequency φ_j and the likelihood of the data in a red noise background. Such likelihood is expressed as the so-called 'Periodogram ratio' that is, the ratio between the periodogram of the data *Cd* and the periodogram of the background red noise *Cb*:

$$p(u) = \prod_{j=1}^{Nf} \int const * \varphi_j((f(u)) * \exp\left[\frac{C_d(f(u))}{C_b(f(u))}\right]$$

where f(u) is the frequency in cycles/My, const is a normalization factor, Nf is the number of tuning frequencies used.

So, the ingredients to evaluate the likelihood are basically:

1) A set of possible tuning frequencies with their uncertainty.

   In this case they were evaluated from the orbital solutions of Laskar et al. (2004) in a 10My interval from 100My to 90My. Periodograms of the orbital solutions in 2My windows were used for picking the frequencies of periodogram peaks corresponding to the orbital periods. The average peak frequencies, together with the associated standard deviations, were computed in the full 10My interval. The table below reports the resulting frequencies and their standard deviations used for tuning:

Orbital cycle	Mean Period (ky)	Mean Frequency (cycles/My)	Standard Deviation (cycles/My)
Long Eccentricity	403.9	2.476	0.050
Short Eccentricity	126.26	7.739	0.047
Short Eccentricity	97.81	10.223	0.075
Obliquity	37.58	26.608	0.082
Precession	22.57	44.305	0.049
Precession	21.39	46.762	0.121
Precession	18.33	54.545	0.094

Table A.12: Used *tuning frequencies*.

2) The periodogram of the data, relative to a stratigraphic interval that can be assumed homogeneous from the sedimentation rate point of view (herein after such interval will be referred as ‘block’);

3) The estimation of the periodogram of the red noise background associated to the data.

Before describing the workflow in detail, the choice of the dataset must be discussed. In the literature, cyclostratigraphic analysis devoted to orbital tuning is commonly applied to continuous profiles of data, e.g. petrophysical logs (Locklair and Sageman, 2008), geochemical logs (Westerhold and Röhl, 2009), layer thickness (Claps and Masetti, 1994), bioturbation density (Erba and Premoli Silva, 1994), etc. In this work, as will be better explained in Chapter 9, thanks to the extremely high-resolution sedimentological description, I considered the carbonate content variation throughout individual section. So, for each section, starting from the available stepwise sedimentological description, a set of carbonate content profiles were extrapolated according to the uniform distributions assigned to seven macro-classes of lithology. In particular, for limestone the carbonate content was assumed to be distributed uniformely between 90% and 97%, for cherty limestone the uniform distribution ranges from 60% to 70%, for marly limestone a uniform distribution from 60% to 80% was used. Marly carbonate content was chosen to distribute uniformely in the 40% - 60% range, while to radiolarian layers and cherts a uniform distribution between 0% and 2% was chosen. Most of the black shales were directly measured for their carbonate content, so there was no need to simulate the values for this lithology. Only for the few black shales without direct calcimetry data, values randomly distributed within the range of the measured ones were chosen. An example of the obtained carbonate content profile is shown in Figure A.13a. Two remarks can be raised: first, as this generated signal is highly correlated with the stratigraphic record, the interpretations reached during analysis must allow for the imperfections inherent in the sampling process. Second, non-deposition, erosion, seafloor dissolution and other geological processes that might have occurred during sedimentation could have partially corrupted the continuity of the signal (Weedon, 2003).

The following steps were applied (Figs. A.13 and A.14):

1) Block selection by trial and error. Assuming a piecewise constant model for the distribution of the sedimentation rate, it is necessary to identify the locations of the sedimentation rate changes along the sections, in order to perform the likelihood computation on a homogeneous block. By observing the available high-resolution sedimentological description, it is intuitive to set such interfaces in correspondence to the main sedimentological changes, like colour changing, presence of different lithologies and so on. Nonetheless, from this initial tentative

guess, block number and definition were chosen after several trial and error runs to obtain comparable spectra. Therefore, the criteria for the block selection were based both on lithological evidence and on spectral estimation optimization. For sake of simplicity, in the example sketched in Fig. A.13 and A.14 a case with a single block is reported.

2) Spectral estimation. In order to identify the main frequency components of the signal, the data belonging to each block were projected to the frequency domain by computing periodograms. The periodogram is one way of estimating the power spectral density of a process, by finding the discrete-time Fourier transform of the samples of the process itself and then appropriately scaling the magnitude squared of the result. The periodogram estimate of the power spectral density of a length-L signal xL[n] with Fs sampling frequency is:

$$P_{xx}(\mathrm{f}) = \frac{1}{LF_S}\left|\sum_{n=0}^{L-1} x_L(\mathrm{n}) e^{-\frac{j2\pi fn}{F_x}}\right|^2$$

As the carbonate content was mainly simulated and not directly measured, in order to refine the periodogram estimation a Montecarlo approach was used. For each section, 30 different realizations of the calcimetry profile were generated and their individual periodogram computed and averaged to obtain the average periodogram (Fig. A.13b). In order to filter the natural background red-noise within the signal and to get a more representative estimation of the frequency content of the studied record, the so-called 'Periodogram ratio', was computed (Fig. A.13e). It consists in the ratio between the average periodogram and a background component representing the red noise to filter (red curve in A.13d). Such background was estimated via non-linear least square fitting on the logarithm of the average periodogram (Fig. A.13c), according to the following formula:

$$C_b(f) = \frac{a}{(f_0^2 + f^2)^b}$$

where f_0, a and b are fitting parameters. The resulting exponential of the Periodogram ratio, which will enter in the likelihood computation, is represented in Fig. A.13f.

3) Likelihood computation and block optimal sedimentation rates estimation. This step consists in the computation of the likelihood function for each block, according to Malinverno et al. (2010) and in the evaluation of the sedimentation rate that maximizes the likelihood itself. In Fig. A.14g1 and in Fig. A.14g2 the match between the Periodogram ratio (in black) and

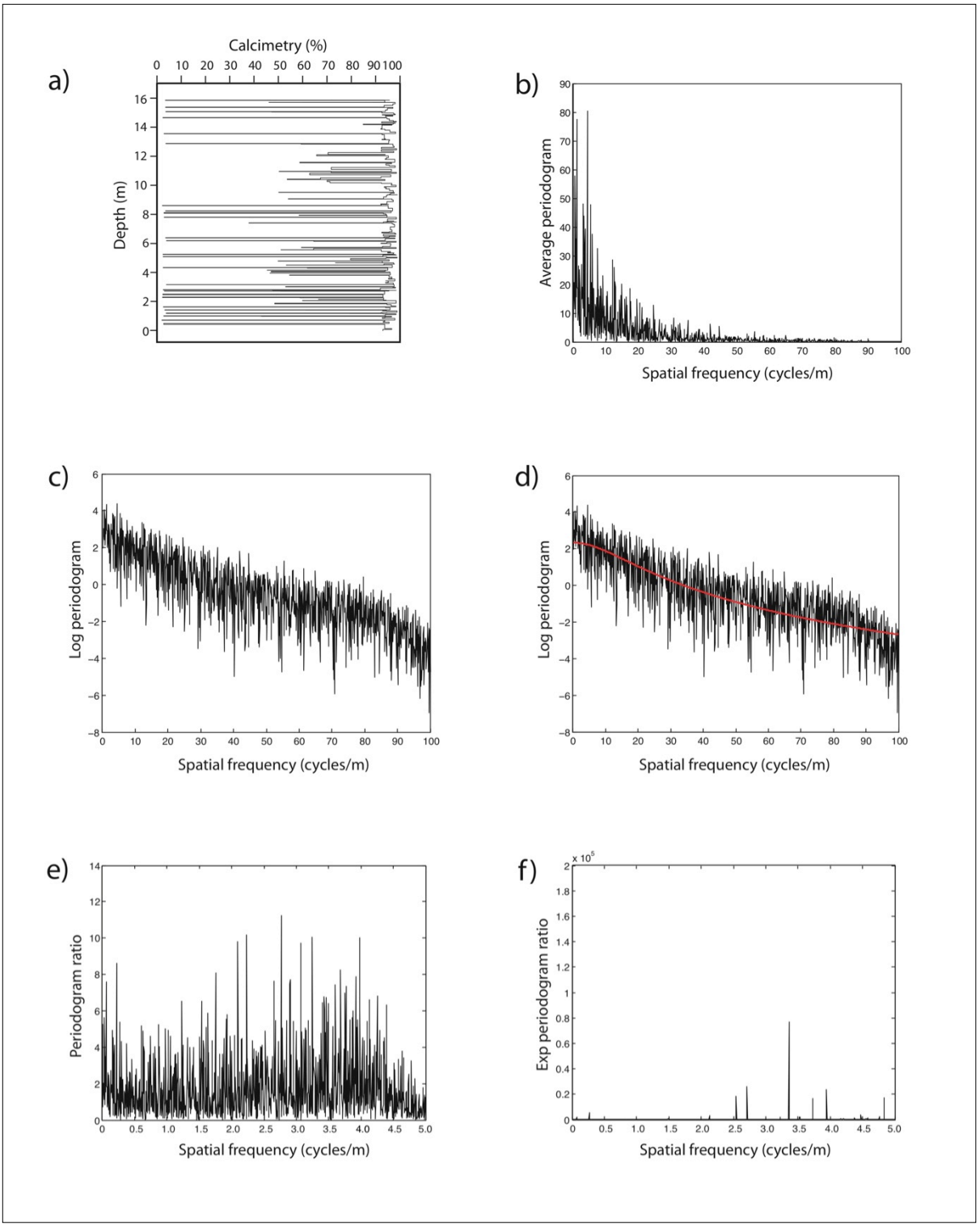

Figure A.13: *Workflow applied for the cyclostratigraphic analyses (steps a) to f)).*

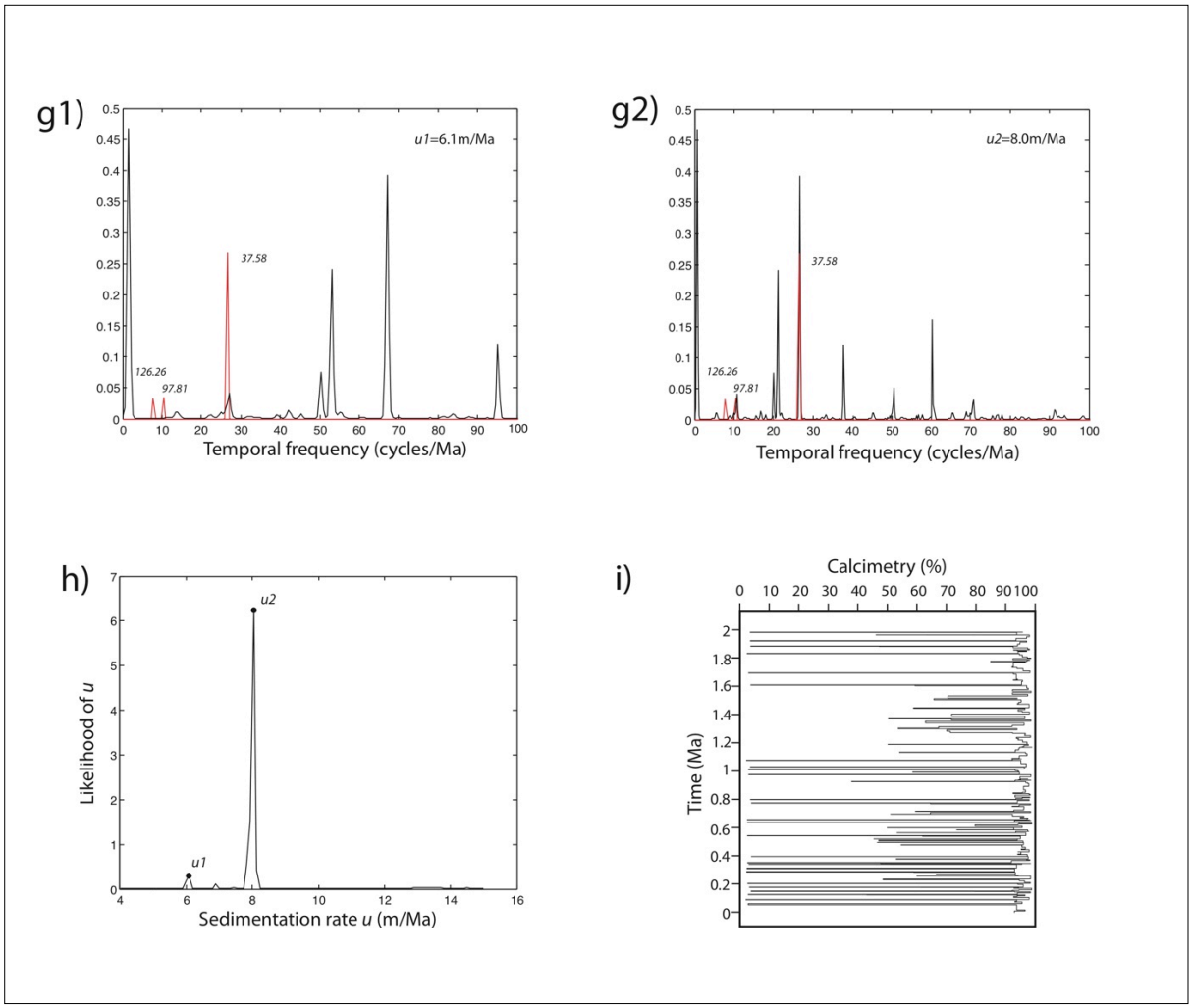

Figure A.14: *Workflow applied for the cyclostratigraphic analyses (steps g) to i)).*

uncertainty of tuning frequencies (in red) can be seen for two different sedimentation rates. The likelihood (Fig. A.14h) is higher in the second case, as there is more overlap between the curves, thus meaning that the second sedimentation rate is the most likely.

4) Time conversion. Finally, the sedimentation rate model (one sedimentation rate per block) was used for converting the stratigraphic record to time. The result is shown in Fig. A.14i.

References

Abineri, K.W. (1986a) – The preparation of cellulose lacquer rock peels. *Microscopy*, 35, 451-459.

Abineri, K.W. (1986b) – Notes on methods of staining lacquer rock peels. *Microscopy Bulletin*, 11, 3-5.

Abineri, K.W. (1989) – Photomicrographs of cellulose peels from the Mesozoic rocks of Dorset. *Proceeding of the Geologist's Association*. 100, 161-174.

Behar, F., Beaumont, v., Penteado, H.L. De B. (2001) – Rock-Eval 6 Technology: performances and developments. *Oil and gas Science and Technology – Revue de l'Institut Francais du Petrole*, 56, 111-134.

Berger, A. and Loutre, M.F. (1994) – Astronomical forcing through geological time. *In:* de Boer, P.L. and Smith, D.G. (Eds.), *Orbital forcing and cyclic sequences*, Special Publication of the Interational Association of Sedimentologists, 19, 15-24.

Claps, M. and Masetti, D. (1994) – Milankovitch periodicities recorded in Cretaceous deep-sea sequences from the Southern Alps. *In:* de Boer, P.L. and Smith, D.G. (Eds.), *Orbital forcing and cyclic sequences*, Special Publication of the Interational Association of Sedimentologists, 19, 99-107.

Coplen T.B. (1994) – Reporting of stable hydrogen, carbon, and oxygen isotopic abundances. *Pure and Applied Chemistry* 66, 273-6.

Davies, P.J. and Till, R. (1968) – Stained dry cellulose peels of ancient and recent impregnated carbonate sediments. *Journal of Sedimentary Petrology*, 38, 234-237.

de Boer, P.L. and Smith, D.G. (1994) – Orbital forcing and cyclic sequences. *In:* de Boer, P.L. and Smith, D.G. (Eds.), *Orbital forcing and cyclic sequences*, Special Publication of the Interational Association of Sedimentologists, 19, 1-14.

Erba, E. and Premoli Silva, I. (1994) – Orbitally driven cycles in trace-fossil distribution from the Piobbico core (late Albian, central Italy). *In:* de Boer, P.L. and Smith, D.G. (Eds.), *Orbital forcing and cyclic sequences*, Special Publication of the Interational Association of Sedimentologists, 19, 211-225.

Espitalie, J., Deroo, G. and Marquis, F. (1985) – Rock Eval Pyrolysis and its applications. *Preprint: Institut Francais du Petrole, Geologie*, No. 27299, 72pp. English translation of: La pyrolyse Rock Eval et ses applications. *Premiere, Deuxieme et Troisieme Parties, in Revue de l'Institut Francais du Petrole*, 40, 563-579 and 755-784, 41, 73-89.

Germann, K. (1965) – Die techniek des Folienabzuges und ihre Ergänzung durch Anfarbemethoden. *Neues Jahrbuch Geologie und Paläontologie Abhandlungen, 121, 293-306.*

Graham, A.R. (1963) – Routine preparation of polished thin-sections. *The Canadian Mineralogist*, 7, 375-377.

Gutteridge, P. (1985) - Grain-size measurement from acetate peels. *Journal of Sedimentary Petrology*, 55, 595-596.

Laskar, J., Robutel, P., Joutel, F., Gastineau, M., Correia, A.C.M., Levrard, B. (2004) – A long-term numerical solution for the insolation quantities of the Earth. *Astronomy and Astrophysics*, 428, 261-285.

Locklair, R.E. and Sageman, B.B. (2008) – Cyclostratigraphy of the Upper Cretaceous Niobrara Formation, Western Interior, U.S.A.: A Coniacian–Santonian orbital timescale. *Earth and Planetary Science Letters*, 269, 540-553.

Malinverno, A., Erba, E., Herbert, T.D. (2010) - Orbital tuning as an inverse problem: Chronology of the early Aptian oceanic anoxic event 1a (Selli Level) in the Cismon APTICORE. *Paleoceanography*, 25, PA2203, doi:10.1029/2009PA001769.

McCrone, A.W. (1963) – Quick preparation of peel-prints for sedimentary petrography. *Journal of Sedimentary Petrology*, 33, 228-230.

Schnetger, B., Brumsack, H.-J., Schale, H., Hinrichs, J., Dittert, L. (2000) – Geochemical characteristics of deep-sea sediments from the Arabian Sea: a high-resolution study. *Deep-Sea Research II*, 47, 2735-2768.

Peters, K.E. (1986) – Guidelines for evaluating petroleum source rock using programmed pyrolysis. *American Association of Petroleum Geologists, Bulletin*, 70/3, 318-329.

Pimmel, A., and Claypool, G. (2001) – Introduction to shipboard organic geochemistry on the JOIDES Resolution. *ODP Tech. Note*, 30, doi:10.2973/odp.tn.30.2001.

van Krevelen, D.W. (1950) – Graphical-statistical method for the study of structure and reaction processes of coal. *Fuel*, 29, 269-284.

Weedon, G.P. (2003) - *Time-Series Analysis and Cyclostratigraphy: Examining Stratigraphic records of Environmental Cycles*, pp. 1-259.

Westerhold, T. and Röhl, U. (2009) – High resolution cyclostratigraphy of the early Eocene – new insights into the origin of the Cenozoic cooling trend. *Climate of the Past*, 5, 309-327.

Wilson, M.A. and Palmer T.J. (1989) – Preparation of acetate peels. *In:* Feldmann, R.M., Chapman, R.E., Hannibal, J.T. (Eds.), *Paleotechniques*, The Paleontological Society, Special Publication, 4, 142-145.

Appendix B
Sensitivity tests on cyclostratigraphy

This appendix reports a short discussion about the sensitivity of the method applied for the cyclostratigraphic analysis. In particular, in order to be able to control the output of the method, an artificial dataset is constructed from ETP curve (Section B.1) and then it is used to explain how the process of block choice has been performed (Section B.2). Finally, a brief discussion of the impact of the parameters choice is presented (Section B.3)

B.1 Dataset construction

In this section, the description of the construction of an artificial dataset is illustrated. The idea is to built a dataset in such a way that it is able to:

• have a known frequency content, so that the result of the cyclostratigraphic analysis is known *a priori*;

• mimic the data measured in nature- that is, it can be compared with the calcimetry records used for the cyclostratigraphic analysis of the sections illustrated in Chapter 8.

In order to fullfil the first requirement, the astronomic solution of Laskar (2004) has been considered. In particular, a time frame of 10My from 100 My to 90 My has been considered and the correspondent Laskar solutions for eccentricity, obliquity and precession have been extracted. For each of the considered astronomical parameters, the characteristic frequencies are known (see Figure B.1, where the power spectrum density (PSD) estimates of such solutions are represented).

In Figure B.2 the convolution of the three orbital parameters is reported, together with its PSD estimate. In the following, such signal will be identified as *ETP*. It has been constructed by summing the normalized astronomical parameters. As it can be appreciated, the power spectrum density of ETP is characterized by seven peaks are present, each of which corresponds to a characteristic frequency of the astronomical parameters.

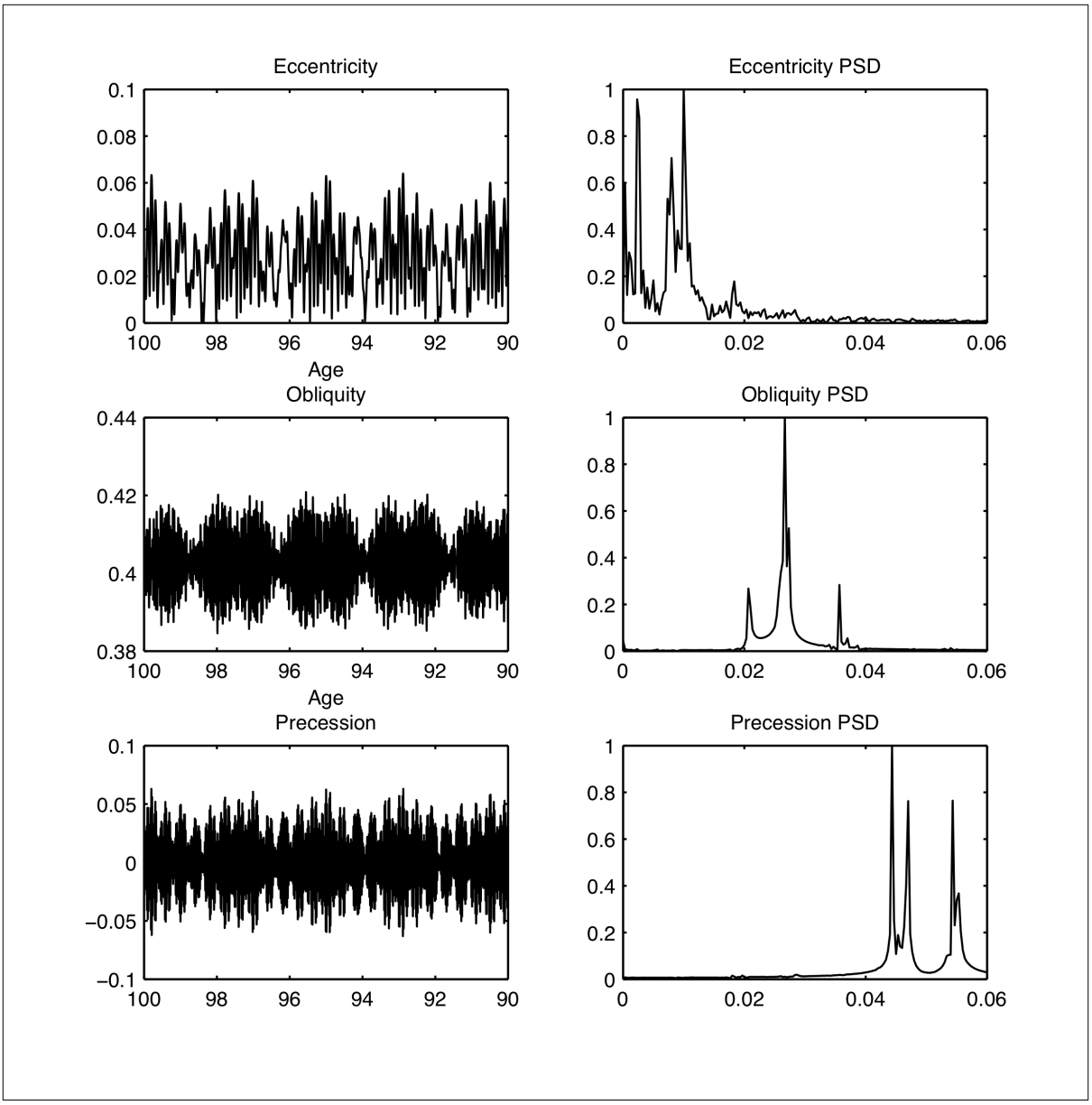

Fig. B.1: Power spectrum density estimation of Laskar solutions and correspondent frequencies.

ETP is the astronomic record that will be carried by the artificial signal. For the moment, it is expressed as a function of time and its value has no geological meaning. Therefore, firstly it is necessary to transform it as a function of depth by multiplying it for an appropriate sedimentation rate model, secondly it should be converted to calcimetry.

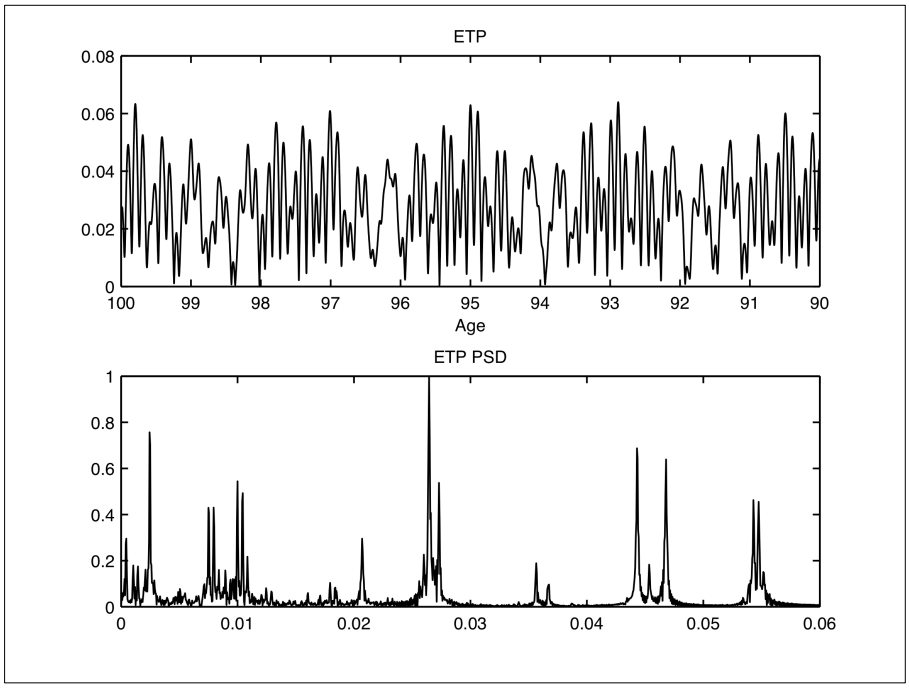

Fig. B.2: ETP curve and its power spectrum density estimation.

As discussed in Chapter 8, a constant sedimentation rate model is not a realistic assumption because of the duration of the considered period. So, in order to reproduce as much as possible what has been observed in the real data, it has been chosen a piecewise constant sedimentation rate model, as follows:

- 7.5 m/My for 3My, from 100 My to 97 My
- 5 m/My for 4.5My, from 97 to 92.5My
- 9 m/My for 2.5My, from 92.5 to 90My

The resulting ETP record converted to depth domain is represented in Figure B.3. The total thickness is 67.5m and the exact block interfaces lie respectively at 22.5m and at 45m.

At this point, the ETP values must be mapped into the scale of carbon content, preferably in such a menner as to respect the proportions of carbon content distribution observed in the considered sections.

For this purpose, Figure B.4 reports the histograms of the distributions of calcimetry for four out of the five sections considered in this work.

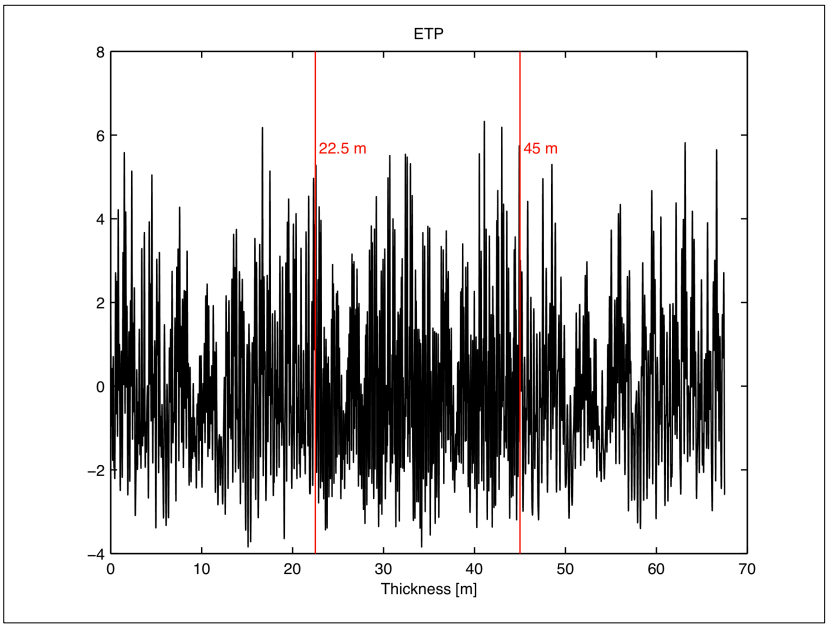

Fig. B.3 – Power spectrum density estimation of Laskar solutions and correspondent frequencies.

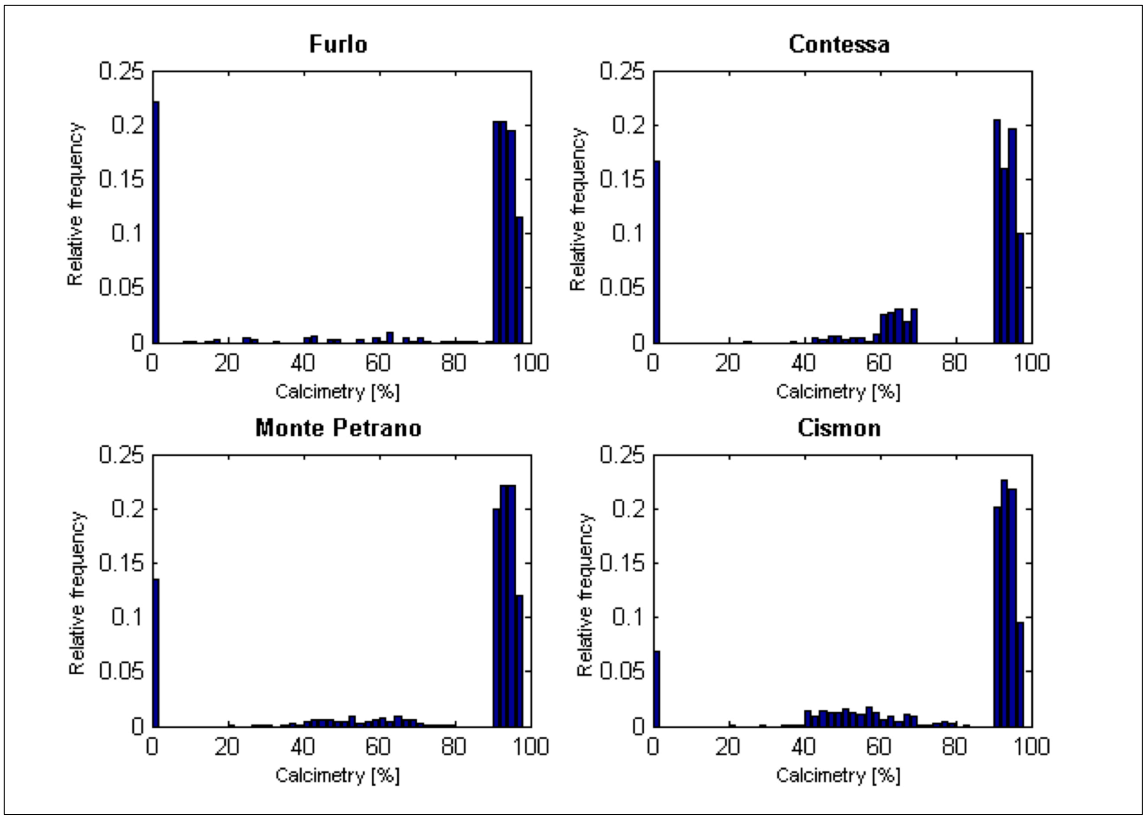

Fig. B.4 – Histograms of calcimetry distributions for the studied sections.

As it can be noticed, the comparison of the histograms highlights that the calcimetry distribution is very similiar for the considered sections, thus enforcing the idea that it makes sense considering them together. By analogy of what has been done in Chapter 8 for transforming the high-resolution sedimentological description into calcimetry, four classes of calcimetry have been identified. They should correspond to the macro lithology identified in the section. It must be noted that in this case an approxi- mation is done, as the calcimetry ranges associated to the lithology classes overlap, while here we need to build disjointed classes. The relative frequency of each class has been computed for each section and an average relative frequency class has been estimated. The results are reported in Table B.1:

calcimetry class %	Furlo	Contessa	Monte Petrano	Cismon	Average relative frequency
$0-2\%$	22.02%	16.60%	13.51%	6.94%	**14.77%**
$2-60\%$	3.45%	4.04%	6.19%	13.72%	**6.85%**
$60-90\%$	2.98%	13.25%	4.04%	5.41%	**6.42%**
$90-97\%$	71.55%	66.11%	76.25%	73.93%	**71.96%**

Table B.1 – Relative frequency of classes of calcimetry estimated for the sections.

Finally, the ETP values has been first sorted and then divided into four groups- that is, the four calcimetry classes. The entity of each group has been determined by the relative frequency of the calcimetry classes of the observed sections. In this way, it is possible to simulate the calcimetry value as it has been done for the section. The distribution has been uniformely sampled in the correspondent calcimetry class. The resulting calcimetry profile is reported in Figure B.5 (left) together with one of the simulated calcimetry profile for Monte Petrano section (Figure B.5 (right)). As it can be seen, the two profiles are very similar.

In the next, the simulated profile will be used for testing the cyclostratigraphic method applied in this work, after having. It contains the astronomic frequencies of eccentricity, obliquity and precession and its values have been transformed in order to resemble a realistic geological record.

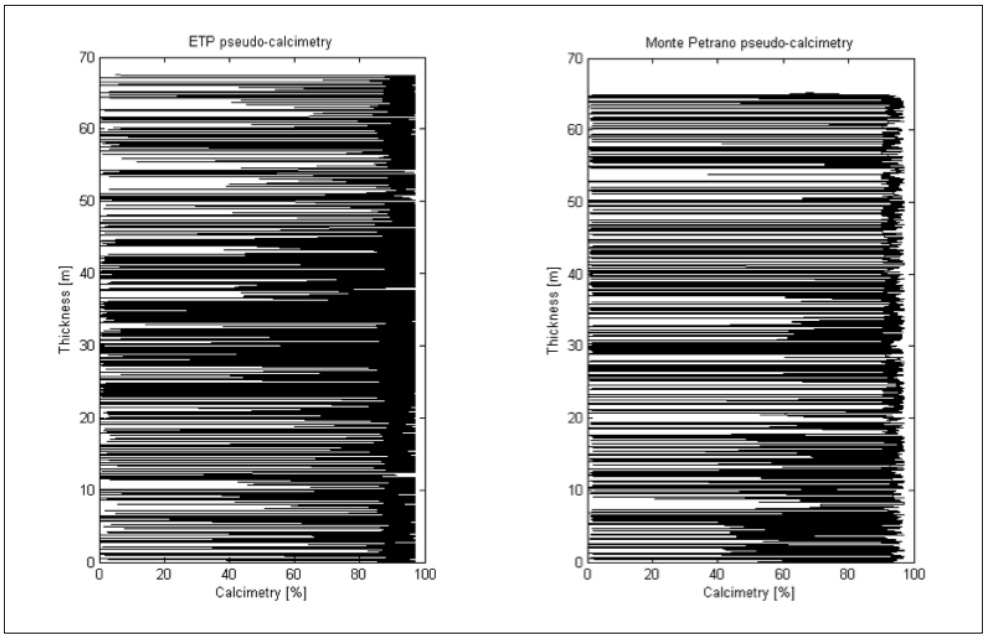

Fig. B.5 – Left: Artificial calcimetry profile simulated from ETP. Right: Calcimetry profile of Monte Petrano section.

B.2 Results

In this section, the cyclostratigraphic method illustrated in Chapter 3 is applied to process the artificial dataset constructed in Section A.1. Although such dataset contains all the astronomical frequencies, in the following only the ones used in the analysis of Chapter 8 will be considered, in order to reproduce exactly what has been run for the real data. In particular, the considered frequencies correspond to two short eccentricity periods (126.26 ky with standard deviation 0.1 and 97.81 ky with standard deviation 0.075) and obliquity (37.58 ky with standard deviation 0.082).

The process is basically a trial and error scheme: starting from an initial guess on the number and placement of the blocks, the likelihood function is computed and analised. The aim is finding the best block distribution and associated sedimentation rate that is able to convert the data from depth to time domain, given the uncertainty on the astronomical frequencies. In this case, the initial run is perfomed on the entire section, thus considering one single block. As it can be seen in Figure B.6a, where the computed likelihood is represented, three distinct peaks are detected by the procedure: they are exactly the sedimentation rates used for the construction of the dataset (respectively, 7.5m/My, 5m/My and 9m/My). The fact that there are multiple peaks indicate that the spectrum of the data is the convolution of three signals. In the case of a geological record, the high-resolution sedimentological description is available. Thanks to this, it is possible to choose the block interfaces in a geologically sensible way. In

the case of this artificial dataset, where no other information is available, the choice is to follow what the data is suggesting: three likely sedimentation rates are evidence of three distinct blocks. Hence, the procedure has been run separately on three blocks, defined as in Figure B.6b). The result is again unsatisfactory, because for each block at least two distinct peaks are present. This means that the choice of blocks is still not optimal. Once identified a reasonable number of blocks, the effort is focused in the calibration of one interface at a time. For example, several trial and error likelihood computations are performed in order to get to a satisfactory result for one interface, like in Figure B.6c). In this case, the lilekihood for the lowermost block is carachterized by a single peak. Repeating the method by changing the uppermost block interface, it is possible to tune the model up to the exact solution, reported in Figure B.6d).

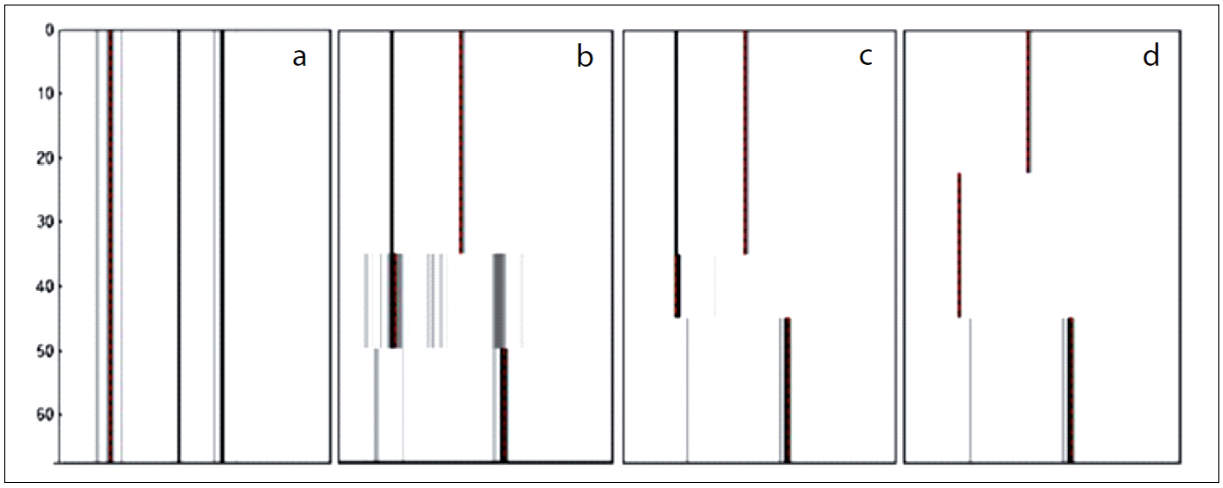

Fig. B.6 – Likelihood image with the change in block interface locations.

B.3 Discussion and conclusions

In this section, the attention is drawn on the impact of the choice of the parameters for the computation of the likelihood function. In particular, a brief discussion of the main critical steps of the procedure is listed here below.

• **Resolution of the dataset** The dataset has a *mm* resolution, that reflects the resolution of the sedimentological description. Of course, the original data is not sampled on a uniformely spaced grid, so a resampling has been performed. With the purpose of avoiding artifacts in the signal, the grid step for every section has been set to 1mm.

• **Periodogram estimation** Periodogram estimation is performed using the Discrete Fourier transform (DFT) algorithm. In this case the main parameter is the number of points of the transfor- mation. The higher the number of points is, the higher the computational time. Therefore, such parameter has been chosen in such a way that the periodogram estimation resulted both accurate enough for the likelihood computation and faster enough to allow a trial and error analysis.

• **Background periodogram estimation** The background estimation has been performed by means of non linear regression fitting. Such algorithm requires an initial guess of the objective parameters. The closer to the solutionthe initial guessis, the better the fitting performances. For this reason, the initial guess has been tuned on each section and optionally on each block.

In conclusion, this appendix has shown how the methodology for cyclostratigraphic analysis works. The algorithm is far from being automatic, as a lot of attention has been drawn in the choice of the initial parameters, like block number and location and periodogram estimation parameters. Applied to an articial case, the procedure is able to detect the exact piecewise sedimentation rate model that determines the given astronomical frequencies. For this reason, there is a good degree of confidence in using it on real datasets, as presented in Chapter 8.

List of attachments

The following documents are available in the CD attached to this thesis:

Attachment 1a – Detailed sedimentological log of the Furlo section
Attachment 1b – Detailed sedimentological log of the Contessa section
Attachment 1c – Detailed sedimentological log of the Le Brecce section
Attachment 1d_lower and **1d_upper** – Detailed sedimentological log of the Monte Petrano section
Attachment 1e_lower and **1e_upper** – Detailed sedimentological log of the Cismon section
Attachment 1f – Detailed sedimentological log of the Bonarelli Level at the Furlo section
Attachment 1g – Detailed sedimentological log of the Bonarelli Level at the Contessa section

Attachment 2 – Stable isotopes of oxygen and carbonate- and organic- carbon data

Attachment 3 – Rock Eval pyrolysis data

Attachment 4 – Calcimetry data

Attachment 5 – X-ray fluorescence (XRF) data

For request of additional supplementary material and data please contact the author at gabriele.gambacorta@unimi.it

Acknowledgments

"It is good to have an end to journey toward; but it is the journey that matters, in the end."

— Ernest Hemingway

The completion of this thesis represents the end of a long journey.

First, I would like to deeply thank my supervisor Prof. Elisabetta Erba. Words cannot express all my gratitude for having constantly trusted in me. Your continuous support, generous sharing of your knowledge and friendship have made this PhD so precious to me. You're a great teacher and a special person: I'm so proud of being one of your students.

A great thank goes to Prof. Riccardo Bersezio: you are a truly example of continuous dedication and passion. I will take care of all your precious teachings in the forthcoming years.

It's my honour to thank Prof. Isabella Premoli Silva for all the suggestions that with affability and modesty she gave me during my research.

I gratefully acknowledge Prof. Hugh Jenkyns for hosting me in Oxford and all the support he gave me since the beginning of this PhD: it has been an incredible experience working with you side by side.

I would like also to extend my gratitude to Prof. Hans Brumsack and Dr. Barnie Schnetger for being so willing to share their knowledge with me. I really enjoyed my time in Oldenburg at ICBM: you both made my stay a really enjoyable experience.

My appreciation goes to Dr. Alberto Malinverno for his kind support and suggestions. I really appreciated your exquisite willingness and the interesting discussions we had together.

I would like to give special thanks to my dissertation committee: Prof. Laura Scesi, Prof. Giancarlo Della Ventura and Prof. Helmut Weissert.

I am indebted to Dr. Giancarlo Davoli, Dr. Sergio Nardon and Dr. Paolo Ruffo for their useful suggestions and confidence.

Additionally I expand my thanks to Dr. Norman Charnley, Dr. Chiara Compostella, Dr. Chris Day, Dr. Peter Ditchfield, Curzio Malinverno, Dr. Maria Rose Petrizzo, Steve Wyatt for their help and assistance.

Thanks to my roommates Cristina, Fabio, Sara and Silvia for all these years together and for tolerating the hundreds of samples I scattered all around our room… You made my time at the university enjoyable. I extend my thanks also to Alessia, Cinzia, Dario, Francesca, Gaia, Giulia and Irene.

In order to accompany me over these years, many friends have become familiar with terms before unknown to them, such as Bonarelli, black shale or radiolarian layer. It must have been a real nightmare for you all! Jokes apart, I'm grateful with you for all the support and attachment you gave me during this long path. In particular I would like to mention: Andrea P., Andrea L., Davide, Doriana, Eleonora, Paola, Sergio, Sandro, Simone and all those fantastic people that every Wednesday share with me the incredible experience of ambulance volunteering (I hope I did not forget anyone). I'm so happy of having you all as friends.

A special thank goes to Silvia and Enzo for their kind and affectionate help.

I am deeply and forever indebted to my family who instilled within me the love for nature and science. I am deeply proud of you all. During the inevitable ups and downs of conducting my research they often reminded me life's true priorities.

At last, my biggest thank is for the person that throughout my PhD have shared with me satisfaction and frustration, sun and rain, happiness and sadness… Matilde, with your love, continuous support and encouragement, you made this journey unique.